

Politechnika Wrocławska

Field: Chemistry
Discipline: Chemical science
PhD thesis

Heterogeneous catalysts based on plant biomass accumulating metals: preparation and application in organic chemistry.

M.Sc. Pola Cybulska

Promotor: prof. dr hab. inż. Tomasz Olszewski
keywords: organic chemistry, ecocatalysis, organophosphorus compounds, phospha-Michael addition, Knoevenagel-phospha-Michael addition

WROCŁAW 2026

Abstract

The work presents an ecocatalysis concept that links metal phytomanagement with efficient and green synthesis of organophosphorus compounds. As the metal source, biomass of the hyperaccumulator, *Arabidopsis halleri*, was used. After simple calcination, a polymetallic heterogeneous catalyst Eco-MgZnOx was obtained, in which basic MgO sites neighbor Lewis-acidic ZnO sites. This bifunctionality gives synergy: simultaneous activation of the nucleophile (P-H or CH acid) and electrophiles ($C{=}O$, $C{=}C$), lowering reaction barriers and increasing selectivity.

The material's effectiveness was verified in three reaction classes: hydrophosphonylation of aldehydes (Pudovik reaction), phospha-Michael addition to activated alkenes, and the Knoevenagel-phospha-Michael cascade run in one- or two-step modes. In all cases, very high conversions (often reaching 95-100%) and clean product profiles were obtained under mild conditions (50-70℃, solvent-free, with catalyst loading of about 5 mol% relative to Zn). A broad substrate tolerance was demonstrated (aromatic, heteroaromatic, aliphatic compounds, various H-phosphonates), multiple recycling of the catalyst with minimal loss of activity, and scale-up to the gram scale without loss of efficiency. DFT calculations and structural analyses confirmed the presence of a solid-solution $Mg(Zn)O$ phase responsible for the observed synergy.

This solution addresses the problems outlined in the introduction: declining availability and rising costs of metals, and the high environmental footprint of their extraction. Phytoextraction provides a green metal source, and the product - a durable catalyst - closes the value loop by coupling remediation with useful synthesis. The main limitation is the need for strongly activated alkenes and a moderate sensitivity to sterics. Nevertheless, applicability remains broad. Altogether, the results show that ecocatalysts from *A. halleri* biomass constitute a practical, scalable, and green-chemistry-compliant platform for forming C-P and C-C bonds.

Streszczenie

Praca przedstawia koncepcję ekokatalizy łączącą fitogospodarowanie metali z efektywną i „zieloną” syntezą związków fosforoorganicznych. Jako źródło metali wykorzystano biomasę hiperakumulatora, Rzeżusznika Hallera (*Arabidopsis halleri*). Po prostej kalcynacji biomasy uzyskano polimetaliczny, heterogeniczny katalizator Eco-MgZnOx, w którym sąsiadują zasadowe centra MgO i kwasowe centra Lewisa ZnO. Ta dwufunkcyjność daje efekt synergii: jednoczesną aktywację nukleofila ($P-H$ lub CH-kwasu) i elektrofili ($C=O$, $C=C$), co ułatwia zajście reakcji i zwiększa ich selektywność.

Skuteczność materiału zweryfikowano w trzech klasach reakcji: hydrofosfonylacji aldehydów (reakcja Pudovika), addycji fosfa-Michaela do aktywowanych alkenów, oraz w kaskadzie Knoevenagel-fosfa-Michael prowadzonej jedno- lub dwustopniowo. We wszystkich przypadkach uzyskano bardzo wysokie konwersje, często sięgające 95-100%, i czyste profile produktów w łagodnych warunkach (50-70℃, bez rozpuszczalnika, z katalizatorem w ilości około 5 mol% względem Zn). Wykazano szeroką tolerancję substratową (związki aromatyczne, heteroaromatyczne, alifatyczne, różne H-fosfoniany), wielokrotny odzysk katalizatora z minimalnym spadkiem aktywności oraz skalowanie do skali gramowej bez utraty wydajności. Obliczenia DFT i analizy strukturalne potwierdziły istnienie fazy $Mg(Zn)O$ odpowiedzialnej za obserwowaną synergię.

Opisane w ramach rozprawy rozwiązanie odpowiada na problemy opisane we wstępie: malejącą dostępność i rosnące koszty metali oraz wysoki ślad środowiskowy ich wydobycia. Fitoekstrakcja stanowi zielone źródło metali, a produkt - trwały katalizator - zamyka obieg wartości, łącząc remediację z użyteczną syntezą. Ograniczeniem metody jest potrzeba silnie aktywowanych alkenów i umiarkowana wrażliwość na zawadę steryczną, jednak stosowalność pozostaje szeroka. Łącznie wyniki dowodzą, że ekokatalizatory z biomasy *A. halleri* stanowią praktyczną, skalowalną i zgodną z zasadami zielonej chemii platformę do tworzenia wiązań $C-P$ i $C-C$.

Preface

The rapid progress of modern organic chemistry is closely tied to advances in catalysis. Catalysts, particularly those based on transition metals, have enabled the development of numerous methods for synthesizing compounds of high biological and industrial value. At the same time, the growing demand for metals, their fluctuating availability, the costs of extraction, and the environmental burdens of mining and processing pose serious challenges both for fundamental research and industrial practice. In response to these issues, new concepts such as ecocatalysis have emerged. This strategy is based on the use of biomass from metal-hyperaccumulating plants to obtain active, polymetallic heterogeneous catalysts.

This dissertation contributes to this research field by bridging phytomanagement of metals, sustainable catalysis, and the synthesis of organophosphorus compounds-molecules of great importance in biological, pharmaceutical, and agrochemical contexts. The work is organized into five main chapters, which guide the reader from the problem and scientific context, through the proposed biomaterial-based solution, to practical demonstrations of efficiency and perspectives for further development.

Chapter 1 provides the introduction and theoretical background. It outlines the global challenges of metal scarcity and increasing costs, as well as the environmental footprint of metal extraction. The concept of phytomanagement is introduced as a strategy that can simultaneously remediate heavy metal-contaminated soils and generate biomass enriched in these elements. Special emphasis is placed on *Arabidopsis halleri* - a model Zn/Cd hyperaccumulator-and the molecular mechanisms behind its metal uptake and storage capacity. Against this background, the concept of ecocatalysis is introduced as a potential response to the demands of green chemistry.

Chapter 2 presents the first application of the biogenic Eco-MgZnOx catalyst, obtained from *A. halleri* biomass, in the hydrophosphonylation of carbonyl compounds (Pudovik reaction). Detailed optimization studies are reported, including reaction conditions, substrate scope, functional group tolerance, stereochemical aspects, and catalyst stability. The possibility of recycling and reusing the catalyst, as well as scaling up the reaction to the gram scale, are demonstrated. The chapter also discusses theoretical calculations that provided mechanistic insights and explained the bifunctional synergy between MgO and ZnO sites.

Chapter 3 focuses on the Knoevenagel condensation, a classic $C-C$ bond-forming reaction between aldehydes and activated methylene compounds. It is shown that Eco-MgZnOx, due to its coexistence of basic and Lewis acidic sites, significantly out-

performs single-component catalysts such as MgO or ZnO. The chapter highlights a broad substrate scope, covering aromatic, heteroaromatic, and aliphatic aldehydes, as well as different methylene donors (malononitrile, cyanoacetates). Catalyst stability over several reaction cycles and successful scale-up are also demonstrated.

Chapter 4 explores the phospha-Michael addition, a reaction forming $C-P$ bonds through the addition of H-phosphonates to activated alkenes. The chapter presents reaction optimization, comparison with simpler oxide catalysts, and studies of catalyst stability and regeneration. Eco-MgZnOx is shown to efficiently catalyze the addition of phosphonates to a wide range of arylidene malononitriles and cyanoacrylates, achieving high yields even in preparative-scale experiments.

Chapter 5 discusses the combined Knoevenagel-phospha-Michael cascade reaction, an example of a multicomponent one-pot process. Particular attention is paid to the competing Pudovik reaction, which in non-catalyzed systems reduces selectivity. The results demonstrate that Eco-MgZnOx enables the cascade to proceed either sequentially or in a single step, with high selectivity and excellent yields. Catalyst recycling, gram-scale synthesis, and tolerance to different substrates confirm the practical utility of this approach.

The final section of the dissertation integrates results from all studies and formulates general conclusions. It emphasizes that the biogenic Eco-MgZnOx catalyst represents a universal catalytic platform for $C-C$ and $C-P$ bond formation. The material combines high efficiency and selectivity with recyclability and straightforward regeneration, while its production is based on hyperaccumulator biomass-a byproduct of phytoremediation. The work thus demonstrates that it is possible to combine environmental remediation with the development of modern, sustainable catalytic methods in organic synthesis.

This dissertation not only delivers detailed studies of a new type of catalyst but also situates them in the broader context of transforming chemistry toward sustainability. It shows that biomass often regarded as waste can be turned into a valuable resource, and that environmental solutions may serve as inspiration for innovative advances in organic synthesis.

- Pola Cybulska, Yves-Marie Legrand, Alicja Babst-Kostecka, Sébastien Diliberto, Anna Leśniewicz, Erwan Oliviero, Valérie Bert, Clotilde Boulanger, Claude Grison, Tomasz K. Olszewski. *Green and effective preparation of α-hydroxyphosphonates by ecocatalysis.* Molecules 2022, 27(10), 3075, 1-19.

- Pola Cybulska, Tomasz K. Olszewski. Biomasa zanieczyszczona metalami jako odnawialne źródło metali do wytwarzania katalizatorów polimetalicznych oraz ich zastosowanie w chemii organicznej. VII Łódzkie Sympozjum Doktorantów Chemii, University of Łódź, Poland, May 9-10, 2019 (poster).
- Pola Cybulska, Tomasz K. Olszewski. Utility of biomass from metal hyperaccumulating plants for preparation of polymetallic catalysts and their application in organic synthesis. 21st Tetrahedron Symposium, June 21-24, 2021, [abstract in: Elsevier, 2021] (poster).
- Pola Cybulska, Tomasz K. Olszewski. Catalysts prepared from metal hyperaccumulating plants and their application in phosphorus chemistry. 23rd International Conference on Phosphorus Chemistry, Częstochowa, July 5-9, 2021 [abstract in conference materials, eds. Tomasz Cierpiał et al., Częstochowa: Jan Długosz University Press, 2021, p. P-003] (poster).
- Pola Cybulska, Tomasz K. Olszewski. Wykorzystanie odpadowej biomasy po fitoremediacji ziem zanieczyszczonych metalami do przygotowania katalizatorów polimetalicznych i ich zastosowanie w syntezie organicznej. 63rd Meeting of the Polish Chemical Society, Łódź, September 13-17, 2021 [abstract in: Book of Abstracts, eds. Tomasz Cierpiał, Paweł Tokarz, Sebastian Rykowski, Warsaw: PTChem, 2021, p. S08-P001] (poster).
- Pola Cybulska, Tomasz K. Olszewski. Przygotowanie katalizatorów polimetalicznych z biomasy roślinnej i ich zastosowanie w reakcjach tworzenia wiązania C-P. IX Łódzkie Sympozjum Doktorantów Chemii, University of Łódź, May 19-20, 2022 (poster).
- Pola Cybulska, Tomasz K. Olszewski. Katalizatory otrzymywane z roślin hiperakumulujących metale i ich zastosowanie w syntezie związków fosforoorganicznych. VII Szczecińskie Sympozjum Młodych Chemików, Szczecin, May 23-27, 2022 [abstract in: Book of Abstracts, eds. Elwira K. Wróblewska, Łukasz Struk, Szczecin: West Pomeranian University of Technology Press, 2022, p. 12] (oral presentation).

- Pola Cybulska, Tomasz K. Olszewski. Use of waste biomass after phytoremediation for the preparation of polymetallic catalysts and application in C-P bond formation. Balticum Organicum Syntheticum (BOS), Vilnius, Lithuania, July 3-6, 2022 [abstract in: Program and Abstract Book, Vilnius: UAB Kalanis, 2022, p. 61] (poster).
- Pola Cybulska, Tomasz K. Olszewski. Tworzenie wiązania C-P przy użyciu nowych katalizatorów polimetalicznych pochodzenia naturalnego. 64th Meeting of the Polish Chemical Society, Lublin, September 11-17, 2022 [abstract in: Book of Abstracts, Warsaw: PTChem, 2022, p. 589] (poster).

In 2020, I was awarded a French Government Scholarship (Bourse du Gouvernement Français) granted by the Embassy of France in Poland. The scholarship was allocated for a total of 12 months across 2021, 2022, and 2023. My planned research stay was to take place at CNRS in France. However, due to the outbreak of the COVID-19 pandemic, the scholarship was suspended. Instead, I collaborated remotely with CNRS professors, and this collaboration resulted in the theoretical calculations included in this dissertation.

Research goals

The main aim of this dissertation was to develop and validate the concept of ecocatalysis, understood as the use of biomaterials obtained from metal-hyperaccumulating plants for the preparation of effective, selective, and recyclable heterogeneous catalysts. The research addresses the dual challenge outlined in the introduction: the increasing scarcity and cost of critical metals for catalysis, and the need for sustainable, low-waste solutions in synthetic organic chemistry.

The specific objectives were as follows:

I Design and preparation of biogenic catalysts

1. To obtain polymetallic oxide catalysts (Eco-MgZnOx) from the biomass of *Arabidopsis halleri*, a model Zn/Cd hyperaccumulator, through controlled thermal processing.

2. To characterize the structural, textural, and compositional properties of these materials, and to identify the presence of synergistic phases responsible for catalytic activity.

II Evaluation of catalytic performance in $C-P$ bond formation in hydrophosphonylation

1. To test the activity of Eco-MgZnOx in the hydrophosphonylation (Pudovik reaction) of aldehydes, focusing on substrate scope, reusage of the catalyst and mechanistic features.



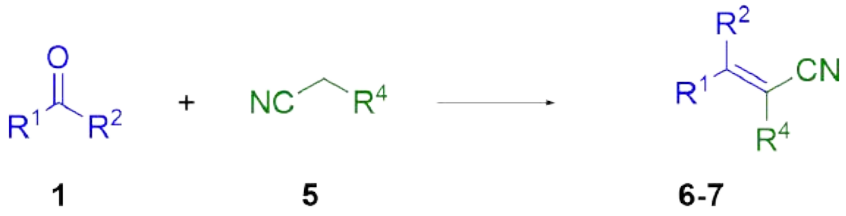
1 2 3-4

Scheme 1. Hydrophosphonylation (Pudovik reaction)

2. To compare the efficiency of biogenic catalysts with conventional single-component oxides (MgO, ZnO, CaO) and to evaluate the role of cooperative active sites.

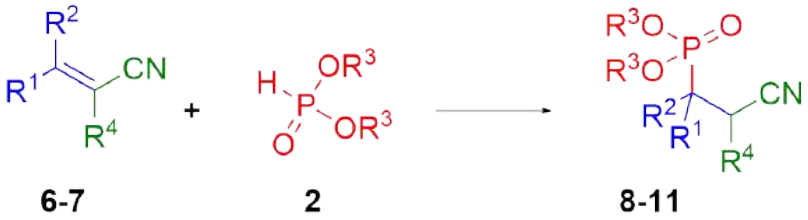
III Exploration of catalytic activity in $C-C$ and $C-P$ bond formation in Knoevenagel-phospha-Michael reaction

1. To investigate the catalytic properties of Eco-MgZnOx in the Knoevenagel condensation (C-C bond formation).



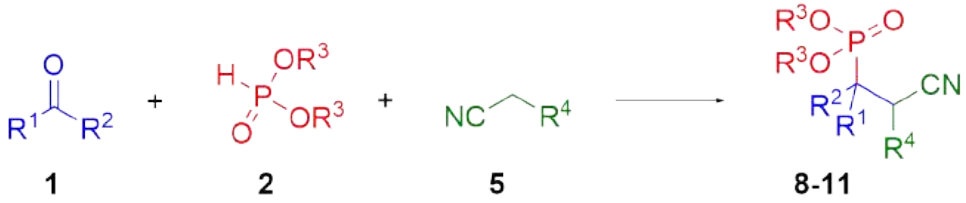
Scheme 2. Knoevenagel condensation

2. To study the activity of Eco-MgZnOx in the phospha-Michael addition ($C-P$ bond formation to activated alkenes).



Scheme 3. Phospha Michael addition

3. To combine these transformations in a one-pot Knoevenagel-phospha-Michael cascade demonstrating the versatility of the catalyst in complex multicomponent reactions.



Scheme 4. Knoevenagel phospha-Michael condensation

IV Assessment of sustainability and practical utility

1. To verify the recyclability and long-term stability of Eco-MgZnOx through repeated catalytic cycles and regeneration procedures.

2. To evaluate the scalability of reactions up to the gram scale, demonstrating preparative potential.

3. To analyze the ecological and economic benefits of using plant-derived catalysts, linking phytomanagement of contaminated soils with high-value chemical synthesis.

V Understanding of the mechanism

1. To perform theoretical calculations aimed at discover the nature of active sites and the origin of bifunctional synergy.

2. To integrate experimental and computational results into a coherent mechanistic model of catalysis.

Together, these goals were designed not only to confirm the feasibility of ecocatalysis in practice but also to position it as a green and scalable alternative to conventional metal-based catalysis, bridging the gap between environmental remediation and sustainable organic synthesis.

Contents

Abstract **3**

Streszczenie **5**

Preface **7**

Research goals **11**

Chapter 1: Introduction **19**

1.1 Introduction to organophosphorus compounds **21**
1.1.1 Organophosphorous compounds overview 21
1.1.2 Applications in industry and research 32
1.1.3 Synthetic and biological research 45
1.1.4 Catalysis in organophosphorus synthesis 51

1.2 Introduction to ecocatalysis **55**
1.2.1 Fundamentals of catalysis 55
1.2.2 Challenges in catalysis: metal availability and sustainability 58
1.2.3 Fundamentals of phytomanagement techniques 66
1.2.4 Overview of ecocatalysis 74
1.2.4.1 Copper-based ecocatalysts 77
1.2.4.2 Manganese-based ecocatalysts 89
1.2.4.3 Zinc-based ecocatalyst 97
1.2.5 Arabidopsis haleri 103

Chapter 2: Hydrophosphonylation **107**

2.1 Hydrophosphonylation - chemical basics **109**

2.2 Hydrophosphonylation - application **112**

2.3 Hydrophosphonylation - catalysts **119**

2.4 Hydrophosphonylation - results and discussion on use of ecocatalysis **124**
2.4.1 Methodology 124

2.4.1.1 Preparation of Eco-MgZnOx catalyst derived from *Arabidopsis halleri* 124
2.4.1.2 General procedure for the reactions 126
2.4.1.3 Analysis of catalyst, reaction mixtures and products 127
2.4.1.4 Modeling 128
2.4.2 Composition and structure of the ecocatalyst 129
2.4.3 Optimization results of the hydrophosphonylation 133
2.4.3.1 Optimization results of the hydrophosphonylation with an optically active substrate 142
2.4.4 Scale-up of the hydrophosphonylation 145
2.4.5 Reusage of the catalyst in the hydrophosphonylation 146
2.4.6 Substrate scope of the Hydrophosphonylation 151
2.4.7 Theoretical calculations of the catalytic mechanism of the hydrophosphonylation 156
2.4.8 Conclusions 160

Chapter 3: Knoevenagel condensation 163

3.1 Knoevenagel condensation - chemical basics 165

3.2 Knoevenagel condensation - application 169

3.3 Knoevenagel condensation - catalysts 174

3.4 Knoevenagel condensation - results and discussion on use of ecocatalysis 182
3.4.1 Methodology 182
3.4.2 Optimization results of the Knoevenagel condensation 183
3.4.3 Reusage of the catalyst in the Knoevenagel condensation 188
3.4.4 Scale-up of the Knoevenagel condensation 189
3.4.5 Substrate scope of the Knoevenagel condensation 189
3.4.6 Conclusions 194

Chapter 4: Phospha-Michael addition reaction 197

4.1 Phospha-Michael addition reaction - chemical basics 199

4.2 Phospha-Michael addition reaction - application 204

4.3 Phospha-Michael addition reaction - catalysts 207

4.4 Phospha-Michael addition reaction - results and discussion on use of eco-catalysis 214

4.4.1 Methodology 214
4.4.2 Optimization results of the phospha-Michael addition reaction 214
4.4.3 Reusage of the catalyst in the phospha-Michael addition reaction 221
4.4.4 Scale-up of the phospha-Michael addition reaction 221
4.4.5 Substrate scope of the phospha-Michael addition reaction 222
4.4.6 Conclusions 230

Chapter 5: Knoevenagel-phospha-Michael reaction 233

5.1 Knoevenagel-phospha-Michael - chemical basis 235

5.2 Knoevenagel-phospha-Michael - applications 236

5.3 Knoevenagel-phospha-Michael reaction - catalysts used 237

5.4 Knoevenagel-phospha-Michael - results and discussion on use of ecocatalyst 243

5.4.1 Methodology 243
5.4.2 Optimization results of the Knoevenagel-phospha-Michael reaction . . . 243
5.4.3 Reusage of the ecocatalyst in the Knoevenagel-phospha-Michael reaction 252
5.4.4 Scale-up of the Knoevenagel-phospha-Michael reaction 253
5.4.5 Substrate scope of the Knoevenagel-phospha-Michael reaction 254
5.4.6 Conclusions 259

Conclusion 261

Experimental section 283

General experimental methods and procedures 285
Products of hydrophosphonylation catalyzed by *Arabidopsis halleri*-derived biogenic Eco-MgZnOx catalyst 290
Products of Knoevenagel condensation catalysed by *Arabidopsis halleri*-derived biogenic Eco-MgZnOx catalyst 299
Products of phospha-Michael addition catalysed by *Arabidopsis halleri*-derived biogenic Eco-MgZnOx catalyst 305

Products of Knoevenagel-phospha-Michael reaction catalysed by *Arabidopsis halleri*-derived biogenic Eco-MgZnOx catalyst 315

References **321**

Chapter 1:
Introduction

1.1 Introduction to organophosphorus compounds

1.1.1 Organophosphorous compounds overview

Organophosphorus compounds (OPCs) hold a contradictory place in science and society. They are essential building blocks of life, forming the structure of DNA and providing energy through molecules like adenosine triphosphate (ATP) [1]. However, synthetic OPCs include some of the most dangerous toxins ever made by humans, used as lethal nerve agents in chemical warfare and as key ingredients in pesticides, causing hundreds of thousands of deaths each year [2–4].

What defines OPCs is the phosphorus atom, which has unique chemical features. It can form multiple bonds, exist in different oxidation states, react strongly as a nucleophile in its trivalent state, and create very stable bonds [5–7]. These characteristics makes OPCs spread widely across numerous fields-from industrial applications such as flame retardants, plasticizers, and metal extraction agents, to specialized research uses as synthetic reagents, catalytic ligands, and tools in biochemical studies [1, 8].

The story of organophosphorus chemistry begins in the 19th century, when the phosphorus are bonded to the organic groups for the first time. One of the earliest recorded syntheses was achieved by Jean Louis Lassaigne in 1820, who reacted ethanol with phosphoric acid to form triethyl phosphate (TEP), marking a key step in the formation of organophosphorus esters [9]. Franz Anton Voegeli continued this line of research and successfully produced TEP in 1848 [10]. Another significant milestone came in 1854 with the synthesis of tetraethyl pyrophosphate (TEPP). Philippe de Clermont is often credited with its discovery, but historical records suggest it was actually Vladimir Moschnin, working under Adolphe Wurtz, who first produced TEPP [11]. At the time, the toxic properties of such compounds were largely unknown, and Clermont described TEPP as having a pungent taste and an irritating smell. Another important time for organophosphorus history, is the 1930s. In 1932, while synthesizing phosphofluoridate compounds at the University of Berlin, Willy Lange and his graduate student Gerda von Krueger noted the powerful physiological effects of the vapors, describing a "marked pressure in the larynx combined with breathlessness" and visual disturbances from even minute quantities [4, 12].This observation of toxicity set the stage for the work of Gerhard Schrader, who is now widely considered the father of modern organophosphorus insecticides as while searching for new insecticides, Schrader synthesized thousands of OPCs. His work led to the first commercial OP insecticide, Bladan, a mixture containing TEPP, and in 1944, the "breakthrough" compound E605,

which was later introduced to the global market as parathion, one of the most widely used insecticides of its class [4, 13]. In 1938, the German government declared all research on OPCs a state secret, initiating a dual-use development program. One arm of the research focused on developing compounds with high insect selectivity for agricultural use, while the other focused on compounds of maximum human toxicity for use as chemical warfare agents. This program starts the infamous "G-series" nerve agents, named for "German," which included Tabun (1936), Sarin (1939), and Soman (1944) [13–16]. Later, British and American research would lead to the even more potent "V-series" agents, with the "V" standing for "venomous" [15, 16].

Phosphorus compounds show a wide range of chemical and physical properties due to different oxidation states and coordination numbers that the phosphorus atom can adopt. Common phosphorus compounds cover oxides, halides, sulfides, hydrides, nitrogen compounds, metal derivatives, and organic derivatives, all of which are widely used in industrial applications. Among these, halides, hydrides, and metal derivatives - and to a lesser degree oxides and sulfides - are especially reactive intermediate compounds that promote the formation of phosphorus bonds with other elements [17].

The vast and diverse family of organophosphorus compounds requires a systematic classification scheme. The most fundamental approach categorizes them based on the oxidation state of the central phosphorus atom, with phosphorus(V) and phosphorus(III) compounds being the most common and important classes [18]. Valency of phosphorous +1, +4, and 0 are occasionally encountered. These states strongly influence reactivity, coordination behavior, and the types of bonds phosphorus can form [19].

Phosphorus (V) acids are compounds where the phosphorus is in the +5 oxidation state. These acids and their derivatives play crucial roles in biochemistry and industrial applications. Their structure is shown on the figure 1.

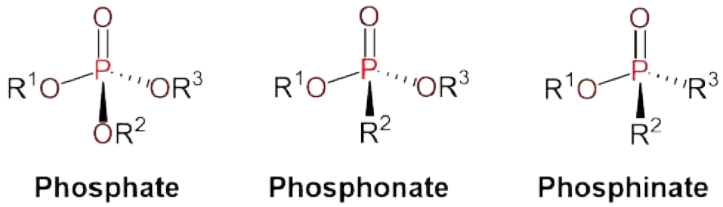


Figure 1. Basic structures of phosphoryl-based (P=O) pentavalent organophosphorus compounds. Based on [20]

Phosphates ($(RO)_3P = O$) are fully oxygenated organophosphorus compounds in which the phosphorus atom adopts a tetrahedral geometry. These are esters of phosphoric acid, which lack a direct phosphorus-carbon bond. Three alkyl or aryl groups are

connected with phosphorous atom via $P-O$ bonds, along with a terminal $P=O$ double bond. These compounds are chemically stable and resistant to hydrolysis, which makes them valuable in applications such as flame retardants, plasticizers, and solvents, but due to their low toxicity and biological compatibility, organophosphate esters are also explored in medicinal chemistry and material science. These compounds form also vital biological molecules such as ATP and the sugar-phosphate backbone of DNA [21].

Phosphonates $RP(=O)(OR')_2$ are characterized by a highly stable, direct phosphorus-carbon $P-C$ bond and have two $P-O$ ester bonds, along with a terminal $P=O$ bond. This structural feature provides significant chemical and thermal stability [22]. The presence of a $P-C$ bond makes them more hydrolytically stable. They are used in agriculture and are also studied as enzyme inhibitors and analogues of phosphate esters in biological systems [23].This class includes one of the world's most widely used herbicides, glyphosate $(HO)_2P(O)CH_2NHCH_2CO_2H)$, as well as the potent nerve agent sarin, which possesses both $C-P$ and $F-P$ bonds. Bisphosphonates are an important class of drugs for treating osteoporosis [24].

Phosphinates $R_2P(=O)OR'$ contain two organic groups directly bonded to phosphorus and one ester-like OR' group. Phosphinates are considered structurally intermediate between phosphines and phosphonates. These compounds are valued in synthetic organic chemistry and are used in medicinal and agrochemical applications. Their lipophilic character and moderate reactivity make them suitable for esterification, substitution, and metal coordination reactions [21, 25].

Trivalent phosphorus compounds include phosphines, phosphites, phosphonites, and phosphinites, what is presented in the 1, while pentavalent phosphorus compounds comprise phosphates, phosphine oxides, and derivatives of phosphonic and phosphinic acids and their amides according to [20]. Compounds with phosphorous in the +5 state, are generally more oxidized and stable ([26]).

Table 1. Comparison of trivalent organophosphorus compound classes

Compound class	**Formula**	**Bond types**	**Reactivity / use**
Phosphines	R_3P	up to 3 × $P-C$	Strong Lewis base, used as ligand in catalysis ([27])
Phosphinites	$R_2P(OR')$	2 × $P-C$, 1 × $P-O$	Moderately reactive, ligands with lower stability ([25])
Phosphonites	$RP(OR')_2$	1 × $P-C$, 2 × $P-O$	Intermediates in pesticide synthesis and catalysis ([28])
Phosphites	$P(OR')_3$	3 × $P-O$	Less nucleophilic, used in reductions and phosphorylations ([21])

Phosphines are a class of organophosphorus compounds where the phosphorus atom is bonded directly to carbon atoms. It forms compounds such as primary, secondary, and tertiary phosphines (RPH_2, R_2PH, and R_3P, respectively). Chalcogenide derivatives of phosphines include compounds where phosphorus forms bonds with sulfur, selenium, or tellurium, leading to structures like phosphine sulfides $R_3P{=}S$ [20].

Other trivalent phosphorous compounds are phosphorus (III) acid derivatives. Phosphinites ($R_2P(OR')$) consist of two organic substituents (R) bonded directly to the phosphorus atom and one alkoxy or aryloxy group (OR') attached via a $P-O$ bond. These compounds are typically more reactive than phosphines and are more prone to oxidation. Phosphinites are occasionally used as ligands in catalysis, although they are generally less stable than phosphines [25]. Phosphonites $RP(OR')_2$ contain one organic group R and two alkoxy or aryloxy substituents OR' attached to the phosphorus atom. These ligands are less basic compared to phosphines but still find some use in coordination chemistry. Phosphonites may act as precursors in phosphorylation reactions and are occasionally employed in the synthesis of pesticides [28]. Phosphites $P(OR')_3$ are fully substituted by alkoxy or aryloxy groups OR'. Each of the three substituents is bonded through a $P-O$ bond. These compounds are more electron-withdrawing and exhibit lower donor ability compared to phosphines. Phosphites are commonly used as reagents in organic synthesis, particularly in Arbuzov-type reactions, Michaelis-Arbuzov rearrangements, or as mild reducing agents [21].

The chemistry of trivalent phosphorus compounds, such as phosphines and phosphites, is dominated by their strong nucleophilicity and character as reducing agents [7]. Unlike the lone pair on the nitrogen in triphenylamine, which is delocalized into the aromatic rings and relatively unreactive, the lone pair on the phosphorus in triph-

enylphosphine is highly available for nucleophilic attack. This results in rapid, often exothermic, reactions with alkyl halides to form phosphonium salts, a key first step in the synthesis of Wittig reagents [7]. The ease with which P(III) is oxidized to P(V) is a powerful thermodynamic driving force in organic synthesis. The formation of the exceptionally stable phosphoryl bond in triphenylphosphine oxide $Ph_3P = O$ propels numerous named reactions, including the Wittig, Mitsunobu, and Appel reactions [7]. This $P = O$ bond is highly polar and more accurately described as a resonance hybrid with significant $P^+ - O^-$ character, rather than a simple double bond, due to the involvement of phosphorus's d-orbitals in p-d bonding [7]. This inherent reactivity of P(III) compounds contrasts with the stability of many P(V) species, but this stability is highly dependent on the nature of the bonds to phosphorus. The P-O-C ester linkage found in organophosphates is susceptible to hydrolysis, a process that can be catalyzed by both acid and base [29, 30]. This hydrolytic lability is precisely why OP pesticides were favored over persistent organochlorines. They were designed to break down in the environment [15]. The rate of this hydrolysis is highly dependent on pH and temperature - for example, many OP esters are relatively stable for days at neutral or acidic pH but degrade in minutes at high pH [30]. Furthermore, phosphites $(P(OR)_3)$ hydrolyze much more rapidly than their corresponding phosphates $(O = P(OR)_3)$ [30].

Phosphonium salts are characterized by the presence of a positively charged phosphorus atom P^+ bonded to four organic groups, forming structures like $R_4P^+X^-$. These salts are often used as phase-transfer catalysts in organic synthesis.

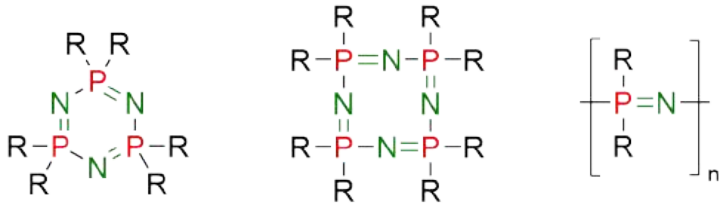


Figure 2. Example of phosphazenes structures [31].

Phosphorus is able to build coordination complexes where the phosphorus atom can exhibit penta- or even hexacoordination, forming five or six bonds. These hypervalent species are typically found in oxyacid derivatives, polyphosphates, and coordination complexes, and they are stabilized by highly electronegative substituents such as oxygen or fluorine. Depending on their electronic and steric environment, such compounds adopt trigonal bipyramidal or octahedral geometries [19]. The important example of pentacoordinated phosphorus compounds is the class of phosphazenes, which can be linear or cyclic and includes the formula $(PN)_n$. Examples are presented

on Figure 2. In these systems, phosphorus atoms often exhibit bonding beyond classical tetrahedral coordination, especially when substituted with various organic groups. Phosphazenes are renowned for their thermal and chemical stability, which has led to their use in flame-retardant polymers, elastomers, membranes, and advanced biomaterials [32].

Phosphorus oxides and their derivatives are among the most structurally diverse phosphorus-containing compounds, primarily because of the strength of the $P{-}O$ and $P{=}O$ bonds. The chemistry of phosphorus oxyacids forms the basis of systematic phosphorus nomenclature, although inconsistencies remain common. For example, the compound traditionally called “phosphorous acid” is more accurately described as phosphonic acid, with the stable tautomer being $HP(=O)(OH)_2$ rather than $P(OH)_3$. Likewise, “hypophosphorous acid” refers to H_3PO_2, also known as phosphinic acid [33]. Many of these acids are encountered more frequently in the form of their salts or esters rather than as free acids. Esters derived from phosphinous acid ($H_2P{-}OH$) and phosphorous acid give rise to phosphite esters ($P(OR)_3$), which are widely used in organic synthesis. Complex examples include hypodiphosphoric acid or diphosphoric(III,V) acid, one $P{-}O{-}P$ and second containing $P{-}P$ linkages. Such species are usually observed as unstable intermediates during the hydrolysis of phosphorus halides and oxohalides [34].



Figure 3. Structures of diethyl phosphonate and triethyl phosphite [32].

The nomenclature of organoderivatives of phosphorus oxyacids without $P{-}C$ bonds-such as esters-is traditionally based on modifying the name of the parent acid: "-ic" becomes "-ate" and "-ous" becomes "-ite". For instance, diethyl phosphonate $(C_2H_5O)_2P(=O)H$ and triphenyl phosphite $(C_6H_5O)_3P$ (Figure 3) are well-known examples used in catalysis and synthesis [32]. Derivatives containing direct phosphorus-carbon bonds are generally classified as organophosphorus compounds or carbophosphorus compounds. Their reactivity, electronic properties, and coordination behavior depend heavily on the phosphorus oxidation state and the surrounding ligands [33].

Phosphorus can form single or double bonds with either oxygen or sulfur. It is common to refer to the $P = O$ bond in a formal sense, in phosphoryl chemistry the bond is the result of an electron pair being donated from the phosphorus atom to oxygen, what creates a bond with strong coordinate character - can be shown as $P \rightarrow O$ or sometimes as $P^{+} - O^{-}$. In the phosphate ion PO_4^{3-} all $P - O$ bonds are energetically equivalent, even though they are often written as one double bond and three singles. Oxygen has a strong natural tendency to bond with phosphorus, and this preference for forming $P = O$ - phosphoryl bonds plays a central role in phosphorus chemistry. Both $P = O$ and $P = S$ bonds can act as electron donors. However, the complexes they form tend to be rather weak because they typically interact with hard Lewis acids, electron-poor species that are not easily polarizable. This property turns out to be pretty useful - for instance, in the extraction of uranium or rare-earth metals using compounds like TOPO - trioctylphosphine oxide or DEHPA - di(2-ethylhexyl) phosphoric acid. Their structures are presented on Figure 4. $P = S$ bonds are generally more reactive than the $P = O$ linkage, but also less stable-they break down more easily, hydrolyze faster, and do not hold up as well under heat. On the flip side, because they are stronger electron donors, P=S bonds can form more robust complexes. That's why they are often used as "protective blocks"-a kind of shielding to prevent the unwanted involvement of the lone phosphorus electron pairs in sensitive reactions [35].

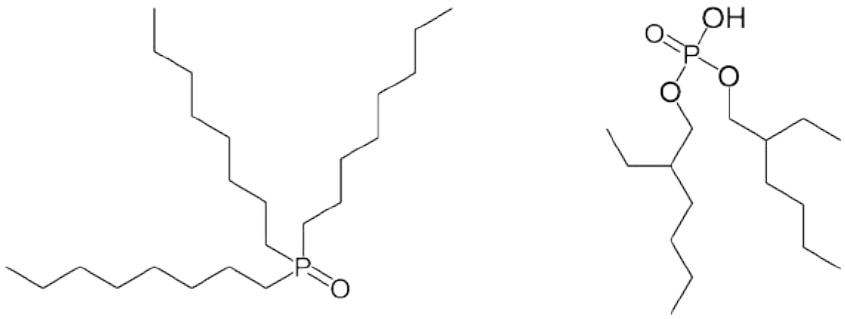


Figure 4. Structures of TOPO - trioctylphosphine oxide and DEHPA - di(2-ethylhexyl) phosphoric acid [35].

The physicochemical properties of organophosphorus compounds, such as hydrophobicity, polarity, solubility, volatility, acidity, and thermal stability, are heavily influenced by the nature of the substituents bonded to the phosphorus atom. Electron-withdrawing groups - for example alkoxy groups - increase compound polarity and acidity, leading to greater water solubility but lower volatility. On the contrary, bulky alkyl or aryl groups typically enhance hydrophobicity and thermal resistance, while re-

ducing aqueous solubility [5, 19]. Trialkyl and aryl phosphates exhibit high polarity due to multiple $P - O$ bonds, with trialkyl phosphates being significantly more hydrophilic. Phosphonates, with one direct P-C bond and two esterified oxygens, combine high polarity with moderate hydrophobicity and display excellent thermal stability, making them suitable for drug and agrochemical development [28]. In contrast, phosphines and phosphites, which lack full oxygen coordination, are more hydrophobic and volatile, with lower thermal stability and reduced polarity. These trends are summarized in the Table 2.

Table 2. Physicochemical properties of selected organophosphorus compounds

Compound Type	Hydrophobicity	Polarity	Acidity (pKa)	Water solubility	Volatility	Thermal stability
Trialkyl phosphates	Moderate	High	∼1–2	Good	Low	High
Aryl phosphates	High	Moderate	∼3–4	Poor	Low	High
Phosphonates	Low–Moderate	High	∼2–3	Good	Low	Very high
Phosphinates	Moderate	Moderate	∼5–6	Moderate	Moderate	Moderate
Phosphites	Low	High	∼2–3	Good	High	Low
Phosphines	High	Low	Very weak base	Poor	High	Low

The industrial production of organophosphorus compounds involves a well-established network of synthetic routes. These pathways typically begin with the transformation of naturally occurring phosphate minerals into elemental white phosphorus (P_4), using high-temperature reduction known as the Wöhler process [33]. From this central starting point, a wide range of phosphorus-containing intermediates and final products can be synthesized. Elemental form undergoes transformation into phosphorus trichloride (PCl_3), phosphine (PH_3), or phosphorus oxide (P_4O_{10}), which structures are presented on Figure 5. These intermediates serve as basic substrates in the production of various organophosphorus compounds. However, conventional methodologies associated with these processes present several sustainability and safety challenges. The production of PCl_3 involves the chlorination of white phosphorus using gaseous chlorine. This reaction not only poses significant safety risks as result of the toxic and reactive nature of the reagents but also generates hazardous by-products that require careful handling and disposal. The entire process is energy-intensive and has significant influence on the environment. The phosphine gas (PH_3) is highly toxic and pyrophoric, so the synthesis of this gas from white

phosphorus and alkali hydroxides also must face safety challenges [36]. Elemental phosphorus (P_4) can react with oxygen, leading to the formation of phosphorus oxides. This reaction is highly exothermic and emits a bright light. Phosphorus oxide (P_4O_{10}) is a potent dehydrating agent and reacts with organic substrates like ethers or alcohols. Those reactions are leading to phosphate esters - mono-, di- or trisubstituted acid phosphates [37].

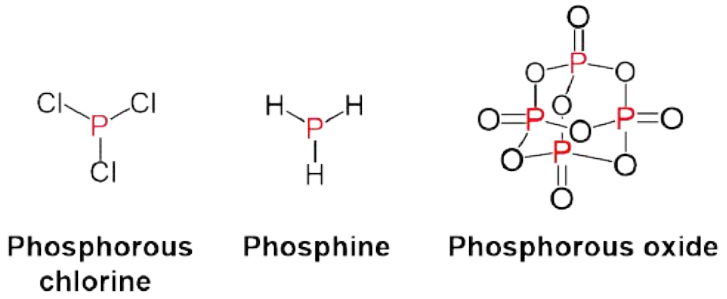
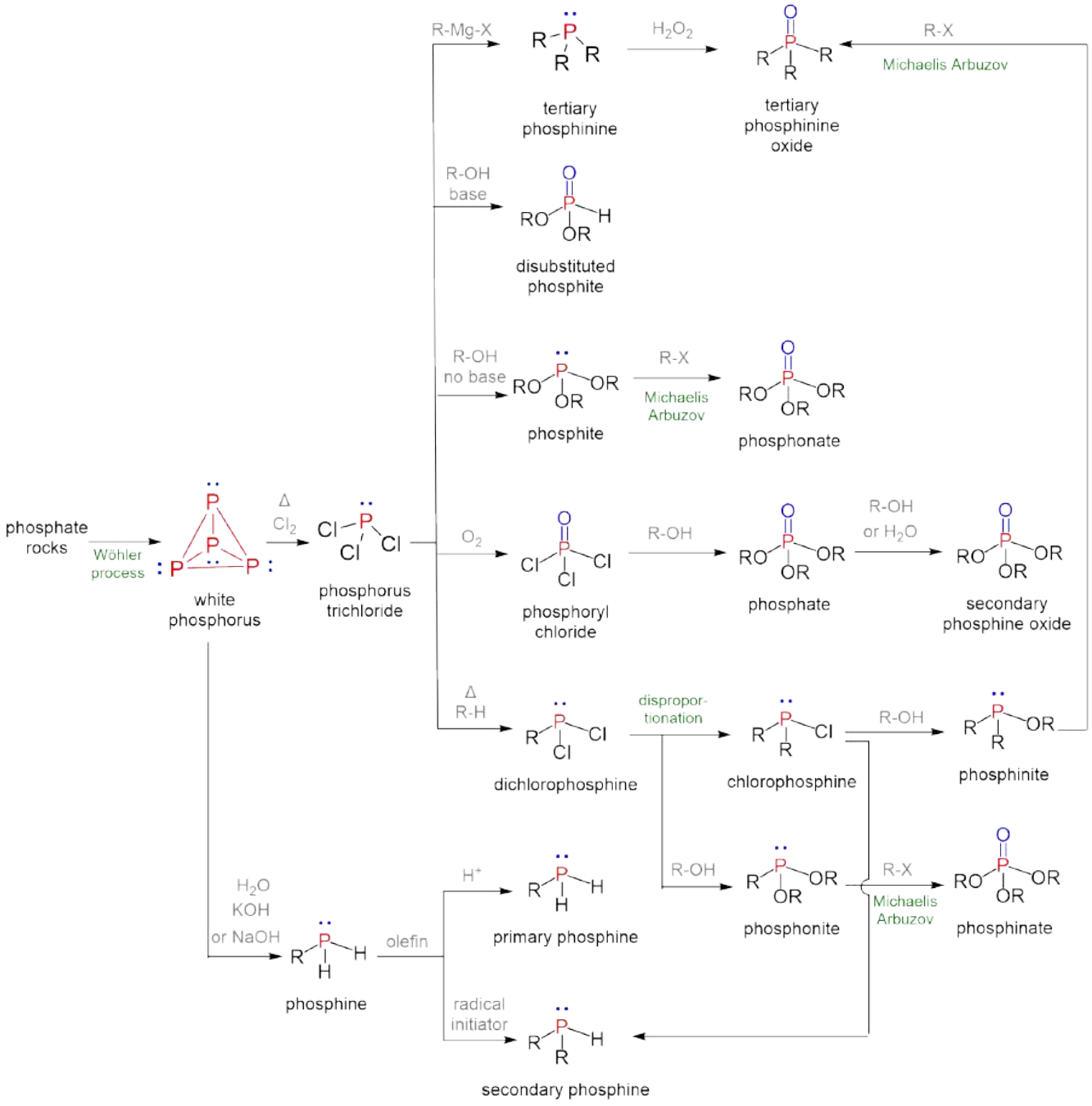


Figure 5. Structures of phosphorus trichloride, phosphine and phosphorus oxide [33].

PCl_3 is a versatile intermediate that can be variously modified. It reacts with alcohols to form various phosphites and phosphates, undergoes alkylation when heated with alkanes, or can be oxidized to generate phosphine oxides. These transformations enable access to a broad array of organophosphorus compounds [33]. Some of the main synthetic pathways leading to various organophosphorus compounds, in which either PCl_3 or PH_3 act as intermediates, are illustrated in the scheme 5.



Scheme 5. Synthetic strategies for the preparation of organophosphorus compounds [33].

PCl_3 participates in a variety of nucleophilic substitution reactions with alcohols, alkanes, or Grignard reagents. Reaction with alcohols in the absence of a base yields fully substituted phosphites, whereas the presence of a base allows formation of disubstituted phosphites bearing a reactive $P-H$ bond. Following alkylation of these phosphites with alkyl halides ($R-X$) via the Michaelis-Arbuzov reaction leads to the formation of phosphonates [33]. During the reaction of PCl_3 with Grignard reagents $R-MgX$, tertiary phosphines R_3P are obtained [38]. These compounds serve as both reagents and ligands in catalysis. Further oxidation using hydrogen peroxide leads to

their respective phosphine oxides $R_3P = O$. Alternatively, when elemental sulfur S_8 will be used, it will lead to phosphine sulfides $R_3P = S$. Both products have higher stability and water solubility [39]. Other option for PCl_3 as substrate, is oxidation with molecular oxygen to phosphoryl chloride $POCl_3$. This intermediate can be further functionalized with alcohols to form trialkyl phosphates, or hydrolyzed to generate secondary phosphine oxides, depending on the nucleophile involved. These pathways are critical for producing stable, highly oxidized phosphorus species. Intermediate compounds such as dichlorophosphines $PRCl_2$ can undergo disproportionation, leading to chlorophosphines PR_2Cl and phosphines. Chlorophosphines can be transformed into phosphinites by reaction with alcohols [33].

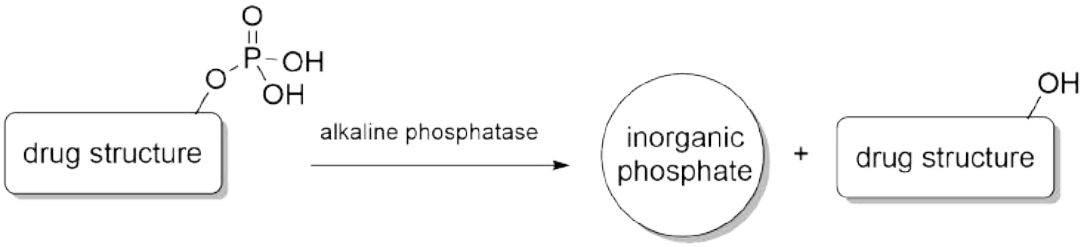
In contrast to phosphorus trichloride, which acts as an electrophile due to the presence of $P-Cl$ bonds, phosphine PH_3 exhibits different reactivity - it is a weak base and a nucleophile, and it engages in reactions characteristic of lone-pair donor systems, especially in coordination chemistry and reduction pathways. PH_3 can be converted into primary and secondary phosphines via hydrophosphination [40].

Phosphorus can be incorporated into a wide variety of organic substituents, where it plays a crucial role in modulating the electronic structure, reactivity, and stability of the overall molecule. The phosphorus atom plays the dominant role in shaping the behavior of substituents as $-PH_Y$, $-PY_2$, and $-POY_2$ (where Y = $-OH$, $-NH_2$, $-CH_3$, or $-F$), more than the attached Y group. Due to its low electronegativity and high polarizability, phosphorus tends to accumulate most of the charge within the functional group, which makes its influence consistent across various chemical environments [41, 42]. For instance, substituents bearing a $P = O$ unit, such as POY_2 groups, demonstrate higher electronegativity compared to $P(III)$-based groups, a feature attributed to the semi-polar $P\rightarrow O$ bond that draws electron density toward the oxygen atom. In neutral organic frameworks - whether saturated like $-CH_3$ or unsaturated like vinyl ($-CH = CH_2$), butadiene ($-CH = CH-CH = CH_2$), or even phenyl rings ($-C_6H_5$) - there is virtually no conjugation between the phosphorus group and the π-system. This conclusion is based on both electronic and geometric data, as there is no planarity observed where one would expect delocalization, and bond lengths and rotational barriers remain small, unlike those seen in strongly conjugated systems like aldehydes $-CHO$. However, when these substituents are adjacent to negatively charged carbon (such as in a carbanion: $-CH_2^-$), the phosphorus-containing groups show a strong ability to stabilize the negative charge, especially when the Y group is less electronegative (e.g., $-CH_3$ or $-NH_2$). This stabilization is not driven by the classical π-conjugation, but rather by electrostatic effects and charge delocalization within the substituent. The

added electron density tends to localize primarily on the phosphorus atom, sometimes exceeding a charge of -2, which underscores its electron-accepting character in such cases. This behavior is nearly the opposite of what is observed in neutral systems. Although neutral molecules see only minor polarization effects from phosphorus substituents, the anionic systems show a much more significant structural and energetic response. In summary, phosphorus-centered groups are soft, low-electronegativity substituents with strong internal polarization and ability to stabilize negative charge, but only in systems where such charge is present or introduced [41, 42].

1.1.2 Applications in industry and research

Phosphorus compounds have numerous applications in crucial areas, one of which is medicine and drug production. Phosphonates are often used in the treatment of bone diseases like osteoporosis due to their ability to inhibit bone resorption. Phosphates are commonly used as prodrugs, inactive compounds that metabolize into active drugs, to enhance the solubility and bioavailability of certain medications, while phosphinates and phosphonamidates are applied in various therapeutic areas, including antiviral and anticancer treatments [43].



Scheme 6. Interconversion of phosphomonoesters prodrugs into drugs and inorganic phosphonate [43].

Prodrugs, phosphomonoesters are formed by directly attaching a phosphate group to a hydroxyl group already present in the drug molecule. This modification is used to overcome the poor solubility of the original drug. Adding the phosphomonoester fragment increases both the water solubility and the effectiveness of the drug during absorption and distribution, as shown in the Scheme 6. In the body, the phosphate prodrug is enzymatically converted back to the active parent drug and inorganic phosphate by alkaline phosphatase, a widely present enzyme in humans.

This kind of prodrugs are widely used to improve the bioavailability and efficacy of alcohol-, phenol-, and steroid-based drugs, presented on Figure 6. A representative example is fosfluconazole [6.(I)], a phosphate prodrug of fluconazole, which shows en-

hanced in vivo efficacy due to improved membrane transport and is used against Cryptococcus neoformans and Candida infections [44]. Similar benefits are observed for primary alcohol derivatives, such as vidarabine monophosphate [6.(II)], an active antiviral agent for systemic herpes infections. Example of phenol-derived phosphomonoesters is fosfosal [6.(III)], a salicylic acid phosphate used as a nonsteroidal anti-inflammatory and analgesic drug. In the case of steroid hormones, conversion to sodium or calcium phosphate salts increases aqueous solubility and reduces irritation. Classic examples include betamethasone sodium phosphate and dexamethasone sodium phosphate [6.(IV)], which enable parenteral administration and broaden clinical applicability when oral therapy is not feasible [45].

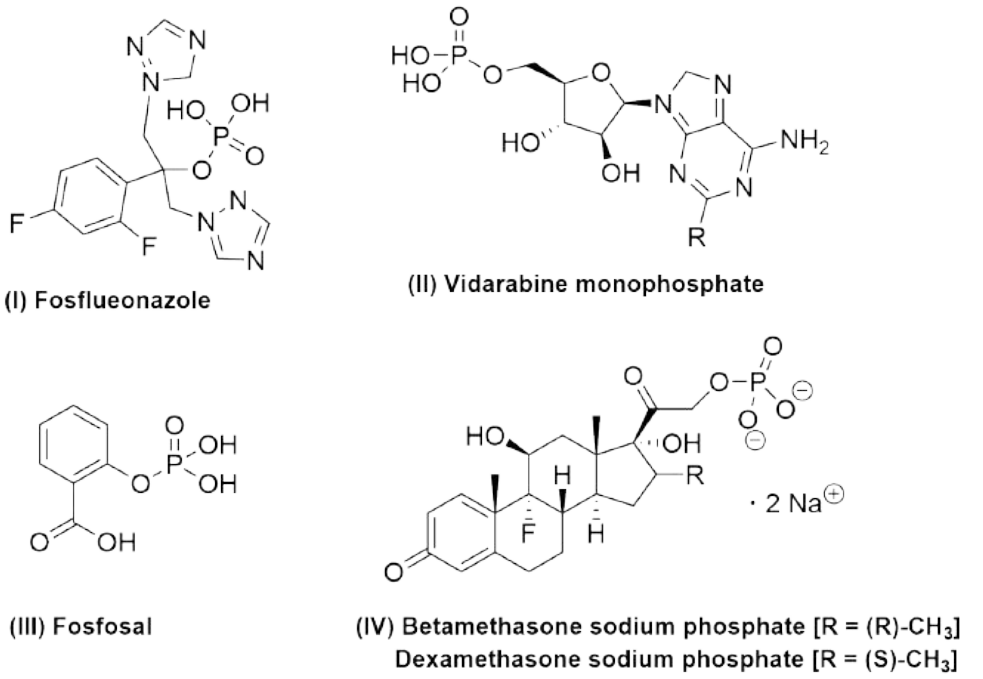


Figure 6. Structures of (I), (II) alcohol-derived phosphomonoester drugs, (III) phenol-derived phosphomonoester drug and (IV) steroid hormone-derived sodium phosphate drug [43].

Most phosphomonoester drugs are obtained by phosphatization of existing drugs or natural compounds, typically as sodium or calcium phosphate salts, to improve water solubility and delivery. A classic example is phosphenytoin disodium [7.(V)], which is a phosphomonoester prodrug developed to improve the water solubility and intravenous delivery of phenytoin. (S)-ethylisothiouronium diethylphosphate [7.(VI)] represents a phosphodiester drug that selectively inhibits inducible nitric oxide synthase, reducing hepatic nitric oxide production. Creatine phosphate sodium [7.(VII)] is based on an endogenous metabolite and supports ATP recycling, lowering the risk of muscular and cardiovascular disorders. Among phosphorodiamidates, cyclophosphamide [7.(VIII)] acts as a nitrogen mustard prodrug that is enzymatically activated in tumor

cells to alkylate DNA and suppress immune function. Finally, phosphorotriamidate alkylating agents such as azetepa [7.(IX)] or uredepa [7.(X)] contain aziridine rings and are used as antineoplastic agents, further highlighting the therapeutic scope of phosphorus-based prodrugs [43].

.

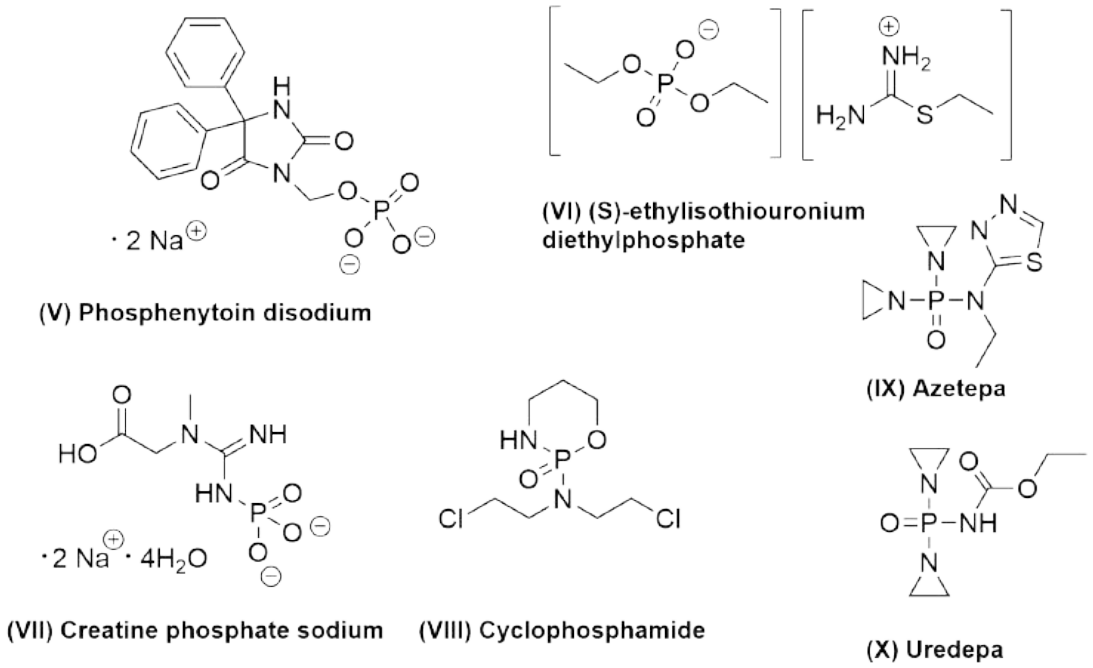


Figure 7. Structures of (V) sodium phosphate drug, (VI) phosphodiester drug, (VII) phosphoromonoamidate (VIII) phosphorodiamidate and (IX, X) phosphorotriamidate drugs [43].

Synthetic phosphonate analogues form an important class of enzyme inhibitors, mainly used as phosphonate prodrugs. A key example is foscarnet sodium [8.(XI)], developed from phosphonomethanoic acid and used to treat herpes viruses, including drug-resistant CMV and HSV, by mimicking pyrophosphate at viral polymerase binding sites. Phosphonated heterocyclic base analogues further extend this concept. For instance, (S)-HPMPA [8.(XII)] shows potent and selective activity against a broad range of DNA viruses. Bioactive fosfomycin sodium [8.(XIII)], a phosphoenolpyruvate analogue that inhibits bacterial cell wall biosynthesis by covalent modification of MurA and is used mainly in urinary tract infections. Replacement of P–O bonds with multiple P–C bonds has also been exploited in CNS-active drugs [46]. Fosazepam [8.(XIV)] is a water-soluble phosphine oxide derivative of diazepam acting as a positive allosteric modulator of GABA receptors [47]. Dyflos [8.(XV)] acts as a parasympathomimetic agent and irreversible anticholinesterase, with known risk of delayed peripheral neuropathy. Finally, stable bisphosphonates such as etidronate disodium [8.(XVI)] inhibit

bone resorption by osteoclasts and are used in the treatment of osteoporosis and Paget's disease, highlighting the broad therapeutic relevance of phosphonate chemistry [43].

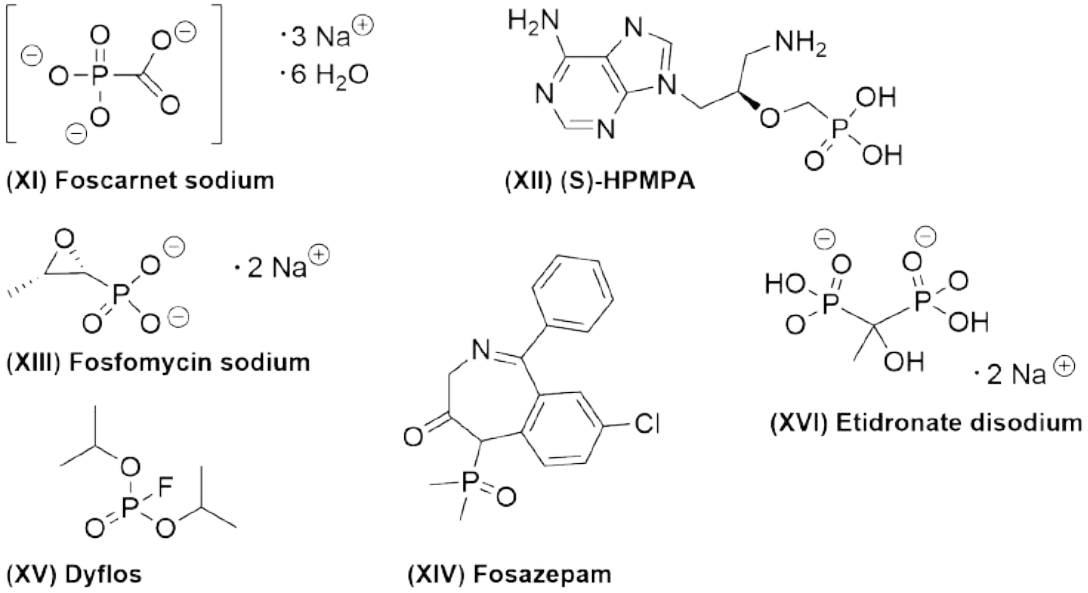
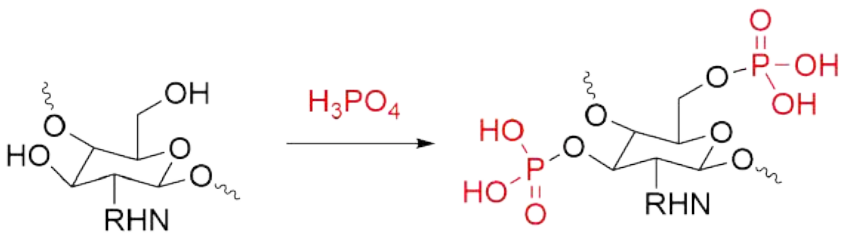


Figure 8. Structures of (XI) synthetic phosphonate drug, (XII) antiviral phosphonate drug, (XIII) bioactive phosphonate drug, (XIV) phosphine oxide drug, (XV) phosphorofluoridate drug and (XVI) non-nitrogenous bisphosphonate drug [43].

Inhibition of bone resporption is the ability of mimicking pyrophosphate, which is a natural bone metabolism regulator. Pyrophosphate mimicking groups help in controlling how synthetic substances interact with specific target enzymes. These interactions can help regulate the harmful effects of enzymes. Scientists develop molecules that look like pyrophosphate, which are similar to natural substances or known inhibitors that the enzymes usually interact with. This process makes it easier to create and test new compounds without necessity to go through long and complicated testing procedures. The natural substances that interact with the enzymes served as models for creating synthetic versions by changing the pyrophosphate parts of the molecules. This helps control the activity of enzyme, which is useful if the enzyme is linked to diseases caused by its overactivity [48]. This method has been successful in creating antiviral drugs, aiding in DNA synthesis [49], targeting cancer pathways [50], and disrupting harmful microbes [51].

Other application of organic compounds containing phosphorus is clinical dentistry. One of them is usage of phosphorylated chitosan films in development biomimetic hydroxyapatite (HA) crystals through an in vitro mineralization process. The key point is creating dental substitute materials that mimic the natural mineralization process

of human teeth to improve their compatibility and functionality. Chitosan is a biopolymer derived from chitin and its biocompatibility makes it a suitable candidate for various biomedical applications. Phosphorylation of chitosan, presented on Scheme 7 enhances its ability to bind calcium ions, which is crucial for initiating the mineralization process that leads to the formation of hydroxyapatite crystals [52]. Recently, researchers aim to assess the suitability of carbomer-based hydrogels for biomedical applications, particularly in areas where biocompatibility and safety are the most important features, such as in wound healing, drug delivery, and dental applications. Carbomers are synthetic high-molecular-weight polymers of acrylic acid commonly used in the pharmaceutical and cosmetic industries as gelling agents due to their ability to swell and form gels when dispersed in water, viscosity-modifying properties and ability to stabilize emulsions. In Zakzak's study (2024), carbomer-based hydrogels are prepared by incorporating phosphorus derivatives into the polymer network to enhance the bioactivity of the hydrogels. Phosphorus contributes to the formation of hydroxyapatite, a major component of bone and enamel. The phosphorus derivatives include acidic functional groups that can interact with calcium ions, promoting bioactivity and potentially enhancing the hydrogel interaction with biological tissues [53].



Scheme 7. Phosphorylation of chitosan [52].

Organophosphate esters (OPEs) have become one of the primary classes of flame retardants, largely replacing polybrominated diphenyl ethers after they were banned due to their persistence and toxicity [54, 55]. Organophosphate esters, such as tris(2-chloroethyl) phosphate (TCEP) and tris(1,3-dichloroisopropyl) phosphate (TDCP), presented on Figure 9, are added to polyurethane foams, plastics, textiles, and electronics to meet fire safety standards [54, 55]. They act through two main mechanisms, different in the solid (condensed) phase and in the gas phase. Of course. In the condensed phase, organophosphorus esters thermally decompose to form phosphoric acid. This acid acts as a catalyst to promote the cross-linking and charring of the polymer, creating a protective insulating layer that shields the material from heat and oxygen. In the gas phase, halogenated organophosphorus esters release reactive phosphorus and halogen species into the flame. These species act as radical scavengers, interrupting

the chemical chain reactions of combustion by quenching high-energy radicals such as $H\cdot$ and $OH\cdot$ [56].

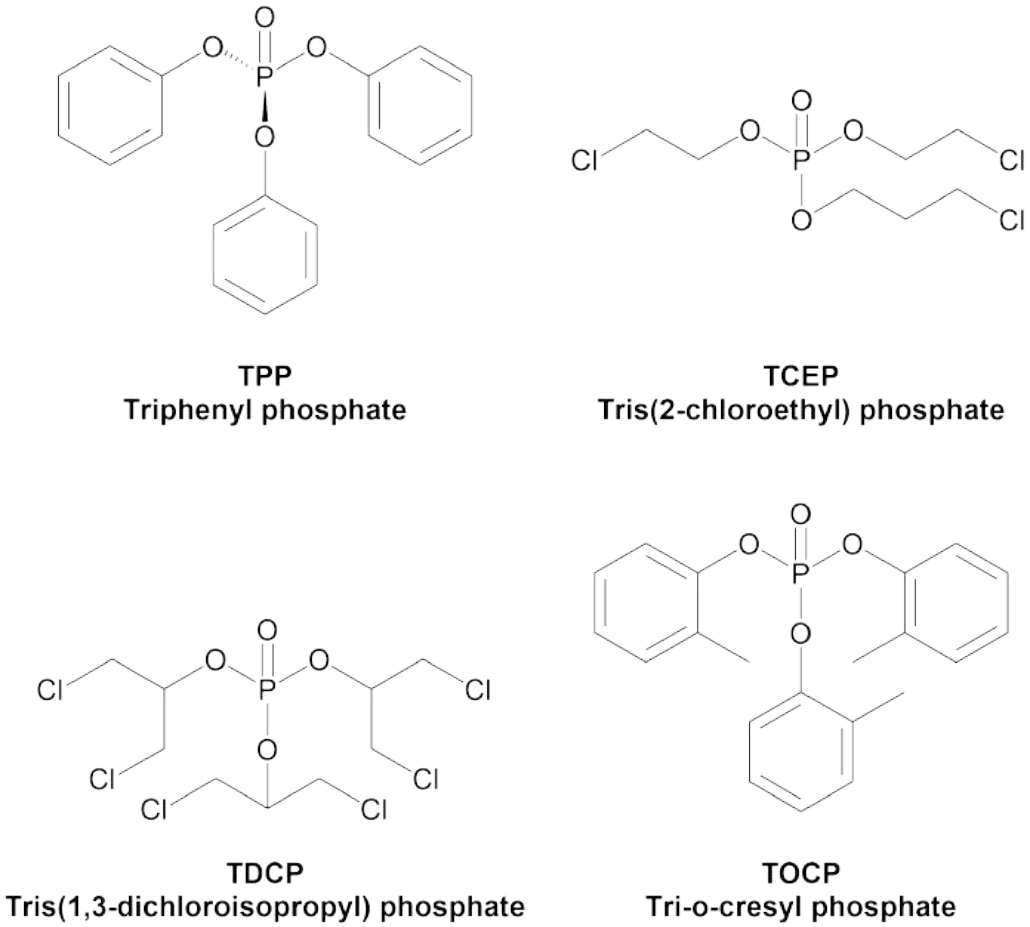


Figure 9. Examples of organophosphorus compounds used as flame retardants: triphenyl phosphate (TPP), tris(2-chloroethyl) phosphate (TCEP), tris(1,3-dichloroisopropyl) phosphate (TDCP), and tri-o-cresyl phosphate (TOCP) [57].

Among phosphorus-containing halogen free flame retardants, the caged bicyclic phosphates like PEPA (1-oxo-4-hydroxymethyl-2,6,7-trioxa-l-phosphabicyclo [2.2.2] octane) is key building blocks for their synthesis. Its rigid cage-type structure enable the development of flame retardants with high phosphorus content by grafting additional flame-retardant functional groups For example Trimer is bicyclic phosphate flame retardant, synthesized using PEPA and phosphorus oxychloride. PEPA and Trimer are presented on Figure 10. This highly symmetric molecule contains three bicyclic phosphate units, a high phosphorus content and exhibits excellent thermal stability and char-forming ability [58]. Jiang with coworkers [59] further demonstrated the effectiveness of this system by combining Trimer with ammonium polyphosphate in a 2:1 weight ratio as a flame retardant for polypropylene. With a total loading of 25 wt.%, the composite achieved a limiting oxygen index (LOI) of 28.8% and a UL-94 V-0 rating,

confirming its high flame-retardant efficiency.

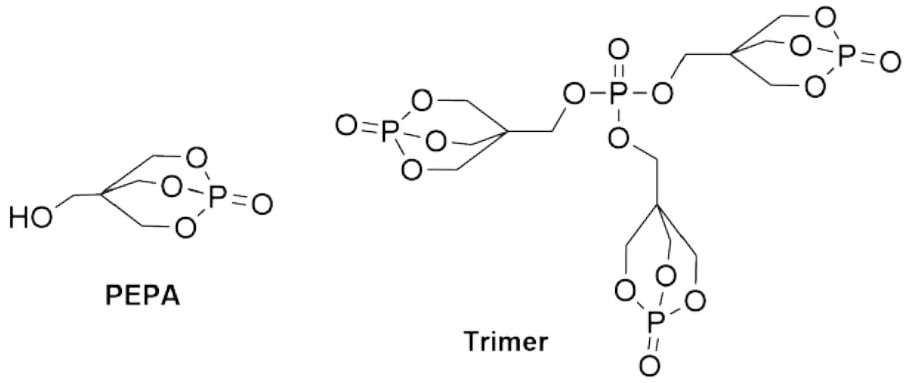


Figure 10. Examples of organophosphorus compounds used as flame retardants: PEPA and Trimer [58].

Because these OPEs are used as additives rather than being chemically bonded to the polymer matrix, they can leach, abrade, and volatilize from products over their lifespan [55]. This has led to their ubiquitous presence in indoor environments, with high concentrations found in household dust, air, and even human tissues, raising concerns about the health effects of chronic, low-level exposure [54, 55].

Phosphorus in fluorinated (co)polymers provides them with high acidity, complexation ability, as well as anti-corrosive, flame-retardant, and biomedical properties. These characteristics enable the use of such fluoro-phosphorus (co)polymers as advanced materials for polymer exchange membranes for fuel cells, self-etching adhesives used in dentistry, anti-corrosive coatings adhesion activators, flame retardants and polymer composites [60].

A range of organic compounds containing phosphorus also have been evaluated as effective corrosion inhibitors like α-aminophosphonate [61], aminomethylenediphosphonic acid (AMDP) [62], piperidin-1-yl-phosphonic acid (PPA) and (4-phosphono-piperazin-1-yl) phosphonic acid (PPPA) [63], as presented on Figure 11

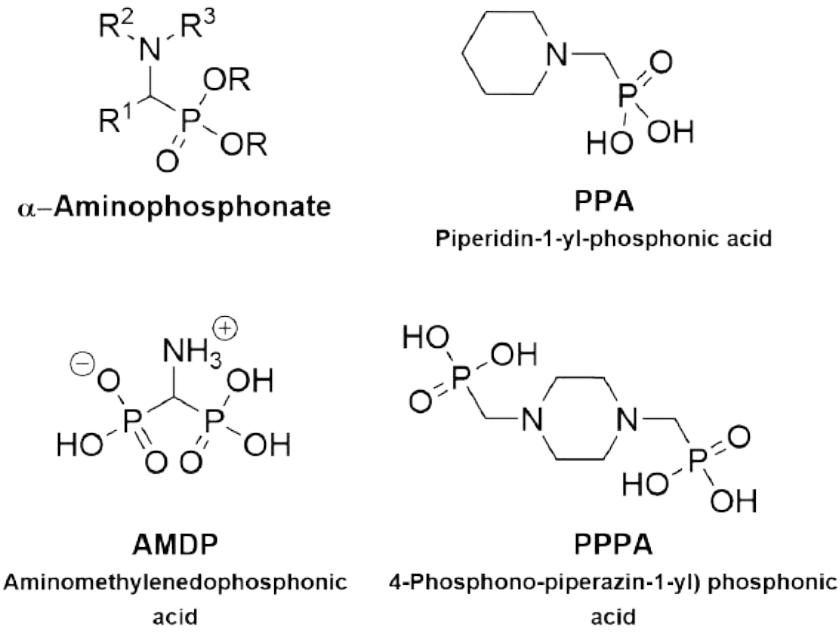


Figure 11. Examples of organophosphorus compounds used as corrosion inhibitors: α-aminophosphonate [61], aminomethylenediphosphonic acid (AMDP) [62], piperidin-1-yl-phosphonic acid (PPA) and (4-phosphono-piperazin-1-yl) phosphonic acid (PPPA) [63].

Certain OPCs are also used as plasticizers, primarily in PVC and other polymers, to increase flexibility, durability, and elasticity [16, 22]. The low cost and compatibility with many polymers make them industrially attractive. Zinc dithiophosphates are another major class of industrial OPCs, produced on a massive scale as anti-wear and antioxidant additives for motor oils [18]. As with flame retardants, the use of OPEs as plasticizers can lead to human exposure through leaching, with recent studies identifying industrial food processing equipment as a potential source of contamination in novel plant-based foods [64].

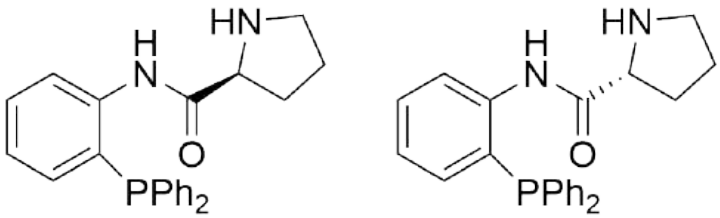


Figure 12. Chiral phosphine-prolineamide [65].

Ogranophosphorous compounds can also be applied as catalysts. Chiral phosphine-prolineamide, presented on Figure 12 can be used as an organocatalyst in direct asymmetric aldol reactions. The research demonstrates that this catalyst is effective in promoting the formation of aldol products with high enantioselectivity and good diastereoselectivity [65]. Other area of organophosphorus catalysis is redox

catalysis P(III)/P(V). For example, Wittig reaction involves the conversion of aldehydes or ketones into alkenes using phosphorylated compounds known as phosphonium ylides $Ph_3P{=}R$. This is concerned as one of the most important methods for alkene synthesis in organic chemistry. This reaction allows for the direct conversion of a carbonyl group into an alkene with control over the stereochemistry of the resulting double bond. It is a highly valued method in organic synthesis, especially in the production of natural compounds and pharmaceuticals [66].

Organophosphorus compounds have found wide use both in agriculture and as chemical weapons, due to their powerful activity against the nervous system in insects and humans. They are still one of the most commonly used insecticides in agriculture. Compounds such as chlorpyrifos, parathion, and dimethoate (their structure is presented in the Figure 13) act by blocking acetylcholinesterase (AChE), which causes a buildup of acetylcholine and leads to uncontrolled nerve signaling. The mechanism of this blockage is presented in the Scheme 8. This eventually results in paralysis and death of the insect [4]. Some of the most popular organophosphorus compounds in agriculture include:

- Parathion (O,O-diethyl O-(4-nitrophenyl) phosphorothioate, $(EtO)_2P(S) - O - C_6H_4NO_2$), structure presented in the Figure 13, which was widely used as an insecticide in the mid-20th century. However, due to its extremely high toxicity to humans and animals, its use has been phased out or banned in many countries. Exposure to this compound can lead to rapid cholinergic overstimulation, often resulting in respiratory failure and death [67].

- Chlorpyrifos (O,O-diethyl O-(3,5,6-trichloro-2-pyridyl) phosphorothioate, $(EtO)_2P(S) - O - C_5H_2Cl_3N$), structure presented in the Figure 13, was used globally for decades in fruit and vegetable farming. It acts by inhibiting acetylcholinesterase, disrupting nerve function in target pests. However, due to growing evidence linking chlorpyrifos to neurodevelopmental harm, particularly in fetuses and young children, many countries, including the United States (2021) and European Union (2020), have implemented bans or severe restrictions on its use [68].

- Dimethoate (O,O-dimethyl S-(N-methylcarbamoyl) methyl phosphorodiamidate, $(MeO)_2P(=O) - SCH_2N(CH_3)C(=O)NH_2$), structure presented in the Figure 13, remains in use in several agricultural regions due to its effectiveness against aphids and other pests. However, its environmental persistence and detection in food and water samples have raised significant concerns regarding

long-term exposure risks, as dimethoate is toxic to many organisms. It disrupts the photosynthetic process in plants and inhibits their growth. In birds, it suppresses brain enzyme activity, leading to sublethal effects - not immediately fatal, but still impairing normal functioning. Aquatic organisms are especially sensitive - following direct exposure to the substance, they often show behavioral changes, particularly in their swimming patterns [69].

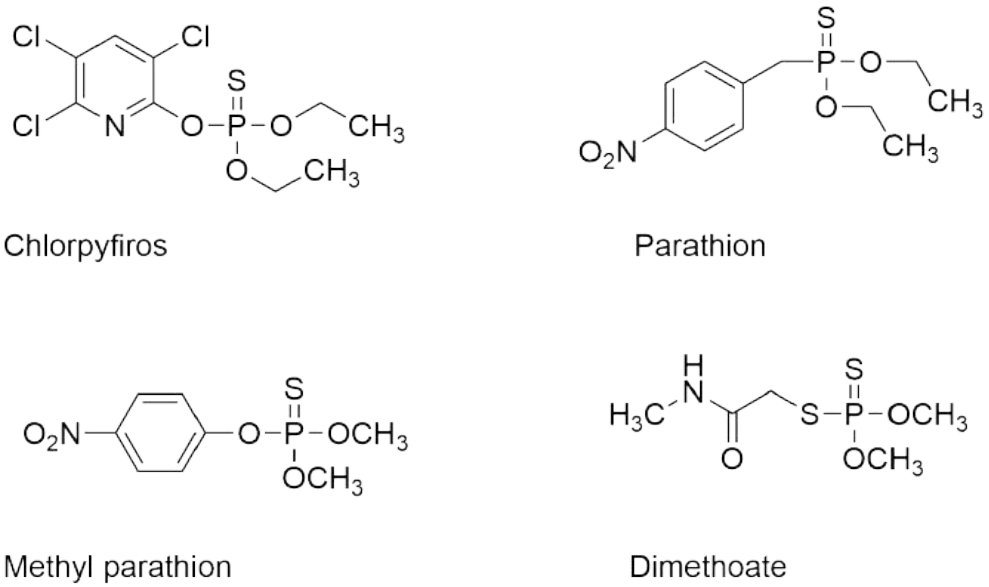
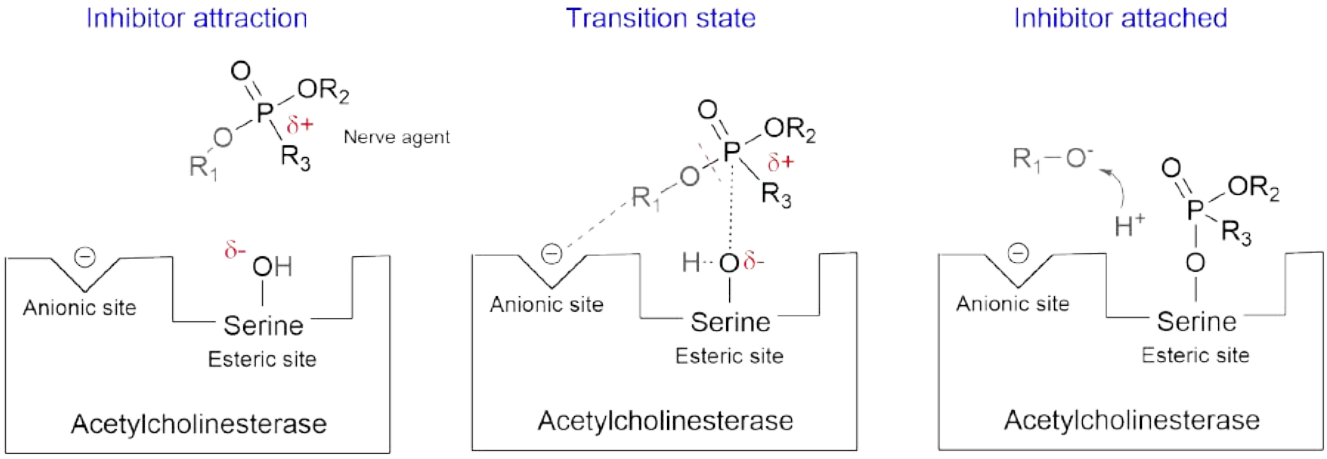


Figure 13. Examples of organophosphorus compounds used in agriculture: chlorpyrifos, parathion, methyl parathion, dimethoate [70].



Scheme 8. Mechanism of cholinesterase inhibition: stepwise interaction between inhibitors and acetylcholinesterase [71].

To improve safety and selectivity, modern insecticide design often employs a strategy similar to the pro-drug concept in medicine. Many widely used OP insecticides, like malathion (Figure 14), are synthesized as thiophosphates, containing a $P = S$ bond

instead of the more reactive $P = O$ (oxon) bond [18]. These thiophosphates are significantly weaker AChE inhibitors. Their toxicity is achieved through in vivo metabolic bioactivation, primarily by cytochrome P450 enzymes in the target organism, which oxidize the $P = S$ group to the highly potent $P = O$ analogue. The effectiveness of this strategy relies on the differential metabolic rates between insects and mammals. An ideal insecticide is one that is rapidly activated in the insect but slowly activated or rapidly detoxified in mammals, creating a margin of safety [30].

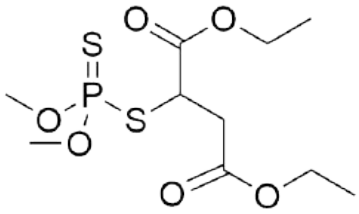


Figure 14. Structure of malathion [18].

Several organophosphorus compounds were developed for military purposes, especially due to their ability to quickly and irreversibly block AChE in humans:

- Sarin (isopropyl methylphosphonofluoridate) (Figure 15) is one of the most well-known organophosphorus nerve agents. As mentioned before, developed during the 1930s, it is a colorless and volatile liquid that inhibits acetylcholinesterase irreversibly, leading to rapid overstimulation of the nervous system. Sarin has been used in several high-profile chemical attacks [72].

- VX (O-ethyl S-(2-diisopropylaminoethyl) methylphosphonothioate) (Figure 15) is a persistent nerve agent with extremely high potency. Unlike sarin, it is oily and poorly volatile, making it particularly dangerous upon skin contact. VX was developed in the 1950s and is classified as a weapon of mass destruction under international law [73].

- A-234, a Novichok agent (N-[1-(diethylamino)ethylidene]-N-methylphosphoramidofluoridate) (Figure 15) belongs to a newer class of nerve agents that emerged from secret Soviet chemical weapons programs. These agents are believed to be more toxic than sarin or VX and have been involved in recent political poisonings, reigniting international concern over chemical warfare [74].

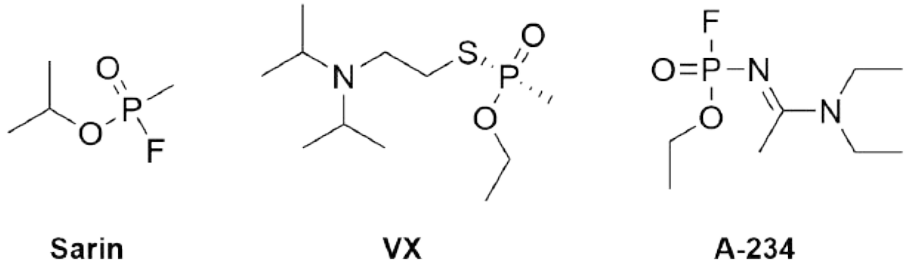


Figure 15. Structures of Sarin (isopropyl methylphosphonofluoridate) [72], VX (O-ethyl S-(2-diisopropylaminoethyl) methylphosphonothioate) [73] and A-234, a Novichok agent (N-[1-(diethylamino)ethylidene]-N-methylphosphoramidofluoridate) [74].

The ethical dimension of these dual-use compounds is hard to ignore: on the one hand, they have helped increase crop yields and food security, but on the other hand, they remain an enduring threat as tools of war. This makes ongoing research into safer, non-toxic alternatives not just important, but urgent.

In contrast to the AChE-inhibiting insecticides, the most prominent OP herbicide, glyphosate, is a phosphonate that operates through a completely different mechanism. Glyphosate inhibits the enzyme 5-enolpyruvylshikimate-3-phosphate synthase (EPSPS), which is a key component of the shikimate pathway for aromatic amino acid synthesis in plants and some microorganisms [75–78]. Glyphosate and 5-enolpyruvylshikimate-3-phosphate, product of the reaction inhibited by glyphosate are presented on Figure 16. Since this pathway does not exist in animals, glyphosate has a much lower acute toxicity to mammals than OP insecticides [79]. The introduction of glyphosate-resistant transgenic crops revolutionized agriculture, allowing for broad-spectrum weed control [80]. However, its widespread use has led to significant controversy. The International Agency for Research on Cancer (IARC) classified glyphosate as probably carcinogenic to humans in 2015, a conclusion disputed by other regulatory bodies [81].

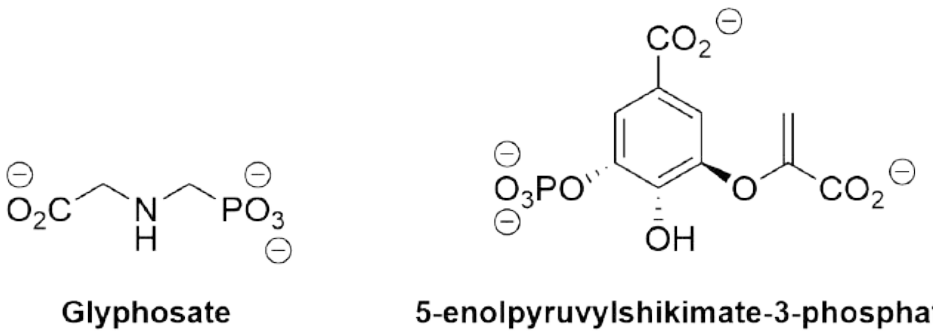


Figure 16. Structure of glyphosate and 5-enolpyruvylshikimate-3-phosphate [82].

The environmental fates of these two classes of agricultural OPCs are explicitly

different, illustrating the two models of risk. Ester-based insecticides like malathion are designed to be non-persistent. Their primary degradation pathway is hydrolysis, which is sensitive to environmental pH and temperature, along with microbial breakdown [18, 83, 84]. While this lability reduces long-term accumulation of the parent compound, their high acute toxicity means that runoff from agricultural fields can pose a significant threat to aquatic ecosystems [85, 86]. Glyphosate, on the other hand, is a phosphonate with a highly stable $P - C$ bond, making it much more resistant to chemical hydrolysis [87]. Its primary degradation route is microbial action in the soil, which can be slow, leading to greater persistence. Its main metabolite, aminomethylphosphonic acid (AMPA) (Figure 17), is also persistent and more mobile in soil. Consequently, the environmental concern with glyphosate is not primarily acute toxicity but rather its widespread presence in soil and water systems and the potential long-term ecological and health effects of chronic exposure [87].

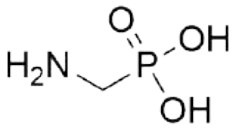
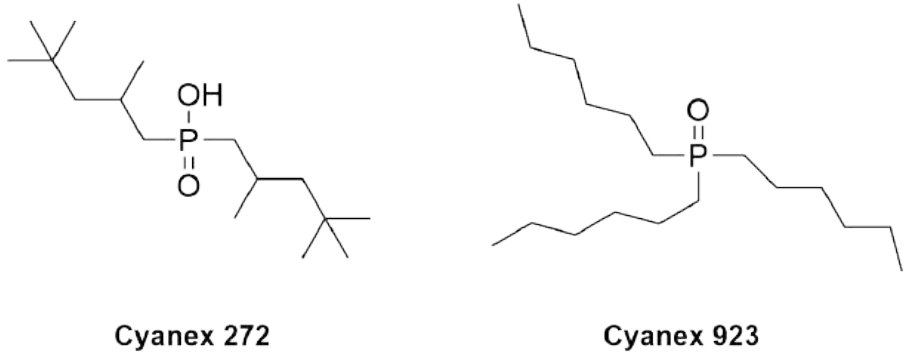


Figure 17. Structure of aminomethylphosphonic acid (AMPA) [87].

In the field of hydrometallurgy, specific organophosphorus compounds are prized for their ability to act as highly selective extractants for separating and purifying metals, including valuable heavy metals and rare-earth elements [88]. Acidic extractants like phosphinic acids, such as Cyanex 272 (Figure 18), and neutral extractants like phosphine oxides, such as Cyanex 923 (Figure 18), function via cation exchange or solvation mechanisms [88]. Their selectivity can be tuned based on chemical principles like the Hard and Soft Acids and Bases (HSAB) theory. Hard oxygen-based ligands preferentially bind to hard metal ions, such as Fe^{3+}, while softer sulfur-based ligands show higher affinity for soft metal ions, such as Cu^{+} [88]. This tunability makes them vital reagents in mining and electronics recycling industries.



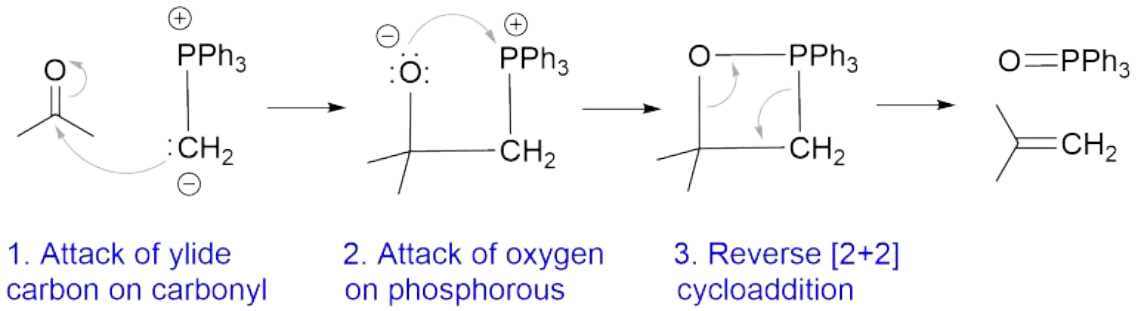
Cyanex 272 Cyanex 923

Figure 18. Structures of Cyanex 272 and Cyanex 923 [88].

1.1.3 Synthetic and biological research

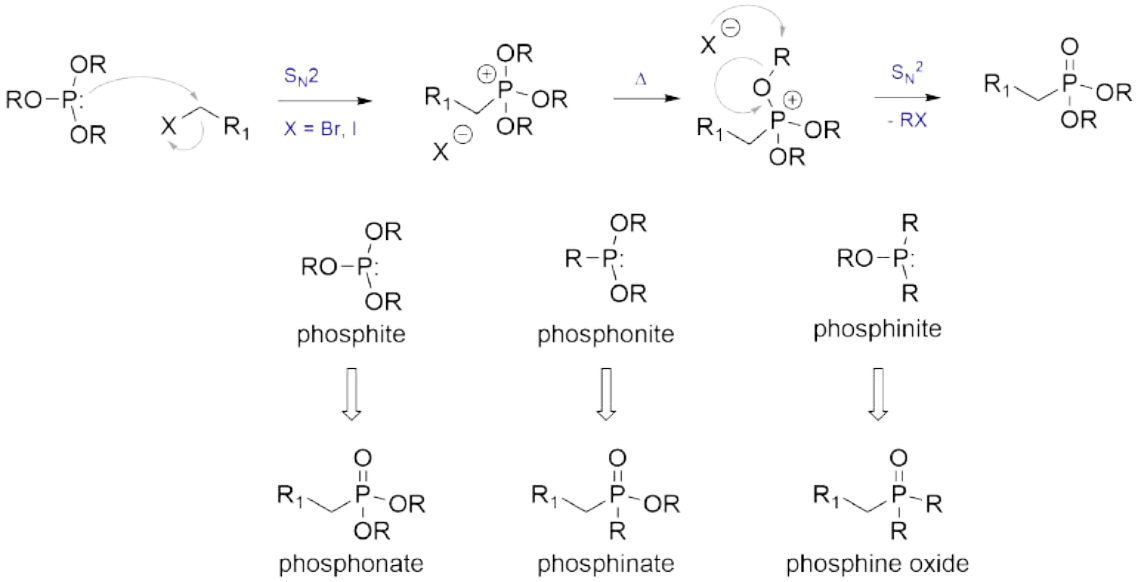
Beyond their large-scale industrial roles, organophosphorus compounds are indispensable tools in the research laboratory. They function as powerful reagents that enable the construction of complex molecules, as highly tunable ligands that are central to modern catalysis, and as sophisticated probes for interrogating biological systems. Several of the most important and widely used transformations in modern organic synthesis rely on the unique reactivity of organophosphorus reagents. A unifying theme across many of these reactions is a $P(III)$ to $P(V)$ redox cycle, where the formation of the exceptionally stable $P = O$ bond in a phosphine oxide byproduct provides the thermodynamic driving force for the overall transformation [89, 90].

Discovered by Georg Wittig, the Wittig reaction is a premier method for synthesizing alkenes from aldehydes or ketones [91], presented on Scheme 9. It utilizes a phosphorus ylide or Wittig reagent, typically prepared by treating a phosphonium salt with a strong base. The nucleophilic carbanion of the ylide attacks the electrophilic carbonyl carbon, leading to an intermediate oxaphosphetane. This four-membered ring then collapses in an irreversible, exothermic step to yield the desired alkene and the highly stable byproduct, triphenylphosphine oxide $Ph_3P = O$ [92]. A key advantage of the Wittig reaction is that the position of the new double bond is unambiguously defined, avoiding the mixtures of isomers often seen in elimination reactions [92].



Scheme 9. General scheme of Wittig reaction [92].

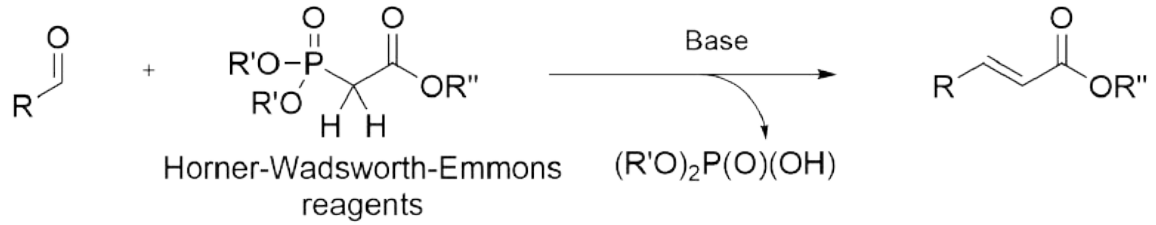
The Michaelis-Arbuzov reaction is the most fundamental and widely used method for forming the robust phosphorus-carbon bond [93, 94]. In its classical form, a trivalent phosphorus ester, such as a trialkyl phosphite, acts as a nucleophile, attacking an alkyl halide in an SN2 reaction to form a phosphonium salt intermediate. A halide anion then dealkylates this intermediate in a second SN2 step, yielding a pentavalent phosphonate and a new alkyl halide [95, 96] as presented in the Scheme 10. This reaction is the entry point for producing the phosphonate precursors used in many other synthetic methods [95, 96].



Scheme 10. General scheme of Michaelis-Arbuzov reaction [95].

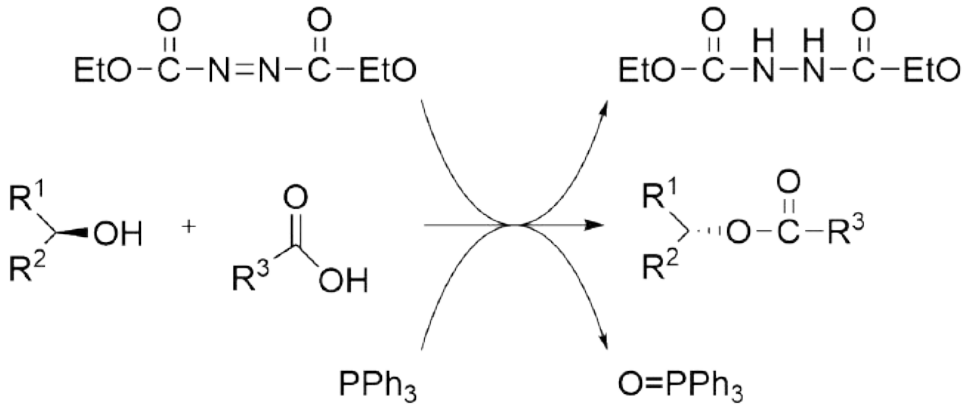
The Horner-Wadsworth-Emmons (HWE) reaction is a powerful modification of the Wittig reaction that uses phosphonate-stabilized carbanions instead of ylides [97–99]. These carbanions are generated by deprotonating a phosphonate ester (often made via the Michaelis-Arbuzov reaction). Scheme is presented on the Scheme 11. The HWE reaction typically provides excellent control over alkene geometry, often favoring the formation of (E)-alkenes, and its water-soluble phosphate byproduct is much easier

to remove from the reaction mixture than the triphenylphosphine oxide generated in the classical Wittig reaction [97, 99].



Scheme 11. General scheme of the Horner-Wadsworth-Emmons Reaction [100].

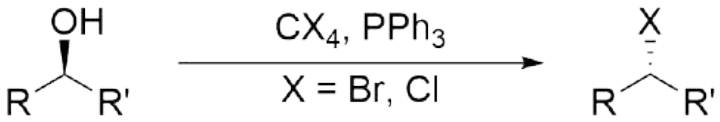
Other important reaction is the Mitsunobu reaction, which is a versatile and powerful redox condensation that converts primary and secondary alcohols into a wide array of other functional groups, including esters, ethers, azides, and thioethers [101]. The reaction employs a combination of a phosphine, typically PPh_3, and an azodicarboxylate - diethylazodicarboxylate (DEAD). The phosphine and DEAD combine to activate the alcohol, converting the hydroxyl group into an excellent leaving group. A key feature of the reaction is that the subsequent nucleophilic substitution occurs with a clean inversion of stereochemistry at the alcohol carbon, making it an invaluable tool for controlling stereocenters in the synthesis of complex natural products [101, 102]. Scheme 12 presents the scheme of the reaction. Like the Wittig reaction, the process is driven by the formation of triphenylphosphine oxide [102].



Scheme 12. General scheme of the Mitsunobu reaction [103].

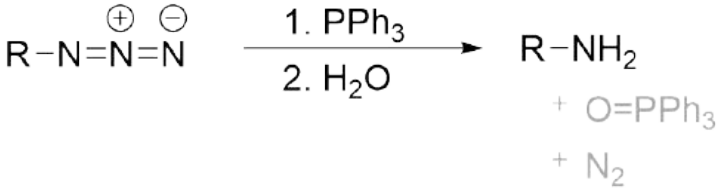
The Appel reaction provides a mild and efficient method for converting alcohols into alkyl halides [104, 105]. It uses a combination of a phosphine, typically PPh_3, and a tetrahalomethane, such as CCl_4 or CBr_4. General scheme is presented on Scheme 13. The reaction proceeds via an oxyphosphonium intermediate, which is then displaced by a halide ion in an SN2 reaction. For chiral secondary alcohols, this

proceeds with inversion of configuration, similar to the Mitsunobu reaction [105]. The driving force is the formation of triphenylphosphine oxide [105].



Scheme 13. General scheme of Appel reaction [106]

The Staudinger reaction involves the reaction of a phosphine with an organic azide to form an iminophosphorane intermediate [107, 108]. This intermediate can then be hydrolyzed with water to yield a primary amine and a phosphine oxide byproduct, providing a very mild and chemoselective method for reducing azides. The scheme is presented in the Scheme 14 This reaction has been ingeniously adapted for bioconjugation in a process known as the Staudinger ligation, where the iminophosphorane is trapped by an intramolecular ester to form a stable amide bond, allowing for the specific labeling of biomolecules in complex biological environments [107, 108].

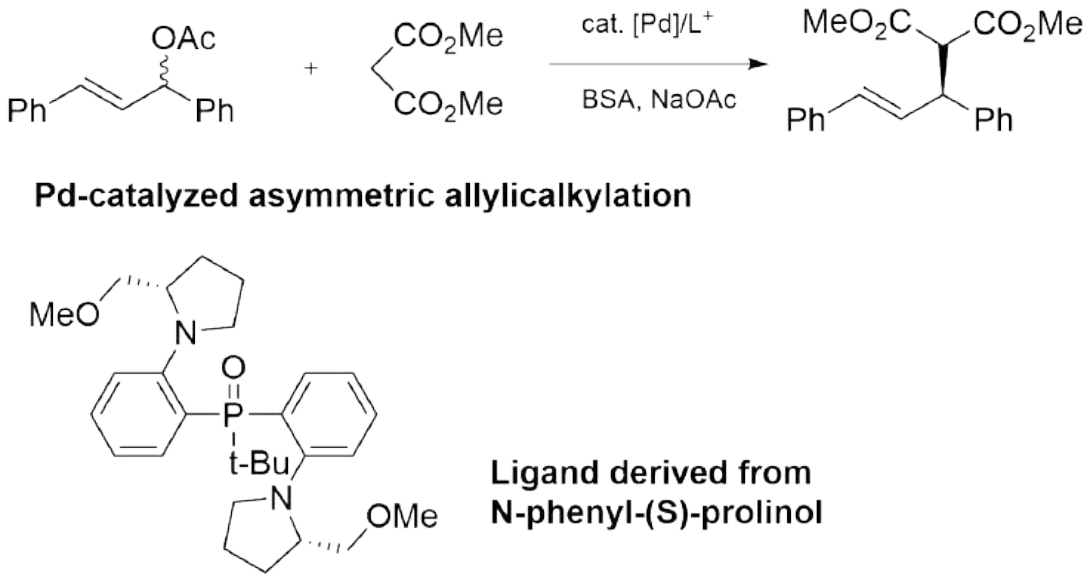


Scheme 14. General scheme of Staudinger reaction [108].

The development of transition metal catalysis has revolutionized organic synthesis, and organophosphorus compounds, specifically phosphines, have been at the very heart of this revolution. A fascinating symbiotic relationship within the field exists: the most advanced methods for synthesizing complex organophosphorus compounds often rely on transition metal catalysis, which, in turn, is enabled by sophisticated organophosphorus ligands [109].

Phosphines R_3P are one of the most important classes of ligands in coordination and organometallic chemistry, with a foundational role in homogeneous catalysis dating back to the 1950s. The early exploration of the use of triphenylphosphine PPh_3 in transition metal complexes and the discovery of Wilkinson's catalyst, $RhCl(PPh_3)_3$, laid the foundation for future developments in the field [110]. The effectiveness of phosphines stems from the unique ability to precisely tune their electronic and steric properties by modifying the three R groups attached to the phosphorus atom [111, 112]. Electronically, they act as strong σ-donors through their lone pair, stabilizing the

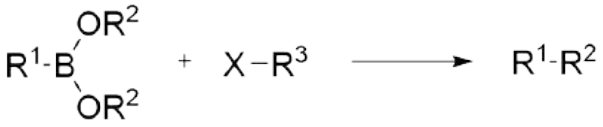
metal center. Sterically, the size of the R groups can be adjusted to control access to the metal, influencing the selectivity of the reaction, with this steric bulk often quantified by the Tolman cone angle [111].



Scheme 15. Scheme of Pd-catalyzed asymmetric allylic alkylation and structure of ligand derived from N-phenyl-(S)-prolinol [113].

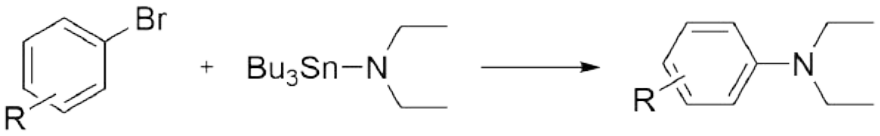
Thanks to this versatility, phosphorus-based ligands have become ubiquitous in catalysis, and contemporary research focuses on designing increasingly advanced structures for specific applications, especially in asymmetric synthesis. For example, the preparation of chiral P, N-ligands derived from N-phenyl-(S)-prolinol (Scheme 15) has been described for use in palladium-catalyzed asymmetric allylic alkylation reactions (Scheme 15), yielding products with high enantiomeric excesses, including an optically active fluorine-containing compound [113]. Other work has focused on the synthesis of atropisomeric aminophosphine ligands with stable configurations, which have also proven effective as ligands in asymmetric catalysis [114].

The impact of phosphine ligands is perhaps most evident in palladium-catalyzed cross-coupling reactions, which are workhorse transformations in the pharmaceutical and materials science industries. One example is Suzuki-Miyaura coupling (Scheme 16). It means the formation of C-C bonds via Suzuki coupling was transformed by the development of bulky, electron-rich dialkylbiaryl phosphine ligands, such as those pioneered by the Buchwald group. These ligands generate highly active Pd(0) catalysts that can facilitate the coupling of previously challenging substrates, such as unactivated and sterically hindered aryl chlorides, often at room temperature and with low catalyst loadings [115–118].



Scheme 16. General scheme of Suzuki-Miyaura coupling [117, 118].

Other example is Buchwald-Hartwig amination (Scheme 17), so the formation of $C-N$ bonds via direct coupling of amines with aryl halides was a long-standing challenge in organic synthesis. The Buchwald-Hartwig amination, a Pd-catalyzed process, provided a general solution. The success of this reaction is almost entirely dependent on the use of specialized, bulky phosphine ligands like XPhos and SPhos, which are designed to promote the difficult reductive elimination step that forms the $C-N$ bond [119, 120].



Scheme 17. General scheme of Buchwald-Hartwig amination [119, 120].

Distinct from their role as ligands for metals, phosphines can also act as nucleophilic organocatalysts in their own right [112, 121, 122]. In this mode of catalysis, the reaction is initiated by the nucleophilic addition of the phosphine to an electrophilic substrate (such as an activated alkene or alkyne), generating a reactive zwitterionic intermediate [121, 122]. This intermediate then engages in a variety of subsequent transformations before the phosphine catalyst is regenerated. Seminal examples of phosphine organocatalysis include the Rauhut-Currier and Morita-Baylis-Hillman (MBH) reactions [121, 122].

The same properties that make organophosphorus compounds (OPCs) potent toxins also make them powerful tools for studying biological systems. The key to this utility is the ability of certain OPCs to irreversibly phosphorylate the active site serine of serine hydrolases, making them highly specific and potent inhibitors [16, 123]. This property is exploited in activity-based proteomics, where OPC-based probes are used to covalently label and identify active enzymes within a complex proteome, providing a snapshot of the functional state of a cell or tissue [123].

OPCs also form the basis of a variety of sensors for detecting enzyme activity or the presence of specific analytes. In one common "signal-off" design, the presence of an OP pesticide inhibits an enzyme, like AChE, which in turn prevents the enzyme from

catalyzing a reaction that would normally produce a colorimetric or fluorescent signal. The absence of a signal therefore indicates the presence of the inhibitor [124, 125].

Another strategy involves creating probes where an enzyme, such as carboxylesterase cleaves a bond in the probe molecule, releasing a quenched fluorophore and "turning on" a fluorescent signal. The presence of an OPC that inhibits the enzyme prevents this fluorescence, allowing for sensitive detection [126–128]. These sophisticated probes are valuable for applications ranging from environmental monitoring to visualizing enzyme activity directly in living cells [126, 129].

1.1.4 Catalysis in organophosphorus synthesis

The synthesis of organophosphorus compounds spans a vast range from multi-ton industrial production to milligram-scale laboratory synthesis. The catalytic strategies employed in this field are diverse and have evolved significantly, driven by unique challenges related to reagent hazards, byproduct management, and the pursuit of novel structures. Catalysis in many industrial sectors focuses on the activation of unreactive substrates, but in phosphorus chemistry the primary challenge is often to moderate the reactivity of highly reactive precursors and manage the safety and selectivity of the process [5]. All the information are summarized in the Table 3.

The traditional foundation of the organophosphorus industry is based on some key highly reactive phosphorus precursors: primarily white phosphorus P_4 and its chlorinated derivatives, phosphorus trichloride PCl_3 and phosphorus oxychloride $POCl_3$. The dominant industrial route for producing the vast majority of organophosphate esters is the alcoholysis of phosphorus oxychloride $POCl_3$. This reaction is often facilitated by Lewis acid catalysts such as aluminum trichloride $AlCl_3$ or magnesium chloride $MgCl_2$ to enhance the reaction rate [16, 19].



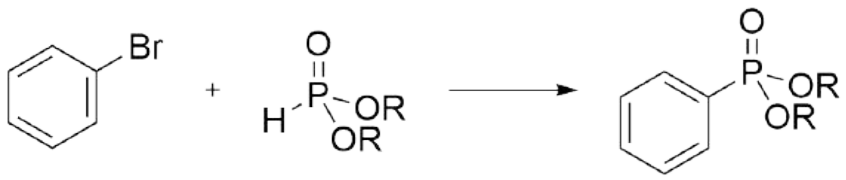
Scheme 18. General scheme of alcoholysis of phosphorus oxychloride [19].

Catalysts play a central role in the synthesis of organophosphorus compounds, enabling efficient and selective formation of $C-P$ and $P-X$ bonds. In classical and modern methodologies, three major catalytic domains can be distinguished: transition-metal catalysis, Lewis acid catalysis, and metal-free strategies including organocatalysis and biocatalysis. Additionally, recent advances in photoredox and electrochemical

Table 3. Summary of catalytic strategies in the synthesis of organophosphorus compounds.

Type of catalysis	Reaction	Example catalysts	Key features / application	Ref.
Transition-metal catalysis	Hirao cross-coupling	Pd, Ni, Cu complexes (e.g., $Pd(PPh_3)_4$, $NiCl_2(dppe)$)	Key method for forming $C-P$ bonds, esp. $C(sp^2)-P$; newer Ni/Cu variants lower costs.	[130, 131]
	Atherton–Todd reaction	Cu complexes (Cu/O_2)	Greener alternative to classical halogenation route for phosphoramidates.	[132]
	Direct $C-H$ phosphorylation	Ru, Rh with photocatalysis	Atom economy via activation of unmodified $C-H$ bonds; reduced waste.	[133]
Lewis acid catalysis	Alcoholysis of $POCl_3$	$AlCl_3$, $MgCl_2$	Industrial production of phosphate esters; higher rate and yield.	[16, 19]
	Hydrophosphonylation (Pudovik)	Ln triflates (e.g., $Yb(OTf)_3$), Ln amides	Activates carbonyls/imines; asymmetric access to α-hydroxy- and α-aminophosphonates.	[134, 135]
	Kabachnik–Fields	$Zn(OTf)_2$, $HfCl_4$, zeolites ($H-Y$), TiO_2	Three-component route to α-aminophosphonates; heterogeneous catalysts enable recycling.	[136, 137]
Metal-free (organocatalysis)	Hydrophosphonylation	Thioureas, squaramides, NHCs	Mild conditions; high ee with H-bonding catalysts; NHCs activate ketones.	[138, 139]
	Various transformations	Nucleophilic phosphines (e.g., PBu_3)	Organocatalyzed cycloadditions/annulations to build P-functional frameworks.	[121, 140]
	Phospha-Michael addition	CAL-B (Novozym 435)	Biocatalytic, metal-free $C-P$ formation under mild conditions; high yields.	[128]
Photoredox & electrochemistry	Hydrophosphinylation of alkenes	Organic dyes (e.g., Eosin Y)	P-centered radicals under visible light; addition to unactivated alkenes.	[141]
	Phosphorylation of arenes	Electrochemical (no added catalyst)	Direct $C(sp^2)-H$ phosphorylation in flow; no external oxidants/halogenated precursors.	[142]

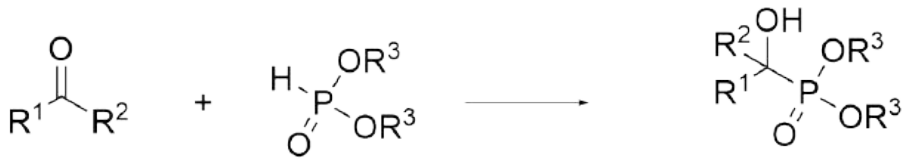
methods have significantly expanded the synthetic toolkit for organophosphorus chemistry [130, 132, 136, 140].



Scheme 19. General scheme of Hirao reaction - cross coupling of dialkyl phosphites with aryl halides catalysed by Palladium [143].

Transition-metal catalysis remains one of the most powerful approaches to $C-P$

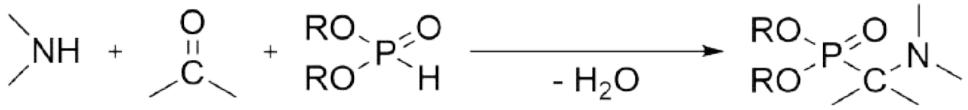
bond construction. The palladium-catalyzed Hirao cross-coupling between aryl halides and dialkyl phosphites (Scheme 19) is a cornerstone reaction, with ligand optimization allowing reduced palladium loadings and activation of less reactive aryl chlorides [130]. More recently, nickel and copper catalysts have emerged as cost-effective alternatives, capable of promoting cross-coupling reactions with a wide substrate scope, including sp2 and sp3 electrophiles [131]. Direct $C-H$ phosphorylation and radical-mediated methods have also gained prominence, especially when integrated with electrochemical or photoredox activation, as they minimize waste and often proceed under milder conditions. Examples include continuous-flow electrochemical arene phosphorylation without the need for metal catalysts or external oxidants [142], as well as visible-light-mediated hydrophosphinylation of unactivated alkenes using inexpensive organic dyes [141].



Scheme 20. General scheme of hydrophosphonylation with carbonyl substrate [134].

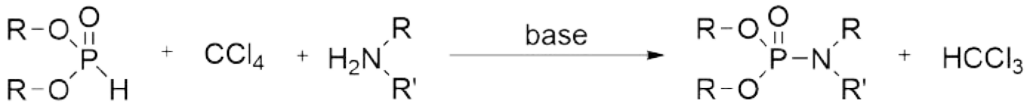
Lewis acid catalysis is particularly valuable in hydrophosphonylation reactions, where activation of carbonyl or imine substrates leads to enhanced reactivity and enantioselectivity. Reaction scheme with carbonyl substrate is presented on Scheme 20. Lanthanide triflates and lanthanide amides are among the most efficient catalysts, with some systems operating at very low loadings and short reaction times [134, 135]. These catalysts also enable asymmetric transformations, making them relevant for the synthesis of optically pure α-hydroxyphosphonates and related compounds.

Metal-free organocatalysis has become an increasingly attractive alternative due to due to decreasing metal resources in the world, mild conditions of metal-free organocatalysis and alignment with green chemistry principles. Nucleophilic phosphine catalysts have been widely applied providing versatile access to P-functionalized frameworks [121, 140]. Hydrogen-bonding catalysts such as squaramides and thioureas enable enantioselective hydrophosphonylation of aldehydes [138], while N-heterocyclic carbenes (NHCs) promote hydrophosphonylation of α-ketoesters and α-trifluoromethyl ketones under ambient conditions [139].



Scheme 21. General scheme of Kabachnik-Fields reaction [136].

The Kabachnik-Fields reaction, presented on Scheme 21, which produces α-aminophosphonates from amines, carbonyl compounds, and dialkyl phosphonate $(RO)_2P(O)H$, is another well-established transformation in organophosphorus chemistry. It can proceed under catalyst-free conditions, especially with microwave heating or solvent-free protocols, but both homogeneous Lewis acids, such as $Zn(OTf)_2$, $HfCl_4$ and heterogeneous solids such as zeolites, TiO_2 and MOFs are frequently used to improve yields and recyclability [136, 137, 144–146]. Mechanistic studies indicate that the reaction often proceeds via imine formation followed by a Pudovik-type addition [136].



Scheme 22. General scheme of Atherton-Todd reaction [132].

In the synthesis of phosphoramidates and phosphates, the Atherton-Todd reaction, presented on Scheme 22, remains a key method. Traditionally employing dialkyl phosphites, amines or phenols, base, and halomethanes, the reaction has been adapted to greener conditions, such as using copper and oxygen as alternatives to toxic halogenated reagents [132].

Biocatalysis has also entered the field of C-P bond formation. For instance, Candida antarctica lipase B (CAL-B, Novozym 435) has been shown to catalyze phospha-Michael additions of phosphine oxides to nitroalkenes and benzylidene derivatives at room temperature with high yields and recyclability, providing a sustainable, metal-free route [128].

Photoredox catalysis, often combined with transition metals or organic dyes, has opened new ways for organophosphorus synthesis, enabling carbophosphorylation, oxyphosphorylation, and direct $C-H$ phosphorylation via P-centered radical intermediates [133, 147]. These strategies, along with electrosynthetic methods [142, 148], illustrate the growing emphasis on mild, selective, and sustainable catalytic systems in organophosphorus chemistry.

1.2 Introduction to ecocatalysis

1.2.1 Fundamentals of catalysis

At the beginning of the 20th century, the primary metric of success in chemical manufacturing was yield. The generation of waste was often viewed as an unavoidable cost of doing business. However, a series of environmental disasters and a growing understanding of the long-term ecological impact of industrial pollution caused a fundamental rethinking of this paradigm [149]. This led to the formalization of green chemistry, a proactive design philosophy aimed at preventing pollution at its source rather than remediating it after the fact [149–151].

Green chemistry is articulated through twelve core principles, which guide chemists in designing safer, more efficient, and environmentally benign products and processes [149, 151]. These principles advocate for actions such as preventing waste, using renewable feedstocks, designing for energy efficiency, and avoiding the use of toxic solvents and reagents [149, 151].

Central to Green Chemistry are quantitative metrics that allow for the objective assessment of a process's environmental performance. Two of the most influential metrics are Atom Economy and the E-Factor. Atom Economy, or atom efficiency, is a theoretical concept that calculates the percentage of atoms from the reactants that are incorporated into the final desired product, assuming a perfect 100% yield [151]. It provides a quick, top-level assessment of how efficiently a reaction uses its raw materials. However, it does not account for real-world inefficiencies like incomplete reactions, side products, or the waste generated from solvents and work-up procedures. To capture this real-world impact, the E-Factor (Environmental Factor) was developed - a simple metric defined as the mass ratio of total waste produced to the mass of the desired product [151]. Unlike atom economy, the E-Factor accounts for all waste streams, including reagent byproducts, solvent losses, and process aids. The ideal E-Factor is zero, but in real world it increases as the complexity of the target molecule grows: bulk chemical production may have an E-Factor of less than 5, while fine chemicals can range from 5 to 50, and the pharmaceutical sector can have E-Factors well over 100 [151]. This massive waste generation, particularly in the fine chemical and pharmaceutical industries, is largely a consequence of the reliance on traditional stoichiometric reagents, which are consumed during the reaction and become part of the waste stream [151].

The principles of green chemistry and the challenge posed by high E-Factors point

directly to catalysis as the most powerful tool for building a sustainable chemical industry. The ninth principle of green chemistry explicitly states a preference for catalytic reagents over stoichiometric ones, as catalysts, by their very nature, are not consumed and can facilitate the transformation of vast quantities of reactants [149, 151]

Catalysts enable sustainability beyond waste reduction. Highly selective catalysts can minimize the formation of unwanted byproducts, simplifying purification and reducing solvent use. By operating under milder conditions of temperature and pressure, catalysts directly address the green chemistry principle of designing for energy efficiency, which in turn reduces the carbon footprint of the manufacturing process. The global push towards a sustainable, low-carbon future-driven by goals like decarbonization, renewable energy integration, and the valorization of biomass-is therefore intrinsically linked to and dependent upon continuous innovation in catalysis [152].

Catalysis sits at the core of modern chemistry and chemical engineering. Catalysts are substances that accelerate a chemical reaction without being depleted in the process and without altering the overall standard Gibbs energy change. It takes part in the elementary steps and is regenerated at the end [153] Catalyst often enables the reaction to proceed along a different, faster pathway. Since a catalyst is not consumed during the reaction, the main advantage of catalyst is that they can be reused in many cycles. There are three types of catalysis: homogeneous catalysis, heterogeneous catalysis and biocatalysis. Catalysts can also be classified into groups, and various substances can act as catalysts, such as protons, Lewis acids, organometallic complexes, organic and inorganic polymers, enzymes, metals, their oxides, and salts [154].

At the molecular level, catalysts lower effective barriers by stabilizing the transition state or providing low-energy pathways. In complex cycles, the turnover frequency and turnover number quantify activity and durability, but their definitions and comparison across subfields require care. Turnover frequency depends on how one counts active sites and on experimental conditions [155]. For multistep cycles, the energetic span model connects a free-energy profile to an apparent turnover frequency by identifying rate- and state-controlling features without invoking a single “rate-determining step,” providing a practical bridge between computation and experiment [156].

Homogeneous catalysts occur in the same phase as the reactants, typically in a liquid form. These catalysts usually involve transition metals paired with organic ligands to create a complex that facilitates chemical reactions. Among their advantages are precise control over reaction conditions and mechanisms, making them suitable for reactions where selectivity and fine-tuning are crucial [157].

Some researchers point out that the science of catalysis has not yet mature enough to be reliably predicted or intentionally developed based on available knowledge. They highlights the need to introduce a degree of chemical complexity into the rigorous domain of physicochemical catalysis [158].

Homogeneous catalysis plays a significant role in chemistry, contributing to various industrial processes like hydroformylation, hydrogenation, carbonylation and metathesis. One advantage over heterogeneous catalysis is the ability to design catalysts with ligands, enabling high activity and selectivity. However, separating catalysts from reaction mixtures can be a challenge [157].

Heterogeneous catalysis is a process in which the catalyst and substrate exist in different phases. Typically, this refers to cases where the catalyst is a solid and the reactants are in a gaseous or liquid state. The combination of solid and gas is commonly concerned as classic heterogeneous catalysis due to its historical development in the petrochemical and bulk chemical industries. Main advantage of heterogeneous catalysis is the ease of separating the catalyst after the reaction. Heterogeneous catalysts rely on active sites on metals, oxides, carbons, and zeolites. Zeolites exemplify how precise pore architectures and Brønsted/Lewis acidity control both activity and shape/selectivity in refinery cracking and methanol-to-hydrocarbons chemistry [159].

Metal oxides are one of the groups of compounds used as catalysts in the industry. These may include oxides of transition metals or main-group metals. The surface, solid state and morphological properties of metal oxides as catalysts are crucial to the execution of complex heterogeneous reactions. Therefore, the relationships between the structural properties and catalytic activity of metal oxides are essential. There are different types of metal oxides with various structural compositions and properties [160].

Transition-metal oxides are widely used as heterogeneous catalysts. The most important attribute of these oxides is stability, which is determined by the oxidation state of the metal. The most commonly used in catalysis are oxides of metals with stable high-oxidation states, such as chromium, zinc, titanium, vanadium, manganese, and aluminum oxides. Metal oxides with intermediate stability are also commonly used as catalysts and this group include: iron, cobalt, nickel and lead. Oxides of metals which form unstable compounds like platinum, palladium, ruthenium, silver and gold are mainly used in nanoparticle form [161].

Thermal stability of metal particles increases, when their size increases in the range from 1 to 6 nm. Particles larger than 6 nm are more resistant to sintering. Oxygen vacancies in metal oxide can also play an important role in enhancing the stability

of nanoparticles [162]. The sintering process of metals is described by the Ostwald ripening and particle migration and coalescence models ([163]).

In the case of metal oxides as catalysts, one of the most important topics is those oxygen vacancies (OVs), which play a significant role in the mechanism and kinetics of reactions catalyzed by these oxides. They are modified to adjust the catalytic efficiency of various materials, such as TiO_2, CeO_2, ZnO, and CuO. It can enhance various aspects of the catalytic process in the same time - for example, in photocatalysis: light absorption, surface reactions or charge transfer and separation. Regulating oxygen vacancies is also often applied in electrocatalysis and thermal catalysis to boost catalytic activity [158].

Metal catalysts can be classified into three main groups: single-atom catalysts, nanoclusters, and nanoparticles. Single atoms are individual metal atoms supported on a solid matrix. This form of catalysts offer maximum metal utilization and exhibit high selectivity due to the ability to form specific active sites. Nanoclusters are clusters including typically less than 20 atoms. Their reactivity is affected by quantum confinement effects. Clusters with fewer than 30 atoms reveal electronic behavior distinct from larger particles. Their size vary from 1 to 100 nm. Nanoparticles are particles larger than nanoclusters. They behave more like bulk metals, and their reactivity is determined by their exposed surface aspects [164].

1.2.2 Challenges in catalysis: metal availability and sustainability

As reported in the CRS report, there has been a steady increase in the prices of minerals and metals in recent years. Some of the main factors driving this trend include the growing global demand, particularly in China, the rising production costs for metals, and the limitations of natural supply. Numerous projects worldwide aim to expand mining and refining infrastructure; however, they face a range of challenges, such as electricity shortages, a lack of skilled labor, equipment issues, labor unrest, weather and transport-related delays, and opposition due to environmental protection policies. These factors can raise costs and intensify supply issues, ultimately leading to higher prices. Higher prices impact materials management, such as reducing the amount of platinum used in automotive catalysts by substituting it with palladium, which is cheaper, where possible, or recovering materials like scrap iron, steel, aluminium, copper and platinum-group metals [165]. Severity of the problem is visible in annual global spending on metal extraction - it increased from 2 billion in 2002 to 10 billion in 2008 [166]. Between 2020 and 2024, the prices of many metals essential for

catalysis and energy transition technologies experienced strong volatility, marked by sharp spikes followed by partial corrections. Even though prices eased in 2023-2024 for several commodities, most metals remain above 2020 levels, and the persistent instability itself has increased risks and costs for catalyst users. Copper illustrates this trend clearly: the COMEX annual average price rose from $2.80 per pound in 2020 to an estimated $4.20 per pound in 2024, a growth of approximately 50% [167]. Nickel followed a similar trajectory, climbing from $13,772 per metric ton in 2020 to about $17,100 per ton in 2024, representing an increase of around 24%, though the peak occurred in 2022 at $25,815 per ton [168]. Lithium carbonate, critical for batteries but also influencing broader chemical supply chains, underwent particularly extreme fluctuations. Its price increased from $10,100 per ton in 2020 to a peak of $71,100 per ton in 2022, before stabilizing near $14,000 per ton in 2024. Even after this correction, lithium remains about 39% more expensive than in 2020, with the 2022 spike representing a staggering 604% increase relative to the baseline year [169]. Cobalt showed a different pattern. From $14.21 per pound in 2020, the price fell slightly to about $12.20 per pound in 2024. However, in 2022 it reached a temporary high of $28.83 per pound, which severely disrupted supply chains and highlighted the risks of short-term scarcity [170]. Platinum Group Metals (PGMs), a family of six elements: platinum, palladium, rhodium, ruthenium, iridium and osmium, are central to catalytic applications, demonstrated some of the most dramatic swings. Palladium fell from $2,205 per ounce in 2020 to an estimated $980 per ounce in 2024, a decline of 56% after record highs [171]. Rhodium prices rose from $9,881 per ounce in 2020 to a peak of $20,254 per ounce in 2021 (an increase of 105%), but later declined to about $4,600 per ounce in 2024, which is still 53% below the 2020 level [171]. In contrast, iridium increased substantially, from $1,623 per ounce in 2020 to roughly $5,200 per ounce in 2024, reflecting a cumulative rise of around 220%. This escalation is strongly connected to iridium's status as a by-product of platinum and nickel mining, where supply cannot be expanded easily in response to demand [171].

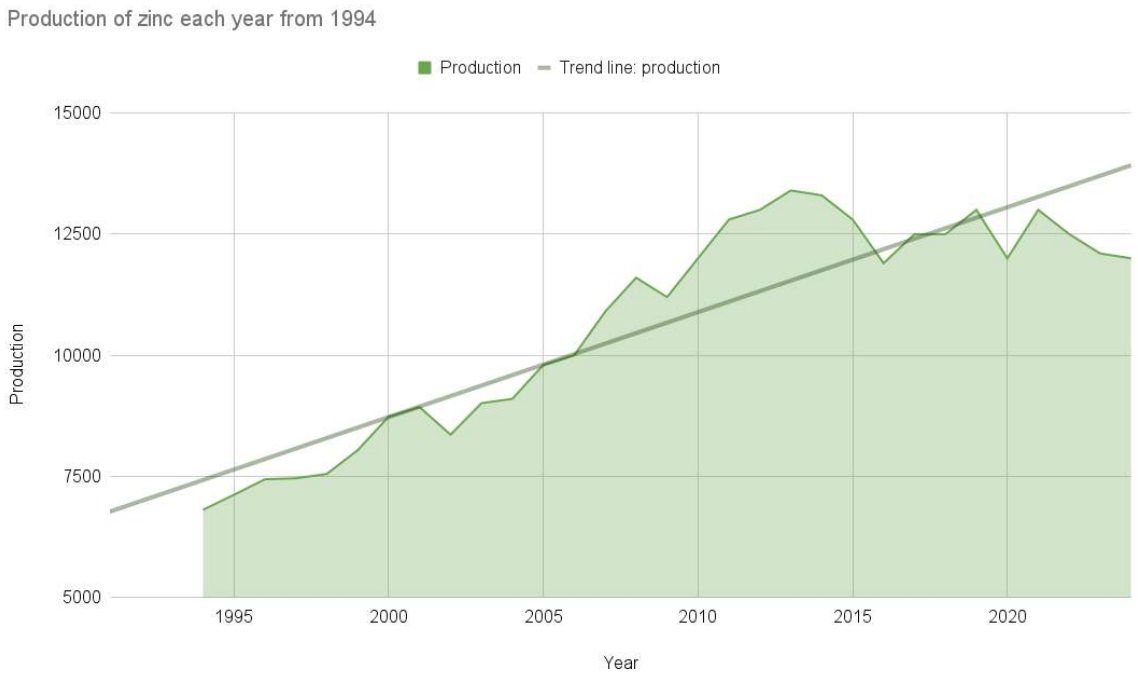


Figure 19. Mine production volumes of zinc yearly from 1994 to 2024 in thousand metric tons, gross weight [166, 169, 172–198].

Between 2020 and 2024, zinc prices displayed moderate fluctuations. According to USGS data, the annual average price for Special High Grade zinc was projected to decrease by about 24% in 2023 compared to 2022 [169]. In 2024, the price decline moderated, with the price projected to fall by approximately 5% compared to 2023 [198]. Price trends are presented on Figure 20 containing information from the Noth America and London markets, year by year from 1991, along with trends in yearly production volume from 1994 presented on Figure 19. Despite these declines, zinc was among the best-performing base metals in 2024, with its price rising roughly 13%, from about $2,621 per metric ton to $2,979 by year-end [199]. According to another source, zinc closed 2024 at around $2,990 per tonne, marking the third-highest year-end price of the past decade, after 2021 and 2017 [200]. It means that zinc experienced a downward drift in 2023 and early 2024, but ultimately rebounded over the year, ending 2024 significantly above 2020 levels.

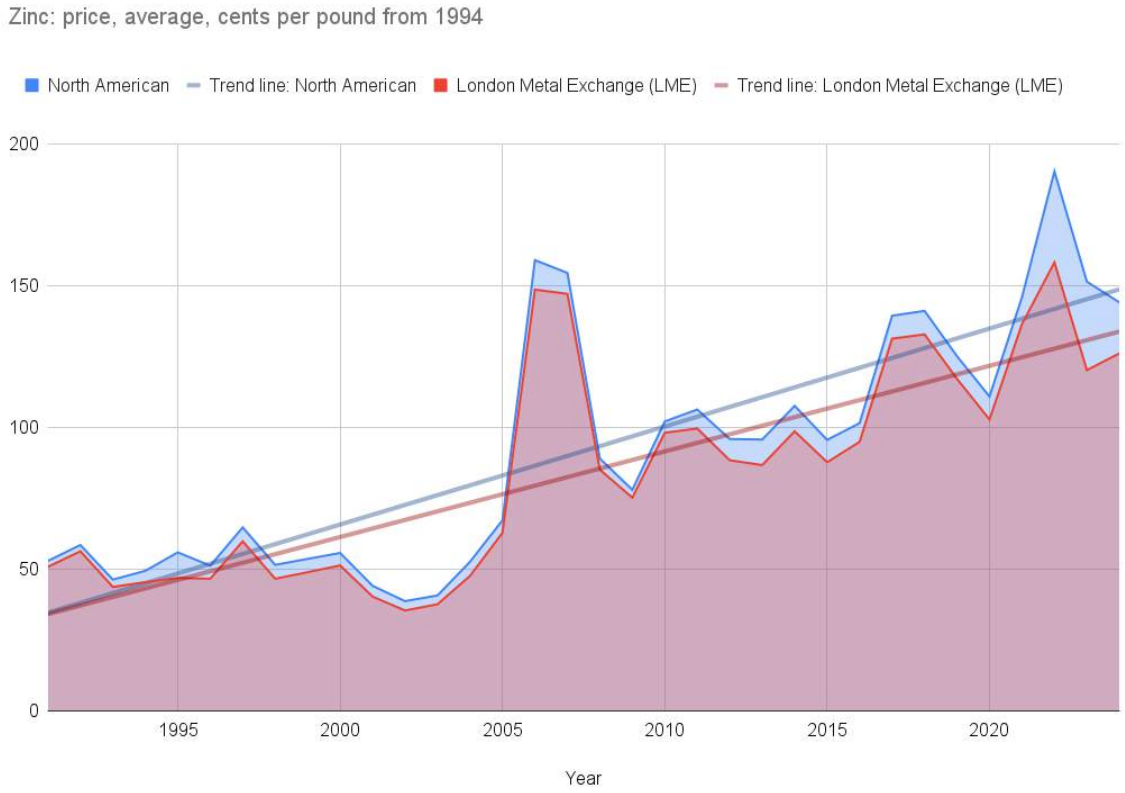


Figure 20. Average price of zinc in cents per pound yearly from 1991 to 2025 [166, 169, 172–198].

The finite nature of metal resources causes a decline in the quality of remaining ores of metals - as the quality of available deposits worsens, the costs and environmental footprint of metal extraction increase. An important issue in this context is the impact on the environment, social responsibility, and management practices, which complicate metal production. For example, stricter environmental regulations and opposition from local communities can limit access to resources, making it difficult to establish new mines or expand existing ones. These issues also significantly impact the economic feasibility of metal production and consequently the global supply chain's ability to meet demand in a sustainable way. The management topics highlighted emphasize the importance of recycling and efficient resource use, which can reduce depence of many industries on new metal extraction and mitigate some challenges resulting from declining resource availability [201].

Some researchers are addressing the problem of decreasing metal availability by exploring the history of technology and its evolution towards the utilization of lower grades deposits. It is one way to expand the availability of both critical raw materials and base metals. Technical problem for treatment of such kind ores is mentioned since

such ores require more energy for treatment, which in turn will increase the production cost [202].

The Platinum Group Metals possess a unique confluence of physical and chemical properties that make them extraordinarily effective catalysts [203–205]. They exhibit high chemical stability, allowing them to withstand the harsh temperatures and corrosive environments of many industrial reactors. Their resistance to oxidation ensures a long operational lifetime, a crucial factor for economic viability [203, 205].

The global metals sector is a major contributor to environmental stress, responsible for an estimated 10% of the world's total energy consumption and a staggering 40% of all industrial greenhouse gas emissions [206]. The Platinum Group Metals extraction is a particularly intensive subset of this industry. They are exceptionally rare, found in very low concentrations in the Earth's crust. To obtain them, vast quantities of ore must be mined, crushed, and processed to extract commercially viable amounts of metal [150]. This is an inherently energy-intensive undertaking. The mining and refining processes not only consume massive amounts of electricity and fuel but also generate enormous volumes of physical waste. For every ton of metal produced, the process can generate 15 to 20 tons of mineral gangue, dusts, and processing residues [206]. These waste tailings can contain harmful substances that pose a risk of contaminating local soil and water systems if not managed meticulously [207].

Platinum Group Metals - PMG are among the rarest elements in the Earth's crust. Their unique properties and indispensable role in key industrial and defense applications have led many governments, including the United States, to classify them as critical minerals. This designation signifies that they are essential to economic and national security and are simultaneously subject to high supply chain risk [205, 208]. The primary source of this risk is the extreme geographical concentration of PGM deposits. The vast majority of the world's economically viable reserves are located in a single geological formation: the Bushveld Igneous Complex in South Africa. Russia is the only other major primary producer, with smaller contributions from Zimbabwe, Canada, and the United States [209, 210]. The combination of tight supply, inelastic industrial demand, and a concentrated production base makes PGM prices notoriously volatile [211]. The concentration of mining operations in South Africa makes the global supply highly vulnerable to local and regional issues. Labor strikes, which have historically plagued the South African mining sector, can halt production for weeks or months, sending shockwaves through the market. Furthermore, challenges such as electricity shortages, mine accidents, and logistical bottlenecks can significantly curtail output with little warning [207, 210, 212]. Other problem is that the automotive industry is

the largest consumer of platinum, palladium and rhodium, and any shifts in this sector have an outsized impact on PGM prices [210, 211]. For example, the global semiconductor chip shortage that began in 2020 constrained automobile production, leading to a decrease in demand for catalytic converters and a subsequent drop in PGM prices [213]

The primary motivation for exploring catalysts based on first-row (3d) transition metals like iron, cobalt, nickel or manganese is rooted in the principles of sustainability and economic viability [150, 214–216]. These metals offer several compelling advantages over their precious PGM counterparts. First and major advantage is their natural abundance. Iron is the most abundant transition metal in the Earth's crust, making it orders of magnitude cheaper than platinum or palladium [**furstner_2016**, 215]. This cost reduction has profound implications, particularly for large-scale industrial processes and for making advanced chemical technologies accessible globally [215, 217]. Their applications are presented on the Figure 21.



Figure 21. Mn, Fe, Co, Ni application in organic catalysis [218].

Second advantage is their significantly lower toxicity profile. Regulatory bodies hold strict limits on residual precious metal content in consumer products, especially pharmaceuticals. For instance, the acceptable limit for residual iron in a drug substance can be as high as 1,300 ppm. In contrast, the limits for most precious metals, including palladium, are often set at or below 10 ppm [217]. This disparity provides a powerful incentive for the pharmaceutical industry to develop iron-based catalytic processes, as it can simplify purification steps and reduce regulatory burdens, contributing to a more sustainable and cost-effective catalyst economy [217]. The use of these more benign metals aligns directly with the green chemistry principle of designing less hazardous

chemical syntheses [216].

Beyond the core 3d transition metals, other earth-abundant elements, particularly zinc and magnesium, along with their respective oxides, are emerging as highly valuable components in the sustainable catalysis toolkit, as they offer unique properties, often complementing the reactivity of iron, cobalt, and nickel, and are especially prominent in heterogeneous and photocatalysis [219–221]. Zinc is an attractive catalytic metal due to its high crustal abundance, low cost, and low toxicity [219, 222, 223]. While zinc complexes are effective catalysts for various organic transformations, including the ring-opening polymerization of lactides and the chemical recycling of plastics [219, 224–226], its oxide, ZnO, is a particularly versatile and widely studied material. Zinc oxide is a stable n-type semiconductor with a wide band, making it an effective photocatalyst for the degradation of organic pollutants and for water disinfection [220, 227]. The photocatalytic mechanism relies on the generation of reactive oxygen species (ROS) under UV irradiation, although its activity can be extended into the visible light spectrum through doping [228, 229]. The efficiency of ZnO nanocatalysts is highly dependent on their morphology and size, which can be controlled through various synthesis methods, including green synthesis routes using botanical extracts [230, 231]. Beyond photocatalysis, ZnO is a crucial component in industrial catalysts for methanol production and is used in the synthesis of biodiesel [127, 232–234]. Magnesium is one of the most abundant metals on Earth, and its compounds are generally non-toxic and environmentally mild [222, 223]. While magnesium complexes have found applications in asymmetric synthesis and polymerization [235, 236], magnesium oxide MgO is a prominent solid base catalyst. Its high thermal stability and basic surface make it an effective heterogeneous catalyst for a range of reactions, including the transesterification of oils to produce biodiesel, where it can outperform conventional catalysts like KOH [237]. MgO is also used as a catalyst or support in the petrochemical industry for processes like methane reforming and catalytic cracking, and its basicity is harnessed for CO_2 capture technologies [221, 238, 239]. In materials science, MgO can be used as a co-activator with ZnO in rubber vulcanization, reducing the required amount of the more ecotoxic zinc oxide while improving material properties [240].

One way of aming more effective catalysis is introduction of nanocatalysis. In traditional heterogeneous catalysis only the atoms on the surface are accessible to reactants and can participate in the catalytic cycle, so the vast majority of atoms in the interior of the particle are catalytically inactive as the active material is often a bulk metal or a large particle supported on a carrier. Nanocatalysis overcomes this limitation by

utilizing metal nanoparticles, typically with diameters in the range of 1-100 nanometers, as the active phase [241]. The key advantage of this approach stems from the dramatic increase in the surface-area-to-volume ratio as particle size decreases [241]. Other way is Single-Atom Catalysis, which represents the logical and ultimate conclusion of catalyst downsizing. In this method, the active phase is not a nanoparticle but individual, isolated metal atoms that are atomically dispersed and anchored onto a carefully chosen support material, such as nitrogen-doped carbon or a metal oxide [242, 243]. This configuration achieves the theoretical maximum in metal utilization efficiency: effectively 100%, as every single precious metal atom is exposed and can function as an active catalytic site [242–244]. This has the potential to dramatically reduce the required loading of expensive metals like platinum, making processes more economical and sustainable [242, 245].

While maximizing efficiency reduces the demand for new metals, it does not eliminate it. The second critical strategy is to create a robust circular economy for catalytic metals, where end-of-life products are not discarded but are instead treated as valuable secondary resources to be recovered and reused. This approach is particularly vital for PGMs, as the concentration of these metals in spent products can be significantly higher than in their natural ores [203, 246, 247]. This concept, known as "urban mining," reframes industrial waste as a rich and strategically important domestic resource [246]. Spent automotive catalysts are the prime example, containing PGM concentrations that can be over 100 times greater than those found in mined ore [203, 246, 247].

Other example of metal recovery is the treatment of aqueous wastewater by electrodialysis containing metal compounds, and recovering metal resources from industrial and municipal wastewater [248]. It is scalable, easy to operate and is run continuously. As a relatively new technology under development, it is efficient for the concentration, separation and selective recovery of metals from acidic wastewater. The general challenges of electrodialysis involve possible scaling within the setup and waste treatment after the process.

The production of metal catalysts can also be challenging. Achieving uniform chemical composition is crucial, but variations in cooling rates and processing steps can create unwanted phase separations. Another topic is control of pore size and distribution in supports or porous structures, which affects the uniformity of active site distribution. Precursor materials, such as metallic glasses, often require activation - like hydrogen reduction or acid etching - to remove passive oxide layers and expose active surface. Industrial-scale production also faces challenges, such as heat transfer control, homo-

geneous heating, and cooling, leading to batch-to-batch inconsistencies [249].

1.2.3 Fundamentals of phytomanagement techniques

The basis for the production of ecocatalysts is plant biomass, which originates from plants utilizing specialized techniques of phytomanagement of the contaminated soils on which they grow, what is the solution for other global problem: an issue of soil and water contamination, driven by centuries of industrial activity, intensive agriculture, and improper waste disposal. It is a challenge to environmental sustainability and human health. Anthropogenic activities, including mining, smelting, manufacturing, and the use of fossil fuels, have led to environmental pollution such as heavy metals, metalloids and organic compounds [250]. These contaminants degrade soil functionality, threaten the integrity of aquatic ecosystems, and pose significant risks of entering the food chain, ultimately impacting human welfare [250, 251]. In response, numerous countries have enacted legislation and established research programs aimed at the remediation and restoration of these vast contaminated areas[250].

Traditionally, the approach to contaminated site cleanup has been dominated by conventional, engineering-based methods. Techniques such as excavation and off-site disposal, soil washing, encapsulation, and vitrification have been the standard of practice [252, 253]. While often effective in reducing contaminant concentrations in the short term, these methods are also typically energy-intensive, often expensive - especially for large or moderately contaminated sites - and destructive to the environment [251–253]. Critically, many of these techniques destroy the soil's natural structure, fertility, and biological activity, leaving behind a sterile medium that is incapable of supporting a functional ecosystem [252, 254]. This approach treats the soil as a disposable matrix rather than a vital, living resource, often simply transferring the pollution problem to a landfill and creating secondary environmental impacts [254]. The inherent unsustainability and high cost of these conventional methods have catalyzed a search for greener, more holistic alternatives, leading to the development of a suite of plant-based technologies.

The concept of phytomanagement techniques emerged in the late 20th century as a promising, nature-based solution to environmental contamination [253]. Defined as the use of green plants and their associated soil microorganisms to eliminate, contain, neutralize, or break down harmful environmental contaminants from the environment or render them harmless, phytoremediation offered a gentler, more ecologically sound alternative to disruptive engineering practices [255]. The most profound conceptual in-

novation of phytomanagement is its reframing of contaminated land. Where traditional remediation sees a problem, which needs to be liminated at great expense, phytomanagement approach gives a resource and an economic opportunity. Instead of focusing solely on the costly removal of total contaminant mass, the phytomanagement approach prioritizes the active management of risk. This is achieved by controlling the bioavailable fraction of contaminants and preventing their migration into water bodies or the food chain, thereby breaking the pathways of exposure[250, 253].

Phytotechnologies are regarded as an environmentally friendly, visually appealing, and cost-effective alternative to more invasive and destructive civil engineering methods. These plant-based approaches not only help restore polluted sites but do so in a way that preserves the natural landscape and reduces the overall environmental impact [256]. One of adventages of phytoremediation is also their ability to be applied directly on-site and on a large scale. However, the time needed to clean up contaminated sites is a significant challenge. For these methods to be viable, the cleanup time should ideally not exceed 10 years. This duration can be reduced if the focus is on reducing the bioavailable pool of contaminants rather than the total concentration of the contaminant in the soil [257]. Climatic conditions, such as temperature and soil moisture, play a critical role in the success of phytoremediation. They influence plant growth, contaminant uptake and overall ecosystem interactions. For example, prolonged drought can stress plants, making them more susceptible to diseases and reducing their effectiveness in remediation efforts. This is specifically problematic in arid and semi-arid regions with low water retention soils [258]. Plants ideal for this purpose should have several key traits, such as the ability to grow beyond their native range, rapid growth, high biomass production, ease of harvesting, and the capacity to accumulate a variety of heavy metals in their harvestable tissues [259].

Heavy metals are resistant to degradation by biological or physical processes and can persist in the soil for extended periods, causing long-term environmental risks. Based on their roles in biological systems, heavy metals can be categorized as essential or non-essential. Essential heavy metals such as copper, iron, manganese, nickel and zinc are necessary for various physiological and biochemical processes in plants. However, excessive amounts of those metals can be toxic. Non-essential heavy metals, including lead, cadmium, arsenic and mercury are highly toxic and have no known beneficial role in plants. These metals can cause significant environmental pollution, disrupt numerous physiological and biochemical processes in crops, and reduce agricultural productivity. Additionally, they can enter the food chain through crops, accumulate in the human body via biomagnification, and pose serious health risks to

humans [260].

Phytomanagement operates through a suite of plant-driven processes that collectively form its technical toolkit, including [261]:

- the extraction of contaminants into harvestable biomass - phytoextraction,
- their immobilization within the soil - phytostabilization,
- their degradation into less harmful substances - phytodegradation,
- and their filtration from water - rhizofiltration.

Each mechanism leverages distinct biological, chemical, and physical properties of the "soil-plant-microbial" system to manage contaminants in different ways[250]. Understanding these foundational processes is essential for designing effective, site-specific phytomanagement strategies that can range from the complete removal of pollutants to their long-term, safe immobilization. These techniques are not mutually exclusive and can often occur simultaneously, contributing to the overall remediation and management of a contaminated site [262].

Phytoextraction is a method that is used to recultivate contaminated soils by growing plants that are tolerant to toxic elements. These plants absorb the contaminants from the soil and store them in their upper parts, such as leaves and stems, which can be harvested. Typically, phytoextraction is effective in removing one or two types of contaminants at a time, rather than a wide range [257]. The primary objective of phytoextraction is the permanent removal of the contaminant mass from the soil ecosystem[263, 264]. Upon harvest, the metal-enriched biomass is removed from the site, thereby incrementally reducing the total pollutant load in the soil over successive growing seasons[265]. The underlying biological mechanisms are complex and involve a coordinated series of physiological events. First, the contaminant must be mobilized from the soil matrix into a bioavailable form that can be taken up by the roots. Once in the root, specialized membrane transporter proteins facilitate its movement across the cell walls and into the vascular system [255, 266]. The contaminant is then loaded into the xylem, the plant's water-conducting tissue, for long-distance transport to the shoots. To prevent cellular damage during this process, the plant employs chelating agents - molecules that bind to the metal ions to safely shuttle them through its tissues. Finally, upon reaching the leaves, the contaminants are typically compartmentalized and sequestered within the cell's vacuole, a large storage organelle, which isolates them from metabolically active parts of the cell and prevents phytotoxicity [255, 266].

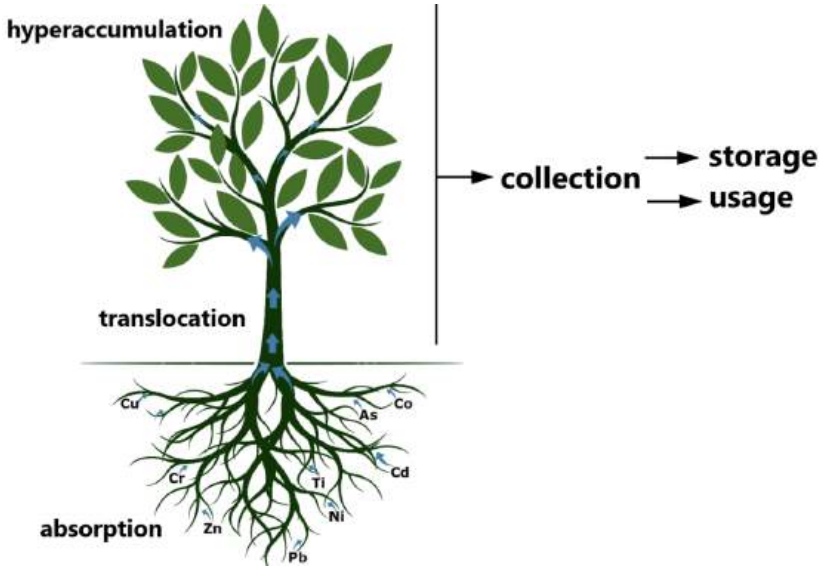


Figure 22. Schematic representation of soil purification by metal hyperaccumulating plants - phytoextraction

Phytoextraction is most applicable to sites with low to moderate levels of contamination, as very high concentrations can be toxic even to tolerant plants[267]. Its success is highly dependent on the selection of appropriate plant species, particularly hyperaccumulators, which have a natural, genetically encoded ability to accumulate extremely high concentrations of specific metals[263].

Phytomining is the related process to phytoextraction focused on recovering valuable metals from contaminated biomass and can make phytoextraction more economically feasible. This process not only addresses the disposal of contaminated biomass but also generates revenue from the recovered metals, making it a profitable venture [268].

Phytostabilization does not aim to remove contaminants from the soil. Instead, its goal is to reduce their mobility and bioavailability, thereby containing them in-situ and minimizing the risk of their migration into groundwater, surface water, or the food chain[254]. Plants are used to create a vegetative cover, which helps prevent erosion, reduce dust, and limit water infiltration. This minimizes the movement of metals into groundwater and the surrounding environment [269]. Phytostabilization is achieved through a combination of physical and biogeochemical processes. Physically, the dense root systems of the selected plants bind soil particles together, significantly reducing wind and water erosion, which are major vectors for the dispersal of contaminated dust and sediment[253, 261]. The plant canopy also overtake rainfall, reducing the amount of water that percolates through the contaminated soil profile and minimizing the leaching of soluble contaminants into underlying aquifers[253].

The process works by adding soil amendments like phosphates, biosolids, zeolites, or ash. These additions bind with metals and make them less available for plant uptake or movement. Plants also play an active role - they stabilize the soil and affect the chemical conditions around their roots. Some plants can trap metals in their root system or change soil pH and redox potential, reducing metal mobility [270].

In trials focused on stabilising polluted soils using plants, a wide range of soil enhancers have been applied. These include materials that raise pH, such as lime, as well as phosphorus-rich substances like apatite, oxides and hydroxides of iron, aluminium and manganese, organic waste, and certain industrial by-products [271–273]. Such treatments work by locking harmful metals and metalloids into forms that are not easily dissolved in water and as a result, these toxic elements are less likely to move downward through the soil layers or be taken up by living organisms. In the studies conducted by Vangronsveld in 1999 in Belgium, soil contaminated with cadmium, lead and zinc in an industrial zinc smelter area was the target of phytostabilization. In this process grass species such as *Festuca rubra*, *Agrostis capillaris*, and *Lolium perenne* combined with additions like compost was utilized [269]. Another studies were conducted in Jales, Portugal. It was focused on arsenic and other metal contamination in mine spoil heaps. The remediation involved tolerant grass species such as *Agrostis castellana* and *Holcus lanatus*, combined with beringite and steel shots. The result of those studies is positive, metal migration into surrounding water systems was reduced [274]. The use of organic inputs, such as compost, animal manure, or treated sewage, also helps improve how the soil behaves. These materials boost water absorption, increase how long the soil holds moisture, and generally make it easier for plants to grow [257, 275]. On top of that, they supply key nutrients and offer an eco-friendly way to reuse organic waste. Another example comes from research by Zanuzzi et al. (2009), where acidic mining waste was treated with pig manure or sewage sludge and topped with marble dust [276]. Within two years, the soil became almost neutral in pH and had much more stable organic matter. Five years later, treated areas showed greater microbial activity, better functioning of soil enzymes, and a richer and more widespread plant cover than untreated sites [277].

In the root zone, the rhizosphere, contaminants can become trapped or immobilized through various processes, including adsorption, where contaminants stick to surfaces, precipitation, where they form solid particles, and accumulation. This is often due to microorganisms that live in symbiosis with plant roots, making contaminants less likely to move or cause harm ([278]). Biogeochemically, plants actively alter the chemistry of the soil zone immediately surrounding the roots. They release root exudates and phy-

tochemicals that can cause contaminants to precipitate out of the soil solution, adsorb onto root surfaces, or form stable, insoluble complexes [261, 279]. Contaminants may also be absorbed into the root tissues and sequestered there, effectively locking them within the below-ground biomass[261]. By converting the contaminants into less mobile and less bioavailable chemical forms, phytostabilization effectively renders them harmless in place[264]. This approach is particularly well-suited for large areas of contamination where complete removal is economically or technically infeasible. However, because the contaminants remain in the soil, phytostabilized sites require long-term monitoring to ensure the continued stability of the immobilized pollutants[254].

Phytodegradation, also known as phytotransformation, is a mechanism that targets organic pollutants, such as pesticides, herbicides, chlorinated solvents and explosives [279]. This process involves the breakdown of complex toxic organic molecules into simpler, less toxic or non-toxic compounds through the plant's own metabolic machinery [264, 279]. Scheme of this process is presented on Figure 23. It begins with the plant taking up the organic contaminant from the soil or water. Once inside the plant tissues, the contaminant is subjected to a series of enzymatic reactions, similar to how the plant metabolizes nutrients and other natural compounds [279]. Specialized plant enzymes, such as dehalogenases, nitroreductases, and laccases, can cleave chemical bonds and transform the structure of the pollutant [279]. The degradation can occur within different parts of the plant, including the roots, stems, and leaves. In some cases, the resulting simpler metabolites are fully mineralized to carbon dioxide and water. In other instances, the metabolites may be incorporated into the plant's own biomass -a process known as phytometabolization- becoming part of the plant's lignin, cellulose, or other structural components [279]. This mechanism effectively detoxifies the contaminant without the need for its physical removal from the site, making it a true in-situ degradation technology for specific classes of organic pollutants[280].

Rhizodegradation is a closely related but distinct mechanism that also focuses on the breakdown of organic pollutants. However, unlike phytodegradation, the primary degradation activity in rhizodegradation does not occur inside the plant itself, but rather in the soil of the rhizosphere[281, 282]. This process leverages the synergistic relationship between the plant and a vast community of soil microorganisms, including bacteria and fungi, that thrive in the root zone[279]. Scheme of this process is presented on Figure 23.

Phytovolatilization is a process where plant roots absorb contaminants from the soil, convert them into a gas, and then release them into the atmosphere. This process is largely driven by the plant's evapotranspiration, which is the combination of water

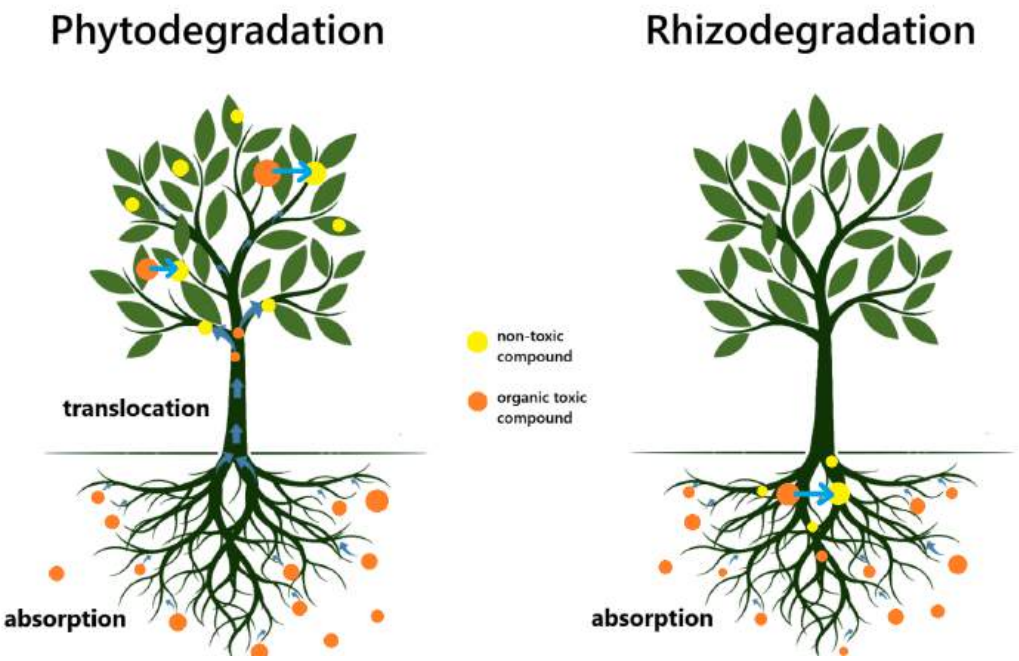


Figure 23. Schematic representation of phytodegradation and rhizodegradation in from soil

evaporation and plant transpiration. Plants with high rates of evapotranspiration are particularly useful for phytovolatilization. This is direct phytovolatilization. Indirect phytovolatilization refers to the increased release of volatile contaminants from beneath the ground due to the activities of plant roots or to the capture of rainfall [283].

Rhizofiltration is primarily an aqueous-phase treatment technology used to remove contaminants from polluted water sources, such as groundwater, surface water, or industrial wastewater [263, 279]. This technique utilizes the extensive surface area of plant root systems to adsorb contaminants from the water[264]. Plants, often grown hydroponically or in constructed wetlands, are placed in contact with the contaminated water. Their roots act as a living filter, with contaminants binding to the root surfaces or being taken up into the root biomass [279]. Terrestrial plants with fibrous, extensive root systems are particularly effective [254]. This method is highly efficient for treating large volumes of water with low contaminant concentrations [263].

The choice of plant species is an important decision in a phytomanagement project. The ideal plant must possess a suite of traits that are often in opposition, requiring a careful balancing act based on the specific goals of the remediation effort. The selection process generally considers two main categories of plants: hyperaccumulators and high-biomass cash crops. Hyperaccumulator plants are a remarkable group of species that have naturally evolved the ability to absorb and concentrate specific elements to exceptionally high levels in their above-ground tissues, often without showing signs of toxicity [284]. The thresholds for classification are element-specific, for ex-

ample, a plant must accumulate over 100 mg/kg of cadmium, 1,000 mg/kg of nickel or 10,000 mg/kg of zinc in its dry shoot biomass to be considered a hyperaccumulator [284]. These plants, such as *Thlaspi caerulescens* for zinc and cadmium or *Pteris vittata* for arsenic, are the champions of phytoextraction [285, 286]. Their unique physiology, which includes highly efficient root uptake transporters, rapid xylem loading, and effective vacuolar sequestration mechanisms, makes them ideal candidates for projects aiming to completely remove metals from the soil, particularly for phytomining applications [266, 286]. However, their primary drawback is that they are often small, slow-growing wild species with low biomass production [251, 284].

High-biomass cash crops, on the other hand, are species selected primarily for their rapid growth and high productivity. This category includes trees like poplar (*Populus spp.*) and willow (*Salix spp.*), often grown in short-rotation coppice systems, and perennial grasses like miscanthus (*Miscanthus x giganteus*) and switchgrass (*Panicum virgatum*) [250]. While these plants typically accumulate much lower concentrations of contaminants in their tissues compared to hyperaccumulators, their enormous biomass yield can compensate for this [265]. The total mass of contaminant removed in a single harvest can be comparable to, or even greater than, that removed by a low-biomass hyperaccumulator. These species form the economic backbone of phytomanagement, as their harvested biomass provides the feedstock for bioenergy, biofuels, fibers, and other marketable products [250].

The most frequently cited advantage of phytomanagement is its significant cost-effectiveness, particularly for large, diffusely contaminated sites [254]. Conventional remediation methods are notoriously expensive. The costs for techniques like excavation and landfilling, soil washing, or vitrification can range from $100 to over $500 per ton of treated soil [287]. These high costs, driven by heavy machinery, high energy consumption, and specialized labor, often render the cleanup of extensive areas of low-to-moderate contamination economically unfeasible [251]. In contrast, the direct costs associated with phytoremediation are substantially lower, with estimates typically falling in the range of $5 to $40 per ton of soil [287]. The primary expenditures are related to standard agricultural practices: site preparation, purchase of seeds or cuttings, planting, irrigation, and periodic monitoring and harvesting [267]. For large-scale projects, these costs are orders of magnitude lower than the equivalent engineering solutions. Furthermore, the economic model of phytomanagement introduces a crucial element that is entirely absent from conventional methods: the potential for revenue generation. By cultivating cash crops, the harvested biomass can be sold into various markets - for bioenergy production, fiber, or other industrial products-creating an income stream

that can offset the operational costs and, in some cases, even generate a net profit [250, 251]. This transforms the contaminated land from a pure financial liability into a low-yield productive asset during the remediation period. For example, one cost estimate for phytoextraction placed total remediation costs at $60,000 to $100,000 per acre, while the use of sunflowers to remove radionuclides from water was estimated at $2 to $6 per thousand gallons treated, including capital and waste disposal costs[267]. When these factors are combined, phytomanagement presents a compelling economic case for sites where immediate cleanup is not a regulatory necessity.

1.2.4 Overview of ecocatalysis

An ecocatalyst is a catalyst derived from natural, renewable, or biosourced materials. Unlike conventional catalysts, which often rely on rare or hazardous materials, ecocatalysts utilize resources such as biomass, phytoremediated metal concentrates, and other plant-based materials to create catalytic systems with unique structural and functional properties [288, 289]. Ecocatalysts are catalysts characterized by lower toxicity, biodegradability, and the possibility of regeneration and reuse. Ecocatalysts can be divided into several categories based on their composition and mode of action. The main types of ecocatalysts include:

- Plant-based catalysts - natural organic compounds derived from plants that are capable of activating chemical reactions [258].
- Microorganism-based catalysts - microorganisms such as bacteria, fungi, or yeasts that use their natural metabolic pathways to catalyze chemical reactions [257].
- Catalysts based on natural materials - catalysts that utilize agricultural waste, biomass, or other natural raw materials as substrates for catalyst synthesis [257, 290].

Ecocatalysis is based on the recycling of mineral resources, specifically through the use of phytoremediation and the subsequent application of biomass contaminated with trace elements in catalysis. The core of this process lies in the remarkable ability of certain plants to thrive in challenging soil conditions by hyperaccumulating metal cations such as zinc, nickel, copper, manganese, cobalt, and palladium. The biomass derived from these plants is then directly used as catalysts in organic synthesis, representing an innovative approach to creating sustainable chemical processes [291].

The biomass - leaves, roots or powders - was subjected to a thermal treatment under air, in order to remove organic matter while retaining the metal oxides or salts. According to the plant species and the treatment, three types of ecocatalysts could be prepared [292]:

- Lewis and/or Brønsted acid ecocatalysts called Eco-MCl,
- reducing ecocatalysts called Eco-M(0),
- oxidative ecocatalysts called Eco-Mox.

Eco-MCl are prepared by adding the hydrogen chloride to thermal residues [293]. Eco-M(0) are obtained from the thermal residues by treating them with formic acid to produce formate salts, which were then subjected to controlled thermal decomposition, resulting in metals in a zero oxidation state [294]. Eco-Mox are made from thermal residues and utilized as catalysts directly without any chemical activation [289].

The production of ecocatalysts relies on hyperaccumulating plants, which have the ability to absorb and concentrate heavy metals from the soil in their tissues. These plants are used for soil remediation and then processed to create catalysts. The example of plant species used in ecocatalysis is *Grevillea* species - this genus includes *Grevillea exul*, *Grevillea meisneri*, *Grevillea rubiginosa*, and *Grevillea gillivrayi*, which can accumulate high levels of manganese [288]. Hyperaccumulating Mustard Plant (HMP) is used for the production of carbon-based catalysts like Cu/HMPC, which are effective in the synthesis of imines [295]. Another example of this kind of plants are *Arabidopsis halleri* and *Salix "Tordis"* (*Salix schwerinii* × *Salix viminalis*), which are known for their ability to accumulate zinc and are often used in contaminated soils [296].

Hyperaccumulating plants are cultivated in contaminated sites as part of phytoremediation strategies, where they accumulate metals from the environment, providing a renewable source of metals for green chemistry applications [258]. The process of transforming plants into ecocatalysts involves multiple steps, each aimed at extracting valuable metals and converting them into functional catalytic materials. The production process is based on phytoextraction, which means that plants are grown in contaminated soil to extract heavy metals from the environment [258]. The aerial parts of the plants, which contain the accumulated metals, are harvested and the biomass is dried, ground, and subjected to thermal treatment to modify its structure and convert it into an activated material [290]. Biomass can also beated with chemical agents, such as acids, to extract metals and create a porous catalyst structure [295]. Extracted metals are converted into polymetallic salts or mixed metal oxides, which serve as active

components in the catalysts. This process transforms what would otherwise be waste material into a valuable resource for the production of green catalysts. The resulting catalysts are versatile, efficient, and reusable, supporting sustainable chemistry [297].

Table 4. Ecocatalysts - hyperaccumulators and good accumulators [292].

Species	Phytotechnology	Catalyst structure
Eco-MCl: Lewis acids / coupling agents - HCl activation		
Noccaea caerulescens	Phytoextraction of Zn	K_2ZnCl_4
Anthyllis vulneraria		$CaMg_2Cl_6$
Arabidopsis halleri	Phytoextraction of Zn	K_2ZnCl_4
Geissospi spuinosa	Phytoextraction of Ni	$KNiCl_3$
Anisopappus chinensis	Phytoextraction of Cu	$CaMg_2Cl_6$
Grevillea exull	Phytoextraction of Mn	$KMnCl_3$
Grevillea exul rubiginosa		$K_3NaMnCl_6$
Grevillea mesneiri		$CaMg_2Cl_6$
Eichhomia crassipes	Rhizofiltration of Pd	K_2PdCl_4
Eichhomia crassipes	Biosorption of Pd	K_2PdCl_6
Eco-M(0): Reducing agents - HCOOH activation		
Psychotria gabrieliae	Phytoextraction of Ni	Ni; $FeNi_3$
Eco-MOx: Oxidizing agents - no activation		
Grevillea exull	Phytoextraction of Mn	$Ca_2Mn_3O_8$
Grevillea exul rubiginosa		$CaMnO_3$

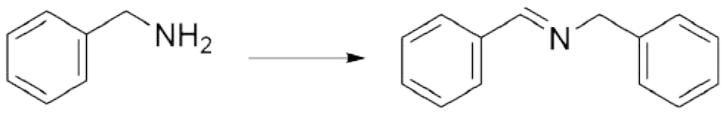
Recent studies emphasize that the metal content and distribution within the plant biomass play a crucial role in determining the properties of the resulting ecocatalysts. Some hyperaccumulators are capable of accumulating technology-critical metals such as cobalt, nickel, and even rare earth elements. This significantly expands the scope of ecocatalysis by enabling the development of catalysts that exhibit distinct redox and electronic properties. The incorporation of TCMs into ecocatalysts may lead to new catalytic functions, such as enhanced selectivity, multistep activation, or improved resistance to deactivation. For example, cobalt and nickel-enriched biomass may be particularly suitable for catalytic hydrogenation or $C-C$ coupling reactions. This opens a new avenue in catalyst design, where specific hyperaccumulator species could be selected and cultivated for their potential to yield highly functional, metal-specific eco-

catalysts [298].

1.2.4.1 Copper-based ecocatalysts

The ecocatalysts derived from plant biomass are often characterized by their polymetallic composition, which enables a broad range of chemical reactivity. Gopiraman and co-workers proposed approach to the preparation of carbon-based ecocatalysts using a copper-hyperaccumulating plant, *Brassica juncea*. The plants were grown under laboratory conditions. One part of the cultivation was carried out in the presence of Cu^{2+} ions introduced as $CuCl_2$, while the rest was grown without added copper as a control. After about 30 days of growth, the biomass was harvested, dried at 60 ℃, and then subjected to preliminary carbonization in air at 300 ℃, followed by grinding to a powder. The resulting material was chemically activated with $NaOH$ in the proportion C to $NaOH$ 1 : 2. Then it was calcined under a nitrogen atmosphere at 600 ℃. In the final step, the material was washed with an HCl solution to remove excess salts [295].

The ecocatalyst obtained from plants grown in the presence of copper was named Cu/HMPC, while the control material was labeled HMPC. Structural studies showed that Cu/HMPC is characterized by the simultaneous presence of three types of morphology: two-dimensional thin carbon sheets, three-dimensional hollow spheres, and one-dimensional needle-like structures. These structures are interconnected, providing a large number of accessible active sites, and they are not observed in the copper-free HMPC material. The copper content in Cu/HMPC is about 1.0 wt% and was confirmed by ICP-MS and EDS analyses. Copper is present mainly as CuO/Cu^{2+} and shows very good dispersion within the carbon matrix, with no visible agglomerates [295].

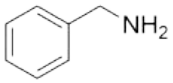
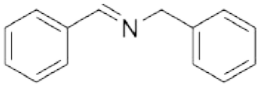
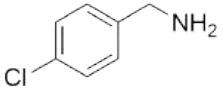
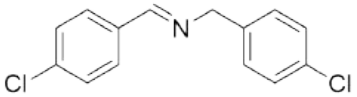
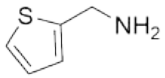
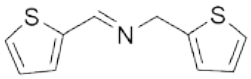
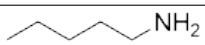
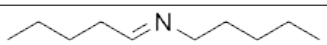
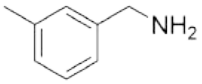
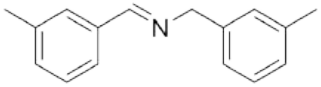


Scheme 23. Scheme of example amine oxidation to imine: oxidation of benzylamine to the corresponding imine with Cu/HMPC as catalyst [295].

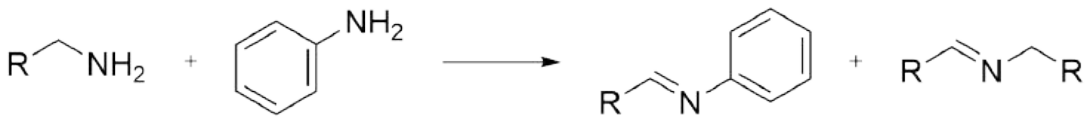
As a model reaction for evaluating catalytic activity, the oxidation of benzylamine to the corresponding imine was selected. Scheme of the reaction is presented on Scheme 23 and examples of results in the Table 5. This reaction is often used in the literature as a standard test for Cu-based catalysts, enabling a direct comparison of the results with other catalytic systems. As part of the optimization of the reaction conditions, the influence of temperature, catalyst loading, reaction time, and atmosphere was investigated. The best results were obtained using 10 mg of the Cu/HMPC catalyst

at 80 ℃ after 4.5 h of reaction, under air and without the addition of a solvent. Under these conditions, a 98% yield with 100% selectivity was achieved. Control experiments demonstrated that in the absence of a catalyst the reaction does not proceed, pure $CuCl_2$ is practically inactive, and the HMPC material without copper exhibits only low activity. Replacing air with a nitrogen atmosphere led to a significant decrease in yield, confirming the crucial role of molecular oxygen.

Table 5. Examples of aerobic oxidation (Scheme 23) results with Cu/HMPC as catalyst [295].

Substrate	Product	Yield	Conditions
		98%	air, $80°$C, 4,5h
		78%	air, $80°$C, 13,5h
		97%	air, $80°$C, 6h
		93%	air, $80°$C, 6h
		92%	air, $80°$C, 6h

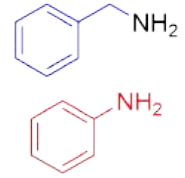
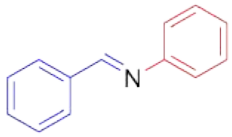
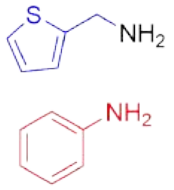
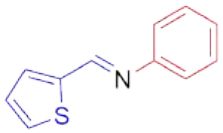
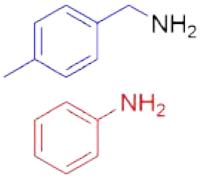
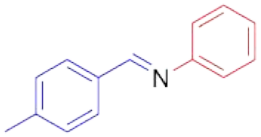
The reaction scope was evaluated by testing various amines. For benzylic amines containing substituents such as $-CH_3$, $-OCH_3$, $-F$, or $-Cl$, high yields in the range of 78–98% were obtained. Good results were also achieved for heterocyclic amines, such as thiophene and pyridine derivatives, where yields reached up to 97%. The ecocatalyst Cu/HMPC was also active toward aliphatic substrates, such as pentylamine and hexylamine, which are challenging. For them moderate results were obtained, while most catalysts reported in the literature show low efficiency in these cases [295].



Scheme 24. General scheme of aerobic oxidative cross coupling of amines with aniline with Cu/HMPC as catalyst [295].

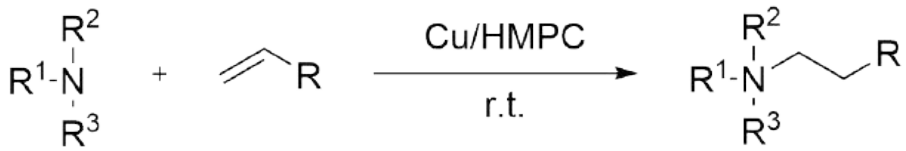
To further expand the applicability of the developed eco-catalyst, the authors investigated its activity in oxidative cross-coupling reactions of amines (Scheme 24 and some example results in the Table 6.). A benzylamine–aniline system was employed, which is particularly challenging due to competing homocoupling reactions. Nevertheless, in the presence of the Cu/HMPC catalyst, high selectivity toward the cross-coupled product was achieved. Under optimized conditions, selective coupling of benzylamine with

Table 6. Examples of aerobic oxidative cross coupling (Scheme 24) results with Cu/HMPC as catalyst [295].

Substrates	Product	Yield	Conditions
		98% (selectivity 98%)	air, $80°$C, 4.5h
		98% (selectivity 98%)	air, $80°$C, 4.5h
		87% (selectivity 87%)	air, $80°$C, 4.5h

aniline to the corresponding imines proceeded with very high yields (up to 98%), while the contribution of the product originating from benzylamine homocoupling remained minimal. Similarly favorable results were obtained for substituted benzylamines and heterocyclic amines, confirming the high level of reaction selectivity control exerted by the Cu/HMPC catalyst [295].

In addition to oxidative transformations, the authors demonstrated that Cu/HMPC is also an efficient catalyst for aza-Michael reactions conducted under exceptionally mild conditions (Scheme 25). The addition of amines to α, β-unsaturated compounds was performed at room temperature, under an air atmosphere, and with very short reaction times on the order of several minutes. Under these conditions, high yields and excellent selectivity of the aza-adducts were obtained for both aliphatic and heterocyclic amines. These results indicate that Cu/HMPC is not a catalyst specialized exclusively in the oxidation of amines to imines, but rather a material with significantly broader synthetic potential, capable of efficiently catalyzing various types of $C - N$ bond-forming reactions under conditions consistent with the principles of green chemistry [295].



Scheme 25. General scheme of aerobic oxidation of amines to imines with Cu/HMPC as catalyst [295].

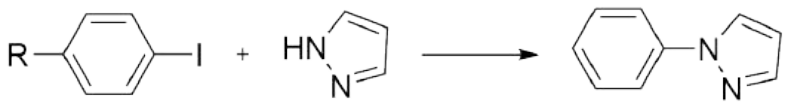
The eco-catalyst Cu/HMPC obtained by Gopiraman and his research group is characterized by good stability and can be reused multiple times without a significant loss of catalytic activity. After completion of the reaction cycles, copper can be easily recovered from the material using an HCl solution, without the need for aggressive reagents and without generating large amounts of waste. The reaction mechanism proposed by the researchers assumes activation of the amine by Cu^{2+} centers in the presence of molecular oxygen from air, leading to the formation of an imine intermediate. The defect-rich carbon matrix stabilizes the individual transformation steps, while oxygen acts as the terminal oxidant. As a result, it was demonstrated that it is possible to obtain a highly efficient catalyst from copper-contaminated plant biomass that is inexpensive, environmentally friendly, efficient, and active under mild reaction conditions [295].

Other set of Cu-based ecocatalysts were prepared by Guillaume Clavé with his research group. They prepared ecocatalysts by phytoextraction and rhizofiltration. First, phytoextraction conducted on soils heavily contaminated with copper from the Mine de l'Etoile area near Lubumbashi in Katanga, where the Cu content reaches 10,000–30,000 mg/kg. Anisopappus chinensis was selected as the model plant and 20 individuals were collected. The copper content in the aboveground parts was determined, yielding an average of approximately 230 μg/g of dry mass, with a relatively large variability among samples. On this basis, the realistic metal removal efficiency was estimated at about 286 g Cu/ha/year, and it was emphasized that this value could be increased through the selection of appropriate populations, genotypes, and multispecies cropping systems. Second method of ecocatalysts deriving is rhizofiltration performed under controlled conditions. For 7 days, *Bacopa monnieri*, *Lolium multiflorum*, and *Eichhornia crassipes* were exposed to a solution of $Cu(NO_3)_2 \cdot 3H_2O$ at a concentration of 40 mg/L (approximately 10.5 mg/L Cu). ICP-MS analyses showed that the highest accumulation of copper in the roots occurred in *E. crassipes*, which additionally produces a very large root biomass. Low TF values indicated that Cu remained mainly in the roots, which is advantageous from the perspective of further utilization [299].

The harvested biomass was subsequently transformed into Eco-Cu® catalysts, which were divided into materials obtained from the leaves of *A. chinensis* ($Eco-Cu1\breve{}2$®) and from the roots of plants used in rhizofiltration ($Eco-Cu3\breve{}8$®). Two preparation variants were applied: simple thermal calcination of the biomass to mineral ashes (odd-numbered catalysts Eco-Cu1/3/5/7) or calcination with additional activation of the ashes with concentrated HCl at about 80℃ for 4 h, leading to the formation of powder containing metal chlorides, including copper, designated by even numbers:

Eco-Cu2/4/6/8. The characterization of the Eco-Cu® materials clearly demonstrates that they are not simple analogues of commercial $CuCl_2$, but rather complex mineral mixtures with a specific surface chemistry resulting from both their biological origin and the preparation method. ICP-MS analyses revealed pronounced differences in elemental composition: materials obtained from rhizofiltration are significantly richer in copper than those derived from phytoextraction. A representative example is Eco-Cu8® obtained from *Eichhornia crassipes*, which contains about 10.37% Cu by weight, compared to approximately 0.26% Cu in Eco-Cu2® derived from *Anisopappus chinensis*. XPS studies of Eco-Cu8® indicate that copper is present predominantly in the $+II$ oxidation state, while signals attributed to $Cu(I)$ are ascribed by the authors to partial reduction of $Cu(II)$ occurring during the analysis itself. At the same time, a strong presence of chlorine confirms the formation of chloride species following HCl activation. Negative-mode ESI mass spectrometry reveals the presence of anionic copper chloride complexes such as $CuCl_3^{2-}$ and $CuCl_2^-$, suggesting that the material contains mixtures of species of the $CuCl_4^{2-}/CuCl_3^-$ type, but the authors note that this technique may promote reduction of $Cu(II)$ to $Cu(I)$. X-ray diffraction shows the presence of several crystalline phases, including $NaCl$, hydrated $CaSO_4$, MnO, and $K_6Fe_2O_5$, whereas copper-containing phases are amorphous in nature, indicating a high degree of dispersion within the matrix. TEM observations further confirm the presence of copper nanoparticles with sizes on the order of 4–8 nm, which are homogeneously distributed and do not undergo significant aggregation [299].

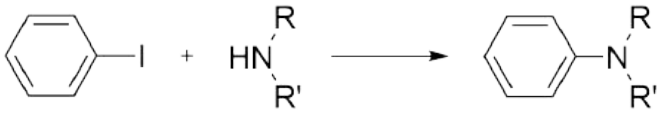
Acidity studies using pyridine-adsorbed FTIR spectroscopy show that although the Lewis acidity strength of Eco-Cu8® is comparable to that of $CuCl_2$, the material also exhibits a pronounced Brønsted acidity component, which is absent in the case of pure copper salts. This is reflected in the acetalization test performed according to the Corma method, where Eco-Cu8® displays a different selectivity than commercial copper chlorides. The authors attribute this behavior to a harder Lewis acidity and to the contribution of Brønsted acid sites arising from the presence of other metals in the matrix, such as Fe or Ca [299].



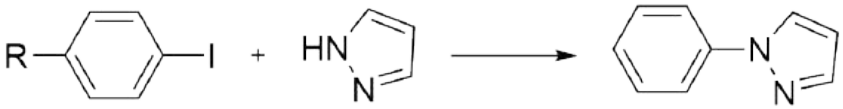
Scheme 26. Scheme of N-arylation of pyrazole with iodobenzen with Eco-Cu as catalyst [299].

In the Ullmann-type $C^{\smile}N$ reaction, N-arylation of pyrazole with iodobenzene was used as a model system to compare Eco-Cu catalysts. Reaction scheme is presented

on Scheme 26. The reaction was carried out in the presence of Cs_2CO_3 as a base in DMF at 90℃ for 15 h under an argon atmosphere, which allowed a direct comparison of the activity of different Eco-Cu catalysts. Screening of Eco-Cu1–8® materials clearly showed that Eco-Cu8®, obtained from Eichhornia crassipesm is the most active catalyst, affording about 85% of the isolated product with only 1 mol% of copper. In general, HCl-activated variants (Eco-Cu2/4/6/8®) are significantly more effective than the corresponding materials obtained solely by biomass calcination (Eco-Cu1/3/5/7®). The catalyst retains useful activity even at very low copper loadings, down to 0.25 mol%, but with a reduced yield [299]. A comparison of Eco-Cu8® with commercial copper sources under the same Ullmann $C^{\smile}N$ reaction conditions showed that CuO is practically inactive, whereas $CuCl$ and $CuCl_2$ catalyze the reaction only moderately and clearly less efficiently than Eco-Cu8®. This indicates that the enhanced activity of the ecocatalytic material does not arise solely from the presence of copper chlorides, but rather from their specific form and environment within the mineral matrix [299].



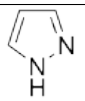
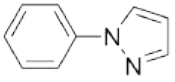
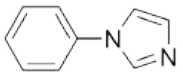
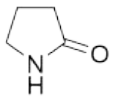
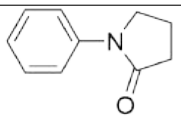
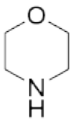
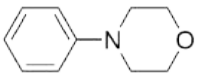
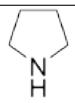
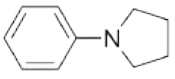
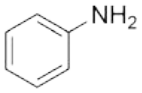
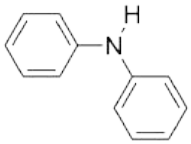
Scheme 27. General scheme of screening of amines in Ullmann reaction with Eco-Cu as catalyst [299].

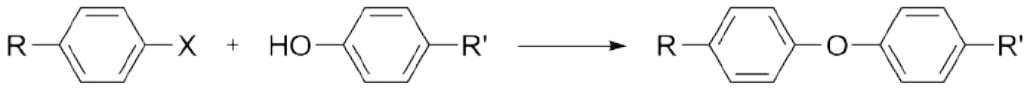


Scheme 28. General scheme of screening of aryl halides in Ullmann reaction with Eco-Cu as catalyst [299].

An analysis of the substrate scope of the Ullmann $C^{\smile}N$ reaction using Eco-Cu8® revealed pronounced differences in the reactivity of nucleophiles (Scheme 27 and examples of results in the Table 7) and aryl halides (Scheme 28 and examples of results in the Table 8). The best results were obtained for azoles such as pyrazole and imidazole, whereas aniline did not undergo coupling, and secondary aliphatic amines, for example morpholine or pyrrolidine, gave only low conversions. For electrophiles, the typical reactivity order iodides > bromides > chlorides was observed. An important achievement is the demonstration that Eco-Cu8® also enables coupling of aryl chlorides, which are considered more challenging substrates in general and often requiring higher temperatures or more strongly activating substituents.

Table 7. Examples of Ullmann reaction results with iodobenzene and different amines as substrates (Scheme 27)and Eco-Cu as catalyst [299].

Substrate	Product	Yield	Conditions
		85%	1 mol% relative to iodobenzene, 0.67 mol% relative to nucleophile, Cs_2CO_3, DMF, 80°C, 15h, argon atmosphere
		54%	
		31%	
		5%	
		6%	
		0%	

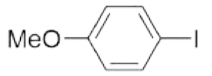
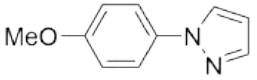
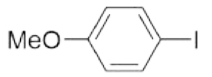
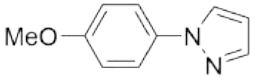
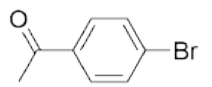
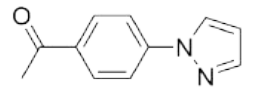
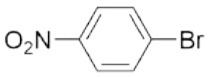
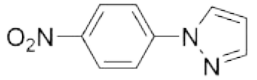
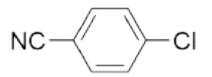
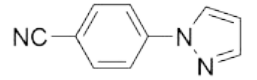


Scheme 29. General scheme of synthesis of alkyl aryl ethers in Ullmann reaction with Eco-Cu as catalyst [299].

In the Ullmann-type $C^{\smile}O$ reaction leading to the synthesis of aryl–alkyl ethers (Scheme 29), Eco-Cu8® also exhibits good catalytic activity under ligand-free conditions, using Cs_2CO_3 as the base, 1 mol% of copper, and DMF as the solvent. High yields are obtained mainly for aryl iodides and bromides at moderate temperatures. In the case of aryl chlorides the use of more strongly activating substituents or an increase in reaction temperature is required. This behavior is consistent with the general trends observed in Ullmann chemistry [299].

Alponti and his team searched for polymetallic ecocatalysts based on plant biomass originating from the mining area of Canaã dos Carajás in northern Brazil, which shall include Cu and Ni. In the first stage, plants were collected and their aboveground parts were analyzed by ICP-OES to determine metal contents, mainly Fe, Cu, and Ni. Among the investigated species, Pluchea sagittalis proved to be the most promising, as its leaves exhibited high metal concentrations [300]:

Table 8. Examples of Ullmann reaction results with pyrazole and different aryl halides as substrates (Scheme 28)and Eco-Cu as catalyst [299].

Substrate	Product	Yield	Conditions
		63%	$90°$C, 15h
		93%	$110°$C, 15h
		31%	$90°$C, 15h
		98%	$90°$C, 4h
		89%	$110°$C, 15h

Reaction conditions: CuHMPC (1 mol %), relative to iodobenzene (1 eq.), nucleophile (1.5 eq.), Cs_2CO_3 (2 eq.), DMF, argon atmosphere.

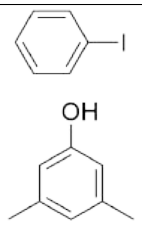
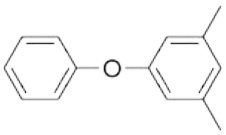
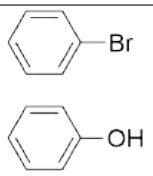
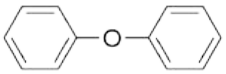
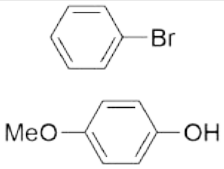
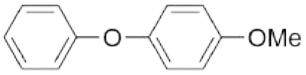
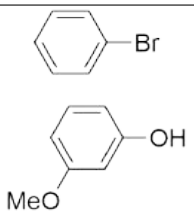
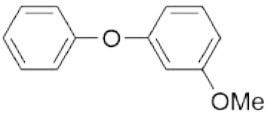
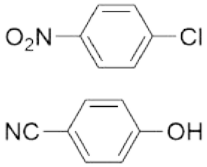
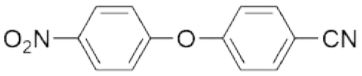
- Cu 567 mg kg^{-1},
- Ni 31.4 mg kg^{-1},
- Fe 10,000 mg kg^{-1}.

The leaves were subjected to calcination in 400℃ for 5 h, yielding crude metal-rich ashes [300]:

- Cu ∼1877 mg kg^{-1},
- Ni ∼118 mg kg^{-1},
- Fe ∼34,491 mg kg^{-1}.

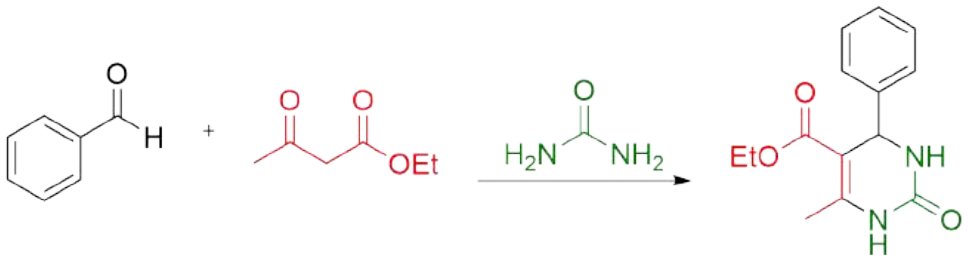
The presence of crystalline metal oxides, including Fe_2O_3 and CuO, was confirmed by XRD analysis. On this basis, three variants of ecocatalysts were prepared, called by researchers Cat A, Cat B and Cat C. In the case of Cat A, treatment with sulfuric acid was applied, however, XRD analysis revealed mainly the presence of mascagnite ($(NH_4)_2\,SO_4$), without distinct transition-metal phases, suggesting either their very low content or strong dispersion. Cat B was obtained by leaching the ashes with HCl for 2 h in 60℃, followed by deposition of the resulting solution onto montmorillonite K10 at 90℃ for 8 h. Despite the low Cu content (∼35 mg kg^{-1}) and undetectable Ni, XRD diffractograms indicated very good dispersion of copper on the support. In contrast,

Table 9. Examples of synthesis of alkyl aryl ethers in Ullmann reaction (Scheme 29) results with Eco-Cu as catalyst [299].

Substrates	Product	Yield	Conditions
		66% 98%	110°C 130°C
		51%	130°C
		82%	130°C
		92%	130°C
		98%	110°C

Cat C was prepared by treating the ashes with concentrated formic acid (85%, 90℃, 18 h). This material contained significantly higher amounts of Cu ($\sim$961 mg kg^{-1}) and Ni ($\sim$32 mg kg^{-1}), but its structural characteristics were similar to those of the raw ashes, indicating poorer dispersion of the active metal species [300].

The activity of the obtained materials was evaluated in two classical multicomponent reactions. In the first stage, the Biginelli reaction leading to the synthesis of dihydropyrimidinone - DHPM derivatives was investigated, using benzaldehyde, a β-ketoester, and urea as a model system, presented on Scheme 27 and examples of results in the Table 10 and Table 11. Initially, the performance of the ecocatalysts was compared with that of classical $CuCl_2 \cdot 2H_2O$ under literature conditions (acidic medium, dioxane/2-MeTHF mixture, room temperature). Under these conditions, in the absence of a Cu(II) catalyst the reaction proceeded very poorly (approximately 21% yield), whereas Cat A enabled a yield of about 60% [300].

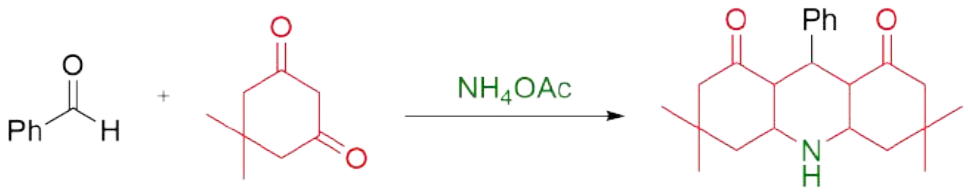


Scheme 30. Scheme of Biginelli reaction - synthesis of DHPM with Eco-Ni, Cu, Fe as catalyst [300].

Table 10. Examples of results of Biginelli reaction (Scheme 30) for different catalysts [300].

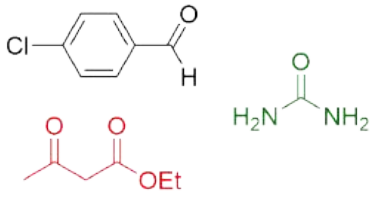
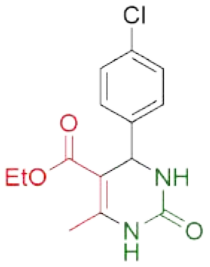
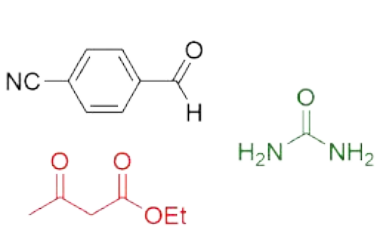
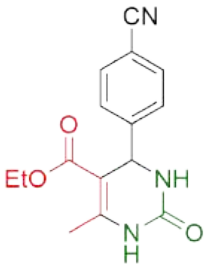
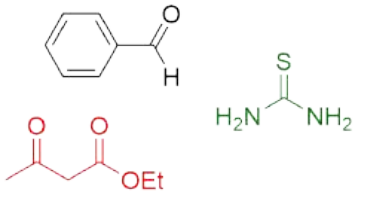
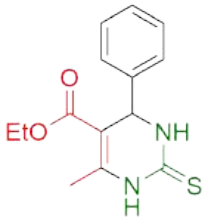
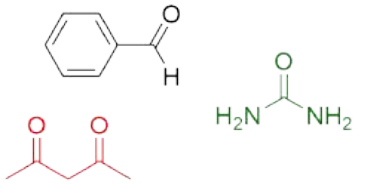
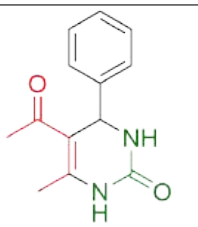
Catalyst	Biomass treatment	Yield	Conditions
Cat A	Treatment with sulfuric acid	60%	24 h, HCl 4M in dioxane and MeTHF, room temperature
Cat B	Treatment with HCl (2 h, 60 °C), deposition onto montmorillonite K10 (90 °C, 8 h)	84%	12 h, 80 °C, solvent free
Cat C	Treatment with 85% formic acid (90 °C, 18 h)	69%	12 h, 80 °C, solvent free
$CuCl_2 \cdot 2H_2O$ (5 mol%)	–	62%	12 h, HCl 4M in dioxane and MeTHF, room temperature

The authors switched to simpler and more green conditions: solvent-free at 80 °C for 12 h. In this setup, the best results were obtained for Cat B, which afforded an 84% yield of the model product. Authors introduced a new parameter, MSMA (mean specific metallic activity). It was defined as the amount of product obtained per total μmol of Cu, Fe, and Ni present in the catalyst. Cat B reached the highest MSMA value (28.7), which the authors interpret as a synergistic effect between the metals and the MK10 support. Extension of the reaction scope to six DHPM derivatives, using various aldehydes and either urea or thiourea, confirmed the general applicability of the system, with yields in the range of approximately 69–88%. In some cases, the addition of a small amount of ethanol (0.5 mL) was necessary to improve the solubility of the reagents.



Scheme 31. Scheme of Hantzsch reaction - synthesis of 1,4-DHP with Eco-Ni, Cu, Fe as catalyst [300].

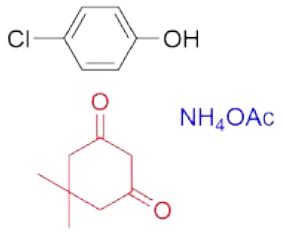
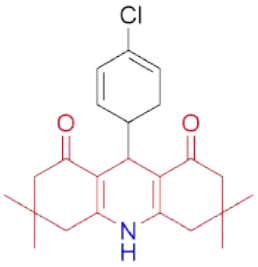
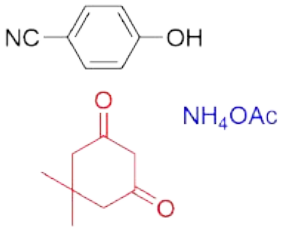
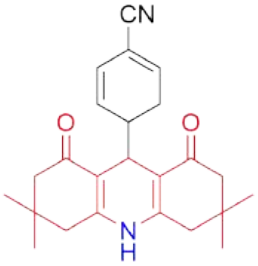
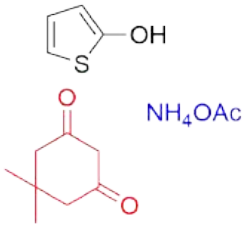
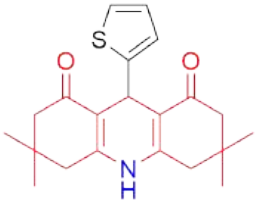
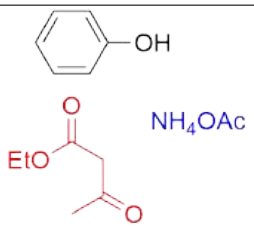
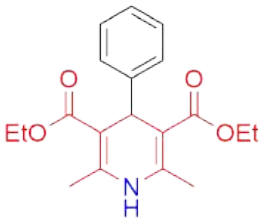
Table 11. Examples of Biginelli reaction (Scheme 30) results with biomass treated with HCl on MK10 as catalyst [300].

Substrates	Product	Yield
		81%
		69%
		79%
		84%

Reaction conditions: $80°$C, 12h

The second catalytic test involved the Hantzsch reaction leading to the synthesis of 1,4-dihydropyridines (1,4-DHP), performed under microwave conditions in ethanol (110℃, 300 W, 20 min). The amount of catalyst was first optimized, revealing that an excess of catalyst reduced the yield, most likely due to adsorption of reagents on the material surface; the optimal mass of ashes was 50 mg. In the comparison of catalyst activities, Cat B again proved to be the most efficient, giving a 98% yield of the model product, compared with 86% for the ashes, 88% for Cat C, and 84% for MK10 alone. This clearly demonstrates the crucial role of copper. Cat B also exhibited good stability: after filtration and washing with ethanol, it could be reused for up to six cycles without significant loss of activity.

Table 12. Examples of results of Hantzsch reaction (Scheme 31) with biomass treated with HCl on MK10 as a catalyst [300].

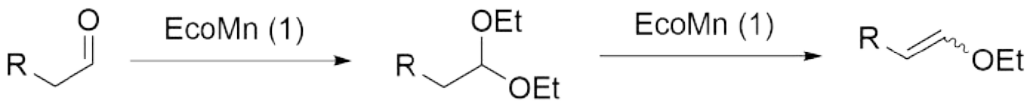
Substrates	Product	Yield
		94%
		79%
		92%
		89%

Reaction conditions: ethanol, microwave irradiation, 110 °C, 300W, 20 min.

Investigation of the reaction scope confirmed broad substrate tolerance, with 1,4-DHP yields in the range of 79–98% for various aldehydes and 1,3-dicarbonyl components. In comparison with literature data, Cat B performs very favorably, enabling rapid product formation (20 min, 98% yield) and multiple reuses. The key conclusion drawn by the authors is that the high activity of Cat B does not result from a high metal loading, but rather from the very good dispersion of active species on the support and favorable textural properties. This demonstrates that the concept of producing efficient heterogeneous catalysts directly from plant biomass is both realistic and practical.

1.2.4.2 Manganese-based ecocatalysts

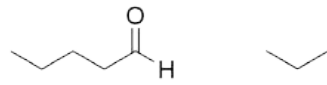
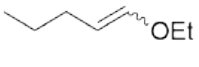
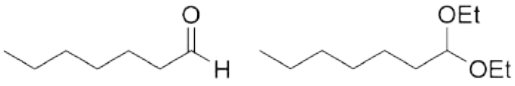
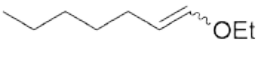
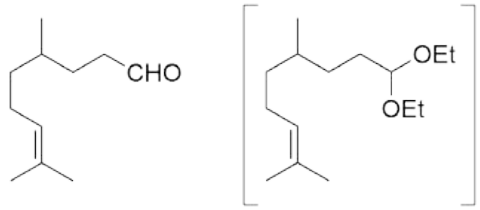
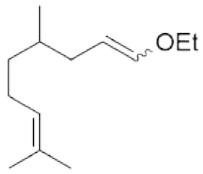
One of the examples of managenese-based ecocatalysts is the Eco-Mn catalyst originates from the plant *Grevillea exul*, known for their ability to accumulate manganese from the soil [301, 302]. Escande et al. used two subspecies of *Grevillea exul* for catalyst preparation: *Grevillea exul exul* and *Grevillea exul rubiginosa*, which grows in post-mining soils in New Caledoni. Their leaves were dried, ground, calcined in air at 400℃, and the resulting ash was treated with diluted HCl. After filtration and solvent removal, a solid Mn-rich material was obtained. Elemental analysis shows manganese as the main component, accompanied by moderate amounts of Mg and Ca and minor quantities of Al, Fe, and Ni. The catalyst derived from *Grevillea exul rubiginosa* contains slightly more Mn and less Fe and Ni than that from *Grevillea exul exul* and this one was chosen for further experiments. FT-IR spectroscopy with pyridine revealed the presence of both Lewis and Brønsted acid sites. This dual acidity, uncommon for simple $Mn(II)$ salts, identifies Eco-Mn (1) as a bifunctional acid catalyst. Eco-Mn (1) efficiently catalyzes the conversion of aldehydes to enol ethers in ethanol via acetal intermediates (Scheme 27 and examples of results in the Table 13) without the use of strong mineral acids, giving good yields and literature-consistent E/Z selectivity. The reactions were carried out using aldehyde and Eco-Mn (1) in amount corresponding to 10 mol% of Mn in anhydrous ethanol at 80℃ for 5h. Aliphatic acetals were formed in good yields (77–96%). In contrast, no ketal formation was observed when ketones were used as substrates, which is consistent with their lower electrophilicity compared to aldehydes. Subsequent alcohol elimination from the acetals afforded the corresponding ethyl enol ethersin good yields (82–89%) [301].

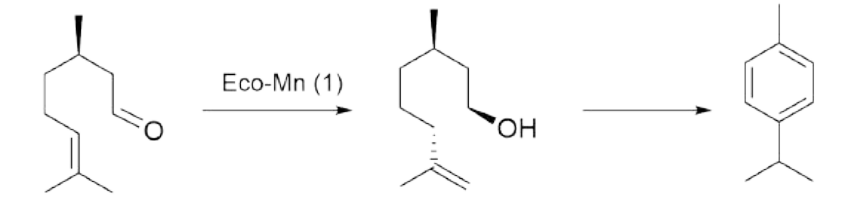


Scheme 32. General scheme of acetalization/elimination of aldehydes catalyzed by Eco-Mn (1) [301].

It also shows high activity in the carbonylene cyclization of citronellal to isopulegol (Scheme 33), where Eco-Mn (1) was co-ground with silica gel and then combined with citronellal. Catalyst was added to achieve 5 mol% of Mn. The mixture was stirred at 90℃ for 1 h, after which it was washed with dichloromethane and filtered through Celite. Removal of the solvent under reduced pressure afforded mainly p-cymene (80% yield), along with 5% of (-)-isopulegol [301].

Table 13. Examples of results of acetalization/elimination of aldehydes (Scheme 32) catalyzed by Eco-Mn (1) [301].

Substrates	Yield	Enol ether	Yield	E/Z
	96%		89%	47/53
	77%		82%	26/74
	–		96%	nd



(R)-(+)-citronellal **R-(-)-isopulegol** ***p*-cymene**

Scheme 33. Scheme of tandem carbonylene cyclization of citronellal to isopulegol catalysed by Eco-Mn (1) leading to p-cymene [301].

Escande and the research team obtained also other version of manganese-based ecocatalyst: Eco-Mn (2). It is obtained from Eco-Mn (1) through a controlled sequence of redox transformations of manganese carried out in an aqueous medium. Eco-Mn (1) is dissolved in water, pH of the solution is raised to 8, which leads to the precipitation of $Mn(II)$ ions in the form of manganese hydroxide. Manganese is progressively oxidized by oxygen from air to higher oxidation states, forming mainly $Mn(III)$ oxides and mixed $Mn(II,III)$ oxides. In the next step, the system is acidified to about pH 3, which triggers the disproportionation of these intermediate manganese species, resulting in the formation of manganese dioxide, MnO_2, containing manganese in the $+IV$ oxidation state:

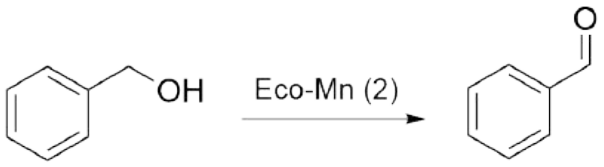
$Mn_3O_4 + 2H^+ \rightarrow Mn^{2+} + Mn_2O_3 + H_2O$

$Mn_2O_3 + 2H^+ \rightarrow Mn^{2+} + MnO_2 + H_2O$

After evaporation of the solvent, a black amorphous powder is obtained - Eco-Mn (2), which acts as a biosourced oxidizing reagent [301].

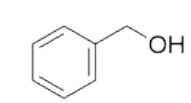
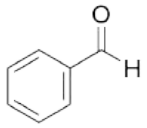
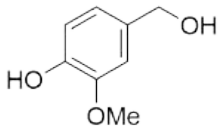
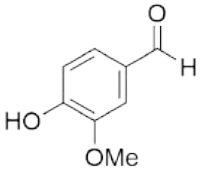
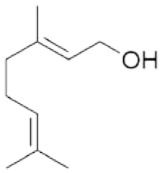
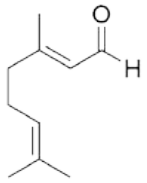
Eco-Mn (2) shows broad applicability as a mild yet highly selective oxidizing reagent in a variety of organic transformations. In the case of benzylic and allylic alcohols, it

enables their quantitative oxidation to the corresponding aldehydes without overoxidation to carboxylic acids, as presented on Scheme 34, clearly outperforming commercial MnO_2 and $MnO_2/FeCl_3$ systems. The reaction was carried out using 3.9 equivalents of Mn from Eco-Mn (2) in EtOAc at 75℃ for 3h and gives yields around 100%. The high efficiency of these reactions is attributed to the synergistic effect arising from the polymetallic composition of Eco-Mn (2). Examples of results of this reaction are presented in the Table 14.



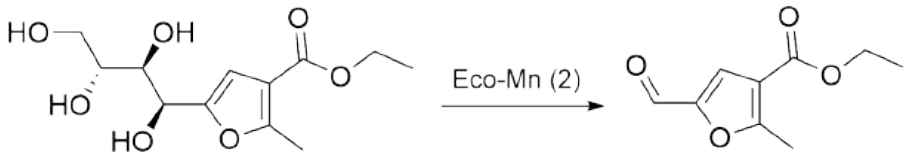
Scheme 34. Scheme of example alcohol oxidation to aldehyde: controlled oxidation of benzylic alcohol into benzaldehyde with Eco-Mn (2) as catalyst [301].

Table 14. Examples of oxidation results with Eco-Mn(2) as catalyst [301].

Substrate	Product	Yield
		100%
		100%
		100%

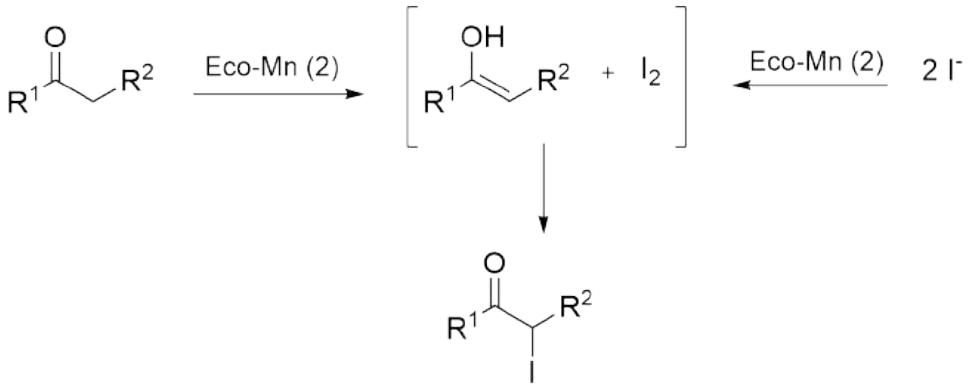
Reaction conditions: 10 mmol of alcohol, 38.8 mmol of Mn, 20 ml of EtOAc, 75 °C, 3 h.

Eco-Mn (2) is also effective in the oxidative cleavage of polyols, providing selective bond scission within polyhydroxy frameworks without degradation of other functional groups, and delivering higher yields than classical $Ce(IV)$- or $Pb(IV)$-based reagents [301]. Example reaction is presented on Scheme 35.



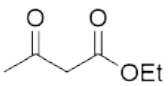
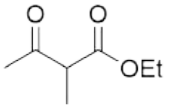
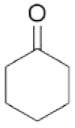
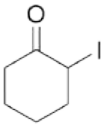
Scheme 35. Scheme of example polyol oxidation to aldehyde: oxidation of polyhydroxyalkyl furan 6 with Eco-Mn (2) as catalyst [301].

In addition, Eco-Mn (2) enables the direct iodination of ketones in the presence of NaI, where iodine is generated in situ from iodide ions, eliminating the need for molecular I_2 and thus complying with current environmental regulations. In this system, Eco-Mn (2) plays a dual role by promoting ketone enolization through its acidic character and oxidizing I^- ions to reactive iodine species, which results in forming the α-iodoketone according to the Scheme 36. Table 15 includes examples of this reaction.



Scheme 36. General scheme of direct oxidative iodination of ketones with NaI and Eco-Mn (2) as catalyst [301].

Table 15. Examples of results of direct oxidative iodination of ketones with Eco-Mn(2) as catalyst.

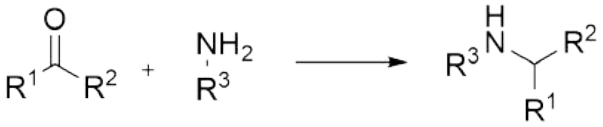
Substrate	Product	Yield
		100%
		64%

Reaction coditions: Conditions: room temperature, 12 h.

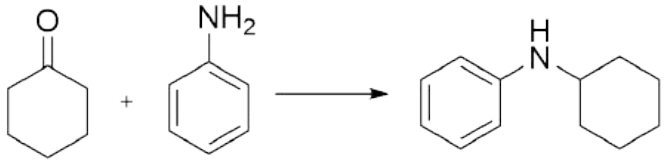
Other work of Escande et al. is focused on Eco-Mn prepared from *Grevinellea exul rubiginosa*. To reduce compositional variability, EcoMn was prepared from several

batches of *Grevillea exul rubiginosa* leaves, allowing homogenization of the material. Eventually, the elemental composition of the catalyst was dominated by alkaline and alkaline earth metals, with calcium (10.44 wt%) as the most abundant component, followed by manganese (6.72 wt%), magnesium (5.26 wt%), and potassium (4.32 wt%) [302].

Due to the fact that Eco-Mn exhibits mixed acidity (both Lewis and Brønsted acid sites), the authors applied this catalyst to the reductive amination of ketones (Scheme 37), a transformation in which simultaneous activation of the carbonyl/imine functionality and the reduction step is crucial. As a model reaction, the amination of cyclohexanone with aniline using the Hantzsch ester (HEH) as the reducing agent was selected (Scheme 38). It was carried out under solvent-free conditions in the temperature range of 80-110℃. Yields were obtained up to 96% and it was achieved at only 0.25 mol% of Mn, which is significantly superior to the performance of $MnCl_2$. A comparative study of example reaction - reductive amination of cyclohexanone with aniline presented on Scheme 38 - showed that $MnCl_2$ is catalytically active, $MnCl_2 \cdot 4H_2O$ performs better, while Eco-Mn is the most efficient, leading to the conclusion that the high catalytic activity arises not from manganese alone but from the specific polymetallic structure of the plant-derived catalyst. In addition, the authors discovered that the presence of a small amount of water - around 10 mol% - enhances the reaction, even though water is theoretically expected to hinder imine formation. Mechanistic investigations demonstrated that water does not improve imine formation, but activates the Hantzsch ester and facilitates the reduction step, most likely through imine protonation and stabilization of transition states via hydrogen bonding [302].



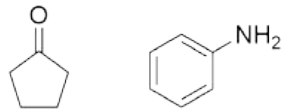
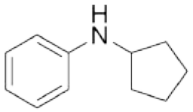
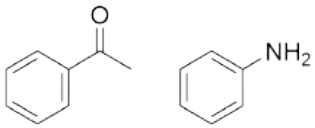
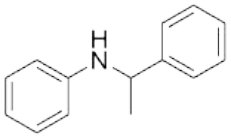
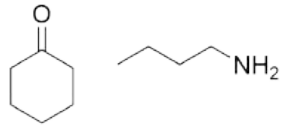
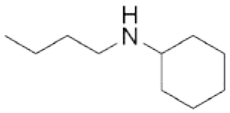
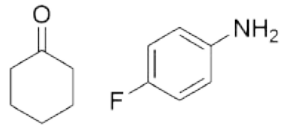
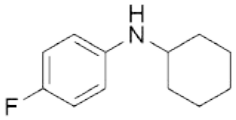
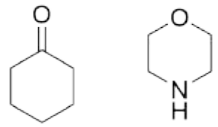
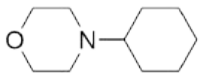
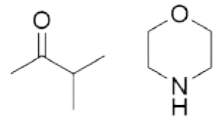
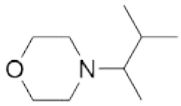
Scheme 37. General scheme of reductive amination of ketones and amines with HEH as reducing agent and Eco-Mn as catalyst [302].



Scheme 38. Scheme of example reaction: reductive amination of cyclohexanone with aniline with HEH as reducing agent and Eco-Mn as catalyst [302].

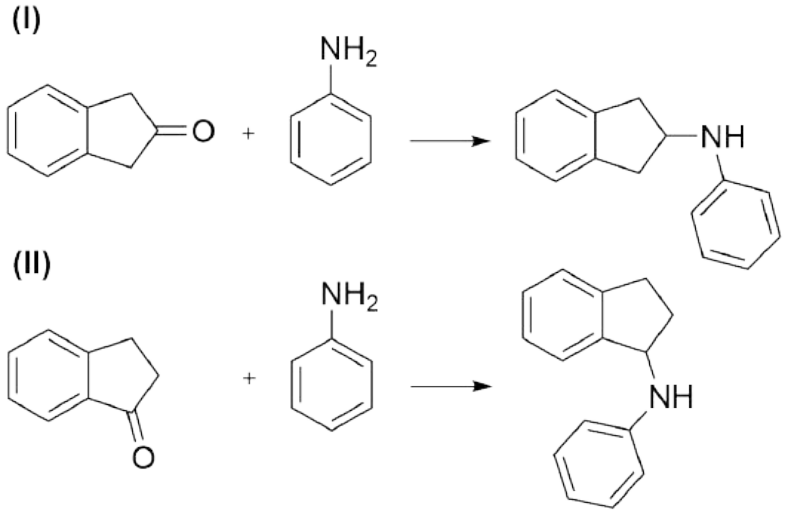
Finally, the practical applicability of the methodology was demonstrated by the syn-

Table 16. Examples of reductive amination results with Eco-Mn as catalyst [302].

Substrates	Product	Yield
		94%
		54%
		77%
		78%
		86%
		83%

Reaction conditions: neat, $110°$C, 4h, HEH (110 mol%), Eco-Mn (100 mol%).

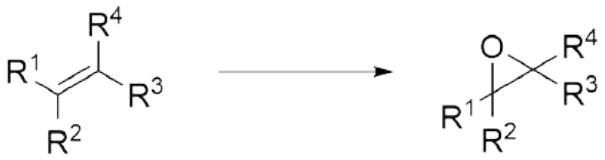
thesis of tetralin-derived and indane-derived amines, which are relevant pharmaceutical precursors, on a gram scale. Synthesis of tetralin-derived secondary amine is presented on Scheme 39.(I). Amine was isolated in 79% yield. It serves as a precursor of antifungal agents as well as dermal anesthetic drugs, meaning that this amine can act as a key intermediate for further functionalization toward pharmaceutically active compounds. The second example, an indane-derived secondary amine, which synthesis is presented on Scheme 39.(II), was obtained in an isolated yield of 67%. The indane scaffold, bearing a secondary aniline-type nitrogen atom, is a well-established motif in medicinal chemistry. It is a precursor of antinociceptive drugs, for example compounds involved in the modulation of pain perception, often through interactions with neuronal ion channels such as sodium channels. In both cases, the successful isolation of these compounds in good yields demonstrates that the ecocatalyst is not limited to model reactions but is also suitable for the preparation of realistic pharmaceutical intermediates [302].



Scheme 39. Scheme of synthesis of tetralin-derived **(I)** and indane-derived **(II)** amines with Eco-Mn as catalyst [302].

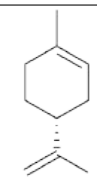
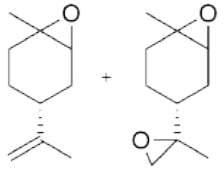
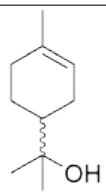
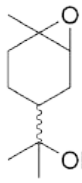
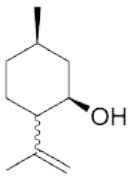
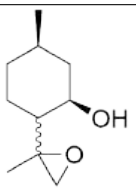
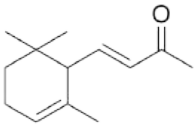
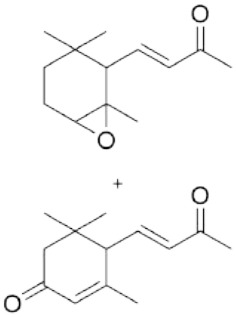
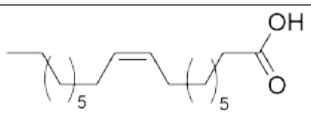
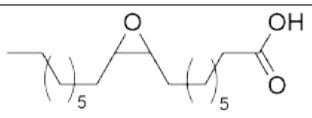
Bihanic et al described catalysts derived from the biomass of four plant species belonging to the *Grevillea genus* have also been reported: *Grevillea exul exul*, *Grevillea exul rubiginosa*, *Grevillea gillivrayi*, and *Grevillea meisneri*. The leaf biomass was dried, ground, and subsequently calcined in air for 6 h at temperatures of 300 ℃, 550 ℃, and 950 ℃. The resulting materials exhibited a polymetallic composition, with manganese as the main transition metal and calcium as the predominant alkaline earth metal, but magnesium, sodium, potassium, and iron were also present. The presence of calcium plays a critical role in stabilizing manganese oxides. The combination of calcium and manganese in the same crystal lattice creates a synergistic effect, enhancing the catalyst's redox capabilities. The elemental composition was reproducible for a given plant species and depended on the calcination temperature. No crystalline manganese oxides were detected after treatment at 300 ℃, where calcination at 550 ℃ led to the formation of $Ca_2Mn_3O_8$, and treatment at 950 ℃ resulted in the formation of $CaMnO_3$ [289].

The catalytic performance of these materials was evaluated in alkene epoxidation reactions using the $H_2O_2/NaHCO_3$ system as the oxidant. Scheme 40 presents general scheme of the reaction and examples of results are shown in the Table 17. It was carried out in the presence of ecocatalyst, used in an amount corresponding to 0.005 equivalents of Mn relative to the substrate. Hydrogen peroxide (30 wt%) was employed as the oxidant in 5 equivalents, activated by sodium bicarbonate in 5 equivalents. The reaction was performed in a water/acetone solvent system at room temperature [289].



Scheme 40. Scheme of alkene epoxidation reactions catalysed by ecocatalyst based on Mn [289].

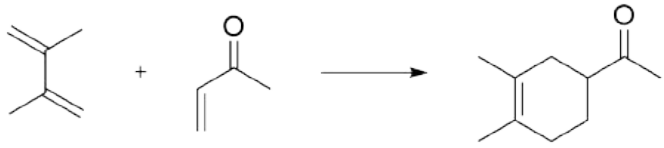
Table 17. Examples of alkene epoxidation results with Mn-based ecocatalyst [289]

Substrate	Product	Yield	Conditions
		15% + 78%	2 h, room temperature
		100%	2 h, room temperature
		100%	4 h, room temperature
		71% + 10%	4 h, room temperature
		66%	4 h, room temperature

All four *Grevillea* species were shown to yield catalytically active materials, while the calcination temperature had only a minor influence on catalytic activity. Temperature 550℃ was identified as the best compromise between catalytic performance and energy input. High conversions and good chemoselectivity were obtained, with the possibility to selectively form mono- or diepoxides. Linalool was converted predominantly to the monoepoxide, which is rare and difficult to achieve due to the high sensitivity of this substrate [289].

1.2.4.3 Zinc-based ecocatalyst

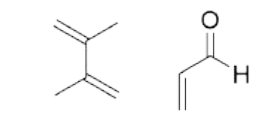
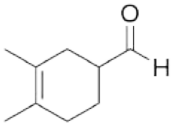
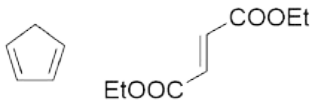
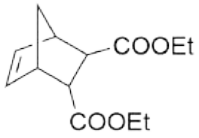
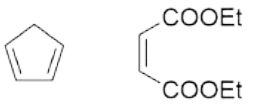
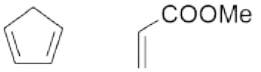
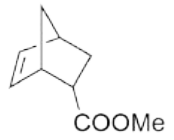
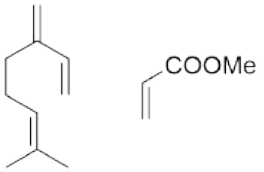
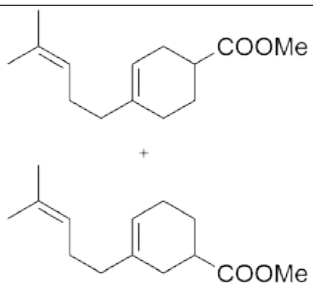
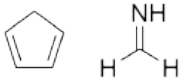
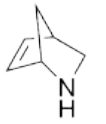
In studies on zinc-based eco-catalysts, Escande and his research team employed biomass from two plant species, *Noccaea caerulescens* and *Anthyllis vulneraria* known for their ability to hyperaccumulate zinc. Leaves were harvested, dried and ground. The prepared biomass was subjected to calcination at 400 °C for several hours. At this stage, complete removal of organic matter occurred. The obtained ash was subsequently extracted with a hydrochloric acid solution (1 M), and the resulting suspension was filtered. The extract contained a mixture of metal chlorides and oxides, primarily zinc, but also iron and calcium. The next step involved depositing the metallic extract onto an aluminosilicate support—montmorillonite K10. In this way, a solid heterogeneous catalytic powder was obtained. XRF and ICP-MS analyses showed that the catalyst contained significant amounts of Zn^{2+} (approximately 6.75%), Fe^{3+} (approximately 2.75%), and Ca^{2+} (approximately 10.3%), as well as trace amounts of other elements. The presence of zinc chloride species, including K_2ZnCl_4, indicates the existence of Lewis acid active sites. Their presence was experimentally confirmed by IR spectroscopy with pyridine adsorption. The observed bands characteristic of pyridine coordinated to Lewis acid sites clearly demonstrate that the obtained material contains real, accessible acidic sites responsible for its catalytic activity [303].



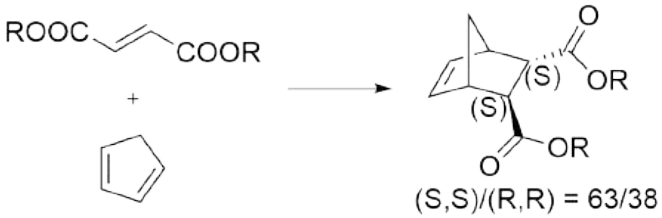
Scheme 41. Scheme of model Diels-Alder reaction between 3-buten-2-one and 2,3-dimethyl-1,3-butadiene catalysed by ecocatalyst based on Zn [303].

The catalytic activity of the obtained ecocatalyst was evaluated in a model Diels-Alder reaction between 3-buten-2-one and 2,3-dimethyl-1,3-butadiene (Scheme 41 and examples of results in the Table 18), carried out in toluene at 110 °C. Under these conditions the $Zn/K10$ catalyst prepared from the biomass of zinc-hyperaccumulating plants provided quantitative substrate conversion and 100% product yield. For comparison, the use of montmorillonite K10 alone resulted in only 44% yield, commercial $ZnCl_2$ gave 67%, while the reaction conducted without any catalyst proceeded to a very limited extent (approximately 6-7%). The catalyst recovered after the reaction and reused retained almost full activity, reaching a 98% yield. Reaction scope studies demonstrated that the catalyst is also effective for other combinations of dienes and dienophiles, affording high yields together with good control of endo/exo stereoselec-

Table 18. Examples of Diels-Alder results with K10-supported Zn-ecocatalyst (0.1 equiv Zn) [303].

Substrates	Product	Yield	Conditions
		100%	110 °C, 4 h, toluene
		93%	5 °C, 1 h, toluene
		91%	25 °C, 0.25 h, toluene
		98%	5 °C, 4 h, CH_2Cl_2
		99% (80%+20%)	110 °C, 4 h, toluene
		84%	25 °C, 6 h, water

tivity [303].

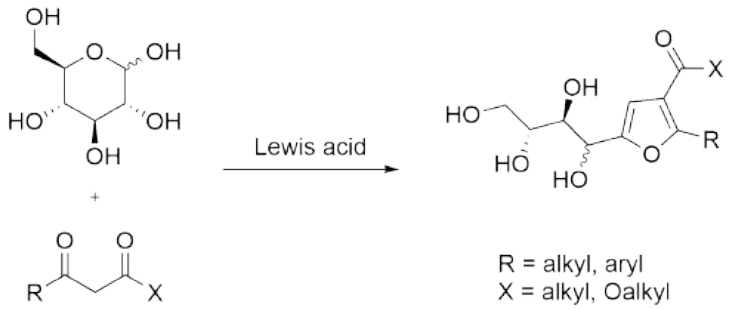


Scheme 42. Scheme of model Diels-Alder reaction between dimethyl fumarate and cyclopentadiene catalysed by ecocatalyst based on Zn [303].

Furthermore, its applicability in hetero-Diels-Alder reactions was demonstrated - these transformations could be performed even in aqueous media and at moderate temperatures. Preliminary asymmetric reaction experiments, carried out with dimethyl fumarate and cyclopentadiene (presented on Scheme 42 at low temperature, showed

a more favorable diastereomeric ratio compared to commercial $ZnCl_2$. The obtained results clearly indicate that the biomass of zinc-hyperaccumulating plants can serve as an effective source of active, selective, and reusable Lewis acid catalysts for cycloaddition reactions [303].

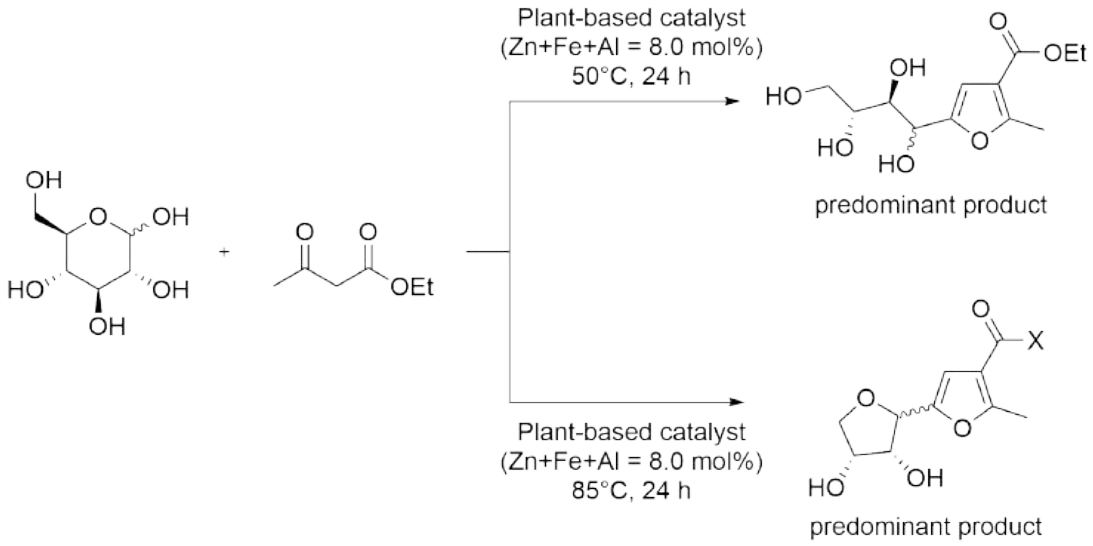
The other idea of Escande and his research group was also conected with Zn-based ecocatalysts. It was obtained from the biomass of *Noccaea caerulescens* and *Anthyllis vulneraria*, collected from a degraded post-mining area in France. Dried and ground leaves were subjected to calcination at 400℃ for 5 h, and the resulting mineral ash was extracted with an aqueous solution of HCl (1 M) at 60℃, leading to the formation of a mixture of metal chlorides exhibiting Lewis acid character. The catalyst composition was analyzed by XRF and ICP-MS, which revealed the presence of Zn as the main transition metal (approximately 6.75 wt%), as well as significant amounts of Fe (approximately 2.75 wt%) and Al (approximately 1.50 wt%). The contents of these elements were relatively reproducible regardless of the plant collection site. XRD analysis indicated the presence of crystalline inorganic phases such as KCl, $CaSO_4$, and K_2ZnCl_4. Furthermore, ESI-MS spectrometry (negative ion mode) confirmed the presence of mono- and polymetallic chloride anions (including $ZnCl_3^-$, $FeCl_4^-$, and $CdCl_3^-$), demonstrating that the catalyst constitutes a complex polymetallic mixture of active Lewis acid centers rather than a simple analogue of a single metal salt [304].



Scheme 43. General scheme of the Garcia Gonzalez reaction catalysed by Zn, Fe, Al based ecocatalyst [304].

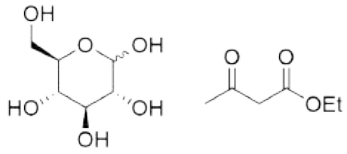
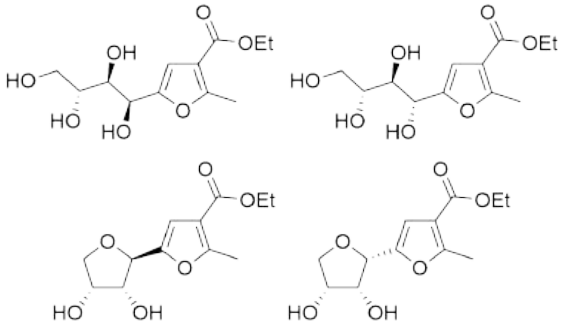
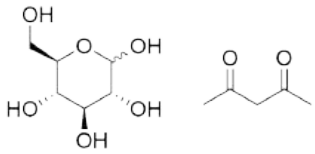
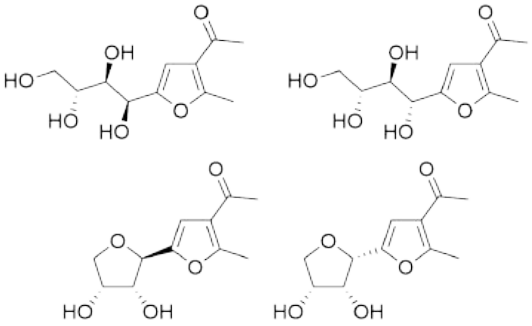
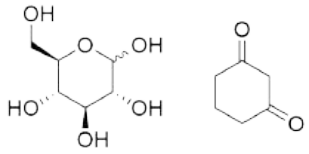
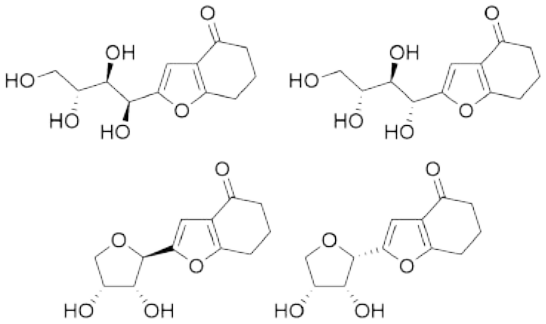
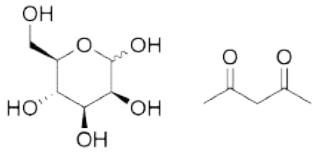
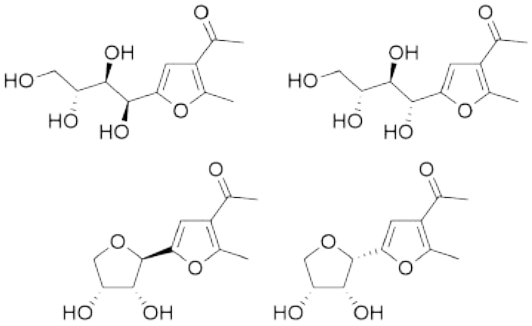
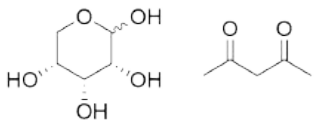
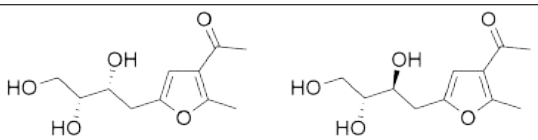
The activity of the obtained plant-derived catalyst was evaluated in the García González reaction between D-glucose and ethyl acetoacetate presented on Scheme 43. Initial experiments conducted in an $H_2O/EtOH$ mixture revealed a significant problem of metal ion leaching into the liquid phase, which prompted the authors to develop a solid-phase reaction variant. In the optimized method, the catalyst and substrates were dispersed on SiO_2 and heated in a closed system, enabling an extraction of the product with ethyl acetate while retaining the metallic components in the solid phase. The catalyst loading was set at 4 mol% with respect to Zn or 8 mol%

with respect to the total amount of Zn+Fe+Al, which were considered the main Lewis acidic centers. Lower loadings resulted in decreased yields, and higher amounts did not provide further improvement. A key feature of the system proved to be the ability to control reaction selectivity via temperature. Performing the reaction at 50℃ for 24 h enabled the selective synthesis of non-cyclized polyhydroxyalkylfurans, but increasing the temperature to 85℃ resulted in nearly quantitative formation of cyclization and dehydration products. This behaviour is shown on the Scheme 44 and examples of results in the Table 19. Such control was not observed for classical catalysts such as SiO_2, $ZnCl_2/SiO_2$, or a mixture of commercial chlorides of Zn^{II}, Fe^{III}, and Al^{III}, indicating that the activity and selectivity arise from the specific polymetallic nature of the plant-derived catalyst [304].



Scheme 44. Scheme of controlling the selectivity of the Garcia Gonzalez reaction catalysed by Zn, Fe, Al based ecocatalyst [304].

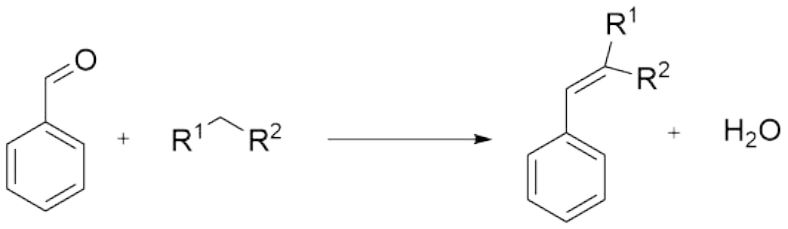
Table 19. Examples of Garcia Gonzalez reaction results with Zn, Fe, Al based ecocatalyst [304].

Substrate	Product	Yield (Selectivity)
		65% (78:22) 2% (98:2)
		72% (75:25) 5% (89:11)
		0% 38% (89:11)
		0% 90% (99:1)
	 no cyclized products	70% (77:23) -

The reaction scope included various hexoses, pentoses, and β-diketone components, affording products in yields ranging from 38% to 98%. In the case of pentoses,

exclusively linear products were observed due to the side chain being too short to undergo cyclization. The products were obtained as mixtures of diastereoisomers, which was attributed to epimerization at the C2'position occurring via a carbocation intermediate. This phenomenon was more pronounced for linear products than for cyclic ones. The catalyst exhibited good stability and could be reused for at least four reaction cycles with only a slight decrease in yield, without significant changes in metal composition. Moreover, ICP-MS analysis of the final products showed no detectable presence of toxic elements such as Cd or Pb [304].

Deyris et al. (2018) presented one of the key conceptual contributions to the field of ecocatalysis. The study employed two plant species from northern France, *Arabidopsis halleri* and *Salix Tordis*, which grow on metal-contaminated sites and exhibit high metal accumulation in their leaves, making them suitable for further processing. Elemental analysis showed that *A. halleri* accumulates very high amounts of zinc, and *S. Tordis* contains less Zn but is rich in Ca, K, and Mg. The preparation of the ecocatalysts involved a multistep process consisting of biomass drying, calcination in air up to 550 °C to obtain ash, acid digestion of the ash in HCl, evaporation of the solution, and final drying to yield a powdered catalyst. The resulting materials contained mixtures of Zn, Ca, K, and Mg, with the *A. halleri*–derived ecocatalyst being significantly richer in zinc, while the *S. Tordis*–based material showed a higher calcium content. Crystalline phase analysis identified, among others, K_2ZnCl_4 present only in the *A. halleri* ecocatalyst, $KMgCl_3 \cdot 6H_2O$ (carnallite), KCl, and $CaSO_4 \cdot 0.5H_2O$. They are unusual salt mixtures, not typically used in catalysis. Acid–base characterization revealed the presence of both Lewis and Brønsted acidity. The *A. halleri*–derived material exhibited a stronger Lewis acidic character due to its higher Zn content, whereas the *S. Tordis* ecocatalyst remained catalytically active despite its lower zinc concentration. Model reaction involving benzaldehyde and various nucleophiles (Scheme 45) was carried out to prove catalytic activity at 100 °C under solvent-free conditions.



Scheme 45. Scheme of alkene epoxidation reactions catalysed by ecocatalyst based on *Zn* [297].

No conversion was observed in the absence of a catalyst, while both ecocatalysts

often outperformed $ZnCl_2$. Ecocatalyst derived from *S. Tordis* was frequently more effective than from *A. halleri* despite its lower Zn content. A particularly important observation was that K_2ZnCl_4 alone showed poor catalytic activity, whereas $KMgCl_3$ exhibited activity comparable to that of the *S. Tordis* ecocatalyst, indicating that zinc is not the key active component and that the magnesium-containing phase plays the dominant role in the catalytic system [297].

1.2.5 Arabidopsis haleri

Arabidopsis halleri was identified for the first time in 1944 at Auby, France, 20 km from Belgium, by a botanist, A. Berton. Since then, the site became an international reference as several metallicolous plants were found, including the Zn- and Cd-hyperaccumulator *Arabidopsis halleri* (formerly *Cardaminopsis halleri (L.) Hayek*) [305]. Ability to hyperaccumulate and tolerate elevated concentrations of heavy metals without exhibiting typical phytotoxic symptoms, begins at the level of the root system, where membrane-bound transport proteins, particularly those from the ZIP (Zrt and Irt-like protein) and HMA (heavy metal ATPase) families, play key roles in the uptake and internal transport of metal ions. Among these, HMA4 has received particular attention in *A. halleri*, as this gene has undergone triplication and exhibits enhanced expression, enabling efficient xylem loading of Zn and its translocation to aerial tissues [306]. In leaf tissues, the accumulated metals are chelated by organic ligands. Those ligans are citrate, malate, and sulfur-containing peptides like phytochelatins or metallothioneins. This prevents free metal ions from interfering with essential cellular processes by sequestering them in vacuoles or binding them in non-toxic forms [307]. In addition, *A. halleri* demonstrates elevated antioxidant activity and enhanced cell wall modifications, which contribute to its metal detoxification capacity and limit oxidative stress.

A. halleri expresses its metal homeostasis as a basic ability rather than as a response to stress, which makes it stand out compared to other metal hyperaccumulating species. This indicates that it is not a stress adaptation but a genetically fixed trait. It could result from natural selection. This enables *A. halleri* to colonize and persist in environments heavily contaminated with heavy metals, where most plant species fail to survive [308]. When comparing *Arabidopsis halleri* with its widely studied relative *Arabidopsis thaliana*, physiological and molecular differences can be observed. Their responses to metal exposure are different. While *A. thaliana* is a non-accumulator and metal-sensitive species, *A. halleri* exhibits a remarkable capacity to tolerate and accu-

mulate toxic metals in concentrations that would severely inhibit or even kill *A. thaliana*. A key difference lies in the regulation and copy number variation of genes associated with metal transport and homeostasis. The HMA4 gene, responsible for loading Zn into the xylem, exists in three tandemly duplicated copies in *A. halleri*, whereas *A. thaliana* has only a single copy with significantly lower expression levels [306]. This genomic expansion enable *A. halleri* to sustain high rates of translocation of Zn without triggering toxicity. Moreover, comparative transcriptomic analyses have shown that many metal-responsive genes in *A. halleri* are constitutively expressed, even in the absence of metal stress, while in *A. thaliana* such genes are only transiently activated under toxic conditions [309]. This difference suggests that *A. halleri* has evolved a genetically fixed state, providing it with a default defense against heavy metal stress. Additionally, *A. thaliana* is characterized by inhibition of growth, chlorosis, and oxidative damage when exposed to elevated levels of Zn or Cd, while *A. halleri* maintains normal development and even benefits from Zn-rich soils in some cases. These observations support the idea that *A. halleri* accumulate metal as its overall strategy, possibly against herbivores or pathogens. It shows a significantly lower expression level of genes involved in iron uptake and the response to iron deficiency, specifically the IRT1 and IRT2 genes. Importantly, in *A. thaliana*, reducing the activity of these genes, for example by adding excess iron to the growth medium, increases zinc tolerance. An excessive amount of zinc leads to a pronounced iron deficiency in *A. thaliana*, resulting in decreased iron content in the shoots. In contrast, *A. halleri* maintains a stable iron level in the shoots regardless of external zinc concentration. In short, *A. halleri* possesses a finely tuned iron regulation system, which, through zinc-responsive ZIP transporters, helps sustain an optimal Fe level, while simultaneously limiting excessive Zn uptake via iron-regulated metal transporters. This coordinated interplay between Zn and Fe regulation may largely contribute to the high zinc tolerance observed in *A. halleri* [310].

In a study comparing the effects of high cadmium and zinc concentrations on the photosynthetic performance of *Arabidopsis arenosa* and *Arabidopsis halleri*, both species-collected from the same contaminated site in Piekary Śląskie, southern Poland-showed visible signs of stress when exposed to either metal. Specifically, in both species, metal treatment led to a clear reduction in chlorophyll levels, along with a noticeable increase in anthocyanin content in leaves, compared to control plants. Cadmium exposure resulted in a significant decrease in energy absorption, the flux of energy trapped in PSII, and the percentage of active reaction centers in both species. Interestingly, the energy dissipation flux in *A. arenosa* leaves was lower than in *A. halleri*, indicating a slightly different photoprotective response. On the other hand,



Figure 24. *A. halleri* on the mine dumps near the ZGH Bolesław zinc mine in Bukowno

zinc had a stronger toxic impact on the electron transport chain in *A. halleri* compared to *A. arenosa*. In *A. arenosa*, exposure to excess Zn triggered a milder response than Cd exposure - only the electron transport flux and proportion of active reaction centers were reduced relative to the control. The two species also differed in how much of each metal they accumulated. Cd content in *A. arenosa* leaves was nearly three times higher than in*A. halleri*, while the opposite trend was observed for Zn-*A. halleri* leaves contained three times more Zn than those of *A. arenosa*. These findings suggest that both *Arabidopsis* metallicolous populations are tolerant to high concentrations of Cd and Zn. However, their photosynthetic machinery appears to respond to metal toxicity in species-specific ways [311].

Dietrich et al. (2021) investigated the relationship between soil metal concentrations and the phytoextraction efficiency of *Arabidopsis halleri*. They analyzed two non-metallicolous and two metallicolous populations, measuring total and bioavailable fractions of Zn and Cd in both soil and plant tissues. Their findings revealed that shoot trace metal element accumulation varied independently of both total and bioavailable soil TME concentrations in metallicolous individuals. One non-metallicolous population exhibited Zn accumulation efficiency comparable to metallicolous populations, despite originating from non-contaminated soil. These results suggest that the plant's inherent physiological traits play a more significant role in phytoextraction efficiency than soil metal content, emphasizing the importance of selecting appropriate plant populations for effective phytoremediation strategies [312].

Chapter 2:
Hydrophosphonylation

2.1 Hydrophosphonylation - chemical basics

Hydrophosphonylation is a broad class of nucleophilic addition reactions in which a phosphorus-based nucleophile, often referred to as a P-nucleophile, is added across a polarized multiple bond such as a $C = O$ or $C = N$. This process represents a key method for constructing C-P bonds and is widely employed in the synthesis of α-substituted phosphonates. Two of the most prominent mechanisms of hydrophosphonylation are the Pudovik and Abramov reactions. While both lead to the formation of $P - C$ bonds, the nature of the phosphorus nucleophile and the electrophilic partner involved differs significantly [313]. This reaction is a cornerstone of organophosphorus chemistry because it provides one of the most direct and efficient routes to forming the hydrolytically stable phosphorus-carbon bond. The stability of the $P - C$ bond, in stark contrast to the labile $P - O$ bond found in biologically ubiquitous phosphates, is the key to the function of many phosphonate-based drugs and probes. It allows these molecules to act as stable analogues of natural phosphates or transition states in enzymatic reactions [314].



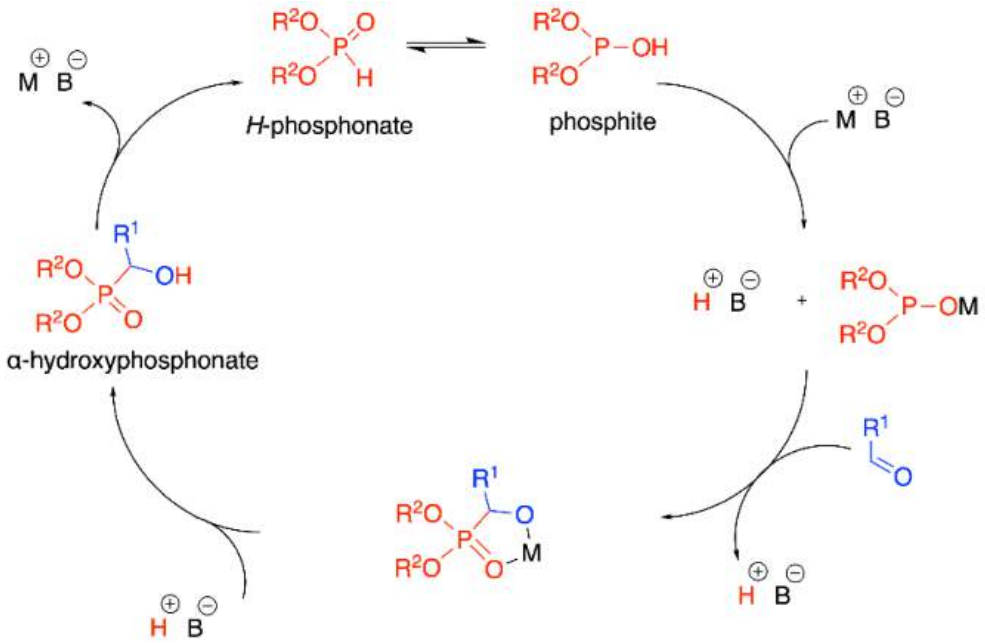
Scheme 1. Hydrophosphonylation, Pudovic reaction

The Pudovik reaction is the most commonly used and best-studied method for the synthesis of α-hydroxyphosphonates [315, 316]. This reaction typically involves the addition of H-phosphonates, such as dialkyl phosphites to imines $-C = N$ or carbonyl compounds $-C = O$ to produce α-aminophosphonates or α-hydroxyphosphonates. Adding dialkyl H-phosphonates $(RO)_2P(O)H)$ to $-C = O$, which gives α-hydroxyphosphonates is the classic Pudovik hydrophosphonylation. Usage of imines instead of aldehydes or ketons will lead to α-aminophosphonates, which is the aza-Pudovik variant of the reaction [135, 317, 318]. Reaction scheme for classic Pudovik reaction with carbonyl compunds is presented on the scheme 1. In contrast, the Abramov reaction classically involves the addition of trialkyl- or triarylphosphites $P(OR)_3$, which are trivalent phosphorus compounds, to carbonyl compounds: aldehydes or ketones [319].

Pudovik reaction is known for its simplicity and high yields, making it a preferred

method for the synthesis of α-hydroxyphosphonates [320]. It proceeds through a four-center cyclic transition state, which is highly sensitive to the structure of the reagents, the nature of the solvent, and the presence of catalysts [321, 322].

The Pudovik reaction is most commonly performed under base-catalyzed conditions [317]. While the precise mechanism has not been definitively proven through experimental means, a plausible pathway is widely accepted in the chemical literature [323]. The first step of the process is believed to be gneration of the nucleophile. The reaction is initiated by the deprotonation of the $P-H$ bond in the phosphorous compound by a base. This step generates a highly reactive anion, which possesses substantial nucleophilicity [323]. The newly formed phosphite anion attacks the electrophilic carbon atom of the carbonyl group. This addition step results in the formation of a new $P-C$ bond and creates a tetrahedral alkoxide intermediate [323].This transition state is highly organized and is influenced by steric and electronic factors. The final step involves a proton transfer, typically from the conjugate acid of the base used in the first step, which neutralizes the alkoxide intermediate to yield the final α-hydroxyphosphonate product [321, 323, 324]. Scheme is presented in the Figure 46.



Scheme 46. Generally accepted mechanism for the Pudovik reaction.

The Pudovik reaction is significantly influenced by the presence of catalysts and solvents. Acidic conditions, such as those provided by the hydrolysis products of dialkyl phosphites, are essential for the reaction to proceed. These conditions facilitate the formation of the transition state and stabilize the intermediate. The choice of solvent also plays a crucial role in the reaction. Polar solvents, such as alcohols, enhance the

reaction rate by stabilizing the transition state and facilitating the proton transfer step. Non-polar solvents hinder the reaction due to the lack of stabilization of the transition state [322].

H-phosphonates exist as a prototropic tautomeric pair: a tetracoordinate $P(V)$, phosphonate form, typically thermodynamically favored in solution, and a trivalent $P(III)$ phosphite form, typically minor. In most common solvents the equilibrium lies strongly to the P(V) side, but the $P(III)$ phosphite tautomer is the species that actually behaves as the P-centered nucleophile [325, 326]. Computational and mechanistic studies show that direct intramolecular H-shift is high-barrier, so tautomerization is often assisted-by bases, Lewis acids, H-bond relays, or self-association/dimers-which is why catalysts and medium effects have such a pronounced impact on rate and outcome [325]. The $P(III)$ phosphite (or its deprotonated equivalent) is the kinetic nucleophile that adds to $C = O$ or $C = N$. If the equilibrium is stuck on $P(V)$, the reaction drags, but if conditions raise the steady-state level of $P(III)$ instead, it accelerates [325, 326]. Brønsted bases, such as amines, DBU, TBD or guanidines, shift the equilibrium toward $P(III)$. They can generate a more reactive phosphite anion, speeding addition and often enabling less reactive ketones or imines [135, 326]. Lewis acids can activate the electrophile by polarizing $C = O$ or $C = N$ and sometimes interact with phosphorus oxygens, effectively stabilizing $P(III)$ character in the reactive complex - both effects lower the addition barrier [135, 326]. Drying agents and molecular sieves can also tilt the equilibrium toward the phosphite and boost rates in phospha-Michael and Pudovik additions [326]. Solvent polarity and H-bonding change the $P(V)$/$P(III)$ balance and the tautomerization barrier. In some systems electron-withdrawing substituents can stabilize $P(III)$ in some systems. These effects translate directly into faster or slower Pudovik reactions and sometimes into different optimal catalysts [325].

Abramov reaction is closely related to the Pudovik reaction, the Abramov reaction involves the addition of a trialkyl phosphite to a carbonyl compound. The mechanism proceeds through an intermediate that undergoes an intramolecular alkyl group transfer from an oxygen atom to the newly formed alkoxide, yielding the phosphonate product [314].

Both of these reactions - Pudovik and Abramov are characterized by a broad substrate scope and have become the starting point for the development of numerous modifications, including stereoselective and environmentally friendly procedures. The variety of catalysts used, from simple bases and acids to complex metal complexes, attests to the maturity and flexibility of these fundamental transformations in organophosphorus chemistry [316].

The main directions of development of these synthesis reactions include asymmetric synthesis, the implementation of green chemistry principles, and the search for innovative catalytic systems. Asymmetric synthesis of α-hydroxyphosphonates is crucial because the biological activity of many chiral compounds is closely related to their absolute stereoisomeric configuration. Obtaining enantiomerically pure hydroxyphosphonates is therefore essential for developing drugs with high selectivity and reduced toxicity [316]. Research in this area focuses on two main approaches. One is the use of chiral resolving agents to separate racemic mixtures. Second is direct asymmetric synthesis using chiral catalysts or substrates [316, 327, 328]. The development of organometallic catalysis, organocatalysis, and biocatalysis has opened up new possibilities in the stereoselective formation of the $C-P$ bond [328, 329]. At the same time, there is a huge emphasis on greening synthetic processes. The pursuit of sustainability is driving research into methods that minimize waste generation, energy consumption, and the use of toxic solvents [89, 144, 315]. In the context of hydroxyphosphonate synthesis, this is manifested in the development of solvent-free procedures, the use of mild and inexpensive catalysts, and the optimization of reaction conditions [315, 316, 330].

Hydroxyphosphonates, products of Pudovik reaction, are known for their high chemical stability, which makes them suitable for various industrial and biological applications. The phosphonate group $-PO_3H_2$ is highly resistant to hydrolysis under mild conditions, ensuring that these compounds remain stable in aqueous environments [316, 317]. However, under specific conditions, such as high temperatures or in the presence of strong acids or bases, hydroxyphosphonates can undergo hydrolysis to form phosphonic acids [331].

The hydroxyl group $-OH$ in hydroxyphosphonates is reactive and can participate in various chemical reactions, such as O-alkylation, O-acylation, and oxidation, which allow the synthesis of a wide range of derivatives, including α-alkoxyphosphonates, α-acyloxyphosphonates, and ketophosphonates [320]. The $-OH$ group can be replaced by other nucleophiles, such as amines, leading to the formation of α-aminophosphonates, which are also biologically active compounds [317, 332].

2.2 Hydrophosphonylation - application

Hydroxyphosphonates have a wide range of applications. As early as the 1950s, their use as insecticides was being written about by Lorenz [333]. Trichlorfon [25.(I)]

also know as O,O'-dimethyl (2,2,2-trichloro-1-hydroxyethyl) phosphonate is the pesticide which was widely used in golf course turf, aquaculture or home lawns [334]. This is connected with broad spectrum of biocidal activity of hydroxyphosphonates, allowing their use as pesticides to control weeds, insects, and pathogenic fungi. Their effectiveness stems from their ability to disrupt key metabolic processes in target organisms [144, 315, 330, 335].

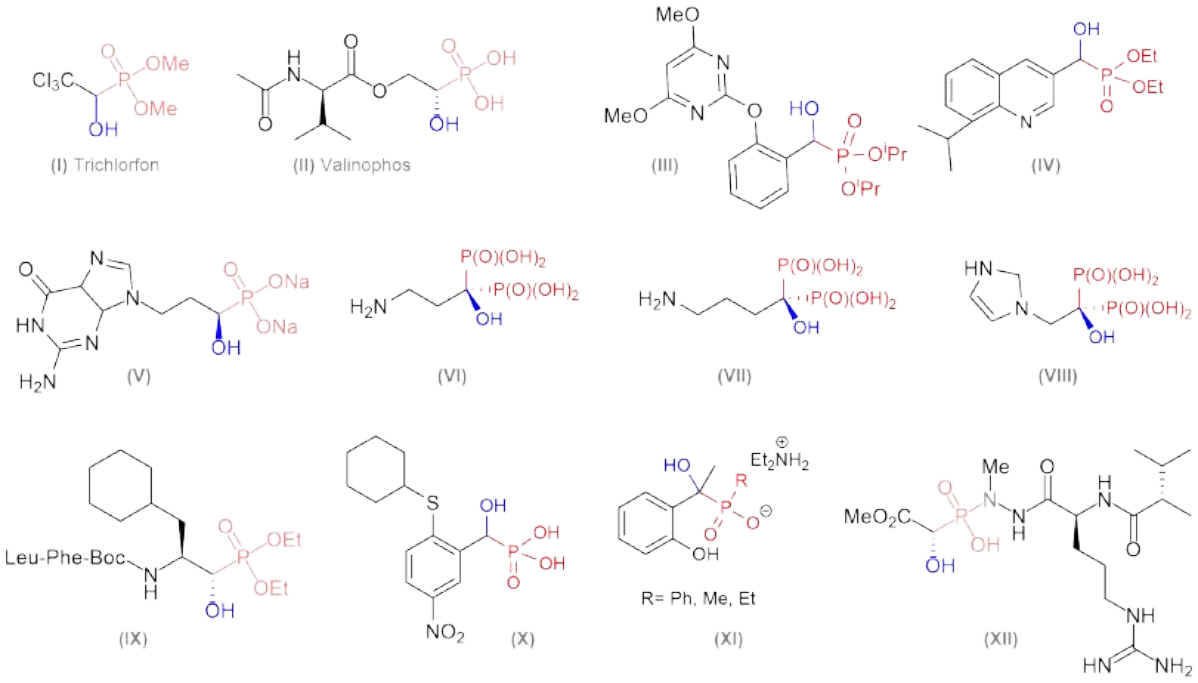


Figure 25. Application of hydroxyphosphonates and phosphonic acids as biologically active compounds

The chemical versatility of hydroxyphosphonates is most fully reflected in their broad applications in the field of medicine and life sciences. The central mechanism underlying the biological activity of hydroxyphosphonates is their ability to act as enzyme inhibitors. This ability stems directly from the principle of bioisosterism, where the phosphonate group effectively mimics naturally occurring phosphate groups [316, 336]. The key difference is the replacement of the enzymatically hydrolyzable $P-O-C$ bond with a stable $P-C$ bond [316]. This allows hydroxyphosphonates to bind to the active site of an enzyme, mimicking the natural substrate, product, and most importantly, the transition state of the reaction, but they do not undergo further transformation. Such molecular mimicry leads to the blockage of the enzyme's catalytic activity, which is of fundamental therapeutic importance [316, 336].

For example valinophos [25.(II)], an N-acetyl-L-Val ester of (R)-2,3-dihydroxypropylphosphonic acid (DHPPA), has slight inhibitory effects on the growth of *Mycobacterium smegmatis* [337]. This suggests that valinophos or its intermediates may have potential antimi-

crobial properties. There are some α-hydroxyphosphonates [25.(III)] and [25.(IV)] which are antibiotic agents against some other bacteria: is an agent for Gram positive bacteria like *Staphylococai* or *Bacillus megtesium-I* and also Gram negative bacteria like *E. coli*, *Salmonella typhi* and *Proteus vulgaris* [338]. β-modified acyclonucleoside phosphonate (ANP) [25.(V)] is hydroxyphosphonate which acts like a drug for malaria. This is significant because the parasite that causes malaria is becoming resistant to existing treatments. This makes the discovery of new drugs increasingly important. ANP has shown the ability to effectively stop the growth of the malaria-causing parasite, even in very small amounts - well when injected, although it also shows some effectiveness when taken orally [339].

There are also hydroxyphosphonates with strong antitumor activity. They are used in oncology treatment. One group of them are hydroxyalkyl-bis-phosphonates: [25.(VI)], [25.(VII)], [25.(VIII)] which have antiproliferative activity so they have the ability to inhibit the growth of several human tumor cell lines what makes them potential drugs in cancer therapy [340].

Some hydroxyphosphonates are renin inhibitors like hydroxyphosphonate [25.(IX)]. A renin inhibitor is a type of medication that blocks renin, an enzyme that starts a chain reaction leading to increased blood pressure. By inhibiting renin, these drugs help lower blood pressure by reducing the production of substances that tighten blood vessels and increase fluid retention [341]. Hydroxyphosphonate [25.(X)] is a compound that blocks the activity of CD-45 tyrosine phosphatase. CD-45 is an enzyme crucial for controlling how blood cells activate and divide. By inhibiting this enzyme, Hydroxyphosphonate can affect the behavior of these cells, potentially influencing immune responses or certain blood disorders [342].

Some hydroxyphosphonates have also antiviral properties like α-γ-dihydroxyphosphinates [25.(XI)] which is a protective agent against influenza A [343]. Influenza A virus causes severe flu outbreaks around the world, leading to health and economic problems. Vaccines target a part of the virus's surface protein to trigger an immune response. However, the virus often changes its surface proteins, making it hard for the immune system to recognize it and for vaccines to stay effective. Using antiviral drugs can be a practical way to help manage and lessen the impact of fast-spreading flu pandemics [344].

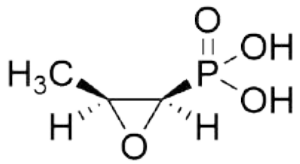


Figure 26. Structure of fosfomycin [345]

Fosfomycin (Figure 26) is hydroxyphosphonate derivative which is applicable as an natural antibiotic that targets the cell wall. It has been isolated from the fermentation products of the bacteria Streptomyces fradiae or Pseudomonas syringae and has attracted significant interest [345].

Hydroxyphosphonates have found extensive applications in the pharmaceutical industry, particularly in the development of drugs for the treatment of bone diseases. Bisphosphonates, a subclass of hydroxyphosphonates, are widely used in the prevention and treatment of osteoporosis. These compounds act by inhibiting bone resorption, reducing the risk of fractures in patients with osteoporosis [346].

The potential of hydroxyphosphonates as enzyme inhibitors translates directly into their wide application in the design and development of new drugs. Their ability to interfere with key metabolic pathways of pathogenic or cancer cells makes them effective candidates for antiviral, anticancer, and antibacterial agents [316].

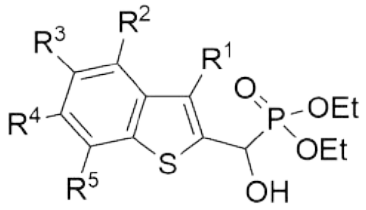


Figure 27. General structure of family of α-hydroxy-α-(benzothiophen-2-yl)-methylphosphonates [347]

In the field of oncology, studies have shown significant cytotoxic activity of some α-hydroxyphosphonates against various cancer cell lines. For example, a newly synthesized family of α-hydroxy-α-(benzothiophen-2-yl)-methylphosphonates (Figure 27) showed promising activity against myeloma U266, melanoma A2058, colon cancer HT-29, and lung cancer EBC-1 cells. Derivatives containing a trifluoromethyl group in the benzene ring were particularly active, indicating the possibility of further structural optimization to increase potency [347]. Furthermore, the ability of bisphosphonates to inhibit farnesyl pyrophosphate synthase, an enzyme crucial for cell proliferation, opens the way for their use as anticancer drugs [336].

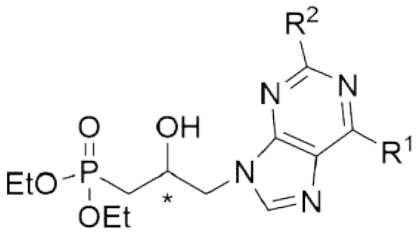


Figure 28. Example of acyclic β-hydroxy- and β-aminophosphonate nucleoside [348]

In the therapy of infectious diseases, hydroxyphosphonates and their derivatives also show great potential. Studies on acyclic β-hydroxy- and β-aminophosphonate nucleosides (Figure 28) have revealed their strong inhibitory effect on the growth of Plasmodium falciparum, the parasite that causes malaria [348]. In the context of the pandemic, phosphonate compounds were studied for their potential activity against the SARS-CoV-2 virus, which highlights their versatility and ability to quickly adapt to new therapeutic challenges [316].

Another important aspect in drug design is the use of hydroxyphosphonates as prodrugs. The phosphonate group, due to its polarity, can be used to modify drug molecules to improve their pharmacokinetic properties. The introduction of a phosphonate group can significantly increase the drug's solubility in water, which facilitates its administration and improves bioavailability. After absorption into the body, the prodrug undergoes metabolic activation to the actual active substance, which ultimately increases its therapeutic efficiency [316].

New and promising applications for those compounds are opening up in the field of medical diagnostics, especially in magnetic resonance imaging. Traditional contrast agents, such as gadolinium complexes, have certain limitations, including non-specific biodistribution and potential toxicity in patients with renal failure [349]. Hydroxyphosphonates can play two key roles in the design of advanced contrast agents. First, they can act as chelating ligands for paramagnetic ions, such as gadolinium Gd^{3+} or manganese Mn^{2+}, forming stable complexes [349]. More importantly, they can be used to functionalize the surface of nanoparticles, particularly superparamagnetic iron oxide nanoparticles - SPIONs [350]. Phosphonate groups, attached to the surface of SPIONs, improve their stability in aqueous solutions, preventing aggregation, and increase their biocompatibility [350]. The greatest potential lies in creating targeted contrast agents. By coupling phosphonate-functionalized nanoparticles with molecules that recognize specific receptors, such as on cancer cells, it is possible to direct the contrast agent directly to the target tissue [336, 350]. Such a strategy allows for much better image contrast at a lower concentration of the agent, which increases diagnostic

sensitivity and specificity. This enables earlier detection of small tumors or metastases that might be invisible using conventional methods [351].

Hydroxyphosphonates and their derivatives are used also as plant growth regulators and components of fertilizers [316]. As plant growth regulators, they can influence various stages of plant development, such as growth rate, flowering, or maturation, by modulating physiological processes [316, 352]. Their use in fertilizers is more complex. On the one hand, the phosphorus content in the molecule suggests potential as a source of this macronutrient, which is one of the most important for plants. The controlled release of phosphorus from the phosphonate molecule could increase the availability of this component in the soil and improve yields [316]. On the other hand, there is a scientific debate about whether plants can effectively metabolize phosphorus from phosphonates to absorbable phosphates. Some studies indicate that this conversion is very slow or does not occur at all, which would mean that phosphonates do not act as a direct source of nutrition for plants [353]. Regardless, their ability to inhibit corrosion and scale formation makes them valuable additives to liquid fertilizers, improving their stability and application properties.

One of the most important and widespread industrial applications of hydroxyphosphonates, but also other phosphonates, is their role as corrosion and scale inhibitors - antiscalants [316, 354, 355]. They are commonly used in water systems, such as cooling circuits, boilers, or water desalination plants, to protect metal surfaces, mainly carbon and mild steel [354, 355]. Their anticorrosive mechanism is based on strong adsorption on the metal surface. Phosphonate molecules, containing heteroatoms such as oxygen and phosphorus with lone pairs of electrons, act as ligands that coordinate with metal cations, such as Fe^{2+}, Fe^{3+}) on the surface, forming a thin, stable, and compact protective layer [354, 355]. This passivating layer acts as a barrier that isolates the metal from the aggressive environment like water containing chloride ions, effectively inhibiting both anodic (metal dissolution) and cathodic (oxygen reduction) corrosion reactions. For this reason, they are often classified as mixed-type inhibitors [355]. The effectiveness of phosphonates is often enhanced by a synergistic effect when used in combination with other substances, especially zinc ions Zn^{2+}. In such systems, zinc ions can precipitate on the cathodic areas of the metal surface as zinc hydroxide, further blocking corrosion reactions and strengthening the action of the phosphonate film [354]. The advantage of phosphonates over traditional inhibitors, such as toxic chromates, is their low toxicity, biodegradability, and relatively low cost, which is consistent with the growing requirements for environmental protection [354–356]. Their ability to prevent the crystallization and deposition of poorly soluble salts, such as calcium

carbonate, their antiscaling action, is an additional advantage in water systems [354].

The versatility of hydroxyphosphonates allows them to be used as precursors or additives in the synthesis of advanced materials with specific properties. Their ability to polymerize or be incorporated into polymer matrices opens the way to creating new functional materials [316]. One of the key applications is their role as flame retardant additives. Incorporating phosphonate groups into the polymer structure can significantly increase its fire resistance. During combustion, phosphorus compounds form a charred protective layer on the material's surface, which limits the access of oxygen and heat to the polymer's interior, inhibiting the burning process [316]. Furthermore, hydroxyphosphonates can be used for the synthesis of biodegradable polymers, which is of great importance in the context of reducing plastic pollution. Their presence in the polymer can also improve its thermal stability and mechanical properties [316].

The development and application of hydroxyphosphonate chemistry are increasingly shaped by the global trend towards sustainable development and green chemistry. This "green pressure" is a pervasive factor driving innovation throughout the field, from basic synthesis to final applications. First, the synthesis of hydroxyphosphonates itself is being re-evaluated from an ecological perspective, which leads to the development of catalytic, solvent-free methods based on renewable raw materials, such as ecocatalysts from biomass [144]. Second, in industrial applications, stringent environmental regulations are forcing the replacement of hazardous substances, such as toxic chromium-based corrosion inhibitors, with more environmentally friendly, biodegradable phosphonates [354, 356]. Third, in agriculture, there is a growing awareness of the negative impact of pesticides on ecosystems, which stimulates research into new, more selective, and less persistent agrochemicals [357]. This observation shows that the future commercial success of products based on hydroxyphosphonates will depend as much on their ecological profile as on their technical effectiveness.

The immediate products of hydrophosphonylation are often not the final target but serve as versatile synthetic building blocks for a wide array of other valuable compounds [317]. Their rich functionality allows for diverse downstream transformations. One of them is O-Functionalization, where the hydroxyl group of an α-hydroxyphosphonate can be readily alkylated or acylated to introduce new functionality or protecting groups [317]. Antoher transformation is oxidation. Mild oxidation converts α-hydroxyphosphonates into the corresponding α-ketophosphonates, which are themselves useful synthetic intermediates [317]. The hydroxyl group can be also replaced by other nucleophiles. For example, treatment with a halogenating agent can produce α-halophosphonates. Importantly, substitution with amines provides a

pathway to convert α-hydroxyphosphonates into α-aminophosphonates [317]. The final and often most critical step for biological applications is the hydrolysis of the phosphonate esters. This is typically achieved under acidic conditions to unmask the phosphonic acid moiety, which is the form responsible for the biological activity of many of these compounds [317].

2.3 Hydrophosphonylation - catalysts

Dialkyl phosphites behave as Brønsted acids ($P-H$) and, under basic or coordinating conditions, as ambident nucleophiles. Many catalysts operate by forming a phosphite/phosphonate anion pair or lowering the LUMO of the $C=O$ or $C=N$ partner through Lewis-acid binding or H-bonding, sometimes in a bifunctional fashion. For imines, stereocontrol typically arises from a chiral pocket around the activated $C=N$ together with a positioned P-nucleophile [358]. The first catalytic systems for the Pudovik reaction were often simple bases or Lewis acids. Alkali metal carbonates, for instance, were used to promote the reaction, though they often suffered from issues related to a competing uncatalyzed background reaction that could erode enantioselectivity in asymmetric variants [359]. Catalysts based on s-block metals, such as alkali and alkaline-earth metal amides, were also explored, but these systems frequently required high catalyst loadings or elevated temperatures and offered limited scope and selectivity [360].

A major breakthrough came with the development of chiral Lewis acid complexes, which enabled the first truly efficient asymmetric hydrophosphonylations. Chiral aluminum (III) complexes have proven to be exceptionally effective. Landmark systems include the aluminum complexes developed by Katsuki - salalen and the aluminum complexes reported by Feng - Schiff base [361, 362]. These catalysts operate through a Lewis acid mechanism, where the aluminum center activates the aldehyde. Crucially, they often function as bifunctional catalysts - the chiral ligand framework can engage in secondary interactions, such as hydrogen bonding, with the phosphite nucleophile, helping to organize the transition state and enforce high stereoselectivity [363].

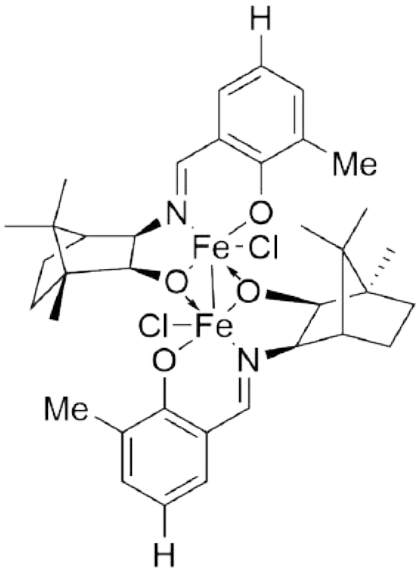
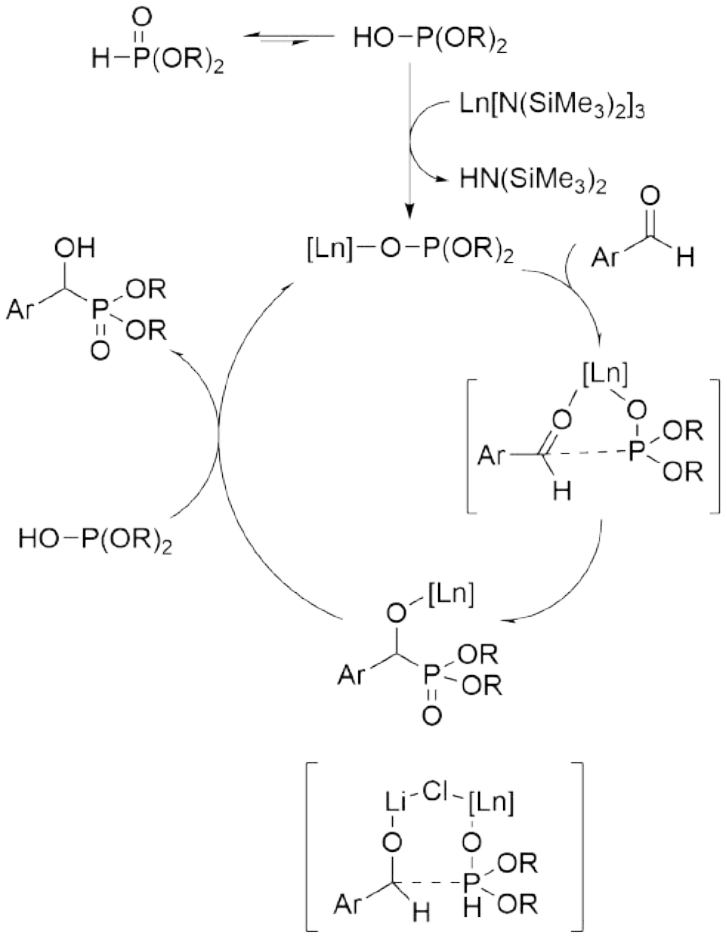


Figure 29. Structure of iron (III) complex with chiral Schiff base ligands which resulted in best yield and enantioselectivity [362]

Seeking more sustainable and practical catalysts, researchers developed systems based on earth-abundant and non-toxic metals. Iron (III) complexes with chiral Schiff base ligands (Figure 29) have emerged as a powerful alternative. These catalysts are advantageous as they are easily synthesized, inexpensive, and robust enough to function effectively under aerobic conditions. With catalyst loadings as low as 5 mol%, they can provide α-hydroxyphosphonates in excellent yields (up to 99%) and with outstanding enantioselectivities (up to 99% ee) [362].

Lanthanide-based catalysts have revolutionized the field by offering unprecedented levels of reactivity, allowing many hydrophosphonylation reactions to proceed under remarkably mild conditions. Complexes such as $3Ln(\mu - Cl)Li(THF)3$ are extraordinarily active catalysts. Mechanism proposed by Wu and the research team is presented on Scheme 47. For the hydrophosphonylation of aromatic aldehydes, these systems can achieve excellent yields - between 91 and 97% in mere minutes at room temperature with catalyst loadings as low as 0.1 mol% [134]. A key discovery was the crucial role of the lithium chloride adduct. This led to the proposal of a cooperative bimetallic mechanism where the lanthanide center acts as a Brønsted base to deprotonate the phosphite, while the smaller, sterically accessible lithium ion functions as a Lewis acid to coordinate and activate the aldehyde. This bifunctional activation within a single complex avoids steric clash and accounts for the dramatic rate enhancement [134]. The utility of lanthanides extends beyond amides. Lanthanide anilido complexes have been shown to efficiently catalyze the hydrophosphonylation of not only aldehydes but also more challenging, unactivated ketones [364]. Asymmetric variants using

chiral heterobimetallic lanthanoid-BINOL complexes (e.g., YbPB) have achieved nearly perfect enantioselectivity (up to 99% ee) in the hydrophosphonylation of cyclic imines [365]. In these systems, the concept of improved rigidity, achieved by using cyclic phosphites instead of acyclic ones, was shown to significantly enhance stereocontrol by pre-organizing the catalytic cycle [365].



Scheme 47. Mechanism of lanthanide amide-catalysed Pudovik reaction [362]

The last two decades have witnessed a paradigm shift towards organocatalysis, which avoids the use of potentially toxic and sensitive metals and often relies on robust, bench-stable small molecules. Many of the most successful organocatalytic systems for hydrophosphonylation converge on a common mechanistic principle: bifunctional activation. This strategy, where a single catalyst molecule simultaneously activates both the nucleophile and the electrophile through non-covalent interactions, has proven to be a powerful approach for achieving high reactivity and stereoselectivity. Chiral thioureas, particularly those derived from cinchona alkaloids, are effective bifunctional catalysts. The two $N-H$ protons of the thiourea moiety are strong hydrogen bond donors, capable of activating the electrophile - an imine or carbonyl and

lowering the energy of the transition state [366]. Simultaneously, a basic site integrated into the catalyst, such as the quinuclidine nitrogen of the cinchona alkaloid, acts as a Brønsted base to deprotonate the phosphite nucleophile. This concerted activation of both reaction partners within a single chiral complex is key to its efficiency [367].

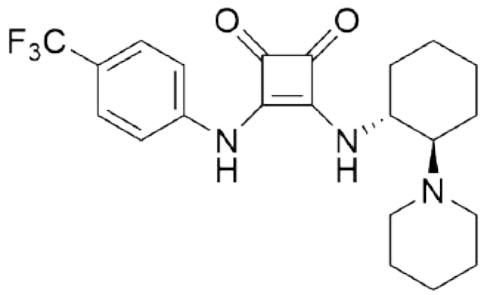
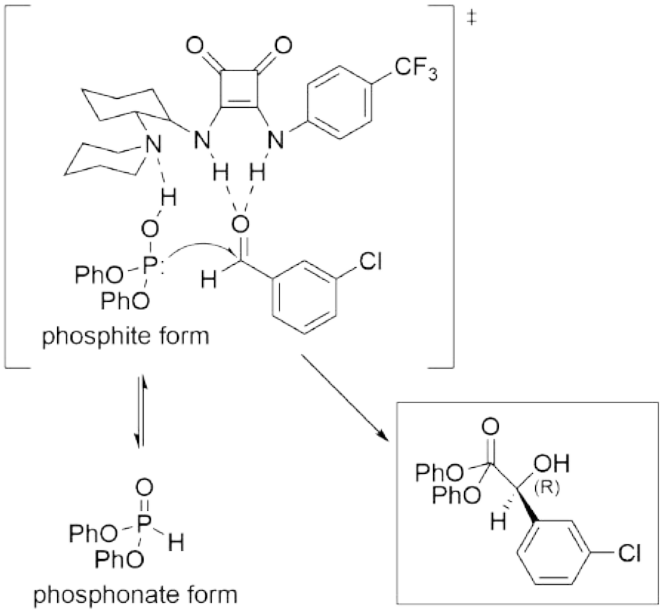


Figure 30. Example of squaramide used as catalyst for hydrophosphonylation [138]

Squaramides (example presented on Figure 30) have emerged as a superior class of hydrogen-bonding catalysts for this transformation. Their rigid, planar structure and the parallel orientation of their two N-H bonds make them exceptionally effective at dual hydrogen-bond activation of the electrophile. This pre-organized geometry often leads to higher reactivity and enantioselectivity compared to the more flexible thioureas [138]. Squaramide-based bifunctional catalysts have been instrumental in solving challenging problems, such as the first highly enantioselective hydrophosphonylation of N-unsubstituted ketimines, providing a direct, deprotection-free route to valuable primary α-aminophosphonates [368]. Alegre-Requena and co-workers [138] demonstrated that squaramide efficiently catalyzes the hydrophosphonylation reaction for a broad range of aldehydes, including both aromatic and aliphatic substrates. Mechanism proposed for this reaction is presented on Scheme 48. In most results, they obtained high yields ranging from 72–98% with reaction times of approximately 88–96 hours. The enantioselectivity of the reaction is good and typically lies around 80–85% ee. The best results were achieved for aromatic aldehydes, such as 4-nitrobenzaldehyde (88% ee), and significantly lower selectivity was observed for the aliphatic substrate $PhCH_2CH_2$ (68% ee). Limitations of the method include long reaction times, somewhat reduced enantioselectivity for certain aliphatic aldehydes, and mild yet demanding conditions, such as low temperature (–38 °C) and a high catalyst loading (20 mol%) [138].



Scheme 48. Mechanism of squaramide-catalysed hydrophosphonylation [138]

The development of axially chiral phosphoric acids derived from BINOL (1,1'-bi-2-naphthol) and SPINOL (1,1'-spirobiindane-7,7'-diol) by groups like Akiyama and Terada marked a seminal moment in organocatalysis [369, 370]. These compounds are strong Brønsted acids capable of protonating an imine to form a reactive iminium ion. The resulting bulky, chiral phosphate anion forms a tight, confined ion pair with the iminium cation, effectively shielding one face of the electrophile and directing the attack of the nucleophilic phosphite to the other. A highly organized, nine-membered transition state has been proposed, in which the catalyst acts bifunctionally: the acidic proton activates the imine, while a phosphoryl oxygen atom acts as a hydrogen-bond acceptor (a Brønsted base) to activate the phosphite nucleophile. This dual activation model accounts for the high enantioselectivities observed, particularly for aldimines [358, 371].

The asymmetric addition to aldehydes is a well-developed area. Aldehydes are highly reactive electrophiles, which presents both an opportunity and a challenge. The high reactivity means that an uncatalyzed background reaction can occur, potentially diminishing the enantioselectivity achieved by a chiral catalyst [359]. Therefore, an effective catalyst must not only be highly stereoselective but also fast enough to outcompete this background process. Both metal-based systems, such as Al(salalen) and Fe(Schiff base) complexes, and organocatalysts, particularly bifunctional squaramides, have proven capable of meeting this challenge, routinely providing α-hydroxyphosphonates with enantiomeric excesses well over 90% for a broad range of aromatic and aliphatic aldehydes [138, 361, 362].

The hydrophosphonylation of ketones is substantially more difficult than that of alde-

hydes. The increased steric hindrance around the carbonyl carbon and the ketone's lower intrinsic electrophilicity combine to make the reaction sluggish and challenging to control [359]. This substrate class represents a frontier in the field. Significant progress has been made using exceptionally active catalysts, such as the lanthanide anilido complexes, which can promote the addition to unactivated ketones [364]. Recently, specialized organocatalysts, such as diaminomethylenemalononitrile, have also been developed to tackle this difficult transformation, marking the first successful asymmetric hydrophosphonylation of ketones using organocatalysis [372].

2.4 Hydrophosphonylation - results and discussion on use of ecocatalysis

2.4.1 Methodology

2.4.1.1 Preparation of Eco-MgZnOx catalyst derived from *Arabidopsis halleri*

In this study, biomass from the plant *Arabidopsis halleri* collected from two distinct locations in Europe was used. The first batch of biomass was obtained from a region in Poland, near the Zn smelter of the Bolesław Mine and Metallurgical Plant, close to the city of Olkusz [373]. This area is highly industrialized and has significant levels of pollution. The second batch was sourced from a former industrial site in Auby, France, specifically from the Bois des Asturies area, which is also known for its heavy soil contamination [374].

The choice to use *A. halleri* in this research was driven by the plant's potential to contribute to new phytomanagement strategies. These strategies focus on the removal of metals from contaminated soils or their recovery from plant biomass. Finding practical applications for the metal-enriched biomass produced through phytoextraction is therefore a key goal.

The sampling included the metal-contaminated locations of *A. halleri* in southern Poland and northern France. The Polish location represents a low elevation site located in one of the most heavily industrialized regions of Poland, the vicinity of the Zn smelter of the Bolesław Mine and Metallurgical Plant near the city of Olkusz [373]. Accordingly, total soil Zn, Cd, and Pb concentrations at this sampling location are as much as 3911 ± 340, 1045 ± 115, 28 ± 3 mg kg^{-1}, respectively ([312]). In France, *A. halleri* plants were collected in a former industrial soil contaminated with zinc and cadm (7000 and

60 mg kg^{-1}, respectively) ([301]). *A. halleri* rosettes were collected from each location in early August 2019. The catalyst derived from the Polish biomass was labeled Eco-MgZnOx-P, while the one from the French biomass was called Eco-MgZnOx-F.

The preparation of the ecocatalyst starts with biomass collected from a metal-hyperaccumulating plant (here *Arabidopsis halleri*). The process involves several steps:

1. Drying and grinding - fresh biomass is first dried in 60 ℃ in an oven and then ground into smaller pieces.
2. Ashing - the dried material is subjected to thermal treatment at 550 ℃ for approximately 6 hours, which removes the organic fraction and yields mineral-rich ash.
3. Final grinding - the obtained ash is ground to produce a fine powder, which constitutes the ecocatalyst.

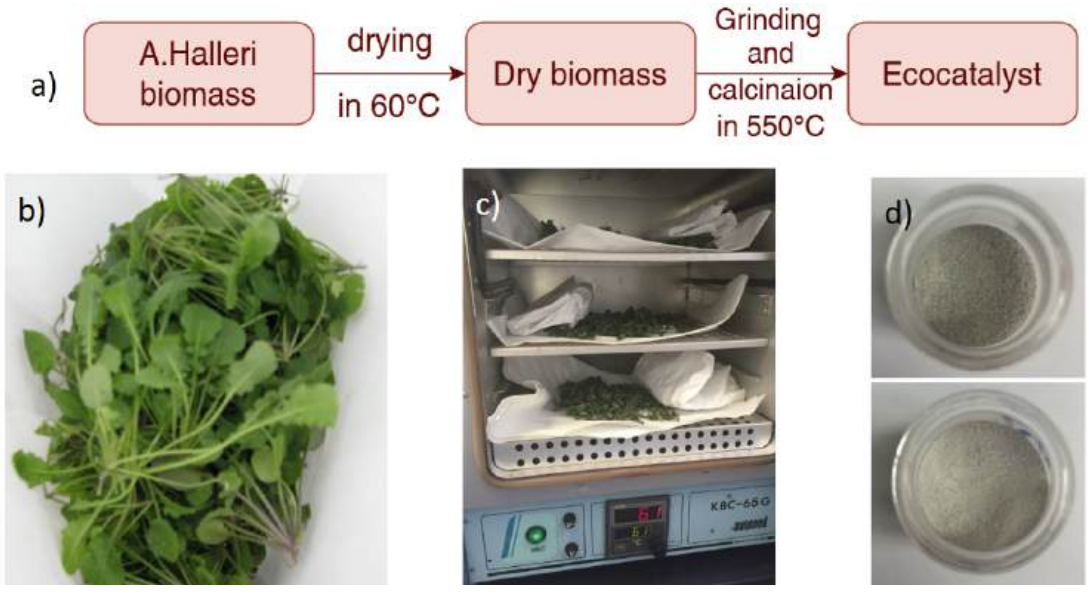


Figure 31. The catalyst preparation process.

The Figure 31 illustrates these process: (a) Schematic representation of the preparation process. (b) Fresh *A. halleri* biomass before drying. (c) Biomass placed in the oven for drying. (d) The final ecocatalyst in powdered form: Eco-MgZnO-F at the top and Eco-MgZnO-P at the bottom.

2.4.1.2 General procedure for the reactions

The reactions were carried out in glass screw-cap test tubes equipped with magnetic stirring bars. Unless otherwise specified, each reaction was performed on a 0.23 mmol scale, with the reagents added in a 1:1 molar ratio. A catalyst, when used, was weighed on an analytical balance and added in an amount corresponding to 5 mol%. For each experiment, three parallel samples were prepared: one containing eco-catalysts derived from the biomass of *A. halleri* plants from Poland (Eco-MgZnOx-P), second containing eco-catalysts derived from the biomass of *A. halleri* plants from France (Eco-MgZnOx-F) and a control sample without any catalyst, which served as a reference. During the course of the reactions, the mixtures were magnetically stirred. When heating was required, the test tubes were placed in a sand-filled heating block and maintained at the desired temperature under continuous stirring.

After the designated reaction time, the test tubes were removed from the heating plate and an appropriate solvent was added to wash the reaction mixture and separate it from the solid catalyst. The suspension was transferred into polypropylene centrifuge tubes, and then centrifuged to sediment the catalyst at the bottom of the tubes. The solvent was chosen so that no further reaction could occur and to ensure good solubility of both the substrates and the products. The supernatant, containing the reaction mixture dissolved in the solvent, was collected for further analysis and product isolation.

For product isolation, standard purification methods were applied. Depending on the physical state of the compounds, purification was achieved either by preparative thin-layer chromatography (for oily products) or by crystallization from diethyl ether/hexane mixtures (for solid products).

Figure 32 presents workflow of the reaction work-up.

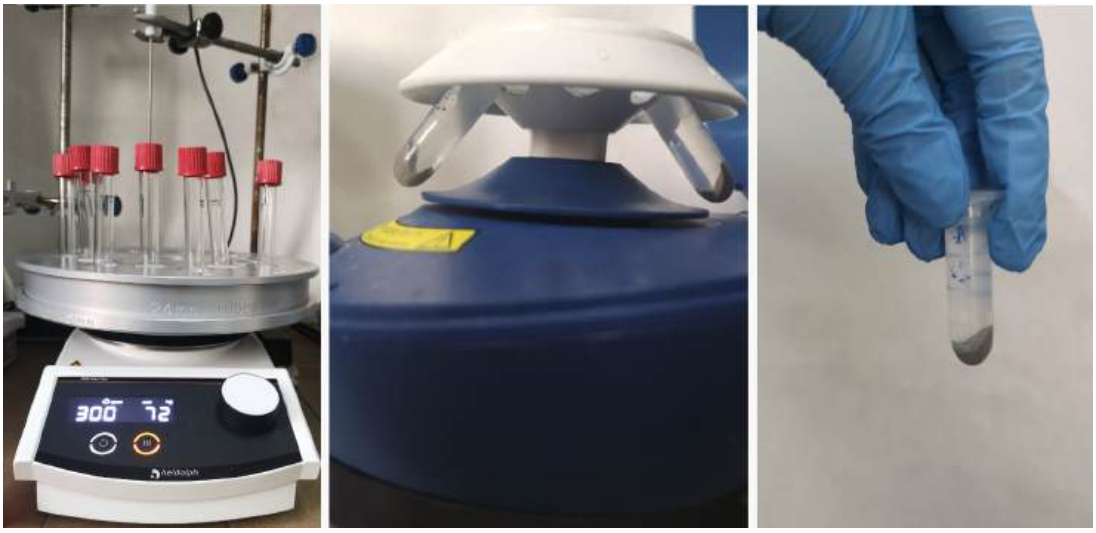


Figure 32. Stages of the experimental procedure. (Left) Reactions carried out in glass screw-cap test tubes equipped with magnetic stirring bars and heated in a sand-filled heating block. (Middle) Centrifugation of the reaction mixtures in polypropylene tubes to separate the solid catalyst. (Right) Reaction mixture after centrifugation, showing the catalyst sedimented at the bottom of the tube and the liquid phase containing the products and unreacted substrates.

2.4.1.3 Analysis of catalyst, reaction mixtures and products

A broad range of complementary analytical techniques was employed to thoroughly characterize the structure, composition, and morphology of the ecocatalysts Eco-MgZnOx-P and Eco-MgZnOx-F. These methods provided insights not only into the elemental and crystalline features of the fresh materials but also into their stability and possible transformations upon recovery and reuse.

Catalyst was analysed via Microwave Plasma-Atomic Emission Spectroscopy (MP-AES). The mineral composition of the catalysts was determined using an Agilent 4200 MP-AES spectrometer equipped with an SPS4 autosampler. This technique enabled the quantification of key elements, including Zn, Mg, Ca, Fe, K, Al, and Na, expressed as weight percentages. To ensure accuracy, samples were subjected to microwave-assisted digestion in reversed aqua regia, followed by filtration and dilution prior to analysis. MP-AES was also applied to assess the elemental composition of catalysts after recovery and reuse, providing information about potential leaching or compositional shifts during catalytic cycles.

Another method of catalyst analysis was X-ray Powder Diffraction (XRPD). Crystalline phases within the catalyst powders were identified using a BRUKER D8 Advance diffractometer with Cu Kα radiation. XRPD allowed for the determination of lattice parameters.

Direct imaging of catalyst particles was provided by High-Resolution Transmission

Electron Microscopy (HRTEM). It enables the visualization of both particle size and distribution.

Scanning Transmission Electron Microscopy with Energy Dispersive X-ray Spectroscopy (STEM-EDX) provided chemical composition mapping was carried out using a JEOL 2200 FS instrument operating at 200 kV, fitted with a Gatan Ultrascan CCD camera and an Oxford Instrument XMaxN 100 TLE EDX spectrometer. For sample preparation, catalyst powders were embedded in LR White resin and ultrathin sections were obtained using a Leica UC7 ultramicrotome.

Product obtained in the ecocatalyzed reactions were comprehensively characterized using standard spectroscopic and analytical methods to confirm their structures and purity: Melting points. Solid products were characterized by melting point determination using a Digimelt apparatus and the standard open capillary method. NMR spectroscopy. Nuclear magnetic resonance spectroscopy was carried out on a Jeol 400 yh instrument. Spectra included ^{1}H NMR (400 MHz, $CDCl_3$) for proton analysis, ^{13}C NMR (100 MHz, $CDCl_3$) for carbon skeleton elucidation, and ^{31}P NMR (243 MHz, $CDCl_3$) for phosphorus characterization. All spectra were referenced to residual solvent peaks. High-Resolution Mass Spectrometry (HRMS). The exact molecular masses of the products were determined using HRMS with electrospray ionization (ESI-TOF), ensuring precise confirmation of molecular formulas.

2.4.1.4 Modeling

Drawing on established methodologies where cluster models have successfully mimicked the active sites of metal oxides like MgO and ZnO, this study adopted a cluster-based approach [375, 376]. An MgO cluster with a 5x2x2 atomic arrangement was constructed to represent the oxide surface.

To simulate the mixed-metal nature of the ecocatalyst, this base MgO cluster was modified by substituting some magnesium atoms with other metals found in the catalyst, creating models for $(Mg_{0.9}Zn_{0.1})O$ and $(Mg_{0.9}Fe_{0.1})O$. The calculations employed the PBE0 hybrid functional, which has been shown to provide a good balance of accuracy and computational cost for reactions catalyzed by metal oxides. For simplicity and to manage calculation times, dimethyl H-phosphonate $(HP(O)(OMe)_2)$ was used as the model phosphonating agent instead of the diethyl ester used in experiments, as the ethyl group is not expected to significantly alter the core reactivity.

2.4.2 Composition and structure of the ecocatalyst

The elemental composition of both catalysts was analysed using Microwave Plasma-Atomic Emission Spectroscopy (MP-AES). Additionally, these catalysts were characterized using various advanced techniques including X-ray Powder Diffraction (XRPD), High-Resolution Transmission Electron Microscopy (HRTEM), Scanning Transmission Electron Microscopy (STEM), and Energy Dispersive X-ray Spectroscopy (STEM-EDX) mapping.

Table 20 shows the mineral composition of Eco-MgZnOx catalysts obtained with *A. halleri* from France (Eco-MgZnOx-F) and Poland (Eco-MgZnOx-P). The applied thermal treatment under air flow leads to a high loss of organic matter (90% to 95% of mass loss) and to a high concentration of mineral residues. Zn concentrations are high and are almost the same in Eco-MgZnOx-F from France (9.89 wt%) and Eco-MgZnOx-P from Poland (11.44 wt%), which confirms the ability of this species to hyperaccumulate zinc. It should be noted that the average Cd concentration remains below 0.2 wt% for both locations. This observation is particularly interesting, considering that Zn-hyperaccumulating plants are often able to coaccumulate cadm in elevated concentrations; however, toxicity is problematic. Mineral compositions of Eco-MgZnOx-F and Eco-MgZnOx-P catalysts are very similar, except for the magnesium content. Eco-MgZnOx-P exhibits twice the amount of Mg when compared to Eco-MgZnOx-F (respectively, 5.24 wt% and 2.64 wt%).

Table 20. Mineral composition of Eco-MgZnOx catalysts determined by MP-AES analyses (wt %) with relative standard deviation percentage (±% RSD, triplicate).

Eco-MgZnOx	Al	Ca	Cd	Fe	K	Mg	Na	Zn
EcoMgZnOx-P								
wt %	0.05	16.71	0.18	0.08	14.41	**5.24**	0.08	**11.44**
%RSD	0.31	0.63	0.72	0.5	0.33	0.39	0.61	0.61
EcoMgZnOx-F								
wt %	0.19	13.95	0.09	0.34	11.53	**2.64**	0.14	**9.89**
%RSD	0.63	1.32	2.37	4.41	1.39	0.19	0.77	0.41

Figure 33 presents the results of the X-ray powder diffraction (XRPD) analysis of Eco-MgZnOx, which was performed to identify metallic species under crystalline form. The XRPD diffractograms of Eco-MgZnOx-P and Eco-MgZnOx-F highlighted the complexity of the samples with a large number of phases (9 in total) as expected for biomass. Both Eco-MgZnOx-F and Eco-MgZnOx-P catalysts clearly exhibited the presence of $CaCO_3$ and K_2SO_4. Very interestingly, a $Mg_{0.88}Zn_{0.12}O$ phase was also observed in both cases and particularly clearly in Eco-MgZnOx-P. This compound is an

isotype of periclase MgO, but the lattice parameter is significantly larger. The diffractogram allowed for determining a parameter equal to 4.232 Å instead of 4.213 Å, which is the lattice parameter of pure MgO. This modification of the structure can easily be explained by the substitution of Mg atoms by Zn atoms, which have a larger atomic radius. The formation of magnesium oxide would be very surprising at 550 °C considering that its standard formation temperature is above 800 °C. Interestingly, the presence of additional metallic species (Zn, Fe) could enhance the reactivity of MgO [374, 377]. Diffractograms showed the expected presence of ZnO, K_2ZnSiO_4, and $ZnSiO_3$, which are zinc silicates and used as antireflection coatings [378].

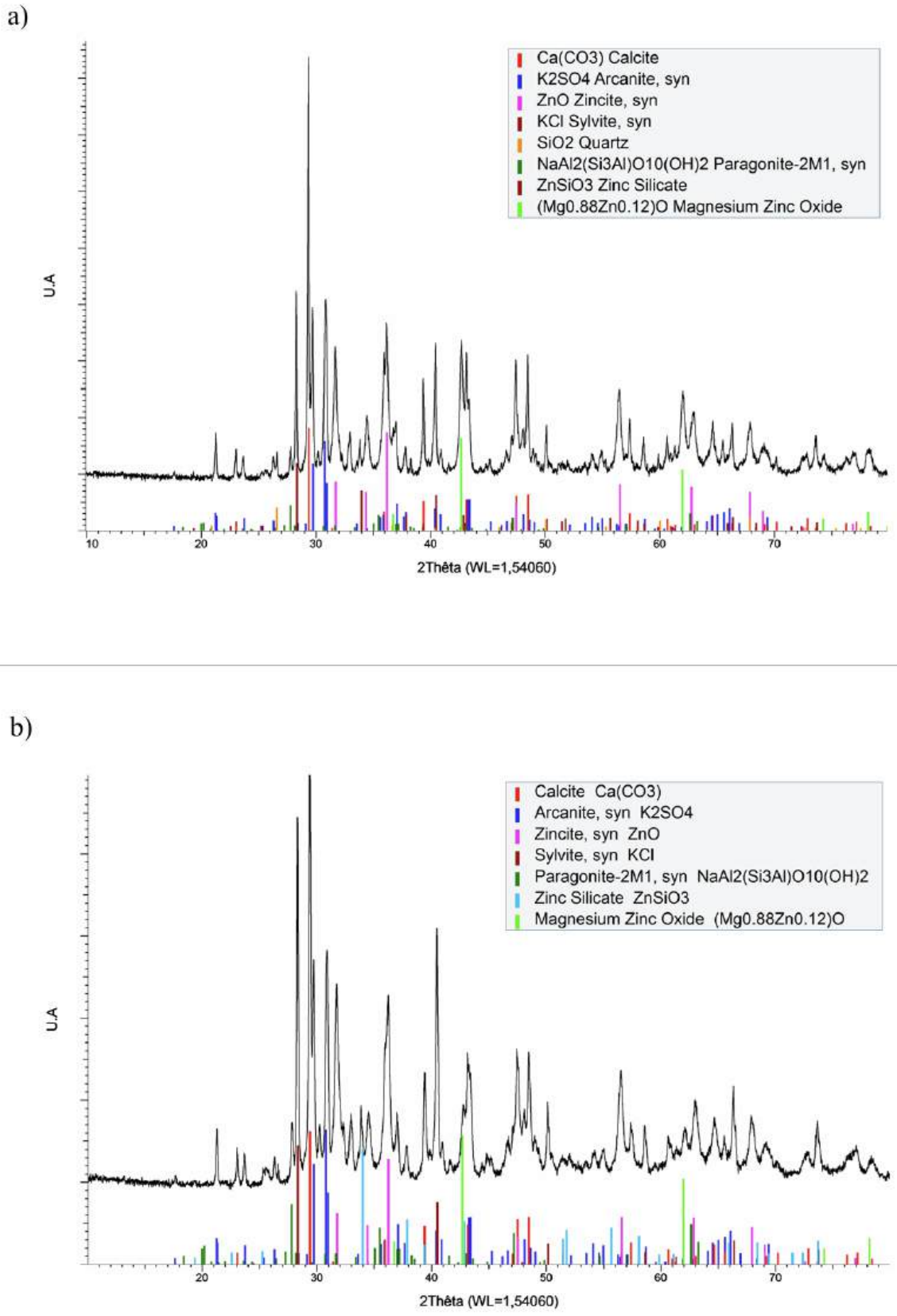


Figure 33. XRPD diffraction pattern of a) Eco-MgZnOx-P and b) Eco-MgZnOx-F

High-resolution transmission electron microscopy (HRTEM) images of Eco-

MgZnOx are presented in the Figure 34. In both Eco-MgZnOx-P (a) and Eco-MgZnOx-F (b), the material is composed of two distinct particle populations. Larger particles, ranging from 100 to 600 nm, form irregular aggregates, while much smaller spherical nanoparticles of 10-50 nm are distributed in close association with them. In Eco-MgZnOx-P, the smaller particles appear mostly embedded within the larger calcite grains, producing dense clusters with a heterogeneous texture. In contrast, Eco-MgZnOx-F shows a more dispersed arrangement, where the nanosized particles are more clearly separated from the larger calcite domains, often forming cloud-like distributions around them.

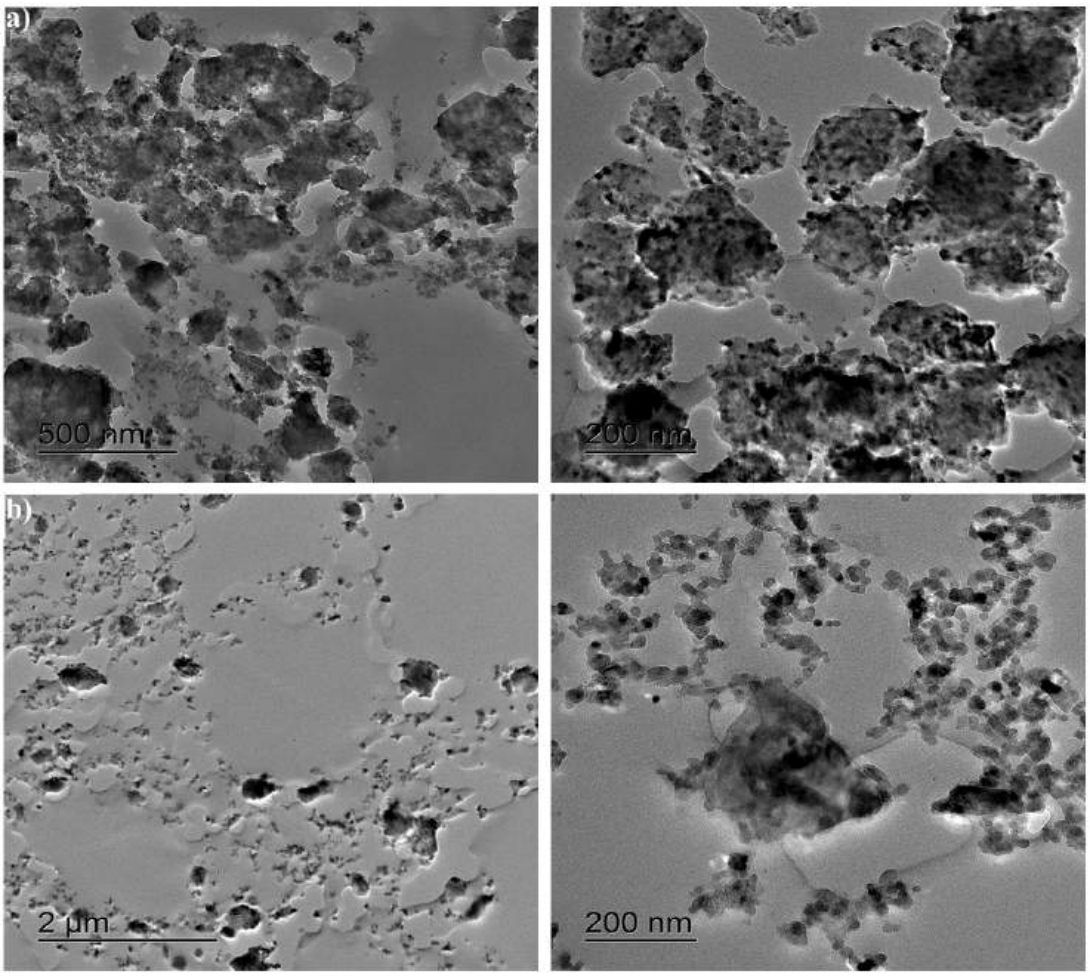


Figure 34. HRTEM images of a) Eco-MgZnOx-P and b) Eco-MgZnOx-F embedded in resin

The elemental composition was examined by scanning transmission electron microscopy coupled with energy-dispersive X-ray spectroscopy (STEM-EDX) (Figure 35). In both Eco-MgZnOx-P and Eco-MgZnOx-F, the larger particles are dominated by Ca and O, corresponding to calcite. For Eco-MgZnOx-F, the EDX maps highlight that calcite also acts as a substrate on which smaller Mg- and Zn-containing particles are deposited, further supporting the more open and separated morphology observed in

the HRTEM images. Overlay images reveal that the nanosized fraction is mainly composed of Mg, Zn, and O, with only minor traces of Fe. This agrees with MP-AES data (Table 20), which confirmed that iron is present only in very low amounts. The poor contrast of Fe in the STEM images is consistent with its trace-level abundance.

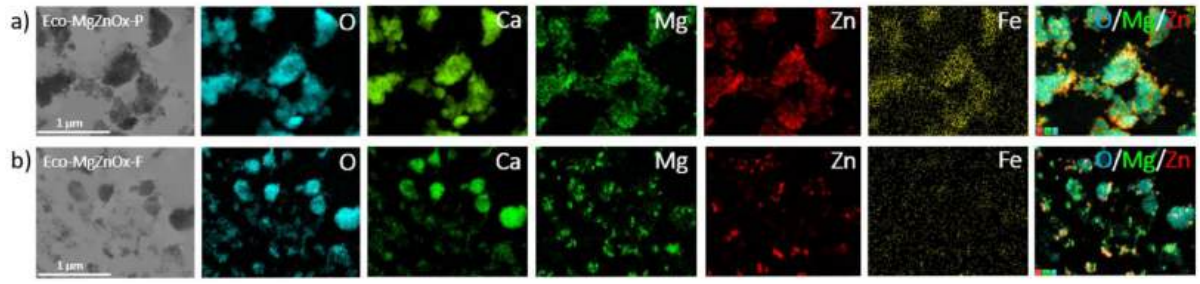


Figure 35. STEM-bright field images of a) Eco-MgZnOx-P and b) Eco-MgZnOx-F. Oxygen, calcium magnesium, zinc and iron elemental STEM-EDX mapping as well as oxygen/magnesium/zinc superposition.

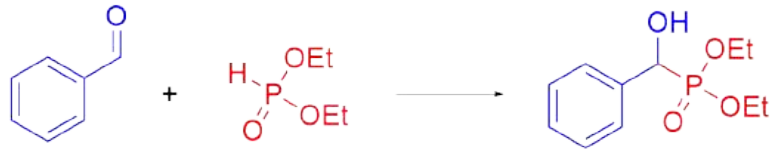
Taken together, these observations confirm that Eco-MgZnOx consists of a composite of large calcite particles and smaller nanoparticles of mixed magnesium oxides, primarily $MgO \cdot ZnO$ with minor contributions from $MgO \cdot FeO$. The structural differences between the two materials lie mainly in the degree of dispersion of the nanosized particles: in Eco-MgZnOx-P they are mostly embedded within calcite grains, whereas in Eco-MgZnOx-F they are more distinct and separated from the larger calcite matrix.

2.4.3 Optimization results of the hydrophosphonylation

The model substrates used for hydrophosphonylation optimization were benzaldehyde (**1a**) and diethyl H-phosphonate (**2a**). The reaction scheme is included in the first row of Table 21. A series of experiments was conducted. Based on the reaction mechanism generally accepted for the hydrophosphonylation reaction, the Eco-MgZnOx could be considered as plurifunctional catalyst. Firstly, the presence of Mg species with basic character should be responsible for activation of the H-phosphonate and formation of a phosphanion (phosphite form). Secondly, the presence of Zn species with Lewis acid character could be responsible for the activation of the carbonyl carbon making it more electrophilic and prone to reaction with phosphorus nucleophile. The simultaneous activation of both substrates can also be envisaged. Initially, the reaction was carried out without a solvent, which proved to be the best choice, as reactions conducted in organic solvents (toluene, ethyl acetate, dichloromethane) did not yield the expected products. Additionally, reactions performed at room temperature resulted in poor to moderate conversion, depending on the reaction time. The variables in the

optimization of eco-catalyst-catalyzed reactions included the presence of a solvent, temperature, reaction time, and the amount of catalyst used. Results are summarized in the Table 21.

Table 21. Preparation of hydroxyphosphonates (Pudovik reaction) - optimization of reaction conditions for model substrates.[a]



1a 2a 3a

Entry	T [°C]	t [h]	Conversion without catalyst[b]	Conversion[b] with EcoCatalyst	
				PL	FR
1	RT	96	8%	93%[e]	97%[f]
2	50	24	19%	97%[e]	100%[f]
3	RT	24	0%[c]	86%[ec]	80%[fc]
4	50	3	2%	93%[e]	100%[f]
5	50	1	0%	76%[e]	80%[f]
6	RT	1	0%	28%[e]	22%[f]
7	50	2.5	0%[d]	65%[ed]	68%[fd]
8	50	3	0%	73%[g]	100%[h]
9	50	3	0%[d]	100%[id]	99%[jd]
10	50	3	0%	47%[k]	0%[l]

a Reaction conditions: aldehyde (0.23 mmol), H-phosphonate (0.23 mmol),
b determined by ^{31}P NMR.
c an average value from 3 experiments.
d an average value from 2 experiments.
e 30 mg of Eco-MgZnOx-P: Mg (28.0 mol%), Ca (54.4 mol%), Zn (22.8 mol%).
f 30 mg of Eco-MgZnOx-F: Mg (14.0 mol%), Ca (45.6 mol%), Zn (19.6 mol%).
g 15 mg of Eco-MgZnOx-P: Mg (14.0 mol%), Ca (27.2 mol%), Zn (11.4 mol%).
h 15 mg of Eco-MgZnOx-F: Mg (7.0 mol%), Ca (22.8 mol%), Zn (9.8 mol%).
i 7.5 mg of Eco-MgZnOx-P: Mg (7.0 mol%), Ca (13.6 mol%), Zn (5.7 mol%).
j 7.5 mg of Eco-MgZnOx-F: Mg (3.5 mol%), Ca (11.4 mol%), Zn (4.9 mol%).
k 1.5 mg of Eco-MgZnOx-P: Mg (1.4 mol%), Ca (2.7 mol%), Zn (1.1 mol%).
l 1.5 mg of Eco-MgZnOx-F: Mg (0.7 mol%), Ca (2.3 mol%), Zn (1.0 mol%).
RT room temperature.

Initially, reaction was performed under solventless conditions, and this resulted in the best choice. The reaction proceeded readily at room temperature but with poor to moderate conversions depending on the reaction time (28% and 80% after 1 h and 24 h, respectively). When heating was applied, conversions were greatly improved and reaction time was limited to only 3h. Importantly, reactions without the plant-based catalysts did not produce any desired α-hydroxyphosphonate.

To sum up, the optimal conditions were determined to be a temperature of 50℃, a reaction time of 3 hours, and an eco-catalyst amount of 5 mol% based on zinc content. For Eco-MgZnOx-P, this corresponds to 7.0 mol% Mg, 13.6 mol% Ca and 5.7 mol% Zn, while for Eco-MgZnOx-F, it corresponds to 3.5 mol% Mg, 11.4 mol% Ca, and 4.9 mol% Zn.

The conversion of the crude reaction mixtures was monitored by ^{31}P NMR spectroscopy on a Jeol 400 yh instrument, which served as a direct and quantitative probe of phosphorus-containing species.

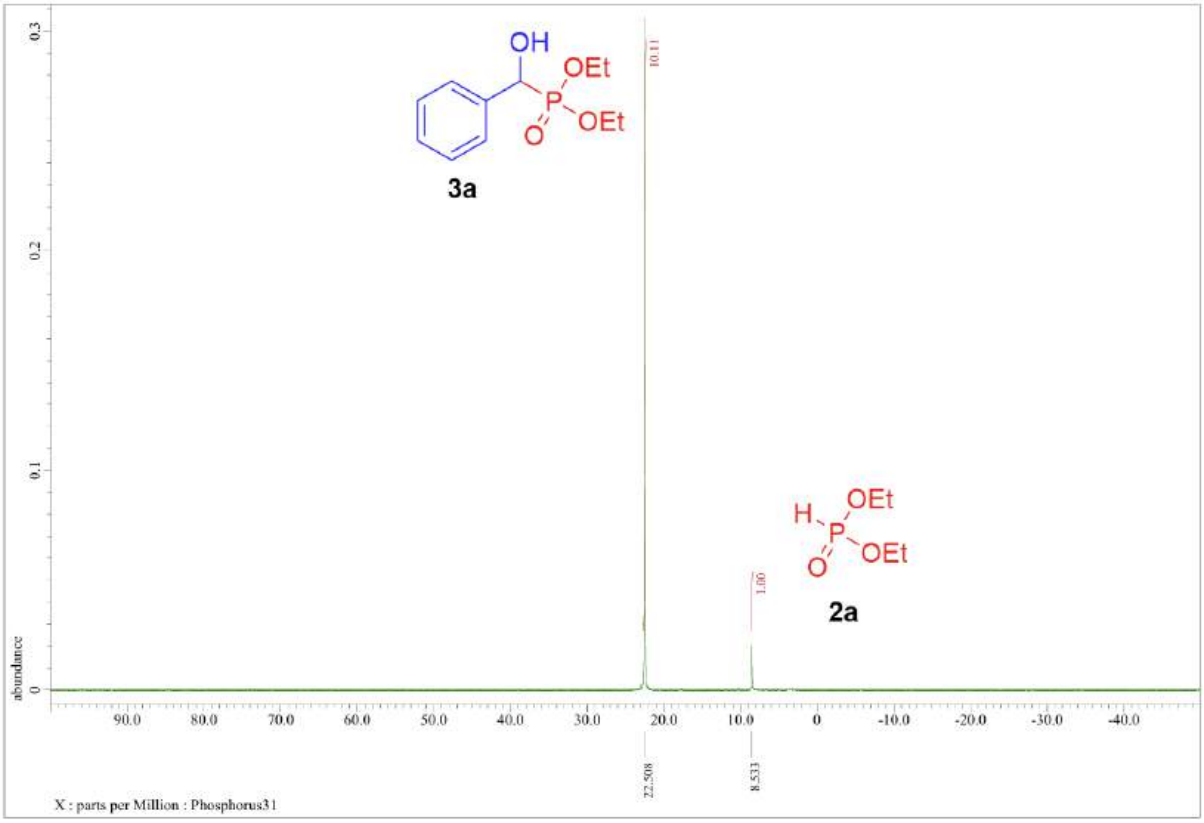


Figure 36. $^{3}1$P NMR spectrum (243 MHz, $CDCl_3$) of crude reaction mixture after the reaction of benzaldehyde with diethyl H-phosphonate.

In the ^{31}P NMR spectrum of the crude mixture, which is presented on the Figure 36, two distinct regions can be assigned unambiguously - signals at 7-9 ppm corresponding to the *H*-phosphonate substrate and signals at 15-25 ppm corresponding to the α-hydroxyphosphonate product. The assignments were verified by recording the spectrum of the pure substrate.

Since one mole of substrate yields one mole of product upon complete conversion, the integrated areas of these signals are directly proportional to their molar ratios in the mixture. The conversion can therefore be calculated according to the following expressions:

$$\text{Product fraction} = \frac{I_{\text{product}}}{I_{\text{product}} + I_{\text{substrate}}},$$

$$\text{Conversion (\%)} = \frac{I_{\text{product}}}{I_{\text{product}} + I_{\text{substrate}}} \times 100,$$

$$\text{Unreacted substrate (\%)} = \frac{I_{\text{substrate}}}{I_{\text{product}} + I_{\text{substrate}}} \times 100,$$

where I_{product} and $I_{\text{substrate}}$ are the integrated peak areas corresponding to the product and substrate, respectively.

In the spectrum shown, the substrate signal at $\delta = 8.533$ ppm was normalized to $I_{\text{substrate}} = 1.00$, while the integral of the product region (15–25 ppm) was $I_{\text{product}} = 10.11$. Thus, the total integral is:

$$I_{\text{total}} = I_{\text{substrate}} + I_{\text{product}} = 1.00 + 10.11 = 11.11.$$

The molar fractions are then:

$$\text{Product fraction} = \frac{10.11}{11.11} = 0.910 \quad \Rightarrow \quad 91.0\%,$$

$$\text{Substrate fraction} = \frac{1.00}{11.11} = 0.090 \quad \Rightarrow \quad 9.0\%.$$

Therefore, the conversion of the example reaction, presented above, as determined from the ^{31}P NMR spectrum, was calculated to be **91.0%**.

The next step involved conducting tests to compare the performance of eco-catalysts with that of commercially available metal oxides. Tests were conducted in optimal conditions. Hydrophosphonylation reactions were carried out using ZnO, MgO, CaO, and $CaCO_3$, as well as a mixture of MgO+ZnO in quantities corresponding to the content of these oxides in Polish and French eco-catalysts, what is summarized in the Table 22. Calcium oxide cannot be included in the final composition of the catalyst due to the mild conditions required for its preparation, and calcium carbonate showed no catalytic activity for the reaction under study; therefore, calcium was excluded from further consideration.

Table 22. Preparation of hydroxyphosphonates (Pudovik reaction) with commercial available compounds as catalysts[a]

Entry	Ecocatalyst	Conversion (%)
1	ZnO[a]	14%
2	MgO[b]	70%
3	ZnO + MgO[c]	78%
4	FeO + MgO[d]	70%
5	FeO + MgO + ZnO[e]	78%
6	K_2CO_f[j]	61%
7	$CaCO_3$[g]	0%

a 5.7 mol% of Zn.

b 7.0 mol% of Mg.

c 5.7 mol% of Zn and 7.0 mol% of Mg.

d 0.05 mol% of Fe and 7.0 mol% of Mg

e 0.05 mol% of Fe, 7.0 mol% of Mg and 5.7 mol% of Zn

f 12.0 mol% of K

g 5.0 mol% of Ca

The results obtained with commercially available oxides were less favorable compared to those achieved with the ecocatalysts. Catalysis with zinc oxide resulted in a 14.5% conversion, with magnesium oxide 69%, and with the ZnO+MgO mixture 76%. It was determined that the use of eco-catalysts leads to better conversion values due to the synergistic effect of the catalytic activities of various metals, with zinc oxide and magnesium oxide playing a significant role.

Subsequently optimization studies were conducted for other substrates: carbonyl compounds, including aliphatic and heteroaromatic aldehydes and ketones, and various H-phosphonates.

The carbonyl substrate for which next optimization studies were conducted was isobutyraldehyde, a representative of aliphatic aldehydes. The reaction scheme is included in the Table 23. The starting point was the optimal conditions obtained for the model reaction with an aromatic aldehyde, but adjustments were necessary as the conversions achieved under those conditions were not sufficiently high. Results are summarized in the Table 23.

Table 23. Pudovik reaction - optimization of reaction conditions, screening of aldehyde scope - aliphatic substrate (**1f**)[a]



1f **2a** **3f**

Entry	T [℃]	t [h]	Catalyst	Conversion[b]	Conversion[b] with EcoCatalyst		Solvent
					PL	FR	
1	50	3	-	0%	70%[e]	79%[f]	None
2	50	5	-	0%	79%[e]	59%[f]	None
3	70	3	-	0%	97%[e]	93%[f]	None
4	50	3	-	0%	75%[g]	85%[h]	None
5	70	3	-	0%	83%[c]	73%[d]	None
6	70	3	ZnO[i]	18%	-	-	None
7	70	3	CaO[j]	99.7%	-	-	None

[a] Reaction conditions: aldehyde (0.23 mmol), H-phosphonate (0.23 mmol)
[b] determined by ^{31}P NMR.
[c] 7.5 mg of Eco-MgZnOx-P: Mg (7.0 mol%), Ca (13.6 mol%), Zn (5.7 mol%).
[d] 7.5 mg of Eco-MgZnOx-F: Mg (3.5 mol%), Ca (11.4 mol%), Zn (4.9 mol%).
[e] 15 mg of Eco-MgZnOx-P: Mg (14.0 mol%), Ca (27.2 mol%), Zn (11.4 mol%).
[f] 15 mg of Eco-MgZnOx-F: Mg (7.0 mol%), Ca (22.8 mol%), Zn (9.8 mol%).
[g] 30 mg of Eco-MgZnOx-P: Mg (28.0 mol%), Ca (54.4 mol%), Zn (22.8 mol%).
[h] 30 mg of Eco-MgZnOx-F: Mg (14.0 mol%), Ca (45.6 mol%), Zn (19.6 mol%).
[i] 20.0 mol% of Zn.
[j] 20.0 mol% of Mg.

Subsequently, it was tested whether the conditions optimized for the model reaction were also optimal for another H-phosphonate, specifically dibutyl H-phosphonate. Table 24 presents reaction scheme and summary of the results.

Table 24. Pudovik reaction - optimization of reaction conditions, screening of H-phosphonate scope.[a]



1a 2b 4a

Entry	T [°C]	t [h]	Conversion without catalyst[b]	Conversion[b] with EcoCatalyst PL	Conversion[b] with EcoCatalyst FR
1	50	3	0%	94%[c]	91%[d]
2	50	3	0%	100%[e]	92%[f]
3	50	3	0%	0%[g]	0%[h]

[a] Reaction conditions: aldehyde (0.23 mmol), H-phosphonate (0.23 mmol)
[b] determined by ^{31}P NMR.
[c] 15 mg of Eco-MgZnOx-P: Mg (14.0 mol%), Ca (27.2 mol%), Zn (11.4 mol%).
[d] 15 mg of Eco-MgZnOx-F: Mg (7.0 mol%), Ca (22.8 mol%), Zn (9.8 mol%).
[e] 7.5 mg of Eco-MgZnOx-P: Mg (7.0 mol%), Ca (13.6 mol%), Zn (5.7 mol%).
[f] 7.5 mg of Eco-MgZnOx-F: Mg (3.5 mol%), Ca (11.4 mol%), Zn (4.9 mol%).
[g] 1.5 mg of Eco-MgZnOx-P: Mg (1.4 mol%), Ca (2.7 mol%), Zn (1.1 mol%).
[h] 1.5 mg of Eco-MgZnOx-F: Mg (0.7 mol%), Ca (2.3 mol%), Zn (1.0 mol%).

The next optimization involved a different carbonyl substrate, a heteroaromatic aldehyde as optimal conditions for model reaction was not enough for those substrates as well. 3-pyridinecarboxaldehyde was an example for this optimization. Table 25 presents reaction scheme and summary of the results.

Table 25. Pudovik reaction - optimization of reaction conditions, screening of aldehyde scope - heterocyclic aldehyde.[a]



1j 2a 3j

Entry	T [℃]	t [h]	Catalyst	Conversion[b]	Conversion[b] with EcoCatalyst	
					PL	FR
1	50	3	-	2.6%	78%[c]	94%[d]
2	70	3	-	12%	95%[c]	100%[d]
3	70	3	ZnO[e]	63%	-	-
4	70	3	CaO[f]	79%	-	-

a Reaction conditions: aldehyde (0.23 mmol), H-phosphonate (0.23 mmol)
b determined by ^{31}P NMR.
c 7.5 mg of Eco-MgZnOx-P: Mg (7.0 mol%), Ca (13.6 mol%), Zn (5.7 mol%).
d 7.5 mg of Eco-MgZnOx-F: Mg (3.5 mol%), Ca (11.4 mol%), Zn (4.9 mol%).
e 20.0 mol% of Zn.
f 20.0 mol% of Ca.

The final step was the optimization for another carbonyl substrate, this time a ketone, with acetophenone serving as the example. Table 26 presents reaction scheme and summary of the results.

Table 26. Pudovik reaction - optimization of reaction conditions, screening of carbonyl compound scope - ketone.[a]



1n **2a** **3n**

Entry	T [℃]	t [h]	Catalyst	Conversion[b]	Conversion[b] with EcoCatalyst	
					PL	FR
1	50	21	-	0%	66%[c]	52%[d]
2	100	21	-	0%	6.2%[c]	16.2%[d]
3	50	117	-	3.5%	78%[c]	49%[d]
4	50	8.5	-	0%	23%[c]	20%[d]
5	50	8.5	-	0%	22%[e]	28%[f]
6	70	9	-	0%	30%[e]	43%[f]
7	70	21	-	0%	39%[e]	46%[f]
8	70	9	-	0%	44%[g]	71%[h]
9	70	21	-	3%	35%[g]	37%[h]
10	70	9	-	-	-	-
11	70	9	ZnO (20 mol% Zn)	-	-	-
12	70	9	CaO (20 mol% Ca)	-	-	-

a Reaction conditions: ketone (0.23 mmol), H-phosphonate (0.23 mmol)
b determined by ^{31}P NMR.
c 30 mg of Eco-MgZnOx-P: Mg (28.0 mol%), Ca (54.4 mol%), Zn (22.8 mol%).
d 30 mg of Eco-MgZnOx-F: Mg (14.0 mol%), Ca (45.6 mol%), Zn (19.6 mol%).
e 7.5 mg of Eco-MgZnOx-P: Mg (7.0 mol%), Ca (13.6 mol%), Zn (5.7 mol%).
f 7.5 mg of Eco-MgZnOx-F: Mg (3.5 mol%), Ca (11.4 mol%), Zn (4.9 mol%).
g 15 mg of Eco-MgZnOx-P: Mg (14.0 mol%), Ca (27.2 mol%), Zn (11.4 mol%).
h 15 mg of Eco-MgZnOx-F: Mg (7.0 mol%), Ca (22.8 mol%), Zn (9.8 mol%).
i 20.0 mol% of Zn.
j 20.0 mol% of Ca.

For aliphatic and heteroaromatic aldehydes, it was necessary to increase the temperature to 70 ℃. The reaction with ketones was also feasible, but it required extending the reaction time to 20 hours and doubling the amount of catalyst. However, the reaction with the ketone did not achieve conversions close to 100%, as was the case with aldehydes. Despite this, the successful formation of the product from the ketone can still be considered an achievement. On the other hand, the use of H-phosphonates other than diethyl H-phosphonate did not affect the optimal conditions. The sum up is presented in the Table 27.

Table 27. Reaction conditions for different carbonyl substrates.

Carbonyl Substrate	Temperature	Time	Catalyst
Aromatic Aldehydes	50℃	3h	Eco-MgZnOx-P^a Eco-MgZnOx-F^b
Aliphatic Aldehydes	70℃	3h	Eco-MgZnOx-P^a Eco-MgZnOx-F^b
Heteroaromatic Aldehydes	70℃	3h	Eco-MgZnOx-P^a Eco-MgZnOx-F^b
Ketones	70℃	20h	Eco-MgZnOx-P^c Eco-MgZnOx-F^d

a 7.5 mg of Eco-MgZnOx-P: Mg (7.0 mol%), Ca (13.6 mol%), Zn (5.7 mol%).

b 7.5 mg of Eco-MgZnOx-F: Mg (3.5 mol%), Ca (11.4 mol%), Zn (4.9 mol%).

c 15 mg of Eco-MgZnOx-P: Mg (14.0 mol%), Ca (27.2 mol%), Zn (11.4 mol%).

d 15 mg of Eco-MgZnOx-F: Mg (7.0 mol%), Ca (22.8 mol%), Zn (9.8 mol%).

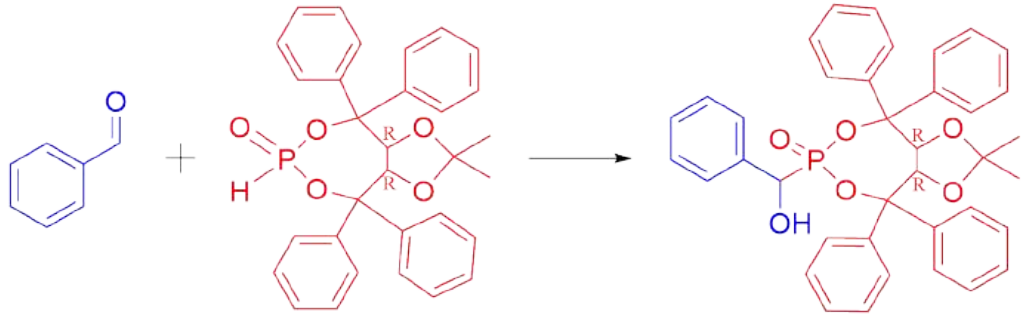
2.4.3.1 Optimization results of the hydrophosphonylation with an optically active substrate

To identify the optimal conditions for the hydrophosphonylation reaction with an optically active phosphite, a series of experiments was performed with different temperatures, catalyst loadings, reaction times, and stoichiometric ratios. The primary goal was to maximize both conversion and stereoselectivity of the reaction, while minimizing the influence of side processes observed in the uncatalyzed pathway or in the presence of simple bases such as Et_3N. Control reactions without catalyst (0) and with Et_3N were included to establish reference points. Particular focus was placed on catalysts P and F, which were systematically tested under varied conditions in order to establish how reaction temperature, time, and aldehyde excess influence conversion and stereoselectivity.

The reaction scheme and results of these optimization studies are summarized in Table 28.

The reference experiments without catalyst and with Et_3N demonstrate that the hydrophosphonylation can proceed either not at all (no catalyst) or in a fast but poorly selective manner (Et_3N). These controls underline the importance of using designed catalysts (P and F) to achieve both high conversion and stereoselectivity.

Table 28. Optimization of the hydrophosphonylation with optically active H-phosphonate with Eco-Catalysts.



Entry	T [°C]	t [h]	Conv./Ratio[a] no catalyst	Conv./Ratio[a] Et_3N	Conv./Ratio[a,b] with EcoCatalyst PL	FR
1	50	3	0% / –	–	27%[d] / 1:4.6	27%[e] / 1:4.8
2[i]	50	3	17% / 1:1.9	–	48%[d] / 1:3.6	30%[e] / 1:3.2
3[j]	60	3	93% / 1:2.2	–	100%[f] / 1:4.2	100%[g] / 1:4.8
4[k]	50	3	69% / 1:2.2	–	100%[d] / 1:5.3	–
5[k]	RT	3	7% / 1:2.4	–	100%[d] / 1:4.4	–
6[k]	0	3	0% / –	100%[h] / 1:2.0	0%[d] / –	–
7	0	96	10% / 1:3.5	100%[h] / 1:2.0	85%[d] / 1:7.8	–
8[l]	0	96	–	–	100%[d] / 1:3.1	100%[e] / 1:3.1
9	0	96	–	–	90%[d] / 1:0.0	89%[e] / 1:0.0
10	0	96	–	–	92%[d] / 1:8.0	91%[e] / 1:7.9

a Determined by ^{31}P NMR.
b Diastereomeric ratio of product (major:minor).
d 7.5 mg of Eco-MgZnOx-P: Mg (28.0 mol%), Ca (54.4 mol%), Zn (22.8 mol%).
e 7.5 mg of Eco-MgZnOx-F: Mg (14.0 mol%), Ca (45.6 mol%), Zn (19.6 mol%).
f 15 mg of Eco-MgZnOx-P: Mg (14.0 mol%), Ca (27.2 mol%), Zn (11.4 mol%).
g 15 mg of Eco-MgZnOx-F: Mg (7.0 mol%), Ca (22.8 mol%), Zn (9.8 mol%).
h 7.5 mg of Et_3N, used as a reference.
i Smaller reactors were used
j Aldehyde were used in excess.
k Aldehyde were used in 4-fold excess.
l H-phosphonate S,S were used.

Catalyst Eco-MgZnOx-P consistently gave the highest activity across a wide temperature range. For example, already at 50°C with 5 mol% and a 4-fold excess of aldehyde (entry 4), full conversion was achieved with a ratio of 1:5.3. At room temperature, P maintained 100 % conversion (entry 5), whereas the blank experiment under the same conditions only reached 7%. This highlights the robustness of P compared to the background pathway.

Catalyst Eco-MgZnOx-F showed a performance similar to Eco-MgZnOx-P in terms of conversion, though typically with slightly lower selectivity. Both catalysts benefited

significantly from excess aldehyde and from longer reaction times at lower temperatures.

A key trend is that lower temperature improves stereoselectivity, but at the cost of longer reaction times. For instance, entry 7 (0℃, 96 h) with P gave 85% conversion and the highest selectivity ratio (1:7.8). This demonstrates that stereocontrol is maximized under kinetic conditions, although conversion is incomplete.

The best overall outcome was obtained in entry 9 and 10 (0℃, 96 h, 5 mol% of P or F), where both catalysts reached very high conversion - 90% for P, 89% for F, combined with outstanding stereoselectivity. This condition represents the optimal compromise between conversion and selectivity, and clearly exceed the reference experiments with no catalyst or with Et_3N.

The progress of the hydrophosphonylation reaction was monitored by quantitative ^{31}P NMR spectroscopy what is presented on Figure 37.

The unreacted H-phosphonate substrate gave a single resonance at -3.42 ppm (normalized to integral = 1.00), whereas the newly formed α-hydroxyphosphonate product appeared as two distinct resonances at 16.119 ppm (integral = 0.72) and 15.165 ppm (integral = 0.19). To determine the conversion, the product integrals were summed:

$$I_{\text{prod}} = 0.19 + 0.72 = 0.91$$

and compared with the total integral of substrate and product:

$$\text{Conversion} = \frac{I_{\text{prod}}}{I_{\text{prod}} + I_{\text{sub}}} \times 100 = \frac{0.91}{0.91 + 1.00} \times 100 = 47.6\%.$$

The diastereomeric ratio was obtained by normalizing signal at 15.165 ppm (integral = 0.19) to 1.00 and expressing the second resonance at 16.119 ppm relative to it:

$$\frac{0.72}{0.19} \approx 3.8,$$

which corresponds to a dr of 1.00 : 3.80. This analysis confirms that the newly formed stereogenic center is located at the benzylic carbon bearing the hydroxyl group in the α-hydroxyphosphonate product.

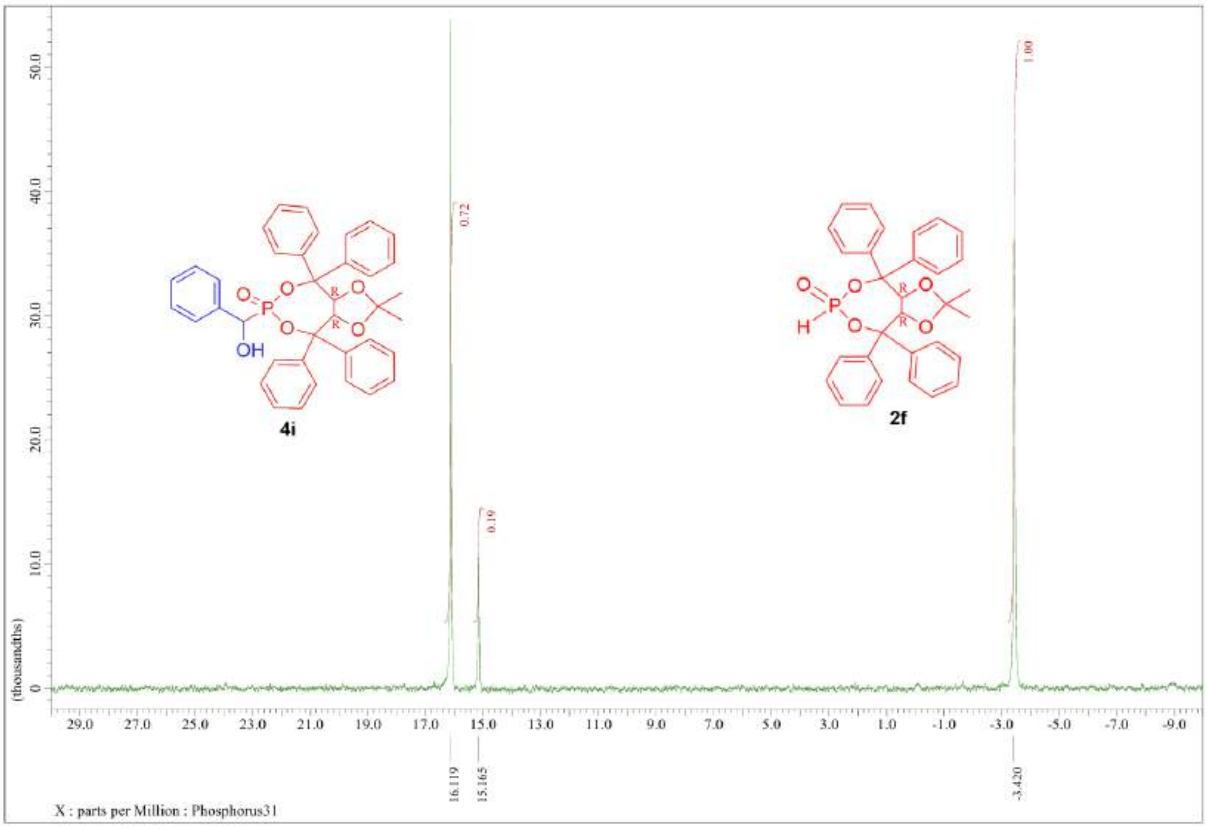


Figure 37. $^{3}1$P NMR spectrum (243 MHz, $CDCl_3$) of crude reaction mixture after the reaction of benzaldehyde with optically active substrate.

2.4.4 Scale-up of the hydrophosphonylation

Finally, scaling-up of the model hydrophosphonylation reaction summarized in Table 21 to 4.6 mmol was performed. It was 20 times larger scale than for optimization experiments with Eco-MgZnOx-P and Eco-MgZnOx-F. The pure desired product 3a was obtained without problems after simple crystallization from the experiment catalysed by Eco-MgZnOx-F with 88% yield (1.0 g).



Scheme 50. Model reaction of hydrophosphonylation

2.4.5 Reusage of the catalyst in the hydrophosphonylation

The possibility of simple and efficient recovery and reuse of the catalyst is a very important aspect of catalysis and green chemistry. Therefore, these experiments for Eco-MgZnOx-P and Eco-MgZnOx-F was performed. For this purpose, hydrophosphonylation of benzaldehyde (**1a**) with diethyl H-phosphonate (**2a**) under optimized conditions was used as the model reaction summarized in Table 21. Aldehyde (0.92 mmol), *H*-phosphonate (0.92 mmol), and appropriate Eco-MgZnOx catalyst (Eco-MgZnOx-P (5.7 mol% of Zn) or Eco-MgZnOx-F (4.9 mol% of Zn)) were placed in a glass vial. The mixture was stirred at 50℃ for 3 h. After that time, ethyl acetate was added (2 mL) and the reaction mixture was centrifuged (6000 rpm/5 min). The organic layer was separated, and an additional portion of ethyl acetate (2 mL) was added to the remaining catalyst and the centrifugation repeated (this process of washing the catalyst was repeated 4 times). The combined organic layers were evaporated under vacuum and the remaining crude product was purified by crystallization or preparative TLC. The remaining solid catalyst was dried in an oven (500℃ for 5 h) and then used for the next reaction. The process could be repeated up to 5 times in the case of Eco-MgZnOx-P.

During these tests a clear difference between reactions catalyzed by Eco-MgZnOx-P and Eco-MgZnOx-F was observed and presented in the Table 29.

Table 29. Recovery and reuse tests of the Eco-MgZnOx catalysts in Pudovik reaction[a].



1a **2a** **3a**

Ecocatalyst	Run	Conversion [b] (%)	Mineral Composition[c] of Eco-MgZnOx		
			Ca	Mg	Zn
Eco-MgZnOx-P	1	97%	16.21%	4.32%	8.02%
	2	96%	15.92%	3.72%	6.96%
	3	94%	13.65%	2.94%	5.87%
Eco-MgZnOx-F	1	96%	14.77%	1.69%	7.22%
	2	58%	14.46%	1.26%	5.23%
	3	14%	15.42%	0.79%	3.45%

a Reaction conditions: aldehyde (0.23 mmol), H-phosphonate (0.23 mmol)

b determined by ^{31}P NMR.

c Mineral compositions were determined by using microwave plasma-atomic emission spectroscopy (MP-AES).

The Eco-MgZnOx catalysts derived from *Arabidopsis halleri* biomass show different reuse behaviors for Pudovik reaction depending on their origin. Eco-MgZnOx-P main-

tains high conversion efficiency over multiple cycles, whereas Eco-MgZnOx-F deactivates rapidly. In the first run, both catalysts achieve 96-97% conversion of the model reaction. Upon reuse, Eco-MgZnOx-F activity plummets - dropping to 58% in the second run and only 14% by the third run. In contrast, Eco-MgZnOx-P retains >94% conversion through the first three cycles and still achieves about 88% conversion by the 5th run, what was also investigated. This divergence in reusability correlates strongly with changes in the catalysts' mineral composition over successive runs.

After each catalytic cycle, the bulk elemental composition, particularly Zn, Mg, and Ca content, of the recovered solids shifts due to loss of material. Atomic emission spectroscopy shows that Zn, Mg, and Ca wt% decrease progressively in both catalysts with each reuse. The magnitude of loss, however, differs. Eco-MgZnOx-F starts with a much lower Mg content (1.7 wt%) than Eco-MgZnOx-P (4.3 wt%). Consequently, after one or two cycles the French catalyst falls below a critical threshold of active Mg and Zn species needed for the reaction. By the third run, Eco-MgZnOx-F has lost over half of its initial Mg and Zn, what resulted its collapse in activity. Eco-MgZnOx-P also loses some Mg and Zn each cycle - for example Mg decreases from 4.3 to 2.9 wt% after three runs, but, because it initially contains more than double the Mg and slightly more Zn compared to the French catalyst, it retains sufficient active components to sustain high conversion. In effect, the Polish-derived catalyst had a larger reservoir of active basic MgO and Lewis acidic ZnO sites to begin with, so the fractional losses over five uses - Zn falling from 8.0 to 5.3 wt% after 3 runs do not inactivate it entirely. Meanwhile, calcium, which is present as $CaCO_3$ shows a modest downward trend in Eco-MgZnOx-P (from 16.2 to 13.7 wt% in three runs) but in Eco-MgZnOx-F the Ca fraction remains roughly constant or even rises slightly in later cycles. This apparent increase is because Mg and Zn are being preferentially stripped out, leaving Ca relatively enriched in the remaining solid. Potassium, also present in the initial ash, was reported to remain constant in wt%, indicating K-containing phases did not leach and thus K was likely not an active phase nor a cause of deactivation. Taken together, the data show that catalyst deactivation correlates with loss of active mineral constituents: rapid Zn and Mg depletion in Eco-MgZnOx-F leads to precipitous activity drop, whereas the slower, limited loss of these components in Eco-MgZnOx-P permits sustained activity. In sum, the Polish ecocatalyst's superior reuse performance is attributed to its higher initial magnesium and zinc content and correspondingly greater resistance to critical depletion of those active species during operation. This analysis underscores that maintaining the mineral composition of the catalyst, especially the MgO and ZnO content, is key to preserving its catalytic efficiency across runs.

The first conclusion based on this fact is that Zn and Mg contents drop from run to run in step with the loss of conversion, while Ca/K remain ineffective, is the classic fingerprint of leaching of the true active sites. And because control experiments show MgO and ZnO, and especially their combination, are the phases that actually promote the hydrophosphonylation, their preferential loss unambiguously identifies MgO (basic) and ZnO (Lewis acidic) as the catalytically relevant components in this system.

The second conslusion is that progressive loss of Zn, Mg, and Ca from the catalyst indicates that leaching is occurring. Leaching in heterogeneous catalysis refers to the undesired removal of active species from the solid catalyst into the reaction solution. In liquid-phase reactions, even a small degree of leaching can deactivate a catalyst by depleting its active components or structural stabilizers. Leaching typically occurs via dissolution or solvolysis of the catalyst material: the solid constituents such as metal ions or oxides are chemically transformed into soluble forms and diffuse into the liquid phase [379]. This phenomenon is one of the major deactivation mechanisms for solid catalysts in liquid media, alongside sintering and poisoning. Sádaba et al. note that leaching often involves breaking the metal-oxygen bonds that anchor metal sites in an oxide or on a support, releasing those metal ions into solution [379]. For example, exposure to acids or water can convert metal oxides into soluble salts or hydroxides. Even in ostensibly neutral conditions, solvent molecules or reactants can coordinate to surface metal sites, weakening their bonds and causing the metal to detach into solution. Leaching is especially pronounced if chelating agents are present: organic molecules with multiple ligating groups can strongly bind metal cations and effectively extract them from the solid lattice [379]. In short, leaching is the loss of active catalyst species like metal ions into the reaction mixture, driven by chemical interactions that render those species soluble. This not only diminishes the solid catalyst activity over time but can also introduce homogeneous activity or metal contaminants in the product. Controlling leaching is therefore critical for catalyst longevity and for preventing metal contamination of products.

In the specific case of the Eco-MgZnOx catalysts leaching is driven by the interaction of these mineral phases with the reaction environment and products. The reaction produces α-hydroxyphosphonate compounds via hydrophosphonylation of aldehydes. Those molecules are potent chelating agents for metal ions. Their metal-binding ability has been directly studied:

- 2-amino-1-hydroxyalkylphosphonic acids obtained via hydrophosphonylation form well-defined $Zn(II)$ and $Cu(II)$ complexes in water, characterized potentiometrically and spectroscopically [327, 380];

- α-hydroxyimino-phosphonate derivatives chelate $Cu(II)$ strongly enough to separate E/Z isomers, with an X-ray-characterized copper complex reported [381];
- chelation by an α-hydroxymethyl-phosphonate/phosphinate motif has been observed directly-Ga(III) induces deprotonation of the α-OH to an alcoholate that binds and closes a chelate ring [382].

As the reaction proceeds, the newly formed hydroxyphosphonate can coordinate strongly to Zn^{2+}, Mg^{2+}, or Ca^{2+} ions on the catalyst surface. This forms soluble organometallic complexes, effectively extracting those metal ions from the solid lattice into the organic phase [379]. In other words, the product itself chelates away the catalyst active ingredients.

The chemical nature of the mineral phases explains their vulnerability. Zinc oxide and magnesium oxide are amphoteric/basic oxides that can be solubilized by acidic or chelating conditions. Zinc oxide is amphoteric and dissolves under acidic or strongly basic/chelating conditions, forming soluble zinc species [383, 384]. Magnesium oxide is a basic oxide that readily dissolves in dilute mineral acids, so even mildly acidic media can mobilize Mg from the surface [385]. Even though the hydrophosphonylation was run under solvent-free, relatively mild conditions, trace moisture or impurities and the H-phosphonate reagent itself can provide acidity and engage in $-P(=O)H \rightleftharpoons -P(OH)$ tautomerism that modulates proton activity. Both effects can promote surface attack on metal oxides [386, 387]. Under such conditions, zinc or magnesium oxides can react to give zinc or magnesium phosph(on)ate or organophosphonate species that remain in the liquid phase, especially because metal-phosphonate coordination is thermodynamically strong [388, 389]. In zinc phosphate systems ZnO can be consumed by phosphoric acids to form zinc phosphates [390]. Moreover, the α-hydroxyphosphonate products possess hard oxygen donors: $P = O$ and $C - OH$ and act as potent metal chelators. Once zinc or magnesium ion is detached, it is efficiently captured and kept in solution [317, 391]. Calcium carbonate, while less catalytically active, can also leach by neutralization with weak acids to release Ca^{2+}, and calcium-phosphonate complexes are stable [391–393]. By contrast, K^+ forms only very weak complexes with phosphonates and, without bulk water, K_2CO_3 remains a stable solid with negligible solubility in non-aqueous or solventless media [393, 394].

The evidence that calcium content decreased or stayed constant while Mg and Zn plummeted suggests that zinc and magnesium oxides were more readily attacked by the product. This selective leaching means the active MgO and ZnO phases are preferentially lost. This explains why the catalyst composition evolves and why activity

degrades: the active base MgO and Lewis acid ZnO sites are progressively removed from the solid, leaving behind less active components like inert $CaCO_3$ or residual K_2CO_3 that cannot sustain the catalytic cycle.

To prolong catalyst life, the dissolution of Zn, Mg, and Ca species from the ecocatalyst must be prevented or minimized. Both experimental and theoretical strategies can be proposed to mitigate or eliminate leaching in such biomass-derived catalysts: Incorporate a support or matrix to immobilize the active species: Dispersing the Eco-MgZnOx components onto or into a more robust solid support can anchor the metal oxides and reduce their direct contact with chelating molecules. For example, earlier work showed that ash-derived Zn/Mg catalyst extracts can be deposited on montmorillonite clay to create a supported ecocatalyst [303]. Using a high-surface-area, inert support, such as mesoporous silica, alumina, or zeolite via impregnation or co-precipitation can immobilize Mg and Zn species and hinder their leaching [395]. The support framework can physically trap metal ions that would otherwise detach, and in some cases can provide binding sites that hold the metal more strongly (making solvolysis less favorable). For instance, CaO on Al_2O_3 or MgO supports shows significantly reduced leaching in biodiesel catalysts because the support stabilizes the Ca/Mg species [395]. Likewise, embedding the mixed Zn/Mg oxides in a porous silica network could confine them and prevent large-scale loss, while still allowing reactants to access catalytic sites. Nevertheless, in experiments described in this chapter of the thesis immobilizing the ecocatalyst on solid supports such as Al_2O_3 and silica gel did not improve stability-the decline in reaction conversion was the same as without immobilization.

Other idea for further stabilization of catalyst is the catalyst composition modification or post-treatment. The minerals can be transformed into phases that are less soluble. Doping or adding a secondary oxide to form a solid solution is a proven strategy. A pertinent example is the incorporation of ZnO into a ZrO_2 lattice: Liguori et al. showed that a $ZnO - ZrO_2$ mixed oxide resists Zn leaching during polyester depolymerization, whereas pure ZnO readily dissolved in the presence of carboxylic acids [396]. Adjusting how the reaction is carried out can also mitigate leaching. For instance, reducing exposure of the catalyst to the product or protic species can help. Conducting the reaction in a continuous flow reactor with the solid packed catalyst could allow the product to be swiftly separated, minimizing contact time for chelation.

2.4.6 Substrate scope of the Hydrophosphonylation

A detailed investigation of the substrate scope was carried out for the hydrophosphonylation reaction (Scheme 1), examining a range of carbonyl substrates (Figure 38) and various H-phosphonates (Figure 39). The results, displayed in the figures below, show the structures of the compounds formed under optimized conditions in accordance with the Table 30. Following each scheme the conversion rates are presented for both catalysts followed with yields in brackets for one catalyst if the product were purified. For example product 3a with catalyst $EcoMgZnO-P$ achieved conversion 97% and with catalyst $EcoMgZnO-F$ achieved conversion 96% and yield 82%.



Scheme 1. Hydrophosphonylation, Pudovic reaction

Table 30. Reaction conditions for different carbonyl substrates.

Carbonyl Substrate	Temperature	Time	Catalyst
Aromatic Aldehydes	50℃	3h	Eco-MgZnOx-P^a Eco-MgZnOx-F^b
Aliphatic Aldehydes	70℃	3h	Eco-MgZnOx-P^a Eco-MgZnOx-F^b
Heteroaromatic Aldehydes	70℃	3h	Eco-MgZnOx-P^a Eco-MgZnOx-F^b
Ketones	70℃	20h	Eco-MgZnOx-P^c Eco-MgZnOx-F^d

a 7.5 mg of Eco-MgZnOx-P: Mg (7.0 mol%), Ca (13.6 mol%), Zn (5.7 mol%).
b 7.5 mg of Eco-MgZnOx-F: Mg (3.5 mol%), Ca (11.4 mol%), Zn (4.9 mol%).
c 15 mg of Eco-MgZnOx-P: Mg (14.0 mol%), Ca (27.2 mol%), Zn (11.4 mol%).
d 15 mg of Eco-MgZnOx-F: Mg (7.0 mol%), Ca (22.8 mol%), Zn (9.8 mol%).

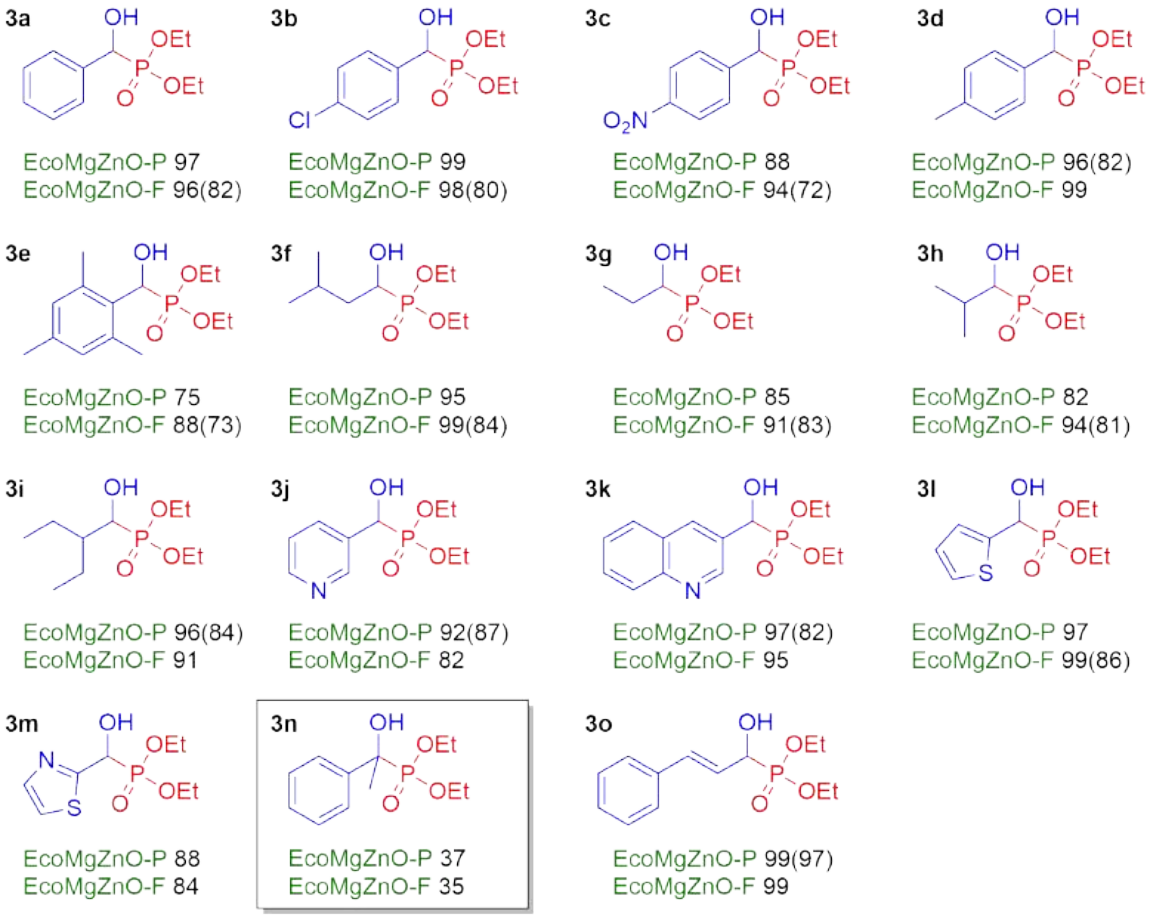


Figure 38. Substrate scope of hydrophosphonylation - scope of carbonyl compounds. Numbers next to each entry are conversions and values in parentheses are isolated yields.

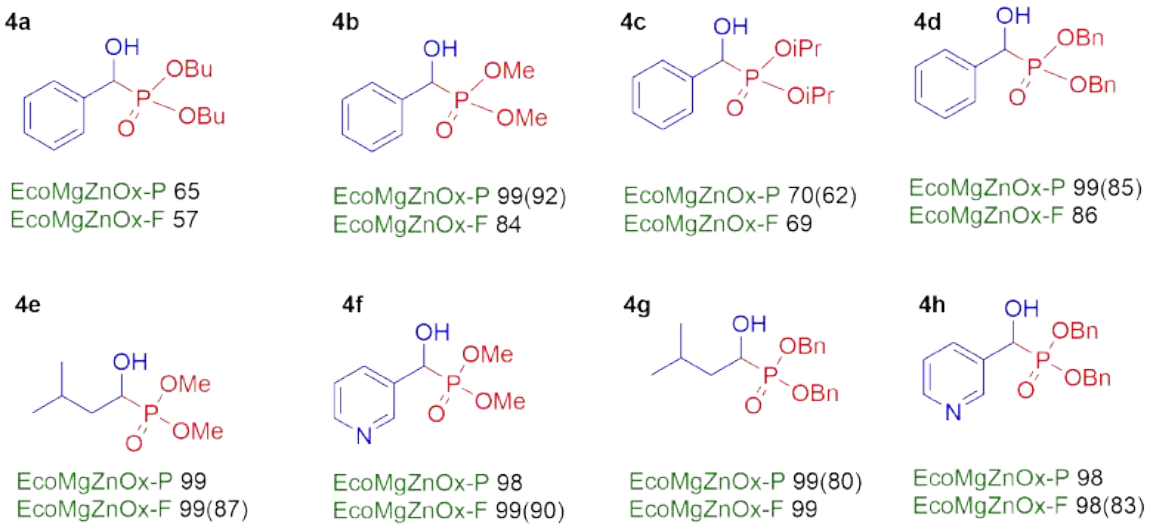


Figure 39. Substrate scope of hydrophosphonylation - scope of H-phosphonates. Numbers next to each entry are conversions and values in parentheses are isolated yields.

The eco-catalyst provides a very effective hydrophosphonylation of aldehydes. The investigated substrate scope was broad for aldehydes - multiple aryl patterns, includ-

ing electron-poor and halogenated, polycyclic aryls, several aliphatic examples, and N- and S-heteroaromatics were covered. Functional-group tolerance is good and the method appears robust to coordinating heteroatoms. Across aryl, aliphatic, and heteroaromatic aldehydes the reaction is usually high-yielding, most entries sit in the 90-99% conversion range and the isolated yields follow closely. Ring electronics have only a small effect - halogenated and even nitrobenzaldehyde work well. Steric hindrance matters more: a heavily crowded mesitaldehyde is clearly slower and gives lower numbers. Heteroaromatics (furan, thiophene, pyridine/indole-type) are well tolerated, which means the oxide surface is not poisoned by N or S donors under these conditions. Polycyclic aryls like naphthyl and simple aliphatic aldehydes also react cleanly. A single ketone control reacts poorly, so the method is chemoselective for aldehydes over ketones. Both catalyst variants perform very similarly.

The H-phosphonate substrate influences rate and yield. Dimethyl and dibenzyl H-phosphonates are consistently the best, giving near-quantitative conversions with both aromatic, aliphatic, and pyridyl aldehydes. Bulky diisopropyl and long-chain di-n-butyl H-phosphonates are slower and give noticeably lower conversions. This pattern points to a steric/acidic balance controlling nucleophile activation on the catalyst.

Isolated products were fully characterized by standard spectroscopic techniques, see Chapter 7 for more details. To illustrate the structural features of the obtained products and to confirm the reliability of the spectroscopic assignments across the series, a representative example was selected for further discussion - compound 3a, a model product (Figure 40). Its structure and purity are confirmed by ^{1}H (Figure 42), ^{13}C (Figure 41), and ^{31}P (Figure 43) NMR spectroscopy, which show the expected signal pattern for the hydroxyphosphonate motif and the absence of detectable side products.

In the ^{1}H NMR spectrum (Figure 42), aromatic protons appear as a multiplet at 7.48–7.28 ppm, while the characteristic hydroxymethine proton is observed at ca. 5.00 ppm. The ethoxy $O\breve{}CH_2$ groups resonate at 4.06–3.97 ppm and the corresponding methyl groups appear as triplets at 1.26–1.18 ppm. The ^{13}C NMR spectrum (Figure 41) shows aromatic carbon signals between 136.8 and 127.2 ppm and the $C\breve{}P$ bonded hydroxymethine carbon in the 71.6–63.1 ppm region, with clear $C\breve{}P$ coupling. A single sharp resonance at 22.05 ppm in the ^{31}P NMR spectrum (Figure 43) confirms a single phosphorus environment and high product purity.

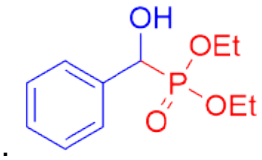


Figure 40. 3a - Diethyl (1-hydroxyphenylmethyl)phosphonate

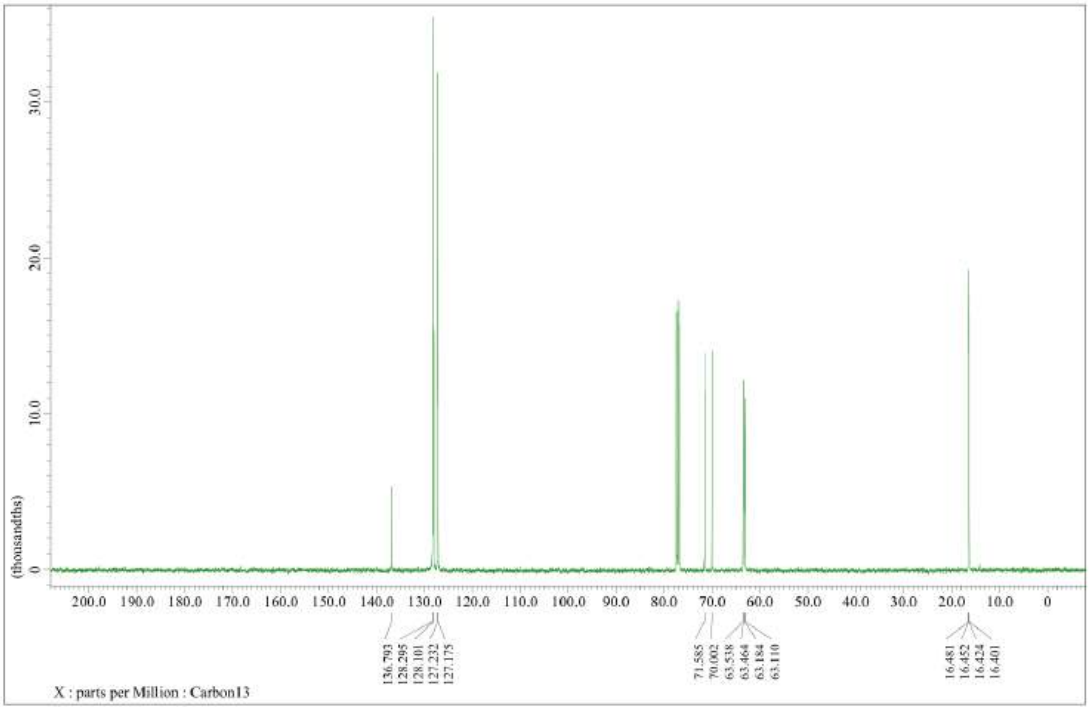


Figure 41. ^{13}C NMR spectrum of 3a - Diethyl (1-hydroxyphenylmethyl)phosphonate

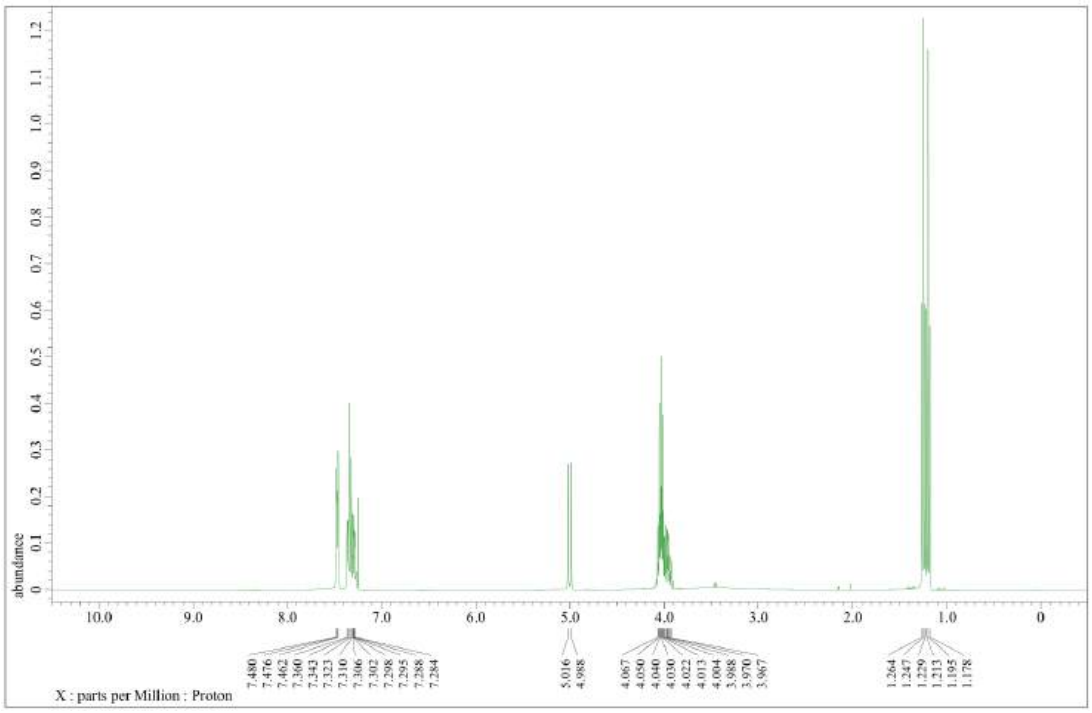


Figure 42. ^{1}H NMR spectrum of 3a - Diethyl (1-hydroxyphenylmethyl)phosphonate

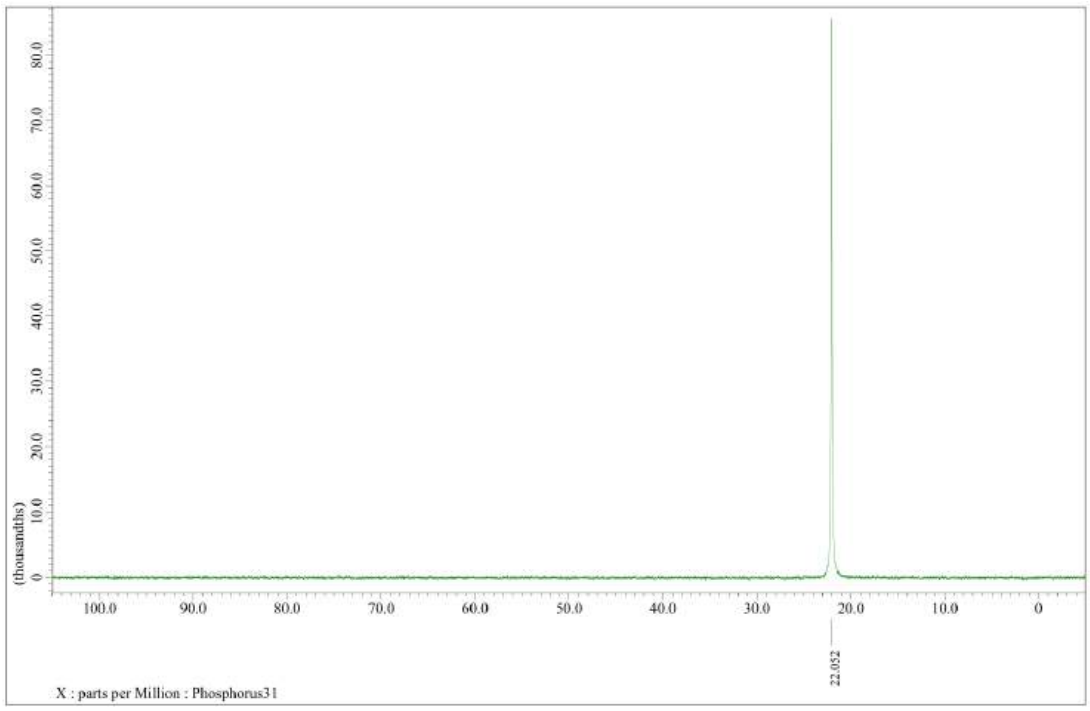


Figure 43. ^{31}P NMR spectrum of 3a - Diethyl (1-hydroxyphenylmethyl)phosphonate

2.4.7 Theoretical calculations of the catalytic mechanism of the hydrophosphonylation

To gain insight into the mechanism of the hydrophosphonylation reaction catalyzed by the EcoCatalyst Eco-MgZnOx at the molecular level and to rationalize its high activity, theoretical calculations were performed. Integrating the results obtained using density functional theory (DFT) with established principles of heterogeneous catalysis allowed for the deconstruction of the reaction mechanism, justification of the computational approach used, and explanation of the synergistic effects arising from the unique, polymetallic composition of the catalyst.

Density functional theory (DFT) is a cornerstone of modern computational catalysis, serving as an indispensable tool for understanding reaction mechanisms at the electronic level [397, 398]. Its utility in the rational design of catalysts lies in identifying key descriptors that determine catalytic activity [398]. For complex, real-world materials such as the Eco-MgZnOx ecocatalyst, which are heterogeneous in structure and composition, direct experimental characterization of the active site during the reaction is extremely difficult. DFT calculations provide a "computational microscope" that enables the study of these transient states. The computational approach employed in the analyzed works a deliberate and necessary strategy aimed at bridging the so-called "materials gap" between idealized models and real catalytic systems [397]. Instead of modeling the entire complex ash, experimental data were used to hypothesize the nature of the active site and construct a simplified yet chemically representative model. This is a classic example of the convergence of theory and experiment to solve a complex problem. The model's success in explaining the experimental results (the superiority of the mixed oxide) retrospectively validates this simplification. The $Mg(Zn)O$ phase was identified by XRPD.

In this study, a finite-size cluster model $522MgO$ was used to represent the catalyst surface. This is a widely accepted and validated methodology in computational catalysis for modeling active centers on metal oxide surfaces [399, 400]. The rationale is that catalysis is often a local phenomenon, and a well-chosen cluster can accurately replicate the geometry and electronic properties of the active site without the computational cost associated with full periodic calculations (slab model) [399]. The choice of a cluster model is a pragmatic compromise. Although a periodic model would better represent the extended surface, it would have precluded the use of advanced, computationally demanding hybrid functionals (such as PBE0) due to excessive costs. By isolating the putative active site in a cluster, it became possible to obtain a more accurate

quantum-mechanical description of the bond-breaking and bond-forming processes that are crucial to the catalytic cycle. This highlights a fundamental decision-making process in computational chemistry: sacrificing the description of long-range periodicity in favor of higher accuracy in the local chemical environment where the reaction actually occurs.

The calculations in this thesis were performed using the hybrid functional PBE0. Hybrid functionals, which mix a portion of exact Hartree-Fock (HF) exchange with a DFT functional, are known to provide a more accurate description of the electronic structures in transition metal oxides compared to standard GGA functionals [401, 402]. Standard GGA functionals often suffer from self-interaction error, leading to an underestimation of band gaps and incorrect localization of d-electrons, which is critical for describing Lewis acidity [401–403]. Although PBE0 is computationally more expensive, its use is justified by the need to accurately model the electronic properties of both the MgO (basic site) and ZnO (Lewis acidic site) interactions. Fabris and his group found that hybrid functionals like PBE0 show good agreement with results from higher-order and much more expensive methods, such as coupled-cluster theory, for reactions on metal oxides [375]. The choice of PBE0 is not arbitrary - for transition metal systems, functionals with about 25% HF exchange, like PBE0, often represent a "sweet spot" that balances the correction of self-interaction error with the inclusion of electron correlation [404]. This is particularly relevant here, where the catalyst's function relies on the subtle electronic interplay between Mg, Zn, and O atoms, creating distinct acidic and basic centers.

The catalytic cycle begins with the activation of the H-phosphonate. DFT calculations showed that upon interaction with the MgO cluster, the H-phosphonate $HP(O)(OMe)_2$ undergoes spontaneous deprotonation. The proton is transferred from the phosphorus atom to a surface lattice oxygen atom of MgO, forming a surface hydroxyl group and a phosphite anion coordinated to the newly exposed, cationic Mg center. This process is highly exothermic, with a calculated stabilization energy of 81.8 kcal/mol. This finding is fully consistent with the known properties of MgO as a solid base catalyst [405]. The MgO surface is rich in basic O^{2-} sites capable of abstracting protons from weakly acidic molecules [405]. This deprotonation step is a classic initiation for base-catalyzed reactions, including the Pudovik reaction [317]. The calculations confirm that the primary role of the magnesium oxide component is to generate a strong phosphite nucleophile, which is essential for the subsequent $C-P$ bond formation. The calculations indicate that the reaction occurs at the "tip of the cluster", which is significant because corners, edges, and defects on oxide surfaces

are known to be more reactive than flat terraces, and these low-coordination sites have enhanced basicity/acidity [376]. DFT calculations revealed a key finding: the nucleophilic attack of the phosphite anion on the carbonyl carbon of benzaldehyde occurs spontaneously only when the model cluster is doped with zinc, in example for the $(Mg_{0.9}Zn_{0.1})O$ model. In the case of pure MgO or iron-doped MgO, no $P-C$ bond formation is observed; the system merely forms a non-bonded complex. This unequivocally demonstrates that zinc is essential for activating the aldehyde. This result provides a molecular explanation for the experimental observation that the $MgO+ZnO$ mixture is more active than either oxide alone (like presented in Table 22). Zinc oxide is known to possess Lewis acid centers that can coordinate to the carbonyl oxygen atom, polarizing the $C=O$ bond and increasing the electrophilicity of the carbonyl carbon [406]. The DFT calculations show precisely this interaction - the zinc atom in the mixed-oxide cluster coordinates to the benzaldehyde oxygen, facilitating the attack of the phosphite nucleophile held by the adjacent MgO portion of the surface.

The full catalytic cycle is depicted in Figure 44. After the $C-P$ bond is formed, an alkoxide intermediate is generated and stabilized by the catalyst surface. The final step is the transfer of a proton from the surface hydroxyl group (formed in step 1) to this alkoxide, which regenerates the basic O^{2-} site of the catalyst and releases the final product, an α-hydroxyphosphonate. This step requires a small amount of energy, likely provided by the reaction conditions (heating to 50-70℃). The proposed mechanism is a textbook example of bifunctional catalysis [407]. The catalyst possesses two distinct types of active sites-basic MgO and acidic ZnO - that work in a coordinated fashion to carry out the different elementary steps of the overall reaction. The key to its efficiency is the spatial proximity of these sites within the mixed-oxide lattice, which allows for the formation of a highly organized transition state where both activated molecules are brought together. This is far more effective than having two separate particles (one MgO, one ZnO), where the reaction would depend on the diffusion of an activated intermediate between them.

The experimental results clearly indicate a synergistic effect. The Eco-MgZnOx ecocatalysts yield >96% conversion, whereas commercial MgO gives 70%, commercial ZnO 14%, and their physical mixture 78%. This proves that the activity of the ecocatalyst is greater than the sum of its parts. Synergy in mixed metal oxide catalysts arises when the interaction between different metal cations creates new structural or electronic properties not present in the parent oxides [408]. The experimental data provide a crucial clue: XRPD analysis of the ecocatalyst identified a $Mg_{0.88}Zn_{0.12}O$ phase,

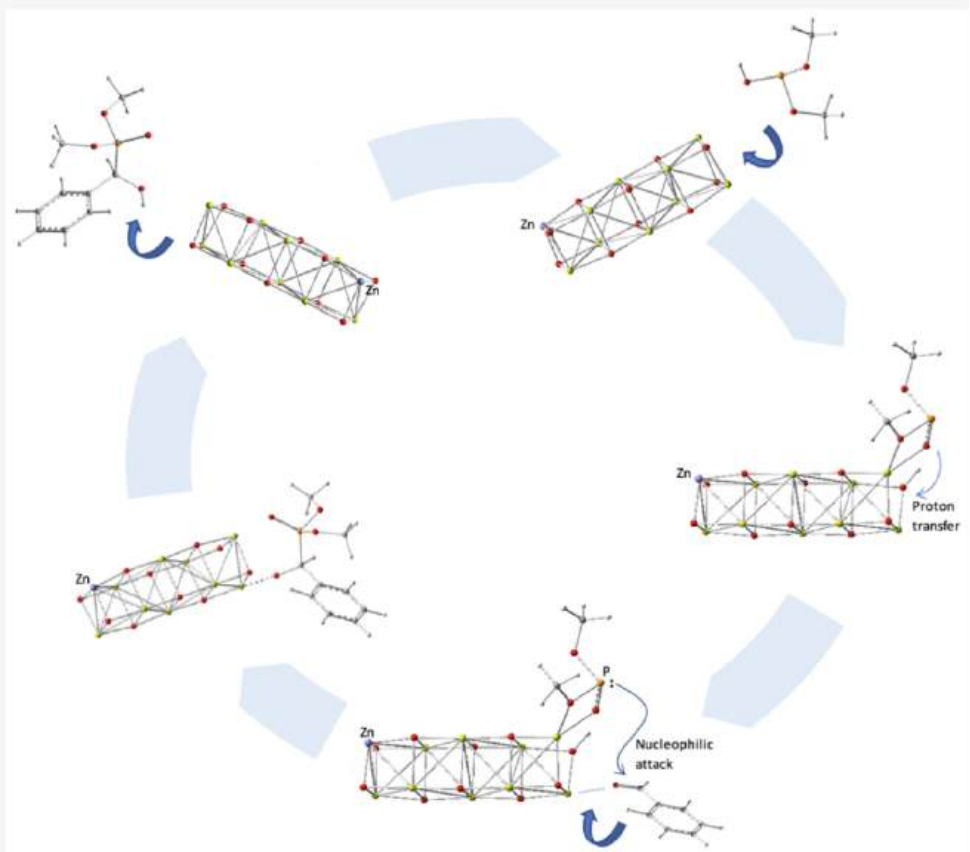


Figure 44. Proposed catalytic cycle for the hydrophosphonylation of benzaldehyde catalyzed by Eco-MgZnOx, based on DFT calculations on a $(Mg_{0.9}Zn_{0.1})O$ cluster model. The cycle illustrates the key steps: (i) deprotonation of the H-phosphonate at a basic MgO site, (ii) coordination and activation of benzaldehyde at an adjacent Lewis acidic Zn site, (iii) nucleophilic attack to form the $C-P$ bond, and (iv) proton transfer to release the product and regenerate the active site.

which is a solid solution of ZnO in the MgO (periclase) lattice. This is not a simple physical mixture. The DFT calculations modeled this scenario (with $(Mg_{0.9}Zn_{0.1})O$ composition). Combining these two pieces of evidence leads to a strong conclusion: the high activity stems from the formation of this unique mixed-oxide phase. In this phase, Zn^{2+} ions are substituted at Mg^{2+} sites, creating bifunctional acid-base pairs at the atomic level. A Zn atom adjacent to an O atom (part of the MgO lattice) forms a Lewis acid center right next to a Brønsted basic site. This atomic-level proximity is the structural origin of the synergy and explains why the ecocatalyst is superior to a simple physical mixture of MgO and ZnO powders [408].

The ecocatalyst is prepared by simple thermal treatment of plant biomass, and the plant, *Arabidopsis halleri*, hyperaccumulates zinc and other metals, incorporating them into its structure. The process of phytoextraction and subsequent calcination is a bottom-up synthesis method in which the plant's biological machinery pre-organizes the metal ions at a molecular level. The plant's metabolic processes distribute metal

ions such as Mg, Zn, Ca in a highly dispersed manner, potentially at the atomic level, within its organic matrix. Upon thermal decomposition of this matrix, the metal ions are in close proximity and can easily form solid solutions of mixed oxides like $Mg(Zn)O$ at relatively low temperatures - 550℃, which might require much higher temperatures or specific precursors in conventional synthesis. In essence, the plant acts as a nanofactory, creating a highly effective precursor for the catalyst. This explains the formation of the unique, highly active $Mg(Zn)O$ phase and provides a compelling argument for the value of ecocatalysis as a green and effective method for preparing catalysts.

In summary, the theoretical assessment has successfully rationalized the high catalytic activity of the Eco-MgZnOx catalyst. It confirmed a cooperative, bifunctional acid-base mechanism where MgO activates the phosphonate nucleophile and ZnO activates the aldehyde electrophile. The calculations pointed to the substitution of Zn into the MgO lattice as the key feature responsible for the observed synergistic effect. This detailed understanding, combining experimental characterization and theoretical modeling, provides a solid foundation for the rational design of future catalysts, suggesting, for example, that tuning the Mg/Zn ratio could optimize performance and that preventing the leaching of these key components is critical for catalyst stability.

2.4.8 Conclusions

Chapter 2 is dedicated to the hydrophosphonylation reaction (Pudovik reaction) using heterogeneous Eco-MgZnOx ecocatalysts. A key element of the research was the preparation of catalysts from the biomass of the zinc hyperaccumulator *Arabidopsis halleri*, harvested from contaminated sites in Poland and France. Advanced physicochemical analyses showed that the obtained materials are composites containing magnesium and zinc oxide phases embedded in a carbonate matrix.

It was demonstrated that the biogenic Eco-MgZnOx catalyst derived from *Arabidopsis halleri* biomass is an efficient and robust heterogeneous catalyst for the hydrophosphonylation of aldehydes (Pudovik reaction). The catalyst enables the formation of $C^{\smile}P$ bonds under mild conditions, providing direct access to α-hydroxyphosphonates in high yields and excellent selectivity.

The developed protocol is based on solvent-free conditions, moderate reaction temperatures (50–70℃), and a low catalyst loading (approximately 5-10 mol% with respect to Zn). Under these conditions, a wide range of aromatic, heteroaromatic, and aliphatic aldehydes reacted smoothly with dialkyl H-phosphonates to afford the corresponding α-hydroxyphosphonates, typically with conversions reaching 95–100% and clean prod-

uct profiles. The products were be isolated by simple crystallization or straightforward purification, highlighting the practical character of the method.

It was shown that the Eco-MgZnOx catalyst exhibits clear bifunctional behavior. The coexistence of basic MgO sites and Lewis-acidic ZnO sites within a mixed $Mg(Zn)O$ oxide phase enables simultaneous activation of the phosphorus nucleophile and the carbonyl electrophile. This cooperative effect results in significantly higher catalytic activity compared to single-component oxides or their physical mixtures. The proposed catalytic mechanism, supported by DFT calculations, explains the observed synergy and the high efficiency of the system.

Furthermore, the catalyst demonstrated good stability and reusability. After simple recovery and thermal regeneration, Eco-MgZnOx could be reused in multiple consecutive reaction cycles with only a minor loss of activity. The material originating from Poland proved to be more durable in repeated use than its French counterpart. The higher stability of the Polish catalyst was explained by a higher initial content of magnesium and zinc, ensuring better resistance to activity loss. The phenomenon of leaching of active metal ions by reaction products, which act as strong chelators, was identified as the main cause of catalyst deactivation. In addition, the hydrophosphonylation was successfully scaled up to the gram scale without deterioration of yield, confirming the applicability of the developed protocol beyond small laboratory experiments.

Overall, the results presented in this chapter confirm that Eco-MgZnOx obtained from hyperaccumulator plant biomass represents a practical, recyclable, and green catalyst for the hydrophosphonylation of aldehydes. This study provides a solid proof of concept for ecocatalysis in $C^{\smile}P$ bond formation and establishes a foundation for further applications of biogenic polymetallic catalysts in organophosphorus chemistry.

Chapter 3:
Knoevenagel condensation

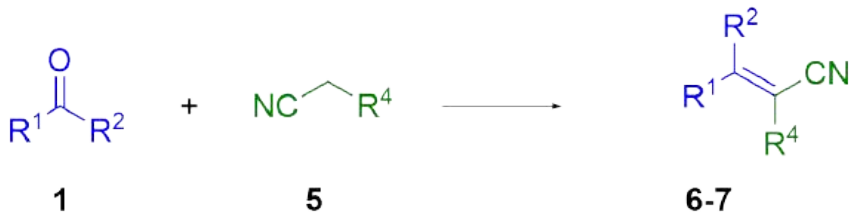
3.1 Knoevenagel condensation - chemical basics

The Knoevenagel condensation stands as a significant reaction of synthetic organic chemistry, known from over a century for its reliability and exceptional versatility in the formation of carbon-carbon double bonds [409]. This reaction facilitates the condensation of an aldehyde or ketone with a compound bearing an active methylene group, culminating in the formation of an α,β-unsaturated product [410].These conjugated systems are not just final products of synthesis but also key intermediates and core patterns found in many important molecules. Because their electronic structure includes an electron-poor double bond, they can easily undergo different follow-up reactions, especially conjugate additions. This makes them very practical building blocks for creating more complex compounds [411].

The reaction was first reported by German chemist Emil Knoevenagel in the 1890s. Knoevenagel discovered that amines could effectively catalyze the condensation between carbonyl compounds and active methylene partners [412]. These early investigations, which often employed primary and secondary amines like piperidine in solvents such as pyridine, laid the foundation for what would later be recognized as the field of organocatalysis [412]. For many decades, the classical Knoevenagel protocol, while effective, relied on reaction conditions that are now considered undesirable from an environmental and safety perspective. The use of large quantities of toxic and carcinogenic solvents like pyridine, coupled with catalysts that were often difficult to recover, presented significant challenges for industrial scale-up and sustainable synthesis [409, 413]. This dissatisfaction was a powerful trigger for innovation. The evolution of the Knoevenagel condensation over the past few decades serves as a starting point for the broader evolution of synthetic organic chemistry itself. The reaction has become a proving ground for major advancements in chemical synthesis, driven by the principles of green chemistry. The journey from stoichiometric, hazardous reagents to modern, highly efficient protocols reflects a paradigm shift in the field. This evolution has encompassed the development of benign metal-free organocatalysts, the rise of recyclable and highly active heterogeneous catalysts, the exploration of green solvents like water and ionic liquids, and the application of alternative energy sources such as microwave and ultrasound irradiation. The reaction has transitioned from a useful but environmentally taxing tool into a sophisticated and sustainable platform for molecular construction [411, 413].

At its core, the Knoevenagel condensation is a nucleophilic addition of a carbanion, derived from an active hydrogen compound, to the carbonyl group of an aldehyde or

ketone, which is typically followed by a dehydration reaction to eliminate a molecule of water. The overall transformation results in the formation of a new carbon-carbon double bond, yielding an α,β-unsaturated product, often a conjugated enone or a related derivative [409]. The general reaction is depicted in Scheme 2.



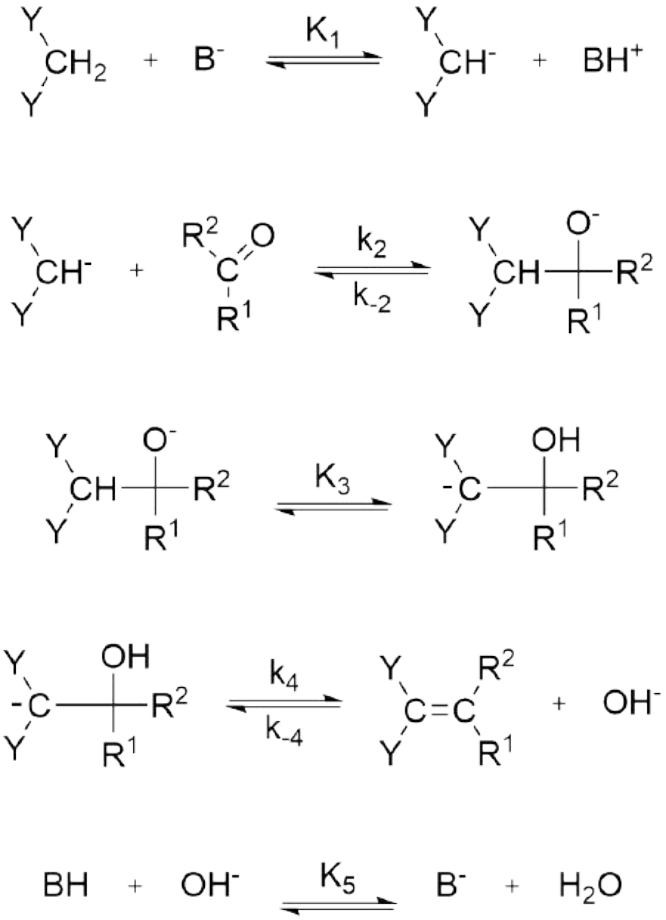
Scheme 2. Knoevenagel condensation

The reaction involves two key substrates: the carbonyl component and the active methylene component. The carbonyl component is typically an aldehyde or, less commonly, a ketone. Aldehydes are generally more reactive than ketones due to reduced steric hindrance and greater electrophilicity of the carbonyl carbon [414]. The active methylene component is the defining feature of the Knoevenagel condensation. It is a compound that possesses a methylene (CH_2) or methine (CHR) group where the hydrogens are rendered acidic. This enhanced acidity arises from the attachment of the carbon to two strong electron-withdrawing groups (EWGs), denoted as Z and Z' [409]. These EWGs stabilize the conjugate base - the carbanion or enolate - formed upon deprotonation through resonance or inductive effects. The EWGs must be sufficiently powerful to permit deprotonation by a relatively weak base, such as an amine. The use of a strong base, such as an alkoxide, is generally avoided as it can induce the self-condensation of the aldehyde or ketone reactant like an aldol condensation. Common examples of such EWGs include ester $COOR$, ketone COR, aldehyde CHO, nitrile CN, and nitro NO_2 groups [409].

While often presented as a single, straightforward process, the mechanism of the Knoevenagel condensation can vary depending on the specific catalyst and reactants employed. The classical textbook mechanism involves the formation of an enolate intermediate, while more recent computational studies have elucidated a distinct and more complex pathway for amine-catalyzed reactions involving an iminium ion intermediate.

The most widely taught mechanism proceeds through three fundamental steps presented on Scheme 51. First step is deprotonation, where a base B : abstracts an acidic proton from the active methylene compound to generate a resonance-stabilized carbanion, also known as an enolate. The stability of this intermediate is crucial for the

reaction to proceed under weakly basic conditions. The next step is nucleophilic addition, where the highly nucleophilic carbanion attacks the electrophilic carbonyl carbon of the aldehyde or ketone. This step forms a new carbon-carbon single bond and generates a tetrahedral alkoxide intermediate, which is an aldol-type adduct. This step is often the slow, rate-determining step of the reaction The last step is dehydration. The alkoxide intermediate is protonated, typically by the conjugate acid of the base, BH^+ to form a β-hydroxy intermediate. Subsequent elimination of a water molecule, often facilitated by the base abstracting a proton from the α-carbon, leads to the formation of the thermodynamically stable, conjugated carbon-carbon double bond of the final product [409].



Scheme 51. Mechanism of Knoevenagel condensation, where Y is electron withdrawing groups, such as $-COOEt$ or $-CN$ [409]

For reactions catalyzed by primary or secondary amines, such as the classic piperidine catalyst mentioned above, a more complicated mechanism is operative known as the amine-catalyzed or iminium ion pathway. This pathway does not simply involve the amine acting as a Brønsted base. The amine functions as a true organocatalyst, actively participating in the reaction cycle by forming a highly reactive intermediate with

the carbonyl compound. Detailed theoretical calculations on the piperidine-catalyzed condensation of benzaldehyde with acetylacetone have provided significant clarity on this pathway. The key steps are as follows [415]:

1. Carbinolamine formation, where the amine catalyst first attacks the carbonyl carbon of the aldehyde to form a tetrahedral carbinolamine intermediate. This step can be catalyzed by the solvent, such as methanol.

2. Iminium ion formation: the carbinolamine undergoes dehydration to form a highly electrophilic iminium ion. This step involves the elimination of a hydroxide ion and is a critical part of the catalytic cycle.

3. Enolate formation: concurrently, a base (which can be a hydroxide ion generated in the previous step or another molecule of the amine catalyst) deprotonates the active methylene compound to form the enolate nucleophile.

4. C-C Bond Formation, which is the result of the enolate attack on the electrophilic carbon of the iminium ion. The new carbon-carbon bond is forming and yielding an addition intermediate.

5. Catalyst regeneration: the final step is the elimination of the amine catalyst from the intermediate, which regenerates the catalyst and forms the final α, β-unsaturated product.

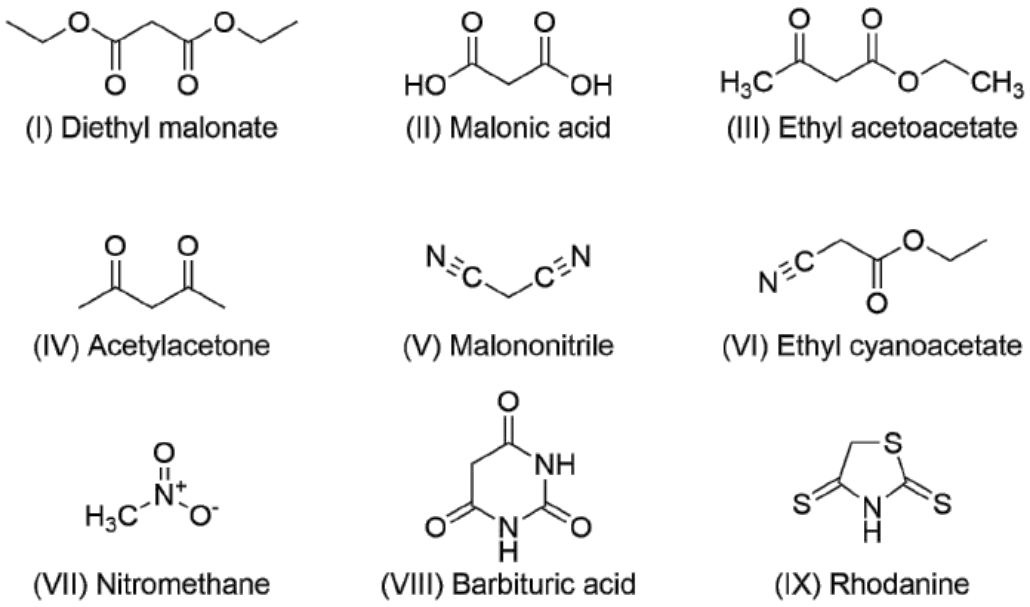


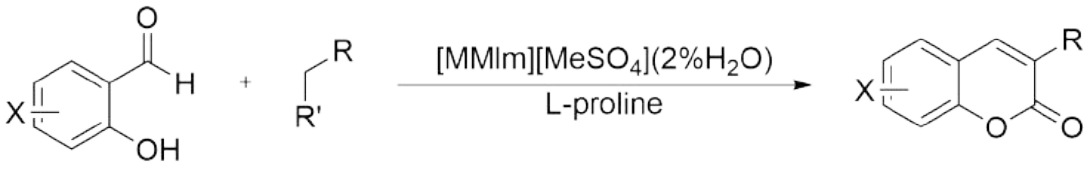
Figure 45. Examples of the active acyclic and cyclic methylene compounds employed in the Knoevenagel condensation.

The active methylene compounds employed in the Knoevenagel condensation can be broadly classified into two major categories: acyclic and cyclic systems. Acyclic systems class includes a range of foundational reactants. Malonic esters and acids are frequently used, with diethyl malonate [45.(I)] serving as a precursor for cinnamic esters and various heterocycles [416]. Malonic acid [45.(II)] itself is central to the Doebner modification, which allows for the direct synthesis of α,β-unsaturated carboxylic acids like cinnamic acids [413]. β-Ketoesters, such as ethyl acetoacetate [45.(III)], are employed in the synthesis of substituted enones and complex dicarbonyl compounds [416]. Similarly, 1,3-diketones like acetylacetone (2,4-pentanedione) [45.(IV)] are used to prepare highly substituted di-acylated alkenes [416]. Cyano-activated compounds represent another vital group. Malononitrile [45.(V)] is a key component in many multi-component reactions and is used to synthesize dicyanoalkenes, including benzylidene malononitrile, the precursor to CS gas [416]. Ethyl cyanoacetate [45.(VI)] is also widely used for the synthesis of α-cyanoacrylates, which are versatile monomers and intermediates [410]. Finally, nitroalkanes such as nitromethane [45.(VII)] are used to synthesize nitroalkenes, which are potent Michael acceptors [417]. Cyclic Systems are the second group. Cyclic active methylene compounds are valuable for constructing complex heterocyclic scaffolds. Among the cyclic 1,3-dicarbonyls, Meldrum's acid is a highly reactive precursor whose products can be easily decarboxylated [416]. Barbituric acid [45.(VIII)] is another important example, used in the synthesis of 5-arylidenebarbiturates, a class of medicinally significant compounds [416, 418]. Other heterocycles also serve as crucial nucleophilic partners. Rhodanine [45.(IX)] is used to synthesize rhodanine-based derivatives that exhibit diverse biological activities and also finds application in polymer synthesis [416, 419]. Oxindole is another key reactant, enabling the synthesis of 3-ylideneoxindoles, a core structure found in many pharmaceuticals, particularly kinase inhibitors used in cancer therapy [416, 420].

3.2 Knoevenagel condensation - application

The Knoevenagel condensation is important reaction in medicinal chemistry and drug discovery, providing access to a vast chemical space of biologically active molecules [411]. Its reliability makes it a key driving force in many multi-component reactions designed to rapidly synthesize compounds for pharmacological screening.

One of the most prominent applications is in the synthesis of heterocyclic compounds. The intramolecular condensation of an active methylene compound with an



Scheme 52. Knoevenagel condensation - synthesis of coumarins [421]

ortho-substituted hydroxybenzaldehyde is a classical and efficient route to coumarins as presented on Scheme 52 [421]. The coumarin core is present in numerous natural products and is the basis for important drugs such as the anticoagulant warfarin (Figure 46) [422].

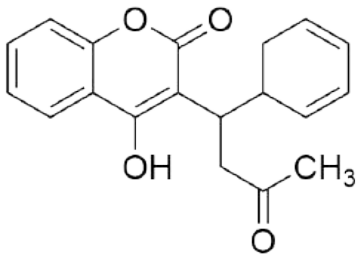
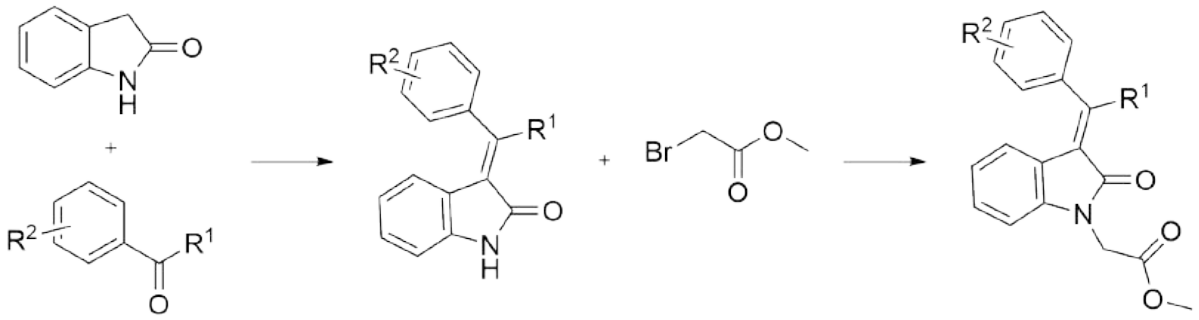


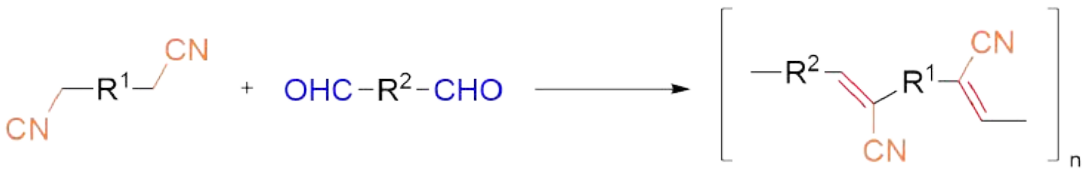
Figure 46. Structure of warfarin - compound with coumarin core [421]

The Knoevenagel reaction is not limited to laboratory-scale synthesis. It has also a key reaction in commercial drug synthesis in the large-scale production of several important drugs. One example is the synthesis of the antimalarial drug lumefantrine, a component of the widely used combination therapy Coartem, where a Knoevenagel condensation is a pivotal bond-forming step. It was employed in the preparation of the C-13 side chain of paclitaxel (Taxol), enabling a more practical and efficient synthetic route [423]. Similarly, the reaction is used in the synthesis of indole-3-acetic acid derivatives, which are further transformed into indomethacin, a well-known anti-inflammatory drug [424]. Important application of Knoevenagel condensation is generation of pharmacological libraries for drug discovery. The modular nature of this reaction makes it ideal for combinatorial chemistry. By reacting a library of diverse aldehydes, often containing known pharmacophores like indole, pyrazole, or benzimidazole, with a library of active methylene compounds, such as oxindoles, barbituric acids, or thiazolidinediones, chemists can rapidly generate large numbers of novel compounds for biological evaluation [255, 411]. This strategy has yielded compounds with potent and varied activities, including anticancer, antioxidant, antimalarial, antidiabetic, and antibacterial properties [411]. For example, Knoevenagel products derived from oxindoles (Scheme 53) have shown significant promise as inhibitors of protein kinases, a critical target in cancer therapy [420].



Scheme 53. Knoevenagel condensation - synthesis of model 3-alkylidene oxindoles [425]

The main problem associated with the Knoevenagel condensation concerns the stereochemistry of the reaction products leading to 3-benzylidene oxindoles and addresses the question of whether it is possible to obtain a product with a defined E or Z configuration in a single synthesis, or whether subsequent isomerization plays the dominant role. Configuration of compounds strongly influences their biological properties. Classical Knoevenagel condensation usually leads to mixtures of isomers, and even after isolation of a pure E or Z form, it may undergo transformations under the influence of UV light, the type of solvent, the pH of the environment, and in certain cases even measurement conditions, such as long-term NMR experiments. For different aldehyde and ketone derivatives, significant differences are observed in the direction and rate of isomerization. A fully stereodefined synthesis of these compounds in a single Knoevenagel reaction is very difficult, and in practice it is often easier to control the configuration of the product through deliberately induced isomerization than through the condensation step itself [425]. Similar application of Knoevenagel reaction is in DNA-encoded libraries. By developing mild reaction conditions that do not damage the DNA barcode, researchers can construct vast libraries of coumarin-conjugated oligonucleotides. These libraries can then be screened against biological targets in a single experiment, representing a powerful new paradigm for hit identification in the early stages of drug discovery [422].



Scheme 54. Scheme of copolimerisation via Knoevenagel polycondensation [426]

The Knoevenagel condensation is a metal-free workhorse for installing vinylene or α,β-unsaturated units directly into polymer backbones and porous networks, enabling extended π-conjugation and reactive handles for post-processing, such as dy-

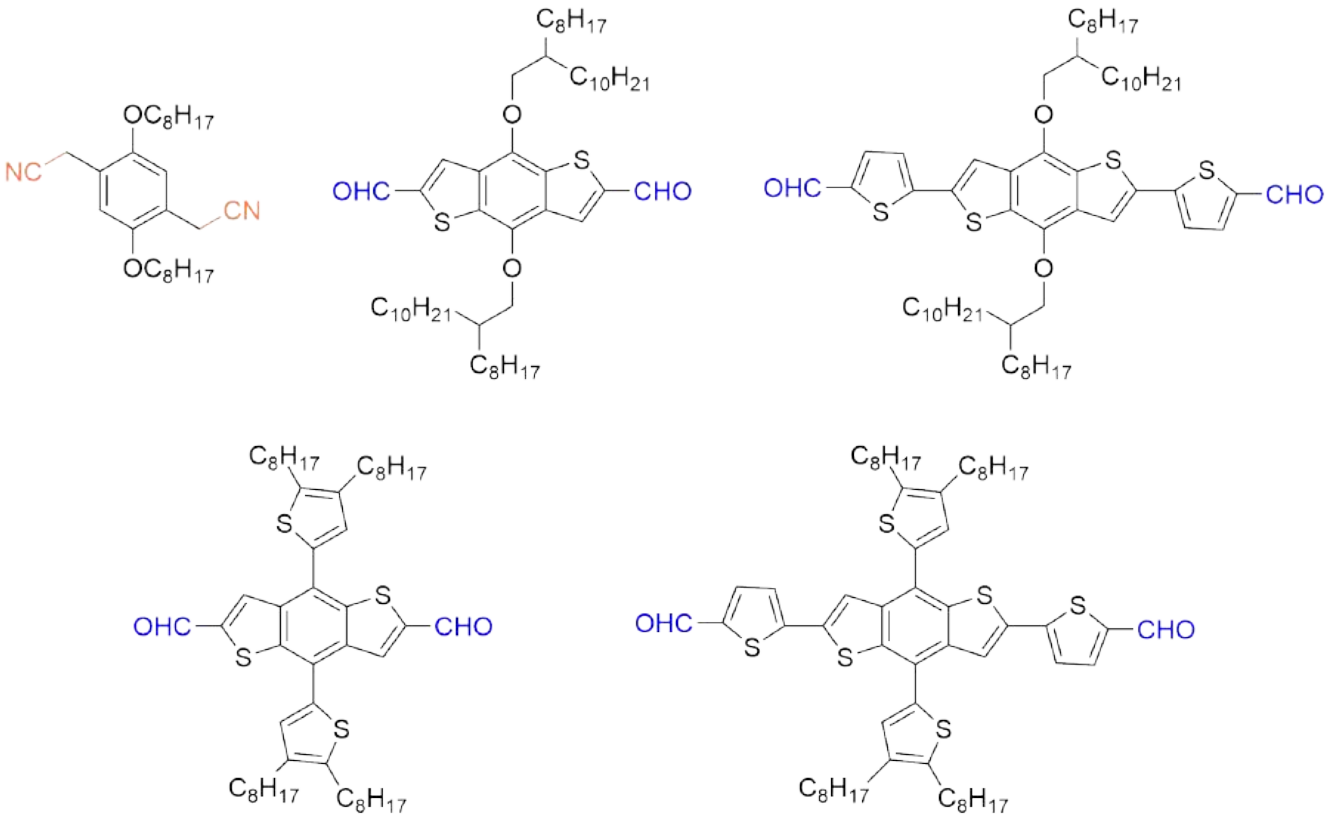


Figure 47. Monomers for copolimerisation via Knoevenagel polycondensation [426]

namic Michael addition-elimination in vinylene-linked COFs [427]. In functional polymer synthesis, tin-free Knoevenagel polycondensation cleanly yields cyanovinylene- or chalcone-type linkers, producing semiconducting conjugated (micro)porous polymers with strong light harvesting and photostability [428, 429]. For organic electronics, Knoevenagel routes have delivered conjugated copolymers used in device-relevant platforms-most visibly polymer solar cells (OPV)-where cyanovinylene-based copolymers have shown high efficiencies without metal residues. Scheme of copolymerisation is presented on Scheme 54 and example of monomers on Figure 47. The same chemistry underpins π-conjugated frameworks and polymers explored for OLEDs and OFETs [426, 430]. Beyond main-chain construction, Knoevenagel-made push-pull chromophores are readily grafted onto high-performance backbones such as poly(aryl ether ketone)s to give robust electro-optic materials with high glass-transition temperatures [431]. A highly innovative application demonstrates the reaction's potential in creating complex polymer architectures. In this approach, a Knoevenagel polycondensation between a bifunctional rhodanine derivative and a dialdehyde is first performed to create a linear polymer backbone containing multiple rhodanine units. This linear polymer then serves as a macroinitiator for a subsequent rhodanine-based anionic ring-opening polymerization (AROP) of thiirane monomers. The result is a complex

multicyclic polymer, where each repeating unit of the original backbone now contains a large cyclic polythioether structure. This tandem strategy provides access to unique polymer topologies that are inaccessible by conventional methods [419].

The Knoevenagel condensation is a versatile transformation that has found widespread industrial use in the production of fine chemicals, agrochemicals, and functional dyes. A prominent example is the Doebner modification, which enables the efficient synthesis of cinnamic acid derivatives through the reaction of benzaldehydes with malonic acid. These cinnamic acid derivatives are important intermediates used in the manufacture of perfumes, cosmetics, and food additives [432, 433]. Beyond fine chemicals, Knoevenagel chemistry provides a valuable route to agrochemically active scaffolds, including cinnamate-type compounds with herbicidal and insecticidal activity, thereby contributing to crop protection strategies [433]. In addition, the extended conjugated π-systems created in this condensation serve as efficient chromophores, which makes the reaction highly relevant to the synthesis of organic dyes and pigments. In particular, it is a key step in the modular synthesis of merocyanine dyes, compounds that exhibit strong charge-transfer absorption and have found applications in dye-sensitized solar cells and organic optoelectronic devices [434].

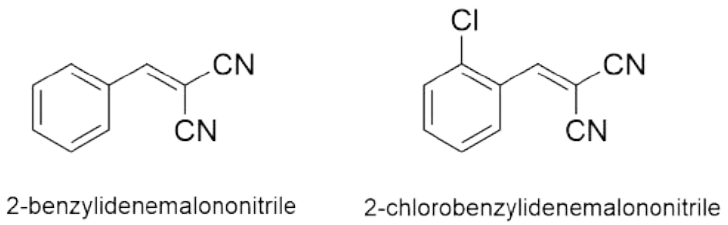


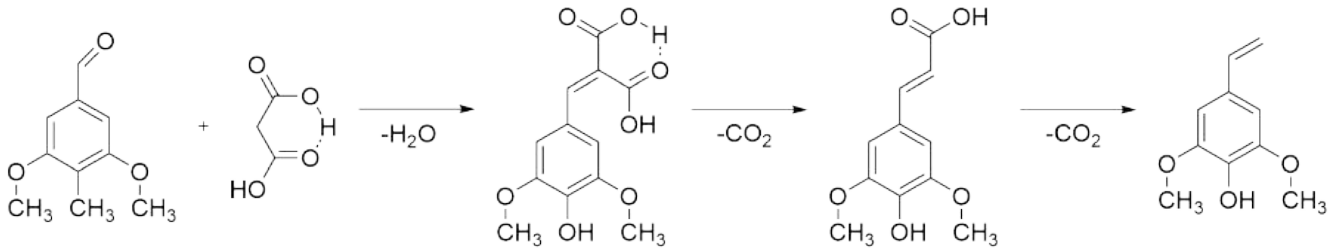
Figure 48. Structure of benzylidenemalononitrile and 2-chlorobenzylidenemalononitrile [418]

The condensation of benzaldehyde with malononitrile is a well-established and important industrial reaction. The product, benzylidenemalononitrile (Figure 48 on left), is a versatile chemical intermediate [435]. It is also known as the precursor to 2-chlorobenzylidenemalononitrile (Figure 48 on right), the chemical agent commonly known as CS gas, which was discovered as a result of this reaction. Research continues to focus on optimizing this specific transformation, with recent efforts developing eco-friendly protocols using catalysts like alum in aqueous media or employing catalyst-free conditions in water to improve sustainability [418, 436].

3.3 Knoevenagel condensation - catalysts

The history and development of the Knoevenagel condensation are linked to the evolution of catalysis. The earliest examples of the Knoevenagel condensation utilized simple, weakly basic homogeneous catalysts. As mentioned in previous subchapters, Knoevenagel's original work identified primary and secondary amines and their salts as effective catalysts for the reaction [437]. For decades, the standard protocol involved using piperidine or pyridine, often with pyridine serving as both the catalyst and the solvent [413].

In 2017, Van Schijndel and co-workers [413] focused on developing a more green version of the Knoevenagel–Doebner condensation, in which pyridine and piperidine were replaced with less toxic catalytic systems. The reaction was carried out under solvent-free conditions As a model reaction, the condensation of syringaldehyde with malonic acid leading to sinapic acid was selected. Reaction scheme is presented on Scheme 55



Scheme 55. Scheme of the Knoevenagel-Doebner reaction served as an example for catalyst examination [413]

Piperidine served as the reference catalyst and, under solvent-free conditions (90℃, 2 h), provided full conversion of the aldehyde and an almost quantitative yield of sinapic acid. In contrast, the absence of any catalyst resulted in a marked slowdown of the reaction and a low product yield, clearly confirming the catalytic role of the basic additive. Piperidine could be replaced by amines primary, secondary, and tertiary amines, such as n-butylamine, dibutylamine, or triethylamine, all enabled the reaction to proceed, although with varied efficiencies, typically in the range of 75-85%. Exact results are presented in the Table 31. Very high activity was observed for 1,2-diaminoethane, but its high toxicity disqualifies it from practical and green applications. A significantly better compromise was 2-aminoethanol, which afforded about 95% conversion and over 90% yield, while posing a much lower environmental risk. Weaker performance was observed for compounds such as TRIS, urea, or glycine, demonstrating that the mere presence of a nitrogen atom is not sufficient; its basicity

and availability under the reaction conditions are crucial. The most important finding reported by Van Schijndel and co-workers in 2017 was the use of ammonium salts as catalysts. Salts such as ammonium chloride, ammonium sulfate, or ammonium bicarbonate were shown to effectively catalyze the Knoevenagel condensation in the solid state. Good results were obtained with ammonium bicarbonate as catalyst, which led to full conversion of syringaldehyde and practically 100% yield of sinapic acid. It was proposed that at elevated temperature this salt decomposes with the release of ammonia, which acts as the actual basic catalytic species. For this reason, NH_4HCO_3 was selected as the catalyst of choice for further studies. Within the investigated substrate scope, it efficiently catalyzed reactions of benzaldehydes bearing both electron-donating and electron-withdrawing groups. In most cases, high substrate conversion was achieved, and reaction selectivity could be controlled by temperature. At lower temperatures, dicarboxylic products predominated, whereas increasing the temperature to about 140℃ favored decarboxylation and led to the corresponding cinnamic acids with isolated yields in the range of 65-90%. For aldehydes containing a hydroxyl group in the para position, a tendency toward secondary decarboxylation and formation of styrene derivatives was observed. The authors proved that the Knoevenagel condensation can be efficiently performed without the use of classical, toxic catalysts, and without solvents, also with simple and inexpensive ammonium salts as catalysts [413].

Table 31. Effect of catalyst on Knoevenagel-Doebner reaction.

Catalyst	Conversion (%)
No catalyst[a]	43
Piperidine	**100**
n-Butylamine	88
Dibutylamine	72
Triethylamine	87
1,2-Diaminoethane	**100**
2-Amino-ethanol	**95**
TRIS	60
Pyridine	88
Benzylamine	**100**
Urea	99
Glycine	57
Ammonium iodide	60
Ammonium sulfate	**98**
Ammonium chloride	**100**
Ammonium bicarbonate	**100**

Researchers have explored even wider range of nitrogen-based catalysts that offer improved performance under milder conditions. For instance, 4,4'-trimethylenedipiperidine - TMDP (Figure 49 has been identified as a highly efficient

and recyclable organocatalyst that provides excellent yields in short reaction times [410]. Other effective organocatalysts include the gentle biological buffer Trizma and carbamic acid ammonium salts, the latter of which can afford product yields up to 98% [410, 438]. A particularly insightful development in this area is the discovery that in more green Knoevenagel protocols using ammonium salts like ammonium bicarbonate, the true catalytic species is not the ammonium ion itself. Instead, it is a double Schiff base - hydrobenzamide formed in situ from the reaction of the aldehyde substrate with ammonia released from the salt. This species then enters a closed catalytic cycle, representing a deeper mechanistic understanding of these seemingly simple systems [412].

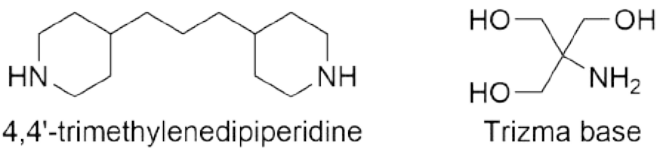


Figure 49. Structures of proposed organocatalysts for Knoevenagel reaction: 4,4'-trimethylenedipiperidine and Trizma base [410]

A major paradigm shift in Knoevenagel catalysis has been the move from homogeneous to heterogeneous systems. Heterogeneous catalysts offer profound advantages that directly address the shortcomings of their homogeneous counterparts and align with the core principles of green chemistry [439, 440].

This has led to the exploration of a wide variety of solid materials as catalysts for the Knoevenagel condensation. One group of those materials are inorganic solid bases and acids. A diverse range of inorganic materials have proven effective. Zeolites and mesoporous silica materials, such as MCM-41 and SBA-15, offer high surface areas and tunable porosity, with their catalytic activity due to basic sites within their frameworks [439, 441].

Coordination polymers can be used as heterogeneous catalysts in the Knoevenagel reaction. They consist of transition metal ions connected by organic ligands into one-, two-, or three-dimensional structures. This combines the potential resulting from the integration of features characteristic of classical organometallic complexes and solid-state materials. The most commonly described metallic centers in coordination polymers are zinc, copper, cobalt, nickel, and manganese ions. These metals primarily act as Lewis acids, activating the carbonyl group of the aldehyde through coordination to the oxygen atom, which facilitates the course of the Knoevenagel condensation. Zinc is particularly frequently employed due to its low toxicity, availability, and good stability under reaction conditions [441, 442]. Example structure of this kind coordination

polymer is presented on Figure 50.

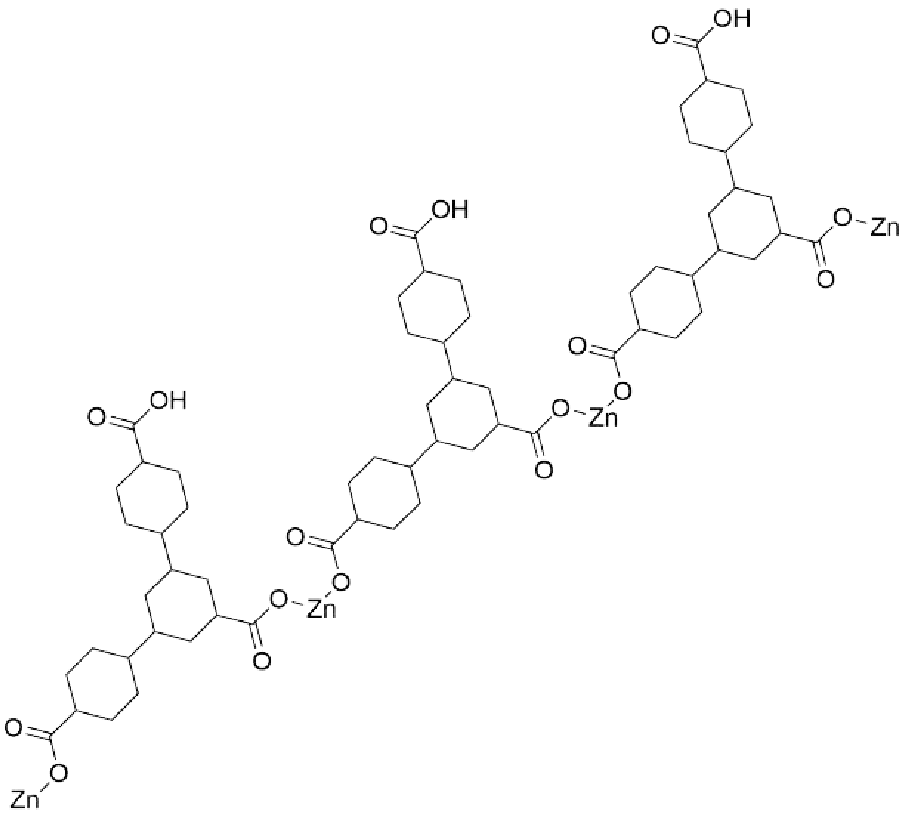
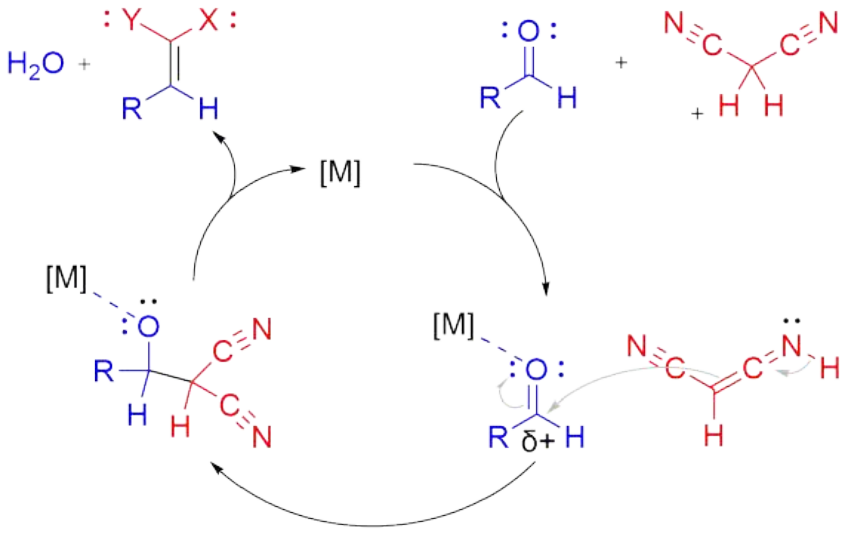


Figure 50. Structure of example monofunctional CP [442]

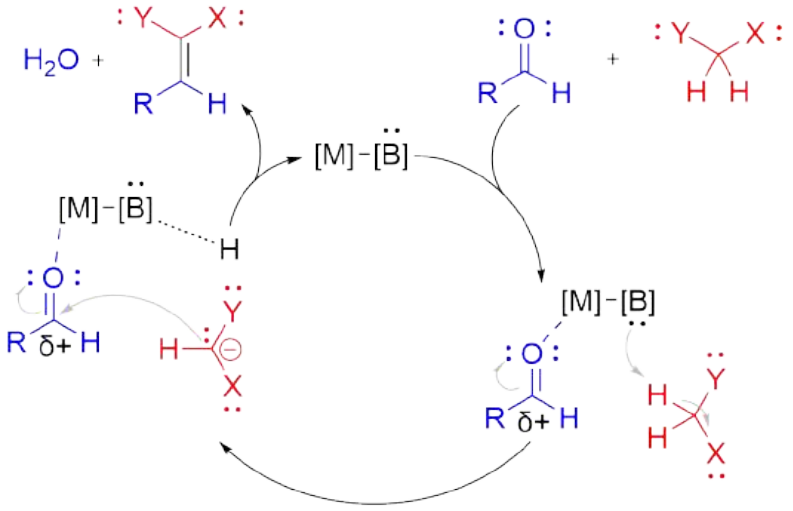
The mere presence of a metal does not guarantee high catalytic activity. Instead, its coordination environment and the accessibility of active sites are of key importance. Organic ligands and the topology of the entire coordination network play a significant role in shaping the catalytic properties. Carboxylate and nitrogen-containing ligands influence not only the structural stability but also the acid–base character of the catalyst. In many cases, ligands may participate in substrate activation as weak bases, assisting the deprotonation of compounds containing an active methylene group. An overly compact structure, despite attractive crystallinity, may limit the access of reagents to the metallic centers, resulting in low catalytic activity. In contrast, moderate porosity and the presence of open metal sites favor an efficient reaction course [441].

The mechanism of the Knoevenagel reaction catalyzed by coordination polymers is most often described as an acid-base process assisted by a metallic center. In the first step, the aldehyde coordinates to the metal ion, which increases the electrophilicity of the carbon atom of the carbonyl group. Subsequently, deprotonation of the compound containing the active methylene group occurs, and the resulting anion attacks the activated aldehyde. After the condensation step and elimination of a water molecule (H_2O), the reaction product detaches from the surface of the catalyst. In some reported sys-

tems, it is suggested that catalysis is not exclusively metal-centered but rather results from the cooperation between the metal and the ligands. Mechanism for monofunctional CPs as catalysts is presented on Scheme 56 and one example mechanism for bifunctional CPs as catalysts is presented on Scheme 57.



Scheme 56. Catalytic cycle for the aldehyde-malononitrile Knoevenagel condensation catalyzed by monofunctional CPs [441]



Scheme 57. Example catalytic cycle for the aldehyde-malononitrile Knoevenagel condensation catalyzed by bifunctional CPs [441]

Many coordination polymers enable the Knoevenagel condensation to be carried out under mild conditions, often in solvents considered more environmentally friendly, such as ethanol or water, and in some cases even without the use of a solvent. Reaction temperatures are usually moderate, and the obtained yields are high, although strongly dependent on the nature of the substrates. At the same time, the lack of standardization of reaction conditions in the literature makes reliable comparison of

the activity of individual catalysts difficult. These catalysts also have significant drawbacks. Some coordination polymers lose activity after only a few reaction cycles, and in certain cases leaching of metal ions into the solution is observed, which undermines the heterogeneous nature of the catalysis. Coordination polymers constitute a promising but still insufficiently explored group of catalysts for the Knoevenagel reaction. Their effectiveness depends largely on rational structural design, the accessibility of active centers, and the stability of the material under reaction conditions.

Metal oxides, particularly in nanoparticulate form, such as $ZnO - NPs$, or MgO, are robust and efficient catalysts [439]. Layered double hydroxides (LDHs), such as $Cu - Mg - AlLDH$, are another important class of solid base catalysts that show excellent activity and retain their structural integrity over many cycles [439]. Another example of a tailored heterogeneous catalyst are porous metal phosphates like porous magnesium aluminum phosphate (MALPO). MALPO is obtained by a hydrothermal method from aqueous solutions of magnesium and aluminum salts and phosphoric acid. First, a solution of H_3PO_4 is prepared, into which solutions of $Mg(NO_3)_2 \cdot 6H_2O$ and $Al(NO_3)_3 \cdot 9H_2O$ are then slowly added simultaneously. During this stage, the pH of the mixture is maintained at approximately 7 by the addition of a concentrated ammonia solution. After the dosing is completed, the mixture is stirred intensively for several more hours at room temperature and subsequently transferred to an autoclave, where it is subjected to hydrothermal treatment at a temperature of about 180℃ for several days. Under these conditions, crystallization of magnesium–aluminum phosphate with a well-developed surface area and acid–base character occurs. After completion of the synthesis, the solid product is separated by filtration, thoroughly washed with water and organic solvents in order to remove residual ions and precursors, and then dried under vacuum, yielding an active heterogeneous MALPO catalyst. In the Knoevenagel reaction, MALPO acts as a solid acid-base catalyst that simultaneously activates both substrates. Basic surface sites facilitate deprotonation of a compound containing an active methylene group, such as malononitrile, while acidic sites coordinate the carbonyl group of the aldehyde, increasing its electrophilicity. As a result, the condensation proceeds efficiently already at room temperature, most often in ethanol as the solvent. After completion of the reaction, the catalyst remains in the solid phase and can be easily separated by filtration, and after simple washing and thermal reactivation, it can be reused in subsequent cycles without significant loss of catalytic activity [440].

Coordination polymers and their sub-class, metal-organic frameworks - MOFs, have emerged as premier platforms for the rational design of high-performance heteroge-

neous catalysts [441]. These crystalline materials are constructed from metal ions or clusters - nodes - connected by organic molecules - linkers. Their features, including extraordinarily high surface areas, tunable pore sizes, and chemical diversity, make them ideal for catalysis. The active sites in metal-organic frameworks can be precisely engineered by judiciously selecting the metal nodes and functionalizing the organic linkers. A key reason for their great performance in the Knoevenagel condensation is their ability to function as bifunctional catalysts. This represents a more sophisticated catalytic strategy than simple base catalysis - different parts of the framework cooperate to activate both reactants simultaneously, creating a synergistic effect that dramatically enhances reaction rates under mild conditions. The mechanism typically involves lewis acid activation, where the exposed metal centers at the nodes, such as Cu^{2+}, Zn^{2+}, Pb^{2+}, act as Lewis acid sites. They coordinate to the carbonyl oxygen of the aldehyde, increasing its electrophilicity and making it more susceptible to nucleophilic attack. From the other side we have Lewis/Brønsted base activation, where basic sites located elsewhere in the framework deprotonate the active methylene compound. These basic sites can be uncoordinated functional groups on the organic linker like an amino group, NH^2 or part of the framework itself, a bridging hydroxide group, $\mu 2 - OH - OH$ [441, 443, 444].

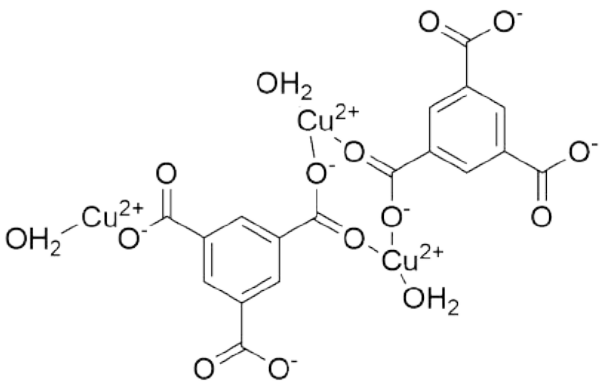
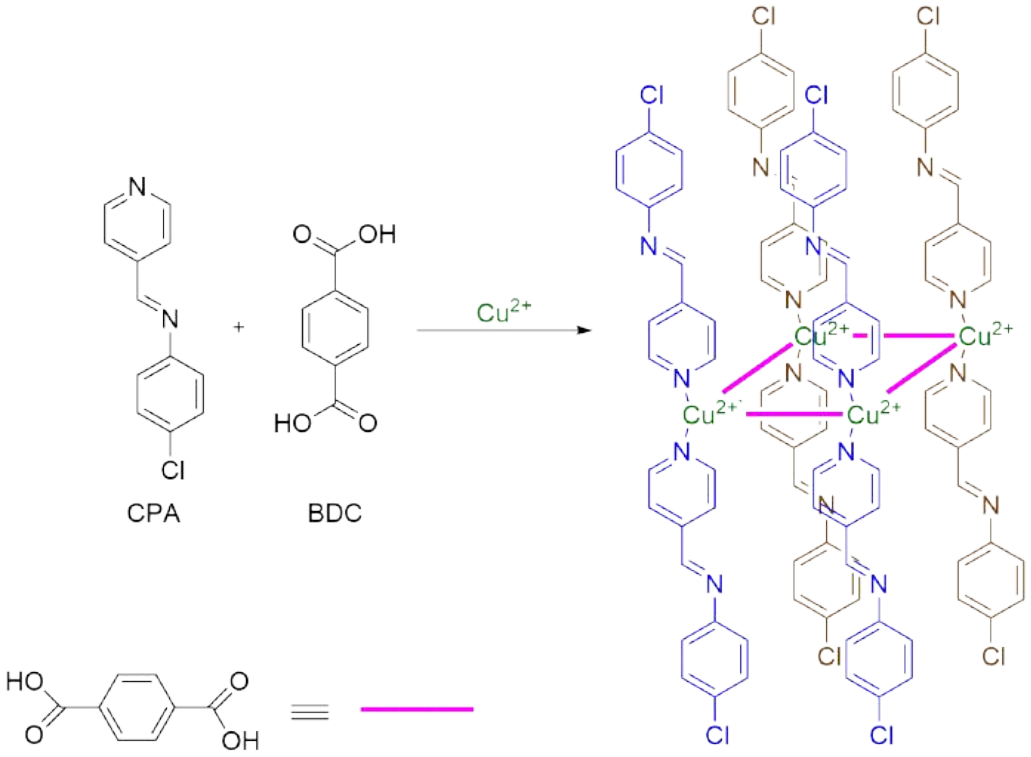


Figure 51. Amino-functionalized HKUST - Cu-based MOF, HKUST-1 used as bifunctional catalyst in Knoevenagel condensation [410]

This cooperative activation on a single, rigid surface is highly efficient. Several case studies illustrate the power of this approach. One example is amino-functionalized HKUST - Cu-based MOF, HKUST-1 (Figure 51), can be post-synthetically modified by grafting various amine-containing molecules onto its unsaturated copper sites. In the resulting material, the $Cu(II)$ centers act as Lewis acids, while the newly introduced amine groups serve as Brønsted basic sites. These bifunctional frameworks are superb catalysts, capable of achieving 100% conversion in the condensation of benzaldehyde

and malononitrile in just 5 minutes at room temperature. They are also highly robust and can be recycled for at least five runs without significant loss of activity [443, 445]. Cu-MOF (Scheme 58) is material containing copper - a metal–organic framework constructed from Cu^{2+} ions and CPA and BDC ligands, forming a two-dimensional network with a (4,4)-type topology. X-ray diffraction studies confirmed its crystalline nature and porous structure, with an average pore diameter of approximately $7, \mathrm{nm}$.

The material exhibits good thermal stability and a high specific surface area, which makes it a promising candidate for heterogeneous catalysis. It is proved that Cu-MOF acts as a highly active heterogeneous catalyst under mild conditions between variously substituted benzaldehydes and compounds containing an active methylene group, malononitrile or ethyl cyanoacetate. The optimal reaction conditions checked by Naskar and the team [445] involved the use of 3 mol % of the Cu-MOF catalyst, a mixed solvent system of H_2O:$MeOH$ in a 3:1 ratio, and room temperature. The reactions proceeded very rapidly— in most cases, full conversion was achieved within 15 minutes, without the need for heating or the addition of any external base [445].



Scheme 58. Scheme of synthesis of Cu-MOF with BDC = 1,4-benzenedicarboxylate [445]

Wide range of aromatic aldehydes, both those bearing electron-donating substituents (–OH, –OMe) and unsubstituted ones, afforded yields in the range of 97 and 99%. The presence of different functional groups on the aromatic ring did not significantly reduce the catalytic activity, indicating good functional group tolerance of the

system. The authors emphasize that the high efficiency of the reaction arises from the presence of Cu^{2+} centers within the MOF structure, which activate the carbonyl group of the aldehyde and facilitate nucleophilic attack by the active methylene compound. At the same time, the porous architecture of the material promotes efficient diffusion of the reactants and contributes to the fast reaction rate. Overall, the Cu-MOF is an efficient, fast, and mild catalyst for the Knoevenagel condensation. It operates in an aqueous medium, at room temperature, with a low catalyst loading, and provides nearly quantitative yields within a very short reaction time [445].

Another example is mixed-linker $Zn(II)$ MOFs. A novel strategy involves constructing MOFs from a single type of metal cluster but two different organic linkers. One neutral linker and one bearing a basic or acidic functional group. This approach has been used to create a series of isoreticular $Zn(II)$ MOFs that contain both cyclic and linear trinuclear zinc clusters. These materials function as Brønsted acid-base bifunctional catalysts and are highly active for solvent-free Knoevenagel condensations [444]. Heterometallic $Pb_{10}K_2$-organic framework (NUC-45a) is the catalyst which introduce multiple metals into a framework what can result with a rich variety of active sites. The framework NUC-45a, built from $Pb_{10}K_2(\mu_2 - OH)_2(COO)_{24}$ clusters, possesses a multitude of Lewis acid sites - Pb^{2+}, K^+) and Lewis base sites, which are the bridging $\mu_2 - OH$ group and the nitrogen atom of the pyridine-based linker. This bifunctionality makes NUC-45a a great catalyst for the Knoevenagel condensation [446].

3.4 Knoevenagel condensation - results and discussion on use of ecocatalysis

3.4.1 Methodology

The same catalyst as in the hydrophosphonylation experiments was employed. For details regarding its preparation, see Section 2.4.1.1 (p. 124) Preparation of Eco-MgZnOx catalyst derived from *Arabidopsis halleri*.

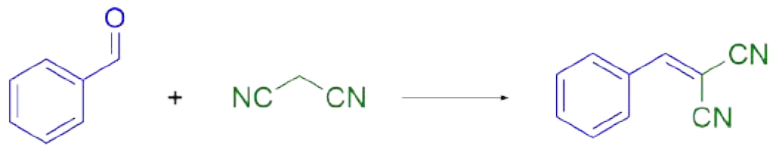
The reactions were carried out according to the same protocol as in the hydrophosphonylation experiments, described in Section 2.4.1.2 (p. 126) General procedure for the reactions.

The same methods were applied as in Section 2.4.1.3 (p. 127) Analysis of catalyst, reaction mixtures and products.

3.4.2 Optimization results of the Knoevenagel condensation

Reaction conditions were first optimized for the model reaction - the Knoevenagel condensation of benzaldehyde with malononitrile, giving benzylidene malononitrile. The reaction scheme is included in the first row of Table 32. Different temperatures, reaction times, solvents, and EcoCatalyst compositions were evaluated in order to determine the most efficient and sustainable conditions, what is sumed up in the Table 32.

Table 32. Knoevenagel addition on model substrates catalyzed by EcoCatalysts[a]



1a 5a 6a

No.	Catalyst	T [℃]	t [h]	Conversion[b]	Conversion with EcoCatalyst[b]		Solvent
					P	F	
1	-	RT	3	0%	67%[c]	81%[d]	None
2	-	RT	24	4%	83%[c]	83%[d]	None
3	-	50	1	25%	89%[c]	94%[d]	None
4	-	50	1	25%	83%[e]	94%[f]	None
5	-	70	1	19%	93%[c]	97%[d]	None
6	-	80	1	0%	91%[c]	94%[d]	None
7	-	80	2	27%	100%[c]	100%[d]	None
8	-	70	1	19%	96%	97%	None
9	-	70	2	28%	100%[c]	100%[d]	None
10	-	70	2	0%	83%	96%	Toluene
11	-	70	2	0%	76%[c]	89%[d]	Ethyl Acetate
12	-	70	2	31%	99%[c]	91%[d]	Methanol
13	MgO[g]	70	2	100%	-	-	None
14	MgO[h]	70	2	72%	-	-	None
15	ZnO[i]	70	2	100%	-	-	None
16	ZnO[j]	70	2	86%	-	-	None
17	$CaCO_3$[k]	70	2	7%	-	-	None
18	$CaCO_3$[l]	70	2	7%	-	-	None
19	MgO+ZnO[m]	70	2	97%	-	-	None
20	MgO+ZnO[n]	70	2	98%	-	-	None

[a] Reaction conditions: benzaldehyde (1): 0.23 mmol, malononitrile (2): 0.23 mmol;
[b] determined by 1H NMR of crude reaction mixture;
[c] 7.5 mg of Eco-MgZnOx-P: Mg (7.0 mol%), Ca (13.6 mol%), Zn (5.7 mol%);
[d] 7.5 mg of Eco-MgZnOx-F: Mg (3.5 mol%), Ca (11.4 mol%), Zn (4.9 mol%);
[e] 15 mg of Eco-MgZnOx-P: Mg (14.0 mol%), Ca (27.2 mol%), Zn (11.4 mol%);
[f] 15 mg of Eco-MgZnOx-F: Mg (7.0 mol%), Ca (22.8 mol%), Zn (9.8 mol%);
[g] 7.0 mol% of Mg;
[h] 3.5 mol% of Mg;
[i] 5.7 mol% of Zn;
[j] 4.9 mol% of Zn;
[k] 13.6 mol% of Ca;
[l] 11.4 mol% of Ca;
[m] 7.0 mol% of Mg + 5.7 mol% of Zn
[n] 3.5 mol% of Mg + 4.9 mol% of Zn

The results show that in the absence of a catalyst the conversion is very low, even after prolonged heating, which confirms that catalysis is essential for this reaction. When EcoCatalysts obtained from hyperaccumulator-derived mixed metal oxides were used, the reaction proceeded with almost complete conversion under relatively mild conditions. Eco-MgZnOx-based catalysts containing magnesium, calcium and zinc oxides exhibited excellent activity, while individual simple oxides such as MgO, ZnO or CaO alone were much less effective, pointing to the importance of synergistic interactions between metals in the eco-derived materials. The reaction was found to work best under solvent-free conditions, since the use of solvents such as toluene, ethyl acetate or methanol did not improve the outcome and in some cases even lowered the conversion. Increasing the temperature to 70℃ significantly enhanced the reaction efficiency, and two hours were sufficient to reach full conversion in the presence of EcoCatalyst. On the basis of these findings, the optimal conditions were established as 70℃ for 2 hours, solvent-free, using an EcoCatalyst corresponding to about 5 mol% Zn, under which the Knoevenagel condensation proceeds nearly quantitatively.

The conversion of the condensation reaction was calculated based on the ^{1}H NMR spectrum of the post-reaction mixture. On the example NMR spectrum (Figure 52) signals from product - benzylidenemalononitrile - and substrates - residual benzaldehyde and unreacted malononitrile - are visible. For this purpose, the methylene signal of malononitrile at 3.59 ppm was chosen as the internal reference and normalized to 2.00, since it corresponds to two protons and shows reliable integration (in contrast to the aldehydic proton, which relaxes slowly and typically integrates lower than expected).

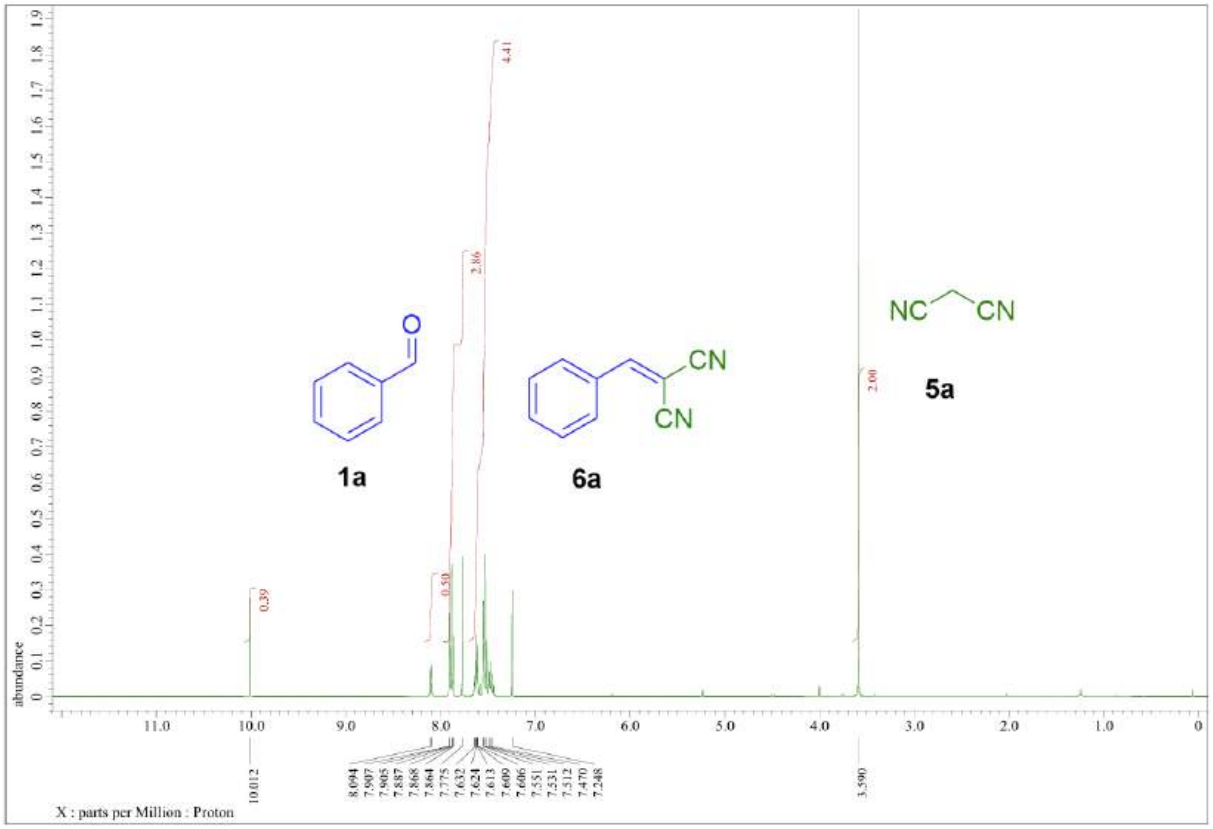


Figure 52. ^{1}H NMR spectrum (400 MHz, $CDCl_3$) of the crude reaction mixture after the condensation of benzaldehyde with malononitrile.

In the aromatic region (7.45-7.90 ppm) both the five aromatic protons of benzaldehyde and the five aromatic protons of the product overlap. After normalization, the integral of this region was 7.27. Subtracting the expected 5.00 protons from benzaldehyde leaves 2.27 protons attributable to the product. Since each mole of product contributes five aromatic protons in this region, the product corresponds to $2.27/5 = 0.454$ mol per 1 mol of starting material. The conversion, calculated as

$$\text{Conversion} = \frac{\text{Product}}{\text{Product} + \text{Substrate}} = \frac{0.454}{0.454 + 1.000} = 0.31\ (31\%),$$

was thus obtained.

This result was cross-checked using the isolated vinylic proton of the product at 8.09-8.11 ppm, which corresponds to one proton per product molecule. In the normalized spectrum, this signal integrated to 0.50, corresponding to 0.50 mol of product. The conversion, calculated as

$$\frac{0.50}{0.50 + 1.00} = 0.33\ (33\%),$$

agrees with the previous estimate.

If the vinylic proton overlaps with the aromatic region, then the product contributes

six protons (five aromatic and one vinylic) in the 7.45-7.90 ppm range. In such a case, the integral of this region was 7.77, from which subtraction of 5.00 protons of benzaldehyde leaves 2.77 protons for the product. Dividing by six gives 0.462 mol of product per 1 mol of substrate, and the corresponding conversion is

$$\frac{0.462}{0.462 + 1.000} = 0.32\ (32\%).$$

In summary, depending on the method of integration, the conversion of the reaction is consistently estimated at about 31-33%. The methylene signal of malononitrile was used as the reference, since the aldehydic proton at 10.01 ppm is not reliable for quantitation due to its long relaxation time T_1.

The second reaction that was subjected to optimization was the Knoevenagel condensation of benzaldehyde with ethyl cyanoacetate, affording the corresponding benzylidene cyanoacetate. The reaction scheme is included in the first row of Table 33, which summarizes the results.

Table 33. Knoevenagel condensation on model substrates catalyzed by EcoCatalysts[a]



1a **5b** **7a**

No.	T [℃]	t [h]	Conversion without catalyst[b]	Conversion[b] with EcoCatalyst	
				P[c]	F[d]
1	RT	1	0%	0%	0%
2	RT	24	0%	67%	53%
3	50	1	0%	62%	59%
4	80	1	0%	84%	85%
5	80	2	18%	92%	100%
6	70	2	0%	92%	100%

[a] Reaction conditions: benzaldehyde (1): 0.23 mmol, ethyl cyanoacetate (4): 0.23 mmol, solvent free.
[b] Determined by ^{1}H NMR of crude reaction mixture.
[c] 7.5 mg of Eco-MgZnOx-P: Mg (7.0 mol%), Ca (13.6 mol%), Zn (5.7 mol%).
[d] 7.5 mg of Eco-MgZnOx-F: Mg (3.5 mol%), Ca (11.4 mol%), Zn (4.9 mol%).

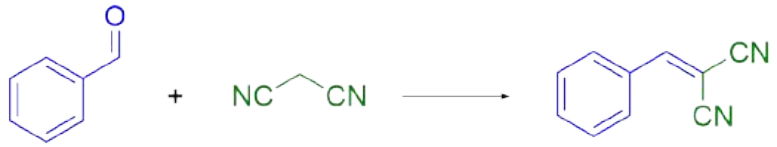
As in the case of malononitrile, for condenstation with cyanoacetate, no conversion was observed without a catalyst, even at elevated temperature. The use of EcoCatalysts led to a significant improvement, with conversions reaching up to 100% under

optimized conditions. The most efficient results were obtained similarly at 70℃ after 2 hours under solvent-free conditions, again highlighting both the high catalytic activity and the sustainable character of the EcoCatalyst system.

3.4.3 Reusage of the catalyst in the Knoevenagel condensation

The reusability of ecocatalysts in the model Knoevenagel condensation between benzaldehyde and malononitrile ($R_1 = CN$) was investigated for the model reaction summarized in Table 32.

Table 34. Recovery and reuse of the catalyst in Knoevenagel condensation - model reaction. R_1 = CN



1a **5a** **6a**

Entry (Run)	Conversion without catalyst[b] [%]	Conversion	
		Eco-MgZnOx-Pc[c]	Eco-MgZnOx-Fd[d]
1.	0%	99%	99%
2.	0%	98%	99%
3.	0%	99%	99%
4.	0%	99%	97%
5.	0%	77%	-

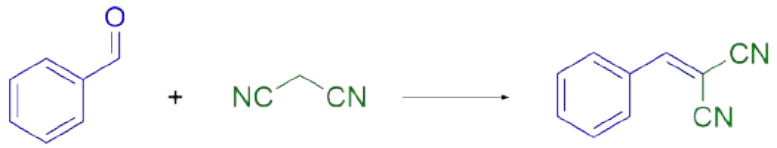
a Reaction conditions: benzaldehyde (1): 1 equiv., malononitrile (2): 1 equiv.
b Determined by ^{1}H NMR of crude react)ion mixture.
c Eco-MgZnOx-P: Mg (7.0 mol%), Ca (13.6 mol%), Zn (5.7 mol%).
d Eco-MgZnOx-F: Mg (3.5 mol%), Ca (11.4 mol%), Zn (4.9 mol%).

Both ecocatalysts: Eco-MgZnOx-P and Eco-MgZnOx-F exhibited excellent catalytic activity, reaching conversions of 97-99% during four runs. High conversions were consistently maintained for four cycles. These results clearly demonstrate that the ecocatalysts obtained from hyperaccumulating biomass are not only highly active in the Knoevenagel reaction but can also be reused multiple times with only a gradual loss of efficiency. This underlines their potential as sustainable heterogeneous catalysts, combining both catalytic effectiveness and reusability.

3.4.4 Scale-up of the Knoevenagel condensation

A model Knoevenagel reaction with malononitrile as a substrate, corresponding to the optimization shown in Table 32, was conducted under optimal conditions on a larger scale to obtain approximately 1 gram of the product. Substrates were used in amounts of 4.6 mmol, analogous to previous studies. Results are shown in the Table 35.

Table 35. Scale-up of the model reaction of Knoevenagel condensation for R_1 = CN[a].



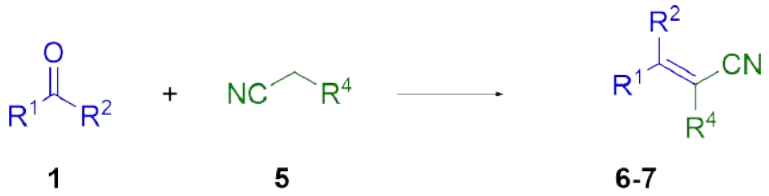
1a 5a 6a

Catalyst	Conversion [%][b]	Yield [%]
Eco-MgZnOx-P[c]	99%	98%[e]
Eco-MgZnOx-F[d]	99%	97%[f]

a Reaction conditions: benzaldehyde (1): 6.4 mmol, malononitrile (2): 6.4 mmol.
b Determined by ^{1}H NMR of crude reaction mixture.
c 210 mg of Eco-MgZnOx-P: Mg (7.0 mol%), Ca (13.6 mol%), Zn (5.7 mol%).
d 210 mg of Eco-MgZnOx-F: Mg (3.5 mol%), Ca (11.4 mol%), Zn (4.9 mol%).
e 976 mg of pure product (3).
f 966 mg of pure product (3).

3.4.5 Substrate scope of the Knoevenagel condensation

The substrate scope of the Knoevenagel condensation catalyzed by the eco mixed-oxide materials (EcoMgZnO-P and EcoMgZnO-F) were investigated and presented below. Two active-methylene substrates were tested: malononitrile (R_4 = CN on Scheme 2, products 6a-6i presented on Figure 53) and ethyl cyanoacetate (R_4 = COOEt on Scheme 2, products 7a-7f presented on Figure 54). The carbonyl set covers a broad range: aryl aldehydes with both donating and withdrawing groups (Me, Cl, NO_2), heteroaromatic aldehydes (pyridyl, thienyl), aliphatic aldehydes (linear and branched), and one ketone. The aim was to probe electronic effects, sterics, tolerance to N/S heteroatoms, and the performance of both catalyst variants. Numbers next to each entry are conversions and values in parentheses are isolated yields.



Scheme 2. Knoevenagel condensation

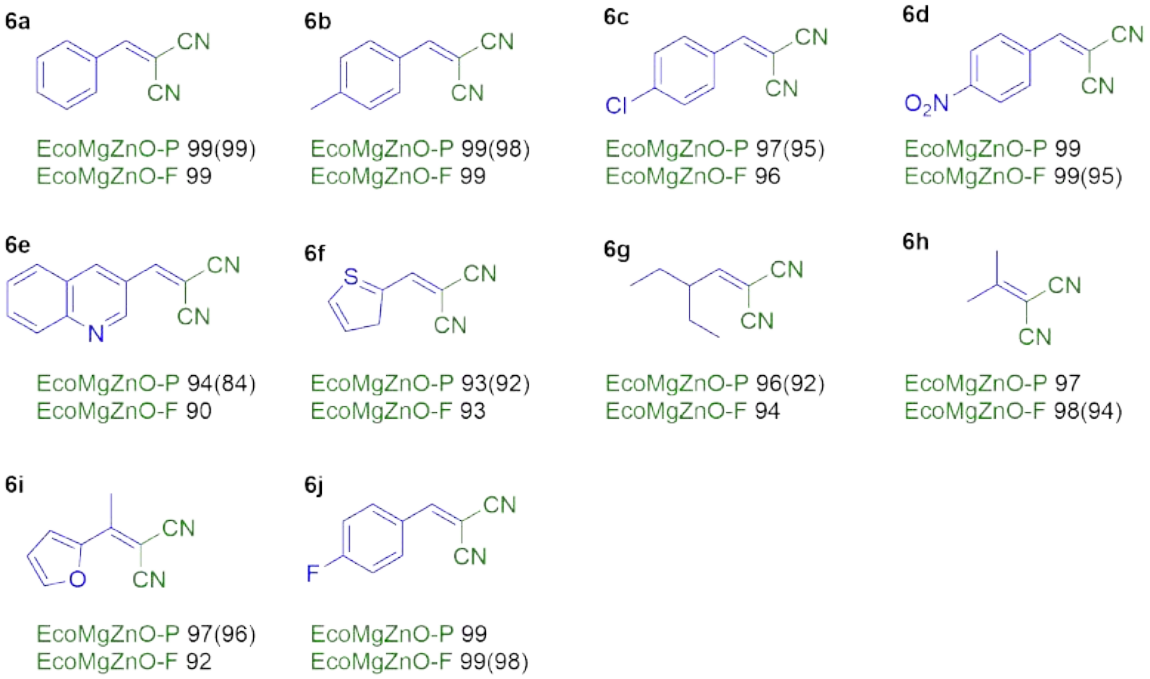


Figure 53. Substrate scope of Knoevenagel condensation - scope of carbonyl compounds with malononitrile. Numbers next to each entry are conversions and values in parentheses are isolated yields.

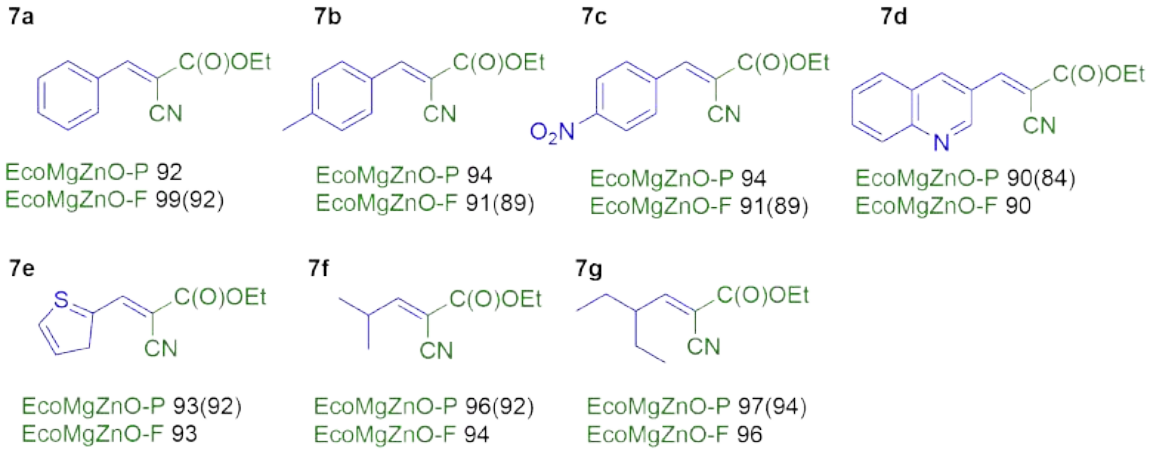
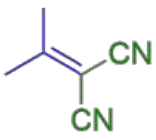


Figure 54. Substrate scope of Knoevenagel condensation - scope of carbonyl compounds with ethyl cyanoacetate. Numbers next to each entry are conversions and values in parentheses are isolated yields.

All aldehydes react with malononitrile giving very high conversions - typically above 90%, often 99% - across aryl, heteroaryl, and aliphatic substrates. The ketone example also performs well. Electronic effects are small: both electron-rich and electron-poor rings work, and halogens and nitro groups are well tolerated. With ethyl cyanoacetate the reaction remains broadly efficient (about 90-99% conversion), though on average it is a little less reactive than with malononitrile, and isolated yields for the harder cases fall to 84-92%. This points to the expected reactivity order of the pronucleophiles: malononitrile is faster and gives near-quantitative outcomes, while ethyl cyanoacetate is slightly slower but still practical. The two eco-catalysts behave very similarly; differences are only a few percentage points ($EcoMgZnO - P$ is sometimes a touch better with malononitrile, while $EcoMgZnO - F$ occasionally edges it with ethyl cyanoacetate). In short, the scope is wide and useful for Knoevenagel condensations - covering diverse aryl patterns, N/S-heteroaromatics, and aliphatic aldehydes - with good functional-group tolerance and even workable reactivity for a representative ketone.

All isolated products were characterized using standard spectroscopic methods (experimental details are given in Chapter 7). To present the key structural features of the products and to demonstrate the consistency of the spectroscopic data across the whole series, one representative compound was chosen for discussion. Compounds 6h and 7c were selected as a model example. They structure and high purity were confirmed by ^{1}H and ^{13}C NMR spectroscopy, which show the expected signals with no evidence of side products or substrates.

For the 6h compound (Figure 55) the ^{1}H NMR spectrum (Figure 57) confirms the high symmetry of the molecule through the presence of only one intense singlet (2.26 ppm), which perfectly corresponds to six chemically equivalent protons originating from two methyl groups. The ^{13}C NMR spectrum (Figure 56) demonstrates the presence of a complete carbon framework, revealing four unique signals, including characteristic resonances for cyano groups (approximately 112 ppm) as well as for a strongly polarized double bond (signals at around 85 ppm and 180 ppm).



.

Figure 55. 6h – 2-(propan-2-ylidene)malononitrile

For the 7c compound (Figure 58 the ^{1}H NMR spectrum (Figure 60) identifies the molecular fragments, showing characteristic signals of an ethyl group (triplet and quar-

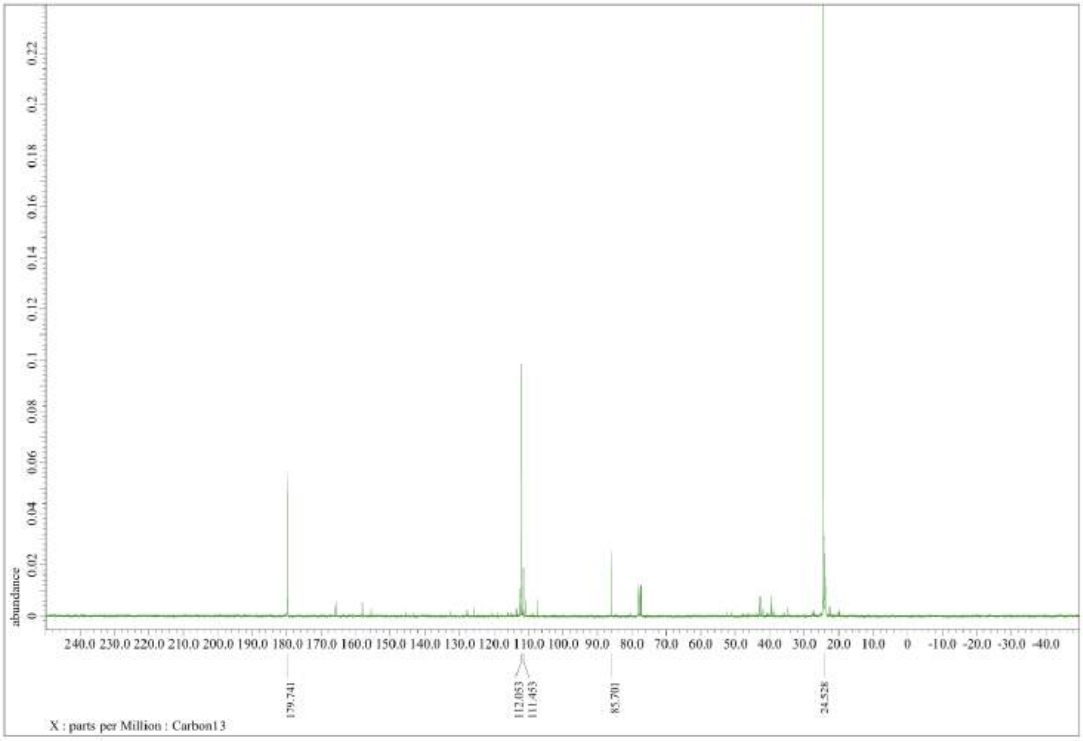


Figure 56. ^{13}C NMR spectrum of 6h – 2-(propan-2-ylidene)malononitrile

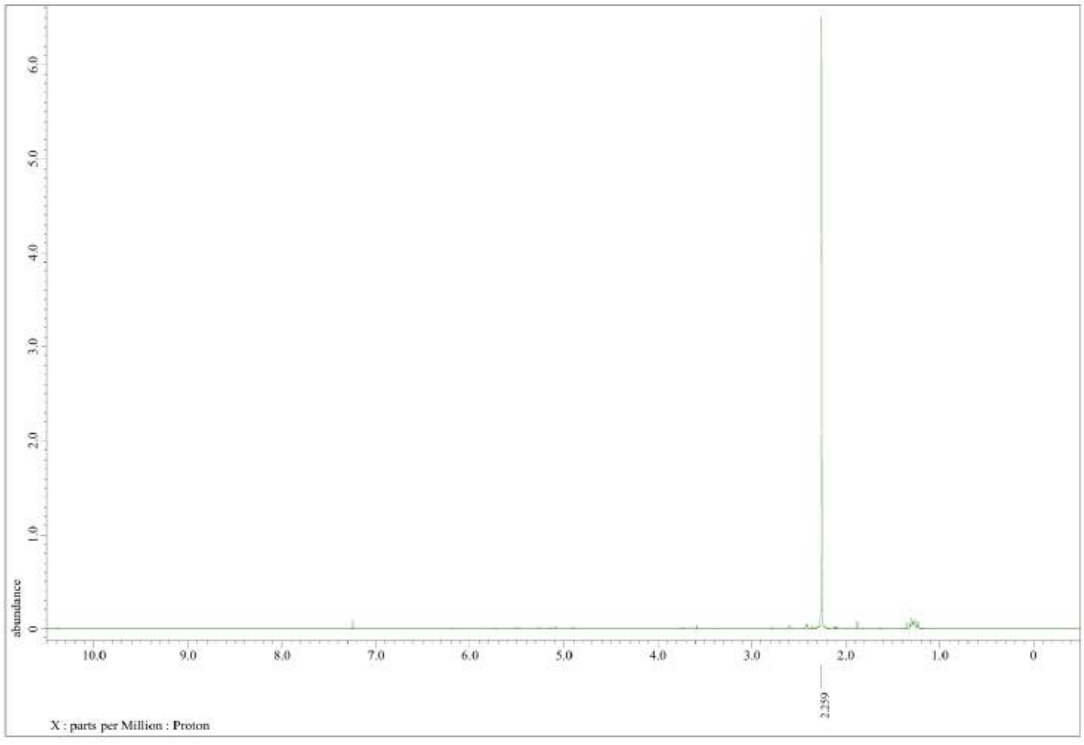
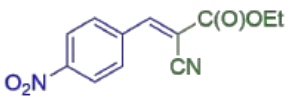


Figure 57. ^{1}H NMR spectrum of 6h – 2-(propan-2-ylidene)malononitrile

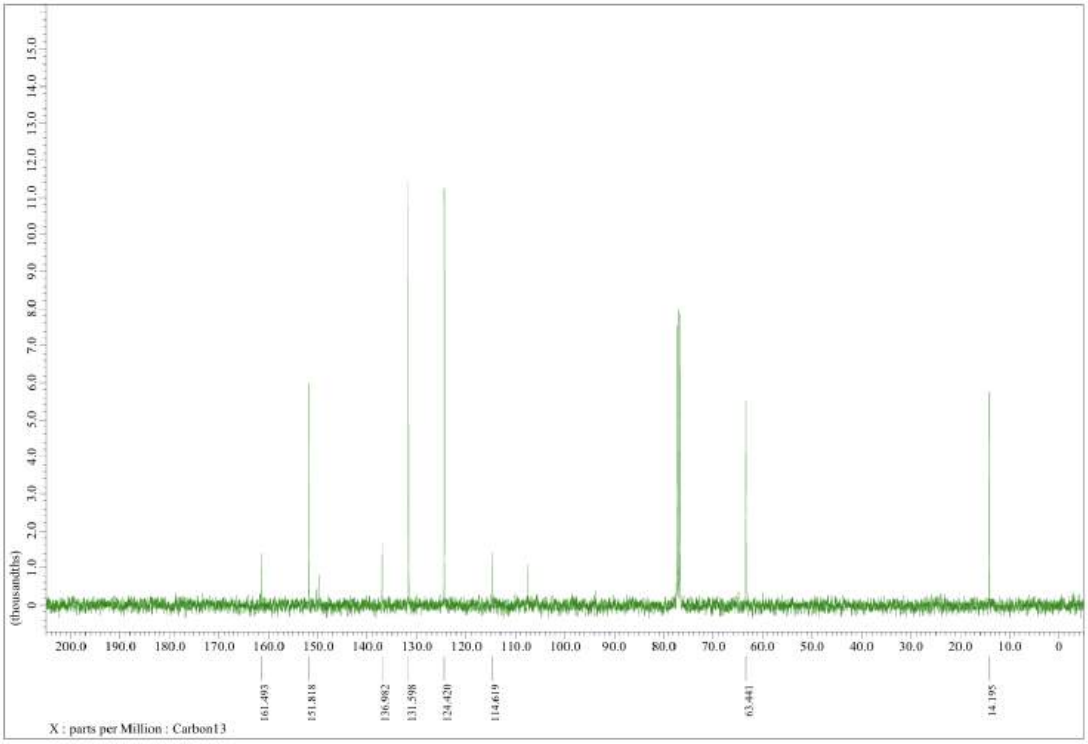
tet) as well as a specific pattern of two doublets in the aromatic region, which is typical for a para-substituted benzene ring. In turn, the ^{13}C NMR spectrum (Figure 59) confirms the presence of all functional groups, revealing unique signals for the carbon of

the cyano group (114 ppm) and for the ester carbonyl carbon (a161 ppm).



.

Figure 58. 7c – ethyl (E)-2-cyano-3-(4-nitrophenyl)acrylate



.

Figure 59. ^{13}C NMR spectrum of 7c – ethyl (E)-2-cyano-3-(4-nitrophenyl)acrylate

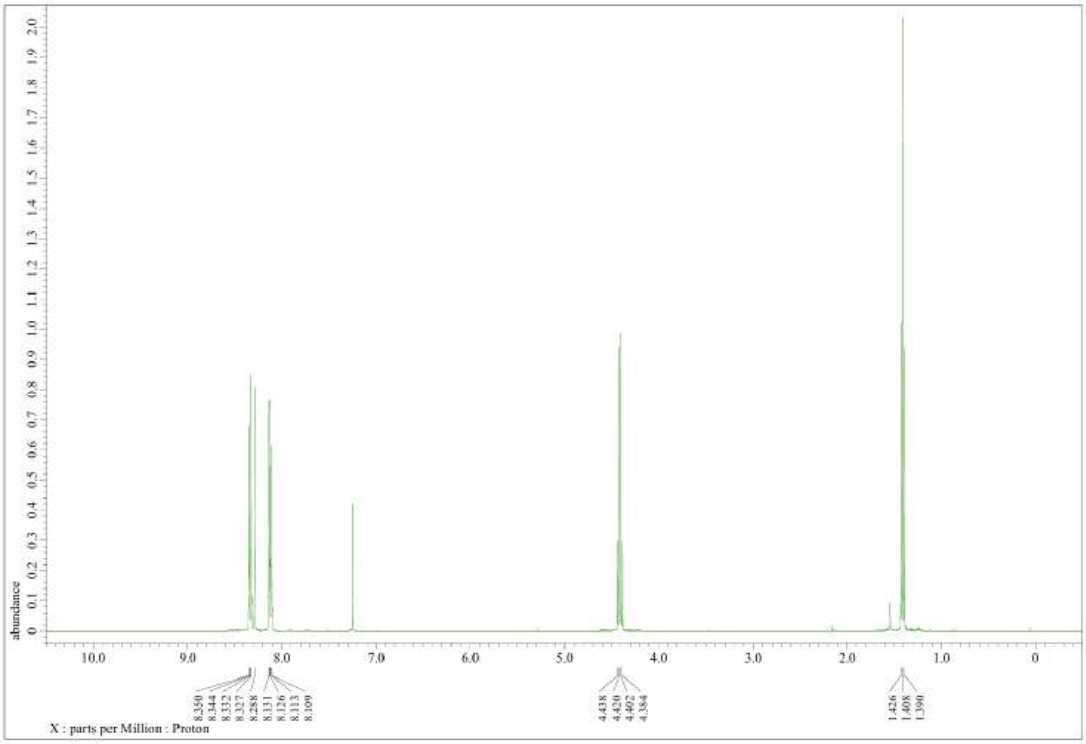


Figure 60. ^{1}H NMR spectrum of 7c – ethyl (E)-2-cyano-3-(4-nitrophenyl)acrylate

3.4.6 Conclusions

It was demonstrated that the ecocatalyst Eco-MgZnOx derived from *Arabidopsis halleri* biomass is an efficient heterogeneous catalyst for the Knoevenagel condensation between aldehydes and activated methylene compounds. The catalyst enables effective $C\breve{}C$ bond formation under mild and solvent-free conditions, in line with the principles of green chemistry.

The developed catalytic protocol operates at moderate temperatures and low catalyst loading, providing the desired Knoevenagel products in high yields and with good selectivity. A broad range of aldehydes, including aromatic, heteroaromatic, and aliphatic substrates, as well as activated methylene donors such as malononitrile and cyanoacetates, were successfully converted. In most cases, high conversions and clean reaction mixtures were obtained, allowing straightforward product isolation.

The catalytic activity of Eco-MgZnOx was shown to be superior to that of single-component oxides such as MgO or ZnO, as well as their physical mixtures. This enhanced performance is attributed to the bifunctional nature of the catalyst, combining basic MgO sites responsible for deprotonation of the methylene compound with Lewis-acidic ZnO sites that activate the carbonyl group of the aldehyde. The close proximity of these sites within the mixed oxide structure enables cooperative activation of both reaction partners and facilitates efficient $C\breve{}C$ bond formation.

It was further shown that the Eco-MgZnOx catalyst exhibits good stability and recyclability in the Knoevenagel condensation. The catalyst could be recovered from the reaction mixture and reused in several consecutive cycles with only a minor decrease in activity. Additionally, the reaction was successfully scaled up to the gram scale without loss of efficiency or selectivity, confirming the robustness and practical applicability of the catalytic system.

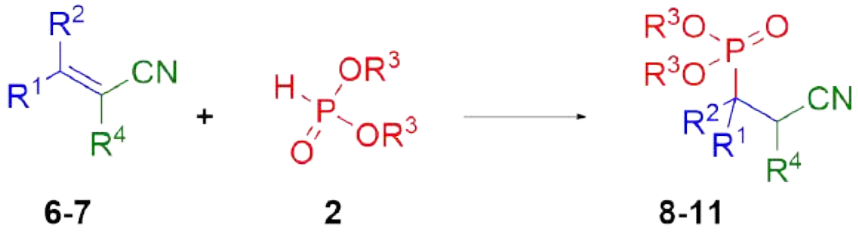
In summary, the results presented in this chapter establish Eco-MgZnOx as a versatile, recyclable, and sustainable catalyst for the Knoevenagel condensation. This study further supports the concept of ecocatalysis and demonstrates that plant-derived polymetallic oxides can serve as effective platforms for key $C^{\sim}C$ bond-forming reactions in organic synthesis.

Chapter 4:
Phospha-Michael addition reaction

4.1 Phospha-Michael addition reaction - chemical basics

Michael addition is a fundamental chemical reaction in organic chemistry. It is nucleophilic addition where nucleophile undergo conjugate addition - reaction of nucleophile with α, β-unsaturated carbonyl compounds. The broad scope of Michael addition is evident in its role in the efficient formation of $C-C$ and $C-X$ bonds, contributing to the synthesis of natural products and drugs through tandem sequences [447].

The phospha-Michael reaction is formally defined as the 1,4-conjugate addition of a phosphorus-based nucleophile to an electron-deficient double or triple carbon-carbon double bond substituted by the acceptor [447–449], as presented on Scheme 3.



Scheme 3. Phospha-Michael addition

This process is highly versatile method for the formation of a new $P-C$ bond, enabling the direct connection of a phosphorus center to a carbon framework. The reaction's strength lies in the vast combination of nucleophiles and electrophiles that can be successfully coupled, leading to a diverse array of functionalized organophosphorus products [449]. The reaction was first reported in the mid-20th century. In 1956, Miller and co-workers demonstrated that disubstituted phosphine oxides $R_2P(O)H$ could add to activated α,β-unsaturated compounds under basic conditions using traces of sodium alkoxide as catalyst to afford β-phosphoryl carbonyl and nitrile adducts [450]. This seminal work represents the discovery of the phospha-Michael type addition. Subsequent early studies in the 1960s extended the concept to other $P(III)$ substrates; for example, Hindersinn reported the addition of trialkyl phosphites to activated alkenes, maleate esters, under thermal conditions, forming phosphonate products [451]. Throughout the 1970s, the scope and mechanism of $P-H$ additions to unsaturated systems were further delineated by Pudovik and Konovalova, who published a comprehensive review in 1979 summarizing the Pudovik reaction, so addition of $P-H$ to $C=O$ or $C=N$ and related additions to $C=C$ [452].

The identity of the phosphorus nucleophile is a key determinant of the reaction con-

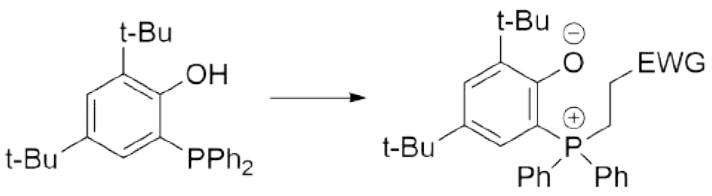
ditions and mechanism. The most commonly employed nucleophiles are hydrophosphoryl compounds, which have a reactive $P-H$ bond. This category includes several groups. One group are secondary phosphine oxides. Species like diphenylphosphine oxide $(Ph_2P(O)H)$ are prototypical nucleophiles in this reaction. They are stable, easy to handle, and readily add to a wide range of Michael acceptors [444, 453, 454]. Another group are dialkyl and diaryl phosphites, so compounds such as diethyl phosphite $(EtO)_2P(O)H$ and diphenyl phosphite $(PhO)_2P(O)H$. They are not expensive, commercially available and serve as excellent nucleophiles, particularly in base-catalyzed variants of the reaction [326, 449]. Primary and secondary phosphines, such as phenylphosphine $PhPH_2$ and diphenylphosphine Ph_2PH are another group which can also serve as nucleophiles. However, due to their lower intrinsic nucleophilicity compared to their deprotonated counterparts and their susceptibility to oxidation, their addition often requires activation by transition metal catalysts or harsh reaction conditions [448, 455]. The last group are tertiary phosphines. While lacking a $P-H$ bond for a net addition, tertiary phosphines, such as triphenylphosphine Ph_3P, or tris(2-carboxyethyl)phosphine, TCEP can act as nucleophilic initiators in catalytic cycles or add to Michael acceptors to form stable, zwitterionic phosphonium adducts. This mode of reactivity is particularly important in organocatalysis and bioconjugation [456–458].

The electrophilic substrates are typically alkenes or alkynes activated by one or more electron-withdrawing groups - EWGs. The degree of activation dictates the required reaction conditions, with more electron-deficient systems reacting more readily. The scope of Michael acceptors is broad. α,β-unsaturated carbonyls and their derivatives are the largest and most classical category of Michael acceptors, encompassing α,β-unsaturated ketones, such as chalcones or methyl vinyl ketone, esters, such as acrylates, cinnamates or crotonates, amides, such as acrylamide, and nitriles such as acrylonitrile [453, 457]. The scope extends to other activated alkenes like vinyl sulfones, nitroalkenes, such as β-nitrostyrenes, and highly activated systems like coumarins and isopropylidenemalononitrile [444, 453]. Modern advancements have significantly expanded the range of accessible Michael acceptors. This includes the successful addition to more complex systems such as β,γ-unsaturated α-ketoesters, which present unique reactivity profiles [455], iminochromenes, which serve as precursors to biologically active heterocycles [459]; and α-fluorinated acrylates, leading to valuable polyfunctionalized products containing contiguous $C-P$ and $C-CFY_2$ bonds [460]. A recent frontier involves the use of activated, electron-deficient alkynes as Michael acceptors. These substrates can undergo a unique and ultrafast organocatalyst-mediated double phospha-Michael addition, where two equivalents of

a $P-H$ nucleophile add across the triple bond, providing a rapid route to geminal bis(phosphorus) compounds [461].

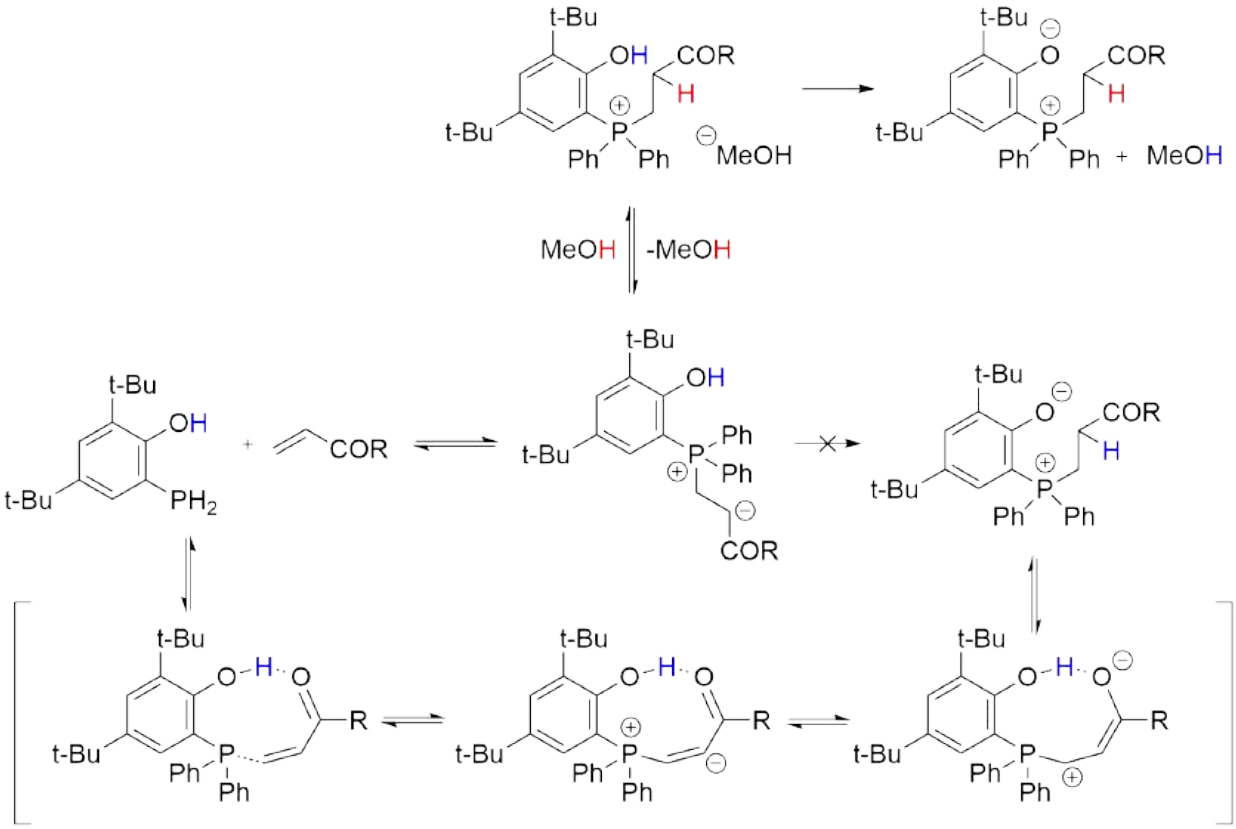
The phospha-Michael reaction includes key steps like the nucleophilic attack of the phosphorus atom at the β-carbon of the Michael acceptor, forming a transient carbanionic or zwitterionic intermediate, which is subsequently protonated to yield the final 1,4-adduct [457, 458]. A crucial mechanistic feature, particularly for hydrophosphoryl compounds like dialkyl phosphites, is the existence of a tautomeric equilibrium. These species exist predominantly in the tetracoordinate phosphonate form $HP(O)(OR)_2$, which is relatively unreactive as a nucleophile. However, they are in equilibrium with a small amount of the trivalent phosphite tautomer $P(OH)(OR)_2$, which is significantly more nucleophilic at the phosphorus center. The actual nucleophilic attack in many base-catalyzed reactions proceeds through this minor but highly reactive phosphite tautomer. This understanding reframes the role of the catalyst: a base does not simply deprotonate the phosphonate to form a phosphite anion - in bifunctional catalytic systems, the basic moiety can actively engage with the hydrophosphoryl compound to shift this tautomeric equilibrium, increasing the concentration of the active phosphite nucleophile. This concept is central to explaining the high efficiency of certain organocatalysts, which are designed with a basic site specifically to facilitate this phosphonate-to-phosphite conversion, thereby priming the nucleophile for the subsequent addition step [459].

It can be intuitively assumed that the formation of the new $P-C$ bond is the slowest, rate-determining step of the reaction, kinetic investigations have revealed a different mechanism. For a wide range of phospha-Michael additions, particularly those involving tertiary phosphines or intramolecular proton sources, the subsequent proton transfer step required to neutralize the initially formed carbanionic intermediate is often the rate-determining step [457, 462]. For instance, in the reaction of 2,4-di-tert-butyl-6-(diphenylphosphino)phenol with various Michael acceptors (presented on Scheme 59), the initial nucleophilic attack forms a zwitterionic intermediate, which is then stabilized by an intramolecular proton transfer from the phenolic hydroxyl group to the carbanion. Kinetic analysis demonstrated that this proton transfer is the rate-limiting event [457].



Scheme 59. Reaction of 2,4-di-tert-butyl-6-(diphenylphosphino)phenol with various Michael acceptors [457].

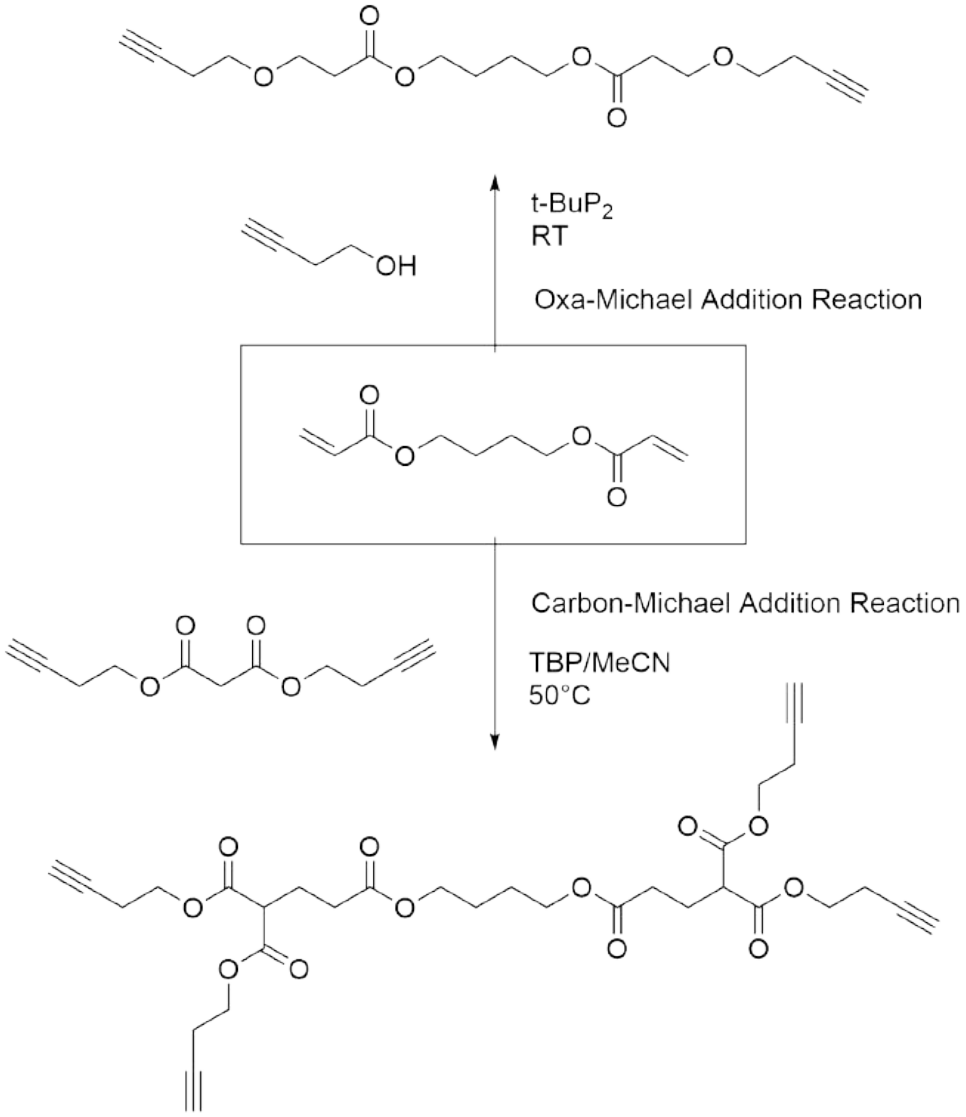
This finding has consequences for catalyst design and reaction optimization. An effective catalyst must not only promote the initial nucleophilic attack but also facilitate an efficient proton transfer - so it explains the success of bifunctional catalysts, which possess both a basic site to activate the nucleophile and a hydrogen-bond donor or Brønsted acid site. Detailed mechanism of this reaction is presented on Scheme 60.



Scheme 60. Mechanism for proton transfer in zwitterion formation with Michael acceptors [457].

The initial conjugate addition step in the phospha-Michael reaction is often reversible. This retro-phospha-Michael reaction, where the adduct reverts to the starting materials, presents both a challenge and an opportunity. From a synthetic point of view, reversibility can lead to incomplete conversions and complex product mixtures, especially under thermodynamic control. It also poses a significant challenge for conducting reproducible kinetic studies, as the concentration of the adduct may not increase linearly. To overcome this, kinetic analyses often employ a trapping agent, such as a Brønsted acid, to irreversibly protonate the zwitterionic intermediate, preventing the back reaction and allowing for the accurate determination of forward rate constants [458]. From other standpoint, this inherent reversibility can be a powerful feature in materials science. While not yet as widely explored for the phospha-Michael reaction as for its oxa- and thiol-Michael counterparts, the principle of dynamic covalent chemistry

applies. The reversible nature of the $P - C$ bond formation could be exploited to create dynamic polymer networks. Such materials could exhibit desirable properties like self-healing, malleability, and recyclability. The bonds within the network could break and reform under specific stimuli like heat or catalyst, allowing the material to be reprocessed or to repair damage. This transforms a mechanistic challenge in traditional synthesis into a desirable design principle for the creation of advanced, sustainable materials [463]. Oxa-Michael and Carbon-Michael reactions were proved to be used for synthesis of multifunctional alkyne building blocks from commercially available acrylate monomers [464], as presented on Scheme 61.



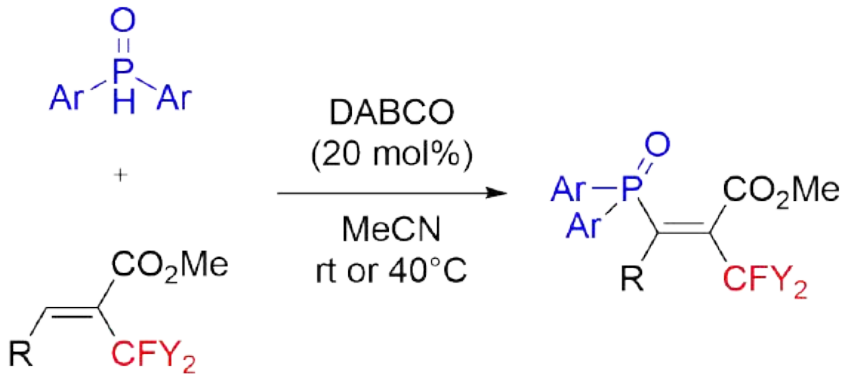
Scheme 61. Oxa- and Carbon-Michael reaction exploited for alkyne building blocks synthesis [464].

The success and efficiency of the reaction depends on the electronic and steric nature of the Michael acceptor, the substituents on the phosphorus atom, and the

specific catalyst and reaction conditions employed [326].

4.2 Phospha-Michael addition reaction - application

Phospha-Michael addition is a versatile and powerful tool in organic synthesis, offering a pathway to a wide array of molecule structures. The usage of this reaction varies from the synthesis of complex molecules with potential pharmaceutical relevance to the creation of materials for advanced technological applications. For instance, α-fluorinated acrylates as Michael acceptors has opened new avenues for synthesizing molecules with $C-P$ and $C-CFY_2$ (where Y = F or H) bonds, demonstrating how phospha-Michael addition can be used to create fluorinated compounds with potential biological activity [465]. General concept of this reaction is presented on Scheme 62.



Scheme 62. Reaction with α-fluorinated acrylates as Michael acceptors [465].

From the other hand Dieter Enders and his colleagues discussed the formation of bioactive phosphonic acids through this reaction [448].

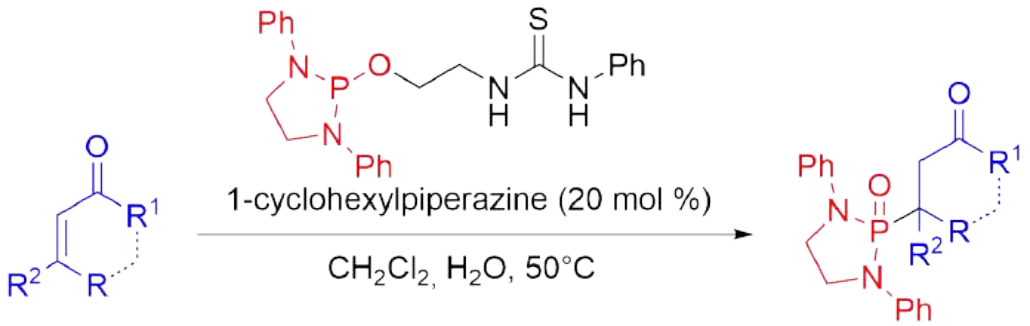
The phospha-Michael addition is crucial for creating ligands for late-transition metals, which are essential in various catalytic processes. Enders et al. also highlight the importance of phosphorus-containing ligands in coordination chemistry [448].

In asymmetric synthesis, the phospha-Michael addition is employed to produce chiral phosphorus compounds with high stereoselectivity [466]. Use of chiral phosphite ligands in asymmetric catalysis was developed. The development of flame retardant materials is another important application. The reaction is used to synthesize flame retardant thermosets by adding phosphorus-containing groups to polymers [467]. In the field of protein functionalization, the phospha-Michael addition serves as a click reaction for modifying protein surfaces with phosphorus groups [456], as presented on Scheme 63.



Scheme 63. Phospha-Michael addition as a click reaction for modifying protein surfaces [456].

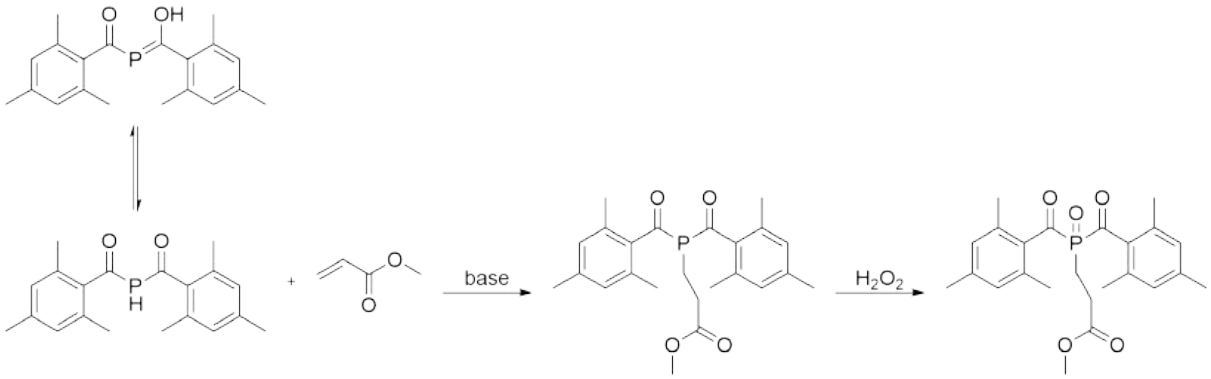
Moreover, the reaction is utilized to synthesize various phosphorus ligands and catalysts used in organic synthesis and industrial applications. Example of this aplication is the synthesis of multifunctional N-Heterocyclic phosphine-thioureas [466] (Scheme 64).



Scheme 64. Synthesis of multifunctional N-Heterocyclic phospine-thioureas [466].

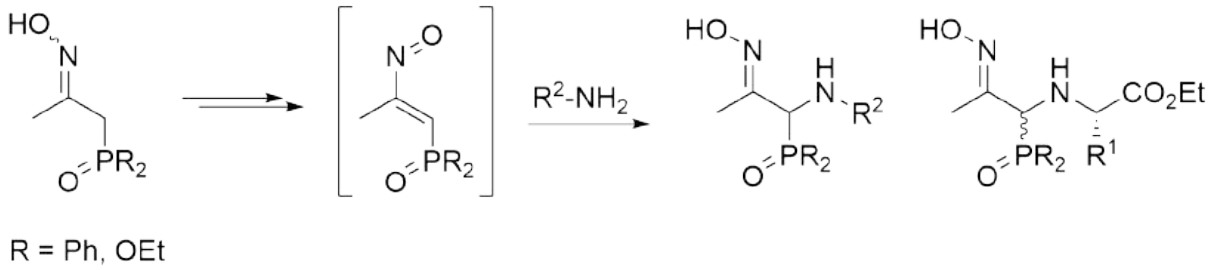
Microwave-assisted reactions also benefit from the phospha-Michael addition. These reactions can enhance reaction rates and yields [468].

The reaction is also used to create flame-retardant materials by incorporating phosphorus groups into polymers [467]. In the development of functional polymers with desired physical and chemical properties, the phospha-Michael addition plays a key role. Xuewen Huang and his team discussed this application in their work on α-fluorinated acrylates [465]. Finally, the phospha-Michael addition is used to synthesize customized bis(acyl)phosphane oxide photoinitiators for photopolymerization applications. Riccardo Conti at al (2022) developed an efficient method for this synthesis [469]. Additionally, the development of bis(acyl)phosphines through phospha-Michael addition, followed by their oxidation to bis(acyl)phosphane oxides, highlights the method's significance in producing potent photoinitiators for radical polymerizations, which are crucial in material science and engineering [469]. Tautomeric structures of BAPH and reaction scheme of its phospha-Michael addition to methyl acrylate followed by oxidation to BAPO are shown on Scheme 65



Scheme 65. Phospha-Michael addition of BAPH and oxidation to BAPO [469].

The transition metal-free synthesis of β-hydrazonophosphine oxides via phospha-Michael reaction further demonstrates the method's applicability in generating precursors for phosphorylated N-heterocycles, α-aminophosphonates, and vinylphosphonates, which are valuable in medicinal chemistry and agriculture [470]. The unusual regioselectivity achieved in the phosphine-catalyzed Michael addition of arylcyanoacetates to allenoates opens new possibilities for accessing molecular structures with quaternary centers, further expanding the synthetic utility of PMA [471]. Functionalized phosphonates, accessible via phosphite addition, demonstrate the method's relevance in producing compounds with applications in various fields, including materials science and drug development [472]. The use of ultrasound activation in phospha-Michael addition, shows the method's adaptability to innovative activation techniques, potentially enhancing reaction efficiency and selectivity [473]. The generation of nitrosoalkenes from phosphine oxides and phosphonates, followed by Michael addition, is another example of the versatility of this method. It enables the synthesis of α-amino phosphine oxides and phosphonates (as presented on Scheme 66), which are valuable compounds in synthetic and medicinal chemistry [470].



Scheme 66. The generation of nitrosoalkenes from phosphine oxides and phosphonates [470].

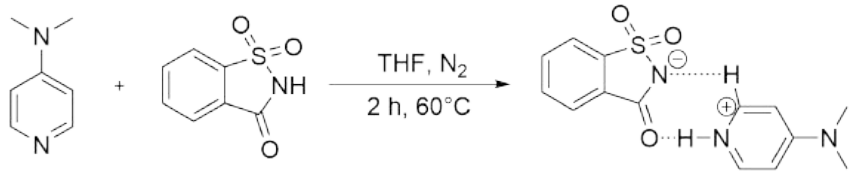
Lastly, the application of phospha-Michael reaction in curable compositions for substrate coating, utilizing a tertiary phosphine catalyst, highlights the method's industrial

relevance, particularly in the development of quick-curing materials for various applications [343]. In summary, the current applications of phospha-Michael addition are multifaceted, ranging from the synthesis of biologically active molecules and materials for technological applications to the development of asymmetric synthesis methods and innovative industrial processes.

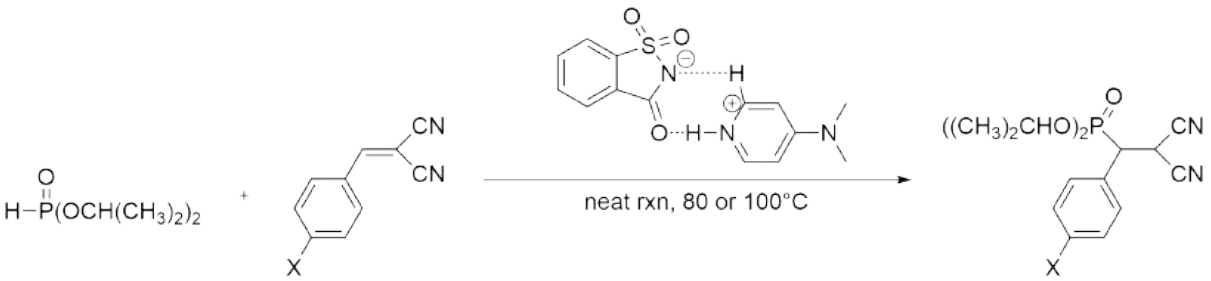
4.3 Phospha-Michael addition reaction - catalysts

In the area of phospha-Michael addition, different catalysts have been used to facilitate the reaction. Basic catalysts are the most classic and widely used for promoting phospha-Michael reactions. The role of a base is typically to deprotonate the $P-H$ compound, generating a highly nucleophilic phosphide or phosphonate anion that can attack the electrophilic double bond. Even a small amount of base can initiate the conjugate addition and drive it to completion. Over the years, numerous bases - both homogeneous and heterogeneous - have been applied [448]. First group is alkali metal alkoxides and hydroxides. In Miller's original 1956 report, catalytic sodium methoxide was used to trigger addition of phosphine oxides to enones and acrylonitrile [450]. Similarly, KOH or $NaOH$ can promote phospha-Michael additions in certain cases, though strong bases can lead to side reactions if not carefully controlled [448, 474].

Another group of bases are tertiary amines such as triethylamine or DABCO (1,4-diazabicyclo[2.2.2]octane) can effectively catalyze $P-H$ additions by base deprotonation. For example, triethylamine is often used in the synthesis of β-phosphonomalonates from diethyl phosphite and activated alkenes, providing moderate to good yields under mild conditions [475]. 4-Dimethylaminopyridine (DMAP) is another effective base catalyst. One of recent ideas is the use of a recyclable DMAP-derived salt. Researchers prepared a 4-(N,N-dimethylaminopyridinium) saccharinate salt that acts as a strong base catalyst but can be precipitated and recovered, enabling multiple uses without significant loss of activity. Such advances combine the efficiency of homogeneous amines with the easy separation of a heterogeneous system [449]. Reaction of catalyst preparation is presented on Scheme 67 and catalysed by DMAP is presented on Scheme 68.



Scheme 67. Synthesis of 4-Dimethylaminopyridine (DMAP) [449].



Scheme 68. Phospha-Michael reaction with 4-Dimethylaminopyridine (DMAP) as catalyst [449].

Interesting group are guanidines and amidines. Strong organic bases like 1,1,3,3-tetramethylguanidine (TMG) (Figure 61) and bicyclic amidines have proven highly efficient. Tetramethylguanidine was presented to catalyze phospha-Michael additions to a broad array of acceptors, such as α,β-unsaturated ketones, nitriles, aldehydes or even imines (as presented on Scheme 69), under mild conditions, in what was one of the earliest demonstrations of organocatalysis for this reaction [476]. The superbasic bicyclic guanidine TBD (1,5,7-triazabicyclo[4.4.0]dec-5-ene) was later reported by Tan and co-workers to facilitate both direct two-component additions and three-component conjugate additions, adding a phosphite in the presence of an enone and an aldehyde, with high efficiency [477]. These bases are strong enough to deprotonate dialkyl phosphites and related $P-H$ compounds, yet often operate under near-ambient conditions [476, 477].

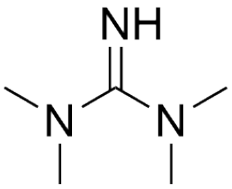
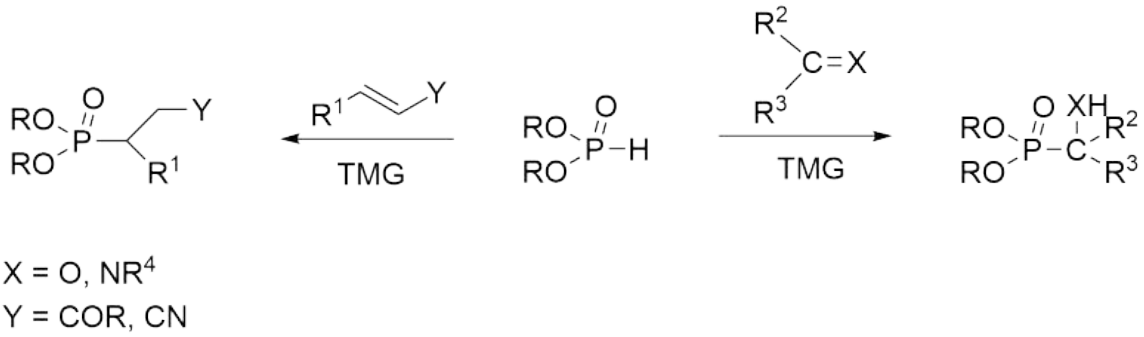


Figure 61. Structure of TMG - 1,1,3,3-tetramethylguanidine [476].



Scheme 69. Reactions with TMG as catalyst [476].

Research continues to discover new organic base catalysts with enhanced activity or special properties. A recent example is the use of 1,1-diamino-2,3-diazene (diaminoazine - Figure 62) derivatives as organocatalysts. Wani et al. (2021)[478] found that 1,1-diaminoazine compounds, diaminated azines are highly effective for phospha-Michael additions of secondary phosphine oxides, providing faster reactions and higher yields than many conventional bases. Reaction is presented on Scheme 70. These catalysts were even able to promote the reaction in aqueous media, demonstrating their strength and unique solubility profile - an advantageous feature for greener chemistry [478].

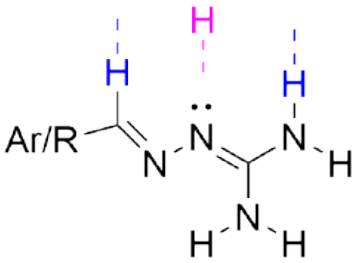
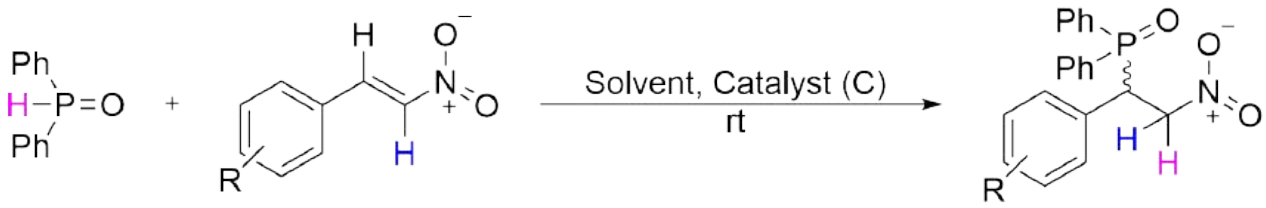


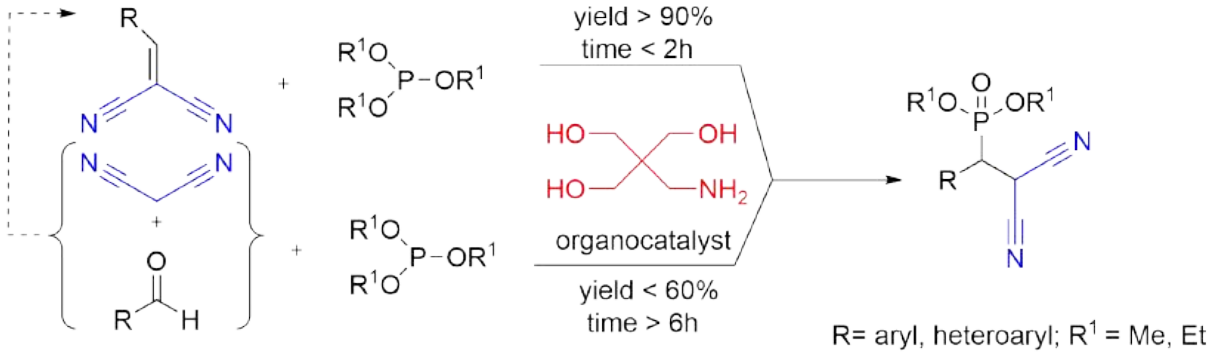
Figure 62. Structure of TMG - 1,1,3,3-tetramethylguanidine [478].



Scheme 70. Phospha-Michael reaction with 1,1-diamino-2,3-diazene (diaminoazine) derivatives as organocatalyst [478].

Another unconventional base that has been explored is tris(hydroxymethyl)aminomethane (TRIS), a common biological buffer. In 2015-2017, Kim and co-workers reported that TRIS can serve as an efficient organobase catalyst for forming β-phosphonomalonates

in one-pot multi-component reactions, as presented on Scheme 71 with the benefit of being low-cost, low-toxicity, and operable under solvent-free conditions [479, 480].



Scheme 71. Synthezis of β-phosphonomalonates in one-pot multi-component reaction with tris(hydroxymethyl)aminomethane as catalyst [480].

To facilitate catalyst recovery, supported base catalysts have been developed. Polymer-supported BEMP, PS-BEMP, where BEMP is a Verkade superbase, is one example, presented on Figure 63. It was demonstrated that PS-BEMP resin could catalyze phospha-Michael additions of various dialkyl phosphites to electron-poor alkenes under solvent-free conditions, giving high yields across aromatic, aliphatic, and cyclic α,β-unsaturated carbonyls [481]. After reaction, the solid base could be filtered off and reused, aligning with green chemistry principles.

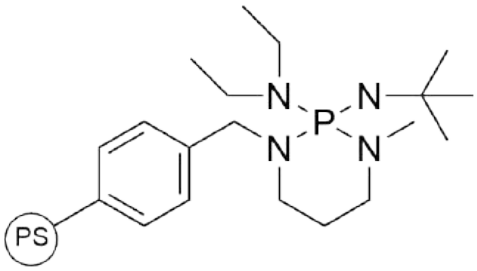
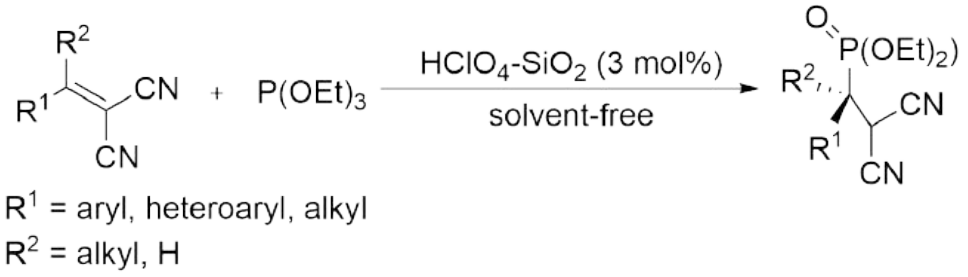


Figure 63. Structure of 2-tert-butylimino-2-diethylamino-1,3-dimethylperhydro-1,3,2-diazaphosphorine supported on polystyrene (PS-BEMP) [481].

Building on the idea of recoverable catalysts, fluorous-tagged bases like long-chain fluorous pyridines have been used to catalyze phospha-Michael reactions and then be separated by fluorous phase extraction [449].

Acidic catalysts can also promote the phospha-Michael reaction in certain cases, although they are less common than bases. The mechanism here is different - a Brønsted or Lewis acid is thought to activate the electrophilic alkene by protonating or coordinating to the electron-withdrawing group, increasing its susceptibility to attack by the P-nucleophile. In some instances, acids may also assist in protonating

intermediate anions or stabilizing transition states. One example is perchloric acid on silica $HClO_4 - SiO_2$ - heterogeneous Brønsted acid catalyst. It was proven in the reaction where dialkyl phosphites is added to α,β-unsaturated malonates to give β-phosphonomalonates in high yields 83-93% under solvent-free and room-temperature conditions (Scheme 72). The catalyst was recovered by simple filtration, dried, and reused several times, making the method eco-friendly and economical [461, 482].



Scheme 72. Synthezis of β-phosphonomalonates in one-pot multi-component reaction with perchloric acid on silica as catalyst [482].

Molecular iodine I_2 has emerged as a mild Lewis acid or halogen-based catalyst for various organic reactions. It was proven that I_2 catalyzes the conjugate addition of H-phosphites to α,β-unsaturated malonates in aqueous micellar solution [483]. Iodine often in the presence of a surfactant like sodium stearate to form micelles likely activates the double bond by forming charge-transfer complexes or iodonium ion intermediates, enabling the phosphite to add. This method avoided strong bases and worked under nearly neutral conditions, plus this catalyst could be recovered by simple workup. The use of elemental iodine exemplifies the drive toward more sustainable and recyclable catalysts in phospha-Michael chemistry [483].

One of the primary roles of metal catalysis in the phospha-Michael addition is to function as Lewis acids. Lewis acidic metal compounds, such as aluminum trimethyl $AlMe_3$ and titanium tetraisopropoxide $Ti(OiPr)_4$, can activate the Michael acceptor by coordinating to its electron-rich heteroatom like the carbonyl oxygen of an enone [326, 448]. This coordination withdraws electron density from the $C = C$ double bond, increasing the electrophilicity of the β-carbon and making it more susceptible to attack by the phosphorus nucleophile. This strategy is particularly useful for reactions involving less reactive Michael acceptors or for promoting additions that are inactive under base-catalyzed conditions [326]. Transition metal complexes, particularly those of platinum and palladium, are often required for the phospha-Michael addition of primary RPH_2 or secondary phosphines R_2PH [448, 474]. Unlike H-phosphonates, these $P(III)$ compounds react through a different mechanism that is effectively facilitated by tran-

sition metal catalysts. Furthermore, specific metal catalysts have been developed for additions involving other classes of phosphorus nucleophiles. For example, an efficient $Ti(OiPr)_4$-catalyzed addition of dimethylphosphine oxide to aldimines has been reported, demonstrating the utility of metal catalysis for specific substrate combinations that are challenging for other systems [448]. While lanthanide-based catalysts have shown immense promise in general Michael additions due to their unique coordination properties, their application specifically to the phospha-Michael reaction remains a relatively nascent and underexplored area [484].

It should be noted that purely acid-catalyzed phospha-Michael additions are less common because most $P-H$ compounds require deprotonation to become nucleophilic. Thus, acid catalysts are typically employed in conjunction with or on bifunctional supports that also have basic sites [482].

In a distinct departure from base catalysis, tertiary phosphines PR_3 can promote the phospha-Michael addition through a nucleophilic catalysis mechanism. In this pathway, the phosphine itself does not act as a Brønsted base to deprotonate the H-phosphonate. Instead, it functions as a potent Lewis base, initiating the catalytic cycle by attacking the β-carbon of the Michael acceptor [457, 485]. This initial conjugate addition step generates a zwitterionic phosphonium enolate intermediate [457, 485]. This highly reactive intermediate is the key to the catalytic cycle. It is sufficiently basic to deprotonate the H-phosphonate, thus generating the nucleophile of the active phosphite anion along with a phosphonium cation [457]. The newly formed phosphite anion then adds to a second molecule of the Michael acceptor to form the final product, regenerating the tertiary phosphine catalyst in the process. The efficacy of this catalytic cycle is critically dependent on the electronic and steric properties of the phosphine. Electron-rich trialkylphosphines like $n-Bu_3P$ are highly nucleophilic and generally exhibit high reactivity, but their pronounced sensitivity to oxidation often necessitates the strict exclusion of air, limiting their practical utility [457, 486]. In contrast, triarylphosphines are far more stable towards oxidation. While standard triphenylphosphine Ph_3P is often insufficiently nucleophilic, the development of electron-rich triarylphosphines, such as tris(4-methoxyphenyl)phosphine (TMTPP) (Figure 64), has provided a class of catalysts that balance high reactivity with operational stability [486].

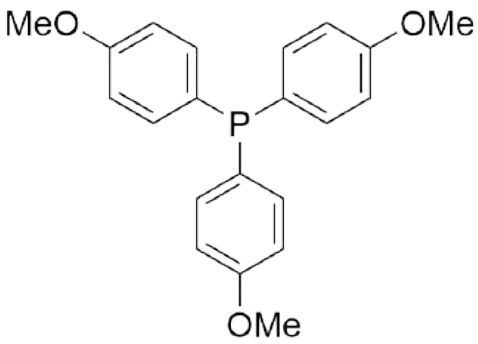


Figure 64. Structure of tris(4-methoxyphenyl)phosphine [486].

The most significant modern advance in phospha-Michael chemistry has been the development of asymmetric organocatalysis, which enables the synthesis of chiral organophosphorus compounds with high levels of enantioselectivity. This has been achieved through the rational design of chiral catalysts that can control the three-dimensional trajectory of the reaction. The breakthrough in asymmetric phospha-Michael additions came with the advent of bifunctional organocatalysts. These molecules possess two distinct functional groups within a single chiral scaffold: a Lewis basic site (typically a tertiary amine) and a Brønsted acidic/hydrogen-bond donor site such as a thiourea or squaramide moiety. This dual-functionality allows the catalyst to perform two essential tasks simultaneously, orchestrating the reaction with remarkable precision [459, 487, 488]. The mechanism of these catalysts is a model of molecular choreography. The basic tertiary amine group, for example the quinuclidine nitrogen in a cinchona alkaloid-derived catalyst (Figure 65), interacts with the H-phosphonate, acting as a general base to facilitate the tautomerization to the nucleophilic phosphite form [488].

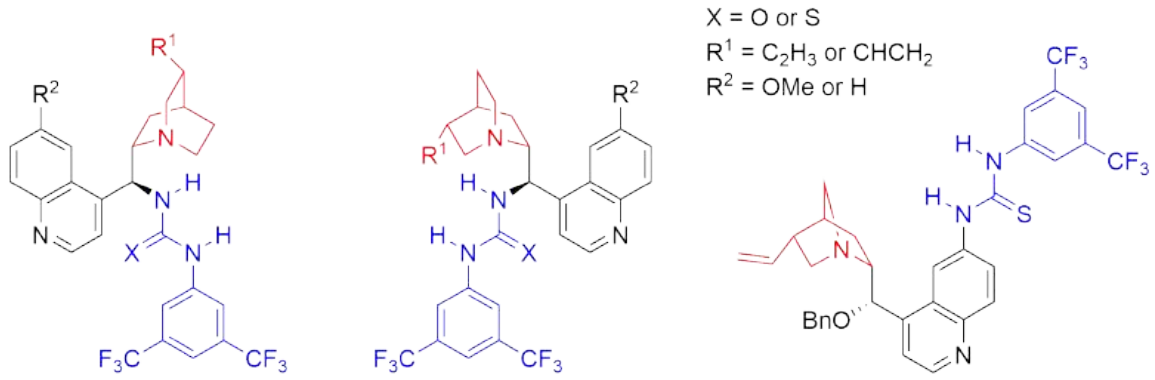


Figure 65. Figures of (thio)urea-substituted bifunctional cinchona alkaloid catalysts [488].

Concurrently, the acidic $N-H$ protons of the squaramide or thiourea moiety engage the Michael acceptor through a network of hydrogen bonds. This non-covalent

interaction serves two purposes: it activates the electrophile by withdrawing electron density, and it holds the substrate in a specific orientation within the catalyst's chiral pocket. This pre-organization of the reactants ensures that the nucleophilic phosphite, generated in close proximity, attacks one of the two enantiotopic faces of the $C = C$ double bond preferentially, leading to the formation of one enantiomer of the product in excess [459, 488, 489]. The success of this strategy represents a triumph of rational catalyst design, where two distinct chemical problems-nucleophile generation and stereocontrol-are solved concurrently by a single, well-designed molecule. This approach moves beyond simple activation to achieve a high level of molecular organization, which is the hallmark of modern asymmetric catalysis [459, 488, 489].

4.4 Phospha-Michael addition reaction - results and discussion on use of ecocatalysis

4.4.1 Methodology

The same catalyst as in the hydrophosphonylation experiments was employed. For details regarding its preparation, see Section 2.4.1.1 (p. 124) Preparation of Eco-MgZnOx catalyst derived from *Arabidopsis halleri*.

The reactions were carried out according to the same protocol as in the hydrophosphonylation experiments, described in Section 2.4.1.2 (p. 126) General procedure for the reactions.

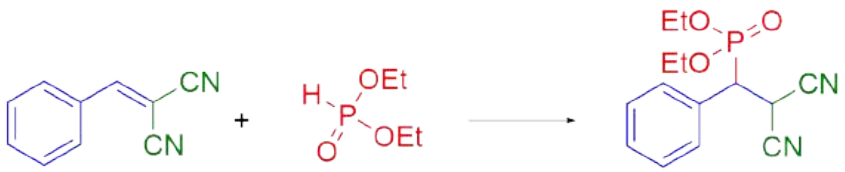
The same methods were applied as in Section 2.4.1.3 (p. 127) Analysis of catalyst, reaction mixtures and products, including the calculation of conversion. In this case, however, in some cases an optically active product was obtained, for which an additional calculation method was applied.

4.4.2 Optimization results of the phospha-Michael addition reaction

The Table 36 presents the optimization results of the phospha-Michael reaction, including the choice of optimal conditions and reactions with commercially available oxides. The data includes conversion rates both without a catalyst and with the use of Ecocatalysts (coming from Poland - P and coming from France - F). Different solvents were also tested in some reactions. The study was carried out using a model phospha-

Michael reaction between malononitrile derivative 6a and diethyl phosphite 2a, leading to the formation of the corresponding adduct 8a, and it is called in this thesis as model reaction of phospha Michael addition (A). This transformation involves the addition of a P-H bond across an activated double bond, representing a typical example of the phospha-Michael reaction. The reaction scheme is included in the first row of Table 36.

Table 36. Optimization results of the phospha-Michael reaction



6a **2a** **8a**

No.	Catalyst	T [°C]	t [h]	Conversion[k]	Conversion[k] with EcoCatalyst		Solvent
					PL	FR	
1	-	50	3	16%	70%[a]	71%[b]	None
2	-	50	4	21%	57%[a]	68%[b]	None
3	-	50	3	16%	82%[c]	81%[d]	None
4	-	50	4	21%	89%[c]	85%[d]	None
5	-	50	4	0%	0%[a]	0%[b]	Ethyl acetate
6	-	RT	4	0%	0%[a]	0%[b]	Ethyl acetate
7	-	RT	4	0%	30%[a]	33%[b]	None
8	-	RT	24	10%	68%[a]	73%[b]	None
9	-	RT	24	0%	7%[a]	7%[b]	Ethyl acetate
10	-	60	3	23%	84%[a]	72%[b]	None
11	-	50	5	19%	91%[a]	90%[b]	None
12	-	50	5	19%	91%[c]	83%[d]	None
13	-	70	4	43%	100%[c]	95%[d]	None
14	-	70	3	28%	100%[a]	100%[b]	None
15	-	70	4	42%	100%[a]	100%[b]	None
16	-	70	3	16%	100%[c]	100%[d]	None
17	-	70	3	0%	4%[a]	6%[b]	Toluene
18	-	70	3	2%	-[a]	-[b]	Methanol
19	-	RT	3	0%	4%[a]	6%[b]	Dichloromethane
20	MgO[e]	70	3	93.5%			None
21	MgO[f]	70	3	60.6%			None
22	ZnO[g]	70	3	61.8%			None
23	ZnO[h]	70	3	53.9%			None
24	MgO+ZnO[i]	70	3	92.2%			None
25	MgO+ZnO[j]	70	3	87.8%			None
26	$CaCO_3$[l]	70	3	47.9%			None
27	$CaCO_3$[m]	70	3	48.2%			None

a 7.5 mg of Eco-MgZnOx-P: Mg (7.0 mol%), Ca (13.6 mol%), Zn (5.7 mol%);
b 7.5 mg of Eco-MgZnOx-F: Mg (3.5 mol%), Ca (11.4 mol%), Zn (4.9 mol%);
c 15 mg of Eco-MgZnOx-P: Mg (14.0 mol%), Ca (27.2 mol%), Zn (11.4 mol%);
d 15 mg of Eco-MgZnOx-F: Mg (7.0 mol%), Ca (22.8 mol%), Zn (9.8 mol%);
e Mg (7.0 mol%);
f Mg (3.5 mol%);
g Zn (5.7 mol%);
h Zn (4.9 mol%);
i Mg (7.0 mol%), Zn (5.7 mol%);
j Mg (3.5 mol%), Zn (4.9 mol%);
l Ca (13.6 mol%);
m Ca (11.4 mol%);
k Conversion determined by ^{31}P NMR of the crude reaction mixture;
RT room temperature.

Among the different sets of parameters tested, the most efficient conditions were identified as 70 ℃, 2 h, under solvent-free conditions, with a catalyst loading corresponding to 5 mol% of Zn (calculated based on the metal content of the eco-catalyst). Under these optimized conditions, both Eco-MgZnOx-P and Eco-MgZnOx-F provided nearly quantitative conversions with excellent selectivity. These conditions were subsequently applied in all further catalytic studies, including reusability tests and scale-up experiments.

The optimization results of the phospha-Michael reaction with malononitrile as a substrate show clear differences depending on the reaction conditions, the use of ecocatalysts, and the choice of commercial oxides. Without any catalyst, the reaction proceeds only to a limited extent. At room temperature no significant conversion was observed (0-10%), while at elevated temperatures (50-70 ℃) the conversion increased slightly but remained low, reaching a maximum of 43% after 5 hours at 70 ℃. In contrast, the introduction of ecocatalysts, led to a dramatic improvement in efficiency.

The influence of solvents was negative. Ethyl acetate completely suppressed the reaction, while other tested solvents such as toluene, methanol, and dichloromethane resulted in very low conversion values. The best results were therefore obtained under solvent-free conditions.

Commercially available oxides were also investigated as catalysts. Magnesium oxide showed the highest activity, giving almost 94% conversion. Zinc oxide was moderately active, with conversion between 54% and 62%, while mixtures of both oxides reached high values of 88-92%. Calcium carbonate exhibited only moderate efficiency, with conversions below 50%.

In phospha-Michael reactions, the conversion of diethyl H-phosphonate into the corresponding addition products was determined by quantitative ^{31}P NMR spectroscopy. Since both the starting material and the products contain exactly one phosphorus atom, the molar ratios can be directly obtained from the integrals of their ^{31}P resonances. After baseline correction and phase adjustment, integrals were measured for the signals corresponding to the substrate and the product. The molar conversion was calculated according to the general formula:

$$\text{Conversion (\%)} = \frac{I_{\text{product}}}{I_{\text{product}} + I_{\text{substrate}}} \times 100\%$$

where I_{product} and $I_{\text{substrate}}$ denote the integrals of the respective signals.

As an example, the phospha-Michael addition of benzylidene malonitrile to diethyl H-phosphonate (2a) afforded the product 8a. The crude reaction mixture after the reac-

tion is presented in the Figure 66. In the ^{31}P NMR spectrum, the signals were observed at $\delta = 8.18$ ppm (substrate 2a) and $\delta = 21.20$ ppm (product 8a). The corresponding integrals were 1.00 (2a) and 2.36 (8a). Substitution into the formula gave:

$$\text{Conversion} = \frac{2.36}{2.36 + 1.00} \times 100\% \approx 70.2\%.$$

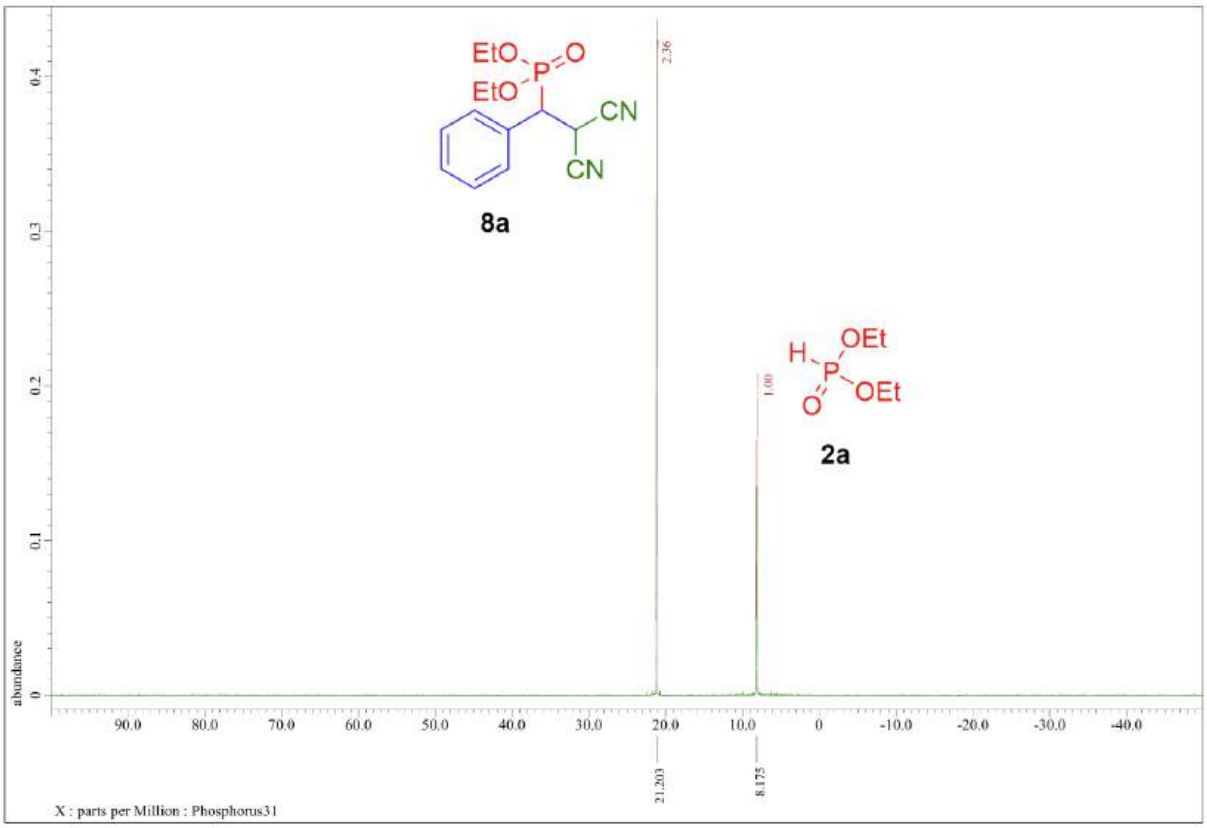
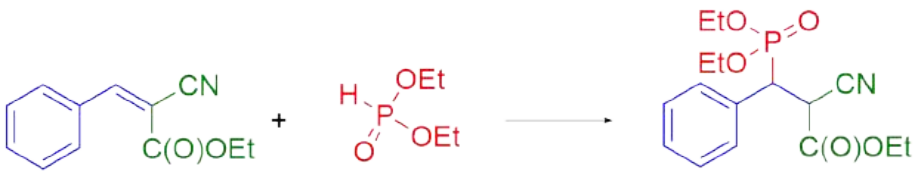


Figure 66. ^{31}P NMR spectrum (243 MHz, $CDCl_3$) of the crude reaction mixture after the reaction of benyzlidene malononitrile with diethyl H-phosphonate.

The second model reaction of phospha-Michael addition was carried out between ethyl cyano(phenylmethylene)acetate **7a** and diethyl H-phosphonate **2a**, affording the adduct **9a**. Similar to the first model system, the optimization focused on determining the influence of temperature, reaction time, solvent, and the application of ecocatalysts,

Table 37. Optimization results of the phospha-Michael reaction (Reaction B), without solvent



7a **2a** **9a**

No.	Catalyst	T [℃]	t [h]	Conversion[k]	Conversion[k] with Ecocatalyst	
					PL	FR
1	-	50	3	0%	94%[a]	94%[b]
2	-	50	4	2%	95%[a]	94%[b]
3	-	70	3	6%	100%[a]	100%[b]
4	-	70	3	5%	100%[a]	100%[b]
5	MgO[c]	70	3	96%		
6	MgO[d]	70	3	96%		
7	ZnO[e]	70	3	96%		
8	ZnO[f]	70	3	17%		
9	MgO+ZnO[g]	70	3	99%		
10	MgO+ZnO[h]	70	3	88%		
11	$CaCO_3$[i]	70	3	7%		
12	$CaCO_3$[j]	70	3	6%		

as well as the activity of commercially available oxides.

a 7.5 mg of Eco-MgZnOx-P: Mg (7.0 mol%), Ca (13.6 mol%), Zn (5.7 mol%);
b 7.5 mg of Eco-MgZnOx-F: Mg (3.5 mol%), Ca (11.4 mol%), Zn (4.9 mol%);
c Mg (7.0 mol%);
d Mg (3.5 mol%);
e Zn (5.7 mol%);
f Zn (4.9 mol%);
g Mg (7.0 mol%), Zn (5.7 mol%);
h Mg (3.5 mol%), Zn (4.9 mol%);
i Ca (13.6 mol%);
j Ca (11.4 mol%);
k Conversion determined by ^{31}P NMR of the crude reaction mixture;
RT room temperature.

The results presented in Table 37 show that, in the absence of a catalyst, the reaction proceeds very poorly, with conversions between 0 and 6% even at elevated temperatures. However, the introduction of ecocatalysts, either from Poland (P) or from France (F), led to excellent results, with conversions reaching 94-100% under the same conditions. This again confirms the high catalytic efficiency of ecocatalysts, comparable or superior to conventional catalysts.

Commercial oxides demonstrated significant differences in activity. Magnesium oxide exhibited very high conversions, while zinc oxide was less effective, giving values between 17% and 96% depending on the conditions. A mixed $MgO + ZnO$ system

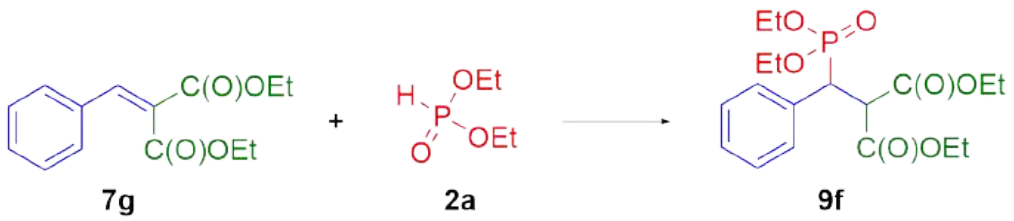
performed particularly well, achieving conversions of 88-99%. In contrast, calcium carbonate proved to be much less active, with conversions not exceeding 7%.

Overall, the optimization results confirm that the phospha-Michael reaction is strongly dependent on catalysis. Ecocatalysts ensured almost complete conversion under mild, solvent-free conditions.

Optimized conditions were decided for as 70 °C, 3 h, under solvent-free conditions, with a catalyst loading corresponding to 5 mol% of Zn (calculated based on the metal content of the eco-catalyst) for both substrates.

The third model reaction of the phospha-Michael addition was carried out between benzylidenemalonic acid diethyl ester (**7g**) and diethyl H-phosphonate (**2a**). Similar to the previous model system, the optimization focused on determining the influence of temperature, reaction time, solvent, and the application of EcoCatalysts. The reaction scheme is included in the first row of Table 38. Results are presented in Table 38.

Table 38. Optimization results of the phospha-Michael reaction (Reaction C), without solvent



7g **2a** **9f**

No.	T [°C]	t [h]	Conversion without catalyst[b]	Conversion with EcoCatalyst[b]	
				PL	FR
1	50	3	0%	0%[c]	0%[d]
2	50	48	0%	13%[e]	7%[f]
3	70	4	0%	0%[e]	2%[f]
4	70	20	0%	17%[g]	12%[h]
5	70	20	0%	14%[e] (6.4:1)	10%[f] (6.0:1)

[a] Reaction conditions: substrate (0.23 mmol), diethyl phosphite (0.23 mmol);
[b] determined by ^{31}P NMR of crude reaction mixture;
[c] 7.5 mg of Eco-MgZnOx-P: Mg (7.0 mol%), Ca (13.6 mol%), Zn (5.7 mol%);
[d] 7.5 mg of Eco-MgZnOx-F: Mg (3.5 mol%), Ca (11.4 mol%), Zn (4.9 mol%);
[e] 15 mg of Eco-MgZnOx-P: Mg (14.0 mol%), Ca (27.2 mol%), Zn (11.4 mol%);
[f] 15 mg of Eco-MgZnOx-F: Mg (7.0 mol%), Ca (22.8 mol%), Zn (9.8 mol%);
[g] 30 mg of Eco-MgZnOx-P: Mg (28.0 mol%), Ca (54.4 mol%), Zn (22.8 mol%);
[h] 30 mg of Eco-MgZnOx-F: Mg (14.0 mol%), Ca (45.6 mol%), Zn (19.6 mol%).

Despite increasing the catalyst loading and prolonging the reaction time, the results of this model system were not satisfactory. Conversions remained low, and only in the final entry a diastereomeric ratio (6.4:1 for Eco-MgZnOx-P and 6.0:1 for Eco-MgZnOx-F) could be determined, confirming the formation of the expected product. However,

this observation did not outweigh the general lack of efficiency. Moreover, performing reactions with higher catalyst amounts (20-30 mg) proved experimentally inconvenient, as the reaction mixtures became difficult to stir with a magnetic stir bar. For these reasons, benzylidenemalonic acid diethyl ester was not selected for further studies.

4.4.3 Reusage of the catalyst in the phospha-Michael addition reaction

To evaluate the recovery and reuse of Eco-MgZnOx-P and Eco-MgZnOx-F in this process, the phospha-Michael addition of ethyl 2-cyano-3-phenylacrylate (**7a**) with diisopropyl H-phosphonate (**2c**) under optimized conditions was employed as a model reaction (Figure 8). The reaction conditions were as follows: 3 hours, 70℃, neat, with Eco-MgZnOx. The appropriate Eco-MgZnOx catalyst (Eco-MgZnOx-P (5.7 mol% of Zn) or Eco-MgZnOx-F (4.9 mol% of Zn)) was added to a glass vial containing the alkene (**7a**, 5.52 mmol) and H-phosphonate (**2c**, 5.52 mmol). The mixture was stirred at 70℃ for 3 hours, as determined from reaction optimization.

After the reaction time elapsed, methanol (2 mL) was added, and the mixture was centrifuged at 6000 rpm for 5 minutes. The organic layer was separated, and an additional portion of ethyl acetate (2 mL) was added to the remaining catalyst, followed by repeated centrifugation. This catalyst washing process was repeated four times. The combined organic layers were evaporated under vacuum, and the resulting crude product was purified by crystallization. The remaining solid catalyst was dried in an oven at 500℃ for 5 hours and then reused in subsequent reactions. This process was repeated four times.

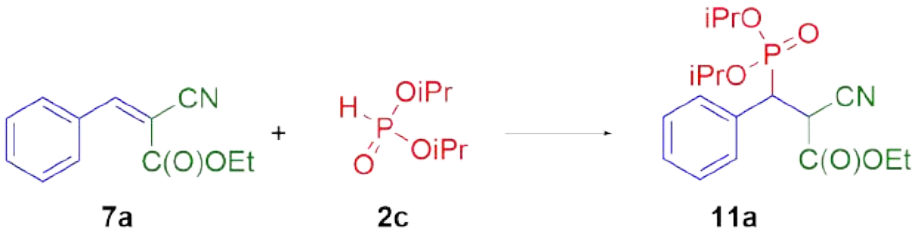
During these tests, no significant difference between the reactions catalyzed by Eco-MgZnOx-P and Eco-MgZnOx-F was observed, as presented in the Table 39.

a Reaction conditions: aldehyde (0.23 mmol), diethyl acetate (0.23 mmol).
b Determined by ^{31}P NMR.

4.4.4 Scale-up of the phospha-Michael addition reaction

Scaling the reaction from 0.23 mmol to 6.4 mmol (1.8 g of product) worked just as well: 99% conversion and 96-97% yield for both Eco-MgZnOx-P and Eco-MgZnOx-F what was presented in the Table 40. This shows that ecocatalyst usage in phospha-Michael reaction is robust on larger batches and has clear potential for further scale-up

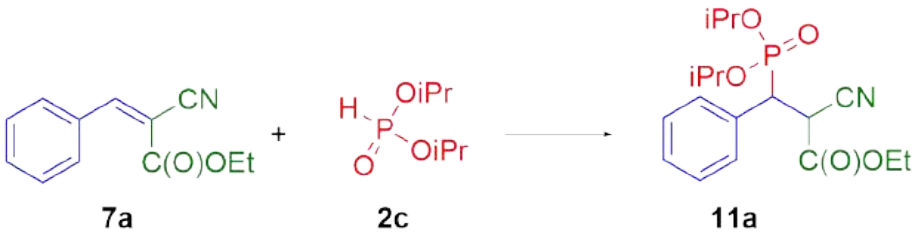
Table 39. Recovery and reuse tests of the Eco-MgZnOx catalysts in phospha-Michael addition reaction[a].



7a **2c** **11a**

Ecocatalyst	Run	Conversion[b] (%)	Ca (wt%)	Mg (wt%)	Zn (wt%)
Eco-ZnOx-P	Reaction 0	97.0	14.1	5.0	10.6
	Reaction 1	95.9	14.4	4.4	9.9
	Reaction 2	96.0	15.0	4.4	9.8
	Reaction 3	95.6	12.7	3.9	8.1
Eco-ZnOx-F	Reaction 0	94.0	14.3	2.2	10.1
	Reaction 1	93.1	14.4	1.9	9.5
	Reaction 2	92.8	14.8	1.9	9.6
	Reaction 3	92.9	11.9	1.8	8.7

Table 40. Scale-up of the model reaction of phospha-Michael addition



7a **2c** **11a**

Catalyst	Conversion [%][b]	Yield [%]
Eco-MgZnOx-P[c]	99%	96%[e]
Eco-MgZnOx-F[d]	99%	97%[f]

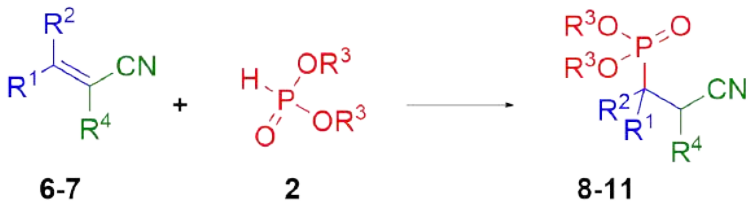
and preparative or pilot-scale use.

a Reaction conditions: benzaldehyde (1): 6.4 mmol, malononitrile (2): 6.4 mmol, H-phosphonate (3): 6.4 mmol.
b Determined by $^{3}1$P NMR of crude reaction mixture.
c 210 mg of Eco-MgZnOx-P: Mg (7.0 mol%), Ca (13.6 mol%), Zn (5.7 mol%).
d 210 mg of Eco-MgZnOx-F: Mg (3.5 mol%), Ca (11.4 mol%), Zn (4.9 mol%).
e 1795 mg of pure product (3).
f 1795 mg of pure product (3).

4.4.5 Substrate scope of the phospha-Michael addition reaction

A comprehensive substrate scope investigation was conducted for the phospha-Michael reaction, exploring various carbonyl substrates and different H-phosphonates.

The results, presented in the Figures 67 and 68, illustrate the structures of the compounds obtained under optimized conditions for both reactions - Reaction A and Reaction B. Each figure also specifies the conversion and yield for the reaction, providing a detailed assessment of the process efficiency across different substrate combinations. All reactions were performed in optimized conditions (70℃, 3 h, solvent-free, catalyst loading corresponding to 5 mol% of Zn).



Scheme 3. General scheme of phospha-Michael addition reaction catalysed with Eco-MgZnOx

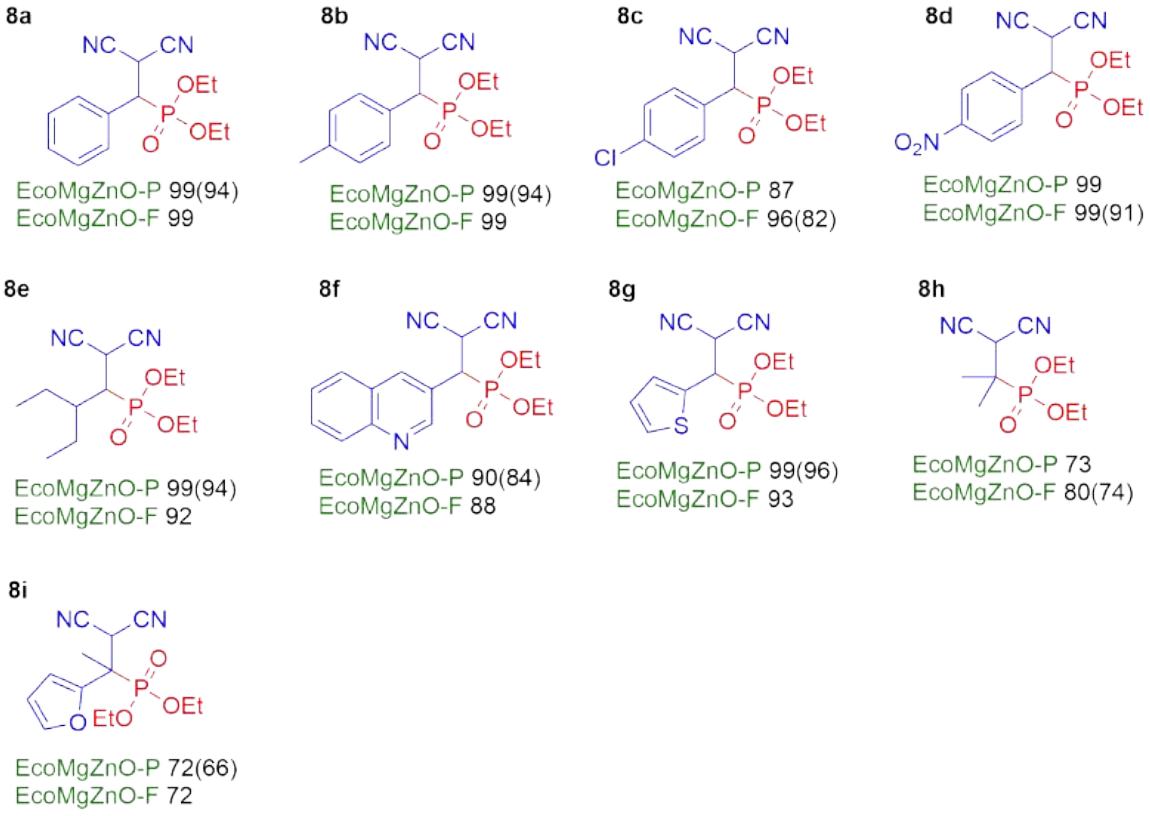


Figure 67. Substrate scope of phospha-Michael reaction - scope of carbonyl compounds (Reaction A). Numbers next to each entry are conversions and values in parentheses are isolated yields.

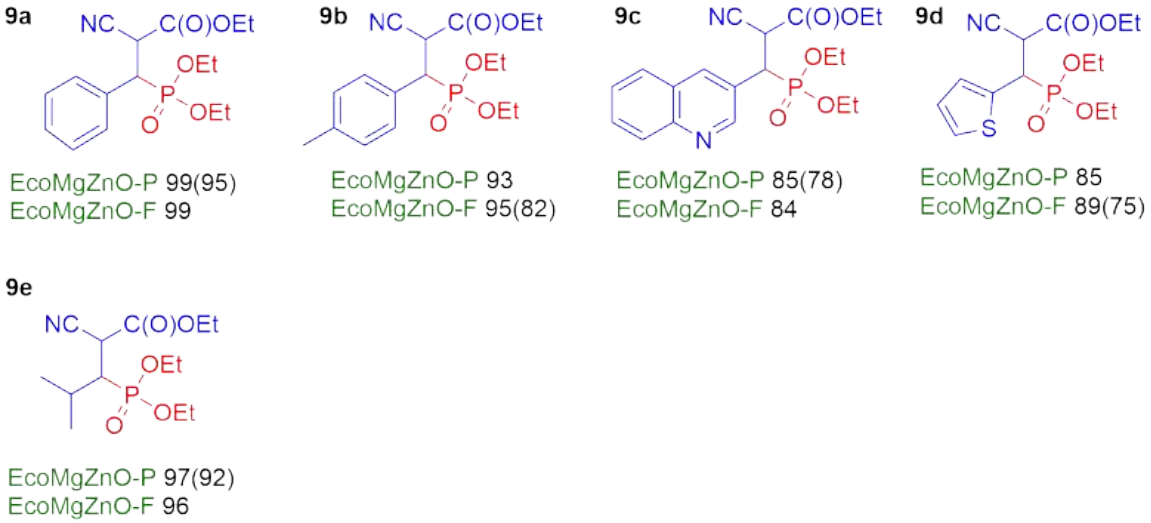


Figure 68. Substrate scope of phospha-Michael reaction - scope of carbonyl compounds (Reaction B). Numbers next to each entry are conversions and values in parentheses are isolated yields.

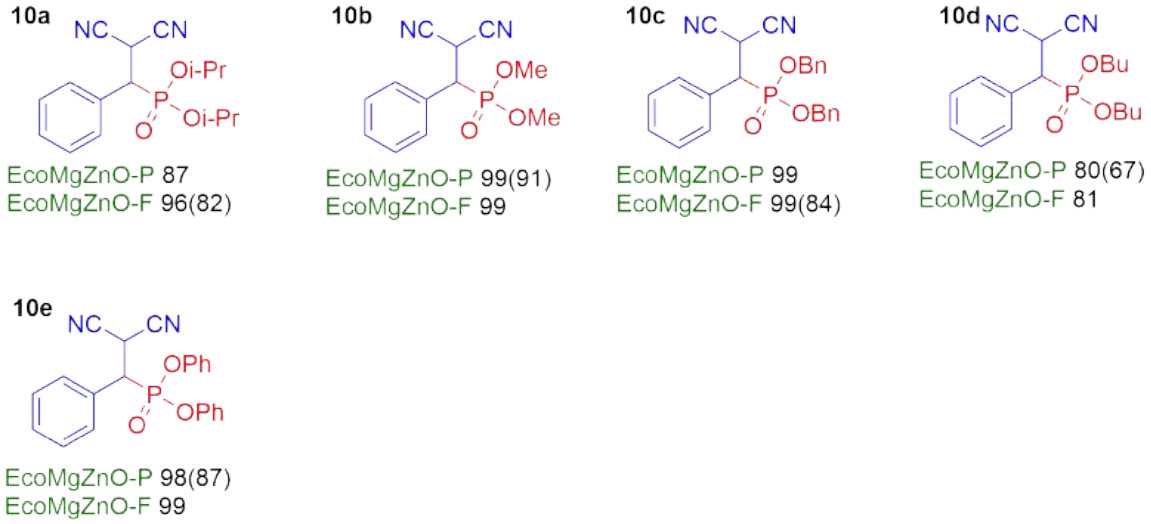


Figure 69. Substrate scope of phospha-Michael reaction - scope of H-phosphonates (Reaction A). Numbers next to each entry are conversions and values in parentheses are isolated yields.

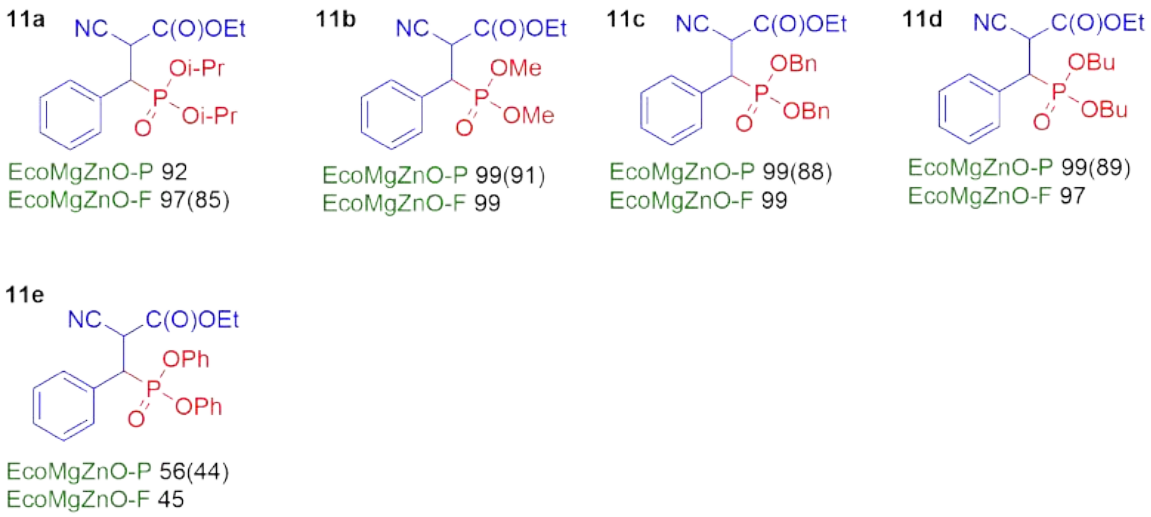


Figure 70. Substrate scope of phospha-Michael reaction - scope of H-phosphonates (Reaction B). Numbers next to each entry are conversions and values in parentheses are isolated yields.

The reaction works across simple phenyl (**8a**) and substituted arenes bearing halogen (**8c**) and strongly electron-withdrawing nitro (**8d**) groups, as well as alkyl substitution (**8e**). Heteroarenes are tolerated, including quinolinyl (**8f**) and thienyl (**8g**) motifs. Yields are generally very high (typically 87-99%). More congested alkenes show some drop: a tetrasubstituted acceptor (**8h**) gives 73-80%, and an ortho-alkoxy substrate (8i) gives 72%.

The method also covers Michael acceptors that include a cyano-ester group. Overall, both electron-rich, electron-poor and heteroaryl systems are compatible.

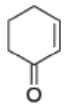
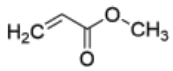
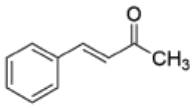
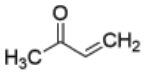
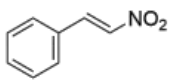
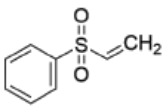
From the nucleophile scope most conversions are high 98-99% (Figures 69 and 70). Bulkier diisopropyl H-phosphonate gives 87-97%, and dibutyl H-phosphonate with malononitrille is the lowest but still good (80-81%), indicating some steric sensitivity at phosphorus.

Both eco-catalysts (EcoMgZnO-P and EcoMgZnO-F) perform similarly across the board; in a few cases the F-variant is slightly higher, especially with more demanding substrates, but differences are small.

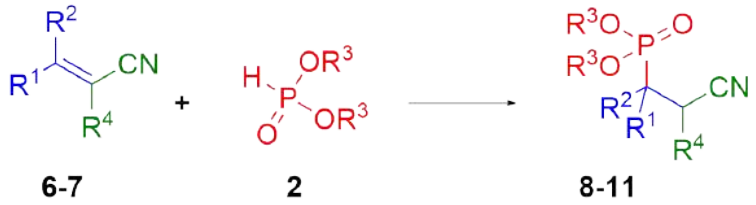
The phospha-Michael addition is broadly applicable to activated alkenes (arylidenemalononitriles and aryl cyanoacrylates) and to a wide range of H-phosphonates. It tolerates electron-withdrawing and electron-donating groups, halides, and heteroarenes, delivering mostly high to near-quantitative yields, with only sterically crowded cases giving lower (yet still useful) conversions.

To further evaluate the substrate scope of the developed methodology, additional alkenes were tested in the phospha-Michael addition reaction (Scheme 3). These experiments were carried out under the conditions optimized for the model substrates.

Table 41. Phospha-Michael addition reaction of different alkenes with diethyl phosphite.

Alkene[a]	**Phosphonate**[b]	**Conversion**	**Conversion**[c] **with EcoCatalyst**	
		without catalyst[c]	**PL**[d]	**FR**[e]
2-cyclohexen-1-one 	diethyl phosphite	0%	19%	17%
cyclohexene 	diethyl phosphite	0%	9%	0%
methyl acrylate 	diethyl phosphite	0%	0%	0%
trans-4-Phenyl-3-buten-2-one 	diethyl phosphite	0%	36%	50%
3-buten-2-one 	diethyl phosphite	0%	45%	35%
trans-β-nitrostyrene 	diethyl phosphite	0%	12%	11%
phenyl vinyl sulfone 	diethyl phosphite	0%	35%	26%

a 0.23 mmol of alkene;
b 0.23 mmol of diethyl phosphite;
c determined by ^{31}P NMR of the crude reaction mixture;
d 7.5 mg of Eco-MgZnOx-P: Mg (7.0 mol%), Ca (13.6 mol%), Zn (5.7 mol%);
e 7.5 mg of Eco-MgZnOx-F: Mg (3.5 mol%), Ca (11.4 mol%), Zn (4.9 mol%).



Scheme 3. General scheme of phospha-Michael addition reaction catalysed with Eco-MgZnOx

For the additional alkenes studied, activation in the presence of EcoCatalysts proved to be much weaker compared to the model substrates. For some compounds only low conversions were observed (below 20%), while in the case of methacrylates or methyl acrylate the reaction practically did not occur. The highest activity among this extended set was observed for 3-buten-2-one, which reached 45% and 35% conversion with Eco-MgZnOx-P and Eco-MgZnOx-F, respectively. The results indicate that the proposed reaction conditions are highly effective for α, β-unsaturated nitriles, ketones, and aromatic derivatives, but are much less suitable for less activated alkenes such as simple alkenes or acrylates.

All the products were subject of NMR spectra confirmation - all the details are described in last chapter. For example, for 8i compound - Diethyl (1,1-dicyano-2-(furan-2-yl)propan-2-yl)phosphonate presented on Figure 71 the structure of the diethyl phosphonate featuring a furan ring and a dicyanomethyl group was proved. The ^{31}P spectrum (Figure 74) contains a single signal at 20.48 ppm, demonstrating the presence of a single, pure phosphorus-containing species. In the ^{1}H spectrum (Figure 73), three signals are visible in the 6.4–7.5 ppm range, which are characteristic of a substituted furan ring. Crucial for verifying the structure are the doublets at 1.87 ppm (methyl group) and 4.69 ppm (proton of the $-CH(CN)_2$ group), both of which exhibit distinct splitting by the phosphorus atom. The complex multiplets of the ethoxy groups (3.8–4.1 ppm) result from the chirality of the molecule, rendering these protons diastereotopic (magnetically non-equivalent). The ^{13}C spectrum (Figure 72) reveals the complete molecular skeleton, including the central quaternary carbon appearing as a doublet around 43 ppm due to $C - P$ bonding. The consistency of the chemical shifts and the presence of spin couplings with phosphorus across all spectra conclusively confirm the correctness of the proposed structure.

Another example is compound 11a (Figure 75) which is an organic phosphonate derivative containing a phenyl ring, a cyano group, and esters.The ^{31}P NMR spectrum (Figure 78 reveals two closely spaced resonance signals at chemical shifts of 21.44 ppm and 21.32 ppm, indicating the presence of a mixture of diastereomers of this compound.In the proton spectrum (Figure 77), in the range of 7.2–7.5 ppm, multiplets

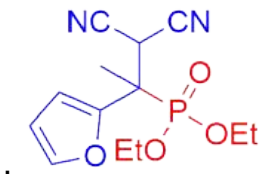


Figure 71. 8i - Diethyl (1,1-dicyano-2-(furan-2-yl)propan-2-yl)phosphonate

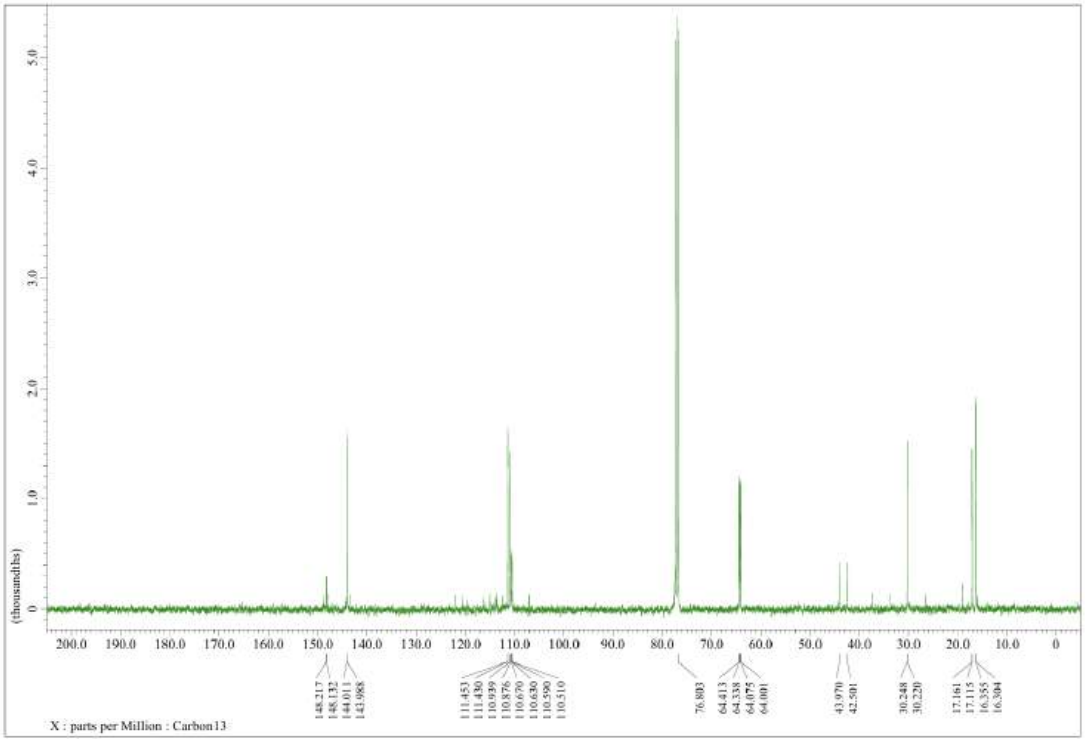


Figure 72. ^{13}C NMR spectrum of 8i - Diethyl (1,1-dicyano-2-(furan-2-yl)propan-2-yl)phosphonate

corresponding to the five aromatic protons of the phenyl ring are visible.The middle region of the ^1H spectrum (3.5–4.6 ppm) contains complex signals of methine protons as well as protons of the OCH and OCH_2 groups, whose complex shape also stems from the presence of isomers.The high-field region (0.7–1.3 ppm) is dominated by intense methyl group signals originating from isopropyl residues and the ethyl group. The carbon spectrum (Figure 76) confirms the backbone structure, showing a carbonyl carbon signal at approx. 164 ppm and a cyano group carbon near 115 ppm. In the ^{13}C spectrum, numerous doublets resulting from J_{C-P} coupling are observed, and the doubling of certain lines further confirms the presence of diastereomers. A comprehensive analysis of chemical shifts in all spectra confirms consistency with the structural formula of the 11a compound, taking into account its stereochemical complexity.

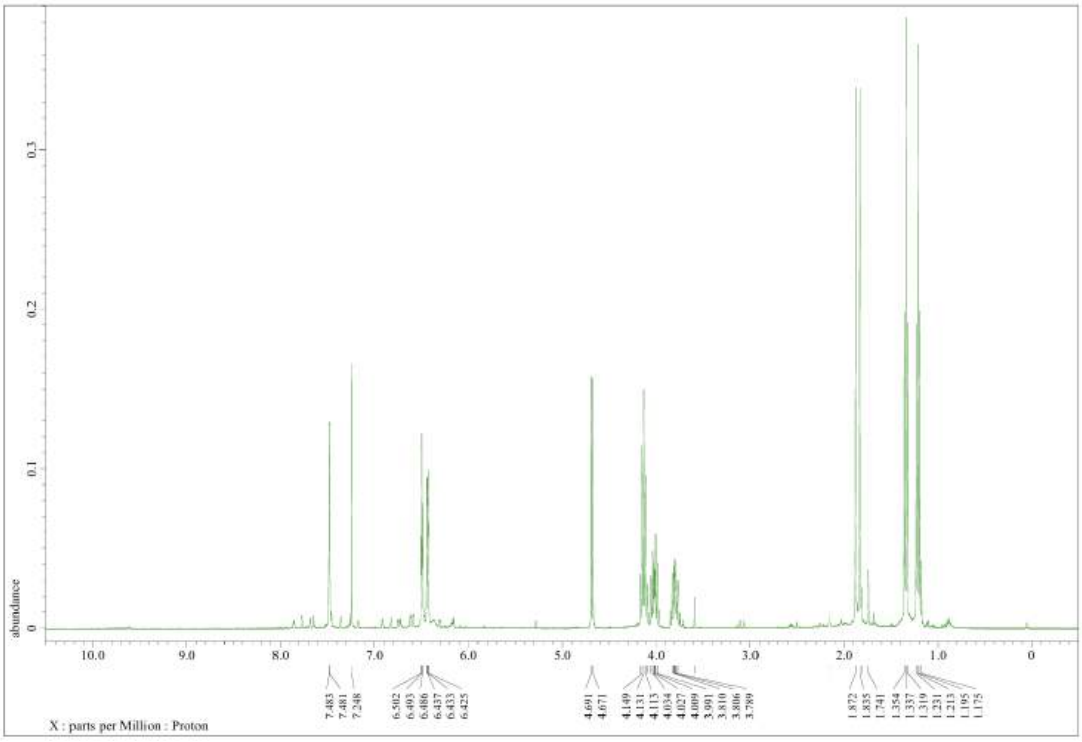


Figure 73. ^{1}H NMR spectrum of 8i - Diethyl (1,1-dicyano-2-(furan-2-yl)propan-2-yl)phosphonate

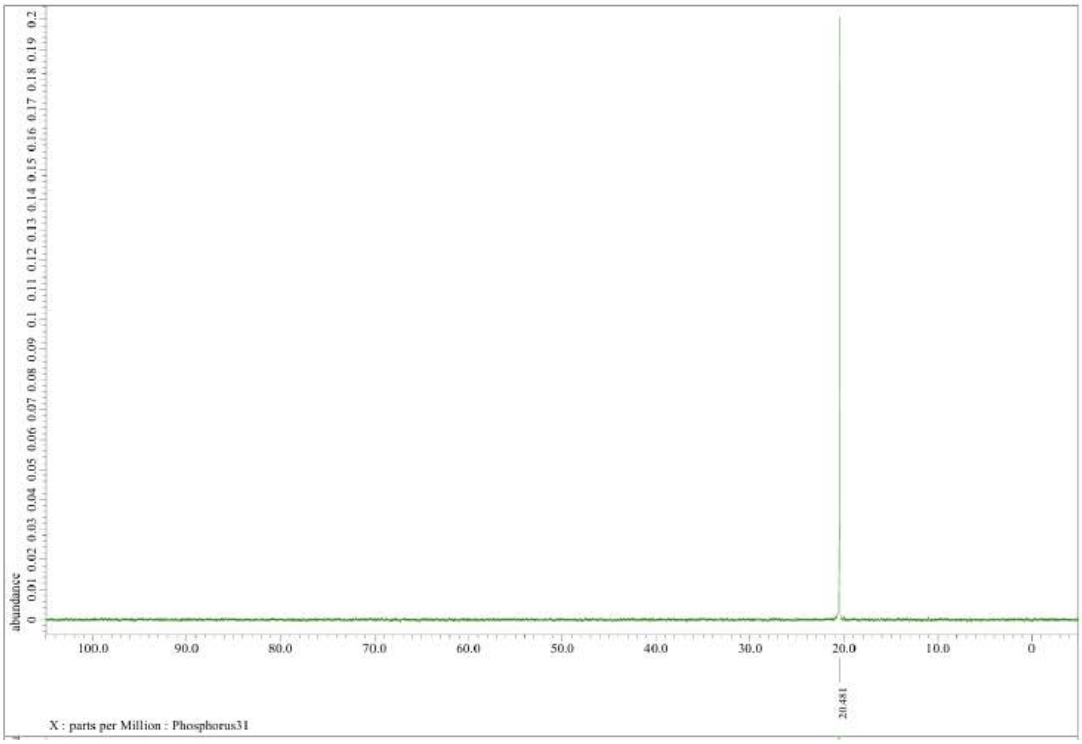


Figure 74. ^{31}P NMR spectrum of 8i - Diethyl (1,1-dicyano-2-(furan-2-yl)propan-2-yl)phosphonate

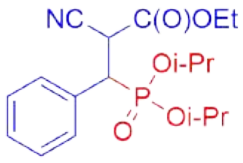


Figure 75. 11a - Ethyl 2-cyano-3-(diisopropoxyphosphoryl)-3-phenylpropanoate

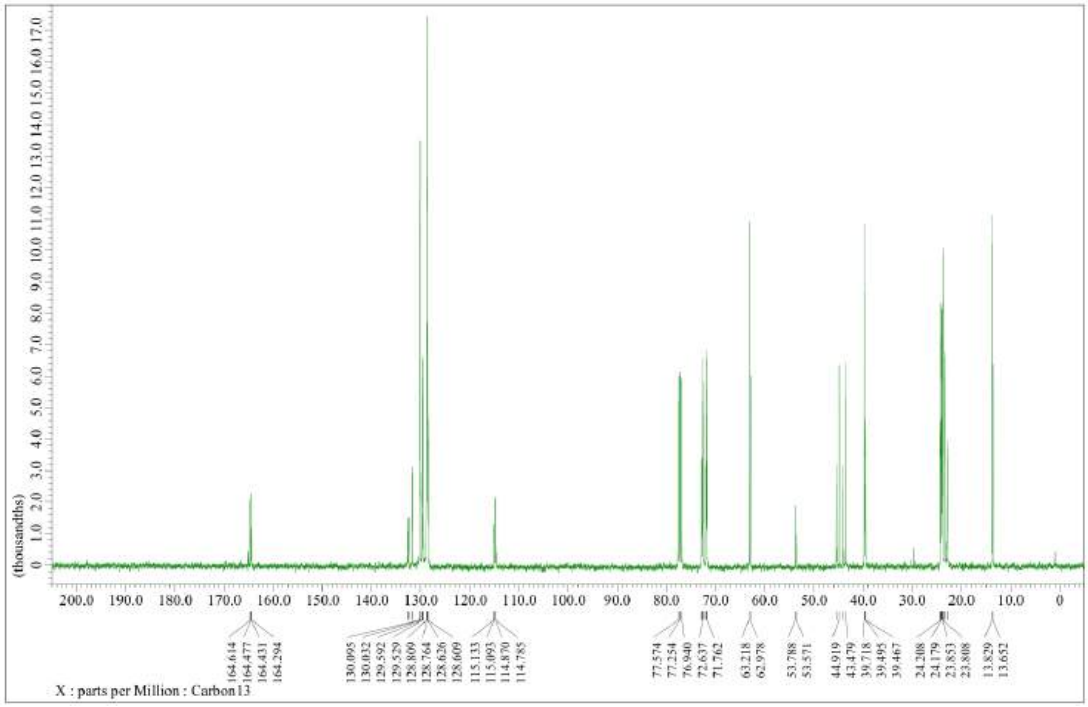


Figure 76. ^{13}C NMR spectrum of 11a - Ethyl 2-cyano-3-(diisopropoxyphosphoryl)-3-phenylpropanoate

4.4.6 Conclusions

In this chapter it was demonstrated that the Eco-MgZnOx catalyst derived from *Arabidopsis halleri* biomass is an effective heterogeneous catalyst for the phospha-Michael addition of dialkyl H-phosphonates to activated alkenes. The catalyst enables efficient $C-P$ bond formation under mild and solvent-free conditions, providing access to phosphonated compounds in high yields and with good selectivity.

The developed catalytic protocol operates at moderate temperatures and requires only a low catalyst loading. A wide range of activated Michael acceptors, including arylidene malononitriles and cyanoacrylates, were successfully converted in the presence of Eco-MgZnOx. The reactions typically proceeded with high conversions and clean product profiles, allowing straightforward isolation of the desired phosphonate products. The method showed good tolerance toward different substituents on the aromatic ring and various dialkyl H-phosphonates as phosphorus nucleophiles.

Comparative studies revealed that Eco-MgZnOx exhibits significantly higher cat-

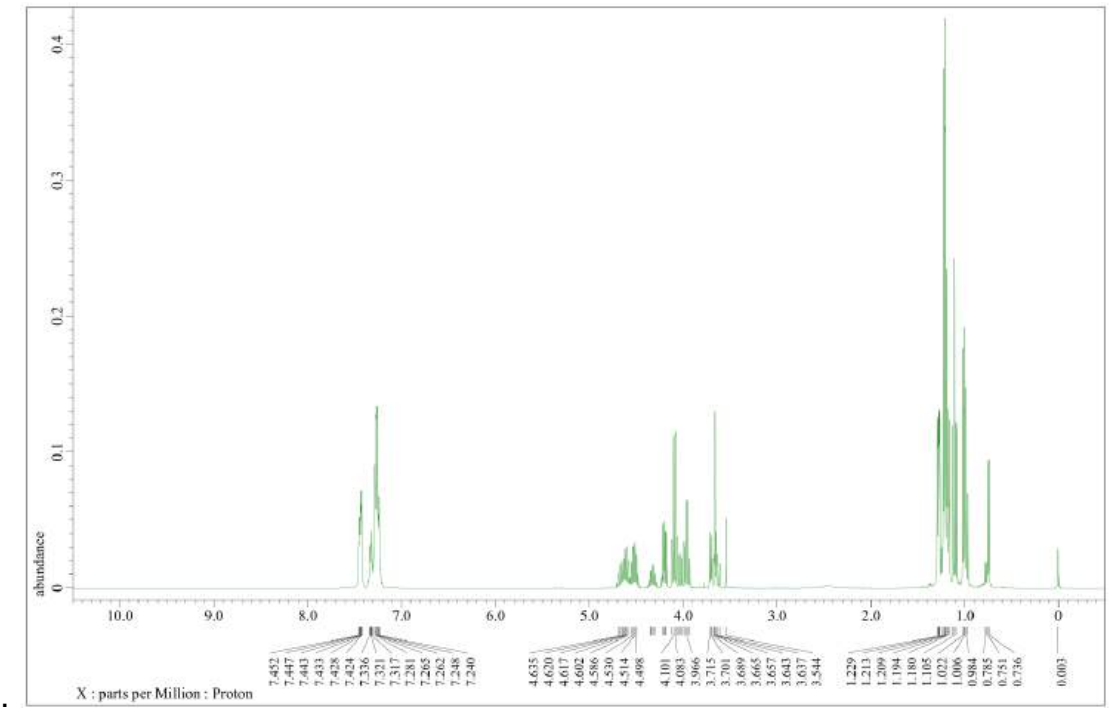


Figure 77. ^{1}H NMR spectrum of 11a - Ethyl 2-cyano-3-(diisopropoxyphosphoryl)-3-phenylpropanoate

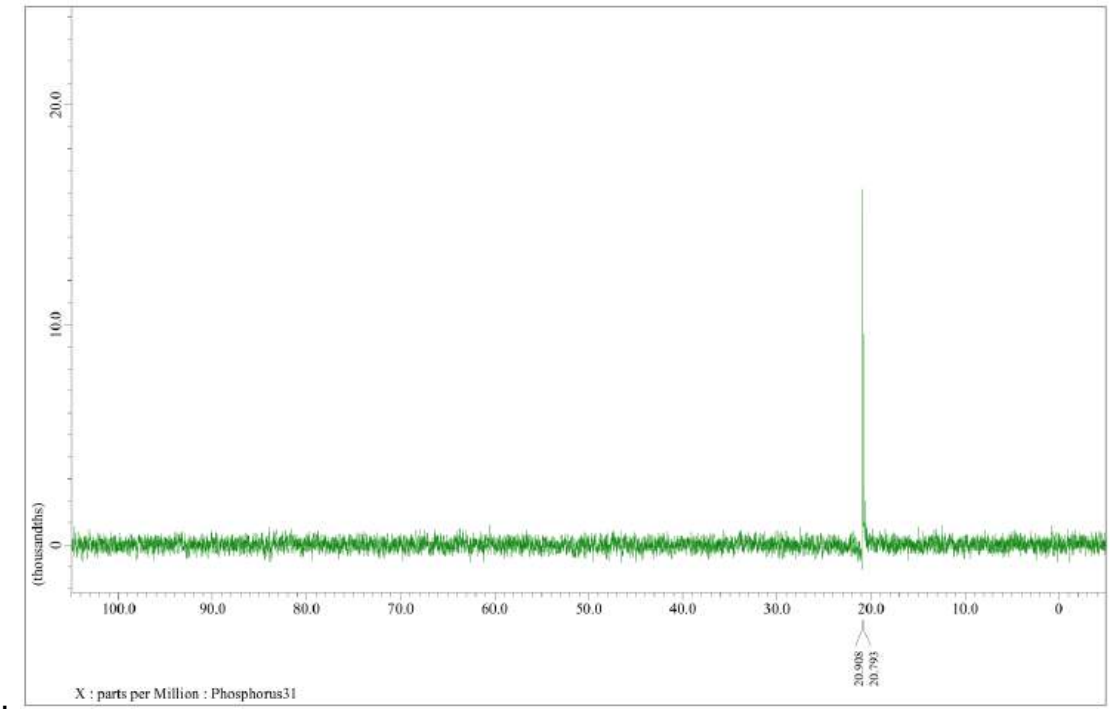


Figure 78. ^{31}P NMR spectrum of 11a - Ethyl 2-cyano-3-(diisopropoxyphosphoryl)-3-phenylpropanoate

alytic activity than single-component oxides such as MgO or ZnO, as well as their physical mixtures. This enhanced performance is attributed to the bifunctional character of the catalyst, combining basic MgO sites responsible for activation of the H-

phosphonate with Lewis-acidic ZnO sites that activate the electron-deficient alkene. The cooperative action of these sites facilitates efficient addition across the $C = C$ bond and accounts for the observed catalytic synergy.

It was further shown that the Eco-MgZnOx catalyst is stable and reusable in the phospha-Michael addition. The catalyst could be easily recovered from the reaction mixture and reused in several consecutive cycles with only a minor decrease in activity. Moreover, the reaction was successfully scaled up to the gram scale without loss of efficiency, confirming the robustness and practical applicability of the catalytic system.

Overall, the results presented in this chapter confirm that Eco-MgZnOx represents a versatile, recyclable, and environmentally benign catalyst for phospha-Michael additions. This study further expands the scope of ecocatalysis in $C\breve{}P$ bond formation and demonstrates the potential of plant-derived polymetallic oxides for sustainable organophosphorus synthesis.

Chapter 5:
Knoevenagel-phospha-Michael reaction

5.1 Knoevenagel-phospha-Michael - chemical basis

Cascade reactions, also referred to as domino or tandem reactions, represent a highly sophisticated and powerful strategy in organic synthesis. Modern organic synthesis aims to be fast, simple, and green, so multicomponent reactions have become very important [490, 491]. These reactions, which combine three or more starting substrates in a single synthetic operation to form a complex product, represent a powerful strategy for rapid molecule construction [492, 493]. The Knoevenagel-phospha-Michael reaction is a prime example of this class, functioning as a domino or tandem multicomponent reaction that integrates two distinct bond-forming events: a carbon-carbon bond formation via the Knoevenagel condensation, followed by a carbon-phosphorus bond formation through a phospha-Michael addition [491]. The overall scheme is presented in the Picture 79 following with general reaction for this thesis presented in the Scheme 4.

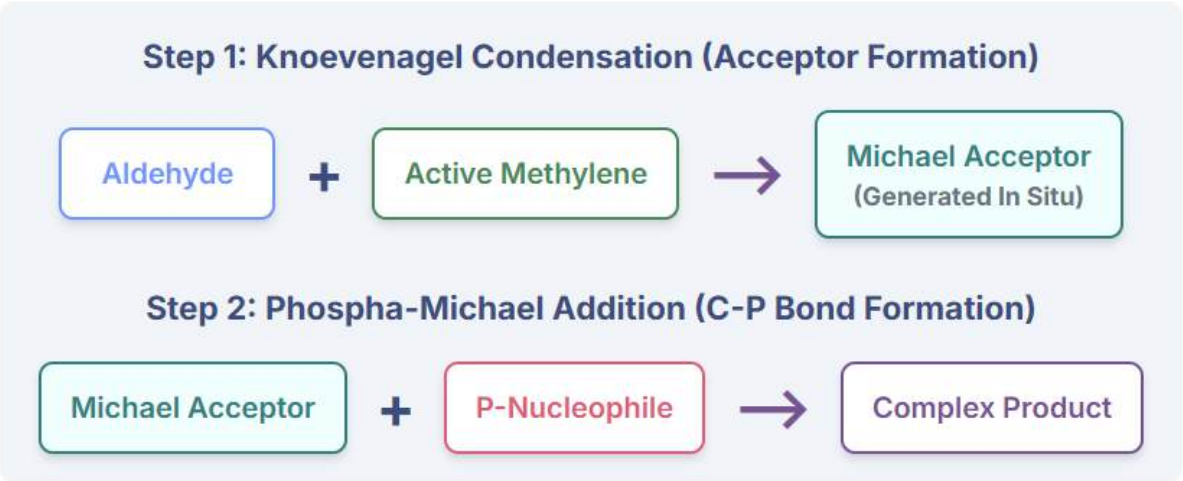
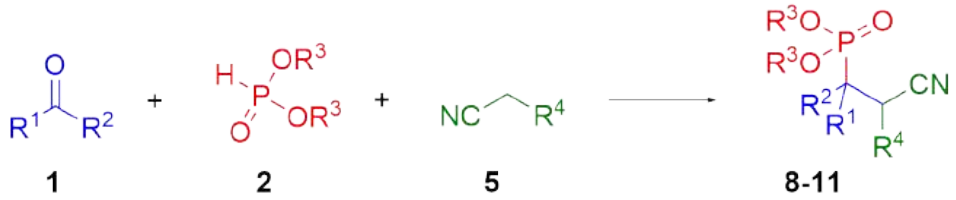


Figure 79. Knoevenagel-phospha-Michael reaction



Scheme 4. Knoevenagel-phospha-Michael model reaction

This approach allows for the assembly of highly functionalized organophosphorus compounds from simple, readily available precursors - typically an aldehyde, an active methylene compound, and a phosphite ester without the need to isolate intermediates

[490]. This reaction is not just a lab novelty - it is central to process intensification - building complex molecules as efficiently as possible, in as few steps as possible [492].

The success of this one-pot process depends critically on the kinetic harmony between the two steps. The catalyst must be capable of promoting both reactions efficiently. If the phospha-Michael addition is significantly slower than the Knoevenagel condensation, the intermediate (I) can accumulate, potentially leading to side reactions or an incomplete conversion. For example, studies using dipropylamine as a catalyst showed significant accumulation of the Knoevenagel intermediate, whereas switching to the more effective catalyst pentamethyldiethylenetriamine (PMDTA) drove the reaction to completion, yielding predominantly the final phosphonate product [468]. This demonstrates that the catalyst's role is not just to initiate the reactions but to effectively couple them in a kinetically efficient cascade.

5.2 Knoevenagel-phospha-Michael - applications

The growing demand for cost-effective and environmentally responsible chemical manufacturing has fueled the development of synthetic methodologies that align with the principles of green chemistry [494]. The one-pot Knoevenagel-phospha-Michael reaction is particularly attractive in this regard for several key reasons. First is atom economy and procedural simplification. By telescoping multiple transformations into a single vessel, the reaction inherently maximizes atom economy, ensuring that a greater proportion of the atoms from the starting materials are incorporated into the final product [490, 492]. This one-pot nature obviates the need for intermediate workup and purification steps, which often require additional resources. This stands in contrast to traditional two-pot procedures, in which the Knoevenagel intermediate is synthesized and isolated first before the subsequent phosphorylation step, leading to increased solvent waste, energy consumption, and time [491]. Another reason is focus on developing catalytic systems that enable the reaction to proceed under mild conditions, such as at room temperature or under solvent-free protocols [475, 490, 494]. The use of water as a reaction medium, which is economical, non-toxic, and non-flammable, represents a particularly significant advance in sustainable synthesis [493]. The reaction frequently delivers the desired products in good to excellent yields, often exceeding 90% and in some cases reaching up to 99% [491, 493]. The high efficiency and clean nature of the transformation simplify the final purification, which can sometimes be achieved through simple crystallization, further reducing the reliance on chromato-

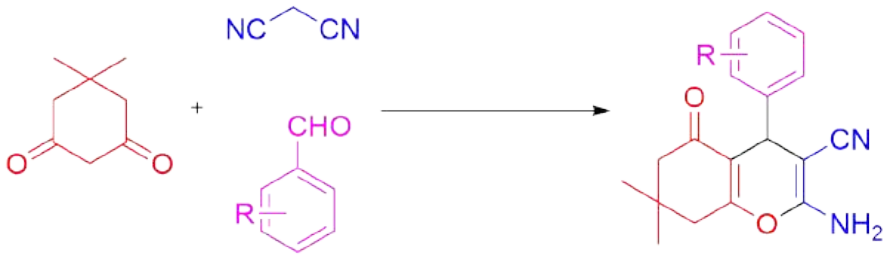
graphic methods [491]. The intense focus on these "green" attributes in the scientific literature is not merely descriptive; it is a primary driver of research in this area. New catalysts and methodologies are consistently evaluated not only on their synthetic efficency - yield and selectivity - but also on their sustainability metrics, including catalyst recyclability, the use of benign solvents, and the avoidance of toxic metals [475, 494, 495]. Consequently, the Knoevenagel-phospha-Michael reaction has become a model system for demonstrating and advancing the practical implementation of green chemistry principles in the synthesis of complex, high-value molecules.

Since the products obtained from this reaction are identical to those produced by the phospha-Michael reaction, their applications are discussed in subchapter 4.2 (p. 204) Phospha-Michael addition reaction - application.

5.3 Knoevenagel-phospha-Michael reaction - catalysts used

In the phospha-Michael addition topic, supported base catalysts were mentioned. Some solid bases include aminopropyl-functionalized silica for conjugate additions to malonate derivatives[496], and basic alkaline earth oxides like CaO or MgO are also good phospha-Michael catalysts. In fact, heterogeneous basic oxides, including natural phosphates and hydroxyapatite doped with base metals, have been tested as reusable catalysts for tandem Knoevenagel-phospha-Michael sequences, as they combine basic sites with Lewis acidic sites to catalyze multi-step processes in one pot [475, 497].

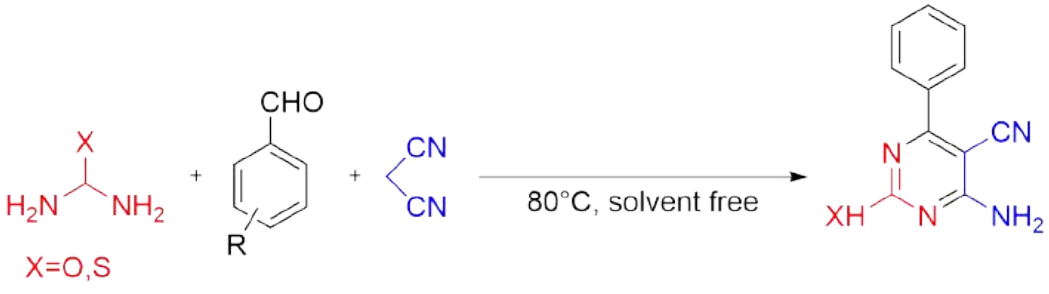
Heterogeneous catalysts are highly valued for their ease of separation from the reaction mixture, potential for recycling, and reduced product contamination. Metal phosphates and doped apatites are some of the examples. Porous metal phosphates and natural phosphate materials have emerged as robust, low-cost, and effective catalysts. For instance, a new porous magnesium aluminum phosphate (MALPO) with a high surface area demonstrated excellent performance, yielding Knoevenagel products with up to 99% yield and showing remarkable recyclability [487, 494]. Example of the one-pot reaction with MALPO was presented by Chowdhury and his team [498]. The aldehyde reactants were all cyclic, but had different substituents, and all showed 98–99% conversion. Reaction is presented on the Scheme 73.



Scheme 73. Scheme of an example of the one-pot reaction with MALPO [498]

Similarly, naturally occurring phosphates, hydroxyapatite, and fluorapatite, particularly when doped with Lewis acidic metal salts such as $ZnCl_2$ or $Cu(II)$, act as powerful catalysts. These systems benefit from a synergistic effect between the basic phosphate support and the acidic metal centers, which co-activate the Knoevenagel-phospha-Michael reaction substrates [494, 499].

The intriguing case of catalyst for the one-pot Knoevenagel-phospha-Michael reaction is modified bone char material functionalized with sulfonic acid groups ($bonechar - nPrN - SO_3H$) [500]. It was investigated as a heterogeneous Brønsted acid catalyst for the synthesis of pyrimidine-5-carbonitrile derivatives. The catalytic system was optimized using a model reaction between 4-chlorobenzaldehyde, malononitrile, and urea, where the best performance was achieved under solvent-free conditions at 80 ℃ with a low catalyst loading of 0.4 mol%. A wide range of aromatic aldehydes bearing both electron-withdrawing and electron-donating substituents such as Cl, Br, Me, NO_2 were efficiently converted with yields above 90% within short reaction times. The catalytic performance was further evaluated using turnover number and turnover frequency, confirming the high efficiency of the system. Proposed mechanism of the process follows a sequence of well-known transformations: initial Knoevenagel condensation between the aldehyde and malononitrile forms an activated intermediate, which subsequently undergoes Michael addition with urea or thiourea, followed by cyclodehydration and tautomerization to afford the pyrimidine-5-carbonitrile product, what was presented on Scheme 74.

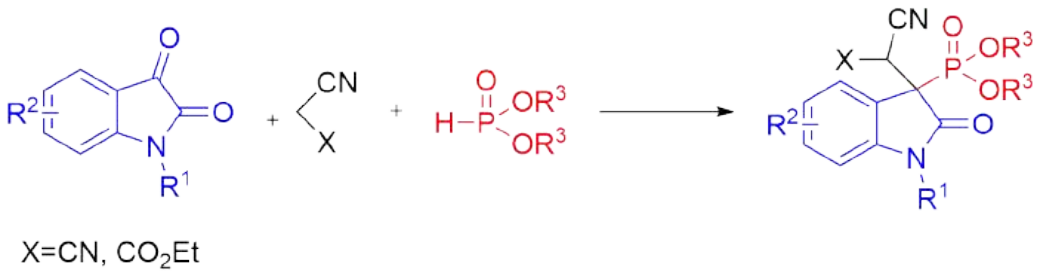


Scheme 74. Reaction scheme of synthesis of pyrimidine-5-carbonitrile derivatives in the presence of $bonechar - nPrN - SO_3$H as catalyst [500].

This approach highlights a simple, economical, and environmentally friendly strategy that combines solvent-free conditions, low catalyst loading, and the use of a biomass-derived material, making it conceptually relevant to the development of sustainable heterogeneous catalytic systems [500].

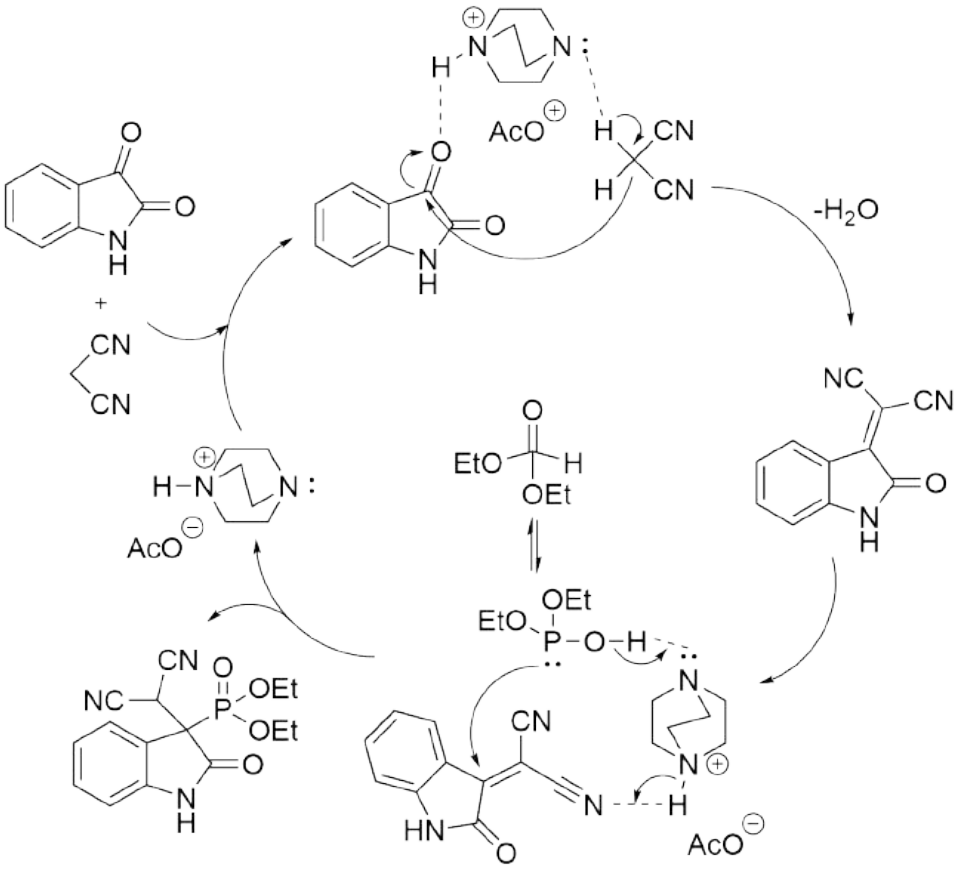
Another type of catalysts for this one-pot reaction are nanocatalysts. The use of nanomaterials, such as ZnO nanorods and functionalized multi-walled carbon nanotubes - MWCNT, leverages an exceptionally high surface-to-volume ratio to achieve enhanced catalytic activity [490, 501, 502]. These catalysts can promote the reaction efficiently under mild, often solvent-free, conditions and are typically recoverable and reusable for multiple cycles [501, 502].

Homogeneous catalysts often exhibit higher activity and selectivity due to the absence of mass transfer limitations, although their separation can be more challenging. Ionic liquids have been extensively explored as both solvents and catalysts for this reaction. In particular, ionic liquids based on 1,4-diazabicyclo[2.2.2]octane (DABCO) have proven to be exceptionally effective, providing excellent yields in short reaction times with low catalyst loadings like 7 mol% [491]. Example reaction of DABCO-based ionic liquid catalyst is presented on Scheme 75.



Scheme 75. Synthesis of 2-Oxindol-3-ylphosphonate with DABCO-based ionic liquid as catalyst [491].

A possible mechanism suggests that the DABCO-based ionic liquids act as a bifunctional catalyst, activating both the carbonyl compound and the active methylene nucleophile via hydrogen bonding, while also serving as a proton shuttle to facilitate the phosphite tautomerization [491], what is presented on Scheme 76.



Scheme 76. Proposed mechanism of Knoevenael-phospha-Michael one-pot reaction catalysed by DABCO [491].

Another catalyst group are amine-based organocatalysts. Simple organic bases like 4-(N,N-dimethylamino)pyridine (DMAP) and pentamethyldiethylenetriamine (PMDTA) are effective and inexpensive for this application [468, 493]. To overcome the separation challenges of traditional homogeneous catalysts, innovative hybrid systems have been developed. These include recoverable catalysts like the 4-N,N-dimethylaminopyridinium saccharinate (DMAP·Hsac) salt, which is soluble during the reaction but can be precipitated by adding a non-polar solvent, and fluorous long-chained pyridines, which are soluble at elevated reaction temperatures but phase-separate upon cooling. This kind of behaviour is called thermomorphic behavior [449, 503]. These systems combine the high activity of homogeneous catalysis with the practical recovery of heterogeneous catalysis. Phosphine catalysts are another potential group of catalyst for Knoevenagel-phospha-Michael reaction. Electron-rich triarylphosphines, such as tris(4-methoxyphenyl)phosphine (TMTPP) outperform the commonly used triphenylphosphine (TPP) in catalyzing Michael additions under mild, solvent-free conditions, showcasing the potential of nucleophilic organocatalysis in this domain [486].

Last important topic is biocatalysis. Perhaps the most significant recent development in the catalysis field is the discovery of the promiscuous catalytic activity of enzymes, particularly lipases, for this non-natural transformation [128, 475]. Lipases, such as those from Candida cylindracea (CcL) and the immobilized Novozym 435, can efficiently catalyze the entire Knoevenagel-phospha-Michael sequence [128, 475]. This biocatalytic approach offers unparalleled advantages. It is metal-free and operates under mild conditions like room temperature, neat or in water [475], the catalyst is biodegradable, renewable, and can be recycled multiple times [475, 494] and it provides a sustainable and cost-effective route to pharmacologically relevant phosphonates, with yields ranging from 43% to 93% [475].

Catalyst Class	Specific Example	Typical Substrates	Reaction Conditions	Yield (%)	Reus. (cycles)	Key Advantages / Disadvantages	Ref.
Heterogeneous							
Doped Phosphate	$ZnCl_2$ / Natural Phosphate	Aldehydes, Malononitrile, Diethylphosphite	EtOH, 25 °C, 9 h	50–90	Not specified	Low cost, synergy between dopant and support	[494]
Nanocatalyst	ZnO Nanorods	Isatins, Malononitrile, Dialkyl phosphonates	Solvent-free, RT, 2–3 h	82–96	$\geq$5	High activity, mild conditions, reusable	[490]
Nanocatalyst	Functionalized MWCNT	Aldehydes, Barbituric acid, Triethylphosphite	EtOH, reflux, 1–2.5 h	88–96	$\geq$4	High efficiency, good yields, heterogeneous	[501]
Homogeneous							
Ionic Liquid	[AcO]	Isatins, Malononitrile, Diethyl phosphite	MeCN, RT, 1–2 h	85–95	$\geq$5	High efficiency, mild conditions, recyclable	[491]
Organocatalyst	DMAP	Salicylaldehyde, Malononitrile, Triethylphosphite	H_2O, microwave, 10–12 min	75–95	Not specified	Aqueous media, fast, high yielding	[493]
Recoverable Organocatalyst	DMAP·Hsac Salt	Benzylidene malonates, Diisopropyl phosphite	Neat, 80–100 °C, 1–4.5 h	up to 99	$\geq$8	Homogeneous activity, heterogeneous recovery	[449]
Biocatalyst							
Lipase	*Candida cylindracea* (CcL)	Aldehydes, Malononitrile, Dimethyl phosphite	Neat, 30 °C, 8 h	43–93	Reusable	Metal-free, mild conditions, sustainable, low cost	[475]

Table 42. Comparison of heterogeneous, homogeneous and biocatalysts used in hydrophosphonylation and related reactions.

Table 42 provides a review of the catalysts discussed above, summarizing the reported reactions from the literature, including experimental conditions, tested substrates, and other relevant details.

5.4 Knoevenagel-phospha-Michael - results and discussion on use of ecocatalyst

5.4.1 Methodology

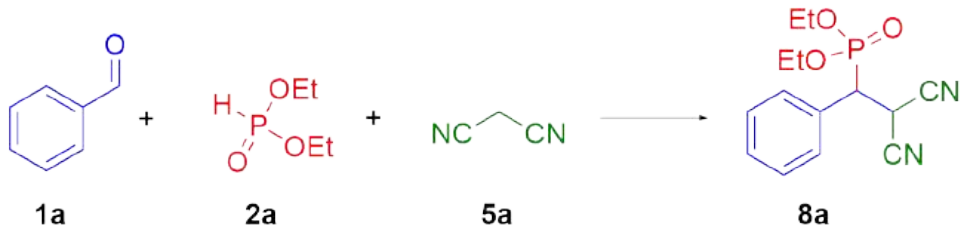
The same catalyst as in the hydrophosphonylation experiments was employed. For details regarding its preparation, see Section 2.4.1.1 (p. 124) Preparation of Eco-MgZnOx catalyst derived from *Arabidopsis halleri*.

The reactions were carried out according to the same protocol as in the hydrophosphonylation experiments, described in Section 2.4.1.2 (p. 126) General procedure for the reactions.

The same methods were applied as in Section 2.4.1.3 (p. 127) Analysis of catalyst, reaction mixtures and products, including the calculation of conversion. In this case, however, in some cases an optically active product was obtained, for which an additional calculation method was applied.

5.4.2 Optimization results of the Knoevenagel-phospha-Michael reaction

The Knoevenagel-phospha-Michael synthesis is a reaction in which three components: a carbonyl substrate, an H-phosphonate, and malononitrile or cyanoacetate, react to give a single product, as illustrated in Scheme 77 using the reaction of benzaldehyde (**1a**), malononitrile (**5a**), and diethyl H-phosphonate (**2a**) as an example. If the reaction between the carbonyl substrate and H-phosphonate were promoted, a side reaction, hydroxyphosphonylation, would occur, leading to the formation of a hydroxyphosphonate (**3a**) instead of the Knoevenagel-phospha-Michael adduct (**8a**), as shown in Scheme 78. This side reaction would inhibit further progress of the Knoevenagel-phospha-Michael reaction.

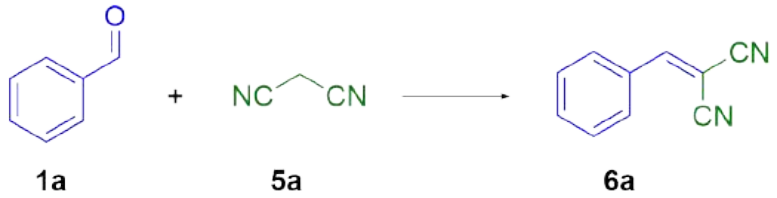


Scheme 77. Model of Knoevenagel-phospha-Michael reaction

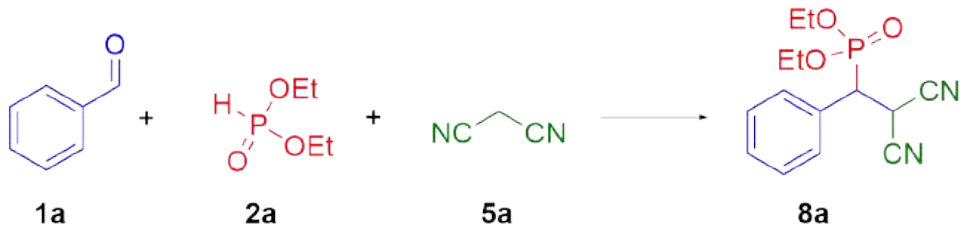


Scheme 78. Hydrofosfonylation as possible side reaction

Therefore, the first step of the Knoevenagel-phospha-Michael synthesis was to carry out this reaction in two steps. Data from previous studies were used to determine the optimal conditions: both the Knoevenagel condensation and the phospha-Michael addition proceed most efficiently at 70℃ in the presence of a catalyst corresponding to approximately 5 mol% Zn (7.5 mg of eco-catalyst per 0.23 mmol of substrate). First, aldehyde and malononitrile were added to the vial (Scheme 79), and after two hours, the H-phosphonate was introduced into the same vial, with the reaction continuing for an additional three hours (Scheme 77). The results of this process are presented in the Table 43.

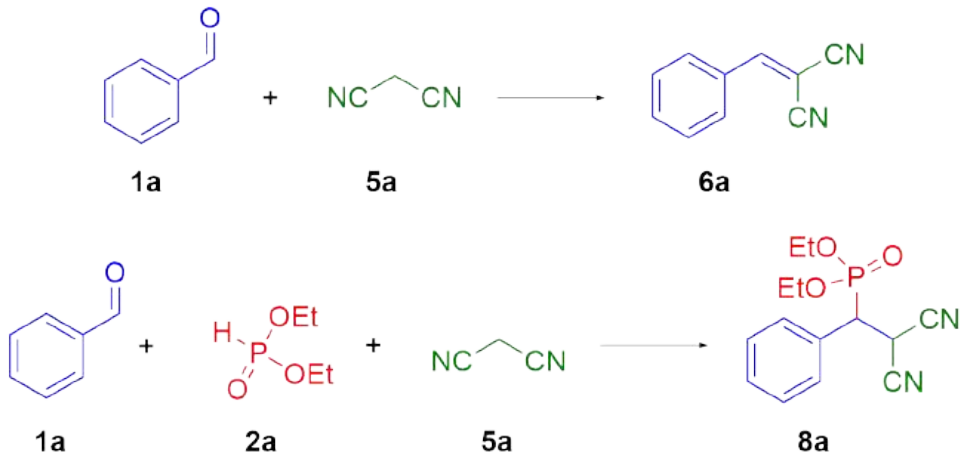


Scheme 79. First step of the process - Knoevenagel condensation



Scheme 77. Second step of the process - phospha-Michael addition

Table 43. Results of two-step Knoevenagel-phospha-Michael reaction.[a]



Entry	Catalyst	Conversion[%][b]	Selectivity [8a:3a]
1.	-	11%	55% : 45%
2.	Eco-MgZnOx-P[c]	100%	100% : 0%
2.	Eco-MgZnOx-F[d]	100%	100% : 0%

a 0.23 mmol of benzaldehyde, 0.23 mmol of H-phosphonate, 0.23 mmol of malononitrile
b Determined by ^{31}P NMR of crude reaction mixture.
c 7.5 mg of Eco-MgZnOx-P: Mg (7.0 mol%), Ca (13.6 mol%), Zn (5.7 mol%).
d 7.5 mg of Eco-MgZnOx-F: Mg (3.5 mol%), Ca (11.4 mol%), Zn (4.9 mol%).

The two-step process yielded satisfactory results. Therefore, the next step was to conduct the reaction as a one-pot process by adding all three substrates to the vial simultaneously (Scheme 77). This reaction was carried out for 5 hours, which is the sum of the times for the two previous steps. The conversions and selectivities, determined by ^{31}P NMR, are presented in the Table 44.

Table 44. Results of one-step Knoevenagel-phospha-Michael reaction.[a]

Conditions	Catalyst	Conversion[%][b]	Selectivity [8a:3a]
5h, T=70℃, neat	-	9%	100% [8a]
	Eco-ZnOx-P[c]	93%	100% [8a]
	Eco-ZnOx-F[d]	99%	100% [8a]

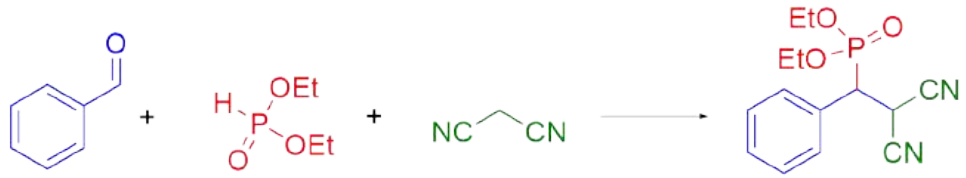
a Reaction conditions: benzaldehyde (1): 0.23 mmol, malononitrile (2): 0.23 mmol;
b Determined by ^{1}H NMR of crude reaction mixture.
c 7.5 mg of Eco-ZnOx-P: Mg (7.0 mol%), Ca (13.6 mol%), Zn (5.7 mol%).
d 7.5 mg of Eco-ZnOx-F: Mg (3.5 mol%), Ca (11.4 mol%), Zn (4.9 mol%).

The next step was to optimize the conditions for the one-pot Knoevenagel-phospha-Michael reaction in terms of temperature, reaction time, and catalyst amount, with a

focus on selectivity due to the potential side reaction leading to the formation of hydroxyphosphonate (Scheme 78). The model reaction chosen for this optimization was the reaction of aldehyde (**1a**), H-phosphonate (**2a**) and malononitrile (**5a**). Results of optimization are presented in the Table 45. The Knoevenagel-phospha-Michael reaction was tested on model substrates and compared with commercially available metal oxides: ZnO, $CaCO_3$, MgO. The comparison was carried out by introducing the metal oxides in amounts corresponding to their proportions in the eco-catalyst derived from *Arabidopsis halleri*. The main product of the desired three-component process is compound **8a**, while hydroxyphosphonate **3a** is treated as the side product formed by direct hydroxyphosphonylation of benzaldehyde with diethyl H-phosphonate.

An analogous approach was conducted for another model reaction - of aldehyde (**1a**), H-phosphonate (**2a**), and cyanoacetate (**5b**), where optimization results are presented in Table 46.

Table 45. Knoevenagel-phospha-Michael reaction on model substrates catalyzed by Eco-Catalysts and comparison with the use of regular ZnO, $CaCO_3$, and MgO for reaction with malononitrile[a]



1a 2a 5a 8a

No.	Catalyst	T [°C]	t [h]	Conversion[b]	Conversion[b] with EcoCatalyst		Solvent	Selectivity 8a:3a [8a:3a]	
					P	F		P	F
1.	-	RT	4	0%	79%	80%	None	19:1	19:1
2.	-	80	1	11%	99%	99%	None	only 8a	31:1, 32:1
3.	-	70	1	3%	84%	86%	None	only 8a	only 8a
4.	-	70	1	5%	89%	91%	None	only 8a	only 8a
5.	-	70	3	9%	100%	100%	None	only 8a	only 8a
6.	-	70	3	0%	100%	90%	None	5:1	4:1
7.	-	70	3	0%	10%	13%	DCM	only 8a	1.4:1
8.	-	70	3	0%	56%	52%	Toluene	2.7:1	3.8:1
9.	-	70	3	0%	77%	70%	Ethyl Acetate	0.8:1	5:1
10.	-	70	3	0%	53%	80%	Methanol	1.8:1	1.3:1
11.	MgO[g]	70	3	92%	-	-	None	only 8a	
12.	MgO[h]	70	3	95%	-	-	None	only 8a	
13.	ZnO[i]	70	3	59%	-	-	None	only 8a	
14.	ZnO[j]	70	3	56%	-	-	None	only 8a	
15.	$CaCO_3$[k]	70	3	52%	-	-	None	only 8a	
16.	$CaCO_3$[l]	70	3	49%	-	-	None	only 8a	
14.	MgO+ZnO[m]	70	3	98%	-	-	None	only 8a	
14.	MgO+ZnO[n]	70	3	98%	-	-	None	only 8a	

a Reaction conditions: benzaldehyde (**1a**): 0.23 mmol, malononitrile (**5a**): 0.23 mmol.
b Determined by ^{1}H NMR of crude reaction mixture.
c 7.5 mg of Eco-MgZnOx-P: Mg (7.0 mol%), Ca (13.6 mol%), Zn (5.7 mol%).
d 7.5 mg of Eco-MgZnOx-F: Mg (3.5 mol%), Ca (11.4 mol%), Zn (4.9 mol%).
e 15 mg of Eco-MgZnOx-P: Mg (14.0 mol%), Ca (27.2 mol%), Zn (11.4 mol%).
f 15 mg of Eco-MgZnOx-F: Mg (7.0 mol%), Ca (22.8 mol%), Zn (9.8 mol%).
g 7.0 mol% of Mg.
h 3.5 mol% of Mg.
i 5.7 mol% of Zn.
j 4.9 mol% of Zn.
k 13.6 mol% of Ca.
l 11.4 mol% of Ca.
m 7.0 mol% of Mg + 5.7 mol% of Zn.
n 3.5 mol% of Mg + 4.9 mol% of Zn.
o 1.5 mg of Eco-MgZnOx-P: Mg (1.4 mol%), Ca (2.7 mol%), Zn (1.1 mol%).
p 1.5 mg of Eco-MgZnOx-F: Mg (0.7 mol%), Ca (2.3 mol%), Zn (1.0 mol%).

As shown in Table 45, Eco-MgZnOx-P and Eco-MgZnOx-F exhibited markedly higher catalytic performance than the corresponding mixtures of single, commercially available oxides introduced in equivalent amounts. While the eco-catalysts achieved conversions above 95% under optimized conditions, the reference oxides alone reached only 49-59% conversion. This indicates that the catalytic activity is not the result of the presence of individual metal oxides, but rather of the synergistic effect created in the mixed-oxide eco-catalyst obtained from *A. halleri*. Importantly, the eco-catalysts also maintained high selectivity towards the desired products, highlighting their robustness and potential as sustainable alternatives to conventional catalysts.

The quantitative analysis of the reaction mixture was performed on the basis of the ^{31}P NMR spectrum (Figure 80). In the ^{31}P NMR spectrum of the reaction mixture, two product signals were observed in the region of 20-22 ppm. Literature data indicate that α-hydroxyphosphonates typically resonate at higher shifts, around 22 ppm, whereas the main Knoevenagel-phospha-Michael adducts give signals slightly upfield, close to 20 ppm [347, 457, 475]. To confirm this assignment, pure diethyl α-hydroxy(phenyl)methylphosphonate was added to the already analyzed crude mixture, and the spectrum was recorded again. A clear increase of the resonance at $\delta \approx 22$ ppm was observed, confirming that this signal corresponds to the hydroxyphosphonate by-product, while the resonance at $\delta \approx 20$ ppm belongs to the main product.

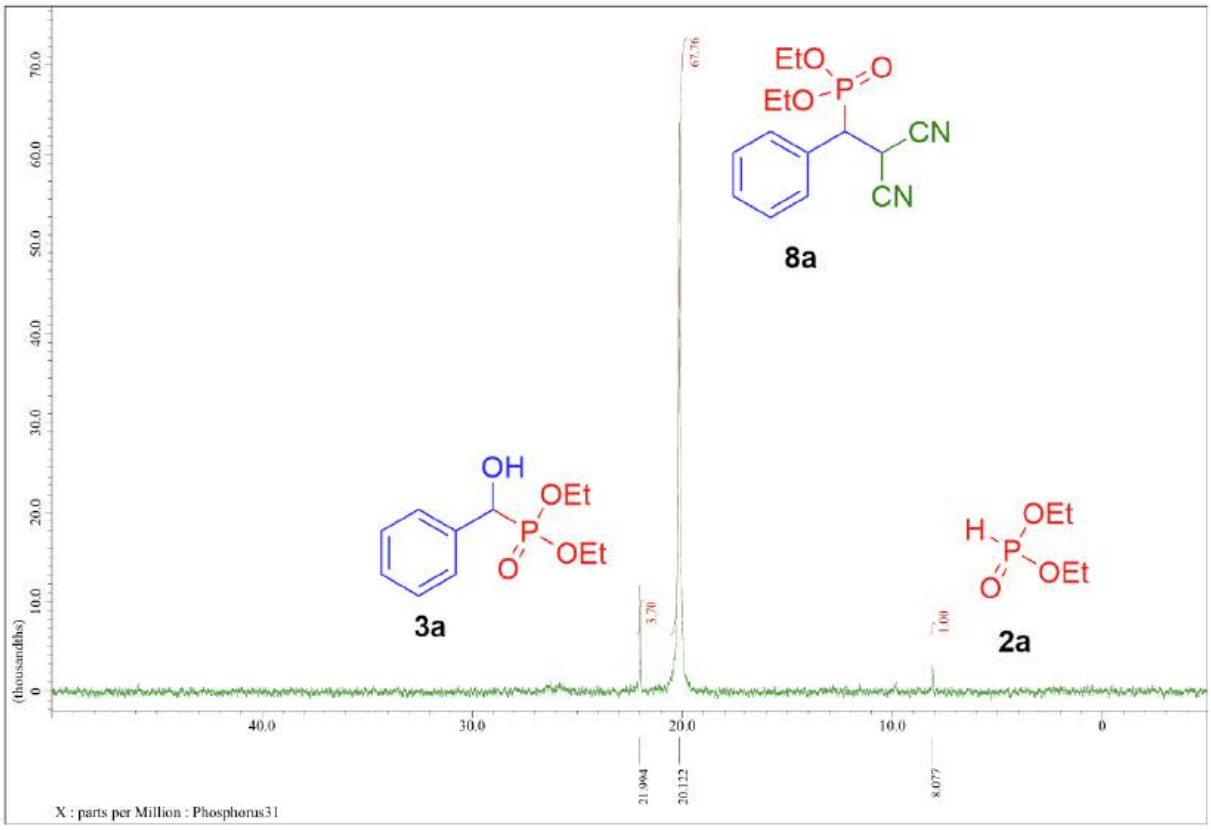


Figure 80. $^{3}1$P NMR spectrum (243 MHz, $CDCl_3$) of crude reaction mixture after the Knoevenavel phospha-Michael reaction of benzaldehyde, malononitrile and diethyl H-phosphonate.

The integrals of the signals were normalized for $\delta = 8.1$ ppm (substrate), so $\delta = 20.1$ ppm (product 8a) = 258.1 and $\delta = 22.0$ ppm (product 3a) = 10.8. The total integral after normalization was:

$$\Sigma I = I_{\text{sub}} + I_{8a} + I_{3a} = 1.0 + 258.1 + 10.8 = 269.9$$

The conversion of diethyl H-phosphonate was calculated according to:

$$\text{Conversion } [\%] = \left(1 - \frac{I_{\text{sub}}}{\Sigma I}\right) \times 100\% = \left(1 - \frac{1.0}{269.9}\right) \times 100\% \approx 99.6\%$$

The selectivity towards each product was determined from the relative integrals:

$$\text{Selectivity}_{8a} = \frac{I_{8a}}{I_{8a} + I_{3a}} \times 100\% = \frac{258.1}{258.1 + 10.8} \times 100\% \approx 95.6\%$$

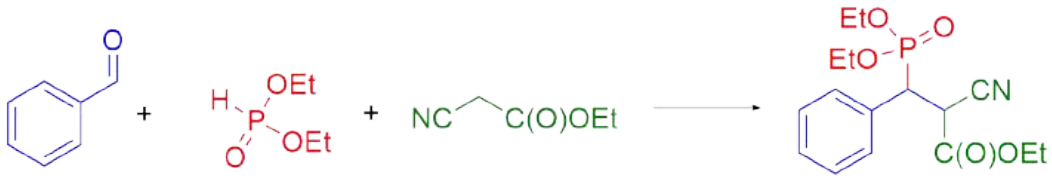
$$\text{Selectivity}_{3a} = \frac{I_{3a}}{I_{8a} + I_{3a}} \times 100\% = \frac{10.8}{258.1 + 10.8} \times 100\% \approx 4.0\%$$

Thus, the molar ratio of the two products was:

$$8a : 3a = \frac{I_{8a}}{I_{3a}} \approx \frac{258.1}{10.8} \approx 24 : 1$$

As a second model, the three-component reaction between benzaldehyde (**1a**), diethyl phosphite (**2a**), and ethyl cyanoacetate (**5b**) was optimized, affording the corresponding product **9a**.

Table 46. Knoevenagel-phospha-Michael reaction on model substrates catalyzed by EcoCatalysts for R^1 = $COOEt$.[a]



1a 2a 5b 9a

Entry	T [°C]	t [h]	Conv./Ratio (0)[b]	Reactions with EcoCatalyst					
				PL (Eco-MgZnOx-P)			FR (Eco-MgZnOx-F)		
				Conv.[b]	Ratio[c]	Sel.$_{KPM}$ [%]	Conv.[b]	Ratio[c]	Sel.$_{KPM}$ [%]
1	50	3	0% / –	17%[d]	1:1.76	83	37%[e]	1:1.62	94
2	50	3	0% / –	6%[f]	–	100	47%[g]	1:1.93	100
3	50	2	0% / –	37%[d]	1:1.65	88	33%[e]	1:1.71	94
4	70	1	0% / –	76%[d]	1:1.78	82	72%[e]	1:1.77	86
5	70	2	2% / –	77%[d]	1:1.77	91	84%[e]	1:1.64	92
6	70	3	4% / –	92%[d]	1:1.78	93	91%[e]	1:1.76	94
7	70	4	6% / –	85%[d]	1:1.74	85	92%[e]	1:1.75	89
8	70	5	8% / –	91%[d]	1:1.58	85	89%[e]	1:1.51	87

[a] Reaction conditions: benzaldehyde (**1a**): 0.23 mmol, diethyl H-phosphonate (**2a**): 0.23 mmol, cyanoacetate (**5b**): 0.23 mmol.
[b] Determined by ^{31}P NMR of the crude reaction mixture.
[c] Diastereomeric ratio of the KPM product (major:minor). A dash indicates the ratio was not determined. Determined by ^{31}P NMR of the crude reaction mixture.
[d] 7.5 mg of Eco-MgZnOx-P (PL): Mg (28.0 mol%), Ca (54.4 mol%), Zn (22.8 mol%).
[e] 7.5 mg of Eco-MgZnOx-F (FR): Mg (14.0 mol%), Ca (45.6 mol%), Zn (19.6 mol%).
[f] 15 mg of Eco-MgZnOx-P (PL): Mg (14.0 mol%), Ca (27.2 mol%), Zn (11.4 mol%).
[g] 15 mg of Eco-MgZnOx-F (FR): Mg (7.0 mol%), Ca (22.8 mol%), Zn (9.8 mol%).

In the absence of the eco-catalyst no product formation was observed. Presence of Eco-MgZnOx-P and Eco-MgZnOx-F provided significant improvements in conversion. Conversion values are slightly lower than those obtained with malononitrile as acceptor, clearly confirm the ability of the eco-catalysts to promote the Knoevenagel-phospha-Michael reaction with different substrates. The trend also highlights the influence of

the electronic properties of the Michael acceptor: the less activated ethyl cyanoacetate gave lower conversions compared to malononitrile, but still demonstrated the efficiency and robustness of the eco-catalysts under these conditions. This underlines the potential of the catalysts derived from *A. halleri* not only for strongly activated acceptors but also for substrates with lower electrophilicity.

Quantitative calculation of conversion and selectivity for this series was performed based on ^{31}P NMR analysis as well what is presented on the example Figure 81.

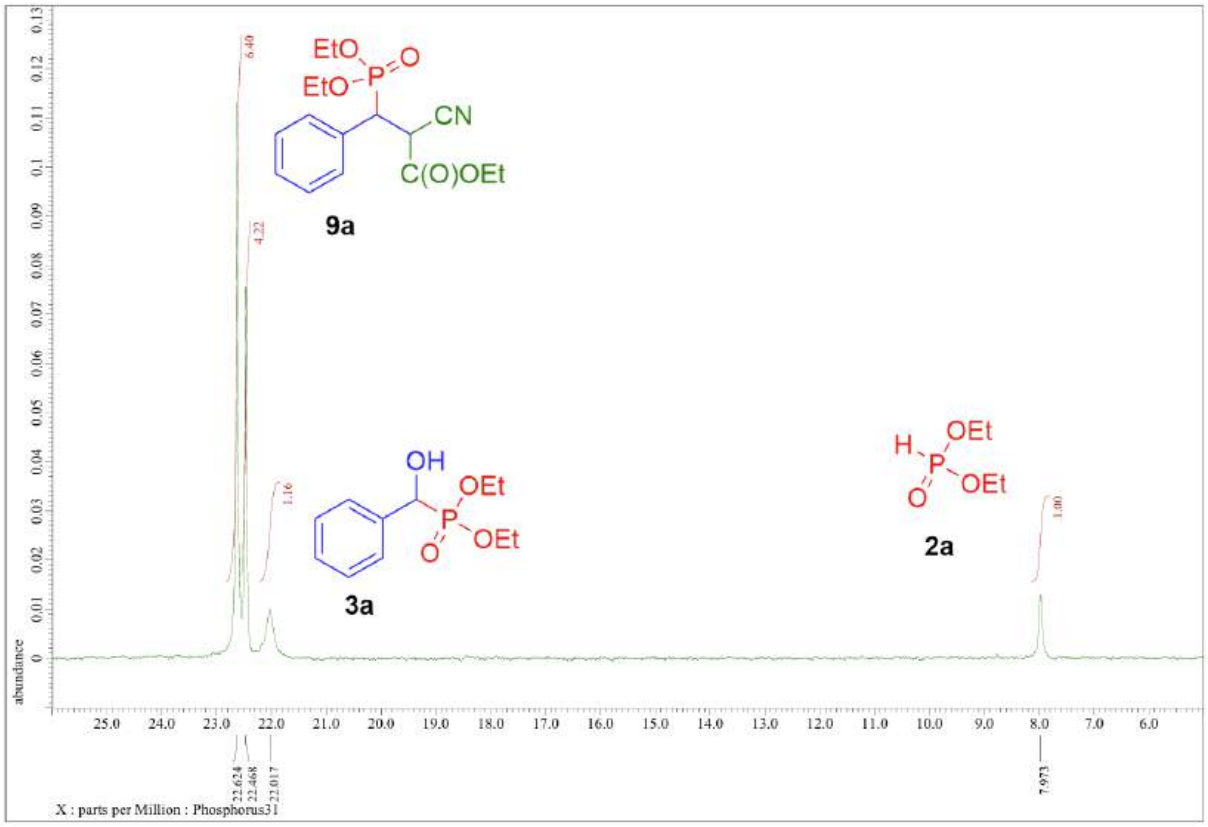


Figure 81. ^{31}P NMR spectrum (243 MHz, $CDCl_3$) of crude reaction mixture after the Knoevenavel phospha-Michael reaction of benzaldehyde, ethyl cyanoacetate and diethyl H-phosphonate.

The ^{31}P NMR spectrum of the crude reaction mixture shows four resonances at

- $\delta = 7.973$ (substrate, normalized to $I_{\text{sub}} = 1$),
- $\delta = 22.017$ (minor α-hydroxyphosphonate, $I_{\text{hyd}} = 1.16$),
- $\delta = 22.468$ and $\delta = 22.624$ ppm (two diastereomers of the Knoevenagel–phospha–Michael adduct, $I_1 = 4.22$, $I_2 = 6.40$).

The duplication of the main-product signal is consistent with the formation of two diastereomers (stereogenic P and adjacent C), each giving a separate ^{31}P resonance.

Assuming quantitative acquisition (gated decoupling, sufficient d_1) and one P nucleus per component, the total integral is:

$$\Sigma I \;=\; I_{\mathrm{sub}} + I_{\mathrm{hyd}} + I_1 + I_2 \;=\; 1 + 1.16 + 4.22 + 6.40 \;=\; 12.78.$$

The overall conversion of diethyl H-phosphonate is:

$$\text{Conversion } [\%] \;=\; \left(1 - \frac{I_{\mathrm{sub}}}{\Sigma I}\right) \times 100\% \;=\; \left(1 - \frac{1}{12.78}\right) \times 100\% \;\approx\; 95.50\%.$$

For the two diastereomers of the Knoevenagel–phospha–Michael adduct, the diastereomeric ratio (d.r.) is:

$$\text{d.r. (major : minor)} \;=\; \frac{I_2}{I_1} \;=\; \frac{6.40}{4.22} \;\approx\; 1.74 : 1,$$

corresponding to mole fractions of $\sim 63.5\%$ (major at $\delta 22.624$ ppm) and $\sim 36.5\%$ (minor at $\delta 22.468$ ppm) within the main-product pair.

For completeness, the product distribution among phosphorus-containing products can be expressed as:

$$\text{Selectivity}_{KPMadduct} \;=\; \frac{I_1 + I_2}{I_1 + I_2 + I_{\mathrm{hyd}}} \times 100\% \;=\; \frac{4.22 + 6.40}{4.22 + 6.40 + 1.16} \times 100\% \;\approx\; 94.70\%,$$

$$\text{Selectivity}_{\alpha-hydroxyphosphonate} \;=\; \frac{I_{\mathrm{hyd}}}{I_1 + I_2 + I_{\mathrm{hyd}}} \times 100\% \;\approx\; 5.30\%.$$

These values support the assignment that the two dominant resonances at $\delta \;\approx\; 22.47$ and 22.62 ppm arise from two diastereomers of the Knoevenagel–phospha–Michael adduct, while the minor peak at $\delta \approx 22.02$ ppm corresponds to the α-hydroxyphosphonate by-product, and the small signal at $\delta \approx 7.97$ ppm to the residual starting diethyl H-phosphonate.

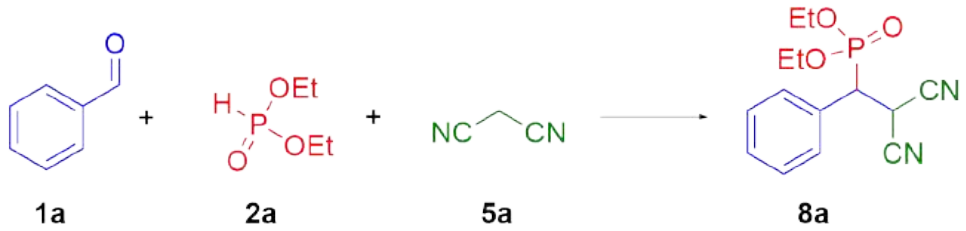
Final optimized conditions for Knoevenagel phospha-Michael reaction were decided to 70℃, 3h, neat, catalyst in mount 5mol% of Zn.

5.4.3 Reusage of the ecocatalyst in the Knoevenagel-phospha-Michael reaction

To evaluate the stability and reusability of the Eco-MgZnOx catalysts, recovery tests were performed in the Knoevenael-phospha-Michael reaction of benzaldehyde (**1a**), malononitrile (**5a**), and diethyl H-phosphonate (**2a**) as illustrated in Scheme 77. After

each run, the catalyst was recovered by centrifugation, followed by calcination at 550 ℃ for 6 h, in order to reproduce the same treatment as during the initial preparation. The results are summarized in Table 47.

Table 47. Recovery and reuse tests of the Eco-MgZnOx catalysts in Knoevenael-phospha-Michael addition[a].



1a 2a 5a 8a

Ecocatalyst	Run	Conversion[b] (%)
Eco-ZnOx-P	1	99%
	2	99%
	3	98%
	4	99%
	5	95%
Eco-ZnOx-F	1	98%
	2	99%
	3	96%
	4	99%
	5	97%

a Reaction conditions: aldehyde (0.23 mmol), H-phosphonate (0.23 mmol).
b determined by ^{31}P NMR.

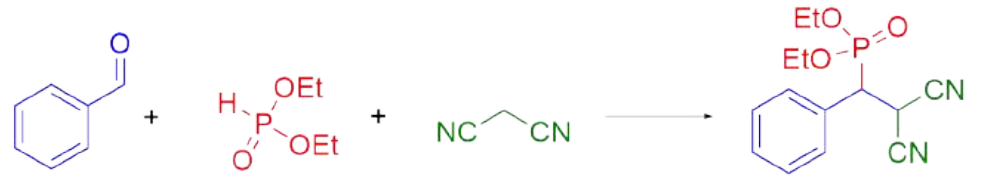
As can be seen from the data, both Eco-ZnOx-P and Eco-ZnOx-F retained high catalytic activity over five consecutive cycles, with only a slight decrease in conversion that remained within the range of experimental error. For Eco-ZnOx-P, the conversion was maintained in the range of 98-99%, while for Eco-ZnOx-F it remained between 96-99%. These results demonstrate that the catalysts derived from hyperaccumulator biomass exhibit not only high activity but also durability under the conditions of the Knoevenael-phospha-Michael reaction.

5.4.4 Scale-up of the Knoevenagel-phospha-Michael reaction

In order to further validate the applicability of the eco-catalysts under more practical conditions, the Knoevenagel-phospha-Michael reaction with malononitrile as the substrate was scaled up from the standard test scale (0.23 mmol) to a preparative scale, targeting the isolation of at least 1 gram of the desired product. For this purpose, benzaldehyde, H-phosphonate and malononitrile were used in equimolar amounts of 6.4

mmol each. The eco-catalysts Eco-MgZnOx-P and Eco-MgZnOx-F were applied in proportions analogous to those previously employed, ensuring consistency of the catalytic conditions. After reaction and work-up, the product was isolated in high purity, and the results are summarized in Table 48

Table 48. Scale-up of the model reaction of Knoevenagel-phospha-Michael reaction for R^1 = CN^a.



1a 2a 5a 8a

Catalyst	Conversion [%][b]	Yield [%]
Eco-MgZnOx-P[c]	98%	96%[e]
Eco-MgZnOx-F[d]	99%	96%[f]

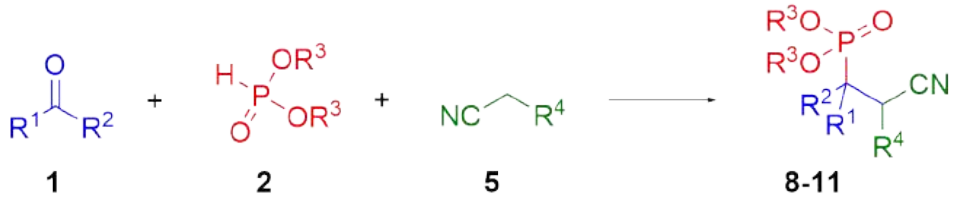
a Reaction conditions: benzaldehyde (1): 6.4 mmol, malononitrile (2): 6.4 mmol, H-phosphonate (3): 6.4 mmol.
b Determined by ^{31}P NMR of crude reaction mixture.
c 210 mg of Eco-MgZnOx-P: Mg (7.0 mol%), Ca (13.6 mol%), Zn (5.7 mol%).
d 210 mg of Eco-MgZnOx-F: Mg (3.5 mol%), Ca (11.4 mol%), Zn (4.9 mol%).
e 1795 mg of pure product (3).
f 1795 mg of pure product (3).

The scale-up experiment clearly demonstrated that both eco-catalysts maintained their excellent activity and selectivity when the reaction was performed at a larger scale. Conversions and yields remained high. These results confirm that the outstanding catalytic efficiency observed on the small scale is fully transferable to preparative conditions. This successful scale-up highlights the practical potential of catalysts derived from *Arabidopsis halleri* biomass, bridging the gap between laboratory-scale experiments and applications closer to real synthetic needs. The consistency of results across scales also emphasizes the reproducibility and stability of the eco-catalysts, which is a crucial factor for their further development in sustainable catalytic processes.

5.4.5 Substrate scope of the Knoevenagel-phospha-Michael reaction

To further evaluate the scope and efficiency of the Knoevenagel-phospha-Michael reaction (Reaction A), a series of substrates was investigated. The study covered different classes of electrophiles, including aromatic aldehydes bearing electron-donating

and electron-withdrawing groups, as well as a set of H-phosphonates with various substituents. Both EcoMgZnO-P and EcoMgZnO-F catalysts were tested to compare their activity and selectivity across the substrate range. All reactions were performed in optimized conditions (70℃, 3 h, solvent-free, catalyst loading corresponding to 5 mol% of Zn).



Scheme 4. General scheme of Knoevenagel-phospha-Michael reaction, where R^4=CN for Reaction A and R^4=COOEt for Reaction B

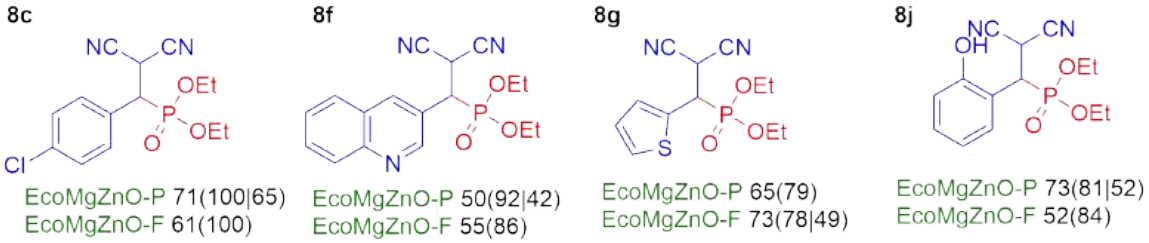


Figure 82. Substrate scope of Knoevenagel-phospha-Michael reaction - scope of aldehydes (Reaction A). Numbers next to each entry are conversions and values in parentheses are isolated yields.

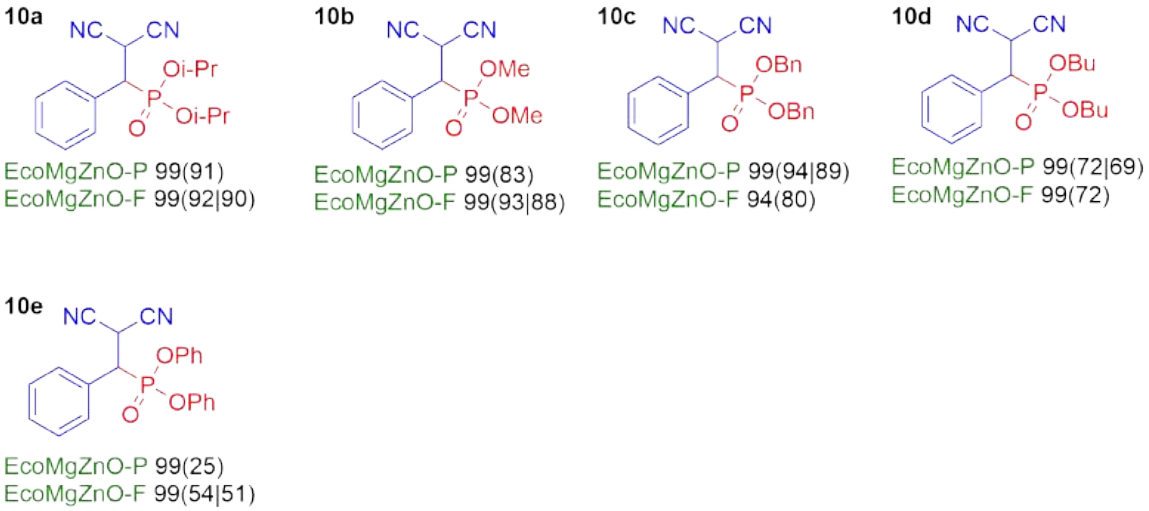


Figure 83. Substrate scope of Knoevenagel-phospha-Michael reaction - scope of H-phosphonates (Reaction A). Numbers next to each entry are conversions and values in parentheses are isolated yields.

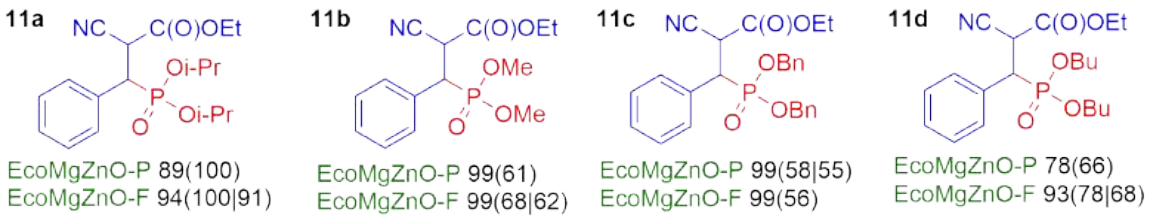


Figure 84. Substrate scope of Knoevenagel-phospha-Michael reaction - scope of H-phosphonates (Reaction B). Numbers next to each entry are conversions and values in parentheses are isolated yields.

Values on Figures 82, 83 and 84 are reported in the format: conversion (selectivity | isolated yield). For example, 95 (90|81) indicates 95% substrate conversion, 90% selectivity toward the main product (KPM adduct), and 81% isolated yield of that product.

The reaction proceeded efficiently across a broad range of carbonyl substrates, from simple aromatics, such as chlorobenzaldehyde or indolecarbaldehyde, to more demanding heteroaromatics like benzothiophene. Conversions were generally high, although selectivity and isolated yields varied depending on the aldehyde structure.

The reaction showed excellent tolerance toward substituents at the phosphorus atom. Regardless of whether alkyl (iPr, OMe, OBn, OBu) or aryl (OPh) groups were present, conversions were nearly quantitative. Isolated yields were usually high, though in the case of bulkier aromatic substituents, a tendency toward reduced selectivity was noted.

The substrate scope included derivatives bearing different ester groups. Conversions were again very high (typically 99%), and isolated yields ranged from good to excellent. Only for the derivative with a bulky butyl substituent (**11d**) was a decrease in conversion observed with EcoMgZnO-P, indicating a limitation related to steric effects.

The Knoevenagel-phospha-Michael reaction catalyzed by EcoMgZnO-P and EcoMgZnO-F displays a broad substrate scope, both with respect to aldehydes and phosphorus derivatives. The substituent effects are visible: heteroatoms like sulfur and sterically demanding alkyl or aryl groups may lead to lower selectivity or yields. Both catalysts perform comparably, although EcoMgZnO-F tends to provide more consistent results in cases involving bulky substrates.

Products were characterized by NMR spectroscopy. The recorded spectral data confirms the structure of the target products obtained via the Knoevenagel-phospha-Michael addition.

As an example, for the **8c** compound - Diethyl [1-(4-chlorophenyl)-2,2-dicyanoethyl]phosphonate (Figure 85), the ^{31}P NMR spectrum (Figure 88) displays a single, sharp resonance at 19.9 ppm, which is characteristic of the expected phospho-

nate functionality and indicates high purity. In the ^{1}H NMR spectrum (Figure 87), the aromatic region features distinct multiplets between 7.4 and 7.5 ppm corresponding to the p-chlorophenyl ring protons. The successful addition is evidenced in the aliphatic region by the specific signals for the methine protons, alongside the diagnostic multiplets and triplets for the diethoxyphosphoryl group. Furthermore, the ^{13}C NMR spectrum (Figure 86) shows the molecular skeleton, clearly showing the characteristic nitrile signals at approximately 111 ppm and the ethoxy carbon signals around 64 and 16 ppm. Splitting patterns observed in the carbon spectrum reveal the expected carbon-phosphorus coupling (J_{C-P}), providing structural verification of the phosphonate attachment to the carbon chain. Collectively, the consistent integration of proton signals and the specific chemical shifts across all three nuclei serve as definitive proof that the reaction proceeded selectively to the desired adduct.

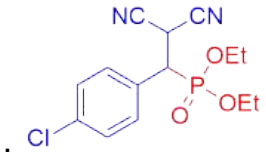


Figure 85. 8c - Diethyl [1-(4-chlorophenyl)-2,2-dicyanoethyl]phosphonate

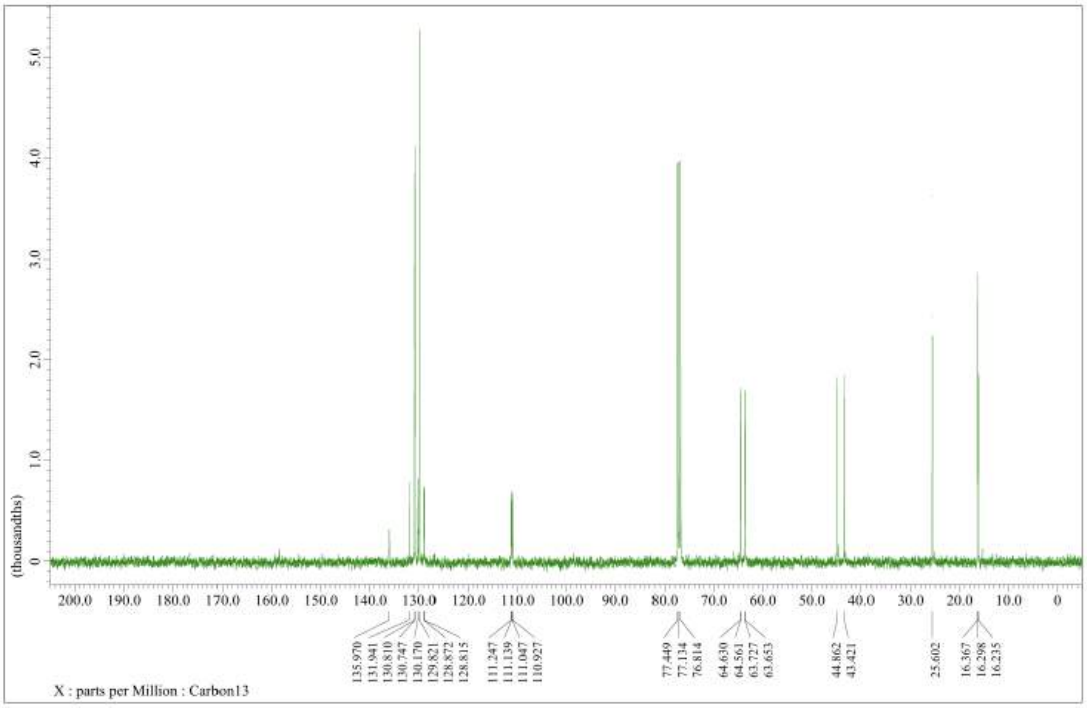


Figure 86. ^{13}C NMR spectrum of 8c - Diethyl [1-(4-chlorophenyl)-2,2-dicyanoethyl]phosphonate

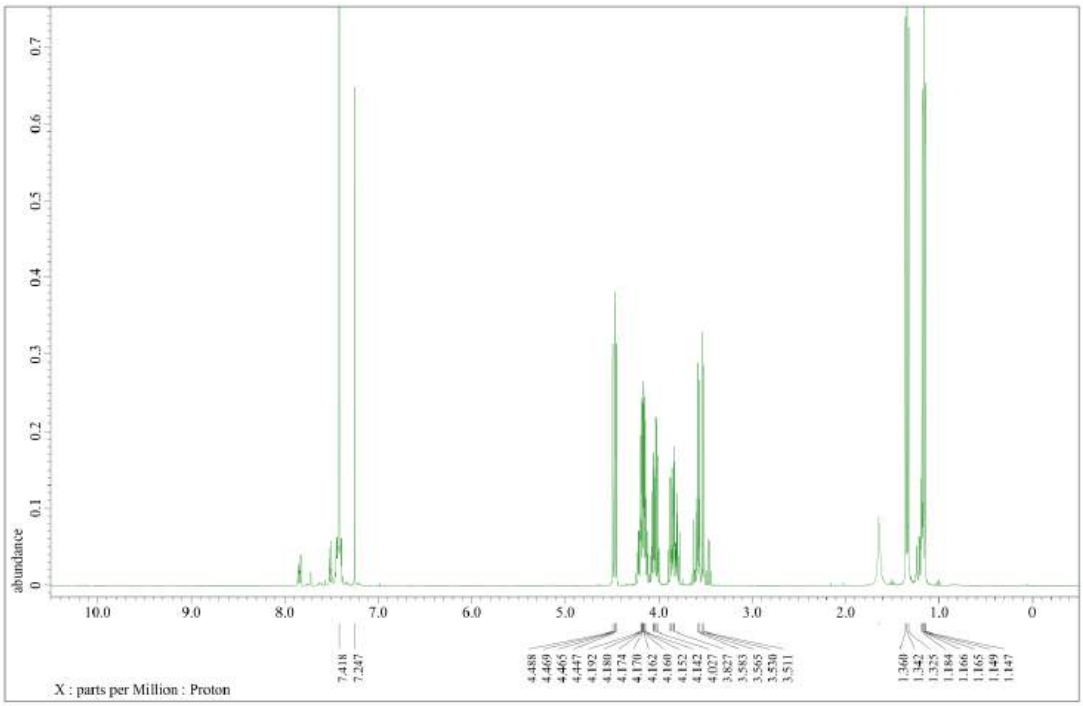


Figure 87. ^{1}H NMR spectrum of 8c - Diethyl [1-(4-chlorophenyl)-2,2-dicyanoethyl]phosphonate

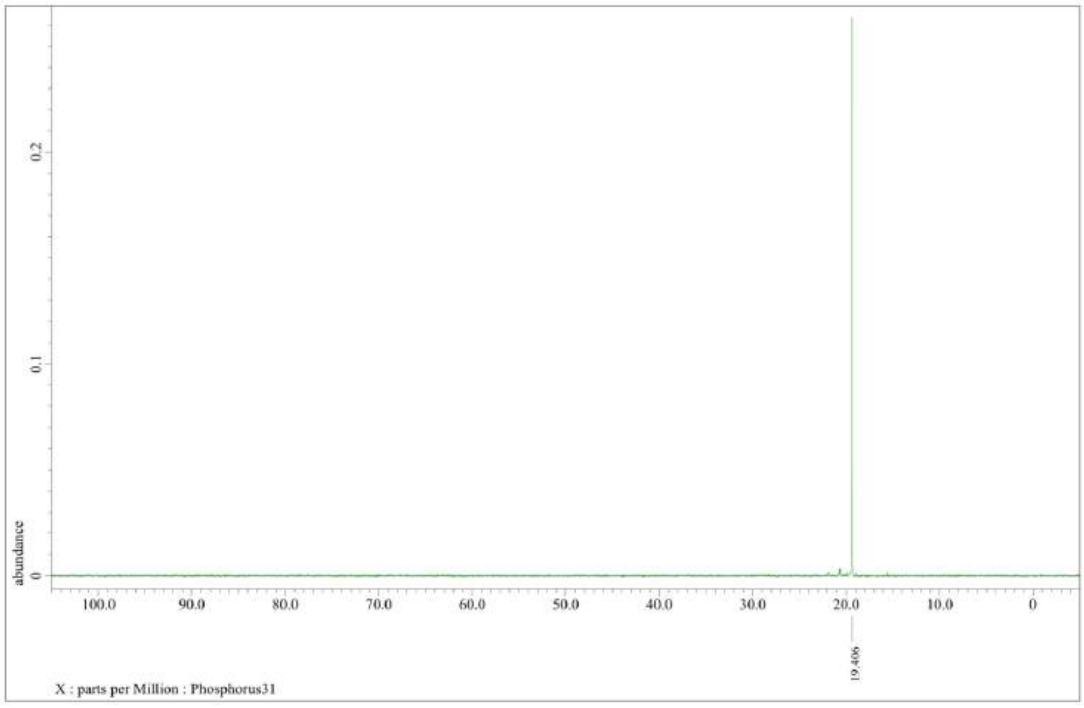


Figure 88. ^{31}P NMR spectrum of 8c - Diethyl [1-(4-chlorophenyl)-2,2-dicyanoethyl]phosphonate

5.4.6 Conclusions

In this chapter, the application of the *Arabidopsis halleri*-derived Eco-MgZnOx catalyst in the Knoevenagel-phospha-Michael reaction was demonstrated. This transformation combines two important bond-forming processes: the Knoevenagel condensation, leading to $C-C$ bond formation, and the subsequent phospha-Michael addition, leading to $C-P$ bond formation. As a result, the reaction gives access to highly functionalized organophosphorus compounds from simple starting materials in a one-pot process.

A key challenge in this reaction system was the possible competition between the desired Knoevenagel-phospha-Michael pathway and the direct hydrophosphonylation of the carbonyl compound. The formation of α-hydroxyphosphonates as side products could reduce the selectivity of the process and block the formation of the expected Michael acceptor. The reaction was first investigated in a two-step variant, in which the Knoevenagel condensation was carried out before the addition of the H-phosphonate. This approach confirmed that the Eco-MgZnOx catalyst efficiently promotes both reaction stages and allows the desired product to be obtained with very high conversion and selectivity.

After confirming the efficiency of the two-step variant, the reaction was successfully transferred to a direct one-pot procedure, in which the aldehyde, the active methylene compound, and the H-phosphonate were added simultaneously. Under optimized conditions, the reaction proceeded efficiently at 70 ℃, under solvent-free conditions, and with a low catalyst loading corresponding to approximately 5 mol% of Zn. These conditions are consistent with the green chemistry approach, as they avoid the use of solvent, require only moderate heating, and use a recyclable heterogeneous catalyst prepared from plant biomass.

Both Eco-MgZnOx-P and Eco-MgZnOx-F showed very high catalytic activity in the model reaction. In the one-pot process with malononitrile, Eco-MgZnOx-F gave nearly quantitative conversion, while Eco-MgZnOx-P also provided very high conversion. The selectivity toward the Knoevenagel-phospha-Michael adduct remained excellent, showing that the catalyst promotes the cascade pathway over the competing hydrophosphonylation reaction. This behavior confirms the important role of the bifunctional acid-base character of the catalyst. Basic sites can activate the H-phosphonate or the active methylene compound, while Lewis-acidic sites can activate the carbonyl group or the electron-deficient alkene. The coexistence of these sites in one material enables efficient cooperation between the two reaction steps.

The substrate scope studies confirmed that the developed method is applicable to a broad range of substrates. Aromatic and heteroaromatic aldehydes were successfully converted, including substrates bearing electron-donating and electron-withdrawing substituents. The reaction also tolerated different H-phosphonates, containing alkyl, benzyl, and aryl substituents. In most cases, high conversions and good to excellent isolated yields were obtained. Some decrease in selectivity or yield was observed for more sterically demanding substrates and for selected heteroaromatic systems, showing that steric and electronic effects influence the reaction outcome. Nevertheless, the general substrate tolerance remained broad, confirming the usefulness of the Eco-MgZnOx catalyst in the synthesis of structurally diverse phosphonated products.

The practical value of the method was further supported by catalyst reuse experiments. Both Eco-MgZnOx-P and Eco-MgZnOx-F could be recovered from the reaction mixture and reused in five consecutive catalytic cycles. Only a small decrease in activity was observed, and the conversions remained high throughout the recycling tests. This confirms that the catalyst is not only active but also stable under the reaction conditions. The possibility of catalyst regeneration by calcination additionally increases the practical potential of the system.

The reaction was also successfully scaled up from the standard analytical scale to a preparative scale. In the gram-scale experiment, both catalysts maintained excellent performance, giving high conversions and isolated yields. This result demonstrates that the catalytic efficiency observed in small-scale optimization experiments can be transferred to larger-scale synthesis without loss of activity or selectivity. The successful scale-up is especially important because it shows that the method is not limited to screening conditions but can be applied to the preparation of useful amounts of product.

Overall, the results presented in this chapter show that Eco-MgZnOx is an efficient, selective, reusable, and scalable heterogeneous catalyst for the Knoevenagel-phospha-Michael reaction. The catalyst enables the formation of both $C-C$ and $C-P$ bonds in a single synthetic sequence under mild and solvent-free conditions. Together with the results from the previous chapters, these findings confirm that catalysts obtained from metal-hyperaccumulating plant biomass can serve as versatile catalytic platforms for sustainable organic synthesis. The Knoevenagel-phospha-Michael reaction is therefore an important example of how ecocatalysis can combine waste biomass valorization, heterogeneous catalysis, and efficient access to valuable organophosphorus compounds.

Conclusion

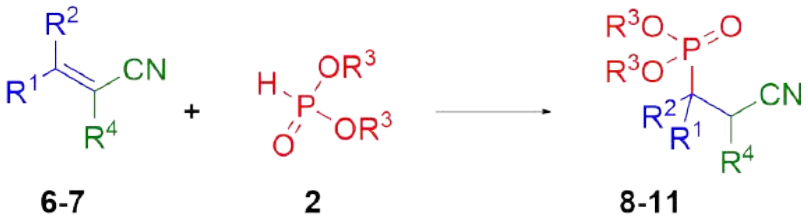
The dissertation demonstrates that plant-derived, polymetallic mixed oxides (Eco-MgZnOx) prepared from *Arabidopsis halleri* biomass act as robust, recyclable heterogeneous Lewis basic/Lewis acidic catalysts for three families of $C-P$ bond forming processes central to organophosphorus synthesis:

- hydrophosphonylation (Pudovik) of carbonyls to give α-hydroxyphosphonates,



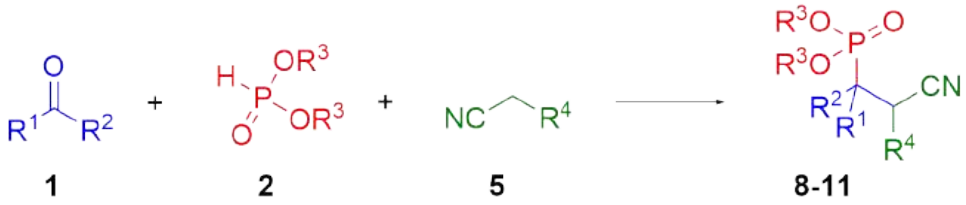
Scheme 1. Hydrophosphonylation (Pudovik reaction) - reaction scheme

- phospha-Michael additions to activated alkenes



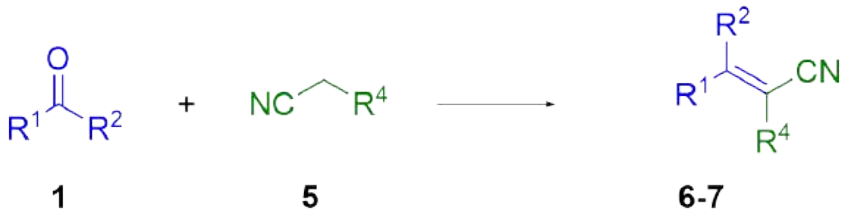
Scheme 3. Phospha Michael addition - reaction scheme

- tandem Knoevenagel-phospha-Michael



Scheme 4. Knoevenagel phospha-Michael condensation - reaction scheme

Additionally Knoevenagel condensation was also demonstrated, which was a natural choice since it was necessary to generate the substrates for the subsequent phospha-Michael reaction. Eco-MgZnOx catalyzed this transformation more efficiently and under milder conditions than other tested methods, making it a natural complement to both the phospha-Michael and the tandem Knoevenagel-phospha-Michael processes.



Scheme 2. Knoevenagel condensation - reaction scheme

Under solvent-free conditions, Eco-MgZnOx promotes fast conversions across electronically diverse substrates, with simple filtration and reusage aligning the chemistry with green-chemistry metrics and extending prior ecocatalysis results to new reaction classes.

The biogenic ecocatalyst Eco-MgZnOx obtained from *Arabidopsis halleri* biomass proved to be highly effective in the hydrophosphonylation (Pudovik reaction) of aldehydes.

- hydrophosphonylation (Pudovik) of carbonyls to give α-hydroxyphosphonates,



Scheme 1. Hydrophosphonylation (Pudovik reaction) - reaction scheme

Under optimized conditions (solvent-free, 50 ℃, 3 h, 5 mol% catalyst relative to Zn), nearly complete conversion of substrates was achieved, typically more than 95% for aromatic aldehydes, with high isolated yields of the products. The method displayed a broad substrate scope - aromatic aldehydes bearing various electronic substituents on the ring, including strong electron-withdrawing nitro and halogens, reacted efficiently without a drop in yield. Functional group tolerance was excellent - the presence of heteroatoms such as nitrogen or sulfur in heteroaromatics, did not suppress the reaction nor poison the catalyst - the oxide surface remained active even in the presence of donor groups. Polycyclic aldehydes (naphthalenes) as well as aliphatic aldehydes also underwent addition with good results under suitably adjusted conditions. Steric hindrance was found to significantly influence reaction rates - for heavily substituted substrates, in example mesitaldehyde with ortho-2,4,6-trimethyl groups (Figure 89), the reaction slowed down, giving lower final conversions. Importantly, the method is chemoselective toward carbonyl groups - aldehydes readily undergo addition, whereas

less reactive ketones remain practically unreacted under these conditions. Tested acetophenone requires significantly higher temperature and longer reaction time, but ketone conversions were able to exceed 40-70% after prolonged runs.

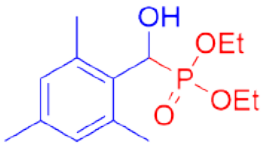
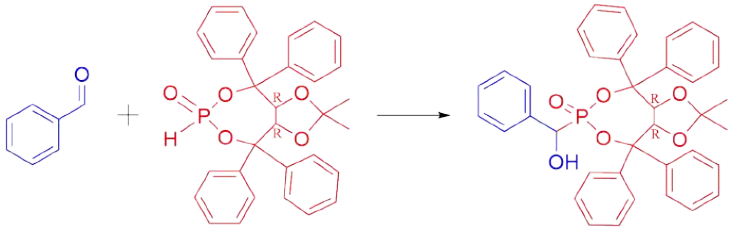


Figure 89. Product of hydrophosphonylation of mesitaldehyde as a heavily substituted substrate

Both studied variants of the catalyst (Eco-MgZnOx-P from Polish biomass and Eco-MgZnOx-F from French biomass) showed comparable activity and efficiency in single-use experiments - no significant differences in yields were observed between them in fresh runs. The nature of the dialkyl H-phosphonate nucleophile affected the efficiency in a steric manner: less hindered H-phosphonates such as dimethyl or dibenzyl, afforded nearly quantitative conversions (99%), even with more challenging aliphatic or heteroaromatic substrates. In contrast, bulkier H-phosphonates - diisopropyl, di-n-butyl - reacted more slowly and gave lower conversions, indicating that excessive steric bulk of the alkyl groups hampers nucleophile activation on the catalyst surface.

Eco-MgZnOx also exhibited aspects of stereoselectivity. While the catalyst itself does not induce chirality, tests with an optically active substrate - a chiral H-phosphonate, as presented on Scheme 80 revealed that the reaction conditions could favor the preferential formation of one diastereomer. In the presence of the catalyst, at lowered temperature and extended reaction time (0℃, 96 h), a high degree of diastereoselectivity (diastereomeric ratio up to 1:7.8) was achieved while maintaining high conversion (85%). In comparison, the uncatalyzed reaction did not proceed at all, and the use of a simple base (Et_3N) did accelerate the addition of the chiral H-phosphonate but at the expense of stereocontrol, giving nearly racemic mixtures. These results highlight that the designed heterogeneous catalyst allows both high efficiency and stereochemical control of the newly formed center, in contrast to either the uncatalyzed or base-catalyzed pathways.



Scheme 80. Model reaction of hydrophosphonylation an optically active H-phosphonate

An important advantage of Eco-MgZnOx is its heterogeneity and durability, enabling easy recovery and reuse. Tests showed that the catalyst derived from Polish biomass could be recycled multiple times ($\geq$5 cycles) without significant loss of activity. In a model reaction (benzaldehyde + diethyl phosphonate, 50℃, 3 h), conversion remained at 94-97% over the first three cycles, and still reached 88% in the fifth run. This demonstrates the high stability of Eco-MgZnOx-P. In contrast, the analogous Eco-MgZnOx-F, ecocatalyst from French biomass, deactivated more rapidly - conversion dropped from 96% in the first use to 58% in the second cycle and as low as 14% in the third.

Post-cycle composition analyses revealed that activity loss correlated with changes in the mineral content, particularly in Mg and Zn. Both catalysts showed gradual leaching of Mg and Zn, but to different extents. Eco-MgZnOx-F started with a significantly lower Mg content (ca. 1.7 wt%) compared to Eco-MgZnOx-P (4.3 wt%). As a result, after only 1-2 uses the French catalyst lost critical amounts of active centers (MgO/ZnO), causing rapid deactivation. In contrast, Eco-MgZnOx-P, with more than double the initial Mg and slightly more Zn, retained a buffer of active sites - even after three cycles, Mg content dropped from 4.3% to 2.9% and Zn from 8.0% to 5.9%, still able to catalyze the reaction efficiently. Thus, the superior durability of Eco-MgZnOx-P stems from its higher initial pool of basic (MgO) and acidic (ZnO) centers, which can partially deactivate or leach without immediate loss of function.

Mechanistic studies (DFT calculations) provided molecular insight into the high activity of Eco-MgZnOx. The proposed mechanism is bifunctional (Figure 44) - the catalyst contains two types of active sites working in concert. Basic MgO centers (O^{2-} anions bound to Mg) deprotonate the $P-H$ group of the H-phosphonate, generating the nucleophilic phosphonate anion, while acidic ZnO centers (Zn^{2+} cations acting as Lewis acids) activate the electrophilic carbon of the aldehyde carbonyl group. Thus, both reactants are simultaneously activated on the surface, brought together in a coordinated transition state where the new $C-P$ bond forms. After addition, the coordinated alkoxide intermediate undergoes protonolysis (a proton from a newly formed -OH group migrates to the alkoxide), releasing the α-hydroxyphosphonate product and regenerating the O^{2-} site. The catalytic cycle thus operates through neighboring basic and acidic sites - a textbook example of bifunctional catalysis, where proximity of complementary sites lowers the activation barrier.

The polymetallic synergy in Eco-MgZnOx was confirmed experimentally and theoretically. Catalytic tests showed that the activity of the ecocatalyst exceeded the sum of its individual components: for benzaldehyde, Eco-MgZnOx gave >96% conversion, whereas MgO alone gave 70%, ZnO 14%, and even a physical mixture $MgO+ZnO$

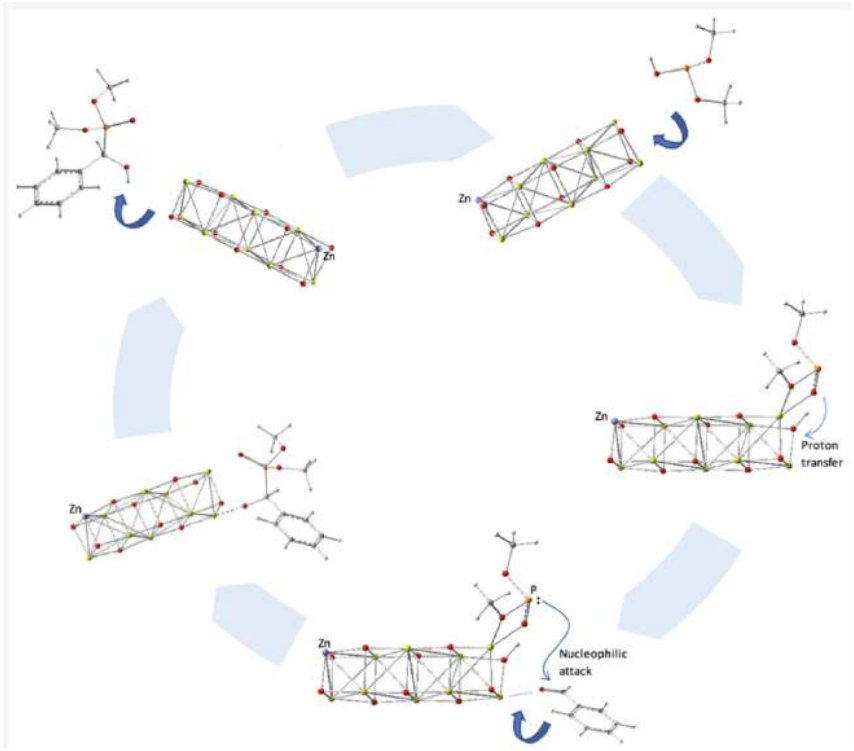


Figure 44. Proposed catalytic cycle for the hydrophosphonylation of benzaldehyde catalyzed by Eco-MgZnOx, based on DFT calculations on a $(Mg_{0.9}Zn_{0.1})O$ cluster model. The cycle illustrates the key steps: (i) deprotonation of the H-phosphonate at a basic MgO site, (ii) coordination and activation of benzaldehyde at an adjacent Lewis acidic Zn site, (iii) nucleophilic attack to form the $C-P$ bond, and (iv) proton transfer to release the product and regenerate the active site.

reached only 78%. This catalytic enhancement arises from the existence of a homogeneous mixed $Mg-Zn-O$ phase. XRPD analysis (Figure 33) confirmed the presence of a solid solution $Mg_{0.88}Zn_{0.12}O$ with periclase structure - Zn^{2+} ions incorporated into the MgO lattice, generating atomic-level adjacency of acidic $Zn(II)$ and basic O^{2-} sites. This structural feature explains the observed synergy: in physical mixtures, the phosphonate anion must migrate between distinct particles, an inefficient process, whereas on the homogeneous $Mg(Zn)O$ surface both steps occur at the same site. DFT calculations on a simplified cluster model ($Mg_{0.9}Zn_{0.1}O$) confirmed that Zn incorporation lowers energy barriers - $C-P$ bond formation was much more facile in the mixed oxide model than on pure MgO. These results provide a consistent mechanistic rationale for the superior activity of the biogenic catalyst, emphasizing the role of polymetallic synergy. Moreover, they suggest routes for further optimization - e.g., tuning the $Mg:Zn$ ratio and minimizing metal leaching are key for performance and durability.

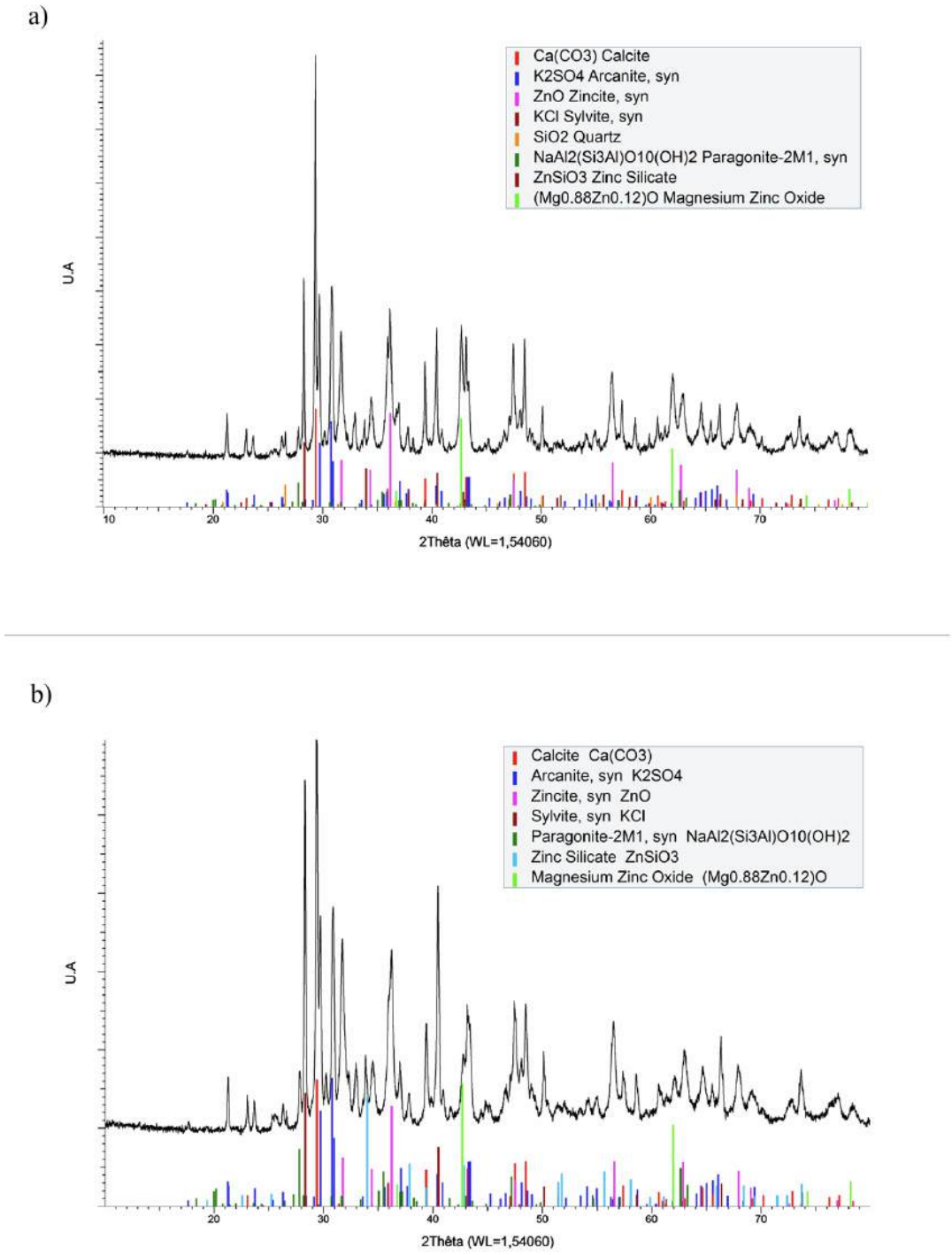


Figure 33. XRPD diffraction pattern of a) Eco-MgZnOx-P and b) Eco-MgZnOx-F

These findings have both scientific and practical significance, advancing the field of sustainable organic catalysis. First, they demonstrate the efficiency of a catalyst obtained from waste plant biomass - material sourced from phytoremediation of metal-contaminated soils. Using ash from *Arabidopsis halleri* as a polymetallic catalyst precursor couples environmental remediation with synthetic chemistry: heavy metals re-

covered from soil are repurposed into a useful catalyst rather than becoming waste. This approach aligns with the principles of green chemistry - using renewable or waste resources and minimizing new waste by enabling catalyst recycling. The Eco-MgZnOx-catalyzed hydrophosphonylation also meets several green chemistry criteria: solvent-free conditions, mild heating, easy catalyst separation by filtration, and minimal work-up (simple centrifugation/filtration and crystallization or chromatography of the product). Together, these features yield high sustainability metrics for organophosphorus synthesis.

It should be noted that using *Arabidopsis halleri* as a biomass source allowed the preparation of a unique catalyst that would be difficult to obtain by conventional routes. Biological hyperaccumulation dispersed and pre-organized metals at the molecular level within plant tissues. Schematic process is presented on Figure 22. Upon calcination (at a relatively mild 550 ℃), this “nanofactory” yielded a multiphase oxide containing Mg, Zn, Ca, Fe. Conventional synthesis of such mixed oxides would typically require multiple steps (co-precipitation, high-temperature calcination >800 ℃, salt precursors), while here nature provided a one-step precursor that, after burning, produced an active catalyst. This opens perspectives for the broader use of ecocatalysis - designing catalysts from biomaterials obtained through phytoremediation or other biological processes, offering an innovative and environmentally friendly approach.

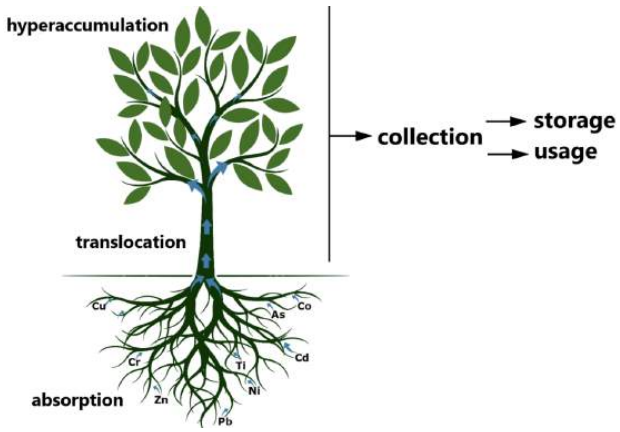
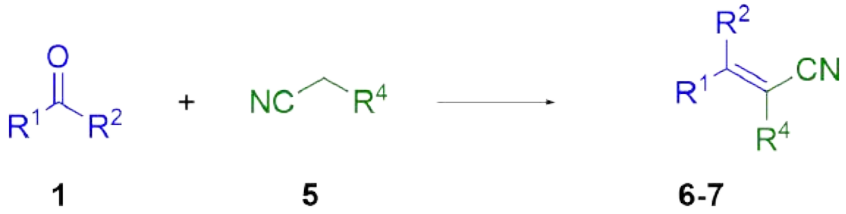


Figure 22. Schematic representation of phytoextraction

Thanks to its high efficiency and simplicity, Eco-MgZnOx has promising practical potential. The hydrophosphonylation reaction was successfully scaled up: in a preparative experiment (20-fold larger scale than the model conditions), about 1 g of product was obtained in 88% yield, with no loss of purity and without elaborate operations (the α-hydroxyphosphonate 3a was isolated by simple crystallization). This demonstrates the scalability of the process and its potential for larger-scale synthe-

sis, in example in pharmaceutical or agrochemical industries. Moreover, the obtained α-hydroxyphosphonates are high-value compounds - stable analogues of phosphates with potential as enzyme inhibitors or nucleotide mimics, finding applications as drugs - phosphonate nucleoside analogues with anticancer and antiviral activity - or agrochemicals. Producing them in a sustainable way - using a recovered plant-derived catalyst, with high efficiency and clean process - represents a significant step toward “green” organophosphorus chemistry.

The Knoevenagel condensation demonstrated the necessity of a catalyst - without the catalyst, conversion was negligible even upon prolonged heating. Employing the Eco-MgZnOx catalyst radically increased the reaction efficiency, enabling near-quantitative conversion to the product under mild conditions. Optimal performance was achieved under solvent-free conditions at 70℃ for 2 h with a catalyst loading corresponding to 5 mol% Zn, resulting in a practically quantitative condensation. Additional tests showed that the presence of a solvent is actually detrimental - e.g., toluene or ethyl acetate lowered conversion relative to neat conditions, underscoring the advantages of running the process without solvent.

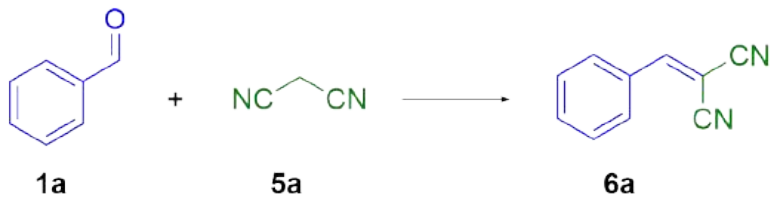


Scheme 2. Knoevenagel condensation - reaction scheme

The Eco-MgZnOx catalyst exhibits synergistic action of its constituents (oxides of Mg, Zn, and Ca). Individual, simple metal oxides (MgO, ZnO, CaO) were clearly less effective - for instance, MgO or ZnO alone reached <100% conversion at comparable concentrations of active sites, and $CaCO_3$ was nearly inactive. In contrast, the catalyst containing Mg, Zn, and Ca simultaneously enabled complete consumption of substrates within a short time. This suggests that the Knoevenagel mechanism is bifunctional: basic sites of MgO activate the donor substrate bearing an active methylene (deprotonation of malononitrile to the carbanion), while Lewis-acidic sites (ZnO) coordinate the carbonyl group of the acceptor, facilitating nucleophilic addition. Such concerted action accounts for the high efficiency and selectivity - the reaction proceeds predominantly to the desired alkene, without byproducts.

The stability and selectivity of the catalyst in the Knoevenagel condensation are very good. Eco-MgZnOx can be reused multiple times - in the model condensation of

benzaldehyde with malononitrile (Scheme 79), high conversions (97–99%) were maintained for at least four consecutive cycles. Only in the fifth cycle was a slight drop in performance observed (to 77% for the Polish catalyst). These results demonstrate that the biogenic Eco-MgZnOx is a durable and renewable heterogeneous catalyst, combining high activity with reusability without substantial loss of efficiency.



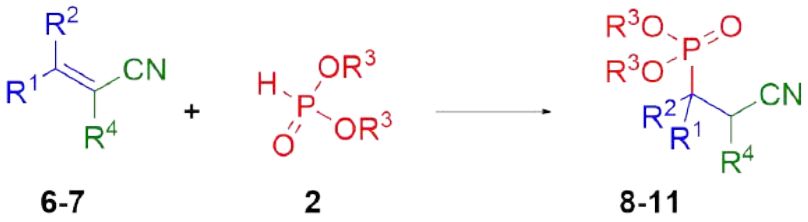
Scheme 79. Model reaction of Knoevenagel condensation with malononitrile

Scaling the process does not negatively impact its efficiency. A 20-fold scale-up of the condensation (to 4.6 mmol, giving 1 g of product) proceeded equally smoothly - 99% conversion and 97–98% isolated yield were obtained with both catalyst variants for model reaction (Scheme 79). The gram-scale yield (≈97% isolated benzylidenemalononitrile) shows that Eco-MgZnOx retains its high activity and selectivity on a preparative scale, which is important for practical applications (no scale effects lowering conversion). Such successful scale-up highlights the reproducibility and reliability of the catalyst, which performs well not only in model trials but also in the synthesis of larger batches.

The substrate scope of the Eco-MgZnOx-catalyzed Knoevenagel condensation is broad. A range of aldehydes (aromatic and aliphatic, including electron-donating Me and electron-withdrawing Cl, NO_2 substituents; as well as heteroaromatics, such as pyridine and thiophene derivatives) was explored with both malononitrile and ethyl cyanoacetate as active-methylene donors. All examined aromatic and heteroaromatic aldehydes reacted smoothly with malononitrile, giving very high conversions 93-99% and high isolated yields. Even for a more demanding carbonyl substrate such as a ketone, successful condensation with high yield was recorded. Electronic effects were minor - substitution of the aromatic ring with electron-donating or electron-withdrawing groups did not significantly affect conversion. Functional groups (halides, nitro) and heteroatoms (nitrogen- and sulfur-containing rings) were also tolerated. The second component - the pronucleophile - had the expected influence on reactivity: malononitrile (strongly activated $-CN$ system) reacted fastest, delivering near-quantitative results, whereas ethyl cyanoacetate (less activated $-COOEt$) was somewhat less reactive. Nevertheless, even for ethyl cyanoacetate, high conversions (typically 90-99%)

and very good isolated yields (84-92% in more challenging cases) were obtained. Differences between catalysts from different sources (Poland vs France) were minimal - both performed almost equally well. Only slight tendencies were noted (Eco-MgZnOx-P sometimes fared marginally better with malononitrile, while Eco-MgZnOx-F occasionally gave slightly higher results with ethyl cyanoacetate). In summary, the Eco-MgZnOx-catalyzed Knoevenagel reaction has wide applicability - it successfully covers diverse substrates (including functionalized systems) and provides high efficiency and selectivity, making it a useful tool in organic synthesis.

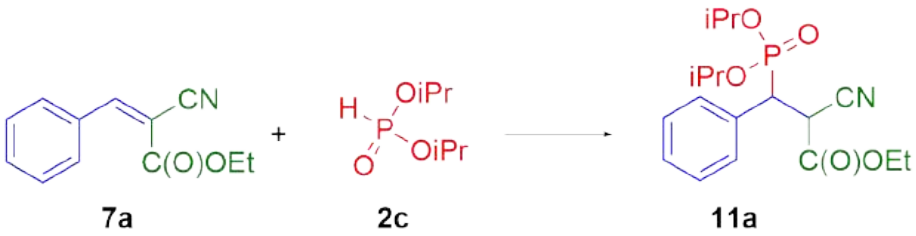
The phospha-Michael addition involves the addition of an H-phosphorus compound to an activated $C = C$ double bond. Optimization showed that without a catalyst the reaction is very slow and inefficient (conversion <10% at room temperature to at most 43% after several hours at 70℃). In the presence of Eco-MgZnOx, however, the efficiency increased dramatically - near-quantitative conversions of the product were achieved in short times. The best conditions mirrored those of the condensation: 70℃, 2-3 h, catalyst loading corresponding to 5 mol% Zn, without solvent. Just 2 h at 70℃ sufficed to reach close to 100% conversion with excellent selectivity - the only product was the desired phosphonate derivative, without side products. Trials run in solvents gave inferior results: for example, the addition of ethyl acetate completely stopped the reaction, while toluene, methanol, or dichloromethane significantly reduced conversions. Solvent-free conditions are therefore crucial for efficient phospha-Michael addition, as in the Knoevenagel condensation.



Scheme 3. Phospha Michael addition - reaction scheme

The EcoCatalyst from *A. halleri* proved markedly more effective than individual oxides ZnO or MgO used in equivalent amounts. Although MgO alone shows some activity as a base (up to 93% conversion) and ZnO as a weak Lewis acid reaches 53-62%, neither alone matched the activity of the biogenic catalyst. Eco-MgZnOx-P and Eco-MgZnOx-F delivered complete conversion (>95%) under the optimized regime, whereas the best simple oxide (MgO) achieved slightly lower performance and others (ZnO, $CaCO_3$) only 50-60%. This again points to the synergy of the multicomponent system - the presence of both basic sites (MgO) to activate the H-phosphonate (de-

protonation of the $P–H$ unit) and acidic sites (ZnO) to activate the electrophilic $C = C$ in the acceptor, which together promote efficient addition. Mechanistically, the catalyst can operate cooperatively: the surface-generated phosphonate anion at MgO attacks the $C = C$ bond activated by ZnO, leading selectively to the phosphonate product (no competing polymerization or hydrolysis is observed, confirming high process selectivity).



Scheme 81. Model reaction of phospha-Michael addition catalysed by Eco-MgZnOx

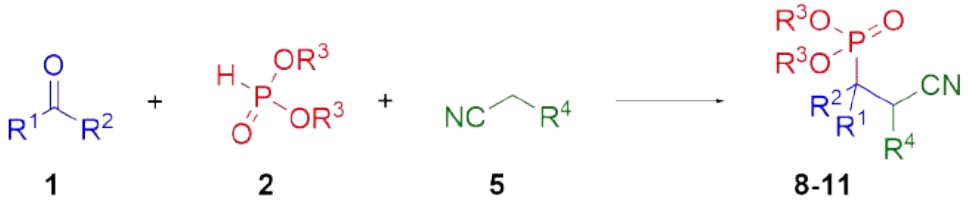
The durability of the catalyst in the phospha-Michael addition is very high. It was performed on model reaction presented on Schema 81. Nearly unchanged activity was observed over successive cycles - both Eco-MgZnOx-P and Eco-MgZnOx-F gave 93-96% conversions across four consecutive runs, essentially identical to initial values. The small drop (from 97% to 95–96% over several cycles) demonstrates stability and the absence of significant deactivation or leaching of active components during reaction. Analysis of the spent solid (Table 21) showed only slight changes in surface metal content (minor Zn loss), which did not affect activity. Thanks to the simple regeneration (reheating), Eco-MgZnOx maintains high durability over use-recovery cycles.

The scalability of the phospha-Michael reaction was also confirmed. It was performed on model reaction presented on Schema 81. Increasing the scale from 0.23 mmol to 6.4 mmol did not deteriorate outcomes - 99% conversion and 96-97% isolated yield were obtained for both catalyst variants. These data indicate that Eco-MgZnOx activity is preserved on a preparative scale, and the catalytic system performs equally well at higher substrate loadings. This is an important demonstration of practical potential - the reaction can be run on larger scale without loss of efficiency, making it attractive for applied synthesis.

The substrate scope in the phospha-Michael addition proved broad, though limited to compounds with strongly activated double bonds. The reaction proceeds efficiently for various Michael acceptors bearing electron-withdrawing groups. Importantly, the method tolerates both electron-donating and -withdrawing substituents and the presence of heteroatoms in aromatic rings - no catalyst inactivation or side products were observed in these varied systems.

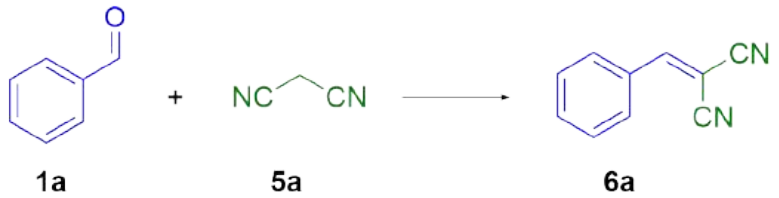
The scope of nucleophilic H-phosphonates is likewise broad. Various dialkyl H-phosphonates were tested - from the typical diethyl H-phosphonate to more branched or aromatic analogues: diisopropyl, dibutyl, dimethyl, dibenzyl, and diphenyl H-phosphonates. In almost all cases conversions were near-quantitative (98–99%), and phosphonate products were obtained in high yields. A modest decrease was observed only for the most sterically demanding substrates - diisopropyl H-phosphonate gave 87-96% conversion, and dibutyl (with the longest alkyl chains) about 80-81%. This indicates moderate sensitivity to sterics at phosphorus. Eco-MgZnOx catalysts from different sources again performed comparably - in most reactions they gave analogous results. In sum, the Eco-MgZnOx-catalyzed phospha-Michael addition is a general reaction for activated alkenes: it tolerates aromatic substrates with various substituents (both withdrawing and donating, including heterocycles) as well as diverse H-phosphonates, delivering predominantly high to near-quantitative yields. The main limitation is the requirement for strong activation of the double bond - for less activated alkenes, such as simple α,β-enones, unactivated alkenes, or acrylates lacking $-$CN groups, catalytic efficiency was low. Additional trials with such substrates (like 2-cyclohexenone, nitrostyrene, methyl acrylate) confirmed that conditions optimized for arylidenemalononitriles do not translate to these less reactive systems. Thus, the practical scope is centered on alkenes conjugated to nitrile or carbonyl groups, which covers many synthetically important substrates.

The tandem Knoevenagel-phospha-Michael reaction merges both steps into a single process, enabling one-pot synthesis of highly functionalized organophosphorus compounds. In this reaction, three components - an aldehyde, an active-methylene compound (malononitrile or cyanoacetate), and an H-phosphonate - react concurrently to give β-phosphonomalonates. A key design challenge was the competing Pudovik reaction (hydrophosphonylation of the aldehyde to α-hydroxyphosphonate), which could consume the aldehyde and undermine the cascade. If the catalyst favored direct aldehyde reaction with the H-phosphonate, the resulting α-hydroxyphosphonate would deplete the aldehyde, preventing downstream steps and lowering the yield of the target adduct. Indeed, a catalyst-free test showed that the mixture benzaldehyde + malononitrile + diethyl H-phosphonate reacts very poorly (only 9% conversion after 5 h at 70℃) and gives a mixture of products, 45% of which is the undesired α-hydroxyphosphonate.

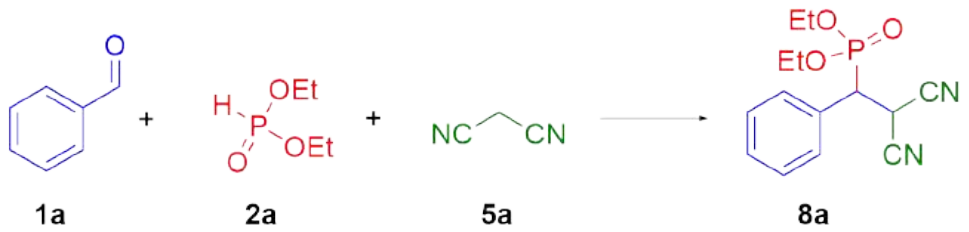


Scheme 4. Knoevenagel phospha-Michael condensation - reaction scheme

To address this, the reaction was initially run in two steps (one-pot, two-steps): first, the Knoevenagel condensation of the aldehyde with malononitrile was conducted in the presence of the catalyst (70℃, 2 h), as presented on Scheme 79, then the H-phosphonate was added to the same mixture and heating continued (70℃, an additional 3 h), which results with the reaction presented on Scheme 77. Such sequential substrate addition prevented the undesired competition - in the first stage the aldehyde was nearly fully converted to the desired product, which in the second stage underwent clean phosphorus addition. The two-step process gave excellent results: with Eco-MgZnOx, 100% conversion to the desired coupled product with full selectivity (no detectable hydroxyphosphonate) was obtained. By contrast, without the catalyst (but still in the two-step sequence, heating for a total of 5 h) conversion reached only 11%, and the **8a**:**3a** ratio was 55:45 - demonstrating that the catalyst is critical both to accelerate the condensation and to steer the pathway toward the tandem outcome.



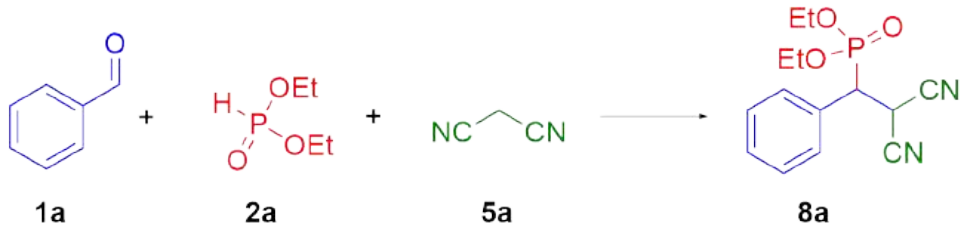
Scheme 79. First step of the process - Knoevenagel condensation



Scheme 77. Second step of the process - phospha-Michael addition

Encouraged by this, a one-step (one-pot, one-step) variant was conducted, adding all three substrates at once in the presence of the catalyst. This mode was also effective - under the established parameters (70℃, 5 h, 5 mol% Zn in the catalyst,

solvent-free) a high degree of conversion and a clean tandem product were obtained. Eco-MgZnOx enabled 93–99% conversion to **8a** in this setup (Scheme 77), leaving no α-hydroxyphosphonate byproduct, which could be produced according to the process presented on Scheme 78 as side reaction - so 100% selectivity to the Knoevenagel-Michael adduct was obtained. This indicates that appropriately chosen kinetic conditions allow the catalyst to direct the reaction along the desired domino pathway - apparently, the Knoevenagel condensation proceeds sufficiently fast thanks to strong basic MgO sites to outpace a potential Pudovik reaction, and the resulting arylidene-malononitrile immediately undergoes P–H addition to C=C, likely assisted by acidic ZnO sites. In other words, the catalyst's bifunctional nature synchronizes both stages in one vessel. Under one-step conditions without the catalyst the reaction is essentially inactive and results with 9% conversion, and contrary to expectation, the undesired **3a** did not dominate, at such low conversion only traces of **8a** formed. This shows Eco-MgZnOx is indispensable for initiating and driving the complex transformation with high efficiency and selectivity.



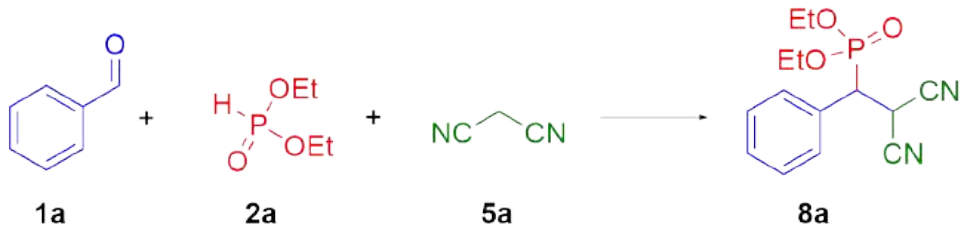
Scheme 77. Model of Knoevenagel-phospha-Michael reaction



Scheme 78. Hydrofosfonylation as possible side reaction

Optimization for the one-pot–one-step mode covered time, temperature, catalyst dose, and solvent effects, analogously to earlier sections. The best results were obtained at 70 ℃ without solvent; a reaction time of 5 h (equal to the sum of the sequential steps) allowed maximal conversion. Variants with different catalyst amounts were also examined - at too low a dose (e.g., 1.5 mg instead of 7.5 mg) conversion decreased and the byproduct **3a** appeared (selectivity degraded to ca. 5:1 in favor of **8a**). This confirms that an appropriate catalyst loading is necessary to carry out both stages simultaneously and efficiently. Studies further showed the negative impact of solvents

- as in the single-step reactions - and the need to maintain anhydrous conditions (the presence of methanol or dichloromethane significantly lowered conversions and promoted trace **3a**). Under all optimal trials, selectivity to the coupled product remained very high (most often 100%, occasionally with undetectable traces of byproduct), evidencing the robustness of the catalyst in channeling the process along the desired pathway. For comparison, tests with single oxides under optimal conditions (70 ℃, 3 h, a dose matching the Mg or Zn content of Eco-MgZnOx) showed that ZnO or $CaCO_3$ individually afford only 50-60% conversion. Neat MgO was more active (up to 92-95% conversion), indicating that basicity is critical. Nevertheless, even MgO does not match the mixed catalyst - Eco-MgZnOx consistently delivered full conversion (>98%). Moreover, conversions with MgO dropped more sharply upon dose reduction than with the mixed system (where synergy sustains activity even at lower individual metal contents). These data clearly highlight the advantage of the biogenic catalyst - its polymetallic character provides both high activity and a unique ability to suppress the side Pudovik pathway, setting it apart from simple metal oxides.



Scheme 77. Model reaction of Knoevenagel-phospha-Michael used for recovery and reuse test of Eco-MgZnOx as a catalyst

Catalyst recycling in the tandem process also proceeds without significant loss of activity. Five consecutive uses of the same Eco-MgZnOx-P and Eco-MgZnOx-F were tested in the model reaction (Scheme 77), with regeneration by calcination (550 ℃, 6 h) after each cycle. The results showed only minimal changes in conversion across cycles. Overall, Eco-MgZnOx maintains catalytic efficiency in the complex reaction, making it a promising candidate for practical applications requiring repeated use of a solid catalyst.

Process scale was verified by synthesizing the product on the 1.8 g scale. The reaction of benzaldehyde, malononitrile, and diethyl phosphite (Scheme 77) was conducted at 6.4 mmol each under optimal conditions (70 ℃, catalyst 210 mg corresponding to 5 mol% Zn). Very high outcomes were obtained: 98–99% conversion (by ^{31}P NMR of the crude mixture) and 96% isolated yield of the target adduct. Both Eco-MgZnOx-P and -F performed equally well at larger scale, delivering virtually identical

results (1.795 g of pure product in both cases). Successful scale-up without loss of selectivity or conversion confirms that the excellent catalytic properties observed on a model scale fully translate to preparative conditions. This underscores the practical potential of catalysts from *A. halleri* biomass - enabling a complex multicomponent transformation on larger scale while retaining all advantages: efficiency, simplicity, and green character.

The substrate scope of the tandem reaction proved broad, encompassing diverse aldehydes and H-phosphonates. A series of carbonyl electrophiles - primarily aromatic - bearing both electron-donating and -withdrawing substituents, as well as heteroaromatics (e.g., indolecarboxaldehyde, benzothiophenecarboxaldehyde), was examined. All these aldehydes (simple aromatics and those containing heteroatoms) enter the tandem reaction with malononitrile and an H-phosphonate efficiently, though some differences in selectivity and isolated yield were observed depending on aldehyde structure. In general, conversions were high, but for more demanding aldehydes (e.g., heterocycle-containing rings such as benzothiophene) somewhat reduced selectivities or isolated yields were noted, suggesting minor side formation or incomplete conversion within the set time. Even so, most aromatic substrates gave excellent results. Only very strongly withdrawing substituents or particularly sterically demanding systems slightly diminished performance.

The diversity of H-phosphonates was also analyzed and Eco-MgZnOx showed tolerance toward these groups - regardless of their nature, conversions were nearly quantitative and isolated yields were generally high. A slight tendency toward reduced selectivity was observed for the bulkiest aromatic substituents such as diphenyl H-phosphonate (Figure 90), indicating that large groups at phosphorus may promote minor competing pathways - perhaps incomplete addition or difficult product desorption. Overall, the tandem Knoevenagel-phospha-Michael reaction features a wide substrate window for both the aldehyde and the phosphorus components. Substituent effects are noticeable mainly in edge cases: the presence of a sulfur heteroatom in the aromatic ring or very bulky alkyl/aryl groups at phosphorus can lead to lower selectivity or yield. However, most standard substrates react efficiently. Both catalyst variants perform similarly - and what is interesting, for more sterically demanding substrates Eco-MgZnOx-F gave slightly more consistent high conversions, while the Eco-MgZnOx-P variant sometimes showed minimal drops, which may arise from compositional and surface differences. Nevertheless, these differences are small, and both catalyst forms can be regarded as equivalently effective across varied substrates.

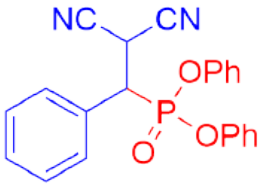


Figure 90. Product of Knoevenagel-Phospha-Michael reaction with diphenyl H-phosphonate as a heavily substituted substrate

All reaction classes exhibit very high efficiencies in the presence of Eco-MgZnOx. Under optimal conditions, nearly complete substrate conversions (often 95–100%) are achieved with excellent selectivity to the desired products - no hydrolysis or polymerization. From a performance perspective, Eco-MgZnOx enables transformations that are inefficient or practically unfeasible otherwise. All reactions reach their best outcomes under closely related conditions (T=50-70℃, 2–5 h, no solvent), indicating that the catalyst operates optimally within a similar regime across mechanistically distinct processes.

The biogenic Eco-MgZnOx has demonstrated high catalytic efficiency in each process discussed. Its advantage stems from multiple active centers of differing character, basic and acidic, enabling cooperative bifunctional mechanisms. As a result, reactions proceed rapidly - within a few hours full conversions are obtained under relatively mild conditions (moderate 50–70℃, no strong reagents or solvents). What is important, conventional single-component catalysts perform markedly worse.

The biogenic Eco-MgZnOx catalyst obtained from the (*Arabidopsis halleri*) proved to be an effective, selective, and versatile catalyst for four important classes of C–C and C–P bond-forming reactions. In all studied processes it enables rapid and complete substrate conversion under solvent-free conditions, is readily recyclable, and aligns with the tenets of sustainable synthesis. Crucially, employing a catalyst produced from waste plant biomass and conducting reactions under green chemistry regimes: no solvents, minimal waste, catalyst reusability significantly enhances the environmental profile of these methods. The work demonstrates that plant-derived biomaterial, transformed into a polymetallic oxide, is a valuable alternative to classical catalysts - a heterogeneous, solvent-free, and reusable catalytic platform delivering excellent conversions and compelling sustainability credentials. All examined reactions achieve high efficiency and selectivity across a wide substrate window, alongside high catalyst durability, positioning Eco-MgZnOx as a practical, green catalyst for key transformations in organophosphorus chemistry and beyond.

An important part of the presented concept is the use of phytoextraction as a sus-

tainable source of metals for catalyst preparation. The increasing demand for metals, together with their limited availability, rising costs, and the environmental impact of conventional mining, creates a need for alternative ways of obtaining catalytically useful elements. At the same time, many post-industrial and mining areas remain contaminated with heavy metals and require long-term remediation. Metal-hyperaccumulating plants, such as *Arabidopsis halleri*, offer a unique solution to both problems. They can grow on contaminated soils and accumulate significant amounts of metals, especially zinc, in their above-ground biomass. In this way, phytoextraction makes it possible to gradually remove metals from polluted sites, while the harvested biomass becomes a valuable secondary resource rather than waste. After drying and calcination of the plant material, the organic fraction is removed and the accumulated elements are converted into a polymetallic mineral residue. This residue can be directly used as a heterogeneous ecocatalyst, such as Eco-MgZnOx, containing naturally combined metal oxides and mineral phases. Therefore, the preparation of the catalyst does not require complex synthetic procedures, expensive metal salts, or additional ligands. This approach links soil remediation with the production of useful catalytic materials and shows how contaminated biomass can be transformed into a practical tool for sustainable organic synthesis.

The work presents a coherent chain of solutions that connects the problems of modern catalysis diagnosed in Chapter 1, such as price and availability instability of metals, and the growing environmental footprint of their extraction, with a practical, low-waste alternative: biogenic, polymetallic oxides Eco-MgZnOx obtained from the biomass and operating as robust, heterogeneous Lewis-acid/basic catalysts for forming C–P and C–C bonds under solvent-free conditions. In this way, the phytomanagement loop of contaminated land ends with a high value-added product - an ecocatalyst - while remaining aligned with green-chemistry metrics (preference for catalysis, low E-factor, simple recovery and reuse).

Instability in the supply and pricing of metals, including metals critical for catalysis, increases risk and costs for catalyst users. Even with temporary dips, many feedstocks remain above their price levels from last years, and the metals sector is highly emissive and energy-intensive. From a green-chemistry perspective, this creates pressure to shift from stoichiometric reagents to catalysis and to circular-economy approaches. Phytomanagement techniques turns degraded land from a costly problem into a resource - it manages risk by reducing the bioavailable fraction of metals, provides scalable and landscape-acceptable solutions, and generates metal-bearing biomass as a feedstock for ecocatalysts. *A. halleri*, presented on Figure 91, which was used as a

model hyperaccumulator, provides a predictable, high metal load. Its molecular mechanisms, such as HMA4 duplication, constitutive expression of homeostasis genes, favor efficient metal acquisition for green calcination of the biomass into a catalytic material.



Figure 91. Biomass from *Arabidopsis Halleri*

The biomass $\rightarrow$ ecocatalyst strategy reduces pressure on primary resources and on the emissive extraction chain, while shifting the burden from costly remediation to waste valorization - what is compatible with green chemistry principles.

Ash obtained by controlled calcination of *A. halleri* biomass (presented on Figure 92) yields a mixture of $Mg/Zn/Ca$ oxides. The key is the periclase solid-solution phase $Mg_{1-x}Zn_xO$, confirmed by XRPD and supported by DFT modeling. This close coexistence of basic (MgO) and Lewis-acidic (ZnO) centers ensures cooperation of active sites: deprotonation of a P–H nucleophile or a CH acid, and activation of the electrophile ($C{=}O$, $C{=}C$), which experimentally translates into synergistic performance surpassing single oxides or their physical mixtures.



Figure 92. Ashes from *Arabidopsis Halleri* biomass - Eco-MgZnOx-F on the left and Eco-MgZnOx-P on the right.

A simple, reproducible preparation protocol (drying $\rightarrow$ calcination at 550 ℃ $\rightarrow$ comminution) affords a material that is easily recovered and regenerated by washing and recalcination, which is critical for longevity in preparative applications.

Bifunctional mechanisms include base and Lewis acid encoded in a polymetallic, solid-solution matrix explain the wide substrate window and high selectivity observed in Chapters 2–5, as well as the advantage over single-component systems. Common features of the green optimum, such as no solvent, moderate temperatures, simple operations, a small catalyst charge calculated at $\sim$5 mol% Zn contained in the material, and recycling/calcination restoring activity, implement in practice the Ninth Principle of Green Chemistry (catalysis over stoichiometric reagents) and help to lower the E-factor at the synthesis and purification stage.

The catalyst has also its limitations and applicability boundaries. The efficiency of the phospha-Michael and the cascade depends on strong activation of the $C{=}C$ bond ($-$CN, $-$COOR). For less activated alkenes, efficiencies fall. Steric hindrance (tetra-substitution of the alkene, bulky phosphonates) lowers yields, but does not disqualify them. Defined substrate limits arise from the nature of the bifunctional mechanism. At the same time, they are broad and cover many synthetically valuable compounds, making the material a platform that is more general than specialized.

The work demonstrates that ecocatalysis responds to the cost-environmental pressure on metals, harnesses the unique biological capacity of *A. halleri* for hyperaccumulation, providing a green metal source, and turns it into a high-performance catalytic platform, under solvent-free conditions and at moderate temperature. It affords high conversions, selectivity, recycling, and reproducibility on the gram scale. This coherent coupling of phytomanagement and catalysis creates a practical pathway toward supply- and eco-resilient organophosphorus chemistry, ready for translation beyond the laboratory.

Experimental section

General experimental methods and procedures

General methods

All reagents and solvents were obtained from commercial suppliers and used without further purification. Reactions were carried out in glass screw-cap test tubes equipped with magnetic stirring bars. Unless otherwise specified, reactions were performed under solvent-free conditions and heated in a sand-filled heating block under continuous magnetic stirring. The progress of phosphorus-containing reactions was monitored mainly by ^{31}P NMR spectroscopy of the crude reaction mixtures, while Knoevenagel condensations were monitored by ^{1}H NMR spectroscopy. Isolated products were characterized by NMR spectroscopy in $CDCl_3$.

Preparation of catalysts

The catalysts Eco-MgZnOx-P and Eco-MgZnOx-F were prepared from the biomass of *Arabidopsis halleri* collected from two metal-contaminated sites. The catalyst marked Eco-MgZnOx-P was obtained from plants collected in Poland, near the Bolesław Mine and Metallurgical Plant in the Olkusz region, while Eco-MgZnOx-F was prepared from plants collected in France, at the former industrial site in Auby. In both cases, the plant biomass was used as a natural source of accumulated metals, mainly Zn and Mg, together with other mineral components naturally present in the plant material.

Fresh plant material was first dried in an oven at 60℃ and then ground into smaller pieces. The dried biomass was subjected to thermal treatment at 550℃ for approximately 6 h. During this step, the organic fraction was removed and a mineral-rich ash was obtained. The resulting ash was used as a polymetallic oxide catalyst. The two catalysts were labelled according to the origin of the biomass: Eco-MgZnOx-P for the material prepared from Polish *A. halleri* and Eco-MgZnOx-F for the material prepared from French *A. halleri*.

The catalyst amount used in catalytic tests was calculated on the basis of the Zn content. Under standard optimized conditions, 30 mg of catalyst was used for a 0.92 mmol reaction scale (or 75 mg of catalyst for a 2.30 mmol reaction scale for Knoevenagel condensation), which corresponded to approximately 5 mol% Zn. For Eco-MgZnOx-P this amount corresponded to 7.0 mol% Mg, 13.6 mol% Ca, and 5.7 mol% Zn, while for Eco-MgZnOx-F it corresponded to 3.5 mol% Mg, 11.4 mol% Ca, and 4.9 mol% Zn.

Characterization of catalysts

The prepared Eco-MgZnOx catalysts were characterized using complementary analytical techniques in order to determine their elemental composition, crystalline phases, morphology, and stability after reuse.

The mineral composition of the catalysts was determined by microwave plasma atomic emission spectroscopy (MP-AES), using an Agilent 4200 MP-AES spectrometer equipped with an SPS4 autosampler. Before analysis, the samples were digested under microwave-assisted conditions in reversed aqua regia, then filtered and diluted. This method allowed the quantification of the main mineral elements present in the catalysts, including Zn, Mg, Ca, Fe, K, Al, and Na. MP-AES was also used to analyze recovered catalysts after catalytic cycles, in order to follow possible changes in composition and leaching of active components.

The crystalline phases present in the catalyst powders were identified by X-ray powder diffraction (XRPD), using a Bruker D8 Advance diffractometer with Cu Kα radiation. XRPD analysis confirmed the complex mineral nature of the plant-derived catalysts. Both Eco-MgZnOx-P and Eco-MgZnOx-F contained several crystalline phases, including $CaCO_3$ and K_2SO_4, as well as Zn-containing phases. Importantly, a $Mg0.88Zn0.12O$ phase was observed, especially clearly for Eco-MgZnOx-P. This mixed Mg–Zn oxide phase was considered one of the key structural features responsible for the bifunctional catalytic behavior of the material.

The morphology of the catalysts was examined by high-resolution transmission electron microscopy (HRTEM). The images showed that both catalysts were composed of larger irregular particles, approximately 100–600 nm in size, associated with smaller spherical nanoparticles of about 10–50 nm. Elemental mapping was performed by scanning transmission electron microscopy coupled with energy-dispersive X-ray spectroscopy (STEM-EDX), using a JEOL 2200 FS microscope operating at 200 kV. This technique confirmed the heterogeneous distribution of mineral components and showed that the larger particles were mainly rich in Ca and O, while smaller particles contained the catalytically relevant Mg and Zn components.

Products of hydrophosphonylation catalyzed by *Arabidopsis halleri*-derived biogenic Eco-MgZnOx catalyst

General procedure for hydrophosphonylation reactions

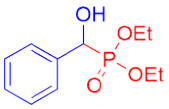
In a typical hydrophosphonylation reaction, the appropriate aldehyde or ketone (0.23 mmol), the H-phosphonate reagent (0.23 mmol), and Eco-MgZnOx catalyst were placed in a glass screw-cap test tube equipped with a magnetic stirring bar. Unless otherwise stated, 7.5 mg of Eco-MgZnOx-P or Eco-MgZnOx-F was used, corresponding to approximately 5 mol% Zn. The reaction mixture was stirred under solvent-free conditions at 50 °C for 3 h.



Scheme 1. Hydrophosphonylation (Pudovik reaction) - reaction scheme

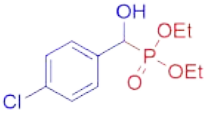
After completion of the reaction, an appropriate solvent was added to dissolve the organic components and wash the reaction mixture from the solid catalyst. The suspension was transferred to a polypropylene centrifuge tube and centrifuged to separate the catalyst. The liquid phase was collected and analyzed by ^{31}P NMR spectroscopy to determine conversion. The product was then isolated from the supernatant. Depending on its physical form, purification was carried out either by preparative thin-layer chromatography for oily products or by crystallization from diethyl ether/hexane mixtures for solid products.

3a - Diethyl (1-hydroxyphenylmethyl)phosphonate



White solid; yield = 82% (148 mg); mp. 83–85 °C; ^{1}H NMR (400 MHz, $CDCl_3$): δ 7.48–7.46 (m, 2H), 7.36–7.28 (m, 3H), 5.00 (d, J = 11.2 Hz, 1H), 4.07–3.92 (m, 4H), 1.25 (t, J = 7.0 Hz, 3H), 1.20 (t, J = 7.0 Hz, 3H); ^{13}C NMR (100 MHz, $CDCl_3$): δ 136.8, 128.1, 127.3, 127.2, 71.6 (d, J = 158.3 Hz), 63.5 (d, J = 7.4 Hz), 63.1 (d, J = 7.4 Hz), 16.4 (d, J = 2.9 Hz), 16.3 (d, J = 2.3 Hz); ^{31}P NMR (243 MHz, $CDCl_3$): δ 22.1 (s); HRMS (ESI-TOF) calcd. for $C_{11}H_{17}O_4PNa$ $[M+Na]^+$ m/z: 267.0762, found: 267.0757.

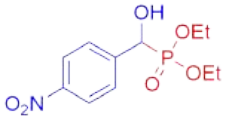
3b - Diethyl [(4-chlorophenyl)(hydroxy)methyl]phosphonate



White solid; yield = 80% (214 mg); mp. 55–58 °C; ^{1}H NMR (400 MHz, $CDCl_3$): δ 7.43–7.38 (m, 2H), 7.32 (d, J = 8.8 Hz, 2H), 5.00 (d, J = 10.8 Hz, 1H), 4.11–3.96 (m, 4H), 1.29–1.20

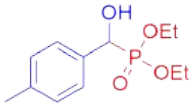
(m, 6H); ^{13}C NMR (100 MHz, $CDCl_3$): δ 135.9, 133.2 (d, J = 3.4 Hz), 128.5 (d, J = 2.9 Hz), 128.4, 70.1 (d, J = 159.5 Hz), 63.8 (d, J = 6.8 Hz), 63.4 (d, J = 7.4 Hz), 16.5 (d, J = 5.2 Hz); ^{31}P NMR (243 MHz, $CDCl_3$): δ 22.1 (s); HRMS (ESI-TOF) calcd. for $C_{11}H_{16}ClO_4PNa$ $[M+Na]^+$ m/z: 301.0372, found: 301.0375.

3c - Diethyl (4-nitro-1-hydroxybenzyl)phosphonate



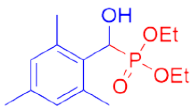
Yellow solid; yield = 72% (200 mg); mp. 86–88 °C; ^{1}H NMR (400 MHz, $CDCl_3$): δ 8.21 (d, J = 8.4 Hz, 2H), 7.66–7.63 (m, 2H), 5.18 (d, J = 12.0 Hz, 1H), 4.99 (bs, 1H), 4.16–4.02 (m, 4H), 1.30–1.22 (m, 6H); ^{13}C NMR (100 MHz, $CDCl_3$): δ 147.6 (d, J = 3.5 Hz), 144.2, 127.8 (d, J = 4.5 Hz), 123.4 (d, J = 2.2 Hz), 70.1 (d, J = 157.7 Hz), 64.2 (d, J = 6.8 Hz), 63.5 (d, J = 8.0 Hz), 16.5 (m); ^{31}P NMR (243 MHz, $CDCl_3$): δ 20.4 (s); HRMS (ESI-TOF) calcd. for $C_{11}H_{16}NO_6PNa$ $[M+Na]^+$ m/z: 312.0613, found: 312.0608.

3d - Diethyl (4-methyl-1-hydroxybenzyl)phosphonate



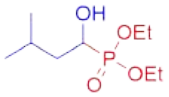
White solid; yield = 82% (203 mg); mp. 94–97 °C; ^{1}H NMR (400 MHz, $CDCl_3$): δ 7.37–7.33 (m, 2H), 7.15 (d, J = 8.0 Hz, 2H), 4.96 (d, J = 10.4 Hz, 1H), 4.08–3.96 (m, 4H), 2.33 (s, 3H), 1.26 (t, J = 7.2 Hz, 3H), 1.20 (t, J = 7.2 Hz, 3H); ^{13}C NMR (100 MHz, $CDCl_3$): δ 137.9, 133.6, 129.1 (d, J = 1.7 Hz), 127.1 (d, J = 6.3 Hz), 70.3 (d, J = 158.9 Hz), 63.4 (d, J = 7.4 Hz), 63.1 (d, J = 7.5 Hz), 21.3, 16.4 (m); ^{31}P NMR (243 MHz, $CDCl_3$): δ 22.2 (s); HRMS (ESI-TOF) calcd. for $C_{12}H_{19}O_4PNa$ $[M+Na]^+$ m/z: 281.0919, found: 281.0914.

3e -Diethyl (2,4,6-trimethyl-1-hydroxybenzyl)phosphonate



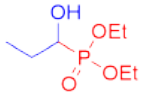
White solid; yield = 75% (201 mg); mp. 90–92 °C; ^{1}H NMR (400 MHz, $CDCl_3$): δ 6.81 (s, 2H), 5.45 (d, J = 15.6 Hz, 1H), 4.16–4.03 (m, 2H), 4.02–3.90 (m, 1H), 3.83–3.72 (m, 1H), 2.45 (s, 6H), 2.23 (m, 3H), 1.29 (t, J = 7.0 Hz, 3H), 1.12 (t, J = 6.8 Hz, 3H); ^{13}C NMR (100 MHz, $CDCl_3$): δ 135.2, 137.6 (d, J = 3.4 Hz), 129.7, 68.7 (d, J = 158.3 Hz), 63.1 (d, J = 6.8 Hz), 62.7 (d, J = 7.5 Hz), 21.1, 20.9, 16.5 (d, J = 5.8 Hz), 16.3 (d, J = 5.7 Hz); ^{31}P NMR (243 MHz, $CDCl_3$): δ 24.3 (s); HRMS (ESI-TOF) calcd. for $C_{14}H_{23}O_4PNa$ $[M+Na]^+$ m/z: 309.1232, found: 309.1240.

3f - Diethyl 1-hydroxy-3-methyl-butylphosphonate



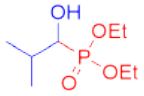
Yellow oil; yield = 84% (181 mg); ^{1}H NMR (400 MHz, $CDCl_3$): δ 4.17–4.06 (m, 4H), 3.93–3.87 (m, 1H), 1.94–1.84 (m, 1H), 1.71–1.60 (m, 1H), 1.44–1.35 (m, 1H), 1.30–1.28 (m, 6H), 0.91 (d, J = 6.8 Hz, 3H), 0.86 (d, J = 6.6 Hz, 3H); ^{13}C NMR (100 MHz, $CDCl_3$): δ 66.0 (d, J = 161.0 Hz), 62.6, 40.0, 24.1 (d, J= 13.7 Hz), 23.5, 21.1, 16.5 (d, J = 4.6 Hz); ^{31}P NMR (243 MHz, $CDCl_3$): δ 24.3 (s); HRMS (ESI-TOF) calcd. for $C_9H_{21}O_4PNa$ $[M+Na]^+$ m/z: 247.1075, found: 247.1070.

3g - Diethyl 1-hydroxypropylphosphonate



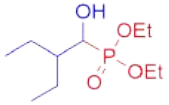
Yellow oil; yield = 83% (156 mg); ^{1}H NMR (400 MHz, $CDCl_3$): δ 4.16–4.07 (m, 4H), 3.78–3.70 (m, 1H), 1.83–1.60 (m, 2H), 1.31–1.26 (m, 6H), 1.04–1.00 (m, 3H); ^{13}C NMR (100 MHz, $CDCl_3$): δ 69.2 (d, J = 159.4 Hz), 62.6 (m), 24.7, 16.5 (d, J = 4.5 Hz), 10.5 (d, J = 13.1 Hz); ^{31}P NMR (243 MHz, $CDCl_3$): δ 26.0 (s); HRMS (ESI-TOF) calcd. for $C_7H_{17}O_4PNa$ $[M+Na]^+$ m/z: 219.0762, found: 219.0760.

3h - Diethyl 1-hydroxy-2-methyl-propylphosphonate



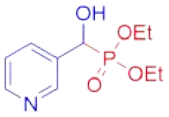
Yellow oil; yield = 81% (164 mg); ^{1}H NMR (400 MHz, $CDCl_3$): δ 4.20–4.10 (m, 4H), 3.65–3.60 (m, 1H), 3.0 (bs, 1H), 2.11–2.00 (m, 1H), 1.33–1.21 (m, 6H), 1.02–1.05 (m, 6H); ^{13}C NMR (100 MHz, $CDCl_3$): δ 72.9 (d, J = 156 Hz), 62.50 (d, J = 7.0 Hz), 30.2 (d, J = 2.3 Hz), 19.9 (d, J = 9.7 Hz), 17.8 (d, J = 7.4 Hz), 16.5 (d, J = 5.7 Hz); ^{31}P NMR (243 MHz, $CDCl_3$): δ 26.0 (s); HRMS (ESI-TOF) calcd. for $C_8H_{19}O_4PNa$ $[M+Na]^+$ m/z: 233.0919, found: 233.0922.

3i - Diethyl 2-ethyl-1-hydroxybutylphosphonate



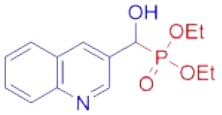
Yellow oil; yield = 84% (192 mg); ^{1}H NMR (400 MHz, $CDCl_3$): δ 4.17–4.07 (m, 4H), 3.89–3.85 (m, 1H), 1.75–1.65 (m, 1H), 1.61–1.32 (m, 4H), 1.29 (t, J = 7.0 Hz, 6H), 0.88–0.84 (m, 6H); ^{13}C NMR (100 MHz, $CDCl_3$): δ 69.4 (d, J = 156.6 Hz), 62.5 (d, J = 7.5 Hz), 42.9 (d, J = 2.8 Hz), 21.9 (d, J = 9.7 Hz), 21.1 (d, J = 5.7 Hz), 16.5 (d,J = 5.7 Hz), 11.4 (d, J = 16.6 Hz); ^{31}P NMR (243 MHz, $CDCl_3$): δ 26.6 (s); HRMS (ESI-TOF) calcd. for $C_{10}H_{23}O_4PNa$ $[M+Na]^+$ m/z: 261.1232, found: 261.1223.

3j - Diethyl 1-hydroxy(pyridine-3-yl)methylphosphonate



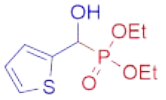
White solid; yield = 87% (205 mg); mp. 125–127°C; ^{1}H NMR (400 MHz, $CDCl_3$): δ 8.60 (s, 1H), 8.47–8.44 (m, 1H), 7.88–7.83 (m, 1H), 7.28–7.24 (m, 1H), 5.04 (d, J = 12.0 Hz, 1H), 4.11–3.99 (m, 4H), 1.25–1.18 (m, 6H); ^{13}C NMR (100 MHz, $CDCl_3$): δ 148.6 (d, J = 2.3 Hz), 148.2 (d, J = 6.2 Hz), 135.4 (d, J = 5.2 Hz), 133.8, 123.4, 68.3 (d, J = 162.9 Hz), 63.6 (d, J = 7.4 Hz), 63.2 (d, J = 7.4 Hz), 16.3 (m); ^{31}P NMR (243 MHz, $CDCl_3$): δ 21.1 (s); HRMS (ESI-TOF) calcd. for $C_{10}H_{16}NO_4PNa$ $[M+Na]^+$ m/z: 268.0715, found: 268.0724.

3k - Diethyl 1-hydroxy(quinolin-3-yl)methylphosphonate



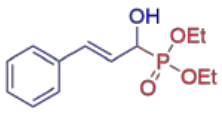
Beige solid; yield = 82% (232 mg); mp. 76–77°C; ^{1}H NMR (400 MHz, $CDCl_3$): δ 9.01 (s, 1H), 8.46–8.38 (m, 1H), 8.22–8.12 (m, 1H), 7.86–7.80 (m, 1H), 7.78–7.70 (m, 1H), 7.61–7.57 (m, 1H), 5.36–5.29 (m, 1H), 4.17–4.06 (m, 4H), 1.29–1.20 (m, 6H); ^{13}C NMR (100 MHz, $CDCl_3$): δ 149.4 (d, J = 4.6 Hz), 146.9, 134.9 (d, J = 6.3 Hz), 130.9, 129.9, 128.5, 128.1, 127.8, 127.1, 68.6 (d, J = 162.8 Hz), 63.7 (d, J = 6.9 Hz), 63.3 (d, J = 7.4 Hz), 16.4 (m); ^{31}P NMR (243 MHz, $CDCl_3$): δ 20.5 (s); HRMS (ESI-TOF) calcd. for $C_{14}H_{18}NO_4PNa$ $[M+Na]^+$ m/z: 318.0871, found: 318.0867.

3l - Diethyl 1-hydroxy(thiophen-2-yl)methylphosphonate



White solid; yield = 86% (207 mg); mp. 28°C; ^{1}H NMR (400 MHz, $CDCl_3$): δ 7.40–7.38 (m, 1H), 7.29–7.26 (m, 1H), 7.19–7.16 (m, 1H), 5.08 (d, J = 10.8 Hz, 1H), 4.14–3.99 (m, 4H), 1.26 (t, J = 7.0 Hz, 3H), 1.20 (t, J = 7.2 Hz, 3H); ^{13}C NMR (100 MHz, $CDCl_3$): δ 137.8, 126.8 (m), 125.7, 123.0 (d, J = 9.2 Hz), 67.4 (d, J = 162.3 Hz), 63.5 (d, J = 6.8 Hz), 63.2 (d, J = 7.4 Hz), 16.5 (m); ^{31}P NMR (243 MHz, $CDCl_3$): δ 21.7 (s); HRMS (ESI-TOF) calcd. for $C_9H_{15}O_4PSNa$ $[M+Na]^+$ m/z: 273.0327, found: 273.0331.

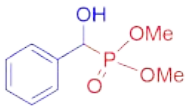
3o - Diethyl (1-hydroxy-3-phenyl)prop-2-enyl-phosphonate



Pale yellow solid, yield = 90% (224 mg); mp. 103–105°C; ^{1}H NMR (400 MHz, $CDCl_3$): δ 7.39–7.18 (m, 5H), 6.80–6.73 (m, 1H), 6.35–6.27 (m, 1H), 4.70–4.64 (m, 1H), 4.21–4.12 (m, 4H), 1.31–1.26 (m, 6H); ^{13}C NMR (100 MHz, $CDCl_3$): δ 136.6 (d, J = 2.8 Hz), 132.2 (d, J = 13.2 Hz), 128.6, 127.9, 126.7, 124.3 (d, J = 4.0 Hz), 70.3, 69.4 (d, J = 160.9 Hz), 63.5 (d, J = 6.8 Hz), 63.2 (d, J = 6.9 Hz), 16.6 (d, J

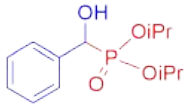
= 5.2 Hz); ^{31}P NMR (243 MHz, $CDCl_3$): δ 22.4.

4b - Dimethyl (1-hydroxyphenylmethyl)phosphonate



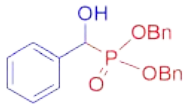
White solid; yield = 92% (182 mg); mp. 84–86 °C; ^{1}H NMR (400 MHz, $CDCl_3$): δ 7.49–7.45 (m, 2H), 7.36–7.24 (m, 3H), 5.06 (d, J = 11.2 Hz, 1H), 3.71–3.64 (m, 6H); ^{13}C NMR (100 MHz, $CDCl_3$): δ 136.9, 128.4, 128.3, 127.1, 70.6 (d, J = 158.8 Hz), 54.1 (d, J = 7.4 Hz), 53.7 (d, J = 7.4 Hz); ^{31}P NMR (243 MHz, $CDCl_3$): δ 24.1 (s); HRMS (ESI-TOF) calcd. for $C_9H_{13}NaO_4P$ $[M+Na]^+$ m/z: 239.0449, found: 239.0445.

4c - Diisopropyl (1-hydroxyphenylmethyl)phosphonate



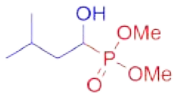
White solid; yield = 62% (203 mg); mp. 93–96 °C; ^{1}H NMR (400 MHz, $CDCl_3$): δ 7.50–7.46 (m, 2H), 7.40–7.26 (m, 3H), 5.05 (d, J = 10.8 Hz, 1H), 4.63–4.50 (m, 2H), 1.26–1.12 (m, 12H); ^{13}C NMR (100 MHz, $CDCl_3$): δ 136.9, 128.2, 128.0, 127.4, 71.5 (m), 24.2 (m); ^{31}P NMR (243 MHz, $CDCl_3$): δ 20.5 (s); HRMS (ESI-TOF) calcd. for $C_{13}H_{21}O_4PNa$ $[M+Na]^+$ m/z: 295.1075, found: 295.1072.

4d - Dibenzyl (1-hydroxyphenylmethyl)phosphonate



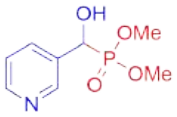
Beige solid; yield = 85% (301 mg); mp. 104–107 °C; ^{1}H NMR (400 MHz, $CDCl_3$): δ 7.46–7.17 (m, 15H), 5.09–4.83 (m, 5H), 3.04 (bs, 1H); ^{13}C NMR (100 MHz, $CDCl_3$): δ 136.1, 128.6 (m), 127.3, 71.1 (d, J = 157.7 Hz), 68.8 (m); ^{31}P NMR (243 MHz, $CDCl_3$): δ 22.7 (s).

4e - Dimethyl 1-hydroxy-3-methyl-butylphosphonate



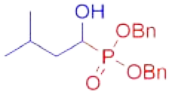
Beige solid; yield = 87% (164 mg); mp. 52–54 °C; ^{1}H NMR (400 MHz, $CDCl_3$): δ 4.00–3.95 (m, 1H), 3.80–3.77 (m, 6H), 1.97–1.85 (m, 1H), 1.75–1.65 (m, 1H), 1.47–1.39 (m, 1H), 0.94–0.88 (m, 6H); ^{13}C NMR (100 MHz, $CDCl_3$): δ 65.8 (d, J = 160.6 Hz), 53.3–53.5 (m), 39.9, 24.1 (d, J = 14.3 Hz), 23.5, 21.1; ^{31}P NMR (243 MHz, $CDCl_3$): δ 28.6 (s); HRMS (ESI-TOF) calcd. for $C_7H_{17}O_4PNa$ $[M+Na]^+$ m/z: 219.0762, found: 219.0760.

4f - Dibenzyl 1-hydroxy-3-methyl-butylphosphonate



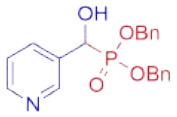
White solid; yield = 80% (168 mg); mp. 72–74 °C; ^{1}H NMR (400 MHz, $CDCl_3$): δ 7.35–7.30 (m, 10H), 5.13–5.00 (m, 4H), 4.01–3.95 (m, 1H), 1.94–1.85 (m, 1H), 1.77–1.65 (m, 1H), 1.48–1.39 (m, 1H), 0.90 (d, J = 6.8 Hz, 3H), 0.83 (d, J = 6.4 Hz, 3H); ^{13}C NMR (100 MHz, $CDCl_3$): δ 136.4 (m), 128.7, 128.5, 128.1 (m), 68.1 (t, J = 6.8 Hz), 66.5 (d, J = 158.3 Hz), 39.8, 24.2, 24.1, 23.5, 21.1; ^{31}P NMR (243 MHz, $CDCl_3$): δ 27.3 (s); HRMS (ESI-TOF) calcd. for $C_{19}H_{25}O_4PNa$ $[M+Na]^+$ m/z: 371.1388, found: 371.1393.

4g - Dimethyl 1-hydroxy(pyridine-3-yl)methylphosphonate



Orange solid; yield = 90% (188 mg); mp. 123–125 °C; ^{1}H NMR (400 MHz, $CDCl_3$): δ 8.61 (s, 1H), 8.49–8.46 (m, 1H), 7.90–7.85 (m, 1H), 7.31–7.27 (m, 1H), 5.10 (d, J = 12.4 Hz, 1H), 3.72–3.70 (m, 6H); ^{13}C NMR (100 MHz, $CDCl_3$): δ 148.8 (d, J = 2.9 Hz), 148.1 (d, J = 6.8 Hz), 135.5 (d, J = 5.1 Hz), 133.4, 123.6, 68.2 (d, J = 162.9 Hz), 54.1 (d, J = 6.8 Hz), 53.8 (d, J = 7.5 Hz); ^{31}P NMR (243 MHz, $CDCl_3$): δ 23.2 (s); HRMS (ESI-TOF) calcd. for $C_8H_{12}O_4PNa$ $[M+Na]^+$ m/z: 240.0402, found: 240.0392.

4h - Dibenzyl 1-hydroxy(pyridine-3-yl)methylphosphonate

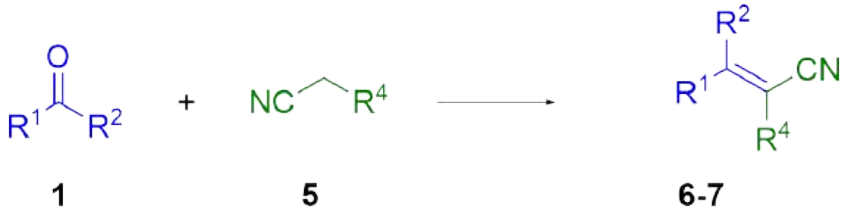


Dark brown solid; yield = 83% (294 mg); mp. 115–118 °C; ^{1}H NMR (400 MHz, $CDCl_3$): δ 8.11 (s, 1H), 8.02 (d, J = 8.4 Hz, 1H), 7.64–7.40 (m, 2H), 7.20–7.10 (m, 10H), 5.31 (d, J = 12.0 Hz, 1H), 5.09–4.88 (m, 4H); ^{13}C NMR (100 MHz, $CDCl_3$): δ 149.7 (d, J = 4.6 Hz), 147.3, 136.0 (d, J = 5.7 Hz), 134.9 (d, J = 6.3 Hz), 130.6, 127.0 (m), 68.8 (m); ^{31}P NMR (243 MHz, $CDCl_3$): δ 22.2 (s); HRMS (ESI-TOF) calcd. for $C_{20}H_{20}O_4PNNa$ $[M+Na]^+$ m/z: 392.1028, found: 392.1020.

Products of Knoevenagel condensation catalysed by *Arabidopsis halleri*-derived biogenic Eco-MgZnOx catalyst

General procedure for Knoevenagel condensation

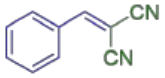
In a typical Knoevenagel condensation, the corresponding aldehyde or ketone (0.23 mmol), the active methylene compound, such as malononitrile or ethyl cyanoacetate (0.23 mmol), and Eco-MgZnOx catalyst were placed in a glass screw-cap test tube equipped with a magnetic stirring bar. The reaction was carried out under solvent-free conditions, typically at 70 ℃, using an amount of catalyst corresponding to approximately 5 mol% Zn.



Scheme 2. Knoevenagel condensation - reaction scheme

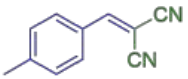
After the required reaction time, the mixture was cooled to room temperature and an appropriate solvent was added to dissolve the organic products and separate them from the catalyst. The suspension was centrifuged, and the supernatant was collected. The crude reaction mixture was analyzed by ^{1}H NMR spectroscopy. The product was isolated from the liquid phase and purified by crystallization or preparative thin-layer chromatography, depending on the physical properties of the compound.

6a - 2-benzylidenemalononitrile



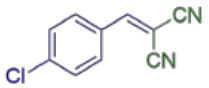
Light yellow solid; yield = 99% (351 mg); ^{1}H NMR (400 MHz, $CDCl_3$): δ 7.71 (s, 1H, =CH), 7.60-7.40 (m, 5H, $H_{arom.}$). ^{13}C NMR (100 MHz, $CDCl_3$): δ 158.0, 134.1, 131.5, 129.8, 129.2, 113.5, 82.0.

6b - 2-(4-methylbenzylidene)malononitrile



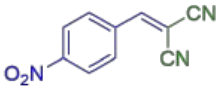
White solid; yield = 98% (379 mg); ^{1}H NMR (400 MHz, $CDCl_3$): δ 7.79 (d, J = 8.2 Hz, 2H, $H_{arom.}$), 7.70 (s, 1H, =CH), 7.32 (d, J = 8.0 Hz, 2H, $H_{arom.}$), 2.44 (s, 3H, CH_3). ^{13}C NMR (100 MHz, $CDCl_3$): δ 159.9, 146.5, 131.0, 130.5, 128.6, 114.2, 113.0, 81.2, 22.1.

6c - 2-(4-chlorobenzylidene)malononitrile



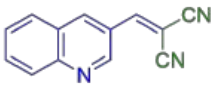
Light yellow solid; yield = 95% (412 mg); ^{1}H NMR (400 MHz, $CDCl_3$): δ 7.85 (d, J = 8.6 Hz, 2H, $H_{arom.}$), 7.73 (s, 1H, =CH), 7.51 (d, J = 8.6 Hz, 2H, $H_{arom.}$). ^{13}C NMR (100 MHz, $CDCl_3$): δ 158.4, 141.2, 131.9, 130.2, 129.4, 113.6, 112.4, 83.4.

6d - 2-(4-nitrobenzylidene)malononitrile



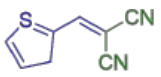
Yellow solid; yield = 95% (435 mg); ^{1}H NMR (400 MHz, $CDCl_3$): δ 8.38 (d, J = 8.8 Hz, 2H, $H_{arom.}$), 8.06 (d, J = 8.8 Hz, 2H, $H_{arom.}$), 7.87 (s, 1H, =CH). ^{13}C NMR (100 MHz, $CDCl_3$): δ 157.0, 150.4, 135.9, 131.4, 124.7, 112.7, 111.7, 87.6.

6e - 2-(quinolin-3-ylmethylene)malononitrile



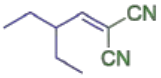
White solid; yield = 84% (396 mg); ^{1}H NMR (400 MHz, $CDCl_3$): δ 9.12 (s, 1H, $H_{arom.}$), 8.95 (s, 1H, $H_{arom.}$), 8.16 (d, J = 8.4 Hz, 1H, $H_{arom.}$), 7.95 (m, 3H, $H_{arom.}$ + =CH), 7.69 (t, J = 7.6 Hz, 1H, $H_{arom.}$). ^{13}C NMR (100 MHz, $CDCl_3$): δ 156.5, 150.6, 150.1, 138.3, 133.6, 129.8, 129.7, 128.6, 126.9, 124.1, 113.3, 112.5, 87.7.

6f - 2-((thiophen-2-yl)methylene)malononitrile



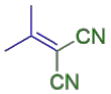
Orange solid; yield = 92% (338 mg); ^{1}H NMR (400 MHz, $CDCl_3$): δ 8.15-8.17 (m, 1H, $H_{arom.}$), 7.78 (s, 1H, =CH), 7.76-7.77 (m, 1H, $H_{arom.}$), 7.48-7.50 (m, 1H, $H_{arom.}$). ^{13}C NMR (100 MHz, $CDCl_3$): δ 152.4, 137.0, 134.1, 128.6, 126.9, 113.9, 113.2, 80.7.

6g - 2-(2-ethylbutylidene)malononitrile



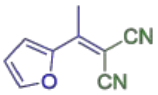
Yellow oil; yield = 92% (313 mg); ^{1}H NMR (400 MHz, $CDCl_3$): δ 7.07 (d, J = 11.0 Hz, 1H, =CH), 2.56-2.52 (m, 1H, CH), 1.64-1.57 (m, 4H, 2×CH_2), 0.86 (t, J = 7.5 Hz, 6H, 2×CH_3). ^{13}C NMR (100 MHz, $CDCl_3$): δ 174.3, 112.2, 111.0, 89.6, 47.3, 26.9, 11.6.

6h - 2-(propan-2-ylidene)malononitrile



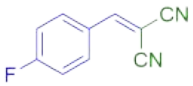
Yellow oil; yield = 94% (229 mg); ^{1}H NMR (400 MHz, $CDCl_3$): δ 2.26 (s, 6H, 2×CH_3). ^{13}C NMR (100 MHz, $CDCl_3$): δ 179.7, 112.1, 85.7, 24.5.

6i - 2-(1-(furan-2-yl)ethylidene)malononitrile



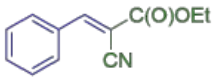
Yellow solid; yield = 96% (349 mg); ^{1}H NMR (400 MHz, $CDCl_3$): δ 7.74 (dd, J = 1.8, 0.8 Hz, 1H, $H_{arom.}$), 7.47 (dd, J = 3.7, 0.8 Hz, 1H, $H_{arom.}$), 6.67 (dd, J = 3.7, 1.8 Hz, 1H, $H_{arom.}$), 2.56 (s, 3H, CH_3). ^{13}C NMR (100 MHz, $CDCl_3$): δ 156.3, 148.2, 120.5, 114.1, 113.7, 113.5, 19.5.

6j - 2-(4-fluorobenzylidene)malononitrile



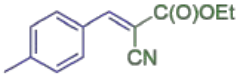
Light yellow solid; yield = 98% (388 mg); ^{1}H NMR (400 MHz, $CDCl_3$): δ 7.96-7.93 (m, 2H, $H_{arom.}$), 7.75 (s, 1H, =CH), 7.24-7.20 (m, 2H, $H_{arom.}$). ^{13}C NMR (100 MHz, $CDCl_3$): δ 166.2 (d, J = 259.0 Hz), 158.6, 133.6 (d, J = 9.7 Hz), 127.5, 117.4 (d, J = 22.0 Hz), 113.7, 112.6, 82.4.

7a - ethyl (E)-2-cyano-3-phenylacrylate



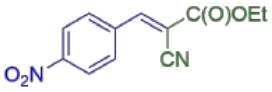
Yellow solid; yield = 92% (425 mg); ^{1}H NMR (400 MHz, $CDCl_3$): δ 8.21 (s, 1H, =CH), 7.90-7.85 (m, 2H, $H_{arom.}$), 7.55-7.45 (m, 3H, $H_{arom.}$), 4.38 (q, J = 7.1 Hz, 2H, OCH_2), 1.40 (t, J = 7.1 Hz, 3H, CH_3). ^{13}C NMR (100 MHz, $CDCl_3$): δ 162.5, 154.5, 133.0, 131.5, 129.3, 115.5, 103.0, 63.0, 14.3.

7b - ethyl (E)-2-cyano-3-(p-tolyl)acrylate



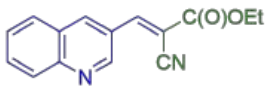
Light yellow solid; yield = 89% (440 mg); ^{1}H NMR (400 MHz, $CDCl_3$): δ 8.20 (s, 1H, =CH), 7.88 (d, J = 8.2 Hz, 2H, $H_{arom.}$), 7.29 (d, J = 8.2 Hz, 2H, $H_{arom.}$), 4.36 (q, J = 7.1 Hz, 2H, OCH_2), 2.42 (s, 3H, Ar-CH_3), 1.38 (t, J = 7.1 Hz, 3H, CH_3). ^{13}C NMR (100 MHz, $CDCl_3$): δ 162.9, 155.1, 144.7, 131.4, 130.1, 129.0, 115.9, 101.7, 62.7, 22.0, 14.3.

7c - ethyl (E)-2-cyano-3-(4-nitrophenyl)acrylate



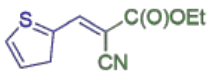
Yellow solid; yield = 89% (503 mg); ^{1}H NMR (400 MHz, $CDCl_3$): δ 8.35 (d, J = 8.8 Hz, 2H, $H_{arom.}$), 8.29 (s, 1H, =CH), 8.13 (d, J = 8.8 Hz, 2H, $H_{arom.}$), 4.41 (q, J = 7.1 Hz, 2H, OCH_2), 1.41 (t, J = 7.1 Hz, 3H, CH_3). ^{13}C NMR (100 MHz, $CDCl_3$): δ 161.5, 151.8, 137.0, 131.6, 124.4, 114.6, 109.2, 63.4, 14.2.

7d - ethyl (E)-2-cyano-3-(quinolin-3-yl)acrylate



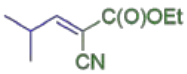
Yellow solid; yield = 84% (487 mg); ^{1}H NMR (400 MHz, $CDCl_3$): δ 9.17 (s, 1H, $H_{arom.}$), 9.06 (s, 1H, $H_{arom.}$), 8.41 (s, 1H, =CH), 8.15-7.64 (m, 4H, $H_{arom.}$), 4.42 (q, J = 7.1 Hz, 2H, OCH_2), 1.42 (t, J = 7.1 Hz, 3H, CH_3). ^{13}C NMR (100 MHz, $CDCl_3$): δ 162.0, 151.7, 151.3, 149.7, 138.0, 132.7, 129.6, 129.5, 128.1, 127.2, 124.6, 115.3, 105.1, 63.2, 14.3.

7e - ethyl (E)-2-cyano-3-(thiophen-2-yl)acrylate



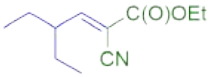
Orange solid; yield = 92% (438 mg); ^{1}H NMR (400 MHz, $CDCl_3$): δ 8.32 (s, 1H, =CH), 7.81-7.76 (m, 2H, $H_{arom.}$), 7.21 (m, 1H, $H_{arom.}$), 4.34 (q, J = 7.1 Hz, 2H, OCH_2), 1.36 (t, J = 7.1 Hz, 3H, CH_3). ^{13}C NMR (100 MHz, $CDCl_3$): δ 162.8, 146.8, 137.3, 136.1, 135.3, 128.7, 115.8, 99.4, 62.6, 14.3.

7f - ethyl (E)-2-cyano-4-methylpent-2-enoate



Light yellow oil; yield = 92% (353 mg); ^{1}H NMR (400 MHz, $CDCl_3$): δ 7.31 (d, J = 10.4 Hz, 1H, =CH), 4.14 (q, J = 7.1 Hz, 2H, OCH_2), 2.83 (m, 1H, CH), 1.20 (t, J = 7.1 Hz, 3H, CH_3), 1.01 (d, J = 6.8 Hz, 6H, 2$\times$$CH_3$). ^{13}C NMR (100 MHz, $CDCl_3$): δ 169.1, 161.4, 113.5, 107.6, 62.4, 31.6, 21.2, 14.1.

7g - ethyl (E)-2-cyano-4-ethylhex-2-enoate

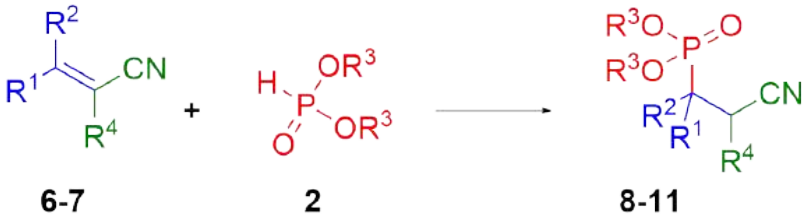


Light yellow oil; yield = 94% (422 mg); ^{1}H NMR (400 MHz, $CDCl_3$): δ 7.31 (d, J = 10.4 Hz, 1H, =CH), 4.22 (q, J = 7.1 Hz, 2H, OCH_2), 2.50 (m, 1H, CH), 1.55 (m, 4H, 2$\times$$CH_2$), 1.34 (t, J = 7.1 Hz, 3H, CH_3), 0.81 (t, J = 7.4 Hz, 6H, 2$\times$$CH_3$). ^{13}C NMR (100 MHz, $CDCl_3$): δ 167.7, 161.2, 114.0, 110.0, 62.3, 46.1, 27.1, 14.0, 11.7.

Products of phospha-Michael addition catalysed by *Arabidopsis halleri*-derived biogenic Eco-MgZnOx catalyst

General procedure for phospha-Michael addition

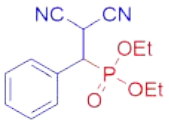
In a typical phospha-Michael addition reaction, the activated alkene, such as an arylidene malononitrile or cyanoacrylate derivative (0.23 mmol), the corresponding H-phosphonate (0.23 mmol), and Eco-MgZnOx catalyst were introduced into a glass screw-cap test tube equipped with a magnetic stirring bar. The catalyst was used in an amount corresponding to approximately 5 mol% Zn, usually 7.5 mg on a 0.23 mmol scale. The reaction was performed under solvent-free conditions at 70 °C for 2–3 h.



Scheme 3. Phospha Michael addition - reaction scheme

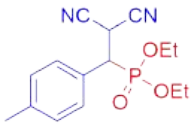
After completion, the reaction mixture was cooled, diluted with a solvent, and transferred to a polypropylene centrifuge tube. The catalyst was separated by centrifugation. The supernatant was analyzed by ^{31}P NMR spectroscopy to determine conversion, based on the integrals of the H-phosphonate substrate and the phosphonate product. The crude product was purified by preparative thin-layer chromatography or crystallization, depending on its physical state. The optimized conditions for this reaction were neat, 70 °C. Reactions carried out in solvents gave lower conversions.

8a - Diethyl (2,2-dicyano-1-phenylethyl)phosphonate



Yellow solid; yield = 94% (254 mg); mp. 55–57 °C; ^{1}H NMR (400 MHz, $CDCl_3$): δ 7.49–7.16 (m, 5H), 4.62–4.59 (m, 1H), 4.18–3.74 (m, 4H), 3.62 (dd, J = 8.0, 21.6 Hz, 1H), 1.36–1.07 (m, 6H); ^{13}C NMR (100 MHz, $CDCl_3$): δ 130.5, 129.5, 129.4, 111.7 (d, J = 9.7 Hz), 111.5 (d, J = 13.4 Hz), 64.5 (d, J = 6.9 Hz), 63.4 (d, J = 6.9 Hz), 44.5 (d, J = 142.9 Hz), 16.3 (d, J = 5.7 Hz), 16.1 (d, J = 5.7 Hz); ^{31}P NMR (243 MHz, $CDCl_3$): δ 20.1.

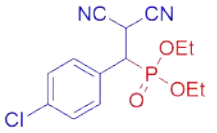
8b - Diethyl (2,2-dicyano-1-(p-tolyl)ethyl)phosphonate



Yellow oil; yield = 94% (253 mg); ^{1}H NMR (400 MHz, $CDCl_3$): δ 7.36–7.31 (m, 2H), 7.23–7.19 (m, 2H), 4.48 (t, J = 8.4 Hz, 1H), 4.19–4.09 (m, 2H), 4.02–3.93 (m, 1H), 3.80–3.69 (m, 1H), 3.58–3.49 (m, 1H), 2.35 (s, 3H), 1.33 (t, J = 7.2 Hz, 3H), 1.11 (t, J

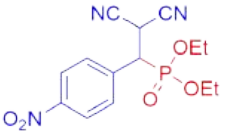
= 7.2 Hz, 3H); ^{13}C NMR (100 MHz, $CDCl_3$): δ 139.7 (d, J_{C-P} = 2.3 Hz, C_{ipso}), 130.2 (s), 129.2 (d, J = 6.3 Hz), 127.2 (d, J = 5.7 Hz); 111.3, 64.4 (d, J = 7.4 Hz, OCH_2), 63.4 (d, $J \approx$ 7.4 Hz, OCH_2), 44.4 (d, $J \approx$ 144 Hz, Cq-P), 21.3 (s lub bardzo małe d, Ar-CH_3), 16.3 (d, 4 $\approx$ 5.7 Hz, CH_3), 16.2 (d, $J \approx$ 5.7 Hz, CH_3). ^{31}P NMR (243 MHz, $CDCl_3$): δ 20.2.

8c - Diethyl [1-(4-chlorophenyl)-2,2-dicyanoethyl]phosphonate



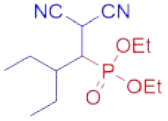
White solid; yield = 82% (242 mg); ^{1}H NMR (400 MHz, $CDCl_3$): δ 7.45-7.35 (m, 4H, $H_{arom.}$), 4.65 (dd, J = 11.5, 10.5 Hz, 1H, P-CH), 4.25-4.05 (m, 3H, O-CH_2 + $CH(CN)_2$), 3.95-3.80 (m, 2H, O-CH_2), 1.32 (t, J = 7.1 Hz, 3H, CH_3), 1.18 (t, J = 7.1 Hz, 3H, CH_3). ^{13}C NMR (100 MHz, $CDCl_3$): δ 136.2, 131.5, 130.9 (d, J = 6.5 Hz), 129.9, 111.2 (d, J=8.0 Hz), 111.0 (d, J=8.2 Hz), 64.8 (d, J = 7.2 Hz), 64.1 (d, J = 7.4 Hz), 44.1 (d, J = 144.1 Hz), 16.4 (d, J = 6.0 Hz), 16.3 (d, J = 6.2 Hz). ^{31}P NMR (243 MHz, $CDCl_3$): δ 19.4.

8d - Diethyl (2,2-dicyano-1-(4-nitrophenyl)ethyl)phosphonate



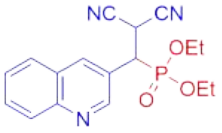
White solid; yield = 91% (221 mg); ^{1}H NMR (400 MHz, $CDCl_3$): δ 8.28–8.32 (m, 2H), 7.68–7.71 (m, 2H), 4.54–4.59 (m, 2H), 4.13–4.24 (m, 2H), 4.06–4.13 (m, 1H), 3.89–3.98 (m, 1H), 3.66–3.75 (m, 1H), 1.35 (t, J = 7.0 Hz, 3H), 1.18–1.22 (m, 3H); ^{13}C NMR (100 MHz, $CDCl_3$): δ 148.6, 137.5 (d, J = 5.7 Hz), 130.6 (d, J = 6.3 Hz), 124.6, 110.8 (d, J = 11.5 Hz), 110.7 (d, J = 10.3 Hz), 64.8 (d, J = 6.9 Hz), 64.1 (d, J = 6.9 Hz), 44.5 (d, J = 142.3 Hz), 25.3, 16.3 (t, J = 6.0 Hz); ^{31}P NMR (243 MHz, $CDCl_3$): δ 18.3.

8e - Diethyl (1,1-dicyano-3-ethylpentan-2-yl)phosphonate



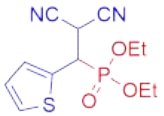
Yellow oil; ^{1}H NMR (400 MHz, $CDCl_3$): δ 4.14–4.29 (m, 5H), 2.43–2.52 (m, 1H), 1.51–1.88 (m, 5H), 1.36 (t, J = 7.2 Hz, 6H), 0.88–0.99 (m, 6H); ^{13}C NMR (100 MHz, $CDCl_3$): δ 112.4 (d, J = 12 Hz), 111.9 (d, J = 6.9 Hz), 63.2 (d, J = 6.9 Hz), 63.0 (d, J = 7.4 Hz), 41.6 (d, J = 2.3 Hz), 40.1 (d, J = 141.7 Hz), 27.0, 23.5 (d, J = 4 Hz), 23.3 (d, J = 6.3 Hz), 22.5, 16.4 (d, J = 6.5 Hz), 11.8, 11.6; ^{31}P NMR (243 MHz, $CDCl_3$): δ 23.8.

8f - Diethyl (2,2-dicyano-1-(quinolin-3-yl)ethyl)phosphonate



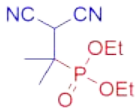
Brown solid; yield = 84% (264 mg); ^{1}H NMR (400 MHz, $CDCl_3$): δ 8.93-7.60 (m, 6H, $H_{arom.}$), 4.67 (dd, J = 8.9, 7.3 Hz, 1H, P-CH), 4.24-3.80 (m, 5H, $CH(CN)_2$ + 2$\times$O-CH_2), 1.35 (t, J = 7.0 Hz, 3H, CH_3), 1.16 (t, J = 7.0 Hz, 3H, CH_3). ^{13}C NMR (100 MHz, $CDCl_3$): δ 150.5, 148.3, 136.8, 131.0, 129.4, 128.3, 127.9, 123.7, 111.1 (d, J=8.1 Hz), 111.0 (d, J=8.5 Hz), 64.7 (d, J = 7.1 Hz), 64.0 (d, J = 7.3 Hz), 42.4 (d, J = 145.2 Hz), 25.6, 16.3 (d, J = 5.9 Hz), 16.2 (d, J = 6.1 Hz). ^{31}P NMR (243 MHz, $CDCl_3$): δ 19.8.

8g - Diethyl (2,2-dicyano-1-(thiophen-2-yl)ethyl)phosphonate



Brown solid; yield = 96% (263 mg); ^{1}H NMR (400 MHz, $CDCl_3$): δ 7.51–7.54 (m, 1H), 7.40–7.43 (m, 1H), 7.22–7.25 (m, 1H), 4.46 (dd, J = 6.6, 9.0 Hz, 1H), 4.03–4.18 (m, 3H), 3.86–3.95 (m, 1H), 3.77 (dd, J = 6.6, 21.4 Hz, 1H), 1.33 (t, J = 7.0 Hz, 3H), 1.19 (t, J = 7.0 Hz, 3H); ^{13}C NMR (100 MHz, $CDCl_3$): δ 129.5 (d, J = 5.7 Hz), 127.8 (d, J = 4.5 Hz), 127.5, 126.3 (d, J = 8.6 Hz), 111.4 (d, J = 12.5 Hz), 111.1 (d, J = 9.7 Hz), 64.5 (d, J = 6.8 Hz), 63.7 (d, J = 6.9 Hz), 40.3 (d, J = 134.7 Hz), 25.8, 16.3 (t, J = 6.0 Hz); ^{31}P NMR (243 MHz, $CDCl_3$): δ 18.1.

8h - Diethyl (1,1-dicyano-2-methylpropan-2-yl)phosphonate



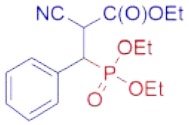
Brown oil; yield = 74% (188 mg); ^{1}H NMR (400 MHz, $CDCl_3$): δ 4.03–4.19 (m, 6H), 1.40 (d, J = 15.6 Hz, 6H), 1.28–1.34 (m, 6H); ^{13}C NMR (100 MHz, $CDCl_3$): δ 111.0 (d, J = 10.8 Hz), 63.7 (d, J = 7.5 Hz), 61.9 (d, J = 5.8 Hz), 37.3 (d, J = 148.0 Hz), 31.2, 20.8–20.6, 16.4–16.3; ^{31}P NMR (243 MHz, $CDCl_3$): δ 21.2.

8i - Diethyl (1,1-dicyano-2-(furan-2-yl)propan-2-yl)phosphonate



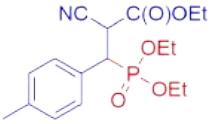
Yellow solid; yield = 88% (180 mg); ^{1}H NMR (400 MHz, $CDCl_3$): δ 7.48 (m, 1H, $H_{arom.}$), 6.50-6.42 (m, 2H, $H_{arom.}$), 4.69 (d, J=5.6 Hz, 0.5H, $CH(CN)_2$), 4.67 (d, J=5.6 Hz, 0.5H, $CH(CN)_2$), 4.17-3.78 (m, 4H, 2$\times$$OCH_2$), 1.87 (s, 1.5H, CH_3), 1.84 (s, 1.5H, CH_3), 1.35-1.17 (m, 6H, 2$\times$$CH_3$-ethyl). ^{13}C NMR (100 MHz, $CDCl_3$): δ 148.2, 144.0, 111.4-110.5 (m), 64.2 (m), 44.0 (d, $J \approx$ 145 Hz), 42.5 (d, $J \approx$ 145 Hz), 30.2, 17.1, 16.3. ^{31}P NMR (243 MHz, $CDCl_3$): δ 20.48.

9a - Ethyl 2-cyano-3-(diethoxyphosphoryl)-3-phenylpropanoate



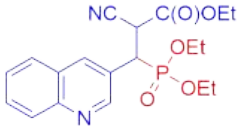
Yellow oil; yield = 95% (296 mg); ^{1}H NMR (400 MHz, $CDCl_3$): δ 7.44-7.27 (m, 5H, $H_{arom.}$), 4.24-3.74 (m, 8H, P-CH, CN-CH, 3$\times$O-CH_2), 1.27-0.97 (m, 9H, 3$\times$$CH_3$). ^{13}C NMR (100 MHz, $CDCl_3$): δ 164.3, 129.9, 129.4, 128.7, 115.0, 63.4, 44.7 (d, $J \approx 140$ Hz), 39.2, 16.2, 13.8. ^{31}P NMR (243 MHz, $CDCl_3$): δ 22.7 (major), 22.6 (minor).

9b - Ethyl 2-cyano-3-(diethoxyphosphoryl)-3-(p-tolyl)propanoate



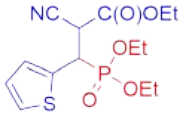
Yellow oil; yield = 82% (266 mg); ^{1}H NMR (400 MHz, $CDCl_3$): δ 7.33-7.07 (m, 4H), 4.21-3.71 (m, 8H), 2.27 (s, 3H), 1.29-1.03 (m, 9H). ^{13}C NMR (100 MHz, $CDCl_3$): δ 164.6 (d, J = 13.1 Hz), 138.7 (d, J = 8.6 Hz), 129.8, 115.1, 63.8 (d, J = 6.8 Hz), 44.2 (d, J = 135.0 Hz), 39.6 (d, J = 4.5 Hz), 21.3, 16.4 (d, J = 9.1 Hz), 14.0. ^{31}P NMR (243 MHz, $CDCl_3$): δ 22.8 (major), 22.6 (minor).

9c - Ethyl 2-cyano-3-(diethoxyphosphoryl)-3-(quinolin-3-yl)propanoate



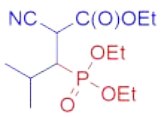
Yellow oil; yield = 78% (280 mg); ^{1}H NMR (400 MHz, $CDCl_3$): ^{1}H NMR (400 MHz, $CDCl_3$): δ 8.86-8.51 (m, 2H, $H_{arom.}$), 8.10-7.55 (m, 4H, $H_{arom.}$), 4.42-3.65 (m, 8H, P-CH, CN-CH, 3$\times$O-CH_2), 1.37-1.02 (m, 9H, 3$\times$$CH_3$). ^{13}C NMR (100 MHz, $CDCl_3$): δ 164.4 (d, J = 14.1 Hz), 151.3, 147.7, 137.1 (d, J = 6.2 Hz), 128.8, 114.5, 64.0 (d, J = 6.9 Hz), 54.1 (d, J = 138.1 Hz), 41.7, 16.3 (d, J = 5.8 Hz), 13.8. ^{31}P NMR (243 MHz, $CDCl_3$): δ 21.9 (major), 21.5 (minor).

9d - Ethyl 2-cyano-3-(diethoxyphosphoryl)-3-(thiophen-2-yl)propanoate



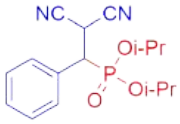
Yellow solid; yield = 75% (238 mg); ^{1}H NMR (400 MHz, $CDCl_3$): δ 7.26-6.92 (m, 3H, $H_{arom.}$), 4.12-3.67 (m, 8H, P-CH, CN-CH, 3$\times$O-CH_2), 1.26-1.13 (m, 9H, 3$\times$$CH_3$). ^{13}C NMR (100 MHz, $CDCl_3$): δ 164.2 (d, J = 15.4 Hz), 131.7, 129.0, 127.4, 126.5, 114.5, 63.5 (d, J = 6.3 Hz), 54.0 (d, J = 154.3 Hz), 40.4 (d, J = 4.8 Hz), 16.3 (d, J = 5.7 Hz), 13.8. ^{31}P NMR (243 MHz, $CDCl_3$): δ 18.1.

9e - Ethyl 2-cyano-3-(diethoxyphosphoryl)-4-methylpentanoate



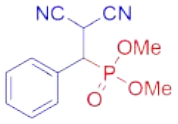
Yellow solid; yield = 92% (258 mg); ^{1}H NMR (400 MHz, $CDCl_3$): δ 4.29-4.07 (m, 6H, 3×O-CH_2), 3.75-3.66 (m, 1H, P-CH or CN-CH), 2.53-2.43 (m, 1H, P-CH or CN-CH), 2.22-2.12 (m, 1H, CH-iPr), 1.33-1.27 (m, 9H, 3×CH_3-ethyl), 1.19-0.99 (m, 6H, 2×CH_3-iPr). ^{13}C NMR (100 MHz, $CDCl_3$): δ 166.0, 115.1, 63.0 (d, J = 6.9 Hz), 44.2 (d, J = 145.0 Hz), 37.1 (d, J = 5.1 Hz), 27.7, 22.0, 21.0, 16.4 (d, J = 5.5 Hz), 14.0. ^{31}P NMR (243 MHz, $CDCl_3$): δ 28.1 (major), 26.8 (minor).

10a - Diisopropyl (2,2-dicyano-1-phenylethyl)phosphonate



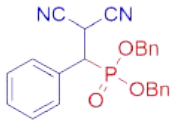
White solid; yield = 82% (243 mg); ^{1}H NMR (400 MHz, $CDCl_3$): δ 7.49–7.40 (m, 5H), 4.80–4.70 (m, 1H), 4.51–4.41 (m, 2H), 3.49 (dd, J = 7.6, 20.8 Hz, 1H), 1.34 (d, J = 6 Hz, 6H), 1.27 (d, J = 6 Hz, 3H), 0.85 (d, J = 6.4 Hz, 3H); ^{13}C NMR (100 MHz, $CDCl_3$): δ 130.7 (d, J = 5.2 Hz), 129.6 (broad signal, 1C), 129.5 (overlapping, 2C), 111.5 (d, J = 10.3 Hz), 111.3 (d, J = 12.0 Hz), 73.9 (d, J = 6.9 Hz), 72.8 (d, J = 7.4 Hz), 45.2 (d, J = 144.6 Hz), 25.9, 24.0 (d, J = 3.5 Hz), 23.9 (d, J = 5.1 Hz), 22.9 (d, J = 6.2 Hz); ^{31}P NMR (243 MHz, $CDCl_3$): δ 22.1 (s).

10b - Dimethyl (2,2-dicyano-1-phenylethyl)phosphonate



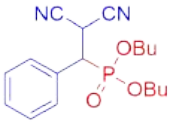
White solid; yield = 91% (221 mg); ^{1}H NMR (400 MHz, $CDCl_3$): δ 7.48–7.42 (m, 5H), 4.51–4.46 (m, 1H), 3.80 (d, J=10.8 Hz, 3H), 3.61 (dd, J=8.4, 21.4 Hz, 1H), 3.53 (d, J=10.8 Hz, 3H). ^{13}C NMR (100 MHz, $CDCl_3$): δ 130.0 (d, J=5.7 Hz), 129.8 (d, J=1.7 Hz), 129.7, 129.3 (d, J=6.9 Hz), 111.3 (d, J=9.8 Hz), 111.1 (d, J=13.2 Hz), 54.7 (d, J=6.8 Hz), 53.6 (d, J=7.4 Hz), 44.2 (d, J=144.0 Hz), 25.6. ^{31}P NMR (243 MHz, $CDCl_3$): δ 22.4 (s).

10c - Dibenzyl (2,2-dicyano-1-phenylethyl)phosphonate



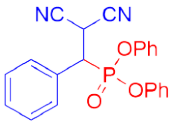
White solid; yield = 84% (320 mg); ^{1}H NMR (400 MHz, $CDCl_3$): δ 7.46–7.26 (m, 13H), 7.10–7.08 (m, 2H), 5.10–4.99 (m, 2H), 4.86–4.81 (m, 1H), 4.63–4.45 (m, 2H), 3.60 (dd, J = 8.0, 21.6 Hz); ^{13}C NMR (100 MHz, $CDCl_3$): δ 135.3, 130.2 (d, J = 5.7 Hz), 129.1, 128.9–128.7, 128.3, 111.6 (d, J = 10.3 Hz), 111.4 (d, J = 12.6 Hz), 69.7 (d, J = 6.9 Hz), 69.0 (d, J = 6.8 Hz), 45.0 (d, J = 143.5 Hz), 25.6; ^{31}P NMR (243 MHz, $CDCl_3$): δ 21.1 (s).

10d - Dibutyl (2,2-dicyano-1-phenylethyl)phosphonate



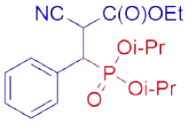
White solid; yield = 67% (214 mg); ^{1}H NMR (400 MHz, $CDCl_3$): δ 7.47-7.37 (m, 5H, $H_{arom.}$), 4.55 (m, 1H, P-CH), 4.08-3.87 (m, 4H, 2×OCH_2), 3.56 (m, 1H, $CH(CN)_2$), 1.66-1.14 (m, 8H, 2×CH_2CH_2), 0.88 (t, J = 7.4 Hz, 3H, CH_3), 0.79 (t, J = 7.4 Hz, 3H, CH_3). ^{13}C NMR (100 MHz, $CDCl_3$): δ 130.5 (m), 129.5 (m), 129.0 (m), 111.5 (m, CN), 67.8 (m, 2×OCH_2), 44.7 (d, $J \approx$ 144 Hz), 44.5 (d, $J \approx$ 144 Hz), 32.3 (m), 18.6 (m), 13.5 (m). ^{31}P NMR (243 MHz, $CDCl_3$): δ 20.2 (major), 20.0 (minor).

10e - Diphenyl (2,2-dicyano-1-phenylethyl)phosphonate



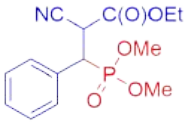
White solid; yield = 87% (312 mg); ^{1}H NMR (400 MHz, $CDCl_3$): δ 7.55–7.08 (m, 13H), 6.79–6.76 (m, 2H), 4.74–4.69 (m, 1H), 3.98 (dd, J = 7.6, 21.6 Hz, 1H); ^{13}C NMR (100 MHz, $CDCl_3$): δ 150.0 (d, J = 9.7 Hz), 149.6 (d, J = 9.7 Hz), 130.2, 129.8, 129.7, 129.2 (d, J = 5.8 Hz), 125.9 (d, J = 32.6 Hz), 120.5 (d, J = 5.6 Hz), 120.1 (d, J = 4.6 Hz), 111.2 (d, J = 10.8 Hz), 110.9 (d, J = 13.1 Hz), 44.9 (d, J = 146.3 Hz), 26.0; ^{31}P NMR (243 MHz, $CDCl_3$): δ 12.51 (s).

11a - Ethyl 2-cyano-3-(diisopropoxyphosphoryl)-3-phenylpropanoate



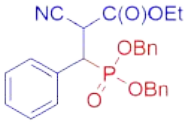
Yellow oil; yield = 78% (287 mg); ^{1}H NMR (400 MHz, $CDCl_3$): δ 7.45-7.24 (m, 5H, $H_{arom.}$), 4.63-3.64 (m, 6H, P-CH, CN-CH, OCH_2, 2×OCH-iPr), 1.23-0.75 (m, 15H, 4×CH_3-iPr + CH_3-ethyl). ^{13}C NMR (100 MHz, $CDCl_3$): δ 164.4 (m), 130.5 (m), 129.5 (m), 128.6 (m), 115.0 (m), 72.3 (m, OCH-iPr), 63.2, 44.5 (d, $J \approx$ 145 Hz), 39.5, 24.1 (m), 13.7. ^{31}P NMR (243 MHz, $CDCl_3$): δ 21.0 (major), 20.8 (minor).

11b - Ethyl 2-cyano-3-(dimethoxyphosphoryl)-3-phenylpropanoate



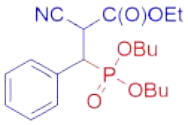
Yellow oil; yield = 84% (260 mg); ^{1}H NMR (400 MHz, $CDCl_3$): δ 7.47-7.29 (m, 5H, $H_{arom.}$), 4.16-3.45 (m, 10H, P-CH, CN-CH, OCH_2, 2×OCH_3), 1.18-1.05 (m, 3H, CH_3). ^{13}C NMR (100 MHz, $CDCl_3$): δ 164.3 (d, $J \approx$ 14 Hz), 132.0 (m), 129.9 (m), 128.8 (m), 114.9 (m, CN), 63.3, 54.0 (m, 2×OCH_3), 45.1 (d, $J \approx$ 145 Hz, C-P), 39.4 (d, $J \approx$ 5 Hz), 13.8. ^{31}P NMR (243 MHz, $CDCl_3$): δ 24.9 (major), 24.8 (minor).

11c - Ethyl 3-(bis(benzyloxy)phosphoryl)-2-cyano-3-phenylpropanoate



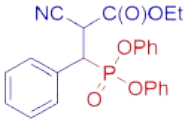
Yellow oil; yield = 81% (376 mg); ^{1}H NMR (400 MHz, $CDCl_3$): δ 7.48-7.02 (m, 15H, $H_{arom.}$), 5.07-4.72 (m, 4H, 2×OCH_2Ph), 4.26-3.81 (m, 4H, P-CH, CN-CH, OCH_2), 1.10 (t, J = 7.0 Hz, 1.5H, CH_3), 1.02 (t, J = 7.0 Hz, 1.5H, CH_3). ^{13}C NMR (100 MHz, $CDCl_3$): δ 164.2 (m), 135.8 (m), 130.0-128.1 (m, $C_{arom.}$), 115.0 (m, CN), 68.8 (m, OCH_2Ph), 63.3, 44.4 (d, $J \approx$ 143 Hz, C-P), 39.4, 13.8. ^{31}P NMR (243 MHz, $CDCl_3$): δ 23.5 (major), 23.4 (minor).

11d - Ethyl 2-cyano-3-(dibutoxyphosphoryl)-3-phenylpropanoate



Yellow oil; yield = 82% (323 mg); ^{1}H NMR (400 MHz, $CDCl_3$): δ 7.48-7.02 (m, 15H, $H_{arom.}$), 5.07-4.72 (m, 4H, 2×OCH_2Ph), 4.26-3.81 (m, 4H, P-CH, CN-CH, OCH_2), 1.10 (t, J = 7.0 Hz, 1.5H, CH_3), 1.02 (t, J = 7.0 Hz, 1.5H, CH_3). ^{13}C NMR (100 MHz, $CDCl_3$): δ 164.2 (m), 135.8 (m), 130.0-128.1 (m, $C_{arom.}$), 115.0 (m, CN), 68.8 (m, OCH_2Ph), 63.3, 44.4 (d, $J \approx$ 143 Hz, C-P), 39.4, 13.8. ^{31}P NMR (243 MHz, $CDCl_3$): δ 23.5 (major), 23.4 (minor).

11e - Ethyl 2-cyano-3-(diphenoxyphosphoryl)-3-phenylpropanoate



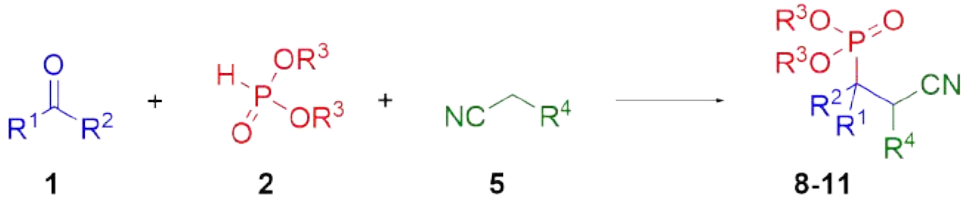
Yellow oil; yield = 44% (192 mg); ^{1}H NMR (400 MHz, $CDCl_3$): δ 7.60-6.77 (m, 15H, $H_{arom.}$), 4.52-4.11 (m, 4H, P-CH, CN-CH, OCH_2), 1.18 (m, 3H, CH_3). ^{13}C NMR (100 MHz, $CDCl_3$): δ 164.1 (m), 150.1 (m), 130.1-120.2 (m, $C_{arom.}$), 114.7 (m, CN), 63.6, 45.0 (d, $J \approx$ 145 Hz, C-P), 39.7, 13.8. ^{31}P NMR (243 MHz, $CDCl_3$): δ 15.4 (major), 14.9 (minor).

Products of Knoevenagel-phospha-Michael reaction catalysed by *Arabidopsis halleri*-derived biogenic Eco-MgZnOx catalyst

General procedure for Knoevenagel-phospha-Michael reaction

The Knoevenagel-phospha-Michael reaction was performed as a two-step one-pot process and then as a direct three-component one-pot reaction. In the two-step procedure, the aldehyde (0.23 mmol), malononitrile or ethyl cyanoacetate (0.23 mmol), and Eco-MgZnOx catalyst were first placed in a glass screw-cap test tube and stirred under solvent-free conditions at 70 ℃. After the Knoevenagel condensation step, the H-phosphonate reagent (0.23 mmol) was added directly to the same reaction vessel, and stirring was continued under the same conditions.

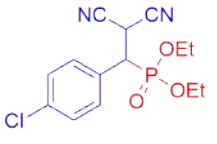
In the one-pot procedure, the aldehyde (0.23 mmol), the active methylene compound (0.23 mmol), the H-phosphonate (0.23 mmol), and Eco-MgZnOx catalyst were added simultaneously to the reaction tube. The reaction was carried out under solvent-free conditions at 70 ℃, typically for 3–5 h, depending on the substrate system. The catalyst loading corresponded to approximately 5 mol% Zn.



Scheme 4. Knoevenagel phospha-Michael condensation - reaction scheme

After the reaction, the mixture was cooled and diluted with an appropriate solvent. The solid catalyst was removed by centrifugation, and the liquid phase was collected. Conversion and selectivity were determined by ^{31}P NMR spectroscopy of the crude reaction mixture, with particular attention to the desired Knoevenagel-phospha-Michael adduct and possible α-hydroxyphosphonate by-product formed through the competing hydrophosphonylation pathway. The final products were purified by crystallization or preparative thin-layer chromatography, depending on their physical state.
Spectra of the Knoevenagel–phospha-Michael products are presented below. Their general spectral pattern is analogous to that observed for the products of the phospha-Michael reaction, as described in the previous section.

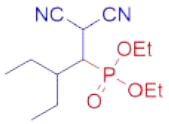
8c - Diethyl [1-(4-chlorophenyl)-2,2-dicyanoethyl]phosphonate



White solid; yield = 82% (242 mg); ^{1}H NMR (400 MHz, $CDCl_3$): δ 7.50-7.40 (m, 4H, $H_{arom.}$), 4.49-3.55 (m, 6H, P-CH, $CH(CN)_2$, 2×OCH_2), 1.33-1.00 (m, 6H, 2×CH_3). ^{13}C NMR (100 MHz, $CDCl_3$): δ 135.8, 131.8, 130.6, 128.7, 111.0 (m), 64.0 (m), 44.7 (d, J=144.0

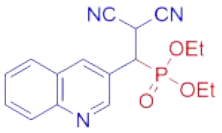
Hz), 43.3 (d, J=144.0 Hz), 25.4, 16.1 (m). ^{31}P NMR (243 MHz, $CDCl_3$): δ 19.9.

8e - Diethyl (1,1-dicyano-3-ethylpentan-2-yl)phosphonate



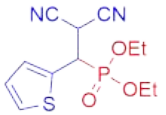
Yellow oil; ^{1}H NMR (400 MHz, $CDCl_3$): δ 4.29-4.16 (m, 6H, P-CH, $CH(CN)_2$, 2×OCH_2), 2.52-2.45 (m, 1H, CH), 1.79-1.53 (m, 4H, 2×CH_2), 1.39-0.90 (m, 12H, 4×CH_3). ^{13}C NMR (100 MHz, $CDCl_3$): δ 112.1 (m), 63.0 (m), 47.3, 41.5 (d, $J \approx$ 145 Hz), 40.7, 39.3, 27.0, 23.4 (m), 22.4, 16.3 (m), 11.6 (m). ^{31}P NMR (243 MHz, $CDCl_3$): δ 23.5.

8f - diethyl (2,2-dicyano-1-(quinolin-3-yl)ethyl)phosphonate



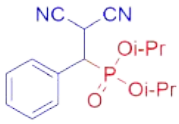
Brown solid; yield = 84% (264 mg); ^{1}H NMR (400 MHz, $CDCl_3$): δ 8.93-7.60 (m, 6H, $H_{arom.}$), 4.67 (dd, J = 8.9, 7.3 Hz, 1H, P-CH), 4.24-3.80 (m, 5H, $CH(CN)_2$ + 2×O-CH_2), 1.35 (t, J = 7.0 Hz, 3H, CH_3), 1.16 (t, J = 7.0 Hz, 3H, CH_3). ^{13}C NMR (100 MHz, $CDCl_3$): δ 150.5, 148.3, 136.8, 131.0, 129.4, 128.3, 127.9, 123.7, 111.1 (d, J=8.1 Hz), 111.0 (d, J=8.5 Hz), 64.7 (d, J = 7.1 Hz), 64.0 (d, J = 7.3 Hz), 42.4 (d, J = 145.2 Hz), 25.6, 16.3 (d, J = 5.9 Hz), 16.2 (d, J = 6.1 Hz). ^{31}P NMR (243 MHz, $CDCl_3$): δ 19.8.

8g - Diethyl (2,2-dicyano-1-(thiophen-2-yl)ethyl)phosphonate



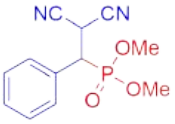
Brown solid; yield = 96% (263 mg); ^{1}H NMR (400 MHz, DMSO-d_6): δ 7.57-7.56 (m, 1H, $H_{arom.}$), 7.25 (m, 1H, $H_{arom.}$), 7.08-7.05 (m, 1H, $H_{arom.}$), 5.45-5.41 (m, 1H, P-CH or $CH(CN)_2$), 4.83-4.76 (m, 1H, P-CH or $CH(CN)_2$), 4.10-3.83 (m, 4H, 2×OCH_2), 1.24-1.07 (m, 6H, 2×CH_3).; ^{13}C NMR (100 MHz, $CDCl_3$): δ 127.7-126.2 (m, $C_{arom.}$), 64.0 (m, 2×OCH_2), 40.2 (m, P-CH), 25.8 ($CH(CN)_2$), 16.2 (m, 2×CH_3). ^{31}P NMR (243 MHz, $CDCl_3$): δ 18.2.

10a - Diisopropyl (2,2-dicyano-1-phenylethyl)phosphonate



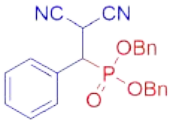
White solid; yield = 82% (243 mg); ^{1}H NMR (400 MHz, $CDCl_3$): δ 7.49-7.40 (m, 5H, $H_{arom.}$), 4.79-4.72 (m, 2H, 2×OCH-iPr), 4.49 (dd, J=11.0, 4.0 Hz, 1H, P-CH), 3.52 (dd, J=11.0, 3.5 Hz, 1H, $CH(CN)_2$), 1.37-0.86 (m, 12H, 4×CH_3-iPr). ^{13}C NMR (100 MHz, $CDCl_3$): δ 130.8 (d, J=5.7 Hz), 129.6, 111.6 (d, J=9.8 Hz), 111.3 (d, J=12.0 Hz), 73.5 (m, 2×OCH), 46.1 (d, J=145.0 Hz), 44.7, 26.0-23.0 (m, 4×CH_3). ^{31}P NMR (243 MHz, $CDCl_3$): δ 18.3.

10b - Dimethyl (2,2-dicyano-1-phenylethyl)phosphonate



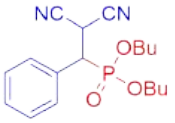
White solid; yield = 91% (221 mg); ^{1}H NMR (400 MHz, $CDCl_3$): δ 7.50-7.44 (m, 5H, $H_{arom.}$), 4.51 (m, 1H, P-CH), 3.81 (d, J=10.8 Hz, 3H, OCH_3), 3.63 (m, 1H, $CH(CN)_2$), 3.54 (d, J=10.8 Hz, 3H, OCH_3). ^{13}C NMR (100 MHz, $CDCl_3$): δ 130.0 (m), 129.8 (m), 129.4 (m), 111.3 (m, 2$\times$CN), 54.2 (m, 2$\times$$OCH_3$), 45.4 (d, $J \approx$ 145 Hz), 44.0 (d, $J \approx$ 145 Hz), 25.7. ^{31}P NMR (243 MHz, $CDCl_3$): δ 22.8 (major), 22.4 (minor).

10c - Dibenzyl (2,2-dicyano-1-phenylethyl)phosphonate



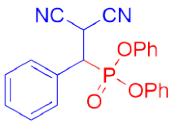
White solid; yield = 82% (243 mg); ^{1}H NMR (400 MHz, $CDCl_3$): δ 7.42-7.06 (m, 15H, $H_{arom.}$), 5.24-4.80 (m, 4H, 2$\times$$OCH_2Ph$), 4.52 (m, 1H, P-CH), 3.60 (m, 1H, $CH(CN)_2$). ^{13}C NMR (100 MHz, $CDCl_3$): δ 135.4 (m), 129.8-128.4 (m, $C_{arom.}$), 111.6 (m, 2$\times$CN), 69.5 (m, 2$\times$$OCH_2Ph$), 45.7 (d, $J \approx$ 145 Hz), 25.7. ^{31}P NMR (243 MHz, $CDCl_3$): δ 21.2 (major), 21.1 (minor).

10d - Dibutyl (2,2-dicyano-1-phenylethyl)phosphonate



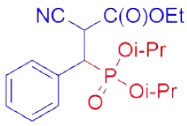
White solid; yield = 67% (214 mg); ^{1}H NMR (400 MHz, $CDCl_3$): δ 7.88-7.24 (m, 5H, $H_{arom.}$), 4.51 (m, 1H, P-CH), 4.18-3.97 (m, 4H, 2$\times$$OCH_2$), 3.54 (m, 1H, $CH(CN)_2$), 1.50-1.08 (m, 14H, 2$\times$$CH_2CH_2CH_3$). ^{13}C NMR (100 MHz, $CDCl_3$): δ 130.6 (m), 129.6 (m), 111.6 (m, 2$\times$CN), 67.7 (m, 2$\times$$OCH_2$), 45.6 (d, $J \approx$ 145 Hz), 44.1 (d, $J \approx$ 145 Hz), 32.4 (m), 25.7, 18.7 (m), 13.6 (m). ^{31}P NMR (243 MHz, $CDCl_3$): δ 20.0.

10e - Diphenyl (2,2-dicyano-1-phenylethyl)phosphonate



White solid; yield = 87% (312 mg); ^{1}H NMR (400 MHz, $CDCl_3$): δ 7.53-6.75 (m, 15H, $H_{arom.}$), 5.27 (m, 1H, CH), 4.70 (m, 1H, CH). ^{13}C NMR (100 MHz, $CDCl_3$): δ 150.0 (m), 130.2-120.1 (m, $C_{arom.}$), 111.3 (m, 2$\times$CN), 45.6 (d, $J \approx$ 145 Hz), 44.2 (d, $J \approx$ 145 Hz), 26.0. ^{31}P NMR (243 MHz, $CDCl_3$): δ 12.97.

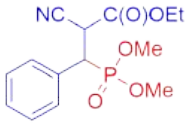
11a - Ethyl 2-cyano-3-(diisopropoxyphosphoryl)-3-phenylpropanoate



Yellow oil; yield = 78% (287 mg); ^{1}H NMR (400 MHz, $CDCl_3$): δ 7.45-7.23 (m, 5H, $H_{arom.}$), 4.60-3.54 (m, 6H, P-CH, CN-CH, OCH_2, 2$\times$OCH-iPr), 1.22-0.73 (m, 15H, 4$\times$$CH_3$-iPr + CH_3-ethyl). ^{13}C NMR (100 MHz, $CDCl_3$): δ 164.4 (m), 132.5 (m), 131.6 (m),

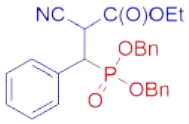
130.0 (m), 129.5 (m), 128.6 (m), 115.0 (m), 72.7 (m, OCH-iPr), 63.2, 45.4 (d, $J \approx$ 145 Hz), 39.5, 24.0 (m), 13.7. ^{31}P NMR (243 MHz, $CDCl_3$): δ 21.4 (major), 21.3 (minor).

11b - Ethyl 2-cyano-3-(dimethoxyphosphoryl)-3-phenylpropanoate



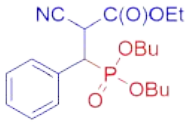
Yellow oil; yield = 84% (260 mg); ^{1}H NMR (400 MHz, $CDCl_3$): δ 7.27–7.49 (m, 5H), 3.42–4.29 (m, 10H), 1.17 (t, J = 7.2 Hz, major, 3H), 1.06 (t, J = 7.0 Hz, minor, 3H); ^{13}C NMR (100 MHz, $CDCl_3$): δ 164.4 (s, major), 164.3 (s, minor), 132.0 (s, major), 131.9 (s, minor), 131.2 (s, major), 131.1 (s, minor), 129.9 (s, major), 129.8 (s, minor), 128.8–129.5 (overlapping), 114.7–115.2 (overlapping), 63.3 (d, J = 20 Hz), 54.1–54.4 (overlapping), 53.2–53.6 (overlapping), 44.2 (d, J = 142.8 Hz, minor), 43.5 (d, J = 144.0 Hz, major), 39.4 (s, major), 39.2 (s, minor), 29.8, 13.9 (s, major), 13.7 (s, minor); ^{31}P NMR (243 MHz, $CDCl_3$): δ 24.9 (s, major), 24.8 (s, minor).

11c - Ethyl 3-(bis(benzyloxy)phosphoryl)-2-cyano-3-phenylpropanoate



Yellow oil; yield = 81% (376 mg); ^{1}H NMR (400 MHz, $CDCl_3$): δ 7.48–7.02 (m, 15H), 5.07–4.72 (m, 4H), 4.26–3.81 (m, 4H), 1.10 (t, J = 7.0 Hz, 3H, major), 1.02 (t, J = 7.0 Hz, 3H, minor); ^{13}C NMR (100 MHz, $CDCl_3$): δ 164.0–164.4 (overlapping), 135.6–135.9 (overlapping), 132.1 (d, J = 6.2 Hz), 131.2 (d, J = 6.3 Hz), 130.0 (d, J = 6.3 Hz), 129.5 (d, J = 6.3 Hz), 129.0, 128.9 (d, J = 2.3 Hz), 128.5–128.8 (overlapping), 128.3 (d, J = 6.3 Hz), 128.1, 115.1 (d, J = 3.5 Hz), 114.8 (d, J = 10.9 Hz), 69.1 (d, J = 6.9 Hz), 69.0 (d, J = 6.9 Hz), 68.4–68.6 (overlapping), 63.4 (s, major), 63.2 (s, minor), 44.7 (d, J = 142.3 Hz, minor), 44.1 (d, J = 142.9 Hz, major), 39.3–39.5 (overlapping), 29.8, 13.8 (s, major), 13.7 (s, minor); ^{31}P NMR (243 MHz, $CDCl_3$): δ 23.5 (s, major), 23.4 (s, minor).

11d - Ethyl 2-cyano-3-(dibutoxyphosphoryl)-3-phenylpropanoate



Yellow oil; yield = 82% (323 mg); ^{1}H NMR (400 MHz, $CDCl_3$): δ 7.47–7.25 (m, 15H), 4.25–3.69 (m, 8H), 1.65–0.73 (m, 17H); ^{13}C NMR (100 MHz, $CDCl_3$): δ 164.4 (d, J = 13.1 Hz, major), 164.2 (d, J = 13.7 Hz, minor), 132.3 (d, J = 6.2 Hz), 131.5 (d, J = 5.7 Hz), 129.9 (d, J = 6.3 Hz), 129.4 (d, J = 6.23 Hz), 128.5–129.1 (overlapping), 128.2, 115.1 (d, J = 3.4 Hz), 114.9 (d, J = 9.1 Hz), 67.2–67.4 (overlapping), 66.5–66.8 (overlapping), 63.3 (s, major), 63.1 (s, minor), 44.4 (d, J = 142.3 Hz, minor), 43.7 (d, J = 142.9 Hz, major), 39.5, 39.2 (d, J = 2.2 Hz), 32.2–32.5 (overlapping), 18.5–18.8 (overlapping), 13.8, 13.5–13.7 (overlapping); ^{31}P NMR (243 MHz, $CDCl_3$): δ 22.5 (s).

References

1. *Organophosphorus Chemistry: From Molecules to Applications* (ed Iaroshenko, V.) (Wiley-VCH, 2019).
2. Delfino, R. T., Ribeiro, T. S. & Figueroa-Villar, J. D. Organophosphorus compounds as chemical warfare agents: a review. *Journal of the Brazilian Chemical Society* **20,** 407–428. doi:10.1590/S0103-50532009000300003 (2009).
3. Eddleston, M., Buckley, N. A., Eyer, P. & Dawson, A. H. Management of acute organophosphorus pesticide poisoning. *The Lancet* **371,** 597–607 (2008).
4. Costa, L. G. Organophosphorus Compounds at 80: Some Old and New Issues. *Toxicological Sciences* **162,** 24–35. doi:10.1093/toxsci/kfx266. (2018).
5. Quin, L. D. *A Guide to Organophosphorus Chemistry* (Wiley-Interscience, 2000).
6. *The Chemistry of Organophosphorus Compounds* (ed Palmer, D.) (States Academic Press, 2023).
7. Reusch, W. *Properties of Phosphorus Compounds* Chemistry LibreTexts. (2023).
8. *Organophosphorus Chemistry: Volume 52* (eds Higham, L. J. & Allen, D. W.) ISBN: 978-1-83767-216-5. doi:10 . 1039 / 9781837672738 (Royal Society of Chemistry, Cambridge, 2024).
9. Chambers, H. W. in *Organophosphates: Chemistry, Fate, and Effects* (eds Chambers, J. E. & Levi, P. E.) 3–17 (Academic Press, San Diego, 1992).
10. Petroianu, G. A. The synthesis of phosphor ethers: who was Franz Anton Voegeli? *Die Pharmazie* **65,** 306–307 (2010).
11. Petroianu, G. A. The history of cholinesterase inhibitors: who was Moschnin(e)? *Die Pharmazie* **64,** 729–730 (2009).
12. Tudosie, G., Serban, D. & Ţincu, R. From the discovery of combat gases to insecticides and bioterrorism - a brief history. *Revista de Medicină Militară* **CXXV,** 112–120 (2022).
13. Moffett, D. B. Public Health Impacts of Organophosphates and Carbamates (ed Gupta, R. C.) 599–606. doi:10.1016/B978-012088523-7/50041-7 (2006).
14. Marrs, T. C., Maynard, R. L. & Sidell, F. R. Chemical Warfare Agents: Toxicology and Treatment. *John Wiley & Sons* (1996).

15. Boczkowski, M., Popiel, S., Nawała, J. & Suska, H. History of Organophosphorus Compounds in the Context of Their Use as Chemical Warfare Agents. *Molecules* **30,** 1615. ISSN: 1420-3049. doi:10.3390/molecules30071615 (2025).

16. Adeyinka, A., Muco, E., Regina, A. C. & Pierre, L. in *StatPearls* Bookshelf ID: NBK499860 (StatPearls Publishing, Treasure Island (FL), 2025).

17. Fee, D. C., Gard, D. R. & Yang, C.-H. in *Kirk-Othmer Encyclopedia of Chemical Technology* (John Wiley & Sons, Inc., 2000). doi:10.1002/0471238961.16081519060505.a01.

18. Sidhu, G. K., Singh, S., Kumar, V., Dhanjal, D. S., Datta, S. & Singh, J. Toxicity, monitoring and biodegradation of organophosphate pesticides: A review. *Critical Reviews in Environmental Science and Technology* **49,** 1–53. doi:10.1080/10643389.2019.1565554 (2019).

19. Corbridge, D. E. C. *Phosphorus: Chemistry, Biochemistry and Technology* (CRC Press, 2016).

20. Balali-Mood, B. in *Basic and Clinical Toxicology of Organophosphorus Compounds* 1–23 (Springer, 2013). doi:10.1007/978-1-4471-5625-3_1.

21. Engel, S. M., Berkowitz, R. M., Barr, D. B., Chevrier, J., Rubinstein, A. M., Wolff, J. M., Wetmur, M. S. & Perera, F. P. Prenatal organophosphate metabolite and organochlorine levels and performance on the Brazelton Neonatal Behavioral Assessment Scale in a multiethnic pregnancy cohort. *American Journal of Epidemiology* **165,** 1397–1404. doi:10.1093/aje/kwm029 (2007).

22. Taylor and Francis. *Organophosphorus compounds* https://taylorandfrancis.com/knowledge/Engineering$_$and$_$technology/Chemical$_$engineering/Organophosphorus$_$compounds/. (2025).

23. Harsági, N. & Keglevich, G. The Hydrolysis of Phosphinates and Phosphonates: A Review. *Molecules* **26,** 2840. doi:10.3390/molecules26102840 (2021).

24. Eriksen, E. F., Díez-Pérez, A. & Boonen, S. Update on long-term treatment with bisphosphonates for postmenopausal osteoporosis: a systematic review. *Bone* **58,** 126–135. doi:10.1016/j.bone.2013.09.023 (2014).

25. Kosolapoff, G. M. *Organophosphorus Compounds* (Wiley, 1950).

26. *Phosphorus(III) Ligands in Homogeneous Catalysis: Design and Synthesis* (eds Kamer, P. C. J. & van Leeuwen, P. W. N. M.) ISBN: 9780470666272. doi:10.1002/9781118299715 (John Wiley & Sons, Ltd, Chichester, 2012).

27. *Phosphorus(III) Ligands in Homogeneous Catalysis: Design and Synthesis* 1st ed. (eds Kamer, P. C. J. & van Leeuwen, P. W. N. M.) ISBN: 9780470666272. doi:10.1002/9781118299715 (John Wiley & Sons, Ltd., Chichester, 2012).

28. Montchamp, J.-L. Phosphinate Chemistry in the 21st Century: A Viable Alternative to the Use of Phosphorus Trichloride in Organophosphorus Synthesis. *Accounts of Chemical Research* **47,** 77–87. doi:10.1021/ar400071v (2014).

29. U.S. Environmental Protection Agency. *Method 8141B: Organophosphorus Compounds by Gas Chromatography* Patent SW-846. (2015).

30. Lockridge, O., Verdier, L. & Schopfer, L. M. Half-life of chlorpyrifos oxon and other organophosphorus esters in aqueous solution. *Chemico-Biological Interactions* **311,** 108788. doi:10.1016/j.cbi.2019.108788 (2019).

31. Karadağ, A. & Akbaş, H. in *Recent Advances in Ionic Liquids* (ed Editors, I.) (InTechOpen, 2018). doi:10.5772/intechopen.76613.

32. Velencoso, M. M., Battig, A., Markwart, J. C., Schartel, B. & Wurm, F. R. Molecular Firefighting—How Modern Phosphorus Chemistry Can Help Solve the Challenge of Flame Retardancy. *Angewandte Chemie International Edition* **57,** 10450–10467. doi:10.1002/anie.201711735 (2018).

33. Ung, S. P.-M. & Li, C.-J. From rocks to bioactive compounds: a journey through the global P(V) organophosphorus industry and its sustainability. *RSC Sustainability* **1,** 11–37. doi:10.1039/D2SU00015F (2023).

34. Nycz, J. E. The Synthesis of Hypodiphosphoric Acid and Derivatives with P–P Bond, including Esters and Diphosphine Dioxides: A Review. *Molecules* **26,** 7286. doi:10.3390/molecules26237286 (2021).

35. Gilmour, R. Phosphorus Compounds. *Kirk-Othmer Encyclopedia of Chemical Technology.* doi:10.1002/0471238961.16081519060505.a01.pub3 (2019).

36. Huangfu, X., Wang, Z., Chen, Y. & Wei, J. Viewpoint on the functionalization of white phosphorus in China. *National Science Review* **11.** CC BY 4.0 license. doi:10.1093/nsr/nwae162 (2024).

37. Ábrányi-Balogh, P., Harsági, N., Drahos, L. & Keglevich, G. A Study on the Direct Esterification of Monoalkylphosphates and Dialkylphosphates; The Conversion of the Latter Species to Trialkylphosphates by Alkylating Esterification. *Molecules* **27.** Editor: Gregory Chatel, 4674. doi:10.3390/molecules27154674 (2022).

38. Wauters, I., Debrouwer, W. & Stevens, C. V. Preparation of phosphines through C–P bond formation. *Beilstein Journal of Organic Chemistry* **10,** 1064–1096. doi:10.3762/bjoc.10.106 (2014).

39. Ma, Y., Chen, F., Bao, J., Wei, H., Shi, M. & Wang, F. Practical way for the synthesis of phosphine oxides and phosphine sulfides from benzyl alcohol derivatives. *Tetrahedron Letters* **57,** 2465–2467. doi:10.1016/j.tetlet.2016.04.035 (2016).

40. Trofimov, B. A., Arbuzova, S. N. & Gusarova, N. K. Phosphine in the synthesis of organophosphorus compounds. *Russian Chemical Reviews* **68,** 215–227. doi:10.1070/RC1999v068n03ABEH000464 (1999).

41. Leyssens, T. & Peeters, D. Theoretical study of the influence of phosphorus containing substituents on organic molecules. *Journal of Molecular Structure: THEOCHEM* **686,** 71–82. ISSN: 0166-1280. doi:10.1016/j.theochem.2004.08.013 (2004).

42. Leyssens, T. & Peeters, D. Negative hyperconjugation in phosphorus stabilized carbanions. *The Journal of Organic Chemistry* **73,** 2725–2730. ISSN: 0022-3263. doi:10.1021/jo7025756 (2008).

43. Yu, H., Yang, H., Shi, E. & Tang, W. Development and clinical application of phosphorus-containing drugs. *Medicine in Drug Discovery* **6,** 100050. doi:https://doi.org/10.1016/j.medidd.2020.100063 (2020).

44. Johnson, D. S. & Li, J. J. *The Art of Drug Synthesis* 80–81. ISBN: 9780471752158 (Wiley-Interscience, Hoboken, NJ, US, 2007).

45. Odlo, K., Klaveness, J., Rongved, P. & Hansen, T. V. Synthesis of combretastatins A-1 and B-1. *Tetrahedron Letters* **47,** 1101–1103. doi:10.1016/j.tetlet.2005.12.037 (2006).

46. Falagas, M. E., Vouloumanou, E. K., Samonis, G. & Vardakas, K. Z. Fosfomycin. *Clinical Microbiology Reviews* **29,** 321–347. doi:10.1128/cmr.00068-15 (2016).

47. Tan, K. R., Rudolph, U. & Lüscher, C. Hooked on benzodiazepines: GABA_A receptor subtypes and addiction. *Trends in Neurosciences* **34,** 188–197. doi:10.1016/j.tins.2011.01.004 (2011).

48. Prasher, P. & Sharma, M. Medicinal chemistry of pyrophosphate mimics: A mini review. *Drug Development Research* **83,** 3–15. doi:https://doi.org/10.1002/ddr.21877 (2022).

49. Yang, S., Froeyen, M., Lescrinier, E., Marliere, P. & Herdewijn, P. 3-Phosphono-L-alanine as pyrophosphate mimic for DNA synthesis using HIV-1 reverse transcriptase. *Organic and Biomolecular Chemistry* **9,** 111–119 (2011).

50. Prasher, P. & Sharma, M. N-acetylgalactosaminyltransferase: a potential target for colorectal adenocarcinoma. *Future Medicinal Chemistry* **12,** 1529–1531 (2020).

51. Teng, K.-H. & Liang, P.-H. Undecaprenyl diphosphate synthase, a cis-prenyltransferase synthesizing lipid carrier for bacterial cell wall biosynthesis. *Molecular Membrane Biology* **29,** 267–273 (2012).

52. Rahmani, F., Bouamrane, O. L. & Bouabdallah, A. B. Biomimetic Hydroxyapatite Crystals Growth on Phosphorylated Chitosan Films by In Vitro Mineralization Used as Dental Substitute Materials. *Polymers* **15,** 1845. doi:https://doi.org/10.3390/polym15112470 (2023).

53. Zakzak, K., Semenescu, A. D., Moacă, E. A. & Predescu, I. Comprehensive Biosafety Profile of Carbomer-Based Hydrogel Formulations Incorporating Phosphorus Derivatives. *Gels* **10,** 477. doi:10.3390/gels10070477 (2024).

54. Bruchajzer, E., Frydrych, B. & Szymańska, J. A. Organophosphorus flame retardants – Toxicity and influence on human health. *Medycyna Pracy* **66,** 235–264. doi:10.13075/mp.5893.00120 (2015).

55. Du, J., Li, H., Xu, S., Zhou, Q., Jin, M. & Tang, J. A review of organophosphorus flame retardants (OPFRs): occurrence, bioaccumulation, toxicity, and organism exposure. *Environmental Science and Pollution Research International* **26,** 22126–22136. doi:10.1007/s11356-019-05669-y (2019).

56. Schartel, B. Phosphorus-Based Flame Retardancy Mechanisms—Old Hat or a Starting Point for Future Development? *Materials* **3,** 4710–4745. doi:10.3390/ma3104710 (2010).

57. Bika, S. H., Adeniji, A. O., Okoh, A. I. & Okoh, O. O. Spatiotemporal Distribution and Analysis of Organophosphate Flame Retardants in the Environmental Systems: A Review. *Molecules* **27,** 573. doi:10.3390/molecules27020573 (2022).

58. Li, Y., Qi, L., Liu, Y., Qiao, J., Wang, M., Liu, X. & Li, S. Recent Advances in Halogen-Free Flame Retardants for Polyolefin Cable Sheath Materials. *Polymers* **14,** 2876. doi:10.3390/polym14142876 (2022).

59. Jiang, W., Hao, J. & Han, Z. Study on the thermal degradation of mixtures of ammonium polyphosphate and a novel caged bicyclic phosphate and their flame retardant effect in polypropylene. *Polymer Degradation and Stability* **97,** 632–637. doi:10.1016/j.polymdegradstab.2012.01.001 (2012).

60. Wehbi, M., Mehdi, A., Negrell, C., David, G., Alaaeddine, A. & Ameduri, B. Phosphorus-containing fluoropolymers: State of the art and applications. *ACS Applied Materials & Interfaces* **12,** 38–59. doi:10.1021/acsami.9b16228 (2020).

61. Benbouguerra, K., Chafaa, S., Chafai, N., Mehri, M., Moumeni, O. & Hellal, A. Synthesis, spectroscopic characterization and a comparative study of the corrosion inhibitive efficiency of an α-aminophosphonate and Schiff base derivatives: Experimental and theoretical investigations. *Journal of Molecular Structure* **1157,** 165–176. doi:10.1016/j.molstruc.2017.12.049 (2018).

62. Carvalho, L. A., Leoni, G. B., de M. Silva, J., da Silva, M. T., Fontes, R. A., Freitas, T. C., de Carvalho, L. J. & Brasil, S. L. D. C. Study of Aminophosphonic Acid Molecules as Corrosion Inhibitors Available to Purchase. *Corrosion,* 1–10. doi:10.5006/C2025-00448 (2025).

63. Amar, H., Benzakour, J., Derja, A., Villemin, D. & Moreau, B. A corrosion inhibition study of iron by phosphonic acids in sodium chloride solution. *Journal of Electroanalytical Chemistry* **558,** 131–139. doi:10.1016/S0022-0728(03)00388-7 (2003).

64. Macan Schönleben, A., den Ouden, F., Yin, S., Fransen, E., Bosschaerts, S., Andjelkovic, M., Rehman, N., van Nuijs, A. L. N., Covaci, A. & Poma, G. Organophosphorus Flame Retardant, Phthalate, and Alternative Plasticizer Contamination in Novel Plant-Based Food: A Food Safety Investigation. *Environmental Science & Technology* **59,** 9209–9220. ISSN: 0013-936X. doi:10.1021/acs.est.4c11805 (2025).

65. Mino, T., Omura, A., Uda, Y., Wakui, K., Haga, Y., Sakamoto, M. & Fujita, T. Chiral phosphine-prolineamide as an organocatalyst in direct asymmetric aldol reaction: An effective method for stereoselective synthesis. *Tetrahedron: Asymmetry* **22,** 2024–2028. doi:10.1016/j.tetasy.2011.11.021 (2011).

66. Coyle, E. E., Doonan, B. J., Holohan, A. J., Walsh, K. A., Lavigne, F., Krenske, E. H. & O'Brien, C. J. Catalytic Wittig Reactions of Semi- and Nonstabilized Ylides Enabled by Ylide Tuning. *Angewandte Chemie International Edition* **53,** 12907–12911. doi:10.1002/anie.201406103 (2014).

67. Ecobichon, D. J. *Toxic Effects of Pesticides* 4th ed. (eds Amdur, M. O., Doull, J. & Klaassen, C. D.) 565–622. ISBN: 9780080402918 (Pergamon Press, New York, 1991).

68. United States Environmental Protection Agency. *EPA Actions to Protect the Public from Exposure to Chlorpyrifos* https://www.epa.gov/ingredients-used-pesticide-products/chlorpyrifos. (2020).

69. Scoy-DaSilva, A. R. V., Pennell, A. & Zhang, X. in *Reviews of Environmental Contamination and Toxicology* 53–70 (Springer, Cham, 2015). doi:10.1007/978-3-319-23573-8_3.

70. Karami-Mohajeri, S., Ahmadipour, A., Rahimi, H.-R. & Abdollahi, M. Adverse effects of organophosphorus pesticides on the liver: a brief summary of four decades of research. *Archives of Industrial Hygiene and Toxicology* **68,** 261–275. ISSN: 0004-1254. doi:10.1515/aiht-2017-68-2989 (2017).

71. Agency for Toxic Substances and Disease Registry (ATSDR). *Part 2: What are Cholinesterase Inhibitors?* https://archive.cdc.gov/www_atsdr_cdc_gov/csem/cholinesterase-inhibitors/inhibitors.html. Last reviewed: June 26, 2023. Accessed: September 7, 2025. U.S. Centers for Disease Control, Prevention, Agency for Toxic Substances, and Disease Registry, (2023).

72. Worek, F., Thiermann, H. & Wille, T. Organophosphorus compounds and oximes: a critical review. *Archives of Toxicology* **94,** 2275–2292. doi:10.1007/s00204-020-02797-0 (2020).

73. *Handbook of Toxicology of Chemical Warfare Agents* Second (ed Gupta, R. C.) ISBN: 978-0-12-800159-2. doi:10.1016/C2013-0-15402-5 (Academic Press, Elsevier Inc., 2015).

74. Jung, H., Heo, J., Park, N., Lim, K. C., Jung, H., Cao, V. D. & Joung, S. Elimination of A-234 from the environment: Effect of different decontaminants. *Journal of Hazardous Materials* **451,** 131150. doi:10.1016/j.jhazmat.2023.131150 (2023).

75. Steinrücken, H. C. & Amrhein, N. The herbicide glyphosate is a potent inhibitor of 5-enolpyruvylshikimic acid-3-phosphate synthase. *Biochemical and Biophysical Research Communications* **94,** 1207–1212. doi:10.1016/0006-291X(80)90547-1 (1980).

76. Maeda, H. & Dudareva, N. The Shikimate Pathway and Aromatic Amino Acid Biosynthesis in Plants. *Annual Review of Plant Biology* **63,** 73–105. doi:10.1146/annurev-arplant-042811-105439 (2012).

77. Kaushal, J., Khatri, M. & Arya, S. K. A treatise on Organophosphate pesticide pollution: Current strategies and advancements in their environmental degradation and elimination. *Ecotoxicology and Environmental Safety* **207,** 111483. ISSN: 0147-6513. doi:10.1016/j.ecoenv.2020.111483 (2021).

78. Duke, S. O. & Reddy, K. N. Glyphosate: Environmental Fate and Impact. *Weed Science* **68,** 213–229 (2020).

79. Williams, G. M., Kroes, R. & Munro, I. C. Safety evaluation and risk assessment of the herbicide Roundup and its active ingredient, glyphosate, for humans. *Regulatory Toxicology and Pharmacology* **31,** 117–165. doi:10.1006/rtph.1999.1371 (2000).

80. Duke, S. O. & Powles, S. B. Glyphosate: a once-in-a-century herbicide. *Pest Management Science* **64,** 319–325. doi:10.1002/ps.1518 (2008).

81. Davoren, M. J. & Schiestl, R. H. Glyphosate-based herbicides and cancer risk: a post-IARC decision review of potential mechanisms, policy and avenues of research. *Carcinogenesis* **39,** 1207–1215. doi:10.1093/carcin/bgy105 (2018).

82. Priestman, M. A., Funke, T., Singh, I. M., Crupper, S. S. & Schönbrunn, E. 5-Enolpyruvylshikimate-3-phosphate synthase from *Staphylococcus aureus* is insensitive to glyphosate. *FEBS Letters* **579,** 728–732. doi:10.1016/j.febslet.2004.12.057 (2005).

83. Kumar, V., Kumar, P. & Singh, J. in *Contaminants in Agriculture and Environment: Health Risks and Remediation* (eds Kumar, V. & Kumar, P.) 269–283 (Agro-bios / Agriculture and Environmental Science Academy, 2019). doi:10.26832/AESA-2019-CAE-0159-01.

84. Singh, B. K. & Walker, A. Microbial degradation of organophosphorus compounds. *FEMS Microbiology Reviews* **30,** 428–471 (2006).

85. Ragnarsdottir, K. V. Environmental fate and toxicology of organophosphate pesticides. *Journal of the Geological Society* **157,** 859–876 (2000).

86. Argüello, M. A. G., Valderrama, J. F. N., Villa, F. A. A. & Pérez, F. J. M. Environmental Risk Assessment of Chlorpyrifos and TCP in Aquatic Ecosystems. *Revista EIA* **17,** 1–12. doi:10.24050/reia.v17i34.1313 (2020).

87. Kanissery, R. G., Gairhe, B., Kadyampakeni, D., Batuman, O. & Alferez, F. Glyphosate: Its Environmental Persistence and Impact on Crop Health and Nutrition. *Plants* **8,** 499. doi:10.3390/plants8110499 (2019).

88. Oulamara, H., Amrane, A. & Benderdouche, N. Advances in Heavy Metal Extraction Using Organophosphorus Compounds: A Comprehensive Review. *Metals* **15,** 524. doi:10.3390/met15050524 (2025).

89. *Organophosphorus Chemistry 2018* (ed Keglevich, G.) ISBN: 978-3-03928-237-1. doi:10.3390/books978-3-03928-237-1 (MDPI, Basel, 2020).

90. Clayden, J., Greeves, N. & Warren, S. *Organic Chemistry* 2nd (Oxford University Press, Oxford, 2012).

91. Wittig, G. & Schöllkopf, U. Über Triphenyl-phosphin-methylen als olefinbildende Reagenzien. *Berichte der deutschen chemischen Gesellschaft (A and B)* **87B,** 1318–1330 (1954).

92. Ilia, G., Simulescu, V., Plesu, N., Chiriac, V. & Merghes, P. Recent Advances in Ultrasound-Assisted Wittig and Aza-Wittig Syntheses. *Molecules* **28,** 1830 (2023).

93. Michaelis, A. & Kaehne, R. U. Ueber das Verhalten der Jodalkyle gegen die sogen. Phosphorigsäureester oder O-Phosphine. *Berichte der deutschen chemischen Gesellschaft* (1898).

94. Arbuzov, A. E. Reactions of Alkyl Halides with Phosphites; On the Structure of Phosphonic Acid and Its Derivatives, Isomerization and Transition of Bonds from Trivalent to Pentavalent Phosphorus. *Journal of the Russian Physical-Chemical Society* **38.** Also published in Chemisches Zentralblatt, 1906, II, 1639, 687 (1906).

95. Kostoudi, S. & Pampalakis, G. Improvements, Variations and Biomedical Applications of the Michaelis–Arbuzov Reaction. *International Journal of Molecular Sciences* **23,** 3395. doi:10.3390/ijms23063395 (2022).

96. Zhang, J., Hu, W., Chen, Z., Wu, N., Li, C., Chen, T. & Han, L.-B. Water-Promoted Mild and General Michaelis–Arbuzov Reaction of Triaryl Phosphites and Aryl Iodides by Palladium Catalysis. *Organic Letters* **26,** 3386–3390. doi:10.1021/acs.orglett.4c00820 (2024).

97. Babar, J., Ahmad, S., Parveen, B., Ali, K. G., Mushtaq, A., Zahoor, A. F., Ahmad, R., Mansha, A. & Irfan, A. Exploring the Synthetic Potential of Horner-Wadsworth-Emmons Reaction Toward the Synthesis of Polyketide Based Natural Products: A Review. *Topics in Current Chemistry (Cham)* **383,** 20. doi:10.1007/s41061-025-00504-0 (2025).

98. IUPAC-IUB Commission on Biochemical Nomenclature. Nomenclature of phosphorus-containing compounds of biochemical importance (Recommendations 1976). *Molecular and Cellular Biochemistry* **21,** 184–192. doi:10.1007/BF00240136 (1978).

99. Jr., W. S. W. & Emmons, W. D. The Horner–Wadsworth–Emmons olefination: A new synthesis of alkenes from aldehydes, ketones, and substituted phosphonate carbanions. *Journal of the American Chemical Society* **83,** 1733 (1961).

100. *Horner–Wadsworth–Emmons Reaction* https://www.tcichemicals.com/TW/en/product/name_reaction/Horner-Wadsworth-Emmons_reaction. Accessed: August 11, 2025. Tokyo Chemical Industry Co., Ltd. (TCI Chemicals), (2025).

101. Bouzina, A., Aouf, Z., Amira, A., Bouone, Y. O., Bentoumi, H., Chemam, Y., Ibrahim-Ouali, M., Zerrouki, R. & Aouf, N.-E. Recent Advances in the Mitsunobu and Related Reactions: A Review from 2010 to 2024. *Topics in Current Chemistry* **383,** —. doi:10.1007/s41061-025-00501-3 (2025).

102. Zhou, X., Xu, L., Ma, Z., Cui, J. & Wang, B. Mitsunobu reaction: assembling C–N bonds in chiral traditional Chinese medicine. *RSC Advances* **15,** 5167–5189. doi:10.1039/D4RA08573F (2025).

103. Mitsunobu, O., Yamada, M. & Mukaiyama, T. Preparation of Esters of Phosphoric Acid by the Reaction of Trivalent Phosphorus Compounds with Diethyl Azodicarboxylate in the Presence of Alcohols. *Bulletin of the Chemical Society of Japan* **40,** 935–939. doi:10.1246/bcsj.40.935 (1967).

104. Tönjes, J., Kell, L. & Werner, T. Organocatalytic Stereospecific Appel Reaction. *Organic Letters* **25,** 9114–9118. doi:10.1021/acs.orglett.3c03463 (2023).

105. Mahata, A., Kumari, N. & Chakraborty, B. Catalytic Appel Reaction Accessing the Mesoporous Substructure of a Robust and Heterogeneous Polyphosphamide. *ChemCatChem* **16,** e202400729. doi:10 . 1002 / cctc . 202400729 (2024).

106. Appel, R. Tertiary Phosphane/Tetrachloromethane, a Versatile Reagent for Chlorination, Dehydration, and P–N Linkage. *Angewandte Chemie International Edition in English* **14,** 801–811. doi:10.1002/anie.197508011 (1975).

107. Chetry, A. B. Cutting-Edge Bioorthogonal Chemistry: Innovations, Practical Applications, and Emerging Trends. *European Journal of Chemistry* **15,** 355–365. doi:10.5155/eurjchem.15.3.355-365.2579 (2024).

108. Zielke, F. M. & Rutjes, F. P. J. T. Recent Advances in Bioorthogonal Ligation and Bioconjugation. *Topics in Current Chemistry* **381.** doi:10.1007/s41061-023-00445-6 (2023).

109. Brodt, N. & Niemeyer, J. Chiral organophosphates as ligands in asymmetric metal catalysis. *Organic Chemistry Frontiers* **10,** 3080–3102 (2023).

110. Duckett, S. B., Newell, C. L. & Eisenberg, R. Observation of New Intermediates in Hydrogenation Catalyzed by Wilkinson's Catalyst, $RhCl(PPh_3)_3$, Using Parahydrogen-Induced Polarization. *Journal of the American Chemical Society* **116,** 10548–10556. doi:10.1021/ja00102a023 (1994).

111. Demchuk, O. M. & Jasiński, R. Organophosphorus ligands: Recent developments in design, synthesis, and application in environmentally benign catalysis. *Phosphorus, Sulfur, and Silicon and the Related Elements* **191,** 245–253. doi:10.1080/10426507.2015.1064921 (2016).

112. Zhao, P.-F., Wang, K., Wen, J.-X., Zhu, Z.-M.-D., Zhang, H., Wang, Z.-H., Liao, Y.-X., Da, C.-S. & Du, Z.-H. Recent advances in chiral phosphoric acids for asymmetric organocatalysis: a catalyst design perspective. *Organic & Biomolecular Chemistry.* doi:10.1039/D5OB00719D (2025).

113. Jiang, B., Huang, Z.-G. & Cheng, K.-J. Preparation of N-phenyl-(S)-prolinol-derived P, N-ligands and their application in Pd-catalyzed asymmetric allylic alkylation. *Tetrahedron: Asymmetry* **17,** 942–951. doi:10.1016/j.tetasy.2006.03.010 (2006).

114. Mino, T., Tanaka, Y., Yabusaki, T., Okumura, D., Sakamoto, M. & Fujita, T. AC(aryl)-N(amine) bond atropisomeric aminophosphine: preparation and use as a ligand in a catalytic asymmetric allylic alkylation. *Tetrahedron: Asymmetry* **14,** 2503–2506. ISSN: 0957-4166. doi:https://doi.org/10.1016/S0957-4166(03)00545-7 (2003).

115. Martin, R. & Buchwald, S. L. Palladium-Catalyzed Suzuki-Miyaura Cross-Coupling Reactions Employing Dialkylbiaryl Phosphine Ligands. *Accounts of Chemical Research* **41,** 1461–1473 (2008).

116. Matsuoka, W., Harabuchi, Y., Nagata, Y. & Maeda, S. Highly chemoselective ligands for Suzuki–Miyaura cross-coupling reaction based on virtual ligand-assisted screening. *Organic & Biomolecular Chemistry* **21,** 3132–3142. doi:10.1039/D3OB00398A (2023).

117. Ohta, H., Tokunaga, M., Obora, Y., Iwai, T., Iwasawa, T., Fujihara, T. & Tsuji, Y. A bowl-shaped phosphine as a ligand in palladium-catalyzed Suzuki–Miyaura coupling of aryl chlorides: effect of the depth of the bowl. *Organic Letters* **9,** 89–92. doi:10.1021/ol0626138 (2007).

118. Lamola, J. L., Moshapo, P. T., Holzapfel, C. W. & Maumela, M. C. Evaluation of P-bridged biaryl phosphine ligands in palladium-catalysed Suzuki–Miyaura cross-coupling reactions. *RSC Advances* **11,** 26883–26891. doi:10.1039/D1RA04947J (2021).

119. Surry, D. S. & Buchwald, S. L. Dialkylbiaryl phosphine ligands in Pd-catalyzed amination: a user's guide. *Chemical Science* **2,** 27–50 (2011).

120. Lundgren, R. J. & Stradiotto, M. Recent advances in the Buchwald–Hartwig amination reaction enabled by the application of sterically demanding phosphine ancillary ligands. *Aldrichimica Acta* **45,** 59–62. doi:10.1002/chin.201333251 (2012).

121. Guo, H., Fan, Y.-C., Sun, Z., Wu, Y. & Kwon, O. Phosphine Organocatalysis. *Chemical Reviews* **118,** 10049–10293. doi:10.1021/acs.chemrev.8b00081 (2018).

122. Lu, X. & Han, X. Nucleophilic Chiral Phosphines: Powerful and Versatile Catalysts for Asymmetric Annulations. *Accounts of Chemical Research* **49,** 2428–2440 (2016).

123. Lockridge, O. & Schopfer, L. M. Review: Organophosphorus toxicants, in addition to inhibiting acetylcholinesterase activity, make covalent adducts on multiple proteins and promote protein crosslinking into high molecular weight aggregates. *Chemico-Biological Interactions* **376,** 110460. doi:10.1016/j.cbi.2023.110460 (2023).

124. Qian, S. & Lin, H. Colorimetric Sensor Array for the Detection and Identification of Organophosphorus and Carbamate Pesticides. *Analytical Chemistry* **87,** 5395–5400. doi:10.1021/acs.analchem.5b00738 (2015).

125. Dhull, V. Acetylcholinesterase Biosensors for Electrochemical Detection of Organophosphorus Pesticides—a Review. *Journal of Analytical Methods in Chemistry* **2013,** 731501. doi:10.1155/2013/731501 (2013).

126. Luo, S., Peng, R., Wang, Y., Liu, X., Ren, J., Li, W., Xiong, Y., Yi, S. & Wen, Q. Enzyme-targeted near-infrared fluorescent probe for organophosphorus pesticide residue detection. *Analytical and Bioanalytical Chemistry* **415,** 4849–4859. doi:10.1007/s00216-023-04801-9 (2023).

127. Rajapaksha, A. A., Fu, Y.-X., Guo, W.-Y., Liu, S.-Y., Li, Z.-W., Xiong, C.-Q., Yang, W.-C. & Yang, G.-F. Review on the recent progress in the development of fluorescent probes targeting enzymes. *Methods and Applications in Fluorescence* **9,** 032001. ISSN: 2050-6120. doi:10.1088/2050-6120/abf988 (2021).

128. Xu, Y., Li, F., Ma, J., Li, J., Xie, H., Wang, C., Chen, P. & Wang, L. Lipase-Catalyzed Phospha-Michael Addition Reactions under Mild Conditions. *Molecules* **27,** 7798. doi:10.3390/molecules27227798 (2022).

129. Li, B., Fu, Y. & Cheng, J. Fluorescent Probes for Detection of Organophosphorus Nerve Agents and Simulants. *Progress in Chemistry* **33,** 1461–1472 (2021).

130. Belabassi, Y., Alzghari, S. & Montchamp, J.-L. Revisiting the Hirao Cross-Coupling: Improved Synthesis of Aryl and Heteroaryl Phosphonates. *Journal of Organometallic Chemistry* **693,** 3171–3178. doi:10.1016/j.jorganchem.2008.07.020 (2008).

131. Ghoghari, R. N. & Chikhalia, K. H. Copper catalysed construction of C–P bond: C–H functionalization. *Journal of Organometallic Chemistry* **1027,** 123512. doi:10.1016/j.jorganchem.2025.123512 (2025).

132. Corre, S. S. L., Berchel, M., Couthon-Gourvès, H., Haelters, J.-P. & Jaffrès, P.-A. Atherton–Todd reaction: mechanism, scope and applications. *Beilstein Journal of Organic Chemistry* **10,** 1166–1196. ISSN: 1860-5397. doi:10.3762/bjoc.10.117 (2014).

133. Holmberg-Douglas, N. & Nicewicz, D. A. Photoredox-Catalyzed C–H Functionalization Reactions. *Chemical Reviews* **121,** 1323–1395. doi:10.1021/acs.chemrev.1c00311 (2021).

134. Wu, Q., Zhou, J., Yao, Z., Xu, F. & Shen, Q. Lanthanide Amides3Ln(μ-Cl)Li(THF)3 Catalyzed Hydrophosphonylation of Aryl Aldehydes. *The Journal of Organic Chemistry* **75,** 7498–7501. doi:10.1021/jo101743e (21 2010).

135. Herrera, R. P. Organocatalytic Hydrophosphonylation Reaction of Carbonyl Groups. *The Chemical Record* **17,** 833–840. doi:10.1002/tcr.201600129 (2017).

136. Keglevich, G. & Balint, E. The Kabachnik–Fields Reaction: Mechanism and Synthetic Use. *Molecules* **17,** 12821–12835. doi:10.3390/molecules171112821 (2012).

137. Varga, P. R. & Keglevich, G. Synthesis of α-Aminophosphonates and Related Derivatives; The Last Decade of the Kabachnik–Fields Reaction. *Molecules* **26,** 2511. doi:10.3390/molecules26092511 (2021).

138. Alegre-Requena, J. V., Marqués-López, E. & Herrera, R. P. Organocatalytic Enantioselective Hydrophosphonylation of Aldehydes Using Squaramides. *Organic & Biomolecular Chemistry* **12,** 1258–1264. doi:10.1039/C3OB42403K (8 2014).

139. He, L., Cai, Z.-H., Pian, J.-X. & Du, G.-F. NHCs Catalyzed Hydrophosphonylation of α-Ketoesters and α-Trifluoromethyl Ketones. *The Scientific World Journal* **2013,** 890187. doi:10.1155/2013/890187 (2013).

140. Xie, C., Smaligo, A., Kalek, M., Smith, A. B. & Denmark, S. E. Phosphorus-Based Catalysis. *ACS Central Science* **7,** 536–558. doi:10.1021/acscentsci.0c01493 (2021).

141. Yoo, W.-J. & Kobayashi, S. Hydrophosphinylation of Unactivated Alkenes with Secondary Phosphine Oxides under Visible-Light Photocatalysis. *Green Chemistry* **15,** 1844–1848. doi:10.1039/C3GC40482J (2013).

142. Long, H., Huang, C., Zheng, Y.-T., Li, Z.-Y., Jie, L.-H., Song, J., Zhu, S. & Xu, H.-C. Electrochemical C–H phosphorylation of arenes in continuous flow suitable for late-stage functionalization. *Nature Communications* **12,** 6629. doi:10.1038/s41467-021-26960-y (2021).

143. Hirao, T., Masunaga, T., Ohshiro, Y. & Agawa, T. A Novel Synthesis of Dialkyl Arenephosphonates. *Synthesis* **1981,** 56–57. doi:10.1055/s-1981-29335 (1981).

144. Demadis, K. D., Adla, S. K., Timonen, J. & Petri A. Turhanen, A. P. Green phosphonate chemistry – Does it exist? *Green Chemistry* **27,** 863–914. doi:10.1039/D4GC02940B (2025).

145. Tillu, V. H., Dumbre, D. K., Wakharkar, R. D. & Choudhary, V. R. One-pot three-component Kabachnik–Fields synthesis of α-aminophosphonates using H-beta zeolite catalyst. *Tetrahedron Letters* **52,** 863–866. ISSN: 0040-4039. doi:10.1016/j.tetlet.2010.11.105 (2011).

146. Hosseini-Sarvari, M. TiO_2 as a new and reusable catalyst for one-pot three-component syntheses of α-aminophosphonates in solvent-free conditions. *Tetrahedron* **64,** 5459–5466. ISSN: 0040-4020. doi:10.1016/j.tet.2008.04.016 (2008).

147. Liu, J., Xiao, H.-Z., Fu, Q. & Yu, D.-G. Advances in radical phosphorylation from 2016 to 2021. *Chemical Synthesis* **1,** 9. doi:10.20517/cs.2021.07 (2021).

148. Kaboudin, B., Behroozi, M., Sadighi, S. & Asgharzadeh, F. Recent advances in the electrochemical synthesis of organophosphorus compounds. *Beilstein Journal of Organic Chemistry* **21,** 770–797. doi:10.3762/bjoc.21.61 (2025).

149. Sharma, S. K., Chaudhary, A. & Singh, R. V. Gray Chemistry Verses Green Chemistry: Challenges and Opportunities. *Rasāyan Journal of Chemistry* **1,** 68–92 (2008).

150. CAS. *Understanding the Power of Catalysis* https://www.cas.org/resources/cas-insights/understanding-power-catalysis. Accessed: September 9, 2025. (2023).

151. Sheldon, R. A., Arends, I. & Hanefeld, U. *Green Chemistry and Catalysis* ISBN: 9783527307159. doi:10.1002/9783527611003 (WILEY-VCH Verlag GmbH & Co. KGaA, Weinheim, Germany, 2007).

152. PwC. *Net zero for the chemicals industry: A transformation in the making* https://www.pwc.com/gx/en/issues/business-model-reinvention/how-we-fuel-and-power/net-zero-chemicals-industry-transformation.html. Accessed: September 7, 2025. (2023).

153. International Union of Pure and Applied Chemistry. *IUPAC Compendium of Chemical Terminology, 5th ed. (the "Gold Book"): catalyst (C00876)* Gold Book. (2025). doi:10.1351/goldbook.C00876.

154. Rothenberg, G. *Catalysis: Concepts and Green Applications* 2nd. ISBN: 978-3-527-80260-9 (Wiley-VCH, Weinheim, 2015).

155. Kozuch, S. & Martin, J. M. L. "Turning Over" Definitions in Catalytic Cycles. *ACS Catalysis* **2,** 2787–2794. doi:10.1021/cs3005264 (2012).

156. Kozuch, S. & Shaik, S. How to Conceptualize Catalytic Cycles? The Energetic Span Model. *Accounts of Chemical Research* (2011).

157. Cornils, B. & Herrmann, W. A. Concepts in homogeneous catalysis: the industrial view. *Journal of Catalysis* **216,** 23–31. doi:10.1016/s0021-9517(02)00128-8 (2003).

158. Zhuang, G., Chen, Y., Zhuang, Z., Yu, Y. & Yu, J. Oxygen vacancies in metal oxides: recent progress towards advanced catalyst design. *Science China Materials* **63,** 2089–2118. doi:10.1007/s40843-020-1305-6 (2020).

159. Vogt, E. T. C. & Weckhuysen, B. M. Fluid catalytic cracking: recent developments on the grand old lady of zeolite catalysis. *Chemical Society Reviews* **44,** 7342–7370. doi:10.1039/C5CS00376H (2015).

160. Mabate, T. P., Maqunga, N. P., Ntshibongo, S., Maumela, M. & Bingwa, N. Metal oxides and their roles in heterogeneous catalysis: special emphasis on synthesis protocols, intrinsic properties, and their influence in transfer hydrogenation reactions. *SN Applied Sciences* **5,** 196. doi:10.1007/s42452-023-05416-6 (2023).

161. Pirkanniemi, K. & Sillanpää, M. Heterogeneous water phase catalysis as an environmental application: a review. *Chemosphere* **48,** 1047–1060. doi:10.1016/S0045-6535(02)00168-6 (2002).

162. Campbell, C. T. The Energetics of Supported Metal Nanoparticles: Relationships to Sintering Rates and Catalytic Activity. *Accounts of Chemical Research* **46,** 1712–1719. doi:10.1021/ar3003514 (2013).

163. Hansen, T. W., DeLaRiva, A. T., Challa, S. R. & Datye, A. K. Sintering of Catalytic Nanoparticles: Particle Migration or Ostwald Ripening? *Accounts of Chemical Research* **46,** 1720–1730. doi:10.1021/ar3002427 (2013).

164. Liu, L. & Corma, A. Metal Catalysts for Heterogeneous Catalysis: From Single Atoms to Nanoclusters and Nanoparticles. *Chemical Reviews* **118,** 4981–5079. doi:10.1021/acs.chemrev.7b00776 (2018).

165. Cooney, S., Pirog, R., Folger, P., Humphries, M. & Nanto, D. K. *Minerals Price Increases and Volatility: Causes and Consequences* tech. rep. RL34695 (Congressional Research Service, 2008).

166. U.S. Geological Survey. *Mineral commodity summaries 2008* Annual report (U.S. Geological Survey, Reston, VA, 2008). doi:10.3133/mineral2008.

167. Flanagan, D. M. in *Mineral Commodity Summaries 2025* (U.S. Geological Survey, 2025).

168. Stewart, A. A. in *Mineral Commodity Summaries 2025* (U.S. Geological Survey, 2025).

169. U.S. Geological Survey. *Mineral commodity summaries 2024* Annual report (U.S. Geological Survey, Reston, VA, 2024), 212. doi:10.3133/mcs2024.

170. Ewing, S. M. in *Mineral Commodity Summaries 2025* (U.S. Geological Survey, 2025).

171. Schulte, R. F. in *Mineral Commodity Summaries 2025* (U.S. Geological Survey, 2025).

172. U.S. Geological Survey. *Mineral commodity summaries 1996* (U.S. Geological Survey, National Minerals Information Center, Reston, VA, 1996). doi:10.3133/mineral1996.

173. U.S. Geological Survey. *Mineral commodity summaries 1997* (U.S. Geological Survey, National Minerals Information Center, Reston, VA, 1997). doi:10.3133/mineral1997.

174. U.S. Geological Survey. *Mineral commodity summaries 1998* (U.S. Geological Survey, National Minerals Information Center, Reston, VA, 1998). doi:10.3133/mineral1998.

175. U.S. Geological Survey. *Mineral Commodity Summaries 1999* Annual report (U.S. Geological Survey, Reston, VA, 1999). doi:10.3133/mineral1999.

176. U.S. Geological Survey. *Mineral Commodity Summaries 2000* Annual report (U.S. Geological Survey, Reston, VA, 2000). doi:10.3133/mineral2000.

177. U.S. Geological Survey. *Mineral Commodity Summaries 2001* Annual report (U.S. Geological Survey, Reston, VA, 2001). doi:10.3133/mineral2001.

178. U.S. Geological Survey. *Mineral Commodity Summaries 2002* Annual report (U.S. Geological Survey, Reston, VA, 2002). doi:10.3133/mineral2002.

179. U.S. Geological Survey. *Mineral Commodity Summaries 2003* Annual report (U.S. Geological Survey, Reston, VA, 2003). doi:10.3133/mineral2003.

180. U.S. Geological Survey. *Mineral Commodity Summaries 2004* Annual report (U.S. Geological Survey, Reston, VA, 2004). doi:10.3133/mineral2004.

181. U.S. Geological Survey. *Mineral Commodity Summaries 2005* Annual report (U.S. Geological Survey, Reston, VA, 2005). doi:10.3133/mineral2005.

182. U.S. Geological Survey. *Mineral commodity summaries 2007* Annual report (U.S. Geological Survey, Reston, VA, 2007). doi:10.3133/mineral2007.

183. U.S. Geological Survey. *Mineral commodity summaries 2009* Annual report (U.S. Geological Survey, Reston, VA, 2009). doi:10.3133/mineral2009.

184. U.S. Geological Survey. *Mineral commodity summaries 2010* Annual report (U.S. Geological Survey, Reston, VA, 2010). doi:10.3133/mineral2010.

185. U.S. Geological Survey. *Mineral commodity summaries 2011* Annual report (U.S. Geological Survey, Reston, VA, 2011). doi:10.3133/mineral2011.

186. U.S. Geological Survey. *Mineral commodity summaries 2012* Annual report (U.S. Geological Survey, Reston, VA, 2012). doi:10.3133/mineral2012.

187. U.S. Geological Survey. *Mineral commodity summaries 2013* Annual report (U.S. Geological Survey, Reston, VA, 2013), 198. doi:10.3133/mineral2013.

188. U.S. Geological Survey. *Mineral commodity summaries 2014* Annual report (U.S. Geological Survey, Reston, VA, 2014), 196. doi:10.3133/70100414.

189. U.S. Geological Survey. *Mineral commodity summaries 2015* Annual report (U.S. Geological Survey, Reston, VA, 2015), 196. doi:10.3133/70140094.

190. U.S. Geological Survey. *Mineral commodity summaries 2016* Annual report (U.S. Geological Survey, Reston, VA, 2016), 202. doi:10.3133/70170140.

191. U.S. Geological Survey. *Mineral commodity summaries 2017* Annual report (U.S. Geological Survey, Reston, VA, 2017), 202. doi:10.3133/70180197.

192. U.S. Geological Survey. *Mineral commodity summaries 2018* Annual report (U.S. Geological Survey, Reston, VA, 2018), 200. doi:10.3133/70194932.

193. U.S. Geological Survey. *Mineral commodity summaries 2019* Annual report (U.S. Geological Survey, Reston, VA, 2019), 200. doi:10.3133/70202434.

194. U.S. Geological Survey. *Mineral commodity summaries 2020* Annual report (U.S. Geological Survey, Reston, VA, 2020), 200. doi:10.3133/mcs2020.

195. U.S. Geological Survey. *Mineral commodity summaries 2021* Annual report (U.S. Geological Survey, Reston, VA, 2021), 200. doi:10.3133/mcs2021.

196. U.S. Geological Survey. *Mineral commodity summaries 2022* Annual report (U.S. Geological Survey, Reston, VA, 2022), 202. doi:10.3133/mcs2022.

197. U.S. Geological Survey. *Mineral commodity summaries 2023* Annual report (U.S. Geological Survey, Reston, VA, 2023), 210. doi:10.3133/mcs2023.

198. U.S. Geological Survey. *Mineral commodity summaries 2025* Annual report (U.S. Geological Survey, Reston, VA, 2025), 212. doi:10.3133/mcs2025.

199. Belder, D. Zinc Price 2024 Year-End Review. *Investing News Network* (2025).

200. Technology, D. P. *Zinc Prices Close 2024 with the Third-Highest Value in the Last Decade* Published January 10, 2025. Accessed: September 7, 2025. (2025).

201. Spooren, J. *et al.* Near-zero-waste processing of low-grade, complex primary ores and secondary raw materials in Europe: technology development trends. *Resources, Conservation and Recycling* **160,** 104919. doi:10.1016/j.resconrec.2020.104919 (2020).

202. Jowitt, S. M., Mudd, G. M. & Thompson, J. F. H. Future availability of non-renewable metal resources and the influence of environmental, social, and governance conflicts on metal production. *Communications Earth & Environment* **1,** 13. doi:10.1038/s43247-020-0011-0 (2020).

203. Yakoumis, I., Panou, M., Moschovi, A. M. & Panias, D. Recovery of Platinum Group Metals from Spent Automotive Catalysts: A Review. *Results in Engineering* **11.** doi:10.1016/j.rineng.2021.100175 (2021).

204. Acres, G. J. K. Platinum Group Metal Catalysis at the End of This Century. Probable Systems and the Processes Based on Them. *Platinum Metals Review* **28,** 150–157. doi:10.1595/003214084X284150157 (1984).

205. Hughes, A. E., Haque, N., Northey, S. A. & Giddey, S. Platinum Group Metals: A Review of Resources, Production and Usage with a Focus on Catalysts. *Resources* **10,** 93. doi:10.3390/resources10090093 (2021).

206. Raabe, D., Tasan, C. C. & Olivetti, E. A. Making Metals Sustainable: The Need for A Fundamental Materials Science-Based Approach. *Chemical Reviews* **123,** 8119–8175. doi:10.1021/acs.chemrev.2c00799 (2023).

207. Smith, B. J., Graziano, D. J., Riddle, M. E., Liu, D.-J., Sun, P., Iloeje, C., Kao, E. & Diamond, D. *Platinum Group Metal Catalysts Supply Chain Deep Dive Assessment* tech. rep. (U.S. Department of Energy, 2022).

208. Barbu, B. The elements of a green catalyst. *C&EN Global Enterprise* **102,** 28–34. doi:10.1021/cen-10205-cover (2024).

209. Schulte, R. F. *Mineral Commodity Summaries 2022: Platinum-Group Metals* tech. rep. (U.S. Geological Survey, 2022), 128–129.

210. Pacific Precious Metals. *Platinum vs. Gold & Silver Volatility* https://www.pacificpreciousmetals.com/blog/platinum-vs-gold-silver-volatility. (2023).

211. Straits Research. Platinum Group Metals Market Size, Growth & Analysis Report (2024).

212. London Platinum and Palladium Market. *The Noble Hedge Companion* White paper. (2012).

213. Schulte, R. F. *Mineral Commodity Summaries 2023: Platinum-Group Metals* tech. rep. (U.S. Geological Survey, 2023), 146–147.

214. Clapson, M. L., Durfy, C. S., Facchinato, D. & Drover, M. W. Base Metal Chemistry and Catalysis. *Cell Reports Physical Science* **4,** 101548. doi:10.1016/j.xcrp.2023.101548 (2023).

215. Bullock, R. M. Earth-Abundant Metal Catalysts for Energy Conversions. *Chem* **2,** 444–446. doi:10.1016/j.chempr.2017.03.019 (2017).

216. Kaplaneris, N. & Ackermann, L. Earth-abundant 3d transition metals on the rise in catalysis. *Beilstein Journal of Organic Chemistry* **18,** 86–88. doi:10.3762/bjoc.18.8 (2022).

217. Fürstner, A. Iron Catalysis in Organic Synthesis: A Critical Assessment of What It Takes To Make This Base Metal a Multitasking Champion. *ACS Central Science* **2,** 778–789. doi:10.1021/acscentsci.6b00272 (2016).

218. Li, L.-J., He, Y., Yang, Y., Guo, J., Lu, Z., Wang, C., Zhu, S. & Zhu, S.-F. Recent Advances in Mn, Fe, Co, and Ni-Catalyzed Organic Reactions. *CCS Chemistry* **6,** 537–584. doi:10.31635/ccschem.023.202303412 (2024).

219. Santulli, F., Pappalardo, D., Lamberti, M., Amendola, A., Barba, C., Sessa, A., Tepedino, G. & Mazzeo, M. Simple and Efficient Zinc Catalysts for Synthesis and Chemical Degradation of Polyesters. *ACS Sustainable Chemistry & Engineering* **11,** 15699–15709. doi:10.1021/acssuschemeng.3c04927 (2023).

220. Zeid, S. A. & Leprince-Wang, Y. Advancements in ZnO-Based Photocatalysts for Water Treatment: A Comprehensive Review. *Crystals* **14,** 611. doi:10.3390/cryst14070611 (2024).

221. Khairudin, N. F., Sukri, M. F. F., Khavarian, M. & Mohamed, A. R. Understanding the performance and mechanism of Mg-containing oxides as support catalysts in the thermal dry reforming of methane. *Beilstein Journal of Nanotechnology* **9,** 1162–1183. doi:10.3762/bjnano.9.108 (2018).

222. U.S. Geological Survey, National Minerals Information Center. *Magnesium Statistics and Information* Website: USGS Mineral Commodity Summaries 2024. (2024).

223. Rosenblum, E. & Ward, D. K. *GreenScreen Chemical Assessment for Magnesium Oxide (CAS RN 1309-48-4)* Assessment prepared for the Tile Council of North America (TCNA); Assessment expiration date: 31 January 2026. Chattanooga, TN, USA, (2021).

224. Kricheldorf, H. R., Weidner, S. M. & Scheliga, F. Ring-opening polymerizations of L-Lactide catalyzed by zinc salts: A reinvestigation. *Journal of Polymer Science* **60,** 3484–3499. doi:10.1002/pol.20220328 (2022).

225. Abbina, S. & Du, G. Zinc-Catalyzed Highly Isoselective Ring-Opening Polymerization of rac-Lactide. *ACS Macro Letters* **3,** 689–692. ISSN: 2161-1653. doi:10.1021/mz5002959 (2014).

226. Cheung, E., Alberti, C. & Enthaler, S. Chemical Recycling of End-of-Life Poly(lactide) via Zinc-Catalyzed Depolymerization and Polymerization. *ChemistryOpen* **9,** 1224–1228. doi:10.1002/open.202000243 (2020).

227. Kedruk, Y. Y., Baigarinova, G. A., Gritsenko, L. V., Cicero, G. & Abdullin, K. A. Facile Low-Cost Synthesis of Highly Photocatalytically Active ZnO Nanoparticles. *Frontiers in Materials* **9,** 869493. ISSN: 2296-8016. doi:10.3389/fmats.2022.869493 (2022).

228. Baig, A., Siddique, M. & Panchal, S. A Review of Visible-Light-Active Zinc Oxide Photocatalysts for Environmental Application. *Catalysts* **15,** 100. ISSN: 2073-4344. doi:10.3390/catal15020100 (2025).

229. Mao, T., Liu, M., Lin, L., Cheng, Y. & Fang, C. A Study on Doping and Compound of Zinc Oxide Photocatalysts. *Polymers* **14,** 4484. doi:10.3390/polym14214484 (2022).

230. Lee, K. M., Lai, C. W., Ngai, K. S. & Juan, J. C. Recent developments of zinc oxide based photocatalyst in water treatment technology: A review. *Water Research* **88,** 428–448. doi:10.1016/j.watres.2015.09.045 (2016).

231. Mutukwa, D., Taziwa, R. T. & Khotseng, L. A Review of Plant-Mediated ZnO Nanoparticles for Photodegradation and Antibacterial Applications. *Nanomaterials* **14,** 1182. ISSN: 2079-4991. doi:10.3390/nano14141182 (2024).

232. Behrens, M., Studt, F., Kasatkin, I., Kühl, S., Hävecker, M., Abild-Pedersen, F., Zander, S., Girgsdies, F., Kurr, P., Kniep, B.-L., Tovar, M., Fischer, R. W., Nørskov, J. K. & Schlögl, R. The Active Site of Methanol Synthesis over $Cu/ZnO/Al_2O_3$ Industrial Catalysts. *Science* **336,** 893–897. doi:10.1126/science.1219831 (2012).

233. Arenas-Quevedo, M. G., Manríquez, M. E., Wang, J. A., Elizalde-Solís, O., González-García, J., Zúñiga-Moreno, A. & Chen, L. F. ZnO–Doped CaO Binary Core–Shell Catalysts for Biodiesel Production via Mexican Palm Oil Transesterification. *Inorganics* **12,** 51. ISSN: 2304-6740. doi:10.3390/inorganics12020051 (2024).

234. Fattah, I. M. R., Ong, H. C., Mahlia, T. M. I., Mofijur, M., Silitonga, A. S., Rahman, S. M. A. & Ahmad, A. State of the Art of Catalysts for Biodiesel Production. *Frontiers in Energy Research* **8,** 101. ISSN: 2296-598X. doi:10.3389/fenrg.2020.00101 (2020).

235. Yang, D., Wang, L., Li, D. & Wang, R. Magnesium Catalysis in Asymmetric Synthesis. *Chem* **5,** 1108–1166. doi:10.1016/j.chempr.2019.02.002 (2019).

236. Wang, L., Lv, J., Zhang, Y. & Yang, D. Asymmetric magnesium catalysis for important chiral scaffold synthesis. *Organic & Biomolecular Chemistry* **22,** 4778–4800. doi:10.1039/D4OB00521J (2024).

237. Eladeb, A. Magnesium Oxide (MgO) as a Sustainable Catalyst for Biodiesel Production from Waste Cooking Oil: A Comparative Study with KOH. *Engineering, Technology & Applied Science Research* **14,** 13751–13756. doi:10.48084/etasr.7055 (2024).

238. Puello-Polo, E., Arias, D. & Márquez, E. Al_2O_3–MgO Supported Ni, Mo, and NiMo Mixed Phosphidic–Sulphidic Phase for Hydrotreating of Stearic and Oleic Acids into Green Diesel. *Frontiers in Chemistry* **10,** 880051. doi:10.3389/fchem.2022.880051 (2022).

239. Ruhaimi, A. H., Kamarudin, N., Kamarudin, M. F. M. F. & Sairin, N. A. Magnesium oxide-based adsorbents for carbon dioxide capture: Current progress and future opportunities. *Journal of CO_2 Utilization* **51,** 101641. doi:10.1016/j.jcou.2021.101641 (2021).

240. Alam, M. N., Asif, M., Tahir, M., Ilyas, M., Khan, M. A. R., Tariq, M., Khan, I., Saeed, F., Alharthi, A., Saeed, K. & Iqbal, J. Advances in Rubber Compounds Using ZnO and MgO as Activators. *Polymers* **14,** 5289. doi:10.3390/polym14235289 (2022).

241. Kashezheva, M., Kedakhezheva, R., Morozov, V., Kolesnikov, R., Voropaev, V., Mezentsev, S., Vasilenko, E., Vernigorova, E., Kuchuk, O. & Simonov, A. Harnessing Nanocatalysts for Sustainable Chemical Processes: Innovations in Green Chemistry. *Asian Journal of Green Chemistry* **9,** 57–82. doi:10.48309/AJGC.2025.483172.1564 (2025).

242. Qiao, B., Wang, A., Yang, X., Allard, L. F., Jiang, Z., Cui, Y., Liu, J., Li, J. & Zhang, T. Single-atom catalysis of CO oxidation using Pt1/FeOx. *Nature Chemistry* **3,** 634–641. doi:10.1038/nchem.1095 (2011).

243. Zhang, Q., Mei, W., Jiang, L., Zheng, Q., Luo, C. & Zhang, G. Environmental fate and effects of organophosphate flame retardants in the soil-plant system. *Soil Ecology Letters* **3,** 178–188. doi:10.1007/s42832-021-0084-4 (2021).

244. Luo, J., Waterhouse, G. I. N., Peng, L. & Chen, Q. Recent progress in high-loading single-atom catalysts and their applications. *Industrial Chemistry & Materials* **1,** 486–500. doi:10.1039/D3IM00062A (2023).

245. Mitchell, S. & Pérez-Ramírez, J. Single atom catalysis: a decade of stunning progress and the promise for a bright future. *Nature Communications* **11.** doi:10.1038/s41467-020-18182-5 (2020).

246. Diac, C., Maxim, F. I., Tirca, R., Ciocanea, A., Filip, V., Vasile, E. & Stamatin, S. N. Electrochemical Recycling of Platinum Group Metals from Spent Catalytic Converters. *Metals* **10,** 822. doi:10.3390/met10060822 (2020).

247. Kamisono, M., Hanada, T. & Goto, M. Platinum Group Metal Recycling from Spent Automotive Catalysts Using Reusable Hydrophobic Deep Eutectic Solvent. *ACS Sustainable Resource Management* **5,** 1021–1028. doi:10.1021/acssusresmgt.4c00100 (1 2024).

248. Juve, J.-M. A., Christensen, F. M. S., Wang, Y. & Wei, Z. Electrodialysis for metal removal and recovery: A review. *Chemical Engineering Journal* **435,** 134857. doi:10.1016/j.cej.2022.134857 (2022).

249. Ertl, G., Knozinger, H. & Weitkamp, J. *Preparation of Solid Catalysts* ISBN: 3-527-29827-4 (WILEY-VCH Verlag GmbH, Weinheim, Germany, 1999).

250. Moreira, H., Pereira, S. I. A., Mench, M., Garbisu, C., Kidd, P. & Castro, P. M. L. Phytomanagement of Metal(loid)-Contaminated Soils: A Review of the Main Promising Cash Crops and the Associated-Cropping Systems. *Frontiers in Environmental Science* **9** (2021).

251. Meers, E., Vandecasteele, B., Ruttens, A., Vangronsveld, J. & Tack, F. Potential of five willow species (*Salix* spp.) for phytoextraction of heavy metals. *Environmental and Experimental Botany* **60,** 57–68. doi:10.1016/j.envexpbot.2006.06.008 (2007).

252. Jones, S., Bardos, R. P., Kidd, P. S., Mench, M., de Leij, F., Hutchings, T., Cundy, A., Joyce, C., Soja, G., Friesl-Hanl, W., Herzig, R. & Menger, P. Biochar and compost amendments enhance copper immobilisation and support plant growth in contaminated soils. *Journal of Environmental Management* **171,** 101–112. doi:10.1016/j.jenvman.2016.01.024 (2016).

253. Garbisu, C., Urra, J., Mench, M. & Kidd, P. *Guide to best phytomanagement practices for the recovery of biodiversity in degraded and contaminated sites* https://www.phytosudoe.eu/wp-content/uploads/2020/05/PRODUCT-WP-2-GUIDE-TO-BEST-PHYTOMANAGEMENT-PRACTICES.pdf. (2020).

254. Pandey, V. C., Bhattacharya, T. & Chakraborty, S. Metal phytoremediation potential of naturally growing plants on fly ash dumpsite of Patratu thermal power station, Jharkhand, India. *International Journal of Phytoremediation* **18,** 87–93. doi:10.1080/15226514.2015.1109605 (2016).

255. Kumar, K., Shinde, A., Aeron, V., Verma, A. & Arif, N. S. Genetic engineering of plants for phytoremediation: advances and challenges. *Environmental Science and Pollution Research* **32,** 12–30. doi:10.1007/s13562-022-00776-3 (2023).

256. Kennen, K. & Kirkwood, N. *Phyto: Principles and Resources for Site Remediation and Landscape Design* 1st. ISBN: 9781315746661 (Routledge, 2015).

257. Vangronsveld, J., Herzig, R., Weyens, N., Boulet, J., Adriaensen, K., Ruttens, A., Thewys, T., Vassilev, A., Meers, E., Nehnevajova, E., van der Lelie, D. & Mench, M. Phytoremediation of contaminated soils and groundwater: Lessons from the field. *Environmental Science and Pollution Research* **16,** 765–794. doi:10.1007/s11356-009-0213-6 (2009).

258. Bhargava, A., Carmona, F. F., Bhargava, M. & Srivastava, S. Approaches for enhanced phytoextraction of heavy metals. *Journal of Environmental Management* **105,** 103–120. doi:10.1016/j.jenvman.2012.04.002 (2012).

259. Seth, C. S. A review on mechanisms of plant tolerance and role of transgenic plants in environmental clean-up. *The Botanical Review* **78,** 32–62. doi:10.1007/s12229-011-9092-x (2012).

260. Fasani, E., Manara, A., Martini, F., Furini, A. & DalCorso, G. The potential of genetic engineering of plants for the remediation of soils contaminated with heavy metals. *Plant, Cell & Environment* **41,** 1201–1232. doi:10.1111/pce.12963 (2017).

261. Pant, M., Dolma, S., Gahlot, M., Sharma, A. & Mundepi, S. Phytoremediation of Heavy Metals (eds Singh, R. P., Singh, P. & Srivastava, A.) 313–340. doi:10.1007/978-981-99-0397-9_15 (2023).

262. Lee, J. H. An overview of phytoremediation as a potentially promising technology for environmental pollution control. *Biotechnology and Bioprocess Engineering* **18,** 431–439. doi:10.1007/s12257-013-0193-8 (2013).

263. Gerhardt, K. E., Huang, X.-D., Glick, B. R. & Greenberg, B. M. Phytoremediation and rhizoremediation of organic soil contaminants: potential and challenges. *Plant Science* **176,** 20–30. doi:10.1016/j.plantsci.2008.09.014 (2009).

264. Alsafran, M., Usman, K., Ahmed, B., Rizwan, M., Saleem, M. H. & Jabri, H. A. Understanding the Phytoremediation Mechanisms of Potentially Toxic Elements: A Proteomic Overview of Recent Advances. *International Journal of Molecular Sciences* **23,** 5633. doi:10.3389/fpls.2022.881242 (2022).

265. Fässler, E., Robinson, B. H., Stauffer, W., Gupta, S. K., Papritz, A. & Schulin, R. Phytomanagement of metal-contaminated agricultural land using sunflower, maize and tobacco. *Agriculture, Ecosystems & Environment* **136,** 49–58. doi:10.1016/J.AGEE.2009.11.007 (2010).

266. Rascio, N. & Navari-Izzo, F. Heavy metal hyperaccumulating plants: How and why do they do it? And what makes them so interesting? *Plant Science* **180,** 169–181 (2011).

267. Miller, R. R. Phytoremediation. *Technology Overview Report* (1996).

268. Kidd, P. S., Mench, M., Álvarez-López, V., Bert, V., Dimitriou, I., Friesl-Hanl, W., Janssen, J. O., Kolbas, A., Muller, I., Neu, S., Renella, G., Rutten, A., Vangronsveld, J. & Puschenreiter, M. Agronomic practices for improving gentle remediation of trace element-contaminated soils. *International Journal of Phytoremediation* **17,** 1005–1037. doi:10.1080/15226514.2014.1003788 (2015).

269. Vangronsveld, J., Assche, F. V. & Clijsters, H. Reclamation of a bare industrial area contaminated by non-ferrous metals: in situ metal immobilization and revegetation. *Environmental Pollution* **87,** 51–59. doi:10.1016/S0269-7491(99)80007-4 (1995).

270. Radziemska, M., Vaverková, M. D. & Baryła, A. Phytostabilization—Management Strategy for Stabilizing Trace Elements in Contaminated Soils. *International Journal of Environmental Research and Public Health* **14,** 958. doi:10.3390/ijerph14090958 (2017).

271. Clemente, R., Escolar, Á. & Bernal, M. P. Heavy metals fractionation and organic matter mineralisation in contaminated calcareous soil amended with organic materials. *Bioresource Technology* **97,** 1894–1901. doi:10.1016/j.biortech.2005.08.018 (2006).

272. Mench, M., Bussière, S., Boisson, J., Castaing, E., Vangronsveld, J., Ruttens, A., Koe, T. D., Bleeker, P., Assunção, A. & Manceau, A. Progress in remediation and revegetation of the barren Jales gold mine spoil after in situ treatments. *Plant and Soil* **249,** 187–202. doi:10.1023/A:1022566431272 (2003).

273. Rinklebe, J. & Shaheen, S. M. Miscellaneous additives can enhance plant uptake and affect geo-chemical fractions of copper in a heavily polluted riparian grassland soil. *Ecotoxicology and Environmental Safety* **119,** 58–65 (2015).

274. Bleeker, P. M., Assunção, A. G. L., Teiga, P. M., de Koe, T. & Verkleij, J. A. C. Revegetation of the acidic, As contaminated Jales mine spoil tips using a combination of spoil amendments and tolerant grasses. *Science of the Total Environment* **300,** 1–13. doi:10.1016/s0048-9697(02)00081-5 (2002).

275. Soriano-Disla, J. M., Navarro-Pedreño, J. & Gómez, I. Contribution of a sewage sludge application to the short-term carbon sequestration across a wide range of agricultural soils. *Environmental Earth Sciences* **61,** 1613–1619. doi:10.1007/s12665-010-0474-x (2010).

276. Zanuzzi, A., Arocena, J. M., van Mourik, J. M. & Cano, A. F. Amendments with organic and industrial wastes stimulate soil formation in mine tailings as revealed by micromorphology. *Geoderma* **154,** 69–75. doi:10.1016/j.geoderma.2009.09.014 (2009).

277. Zornoza, R., Faz, A., Carmona, D. M., Martínez-Martínez, S. & Acosta, J. A. Plant cover and soil biochemical properties in a mine tailing pond five years after application of marble wastes and organic amendments. *Pedosphere* **22,** 22–32. doi:10.1016/S1002-0160(11)60188-4 (2012).

278. Mench, M., Lepp, N., Bert, V., Schwitzguébel, J.-P., Gawronski, S. W., Schröder, P. & Vangronsveld, J. Successes and limitations of phytotechnologies at field scale: Outcomes, assessment and outlook from COST Action 859. *Journal of Soils and Sediments* **10,** 1039–1070. doi:10.1007/s11368-010-0190-x (2010).

279. Nissim, W. G. *Introduction to Phytotecnologies and Phytomanagement* tech. rep. (University of Milano-Bicocca, 2023).

280. Kumar, P. B. A., Dushenkov, V., Motto, H. & Raskin, I. Phytoextraction: The Use of Plants To Remove Heavy Metals from Soils. *Environmental Science & Technology* **29,** 1232–1238. doi:10.1021/es00005a014 (1995).

281. Schwitzguébel, J.-P., Comino, E., Plata, N. & Khalvati, M. Is phytoremediation a sustainable and reliable approach to clean-up contaminated water and soil in Alpine areas? *Environmental Science and Pollution Research* **18,** 842–856. doi:10.1007/s11356-011-0498-0 (2011).

282. Mahar, A., Wang, P., Ali, A., Awasthi, M. K., Lahori, A. H., Wang, Q., Li, R. & Zhang, Z. Challenges and opportunities in the phytoremediation of heavy metals contaminated soils: A review. *Ecotoxicology and Environmental Safety* **126,** 111–121. ISSN: 0147-6513. doi:https://doi.org/10.1016/j.ecoenv.2015.12.023 (2016).

283. Limmer, M. & Burken, J. Phytovolatilization of Organic Contaminants. *Environmental Science & Technology* **50,** 6632–6643. doi:10.1021/acs.est.5b04113 (2016).

284. Akinbile, B. J. & Mbohwa, C. Incorporating hyperaccumulating plants in phytomining, remediation and resource recovery: recent trends in the African region – a review. *RSC Sustainability* **3,** 1652–1671. doi:10.1039/D5SU00021A (2025).

285. *Phytomanagement as a nature-based solution for polluted soils* (ed Chalot, M.) ISBN: 9780443158254 (Elsevier, 2024).

286. Allamin, I. A. Phytoremediation of Heavy Metals in Contaminated Soils: A Review. *Journal of Biochemistry, Microbiology and Biotechnology* **9,** 7–14. doi:10.54987/jobimb.v9i2.610 (2021).

287. Farraji, H., Basheer-Salimia, H. & Faraji, R. Advantages and disadvantages of phytoremediation: A concise review. *International Journal of Environmental Technology and Science* **2,** 35–41 (2016).

288. Bihanic, C., Richards, K., Olszewski, T. K. & Grison, C. Eco-Mn Ecocatalysts: Toolbox for Sustainable and Green Lewis Acid Catalysis and Oxidation Reactions. *ChemCatChem* **12,** 1529–1545. doi:10.1002/cctc.201901845 (2020).

289. Bihanic, C., Pelissier, S. D. F., Petit, E., Boulanger, C. & Grison, C. Eco-CaMnOx: a greener generation of ecocatalysts for ecofriendly oxidation processes. *ACS Sustainable Chemistry & Engineering* **8,** 4044–4057. doi:10.1021/acssuschemeng.9b05444 (2020).

290. Palermo, V., Igal, K., Migliorero, M. B. C., Sathicq, A. G., Quaranta, N., Vázquez, P. G. & Romanelli, G. P. Valorization of Different Wastes and Their Use for the Design of Multifunctional Eco-catalysts. *Waste and Biomass Valorization* **8,** 69–83. doi:10.1007/s12649-016-9634-x (2017).

291. Grison, C., Escande, V. & Biton, J. *Ecocatalysis: A New Integrated Approach to Scientific Ecology* 1–83 (2015).

292. Grison, C. & Ki, Y. L. T. Ecocatalysis, a new vision of Green and Sustainable Chemistry. *Current Opinion in Green and Sustainable Chemistry* **29,** 100461. ISSN: 2452-2236. doi:https://doi.org/10.1016/j.cogsc.2021.100461 (2021).

293. Escande, V., Garoux, L., Grison, C. M., Thillier, Y., Debart, F., Vasseur, J.-J., Boulanger, C. & Grison, C. Ecological catalysis and phytoextraction: symbiosis for future. *Applied Catalysis B: Environmental* **146,** 1–298. doi:10.1016/j.apcatb.2013.04.011 (2013).

294. Escande, V., Poullain, C., Clavé, G., Petit, E., Masquelez, N., Hesemann, P., *et al.* Bio-based and environmental input for transfer hydrogenation using EcoNi(0) catalyst in isopropanol. *Applied Catalysis B: Environmental* **210,** 495–503. doi:10.1016/j.apcatb.2017.04.023 (2017).

295. Gopiraman, M., Wei, K., Zhang, K.-Q., Chung, I.-M. & Kim, I.-S. Cultivation of a Cu/HMPC catalyst from a hyperaccumulating mustard plant for highly efficient and selective coupling reactions under mild conditions. *RSC Advances* **9,** 4531–4547. doi:10.1039/c7ra12470h (2018).

296. Deyris, P., Bert, V., Diliberto, S., Boulanger, C., Petit, E., Legrand, Y. & Grison, C. Biosourced Polymetallic Catalysis: A Surprising and Efficient Means to Promote the Knoevenagel Condensation. *Frontiers in Chemistry* **6,** 48. doi:10.3389/fchem.2018.00048 (2018).

297. Deyris, P.-A. & Grison, C. Nature, Ecology and Chemistry: An unusual combination for a new green catalysis, Ecocatalysis. *Current Opinion in Green and Sustainable Chemistry* **10,** 6–10. doi:10.1016/j.cogsc.2018.02.002 (2018).

298. Rylott, E. L. & van der Ent, A. Harnessing hyperaccumulator plants to recover technology-critical metals. *New Phytologist* **246,** 859–866. doi:10.1111/nph.20449 (3 2025).

299. Clavé, G., Garel, C., Poullain, C., Renard, B.-.-L., Olszewski, T. K., Lange, B., Shutcha, M., Faucon, M.-.-P. & Grison, C. Ullmann reaction through ecocatalysis: insights from bioresource and synthetic potential. *RSC Advances* **6,** 59550–59564. doi:10.1039/C6RA08664K (2016).

300. Alponti, L. H. R., Picinini, M., Urquieta-Gonzalez, E. A., da Silva, C. S., Silva, S. Y. S., Silva, S. C., de Oliveira, M. N., Viera, J., das Graças Fernandes da Silva, M. F. & Corrêa, A. G. Multicomponent Reactions Promoted by Ecocatalyst from Metal Hyperaccumulating Plant *Pluchea sagittalis*. *Reactions* **4,** 552–568. doi:10.3390/reactions4040033 (2023).

301. Escande, V., Renard, B. L. & Grison, C. Lewis acid catalysis and green oxidations: Sequential tandem oxidation processes induced by Mn-hyperaccumulating plants. *Environmental Science and Pollution Research* **22,** 5633–5652. doi:10.1007/s11356-014-3631-z (2015).

302. Escande, V., Velati, A., Garel, C., Renard, B.-L., Petit, E. & Grison, C. Phytoextracted mining wastes for ecocatalysis: Eco-Mn®, an efficient and eco-friendly plant-based catalyst for reductive amination of ketones. *Green Chemistry* **17,** 2188–2199. doi:10.1039/C4GC02193B (2015).

303. Escande, V., Olszewski, T. K. & Grison, C. Preparation of ecological catalysts derived from Zn hyperaccumulating plants and their catalytic activity in Diels–Alder reaction. *Comptes Rendus Chimie* **17,** 731–737. doi:10.1016/j.crci.2013.09.009 (2014).

304. Escande, V., Olszewski, T. K., Petit, E. & Grison, C. Biosourced Polymetallic Catalysts: An Efficient Means To Synthesize Underexploited Platform Molecules from Carbohydrates. *ChemSusChem* **7,** 191–195. doi:10.1002/cssc.201400078 (2014).

305. Lemoine, G. in *Bioremediation and Bioeconomy* (ed Prasad, M. N. V.) 361–388 (Elsevier, 2016). ISBN: 978-0-12-802830-8. doi:10.1016/B978-0-12-802830-8.00015-0.

306. Hanikenne, M., Talke, I. N., Haydon, M. J., Lanz, C., Nolte, A., Motte, P., Kroymann, J., Weigel, D. & Krämer, U. Evolution of metal hyperaccumulation required cis-regulatory changes and triplication of HMA4. *Nature* **453,** 391–395. doi:10.1038/nature06877 (2008).

307. Krämer, U. Metal hyperaccumulation in plants. *Annual Review of Plant Biology* **61,** 517–534. doi:10.1146/annurev-arplant-042809-112156 (2010).

308. Corso, M., An, X., Jones, C. Y., Gonzalez-Doblas, V., Schvartzman, M. S., Malkowski, E., Willats, W. G. T., Hanikenne, M. & Verbruggen, N. Adaptation of *Arabidopsis halleri* to extreme metal pollution through limited metal accumu-

lation involves changes in cell wall composition and metal homeostasis. *New Phytologist* **230,** 669–682. doi:10.1111/nph.17173 (2021).

309. Talke, I. N., Hanikenne, M. & Kramer, U. Zinc-dependent global transcriptional control, transcriptional deregulation, and higher gene copy number for genes in metal homeostasis of the hyperaccumulator Arabidopsis halleri. *Plant Physiology* **142,** 1488–1507 (2006).

310. Shanmugam, V., Lo, J.-C., Wu, C.-L., Wang, S.-L., Lai, C.-C., Connolly, E. L., Huang, J.-L. & Yeh, K.-C. Differential expression and regulation of iron-regulated metal transporters in Arabidopsis halleri and Arabidopsis thaliana – the role in zinc tolerance. *New Phytologist* **190,** 125–137. doi:10.1111/j.1469-8137.2010.03606.x (2011).

311. Szopiński, M., Sitko, K., Gieroń, Ż., Rusinowski, S., Corso, M. & Hermans, C. Toxic Effects of Cd and Zn on the Photosynthetic Apparatus of the Arabidopsis halleri and Arabidopsis arenosa Pseudo-Metallophytes. *Frontiers in Plant Science* **10,** 748. doi:10.3389/fpls.2019.00748 (2019).

312. Dietrich, C. C., Tandy, S., Murawska-Wlodarczyk, K., Banas, A., Korzeniak, U., Seget, B. & Babst-Kostecka, A. Phytoextraction efficiency of Arabidopsis halleri is driven by the plant and not by soil metal concentration. *Chemosphere* **285,** 131437. doi:10.1016/j.chemosphere.2021.131437 (2021).

313. Abramov, V. S. Reaction of Dialkyl Phosphites with Aldehydes and Ketones (A New Method of Synthesis of Esters of Hydroxyalkanephosphonic Acids). *Doklady Akademii Nauk SSSR* **73,** 487–489 (1950).

314. Kolodiazhna, A. O. & Kolodiazhnyi, O. I. Catalytic Asymmetric Synthesis of C-Chiral Phosphonates. *Symmetry* **14,** 1758. doi:10.3390/sym14091758 (9 2022).

315. Keglevich, G. Synthesis and Reactions of α-Hydroxyphosphonates. *Molecules* **23,** 1493. doi:10.3390/molecules23061493 (2018).

316. Kaboudin, B., Daliri, P., Faghih, S. & Esfandiari, H. Hydroxy- and Amino-Phosphonates and -Bisphosphonates: Synthetic Methods and Their Biological Applications. *Frontiers in Chemistry* **10,** 890696. doi:10.3389/fchem.2022.890696 (2022).

317. Radai, Z. & Keglevich, G. Synthesis and Reactions of α-Hydroxyphosphonates. *Molecules* **23.** ISSN: 1420-3049. doi:10.3390/molecules23061493 (2018).

318. Bálint, E., Tajti, Á., Ádám, A., Csontos, I., Karaghiosoff, K., Czugler, M., Ábrányi-Balogh, P. & Keglevich, G. The Synthesis of α-Aryl-α-Aminophosphonates and α-Aryl-α-Aminophosphine Oxides by the Microwave-Assisted Pudovik Reaction. *Beilstein Journal of Organic Chemistry* **13,** 76–86. doi:10.3762/bjoc.13.10 (2017).

319. Thottempudi, V. & Chung, K.-H. Niobium(V) Chloride Catalyzed Abramov Reaction: An Efficient Protocol for the Preparation of α-Hydroxy Phosphonates. *Bulletin of the Korean Chemical Society* **29,** 1781–1784. doi:10.5012/bkcs.2008.29.9.1781 (2008).

320. Radai, Z. α-Hydroxyphosphonates as Versatile Starting Materials. *Phosphorus, Sulfur, and Silicon and the Related Elements* **194,** 425–437. doi:10.1080/10426507.2018.1544132 (2019).

321. Sobanov, A., Zolotukhin, A., Galkina, I., Galkin, V. & Cherkasov, R. Kinetics and Mechanism of the Pudovik Reaction in the Azomethine Series: III. Acid-Catalyzed Hydrophosphorylation of Imines. *Russian Journal of General Chemistry* **76,** 471–475. doi:10.1134/S1070363206030121 (2006).

322. Cherkasov, R., Galkin, V., Khabibullina, A. & Kurdi, K. A. Kinetics and Mechanism of the Pudovik Reaction. *Phosphorus, Sulfur, and Silicon and the Related Elements* **49-50,** 61–64. doi:10.1080/10426509008038907 (1990).

323. Yang, J., Qian, D.-W. & Yang, S.-D. Lewis acid-catalyzed Pudovik reaction–phospha-Brook rearrangement sequence to access phosphoric esters. *Beilstein Journal of Organic Chemistry* **18,** 1188–1194. doi:10.3762/bjoc.18.123 (2022).

324. Sobanov, A., Zolotukhin, A., Galkin, V. I., Cherkasov, R. & Pudovik, A. Kinetics and Mechanism of the Pudovik Reaction in the Azomethine Series: I. Addition of Dimethyl Hydrogen Phosphite to N-Isopropylbenzalimines. *Russian Journal of General Chemistry* **72,** 1067–1070. doi:10.1023/A:1020794530963 (2002).

325. Vincze, D., Ábrányi-Balogh, P., Bagi, P. & Keglevich, G. A Mechanistic Study on the Tautomerism of H-Phosphonates, H-Phosphinates and Secondary Phosphine Oxides. *Molecules* **24,** 3859. doi:10.3390/molecules24213859 (2019).

326. Rulev, A. Y. Recent advances in Michael addition of H-phosphonates. *RSC Advances* **4,** 25671–25688. doi:10.1039/C4RA04179H (2014).

327. Drag, M., Latajka, R., Gumienna-Kontecka, E., Kozlowski, H. & Kafarski, P. Stereoselective Synthesis, Solution Structure and Metal Complexes of (1S,2S)-2-amino-1-hydroxyalkylphosphonic Acids. *Tetrahedron: Asymmetry* **14,** 1837–1845. doi:10.1016/S0957-4166(03)00278-7 (2003).

328. Kolodiazhnyi, O. I. *Asymmetric Synthesis in Organophosphorus Chemistry: Synthetic Methods, Catalysis, and Applications* ISBN: 978-3-527-34150-4. doi:10.1002/9783527341542 (Wiley-VCH, Weinheim, Germany, 2017).

329. *Organophosphorus Chemistry: Volume 44* (eds Allen, D. W., Higham, L. J. & Tebby, J. C.) ISBN: 978-1-78262-111-9. doi:10.1039/9781782622765 (Royal Society of Chemistry, Cambridge, 2015).

330. Szalai, Z., Ábrányi-Balogh, P. & Keglevich, G. Unexpected Reaction of Dialkyl α-Hydroxy-benzylphosphonates with Dialkyl Phosphites and a Few Related Reactions. *The Journal of Organic Chemistry* **90,** 439–447. ISSN: 0022-3263. doi:10.1021/acs.joc.4c02355 (2025).

331. Kiss, N. Z., Rádai, Z., Szabó, R., Kollár, Z. & Keglevich, G. Synthesis of Organophosphates Starting from α-Hydroxyphosphonates. *Phosphorus, Sulfur, and Silicon and the Related Elements* **194,** 370–371. doi:10.1080/10426507.2018.1547722 (2019).

332. Błażewska, K. M. & Gajda, T. Assignment of the Absolute Configuration of Hydroxy- and Aminophosphonates by NMR Spectroscopy. *Tetrahedron: Asymmetry* **20,** 1337–1361. doi:10.1016/j.tetasy.2009.05.021 (2009).

333. Lorenz, W., Henglein, A. & Schrader, G. The new insecticide O,O-dimethyl 2,2,2-trichloro-1-hydroxyethylphosphonate. *Journal of the American Chemical Society* **77,** 2554–2556. doi:10.1021/ja01615a088 (1955).

334. World Health Organization. *Trichlorfon: Environmental Health Criteria 132* International Programme on Chemical Safety (World Health Organization, Geneva, 1992).

335. Kiss, N. Z., Rádai, Z. & Keglevich, G. Green syntheses of potentially bioactive α-hydroxyphosphonates and related derivatives. *Phosphorus, Sulfur, and Silicon and the Related Elements* **194,** 971–976. doi:10.1080/10426507.2019.1630407 (2019).

336. Turhanen, P. A., Demadis, K. D. & Kafarski, P. Editorial: Phosphonate Chemistry in Drug Design and Development. *Frontiers in Chemistry* **9,** 695128. ISSN: 2296-2646. doi:10.3389/fchem.2021.695128 (2021).

337. Ju, K. S., Gao, J., Doroghazi, J. R., Wang, K.-K. A., Thibodeaux, C. J., Li, S. & Metcalf, W. W. Discovery of phosphonic acid natural products by mining the genomes of 10,000 actinomycetes. *Proceedings of the National Academy of Sciences* **112,** 12175–12180. doi:10.1073/pnas.1500873112 (2015).

338. Radai, Z., Kiss, N. Z., Keglevich, G. & Keglevich, G. in *Organophosphorus Chemistry* 91–107 (Walter de Gruyter GmbH, Berlin, 2018). doi:10.1515/9783110535839-005.

339. Cheviet, T., Wein, S., Bourchenin, G., Lagacherie, M., Perigaud, C., Cerdan, R. & Peyrottes, S. β-Hydroxy- and β-aminophosphonate acyclonucleosides as potent inhibitors of *Plasmodium falciparum* growth. *Journal of Medicinal Chemistry* **63,** 8069–8087. doi:10.1021/acs.jmedchem.0c00131 (2020).

340. Bubenik, M., Rej, R., Nguyen-Ba, N., Attardo, G., Ouellet, F. & Chan, L. Novel nucleotide phosphonate analogues with potent antitumor activity. *Bioorganic & Medicinal Chemistry Letters* **12,** 3063–3066. doi:10.1016/s0960-894x(02)00679-0 (2002).

341. Patel, D. V., Rielly-Gauvin, K., Ryono, D. E., Free, C. A., Rogers, W. L., Smith, S. A. & Petrillo, E. W. α-Hydroxy Phosphinyl-Based Inhibitors of Human Renin. *Journal of Medicinal Chemistry* **38,** 4557–4569. doi:10.1021/jm00022a022 (1995).

342. Frechette, R. F., Ackerman, C., Beers, S., Look, R. & Moore, J. Novel hydroxyphosphonate inhibitors of CD-45 tyrosine phosphatase. *Bioorganic & Medicinal Chemistry Letters* **7,** 2169–2172. ISSN: 0960-894X. doi:https://doi.org/10.1016/S0960-894X(97)00390-9 (1997).

343. Bowman, M. P. *Michael addition curing using phosphine catalyst* Patent no. US20100068393A1. (2008).

344. Das, K. Antivirals targeting influenza A virus. *Journal of Medicinal Chemistry* **55,** 6263–6277. doi:10.1021/jm300455c (2012).

345. Fields, S. C. Synthesis of Natural Products Containing a C-P Bond. *Tetrahedron* **55,** 12237–12273. doi:10.1016/S0040-4020(99)00701-2 (1999).

346. Papathanasiou, K. E., Vassaki, M., Spinthaki, A., Alatzoglou, F.-E. G., Tripodianos, E., Turhanen, P. & Demadis, K. D. Phosphorus Chemistry: From Small Molecules, to Polymers, to Pharmaceutical and Industrial Applications. *Pure and Applied Chemistry* **91,** 421–441. doi:10.1515/pac-2018-1012 (2019).

347. Milen, M., John, T. M., Kis, A. S., Garádi, Z., Szalai, Z., Takács, A., Kőhidai, L., Karaghiosoff, K. & Keglevich, G. Synthesis and Cytotoxic Activity of a New Family of α-Hydroxyphosphonates with the Benzothiophene Scaffold. *Pharmaceuticals* **18,** 949. ISSN: 1424-8247. doi:10.3390/ph18070949 (2025).

348. Cheviet, T., Wein, S., Bourchenin, G., Lagacherie, M., Périgaud, C., Cerdan, R. & Peyrottes, S. β-Hydroxy- and β-Aminophosphonate Acyclonucleosides as Potent Inhibitors of Plasmodium falciparum Growth. *Journal of Medicinal Chemistry* **63,** 8069–8087. doi:10.1021/acs.jmedchem.0c00131 (2020).

349. Ramalho, J., Semelka, R. C., Ramalho, M., Nunes, R. H., AlObaidy, M. & Castillo, M. Gadolinium-Based Contrast Agents: What is the Evidence for 'Gadolinium Deposition Disease' and the Use of Chelation Therapy? *American Journal of Neuroradiology* **37,** 1192–1198. doi:10.3174/ajnr.A4615 (2016).

350. Lapusan, R., Borlan, R. & Focsan, M. Advancing MRI with magnetic nanoparticles: a comprehensive review of translational research and clinical trials. *Nanoscale Advances* **6,** 2234–2259. ISSN: 2516-0230. doi:10.1039/D3NA01064C (2024).

351. Gallo, J., Long, N. J. & Aboagye, E. O. Magnetic nanoparticles as contrast agents in the diagnosis and treatment of cancer. *Chemical Society Reviews* **42,** 7816–7833. doi:10.1039/c3cs60149h (2013).

352. Cohrssen, J. J. Regulating the Regulator of Plant Growth Regulators. *Regulation* **45,** 6–7 (2023).

353. Havlin, J. L. & Schlegel, A. J. Review of Phosphite as a Plant Nutrient and Fungicide. *Soil Systems* **5,** 52. doi:10.3390/soilsystems5030052 (2021).

354. Karthik, B., Selvakumar, P. & Thangavelu, C. Phosphonic Acids used as Corrosion Inhibitors – A Review. *Asian Journal of Chemistry* **24,** 3303–3308 (2012).

355. Kiche, R., Ouksel, L. & Bourzami, R. Synthesis and Investigations of Corrosion Inhibition Performance of an Ester and Acid α-Hydroxyphosphonates Combining Experimental, Density Functional, and Monte Carlo Methods. *Russian Journal of Physical Chemistry A* **98,** 331–345. doi:10.1134/S0036024424020171 (2024).

356. Al-Amiery, A. A., Yousif, E., Isahak, W. N. R. W. & Al-Azzawi, W. K. A Review of Inorganic Corrosion Inhibitors: Types, Mechanisms, and Applications. *Tribology in Industry* **45,** 313–339. ISSN: 0354-8996. doi:10.24874/ti.1456.03.23.06 (2023).

357. Li, W., Wilkes, R. A. & Aristilde, L. Effects of Phosphonate Herbicides on the Secretions of Plant-Beneficial Compounds by Two Plant Growth-Promoting Soil Bacteria: A Metabolomics Investigation. *ACS Environmental Au* **2,** 136–149. doi:10.1021/acsenvironau.1c00030 (2022).

358. Akiyama, T., Morita, H., Itoh, J. & Fuchibe, K. Chiral Brønsted Acid Catalyzed Enantioselective Hydrophosphonylation of Imines: Asymmetric Synthesis of α-Amino Phosphonates. *Organic Letters* **7,** 2583–2585. doi:10.1021/ol050695e (13 2005).

359. Suyama, K., Sakai, Y., Matsumoto, K., Saito, B. & Katsuki, T. Asymmetric Hydrophosphonylation of Aldehydes. *Synfacts* **6,** 0448. doi:10.1055/s-0029-1219476 (2010).

360. Fener, B. E., Härling, S. M., Krieck, S., Görls, H. & Westerhausen, M. Scope and Limitations of the s-Block Metal-Mediated Pudovik Reaction. *Chemistry – A European Journal* **26,** 7235–7243. doi:10.1002/chem.201905565 (2020).

361. Saito, B., Egami, H. & Katsuki, T. Synthesis of an Optically Active Al(salalen) Complex and Its Application to Catalytic Hydrophosphonylation of Aldehydes and Aldimines. *Journal of the American Chemical Society* **129,** 1978–1986. doi:10.1021/ja0651005 (7 2007).

362. Chen, C. & Ramalingam, B. Catalytic Enantioselective Hydrophosphonylation of Aldehydes Using the Iron Complex of a Camphor-Based Tridentate Schiff Base $[FeCl(SBAIB\text{-}d)]_2$. *Advanced Synthesis & Catalysis,* 3443–3450. doi:10.1002/adsc.201300653 (2013).

363. Li, G., Liu, F. & Wu, M. BINOLs modified at the 3,3'-positions: chemists' preferred choice in asymmetric catalysis. *ARKIVOC* **2015,** 140–174. doi:10.3998/ark.5550190.p009.060 (6 2015).

364. Liu, C., Qian, Q., Nie, K., Wang, Y., Shen, Q., Yuan, D. & Yao, Y. Lanthanide anilido complexes: synthesis, characterization, and use as highly efficient catalysts for hydrophosphonylation of aldehydes and unactivated ketones. *Dalton Transactions* **43,** 8355–8362. ISSN: 1477-9226. doi:10.1039/C4DT00522H (2014).

365. Schlemminger, I., Saida, Y., Gröger, H., Maison, W., Durot, N., Sasai, H., Shibasaki, M. & Martens, J. Concept of Improved Rigidity: How to Make Enantioselective Hydrophosphonylation of Cyclic Imines Catalyzed by Chiral

Heterobimetallic Lanthanoid Complexes Almost Perfect. *The Journal of Organic Chemistry* **65,** 4818–4825. ISSN: 0022-3263. doi:10.1021/jo991882r (2000).

366. Steppeler, F., Han, X., Kondinski, A. & Tsogoeva, S. B. Chiral Thioureas—Preparation and Significance in Asymmetric Synthesis and Medicinal Chemistry. *Molecules* **25,** 401. doi:10.3390/molecules25020401 (2020).

367. Li, W., Huang, D. & Lv, Y. Theoretical study on the mechanism and stereochemistry of the cinchona–thiourea organocatalytic hydrophosphonylation of an α-ketoester. *Organic & Biomolecular Chemistry* **11,** 7497–7506. doi:10.1039/C3OB41397G (43 2013).

368. Yamada, K., Kondo, Y., Kitamura, A., Kadota, T., Morimoto, H. & Ohshima, T. Organocatalytic Direct Enantioselective Hydrophosphonylation of N-Unsubstituted Ketimines for the Synthesis of α-Aminophosphonates. *ACS Catalysis* **13,** 3158–3163. doi:10.1021/acscatal.2c05953 (2023).

369. Akiyama, T., Itoh, J., Yokota, K. & Fuchibe, K. Enantioselective Mannich-type Reaction Catalyzed by a Chiral Brønsted Acid. *Angewandte Chemie International Edition* **43,** 1566–1568. doi:10.1002/anie.200353240 (2004).

370. Uraguchi, D. & Terada, M. Chiral Brønsted Acid-Catalyzed Direct Mannich Reactions via Electrophilic Activation. *Journal of the American Chemical Society* **126,** 5356–5357. doi:10.1021/ja0491533 (2004).

371. Zhao, Y., Li, X., Mo, F., Li, L. & Lin, X. Highly enantioselective hydrophosphonylation of imines catalyzed by SPINOL-phosphoric acid. *RSC Advances* **3,** 11895–11901. doi:10.1039/C3RA40958A (2013).

372. Hirashima, S.-I. Development of Green Asymmetric Organocatalytic Synthesis. *Yakugaku Zasshi* **141,** 1137–1145. doi:10.1248/yakushi.21-00130 (2021).

373. Babst-Kostecka, A., Schat, H., Saumitou-Laprade, P., Grodzińska, K., Bourceaux, A., Pauwels, M. & Frérot, H. Evolutionary dynamics of quantitative variation in an adaptive trait at the regional scale: The case of zinc hyperaccumulation in Arabidopsis halleri. *Molecular Ecology* **27,** 3257–3273. doi:10.1111/mec.14800 (2018).

374. Gomez-Balderas, C., Cochet, N., Bert, V., Tarnaud, E. & Sarde, C. 16S rDNA analysis of bacterial communities associated with the hyper accumulator Arabidopsis halleri grown on a Zn and Cd polluted soil. *European Journal of Soil Biology* **60,** 16–23. doi:10.1016/j.ejsobi.2013.10.006 (2014).

375. Kwapien, K., Piccinin, S. & Fabris, S. Energetics of Water Oxidation Catalyzed by Cobalt Oxide Nanoparticles: Assessing the Accuracy of DFT and DFT+U Approaches against Coupled Cluster Methods. *The Journal of Physical Chemistry Letters* **4,** 4223–4230. doi:10.1021/jz402263d (2013).

376. Petitjean, H., Guesmi, H., Lauron-Pernot, H., Costentin, G., Loffreda, D., Sautet, P. & Delbecq, F. How Surface Hydroxyls Enhance MgO Reactivity in Basic Catalysis: The Case of Methylbutynol Conversion. *ACS Catalysis* **4,** 4004–4014. doi:10.1021/cs5010807 (2014).

377. Peterson, G. R. & Scarrah, W. P. Rapeseed oil transesterification by heterogeneous catalysis. *Journal of the American Oil Chemists' Society* **61,** 1593–1597. doi:10.1007/BF02541639 (1984).

378. Karazhanov, S. Z., Ravindran, P., Fjellvåg, H. & Svensson, B. G. Electronic structure and optical properties of $ZnSiO_3$ and Zn_2SiO_4. *Journal of Applied Physics* **106,** 123701–123707. doi:10.1063/1.3268445 (2009).

379. Sádaba, I., Granados, M. L., Riisager, A. & Taarning, E. Deactivation of solid catalysts in liquid media: the case of leaching of active sites in biomass conversion reactions. *Green Chemistry* **17,** 4133–4145. doi:10.1039/C5GC00804B (2015).

380. Skropeta, D. & Schmidt, R. R. Chiral, non-racemic α-hydroxyphosphonates and phosphonic acids via stereoselective hydroxylation of diallyl benzylphosphonates. *Tetrahedron: Asymmetry* **14,** 265–273. doi:10 . 1016 / S0957 - 4166(02)00786-3 (2003).

381. Gibson, D. & Karaman, R. Metal Complexes of α-Hydroxyimino Phosphonic Acid Derivatives: Separation of the *E* and *Z* Isomers by Metal Chelation and the Preparation and Characterization of Copper bis[α-(hydroxyimino)benzyl]phosphonate·H_2O. *Inorganic Chemistry* **28,** 1928–1932. doi:10.1021/ic00309a031 (1989).

382. Simecek, J., Schulz, M., Notni, J., Plutnar, J., Kubicek, V., Havlickova, J. & Hermann, P. Complexation of Metal Ions with TRAP (1,4,7-Triazacyclononane Phosphinic Acid) Ligands and 1,4,7-Triazacyclononane-1,4,7-triacetic Acid: Phosphinate-Containing Ligands as Unique Chelators for Trivalent Gallium. *Inorganic Chemistry* **51,** 577–590. doi:10.1021/ic202103v (2012).

383. World Health Organization. *Environmental Health Criteria 221: Zinc* (WHO, Geneva, 2001).

384. U.S. Environmental Protection Agency. *Ambient Water Quality Criteria for Zinc* tech. rep. (EPA, Washington, DC, 1987).

385. American Chemical Society. *Magnesium Oxide | ACS Reagent Chemicals* https://pubs.acs.org/doi/10.1021/acsreagents.4205. (2017).

386. Vincze, D., Ábrányi-Balogh, P., Bagi, P. & Keglevich, G. A Mechanistic Study on the Tautomerism of H-Phosphonates, H-Phosphinates and Secondary Phosphine Oxides. *Molecules* **24,** 3859. doi:10.3390/molecules24213859 (2019).

387. Janesko, B. G., Fisher, H. C., Bridle, M. J. & Montchamp, J.-L. $P(=O)H$ to $P^{\circ}OH$ Tautomerism: A Theoretical and Experimental Study. *The Journal of Organic Chemistry* **80,** 10025–10032. doi:10.1021/acs.joc.5b01618 (2015).

388. Gagnon, K. J., Perry, H. P. & Clearfield, A. Conventional and Unconventional Metal–Organic Frameworks Based on Phosphonate Ligands: MOFs and UMOFs. *Chemical Reviews* **112,** 1034–1054 (2012).

389. Clearfield, A. Recent Advances in Metal Phosphonate Chemistry II. *Coordination Chemistry Reviews* **229,** 371–393 (2002).

390. Park, C.-K., Silsbee, M. R. & Roy, R. Setting Reaction and Resultant Structure of Zinc Phosphate Cement in Various Orthophosphoric Acid Cement-Forming Liquids. *Cement and Concrete Research* **28,** 1555–1567 (1998).

391. Nowack, B. Environmental chemistry of phosphonates. *Water Research* **37,** 2533–2546. doi:10.1016/S0043-1354(03)00079-4 (2003).

392. Hao, J., Feilberg, K. L. & Shapiro, A. Kinetics of Calcite Dissolution and Ca–Mg Ion Exchange on the Surfaces of North Sea Chalk Powders. *ACS Omega* **5,** 17506–17520. doi:10.1021/acsomega.0c02000 (2020).

393. Popov, K., Rönkkömäki, H. & Lajunen, L. H. J. Critical evaluation of stability constants of phosphonic acids (IUPAC Technical Report). *Pure and Applied Chemistry* **74,** 2227. doi:10.1351/pac200274112227 (2002).

394. Armand Products Company. *Potassium Carbonate Handbook* (Armand Products, Cranbury, NJ, 1999).

395. Mazaheri, H., Ong, H. C., Amini, Z., Masjuki, H. H., Mofijur, M., Su, C. H., Badruddin, I. A. & Khan, T. M. Y. An Overview of Biodiesel Production via Calcium Oxide Based Catalysts: Current State and Perspective. *Energies* **14,** 3950. doi:10.3390/en14133950 (2021).

396. Liguori, F., Oberhauser, W., Berretti, E., Poggini, L., Barbaro, P. & Moreno-Marrodán, C. Stabilization of ZnO Catalysts for Polyesters Hydrolytic Depolymerization by Incorporation into ZrO_2 Lattice: A Polylactic Acid Case Study. *Advanced Energy and Sustainability Research* **5,** 2100349. doi:10.1002/aesr.202400349 (2024).

397. Montgomery, R. M. Bridging Scales in Heterogeneous Catalysis: A Multi-scale Computational Framework for Operando Conditions. *ResearchGate.* doi:10.13140/RG.2.2.35798.97602 (2025).

398. Butera, V. Density functional theory methods applied to homogeneous and heterogeneous catalysis: a short review and a practical user guide. *Physical Chemistry Chemical Physics* **26,** 7950–7970. doi:10.1039/D4CP00266K (2024).

399. Czekaj, I., Wambach, J. & Kröcher, O. Modelling catalyst surfaces using DFT cluster calculations. *International Journal of Molecular Sciences* **10,** 4310–4329. doi:10.3390/ijms10104310 (2009).

400. Wang, G.-C., Jiang, L., Pang, X.-Y. & Nakamura, J. Cluster and Periodic DFT Calculations: The Adsorption of Atomic Nitrogen on M(111) (M = Cu, Ag, Au) Surfaces. *The Journal of Physical Chemistry B* **109,** 17943–17950. doi:10.1021/jp0500034 (2005).

401. Vogiatzis, K. D., Polynski, M. V., Kirkland, J. K., Townsend, J., Hashemi, A., Liu, C. & Pidko, E. A. Computational Approach to Molecular Catalysis by 3d Transition Metals: Challenges and Opportunities. *Chemical Reviews* **119,** 2453–2523. doi:10.1021/acs.chemrev.8b00361 (2019).

402. Zhao, Q. & Kulik, H. J. Stable Surfaces That Bind Too Tightly: Can Range-Separated Hybrids or DFT+U Improve Paradoxical Descriptions of Surface Chemistry? *The Journal of Physical Chemistry Letters* **10,** 5090–5098. doi:10.1021/acs.jpclett.9b01650 (2019).

403. Köster, K. D. & Kaghazchi, P. Hybrid functionals with nonempirical Hartree-Fock parameters for electronic structure calculation of layered oxides. *Physical Review B* **109,** 155134. doi:10.1103/PhysRevB.109.155134 (2024).

404. Harvey, J. On the accuracy of density functional theory in transition metal chemistry. *Annual Reports Section "C" (Physical Chemistry)* **102.** doi:10.1039/B419105F (2006).

405. Podobiński, J. & Datka, J. Basic Properties of ZnO, Ga_2O_3, and MgO—Quantitative IR Studies. *Catalysts* **14,** 106. doi:10.3390/catal14020106 (2024).

406. Adet, N., Specklin, D., Gourlaouen, C., Damiens, T., Jacques, B., Wehmschulte, R. J. & Dagorne, S. Towards Naked Zinc(II) in the Condensed Phase: A Highly Lewis Acidic ZnII Dication Stabilized by Weakly Coordinating Carborate Anions. *Angewandte Chemie International Edition* **60,** 2084–2088. doi:10.1002/anie.202012287 (2021).

407. Setoyama, T. Acid–base bifunctional catalysis: An industrial viewpoint. *Catalysis Today* **116,** 250–262. ISSN: 0920-5861. doi:10.1016/j.cattod.2006.01.031 (2006).

408. Rodríguez-Fernández, J., Sun, Z., Zhang, L., Tan, T., Curto, A., Fester, J., Vojvodic, A. & Lauritsen, J. V. Structural and electronic properties of Fe dopants in cobalt oxide nanoislands on Au(111). *The Journal of Chemical Physics* **150,** 041731. doi:10.1063/1.5052336 (2019).

409. Khare, R., Pandey, J., Smriti & Rupanwar, R. The Importance and Applications of Knoevenagel Reaction (Brief Review). *Oriental Journal of Chemistry* **35,** 423–429. doi:10.13005/ojc/350154 (2019).

410. Diksha, D. & Kumar, N. Recent Developments in Knoevenagel Condensation Reaction: A Review. *Journal of Advanced Scientific Research* **13,** 17–25. doi:10.55218/jasr.202213502 (2022).

411. Johari, S., Johan, M. R. & Khaligh, N. G. How Important is the Metal-free Catalytic Knoevenagel Reaction in Medicinal Chemistry? An Updated Review. *Current Medicinal Chemistry* **31,** 4286–4311. doi:10.2174/0109298673260463231122074253 (2024).

412. Van Schijndel, J., Canalle, L. A., Molendijk, D. & Meuldijk, J. Exploration of the Role of Double Schiff Bases as Catalytic Intermediates in the Knoevenagel Reaction of Furanic Aldehydes: Mechanistic Considerations. *Synlett* **29,** A–F. doi:10.1055/s-0037-1610235 (2018).

413. Van Schijndel, J., Canalle, L. A., Molendijk, D. & Meuldijk, J. The green Knoevenagel condensation: solvent-free condensation of benzaldehydes. *Green Chemistry Letters and Reviews* **10,** 404–411. doi:10.1080/17518253.2017.1391881 (2017).

414. Bruice, P. Y. *Organic Chemistry* 8th (Pearson, 2016).

415. Dalessandro, E. V., Collin, H. P., Guimarães, L. G. L., Valle, M. S. & Jr., J. R. P. Mechanism of the Piperidine-Catalyzed Knoevenagel Condensation Reaction in Methanol: The Role of Iminium and Enolate Ions. *The Journal of Physical Chemistry B* **121,** 5300–5307. doi:10.1021/acs.jpcb.7b03191 (2017).

416. Gašparová, R. & Lácová, M. Reactions of 3-Formylchromone with Active Methylene and Methyl Compounds and Some Subsequent Reactions of the Resulting Condensation Products. *Molecules* **10,** 937–960. doi:10.3390/10080937 (2005).

417. Fioravanti, S., Pellacani, L., Tardella, P. A. & Vergari, M. C. Facile and Highly Stereoselective One-Pot Synthesis of Either (E)- or (Z)-Nitro Alkenes. *Organic Letters* **10,** 1449–1451 (2008).

418. Koli, B. P. & Gore, R. P. Alum Catalyzed an Eco-Friendly Synthesis of Benzylidene Malononitrile and Benzylidene Barbituric Acid Derivatives in Aqueous Medium. *Rasayan Journal of Chemistry* **16,** 1734–1740. doi:10.31788/RJC.2023.1638394 (2023).

419. Zhang, Z., Nie, X., Wang, F., Chen, G., Huang, W.-Q., Xia, L., Zhang, W.-J., Hao, Z.-Y., Hong, C.-Y., Wang, L.-H. & You, Y.-Z. Rhodanine-based Knoevenagel reaction and ring-opening polymerization for efficiently constructing multicyclic polymers. *Nature Communications* **11,** Article 3654. doi:10.1038/s41467-020-17474-0 (2020).

420. Dhokne, P., Sakla, A. P. & Shankaraiah, N. Structural insights of oxindole based kinase inhibitors as anticancer agents: Recent advances. *European Journal of Medicinal Chemistry* **216,** 113334. doi:10.1016/j.ejmech.2021.113334 (2021).

421. Verdía, P., Santamarta, F. & Tojo, E. Knoevenagel Reaction in [MMIm][MSO_4]: Synthesis of Coumarins. *Molecules* **16,** 4379–4388. doi:10.3390/molecules16064379 (2011).

422. Osawa, T. & Obika, S. Synthesis of Coumarin-Conjugated Oligonucleotides via Knoevenagel Condensation to Prepare an Oligonucleotide Library. *Chemical and Pharmaceutical Bulletin* **72,** 143–148. doi:10.1248/cpb.c23-00295 (2024).

423. Choudary, B. M., Chowdari, N. S., Madhi, S. & Kantam, M. L. A Trifunctional Catalyst for One-Pot Synthesis of Chiral Diols via Heck Coupling–N-Oxidation–Asymmetric Dihydroxylation: Application for the Synthesis of Diltiazem and Taxol Side Chain. *The Journal of Organic Chemistry* **68,** 1736–1746. doi:10.1021/jo026687i (2003).

424. Magedov, I. V., Hortelano, O., Kuznetsov, A. K. & Kornienko, A. New Procedure for Obtaining Indomethacin. *Chemistry of Heterocyclic Compounds* **41,** 623–625. doi:10.1007/s10593-005-0169-5 (2005).

425. Novikova, D., Grigoreva, T., Gurzhiy, V. & Tribulovich, V. Is It Possible to Obtain a Product of the Desired Configuration from a Single Knoevenagel Condensation? Isomerization vs. Stereodefined Synthesis. *International Journal of Molecular Sciences* **24,** 11339. doi:10.3390/ijms241411339 (2023).

426. Cao, C., Xiao, M., Yang, X., Zhang, J., Huang, F. & Cao, Y. Cyanovinylene-based copolymers synthesized by tin-free Knoevenagel polycondensation for high-efficiency polymer solar cells. *Journal of Materials Chemistry C* **6,** 8020–8027. doi:10.1039/C8TC02021C (2018).

427. Xu, S., Liao, Z., Dianat, A., Park, S.-W., Addicoat, M. A., Fu, Y., Pastoetter, D. L., Fabozzi, F. G., Liu, Y., Cuniberti, G., Richter, M., Hecht, S. & Feng, X. Combination of Knoevenagel Polycondensation and Water-Assisted Dynamic Michael-Addition-Elimination for the Synthesis of Vinylene-Linked 2D Covalent Organic Frameworks. *Angewandte Chemie International Edition* **61,** e202202492. doi:10.1002/anie.202202492 (2022).

428. Wei, Y., Chen, W., Zhao, X., Ding, S., Han, S. & Chen, L. Solid-state emissive cyanostilbene based conjugated microporous polymers via cost-effective Knoevenagel polycondensation. *Polymer Chemistry* **7,** 3983–3988. doi:10.1039/C6PY00614K (2016).

429. Kotnik, T., Žerjav, G., Pintar, A., Žagar, E. & Kovačič, S. Highly Porous Poly(arylene cyano-vinylene) Beads Derived through the Knoevenagel Condensation of the Oil-in-Oil-in-Oil Double Emulsion Templates. *ACS Macro Letters* **10,** 1248–1253. doi:10.1021/acsmacrolett.1c00457 (2021).

430. Kotnik, T. & Kovačič, S. Modern Methods for Conjugated Polymers Preparation: A Concept of Transition Metal-Free Synthesis. *European Journal of Organic Chemistry,* e202400874. doi:10.1002/ejoc.202400874 (2025).

431. Zhou, J., Liu, J., Wang, M., Hou, W., Qin, G., Kityk, I. V., Fedorchuk, A. A., Albassam, A. A., El-Naggar, A. M. & Andrushchak, A. Novel poly(aryl ether ketone) with electro-optic chromophore side chains for light modulators. *Journal of Materials Science: Materials in Electronics* **28,** 18568–18577. doi:10.1007/s10854-017-7805-6 (2017).

432. Gupta, M. & Wakhloo, B. P. Tetrabutylammonium bromide mediated Knoevenagel condensation in water: synthesis of cinnamic acids. *ARKIVOC* **2007,** 94–98. doi:10.3998/ark.5550190.0008.110 (2007).

433. Rioux, B., Peyrot, C., Mention, M. M., Brunissen, F. & Allais, F. Sustainable Synthesis of p-Hydroxycinnamic Diacids through Proline-Mediated Knoevenagel Condensation in Ethanol: An Access to Potent Phenolic UV Filters and Radical Scavengers. *Antioxidants (Basel)* **9,** 331. doi:10.3390/antiox9040331 (2020).

434. Meyer, T., Krug, R. & Müller, T. J. J. Three-Component Suzuki–Knoevenagel Synthesis of Merocyanine Libraries and Correlation Analyses of Their Oxidation Potentials and Optical Band Gaps. *Molecules* **26,** 5149. doi:10.3390/molecules26175149 (2021).

435. Jadhav, A. L. & Yadav, G. D. Clean synthesis of benzylidenemalononitrile by Knoevenagel condensation of benzaldehyde and malononitrile: effect of combustion fuel on activity and selectivity of Ti-hydrotalcite and Zn-hydrotalcite catalysts. *Journal of Chemical Sciences* **131,** 1–14. doi:10.1007/s12039-019-1641-6 (2019).

436. Kolagkis, P. X., Serviou, S. K., Stini, N. A., Demertzidou, V. P., Poursaitidis, E. T., Galathri, E. M., Mountanea, O. G., Skolia, E. & Kokotos, C. G. Deciphering the Knoevenagel condensation: towards a catalyst-free and water-mediated process. *Organic & Biomolecular Chemistry* **22,** 8293–8299. doi:10.1039/D4OB01420K (2024).

437. Knoevenagel, E. Condensationen zwischen Aldehyden und Malonsäure unter dem Einfluss von Ammoniak und organischen Aminen. *Berichte der deutschen chemischen Gesellschaft* **31,** 2596–2619 (1898).

438. Mase, N. & Horibe, T. Organocatalytic Knoevenagel Condensations by Means of Carbamic Acid Ammonium Salts. *Organic Letters* **15,** 1854–1857 (2013).

439. Appaturi, J. N., Ratti, R., Phoon, B. L., Batagarawa, S. M., Din, I. U., Selvaraj, M. & Ramalingam, R. J. A review of the recent progress on heterogeneous catalysts for Knoevenagel condensation. *Dalton Transactions* **50,** 4445–4469. doi:10.1039/D1DT00456E (2021).

440. Chowdhury, A., Bhattacharjee, S., Chongdar, S., Malakar, B. & Bhaumik, A. A New Mixed-Metal Phosphate as an Efficient Heterogeneous Catalyst for Knoevenagel Condensation Reaction. *Catalysts* **13,** 1053. doi:10.3390/catal13071053 (2023).

441. Louzada, L. D. T., Batalha, P. N. & de Almeida, F. B. Coordination Polymers as Catalysts in Knoevenagel Condensations—A Critical Review Analysis under Synthesis Conditions and Green Chemistry. *Crystal Growth & Design* **25,** 1708–1720. doi:10.1021/acs.cgd.5c00033 (2025).

442. Chen, J.-W., Li, X., Feng, A.-S., Zou, X.-Z., Li, Y. & Gu, J.-Z. Four Metal-Organic Architectures from a Triphenyl-Tricarboxylic Acid: Synthesis, Crystal Structures, and Catalytic Features. *Transition Metal Chemistry* **47,** 301–309. doi:10.1007/s11243-022-00513-8 (2022).

443. Li, X., Wang, X., Ren, C., Palansooriya, K. N., Wang, Z. & Chang, S. X. Microplastic pollution: Phytotoxicity, environmental risks, and phytoremediation strategies. *Critical Reviews in Environmental Science and Technology* **54,** 486–507. doi:10.1080/10643389.2023.2252310 (2024).

444. Lu, Z., Yang, C., He, L., Hong, J., Huang, C., Wu, T., Wang, X., Wu, Z., Liu, X., Miao, Z., Zeng, B., Xu, Y., Yuan, C. & Dai, L. Asymmetric Hydrophosphonylation of Imines to Construct Highly Stable Covalent Organic Frameworks with Efficient Intrinsic Proton Conductivity. *Journal of the American Chemical Society* **144,** 9624–9633. doi:10.1021/jacs.2c00429 (22 2022).

445. Naskar, K., Maity, S., Maity, H. S. & Sinha, C. A Reusable Efficient Green Catalyst of 2D Cu-MOF for the Click and Knoevenagel Reaction. *Molecules* **26,** 5296. doi:10.3390/molecules26175296 (2021).

446. Liu, S., Chen, H. & Zhang, X. Bifunctional Pb10K2–Organic Framework for High Catalytic Activity in Cycloaddition of CO2 with Epoxides and Knoevenagel Condensation. *ACS Catalysis* **12,** 10373–10383. doi:10.1021/acscatal.2c02649 (2022).

447. Jyothi, R. S. M., Sripathi, M. P. & Thirupathi, P. Recent Advances in Base-assisted Michael Addition Reactions. *Current Organic Chemistry* **26,** 1264–1293. doi:10.2174/1385272826666220827095110 (2022).

448. Enders, D., Saint-Dizier, A., Lannou, M.-I. & Lenzen, A. The Phospha-Michael Addition in Organic Synthesis. *European Journal of Organic Chemistry* **2006,** 29–49. doi:10.1002/ejoc.200500593 (2006).

449. Tessema, E., Elakkat, V., Chiu, C.-F., Chiu, C.-F., Zheng, J.-H., Chan, K. L., Shen, C.-R., Zhang, P. & Lu, N. Recoverable Phospha-Michael Additions Catalyzed by a 4-N,N-Dimethylaminopyridinium Saccharinate Salt or a Fluorous

Long-Chained Pyridine: Two Types of Reusable Base Catalysts. *Molecules* **26.** doi:10.3390/MOLECULES26041159 (2021).

450. Miller, R. C., Bradley, J. S. & Hamilton, L. A. Disubstituted Phosphine Oxides. III. Addition to α, β-Unsaturated Nitriles and Carbonyl Compounds. *Journal of the American Chemical Society* **78,** 5299–5303. doi:10.1021/ja01601a039 (1956).

451. Hindersinn, R. R. & Ludington, R. S. The reaction of trialkyl phosphites with maleate esters. *Journal of Organic Chemistry* **30,** 4020–4025. doi:10.1021/jo01023a008 (1965).

452. Pudovik, A. N. & Konovalova, I. V. Addition Reactions of Esters of Phosphorus(III) Acids with Unsaturated Systems. *Synthesis* **1979,** 81–96. doi:10.1055/s-1979-28566 (1979).

453. Lenker, H. K., Richard, M. E., Reese, K. P., Carter, A. F., Zawisky, J. D., Winter, E. F., Bergeron, T. W., Guydon, K. S. & Jr., R. A. S. Phospha-Michael Additions to Activated Internal Alkenes: Steric and Electronic Effects. *The Journal of Organic Chemistry* **77,** 1378–1385. doi:10.1021/jo202183u (2012).

454. Hou, L., Kikuchi, J., Ye, H., Bao, M. & Terada, M. Chiral Phosphoric Acid-Catalyzed Enantioselective Phospha-Michael-Type Addition Reaction of Diarylphosphine Oxides with Alkenyl Benzimidazoles. *The Journal of Organic Chemistry* **85,** 14802–14809. doi:10.1021/acs.joc.0c01840 (2020).

455. Chew, R. J., Teo, K. Y., Huang, Y., Li, B.-B., Li, Y., Pullarkat, S. A. & Leung, P.-H. Enantioselective Phospha-Michael Addition of Diarylphosphines to β, γ-Unsaturated α-Ketoesters and Amides. *Chemical Communications* **50,** 8768–8770. doi:10.1039/C4CC01610F (2014).

456. Lee, Y.-J., Kurra, Y. & Liu, W. R. Phospha-Michael Addition as a New Click Reaction for Protein Functionalization. *ChemBioChem* **17,** 456–461. doi:10.1002/cbic.201500697 (2016).

457. Steiner, M. R., Schmallegger, M., Donner, L., Hlina, J. A., Marschner, C., Baumgartner, J. & Slugovc, C. Using the phospha-Michael reaction for making phosphonium phenolate zwitterions. *Beilstein Journal of Organic Chemistry* **20,** 41–51. doi:10.3762/bjoc.20.6 (2024).

458. An, F., Brossette, J., Jangra, H., Wei, Y., Shi, M., Zipse, H. & Ofial, A. R. Reactivities of tertiary phosphines towards allenic, acetylenic, and vinylic Michael acceptors. *Chemical Science* **15,** 18111–18126. doi:10.1039/D4SC04852K (2024).

459. Marqués-López, E., Sonsona, I. G., Garcés-Marín, M., Gimeno, M. C. & Herrera, R. P. Asymmetric Organocatalyzed Phospha-Michael Addition for the Direct Synthesis of Biologically Active Chromenylphosphonates. *Advanced Synthesis & Catalysis* **365,** 3234–3240. doi:10.1002/adsc.202300563 (2023).

460. Huang, X., Besset, T., Jubault, P. & Couve-Bonnaire, S. Phospha-Michael Addition on α-Fluorinated Acrylates: A Straightforward Access to Polyfunctionalized Fine Chemicals. *The Journal of Organic Chemistry* **87,** 9035–9047. doi:10.1021/acs.joc.2c00937 (2022).

461. Sagdic, G., Daglar, O., Cakmakci, E., Findik, V., Erdem, S. S., Tunca, U., Gunay, U. S. & Durmaz, H. New Horizon in Phospha-Michael Reaction: Ultrafast Double Addition of P-H Bond-Bearing Nucleophiles to Electron-Deficient Triple Bonds and Its Use for Functional Monomer Synthesis and Polymer Modification. *Macromolecules* **56,** 7006–7022. doi:10.1021/acs.macromol.3c00625 (17 2023).

462. Salin, A. V., Fatkhutdinov, A. R., Il'in, A. V., Galkin, V. I. & Shamsutdinova, F. G. Solvent Effect on Kinetics and Mechanism of the Phospha-Michael Reaction of Tertiary Phosphines with Unsaturated Carboxylic Acids. *Heteroatom Chemistry* **25,** 205–216. doi:10.1002/hc.21161 (2014).

463. Ratzenböck, K., Uher, J. M., Fischer, S. M., Edinger, D., Schallert, V., Žagar, E., Pahovnik, D. & Slugovc, C. Exploiting retro oxa-Michael chemistry in polymers. *Polymer Chemistry* **14,** 651–661. doi:10.1039/D2PY01345B (2023).

464. Hennen, D., Hartmann, D., Rieger, P. H., Oesterreicher, A., Wiener, J., Arbeiter, F., Feuchter, M., Fröhlich, E., Pichelmayer, M., Schlögl, S. & Griesser, T. Exploiting the Carbon and Oxa Michael Addition Reaction for the Synthesis of Yne Monomers: Towards the Conversion of Acrylates to Biocompatible Building Blocks. *ChemPhotoChem* **4,** 476–480. doi:10.1002/cptc.201900199 (2020).

465. Huang, X., Besset, T. & Jubault, P. Phospha-Michael Addition on α-Fluorinated Acrylates: A Straightforward Access to Polyfunctionalized Fine Chemicals. *The Journal of Organic Chemistry.* doi:10.1021/acs.joc.2c00937 (2022).

466. Huang, H. & Kang, J. Amine-Catalyzed Phospha-Michael Reaction of α,β-Unsaturated Aldehydes and Ketones with Multifunctional N-Heterocyclic Phosphine-Thioureas as Organocatalysts. *Organic Letters.* doi:10.1021/acs.orglett.6b02121 (2016).

467. Moreno, M., Lligadas, G., Ronda, J. C., Galià, M. & Cadiz, V. Phospha-Michael addition to enone-containing triglyceride derivatives as an efficient route to flame retardant renewable thermosets. *Journal of Polymer Science Part A: Polymer Chemistry* **50,** 3206–3213. doi:10.1002/pola.26106 (2012).

468. Mernyák, E., Bartha, S., Kóczán, L., Jójárt, R., Resch, V., Paragi, G., Vágvölgyi, M., Hunyadi, A., Bruszel, B., Zupkó, I. & Minorics, R. Microwave-assisted Phospha-Michael addition reactions in the 13α-oestrone series and in vitro antiproliferative properties. *Journal of Enzyme Inhibition and Medicinal Chemistry* **36,** 1931–1937. doi:10.1080/14756366.2021.1963241 (2021).

469. Conti, R., Widera, A., Müller, G., Fekete, C., Thöny, D., Eiler, F., Benkő, Z. & Grützmacher, H. Organocatalyzed Phospha-Michael Addition: A Highly Efficient Synthesis of Customized Bis(acyl)phosphane Oxide Photoinitiators. *Chemistry - European Journal* **29.** doi:10.1002/chem.202202563 (2022).

470. De los Santos, J. M., Ignacio, R., Aparicio, D. & Palacios, F. Michael Addition of Amine Derivatives to Conjugate Phosphinyl and Phosphonyl Nitrosoalkenes. Preparation of α-Amino Phosphine Oxide and Phosphonate Derivatives. *The Journal of Organic Chemistry* **72,** 5202–5206. doi:10.1021/jo0705521 (2007).

471. Gandi, V. R. & Lu, Y. Phosphine-Catalyzed Regioselective Michael Addition to Allenoates. *ChemInform* **47.** doi:10.1002/CHIN.201613029 (2016).

472. Yong, K. J., Hai, H. & Nagaraju, M. *Functionalized phosphonates via Michael addition* Patent no. US10435423B2. (2018).

473. Martin-Aranda, R. M., E. Ortega-Cantero, M. R.-C., Vicente-Rodríguez, M. & Bañares-Muñoz, M. Sonocatalysis and Basic Clays. Michael Addition Between Imidazole and Ethyl Acrylate. *Catalysis Letters* **84,** 201–204. doi:10.1023/A:1021480020425 (2002).

474. Sobkowski, M., Kraszewski, A. & Stawinski, J. Recent advances in H-phosphonate chemistry. Part 1. H-Phosphonate esters: synthesis and basic reactions. *Topics in Current Chemistry* **361,** 137–177. doi:10.1007/128_2014_562 (2014).

475. Samsonowicz-Górski, J., Koszelewski, D., Kowalczyk, P., Śmigielski, P., Hrunyk, A., Kramkowski, K., Wypych, A., Szymczak, M., Lizut, R. & Ostaszewski, R. Promiscuous Lipase-Catalyzed Knoevenagel–Phospha–Michael Reaction for the Synthesis of Antimicrobial β-Phosphono Malonates. *International Journal of Molecular Sciences* **23,** 8819. doi:10.3390/ijms23158819 (2022).

476. Simoni, D., Invidiata, F. P., Manferdini, M., Lampronti, I., Rondanin, R., Roberti, M. & Pollini, G. P. Tetramethylguanidine (TMG)-catalyzed addition of dialkyl phosphites to α,β-unsaturated carbonyl compounds, alkenenitriles, aldehydes, ketones and imines. *Tetrahedron Letters* **39,** 7615–7618. ISSN: 0040-4039. doi:https://doi.org/10.1016/S0040-4039(98)01656-6 (1998).

477. Jiang, Z., Zhang, Y., Ye, W. & Tan, C.-H. P–C Bond formation via direct and three-component conjugate addition catalyzed by 1,5,7-triazabicyclo[4.4.0]dec-5-ene (TBD). *Tetrahedron Letters* **48,** 51–54. doi:10.1016/j.tetlet.2006.11.019 (2007).

478. Wani, A. A., Chourasiya, S. S., Kathuria, D. & Bharatam, P. V. 1,1-Diaminoazines as organocatalysts in phospha-Michael addition reactions. *Chemical Communications* **57,** 11717–11720. doi:10.1039/D1CC04657H (2021).

479. Kalla, R. M. N., Park, H., Lee, H. R., Suh, H. & Kim, I. Efficient, solvent-free, multicomponent method for organic-base-catalyzed synthesis of β-phosphonomalonates. *ACS Combinatorial Science* **17,** 691–697. doi:10.1021/acscombsci.5b00109 (2015).

480. Kalla, R. M. N. & Kim, I. Tris(hydroxymethyl)aminomethane as an efficient organobase catalyst for the synthesis of β-phosphonomalonates. *Tetrahedron Letters* **58,** 410–414. doi:10.1016/j.tetlet.2016.12.035 (2017).

481. Strappaveccia, G., Bianchi, L., Ziarelli, S., Santoro, S., Lanari, D., Pizzo, F. & Vaccaro, L. PS-BEMP as a basic catalyst for the phospha-Michael addition to electron-poor alkenes. *Organic & Biomolecular Chemistry* **14,** 3521–3525. doi:10.1039/C6OB00242K (2016).

482. Sobhani, S. & Rezazadeh, S. $HClO_4 - SiO_2$ as a Novel and Recyclable Catalyst for the Phospha-Michael Addition of Phosphorous Nucleophiles to α,β-Unsaturated Malonates. *Synlett* **2010,** 1485–1488. doi:10.1055/S-0029-1220069 (2010).

483. Sobhani, S. & Jahanshahi, R. One-pot synthesis of β-phosphonomalonates catalyzed by molecular iodine. *Synthetic Communications* **43,** 3247–3257. doi:10.1080/00397911.2013.768670 (2013).

484. Comelles, J., Moreno-Mãnas, M. & Vallribera, A. Michael additions catalyzed by transition metals and lanthanide species. A review. Part 1. Transition metals. *ARKIVOC (Archive for Organic Chemistry)* **2005,** 207–238. doi:10.3998/ark.5550190.0006.921 (2005).

485. Tam, A. & Raines, R. T. Protein engineering with the traceless Staudinger ligation. **462,** 25–44. doi:10.1016/S0076-6879(09)62002-4 (2009).

486. Fischer, S. M., Renner, S., Boese, A. D. & Slugovc, C. Electron-rich triarylphosphines as nucleophilic catalysts for oxa-Michael reactions. *Beilstein Journal of Organic Chemistry* **17,** 1689–1697. doi:10.3762/bjoc.17.117 (2021).

487. Sharma, P., Gupta, R. & Bansal, R. K. Recent advances in organocatalytic asymmetric aza-Michael reactions of amines and amides. *Beilstein Journal of Organic Chemistry* **17,** 2585–2610. doi:10.3762/bjoc.17.173 (2021).

488. Connon, S. J. Asymmetric catalysis with bifunctional cinchona alkaloid-based urea and thiourea organocatalysts. *Chemical Communications* **2008,** 2499–2510. doi:10.1039/b719249e (2008).

489. Zhu, Y., Malerich, J. P. & Rawal, V. H. Squaramide-Catalyzed Enantioselective Michael Addition of Diphenyl Phosphite to Nitroalkenes. *Angewandte Chemie International Edition* **49,** 153–156. doi:10.1002/anie.200904779 (2010).

490. Haji, M. Multicomponent reactions: A simple and efficient route to heterocyclic phosphonates. *Beilstein Journal of Organic Chemistry* **12,** 1269–1301. doi:10.3762/bjoc.12.121 (2016).

491. Song, L.-L., Yang, C., Yu, Y.-Q. & Xu, D.-Z. A Simple and Green Tandem Knoevenagel-Phospha-Michael Reaction for One-Pot Synthesis of 2-Oxindol-3-ylphosphonates Catalyzed by a DABCO-Based Ionic Liquid. *Synthesis* **49,** 1641–1647. doi:10.1055/s-0036-1588357 (2017).

492. Müller, T. J. J. Multicomponent reactions II. *Beilstein Journal of Organic Chemistry* **10,** 115–116. doi:10.3762/bjoc.10.7 (2014).

493. Kour, P., Kumar, A. & Rai, V. K. Aqueous microwave-assisted DMAP catalyzed synthesis of β-phosphonomalonates and 2-amino-4H-chromen-4-ylphosphonates via a domino Knoevenagel-phospha-Michael reaction. *Comptes Rendus Chimie* **20,** 140–145. doi:10.1016/j.crci.2016.05.013 (2017).

494. Aichi, Y., Rhihil, A., Sebti, S. & Guendouzi, M. E. Effective Catalysis of Knoevenagel-phospha-Michael Addition Reaction by $ZnCl_2$ Doped Natural Phosphate. *European Chemical Bulletin* **12,** 3128–3134 (2023).

495. Ying, A., Ni, Y., Xu, S., Liu, S., Yang, J. & Li, R. Novel DABCO Based Ionic Liquids: Green and Efficient Catalysts with Dual Catalytic Roles for Aqueous Knoevenagel Condensation. *Industrial & Engineering Chemistry Research* **53,** 5678–5682. doi:10.1021/ie500440w (2014).

496. Sobhani, S. & Parizi, Z. P. An eco-friendly procedure for one-pot synthesis of β-phosphonomalonates: micellar solution of sodium stearate catalyzes tandem Knoevenagel–phospha-Michael reaction of aldehydes, malonitrile, and phosphites in aqueous media. *Tetrahedron* **67,** 3540–3545. doi:10.1016/j.tet.2011.03.014 (2011).

497. Youness, A., Rhihil, A., Sebti, S. & Guendouzi, M. E. Effective Catalysis of Knoevenagel-phospha-Michael Addition Reaction by $ZnCl_2$ Doped Natural Phosphate. *European Chemical Bulletin* **12,** 3128–3134 (2023).

498. Chowdhury, A., Bhattacharjee, S., Chongdar, S., Malakar, B., Maity, A. & Bhaumik, A. A New Mixed-Metal Phosphate as an Efficient Heterogeneous Catalyst for Knoevenagel Condensation Reaction. *Catalysts* **13,** 1053. doi:10.3390/catal13071053 (2023).

499. Amini, A., Fallah, A., Cheng, C.-H. & Tajbakhsh, M. Knoevenagel–Michael and Click Reactions on a Cu(II)/Natural Phosphate Catalyst. *Synfacts* **15,** 0412. doi:10.1055/s-0037-1612396 (2019).

500. Siahpour, Z. & Hajjami, M. Highly efficient synthesis of pyrimidine-5-carbonitrile derivatives over a robust biowaste bone char-Bronsted solid acid catalyst. *Scientific Reports* **14,** 30411. doi:10.1038/s41598-024-82040-3 (2024).

501. Homayoun, F. & Ghassamipour, S. A domino Knoevenagel-phospha-Michael reaction: One-pot synthesis of novel organophosphonates in the presence of multi-walled carbon nanotube-$CO-NH(CH_2)_2NH-SO_3H$ as catalyst. *Phosphorus, Sulfur, and Silicon and the Related Elements* **193,** 441–445. doi:10.1080/10426507.2018.1452230 (2018).

502. Ghassamipour, S. Synthesis of new organophosphonates via domino Knoevenagel-Phospha-Michael reaction catalyzed by modified multi-walled carbon nanotube. *Journal of Nano Chemistry and Electrochemistry* **1,** 1–10 (2021).

503. Tedeschi, L. & Enders, D. Asymmetric Synthesis of β-Phosphono Malonates via Fe_2O_3-Mediated Phospha-Michael Addition to Knoevenagel Acceptors. *Organic Letters* **3,** 3515–3517. doi:10.1021/ol016591v (2001).